Lecture Notes in Electrical Engineering 333

Tong-Cun Zhang
Motowo Nakajima
Editors

Advances in Applied Biotechnology

Proceedings of the 2nd International Conference on Applied Biotechnology (ICAB 2014)-Volume II

Springer

Lecture Notes in Electrical Engineering

Volume 333

About this Series

"Lecture Notes in Electrical Engineering (LNEE)" is a book series which reports the latest research and developments in Electrical Engineering, namely:

- Communication, Networks, and Information Theory
- Computer Engineering
- Signal, Image, Speech and Information Processing
- Circuits and Systems
- Bioengineering

LNEE publishes authored monographs and contributed volumes which present cutting edge research information as well as new perspectives on classical fields, while maintaining Springer's high standards of academic excellence. Also considered for publication are lecture materials, proceedings, and other related materials of exceptionally high quality and interest. The subject matter should be original and timely, reporting the latest research and developments in all areas of electrical engineering.

The audience for the books in LNEE consists of advanced level students, researchers, and industry professionals working at the forefront of their fields. Much like Springer's other Lecture Notes series, LNEE will be distributed through Springer's print and electronic publishing channels.

More information about this series at http://www.springer.com/series/7818

Tong-Cun Zhang · Motowo Nakajima
Editors

Advances in Applied Biotechnology

Proceedings of the 2nd International Conference on Applied Biotechnology (ICAB 2014)-Volume II

Springer

Editors
Tong-Cun Zhang
Tianjin University of Science and Technology
Tianjin
China

Motowo Nakajima
SBI ALApromo
Tokyo
Japan

ISSN 1876-1100 ISSN 1876-1119 (electronic)
Lecture Notes in Electrical Engineering
ISBN 978-3-662-46317-8 ISBN 978-3-662-46318-5 (eBook)
DOI 10.1007/978-3-662-46318-5

Library of Congress Control Number: 2014955624

Springer Heidelberg New York Dordrecht London

Printed on acid-free paper

Springer-Verlag GmbH Berlin Heidelberg is part of Springer Science+Business Media (www.springer.com)

Preface

The 2014 International Conference on Applied Biotechnology (ICAB 2014), organized by Chinese Society of Biotechnology and Tianjin University of Science, was held from November 28 to 30, 2014 in Tianjin, China.

The conference served as a forum for exchange and dissemination of ideas and the latest findings in aspects of applied biotechnology. The conference was complemented by talks given by more than 30 professors and researchers.

The conference papers were submitted by more than 100 authors from different universities, institutes, and companies. Numerous fields were covered, ranging from fermentation engineering, cell engineering, genetic engineering, enzyme engineering, to protein engineering.

Special thanks are given to the Secretary Staff of the conference for the commitment to the conference organization. We would also like to thank all the authors who contributed with their papers to the success of the conference.

This book gathers a selection of the papers presented at the conference. It contains contributions from both academic and industrial researchers focusing on the research and development of applied biotechnology from all over the world. The scientific value of the papers also helps researchers in this field to get more valuable results.

Tianjin, China — Tong-Cun Zhang
Tokyo, Japan — Motowo Nakajima

Contents

Part I
Microbial Genetics and Breeding

Chapter 1
Inheritance Analysis for Exserted Stigma Rate in *Japonica* Rice

Ruhua Wang, Na Yan, Xueyan Gao, Jie Yu, Fang Wang and Zetian Hua

Abstract Rice is the main crop in China. Since the discovery and exploitation of sterile strain line, three lines of *Indica* hybrid rice were bred successfully; the *Indica* hybrid rice has made great progress in production. Compared to *Indica* rice, *Japonica* hybrid rice is hard to study because it lacks the restorer gene. The key to promoting development of hybrid *Japonica* rice is to improve the yields of seed production. However, the low stigma exsertion rate of *Japonica* CMS Line is the main cause that restricts the yield of hybrid seed production of *Japonica* rice. As the inheritance mechanism of the stigma exsertion is complicated and difficult to study, the related study is far from enough. In this study, Jinke DS, a sterile line with higher stigma exsertion rate, and C9083, a restorer line with lower stigma exsertion rate, were used as parents for hybrid. P_1, P_2, F_1 and F_2 were chosen as the study materials and major gene plus polygene mixed inheritance model was chosen to analyze the genetic effects. The results showed that glume-opening single exserted stigma rate was in consistence with the E-2 model, glume-closed single exserted stigma rate was in consistence with the E-0 model, glume-opening dual exserted stigma rate, glume-opening exserted stigma rate, glume-closed dual exerted stigma rate and glume-closed exserted stigma rate were in consistence with the E-1 model.

Keywords Rice · Exserted stigma rate · Inheritance analysis

R. Wang · N. Yan · X. Gao · J. Yu · F. Wang (✉) · Z. Hua (✉)
College of Food Engineering and Biotechnology, Tianjin University of Science and Technology, Tianjin 300457, People's Republic of China
e-mail: wangfang@tust.edu.cn

Z. Hua
e-mail: hzetian@tust.edu.cn

F. Wang · Z. Hua
China National Japonica Rice R&D Center, Tianjin 300457, People's Republic of China

T.-C. Zhang and M. Nakajima (eds.), *Advances in Applied Biotechnology*,
Lecture Notes in Electrical Engineering 333, DOI 10.1007/978-3-662-46318-5_1

1.1 Introduction

The key to promoting development of hybrid *Japonica* rice is to improve the yields of seed production. But the low stigma exsertion rate of *Japonica* CMS Line is the main cause that restricts the yield of hybrid seed production of *Japonica* rice.

The exsertion of the stigma can increase the chances of pollination. Especially for the closed glumes, it is a good factor to overcome the barrier of pollination when the parents' flowering periods are different [1]. The average seed set of stigma exserted spikelet is 3–4 times higher than that of stigma non-exserted spikelet, and occupies 70–80 % of the outcrossing rate [2, 3]. As a matter of fact, it is significant to improve the stigma exsertion rate for hybrid rice seed production. Although the stigma exsertion rate is related with the ambient conditions, such as cultivation techniques, exogenous hormones, and so on, it is determined by the genetic factor, the variety itself [4, 5]. As the inheritance mechanism of the stigma exsertion is complicated and difficult to study, the related study is far from enough. In this study, we used mixed genetic model between major gene and multiple minor genes and segregation analysis to study the inheritance mechanism of stigma exsertion to explore the effects and relative importance of the major gene and multiple genes. We hope that this study can provide some theoretical basis for improving this trait.

1.2 Materials and Methods

1.2.1 Experimental Materials

F_1 generation was obtained by crossing Jinke DS with C9083, which is a male sterile line with high percentage of exserted sigma and a restorer line with low percentage of exserted sigma, respectively. F_2 generation was obtained from F_1 generation plants selfing. Jinke DS was photo-thermo sensitive male sterile line japonica rice cultivated by Tianjin University of Science and Technology, with 87 % of exserted sigma rate. C9083 was restorer line rice cultivated by China National Japonica Rice R&D Center, with 3 % of exserted sigma rate.

1.2.2 Field Experiment and Character Investigation

P_1, P_2, F_1 and F_2 groups were cultivated in experiment fields of Tianjin University of science and technology. There were 30 plants in each P_1, P_2 and F_1 groups and 900 plants in F_2 group. The row and individual spacing was 30 cm × 20 cm. The field management was the same as field production. 10 plants in P_1, P_2 and F_1 groups, as well as 204 plants in F_2 group were randomly marked, with 3 spikes marked each. Spikelet quantity, single exserted stigma quantity, and dual exserted stigma quantity were investigated by the early floret opening period. Glume-closed single exserted stigma quantity, dual exserted stigma, and spikelet quantity were investigated by the ending floret opening period. The percentage of exserted sigma was calculated with the formula:

$$\text{single exserted stigma rate} = \frac{\text{single exserted stigma quantity}}{\text{spikelet quantity}} \times 100\,\%$$

$$\text{dual exserted stigma rate} = \frac{\text{dual exserted stigma quantity}}{\text{spikelet quantity}} \times 100\,\%$$

$$\text{exserted stigma rate} = \text{single exserted stigma rate} + \text{dual exserted stigma rate}.$$

1.2.3 Genetic Analysis

The mixed genetic model between major genes and multiple minor genes [6] was applied to analyze the percentage of exserted stigma of P_1, P_2, F_1 and F_2 groups. Iterative algorithm ECM (Iterate expectation and conditional maximization) was applied to evaluate distribution parameters of each generation. Then AIC (Akaike's information criterion) was applied to screen the relatively optimum model. Fit tests, including homogeneity test $\left(U_1^2,\ U_2^2,\ U_3^2\right)$, Smirnov test ($nW^2$), and Kolmogorov test ($D_{n)}$ were then operated to select the optimum model. QTL analysis system of four generation method of major gene plus polygene and the basic symbol and parameters based on presupposition of five categories (A, B, C, D and E), totally 22 genetic models were referred to Gai and Wang [7] and Zhang [8]. Analysis software of Major gene plus polygene mixed genetic model were provided by Prof. Yuanming Zhang of Nanjing Agricultural University.

1.3 Results and Discussions

1.3.1 Character Distribution of Parents and Each Generation

C9083 was characterized as low percentage of exserted stigma (3.5 %). Jinke DS was characterized as high percentage of exserted stigma (87 %). Percentage of exserted stigma between 3.15 and 92.3 % in 204 F_2 individual plants showed a continuous distribution (Table 1.1). As shown in Table 1.1, there was a distinct peak between 30 and 45 % of exserted stigma, which showed a character of quantitative trait.

Table 1.1 Frequency distribution of trail in parents and population

Generation	Percentage of glume-closed exserted stigma								$\sum f$	$\bar{x}$	σ2
	0–10	10–20	20–30	30–40	40–50	50–60	60–70	70–100			
P_1[a]	10								10	6.51	1.007
P_2[b]							2	8	10	74.7	15.029
F_1			7	3					10	24.37	10.927
F_2	18	41	69	34	21	12	7	2	204	22.31	156.89

[a] P_1: C9083
[b] P_2: Jinke DS

1.3.2 Genetic Model

Four generation method of major gene plus polygene mixed inheritance model was applied to analyze the percentage of exserted stigma in four generations of crossing C9083 and Jinke DS. Maximum likelihood function values of a pair of major gene (A), two pairs of major gene (B), polygene (C), a pair of major gene plus polygene (D), and two pairs of major gene plus polygene (E); totally five categories of 22 kinds of genetic models were obtained. The AIC values of total percentage of exserted stigma are shown in Table 1.2. According to genetic model selection principle, minimum AIC value principle, five models with the minimum AIC values were taking the fit tests. Models with least number of statistics with significant meanings were chosen as the optimum model. Statistics $\left(U_1^2, U_2^2, U_3^2, nW^2\right) > 0.05$ was considered as not significant. The results showed that the optimum model for glume-closed exserted stigma rate was mixed genetic model E-1 between two additive-dominance major genes and additive-dominance multiple minor genes (Table 1.3). Optimum models were selected with this method.

Table 1.2 The max-likelihood value and Akaike's information criterion values under various genetic models

Model	Max-likelihood-value	AIC
A-1	−927.14	1880.29
A-2	−963.36	1936.73
A-3	−944.46	1898.92
A-4	−948.65	1967.31
B-1	−879.61	1781.23
B-2	−894.32	1804.64
B-3	−948.15	1906.30
B-4	−944.15	1904.30
B-5	−919.01	1848.02
B-6	−922.27	1852.53
C-0	−878.55	1769.11
C-1	−913.19	1846.37
D-0	−849.06	1754.12
D-1	−899.76	1813.53
D-2	−913.19	1848.48
D-3	−913.19	1848.32
D-4	−913.18	1848.37
E-0	−859.34	1745.38
E-1	−859.80	1751.63
E-2	−891.56	1793.12
E-3	−913.20	1832.44
E-4	−913.20	1823.43

Table 1.3 Tests for fitness about some traits of exserted stigma

Trait	Model	Generation	U_1^2	U_2^2	U_3^2	nW^2	D_n
Glume-opening single exserted stigma rate	E-2	P_1	0.073 (0.7868)	0.089 (0.7660)	5.008 (0.0252)	0.1633	0.2626
		P_2	0.349 (0.5545)	0.064 (0.7999)	1.627 (0.2021)	0.1586	0.2828
		F_1	0.162 (0.6876)	1.402 (0.2364)	10.100 (0.0015)	0.2096	0.2644
		F_2	0.017 (0.8971)	0.008 (0.9271)	0.018 (0.8926)	0.0334	0.0469
Glume-opening dual exserted stigma rate	E-1	P_1	0.269 (0.6037)	0.128 (0.7207)	11.836 (0.0006)	0.8558	0.5474
		P_2	0.963 (0.3265)	0.242 (0.6230)	3.363 (0.0667)	0.2871	0.3675
		F_1	0.246 (0.6200)	0.342 (0.5587)	18.144 (0.0000)	0.3448	0.3305
		F_2	0.799 (0.3714)	1.249 (0.2638)	1.016 (0.3134)	0.9200	0.1721
Glume-opening exserted stigma rate	E-1	P_1	0.013 (0.9092)	0.191 (0.6617)	1.712 (0.1907)	0.0622	0.1659
		P_2	0.009 (0.9257)	0.005 (0.9451)	0.007 (0.9315)	0.0487	0.2016
		F_1	0.002 (0.9669)	0.025 (0.8742)	0.631 (0.4270)	0.0306	0.1653
		F_2	0.001 (0.9749)	0.000 (0.9885)	0.004 (0.9489)	0.0192	0.0284
Glume-closed single exserted stigma rate	E-0	P_1	0.000 (0.9895)	0.506 (0.4768)	8.392 (0.0038)	0.3033	0.3517
		P_2	0.078 (0.7794)	0.250 (0.6168)	0.841 (0.3592)	0.0493	0.1470
		F_1	0.209 (0.6479)	0.007 (0.9349)	2.080 (0.1493)	0.1691	0.3084
		F_2	0.000 (0.9849)	0.000 (0.9862)	0.000 (0.9966)	0.0086	0.0211
Glume-closed dual exerted stigma rate	E-1	P_1	0.952 (0.3292)	3.043 (0.0811)	10.233 (0.0014)	0.9127	0.5891
		P_2	0.886 (0.3466)	0.927 (0.3356)	0.043 (0.8366)	0.1190	0.2627
		F_1	0.006 (0.9379)	0.991 (0.3195)	13.542 (0.0002)	0.2471	0.2861
		F_2	0.186 (0.6665)	3.592 (0.0580)	34.959 (0.0000)	4.9490	0.3355
Glume-closed exserted stigma rate	E-1	P_1	0.015 (0.9010)	0.346 (0.5565)	8.031 (0.0046)	0.2885	0.3356
		P_2	0.158 (0.6912)	0.461 (0.4972)	1.386 (0.2390)	0.0958	0.2058
		F_1	0.059 (0.8088)	0.169 (0.6810)	0.500 (0.4793)	0.0548	0.1739
		F_2	0.015 (0.9018)	0.010 (0.9215)	0.007 (0.9335)	0.0166	0.0303

1.4 Conclusion

In this study, we adopted the major gene plus poly gene mixed genetic model to analyze the characters of exserted stigma. Separately, two pairs of major genes were detected in six characters of exserted stigma, performing higher frequencies of heritability. In case of the target characters of loss and recession from generation to generation, selection should be done in the early generations to obtain the materials with stable higher percentage of exserted stigma. Related genes of high percentage of exserted stigma should be induced into varieties with good comprehensive characters to get more new varieties with higher yields, quality, and resistance in practice.

Acknowledgments This work was supported by National High-tech R&D Program of China (863 Program) (Grant No. 2011AA10A101), Tianjin High School Science & Technology Fund Planning Project (Grant No. 20130616) and the National Natural Science Foundation of China Grant (No. 31271676).

References

1. Li ZY (2004) Aim character disquisition on close-general the seed set of outcrossing sterile line. Reclaiming Rice Cultivation 2004(3):7–10
2. Tian DC (2004) The relationship between flowering and pollination time and outcrossing rate of male sterile lines in hybrid rice seed production. Hybrid Rice 19(3):50–54
3. Virmani SS, Atheval DS (1973) Genetic variability in floral characteristics influencing outcrossing in *Oryza sativa* L. Crop Sci 13(1):66–67
4. Wang YR (2008) Breeding and application of Japonica male sterile lines with high stigma exsertion rate in rice. Hybrid Rice 23(3):4–8
5. Virmani SS, Atheval DS (1974) Introduction of floral characteristics influencing outcrossing in rice. Crop Sci 14(3):350–353
6. Ou HL (2005) Study on the major genes plus polygenes mixed inheritance of yield and panicle traits in rice. Fujian Agric For Univ 2005:24–32
7. Gai J, Wang J (1998) Inheritance of major gene and polygene mixed inheritance model of quantitative traits by using joint analysis of Pl, F1, P2, F2 and F23 Generations. Acta Agronomica Sinica 24(6):651–659
8. Zhang Y (2002) An Expansion of the joint segregation analysis of P1, P2, P3 and F23 generations in the mixed major gene plus polygenes inheritance analysis of quantitative traits. J Biomath 17(3):363–368

Chapter 2
Cloning and Expression of β-Glucosidase from Cassava in *Pichia pastoris* GS115

Dongheng Guo, Hongming Tian, Yanshan Xu and Suiping Zheng

Abstract β-Glucosidases have been widely applied in the synthesis of alkyl polyglucosides. Studies have shown that cassava β-glucosidase has great synthesis ability. This study has realized the secretion of cassava β-glucosidase gene (*mebgl*) in *Pichia pastoris* GS115. The recombinant yeast expression vector pPICZαA-MEBGL has been successfully constructed. The constructed plasmid was linearized and integrated into *P. pastoris* GS115 strain by electroporation. Positive clones were selected on YPDZ plates and then cultured in shake flask. The supernatant was collected and used for alkyl polyglucoside synthesis. The synthesis reaction was conducted under conditions: 40 °C, pH 5.0, 10 % water content, while the conditions have not been optimized. The results of these studies have indicated that 5′AOX promoter was the best one for expression; in the shake flask fermentation, the strain had the maximum hydrolysis activity of 60 U/L, while the optimal temperature was 35 °C, the optimal pH was 6.0, *p*NP-Glc was used as substrate; the molecular mass of the recombinant monomer protein was estimated to be 70 kDa; the recombinant protein showed high ability to transfer glucose from *p*NP-Glc to n-hexyl alcohol with high yields of 60 %, and the yields would substantially increase after optimized. This recombinant cassava β-glucosidase is expected to promote the industrialization process of alkyl polyglucoside enzymatic synthesis.

Keywords Cassava β-glucosidase · *Pichia pastoris* GS115 · Secretory expression · Enzymology properties

2.1 Introduction

β-Glucosidases (E.C. 3.2.1.21) catalyze the hydrolysis of β-D-glucosidic linkages between β-D-glucose and aglycone or sugar. β-Glucosidases exhibit similar specificity for β-glucoside substrates, have a similar molecular weight (about 55–65 kDa)

D. Guo · H. Tian · Y. Xu · S. Zheng (✉)
School of Bioscience and Bioengineering, South China University of Technology, Guangzhou 510006, China
e-mail: spzheng@scut.edu.cn

T.-C. Zhang and M. Nakajima (eds.), *Advances in Applied Biotechnology*,
Lecture Notes in Electrical Engineering 333, DOI 10.1007/978-3-662-46318-5_2

and pH optima (between pH 5 and 6) [1], and are evolutionarily related. However, they may have different substrate specificities, suggesting their diverse biological functions. According to the classification of glycosyl hydrolases based on amino acid sequence similarities [2], β-glucosidases belong to GH1, GH3, GH5, GH9, GH30, GH116 families. A large proportion of β-glucosidases belong to glycoside hydrolase families 1 and 3 (GH1 and GH3), and hydrolyze their substrates via double-displacement mechanism [3]. The crystal structures of β-glucosidases belonging to GH1 family have been reported. But to GH3 family, only four crystal structures have been reported. β-Glucosidases that belong to GH1 and GH3 family can catalyze reverse hydrolysis and transglycosylation reactions, leading to synthesis of oligosaccharides and alkyl polyglucosides.

Cassava β-glucosidase belongs to GH1 family, it can transfer a nonreducing glucosyl group from a glycoside or carbohydrate to water (hydrolysis) or another alcohol (transglycosylation) via retaining mechanism. Cassava β-glucosidase possess $(\beta/\alpha)_8$ barrel structure. It has two carboxylic acid residues on β-strands 4 and 7, which act as the general acid–base catalyst and the nucleophile, respectively [4]. Site-directed mutagenesis is carried out to study the function of active-site amino acid residues based on a homology model, while the MODELLER program is used [5]. The enzyme activity is destroyed when Glu-413 is changed to Gly, which is consistent with that it being the catalytic nucleophile. The Gln-339/Glu mutation also destroys activity, confirming a function in positioning the catalytic diad. The Phe-269 contributes to the cyanogenic specificity of the cassava β-glucosidase. The recombinant cassava β-glucosidase is successfully expressed in *Saccharomyces cerevisiae*. Its Michaelis constants for the natural substrate linamarin (K_m = 1.06 mM) and the synthetic *p*-nitrophenyl β-D-glucopyranoside (*p*NP-Glc; K_m = 0.36 mM) are very similar to the plant enzyme. Linamarase gene is intracellular expressed in *Pichia pastoris* GS115 [6]. SDS/PAGE analysis shows that the molecular weight of recombinant protein is around 71 kDa. The optimal temperature of recombinant protein is about 37 °C, and the optimal pH is about 5. The K_m is 1.70 mmol/L, and V_{max} is 8.36 μmol/(min mg), while *p*NP-Glc is used as the substrate.

The cassava β-glucosidase has very low hydrolysis activity, but shows high synthesis ability [7]. The alkyl polyglucosidase synthesis ability of β-glucosidases from cassava, Thai rosewood, and almond has been compared. Cassava β-glucosidase shows greater ability to transfer glucose from *p*NP-Glc to secondary alcohol acceptors than other β-glucosidases, and it is the only one to synthesize tertiary alkyl β-glucosides with high yields. However, it could not catalyze the synthesis of alkyl polyglucosides through reverse hydrolysis reaction. Cassava β-glucosidase requires active glycosyl donors and could not use mono- or disaccharides as sugar donors in alkyl polyglucoside synthesis.

The *P. pastoris* expression system is widely used as eukaryotic expression system [8, 9]. The system has many advantages, such as relatively simple operation, fast growth, high expression, low miscellaneous proteins, postprocessing, protein folding, and posttranslational modification. And the AOX1 promoter can ensure a high expression of exogenous genes with methanol as the sole carbon and energy source.

In this study, we constructed the recombinant expression vector pPICZαA-MEBGL. The constructed plasmid was integrated into *P. pastoris* GS115 strain. After screened by nutrient deficiencies plate and shake flask fermentation, we got the positive recombinant strains. And we carried out preliminary enzymatic properties study on the recombinant cassava β-glucosidase, such as hydrolysis and synthesis ability.

2.2 Materials and Methods

2.2.1 Materials, Strains, and Media

Escherichia coli Top10F™ was used for the amplification of all plasmids. The *P. pastoris* GS115 strains were used as host strains for β-glucosidase expression. The cloning and expression vector pPICZαA was purchased from Invitrogen.

LB culture medium: 1 % tryprone, 0.5 % yeast extract, 1 % NaCl. Zeocin was added to the medium when the medium was used for screening. In the medium, the concentration of zeocin was 25 μg/mL. YPD, BMGY, BMMY reference Invitrogen company operating manuals. YPDZ medium, which the concentration of zeocin was 100 μg/mL, was used for screening.

2.2.2 PCR of Cassava β-Glucosidase Gene

The Genebank ID of *mebgl* gene was gi:249261. The gene was synthesized after codon optimization. The oligonucleotide primers contain 5′ *Eco*RI and 3′ *Kpn*I restriction endonuclease sites. Upstream primer contains *Eco*RI restriction endonuclease site (outlined by underline), "His" label and protected bases: 5′CAGGAATTCCAT-CATCACCATCACCATACAGATGACGATGACGACAA 3′. Downstream primer contains *Kpn*I restriction endonuclease site and protected bases: 5′CGGGGTA-CCCTACATAACGTAAAACTTTC3′. The PCR amplification of *mebgl* gene was conducted under conditions: 2 μL 100 ng/μL template, 25 μL 2× KOD FX Buffer, 10 μL 2 mmol dNTPs, 2.5 μL 10 μmol/L each primer, 1 μL KOD FX DNA polymerase, 9.5 μL ddH_2O; initial denaturation at 94 °C for 5 min, 30 cycles (10 s at 94 °C, 30 s at 55 °C, and 96 s at 68 °C) were followed by a final incubation at 68 °C for 10 min.

2.2.3 Cloning and Construction of the Yeast Expression Vector

The PCR products were digested with *Eco*RI and *Kpn*I, gel purified, and subsequently inserted into the *Eco*RI–*Kpn*I sites in pPICZαA, giving pPICZαA-MEBGL. The recombinant plasmid was transformed into *E. coli* Top10F™ via $CaCl_2$ transformation method. Single colonies of *E. coli* Top10F™ that contained pPICZαA-MEBGL were grown in LB resistance screening medium, at 37 °C, 200 rpm for 14–16 h. The recombinant plasmid was extracted, confirmed by restriction digestion, and DNA sequencing.

2.2.4 Yeast Transformation and Screening

Electrotransformation was carried out with the Bio-Rad Gene Pulser system (Bio-Rad, Richmond, CA, U.S.A.) according to the manufacturer's instructions, 0.1 μg linearized plasmid was used. After that, the GS115 cells were coated in YPDZ plates. The plates were cultured at 30 °C for 3 days. Single colonies of *P. pastoris* GS115 were grown in YPDZ medium, and confirmed by colony PCR.

2.2.5 Expression of Cassava β-Glucosidase in Pichia pastoris GS115

The strains were cultured at BMGY, at 30 °C, 200 rpm for 20–24 h. Then the culture was transformed into BMMY which contained 2 % (v/v) methanol. The initial OD_{600} was controlled at one. After that, the strains were cultured at BMMY for 144 h, at 30 °C, 200 rpm. 2 % (v/v) fermented liquid was extracted and 2 % (v/v) methanol was added every 24 h for the induction of the recombinant proteins.

2.2.6 Purification of Recombinant Cassava β-Glucosidase

The fermentation liquor was collected after the strains were cultured for 144 h. The supernatant was used for purification after filtered by 0.22 μm filter membrane. Then the supernatant was desalted through desalting crude (HiTrap™). After that, the supernatant was used for Ni-chelating affinity chromatography (HisTrap™FF). The recombinant protein was eluted by 10, 20, 50, 100, 200, 300 mM imidazole. Then the eluent was concentrated through 10 kDa filter membrane bag. The recombinant protein was used for further analysis.

2.2.7 SDS-PAGE Analysis

SDS-PAGE electrophoresis was performed on 6 % spacer polyacrylamide gel and 12 % (w/v) separation polyacrylamide gel. After electrophoresis, proteins were stained in 0.05 % (w/v) Coomassie Brilliant Blue R250 (Sigma-Aldrich) solution.

2.2.8 The Analysis of Hydrolysis and Transglycosylation Activities

The hydrolysis activity of cassava β-glucosidase was assayed with colorimetric method while *p*NP-Glc was used as substrate. The reaction was conducted under conditions: 250 μL cassava β-glucosidase liquid and 250 μL 5 mM *p*NP-Glc were preheated at 40 °C for 5 min, respectively, then they were mixed for reaction at 40 °C for 30 min, 0.2 M sodium acetate (pH 5.0) buffer solution was used. The reaction was stopped by adding 500 μL 1 M sodium carbonate, and the *p*-nitrophenol released was measured by its absorbance at 405 nm. One unit of activity is defined as the amount of enzyme used to release 1 μmol of *p*-nitrophenol in 1 min.

The temperature optimum was determined by measuring *p*-nitrophenol released from *p*NP-Glc at temperatures ranging from 10 to 70 °C at 10 °C increments, and the assay was completed as described above. The pH optimum was determined by hydrolysis of *p*NP-Glc at 40 °C for 30 min in the following 0.2 M buffers: glycine–HCl, pH 2–3; sodium citrate, pH 3–4; sodium acetate, pH 4–5; MES, pH 5–6; sodium phosphate, pH 6–8; Tris–HCl, pH 8–9; and CAPS, pH 9–10.

The preliminary experiments of transglycosylation reaction were conducted under conditions: 30 mM *p*NP-Glc; 10 % (v/v) 0.2 M pH 5.0 sodium acetate (containing recombinant cassava β-glucosidase); 90 % (v/v) n-hexyl alcohol, at 40 °C for various times (from 1 to 6 h) before analysis by HPLC.

Waters 2695, Waters 2424 ELS Detector and C18 chromatographic column were used for HPLC analysis. Samples were filtered by 0.22 μm filter membrane before detected. The mobile phase was methol–water mixture (80:20, v/v). The detection was conducted under conditions: 1.0 mL/min flow rate, 30 °C for C18 column, 60 °C for drift tube, 30 psi for nitrogen pressure.

2.3 Results and Discussions

2.3.1 Construction of Recombinant Expression Vector pPICZαA-MEBGL

The recombinant plasmid pPICZαA-MEBGL (Fig. 2.1) was constructed by the products of PCR based on the method as described by Sect. 2.2.3. Three different recombinant plasmids were constructed, which contain GAP, modified AOX and

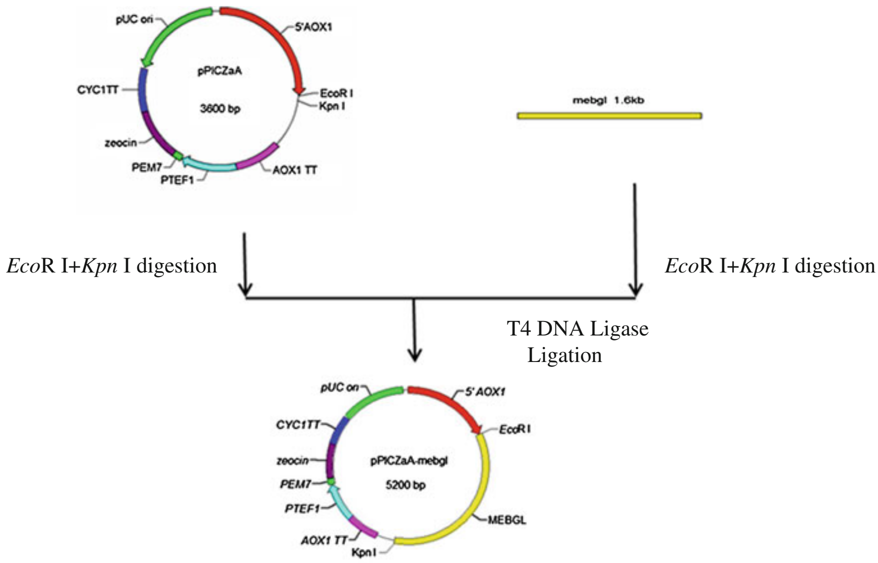

Fig. 2.1 Sketch of construction of recombinant expression plasmid pPICZαA-MEBGL

5′AOX promoter, respectively. The recombinant plasmids were confirmed by restriction digestions (Fig. 2.2a) and DNA sequencing. The targeted band was between 1,500 and 2,250 bp.

2.3.2 *Identification of Recombinant Pichia pastoris GS115/pPICZαA-MEBGL*

Single colonies of *P. pastoris* GS115 were grown in YPDZ medium, and then confirmed by colony PCR (Fig. 2.2b). The results showed that most single colonies were positive clone. The positive clones were used for further screening.

2.3.3 *The Screening of Recombinant Pichia pastoris GS115*

The recombinant and control strains were cultured at the conditions as described by Sect. 2.2.5. There were no difference between their growth situations, but the recombinant strains show better hydrolytic activities, 60 U/L after been induced for 144 h (Fig. 2.3). The hydrolysis activities of recombinant strains were increased along with the induction time, but the control strains were decreased. And among GAP, modified AOX and 5′AOX, 5′AOX promoter was the best one for expression.

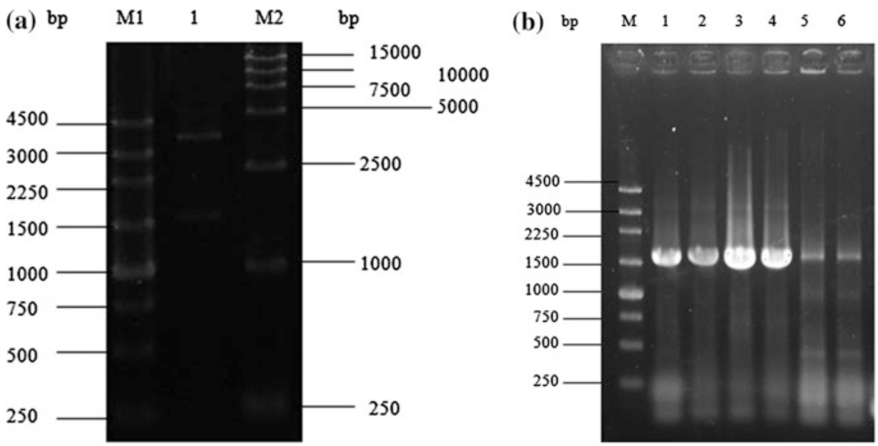

Fig. 2.2 **a** Identification of recombinant plasmid pPICZαA-MEBGL. *M1* 250 bp DNA marker; *1* Double restriction of pPICZαA-MEBGL by *Eco*RI and *Kpn*I; *M2* DL15000 DNA marker. **b** Identification of recombinant *Pichia pastoris* GS115/pPICZαA-MEBGL. *M1* 250 bp DNA marker; *1*, *2*, *3*, *4*, *5*, *6* recombinant *P. pastoris* GS115

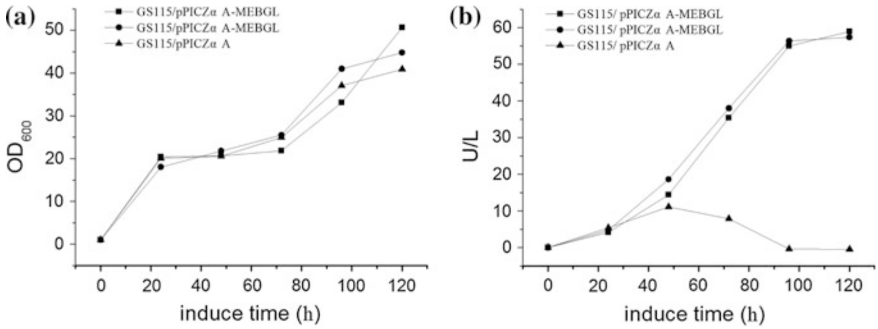

Fig. 2.3 The culture of recombinant *Pichia pastoris* GS12. **a** OD_{600} of recombinant *P. pastoris* GS115/pPICZαA-MEBGL (GS115/pPICZαA as control); **b** supernatant hydrolytic activities of recombinant *P. pastoris* GS115/pPICZαA-MEBGL (GS115/pPICZαA as control)

2.3.4 Analysis of SDS-PAGE

The supernatant of the recombinant and control strains were applied for SDS-PAGE analysis. The molecular mass of the recombinant monomer protein was estimated to be 70 kDa (Fig. 2.4). This is consistent with literature reports that the recombinant protein was 71 kDa [6].

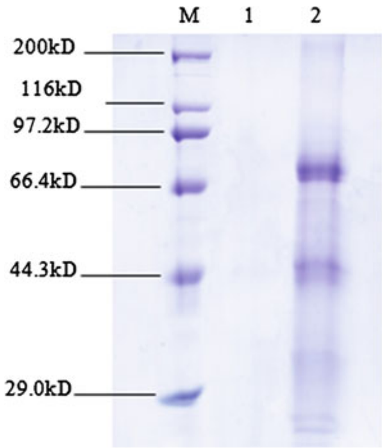

Fig. 2.4 SDS-PAGE analysis of the recombinant cassava β-glucosidase expressed in *Pichia pastoris* GS115 (GS115/pPICZαA as control); *M* protein marker; *1* supernatant of GS115/pPICZαA; *2* supernatant of *P. pastoris* GS115/pPICZαA-MEBGL

2.3.5 Optimization of Temperature and pH for Hydrolytic Activity of Recombinant Cassava β-Glucosidase

The recombinant cassava β-glucosidase was sensitive to temperature and pH values. As shown in Fig. 2.5a, when the temperature increased from 10 to 35 °C, the activity increased gradually. The maximum activity was achieved at 35 °C. If the temperature continued to rise, the activity decreased seriously. At 60 °C, the activity only retained 14.0 % of maximal activity.

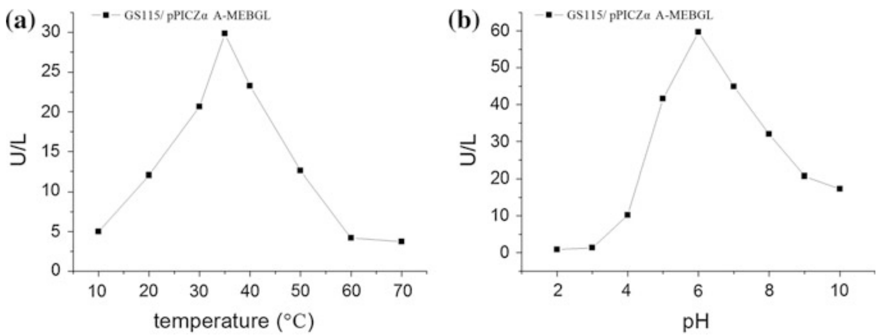

Fig. 2.5 Optimization of temperature and pH for hydrolytic activity of recombinant cassava β-glucosidase. **a** Optimization of temperature for hydrolytic activity of recombinant cassava β-glucosidase. **b** Optimization of pH for hydrolytic activity of recombinant cassava β-glucosidase

As shown in Fig. 2.5b, the recombinant β-glucosidase had an optimal pH of 6. At pH 5.0 and pH 7.0 the activity kept about 60–70 % of the maximum activity. There were only 17.1 and 29.0 % of maximal activity, when the pH values were 4.0 and 10.0.

2.3.6 Purification of Recombinant Cassava β-Glucosidase

The fermentation liquor was desalted through desalting crude, then the supernatant was used for Ni-chelating affinity chromatography. The results indicated that most of the proteins could not bind to nickel column, a few proteins were eluted by 10 mM imidazole, and no proteins were eluted by other concentrations of imidazole. The supernatants that containing unbound proteins were concentrated through 10 kDa filter membrane bag, so were the eluents. Both of the concentrated solutions were used for SDS-PAGE analysis and transglycosylation reactions. The results of SDS-PAGE indicated that most of recombinant cassava β-glucosidase could not bind to nickel column. The concentrated cassava β-glucosidase was used for the synthesis of alkyl polyglycoside.

2.3.7 The Preliminary Experiment: Transglycosylation of Recombinant Cassava β-Glucosidase

A certain amount of cassava β-glucosidase, the hydrolysis activity was 0.1 U, was used for transglycosylation reaction. The preliminary experiment of transglycosylation reaction of cassava β-glucosidase showed great alkyl polyglycoside synthesis ability (Fig. 2.6). This was consistent with literature reports that cassava β-glucosidase showed better alkyl polyglycoside synthesis ability than Thai rosewood and

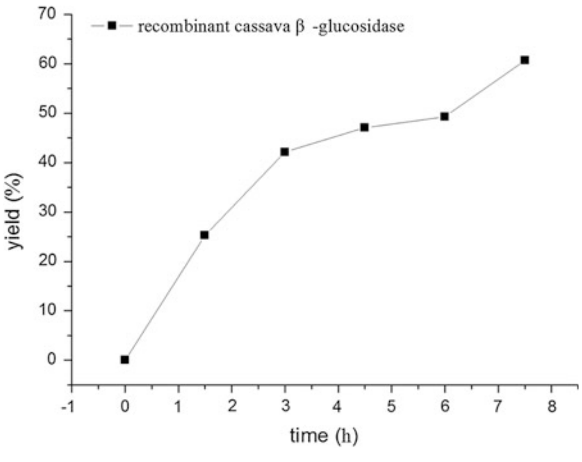

Fig. 2.6 The synthesis of *n*-hexyl β-D-glucopyranoside through transglycosylation, while *p*NP-Glc was used as the substrate

almond β-glucosidases [7]. The cassava β-glucosidase could synthesize tertiary alkyl polyglycosides, while the other two β-glucosidases could not. Cassava β-glucosidase was important to the enzymatic synthesis of alkyl polyglycoside for its high synthesis ability.

2.4 Conclusion

This study realized the expression of β-glucosidase gene *(mebgl)* from cassava in *P. pastoris* GS115. SDS/PAGE analysis showed that the molecular mass of the recombinant monomer protein was around 70 kDa. The optimal temperature of this enzyme was about 35 °C, and the optimal pH was about 6.0, the maximum supernatant hydrolytic activity was 60 U/L, while *p*NP-Glc was used as the substrate. Study had shown that cassava β-glucosidase shows greater ability to transfer glucose from *p*NP-Glc to primary and secondary alcohol acceptors than Thai rosewood and almond β-glucosidases. And it is the only one β-glucosidase that is able to synthesize tertiary alkyl β-glucosides. This β-glucosidase is expected to promote the industrialization process of alkyl glucoside enzymatic synthesis.

References

1. Esen A (1993) β-Glucosidases: overview. In: Esen A (ed) β-Glucosidases biochemistry and molecular biology. American Chemical Society, Washington, DC, pp 1–14
2. Henrissat B (1991) A classification of glycosyl hydrolases based on amino acid sequence similarities. Biochem J 280:309–316
3. Henrissat B, Davies GD (2000) Glycoside hydrolases and glycosyltransferases. Families, modules, and implications for genomics. Plant Physiol 124:1515–1519
4. Keresztessy Z, Kiss L, Hughes M (1994) Investigation of the active site of the cyanogenic β-D-glucosidase (linamarase) from Manihot esculenta Crantz (cassava). II. Identification of Glu-198 as an active site carboxylate group with acid catalytic function. Arch Biochem Biophys 315: 323–330
5. Keresztessy Z, Brown K, Dunn MA, Hughes MA (2001) Identification of essential active-site residues in the cyanogenic β-glucosidase (linamarase) from cassava (Manihot esculenta Crantz) by site-directed mutagenesis. Biochem J 353:199–205
6. Peifeng S, Lili F, Xuepiao S, Jiaming Z (2012) Cloning, expression of linamarase in cassava and characterization of its recombinant protein activity. Chinese Agric Sci Bulleti 28(12): 164–168
7. Svasti J, Phongsak T, Sarnthima R (2003) Transglycosylation of tertiary alcohols using cassava β-glucosidase. Biochem Biophys Res Commun 305:470–475
8. Yan Q, Hua C, Yang S et al (2012) High level expression of extracellular secretion of β-glucosidase gene (PtBglu3) from Paecilomyces thermophila in Pichia pastoris. Protein Expr Purif 84:64–72
9. Ruanglek V, Sriprang R, Ratanaphan N et al (2007) Cloning, expression, characterization, and high cell-density production of recombinant endo-1,4-β-xylanase from Aspergillus niger in Pichia pastoris. Enzyme Microb Technol 41:19–25

Chapter 3
Construction of L-*tert*-Leucine Producing Strain by Expressing Heterologous Leucine Dehydrogenase and Formate Dehydrogenase in *Escherichia coli*

Junzhen Bai, Yajian Song, Xuegang Luo, Haixu Yang, Wen Du and Tongcun Zhang

Abstract L-*tert*-Leucine is an unnatural amino acid that is a key intermediate for the synthesis of several important drugs. The L-*tert*-Leucine synthesis can be performed continuously by the collaboration of leucine dehydrogenase and formate dehydrogenase. In this study, recombinant strains of *Escherichia coli* expressing leucine dehydrogenase (LeuDH) and formate dehydrogenase (FDH), respectively, and the strain co-expressing the two enzymes were constructed. The activity for the two enzymes of the cell extraction from different recombinant strains was determined. L-*tert*-Leucine was successfully synthesized by the recombinant strains, and the yield in different conditions was compared. The production of L-*tert*-Leucine was the highest when cell extraction of strains containing pLeuDH and pFDH, 1 mL cells extract could produce 4.5 mg L-*tert*-Leucine, while 1 mL whole cells could only produce 1.05 mg L-*tert*-Leucine. The yield of L-*tert*-Leucine was 3.375 mg/mL cell extraction of the strain containing pLeuDHFDH when NAD was added, while the yield fell to 1.635 mg/mL when the whole cell was used.

Keywords L-*tert*-Leucine · Leucine dehydrogenase · Formate dehydrogenase

3.1 Introduction

Amino acids are extensively used as chiral starting materials, auxiliaries, and catalysts in modern organic synthesis [1]. Incorporation of unnatural amino acids into peptide has become an important strategy in the synthesis of biologically active

J. Bai and Y. Song—Co-first author.

J. Bai · Y. Song · X. Luo · H. Yang · W. Du · T. Zhang (✉)
Key Laboratory of Industrial Fermentation Microbiology, Ministry of Education and Tianjin City, College of Biotechnology, Tianjin University of Science and Technology, Tianjin 300457, People's Republic of China
e-mail: tony@tust.edu.en

T.-C. Zhang and M. Nakajima (eds.), *Advances in Applied Biotechnology*, Lecture Notes in Electrical Engineering 333, DOI 10.1007/978-3-662-46318-5_3

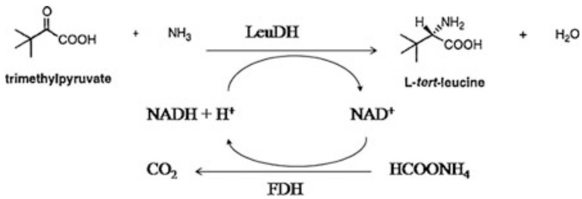

Fig. 3.1 Synthesis of L-*tert*-Leucine by coupling of enzyme reactions

compounds owing to the resistance to enzymatic degradation [2]. One of the most interesting amino acids in this regard is L-*tert*-Leucine, which has a sterically demanding side-chain. L-*tert*-Leucine can be used for templates in asymmetric synthesis and as building blocks for pharmaceutically active compounds. L-*tert*-Leucine itself is a component of several pharmaceutical development projects as tumor fighting agents or HIV protease inhibitors. A whole range of ligands for asymmetric catalysts has also been developed with L-*tert*-Leucine, mostly based on the oxazolidine moiety [3].

A method for enzymatic synthesis L-*tert*-Leucine was performed by reductive amination of trimethylpyruvate with leucine dehydrogenase (LeuDH) [4–6]. However, the cost of coenzyme hampered the application of this method to industrial production. A multi-enzyme reaction system for simultaneous coenzyme regeneration has been proposed to overcome this problem. As shown in Fig. 3.1, L-*tert*-Leucine was produced from trimethylpyruvate with LeuDH and the necessary cofactor NADH is regenerated by a second enzyme, formate dehydrogenase (FDH).

In this study, we constructed recombinant strains of *Escherichia coli* expressing LeuDH and FDH, respectively, and co-expressing the two enzymes together to produce L-*tert*-Leucine. The crude enzyme activity and production of L-*tert*-Leucine were determined and compared.

3.2 Materials and Methods

3.2.1 Bacterial Strains, Plasmids, and Other Materials

Bacillus cereus (TCCC 11114) used in this study was obtained from the preservation management center of College of Biotechnology, Tianjin University of Science and Technology. *Candida boidinii* (2.1645) used in this study was obtained from China General Microbiological Culture Collection Center (CGMCC). Vector plasmids pET-28a used for gene cloning and expression were purchased from YouBio (Changsha, Hunan, China) and host strain *E. coli* BL21 (DE3) was purchased from Invitrogen (Beijing, China). Restriction enzymes and other DNA-modifying enzymes were purchased from Takara (Dalian, China) and used according to the manufacturers’ instructions. NAD and NADH were obtained from

Table 3.1 Primers and template DNAs used for construction of pLeuDH and pFDH

Gener	Primer	Template
LeuDH	Forward 5′-GGCCCATGGCATTAGAAATCTTCGAATAC-3′[a] Reverse 5′-GATGGATCCGCGACGGCTAATA ATGTC-3′[b]	Genome of *Bacillus cereus*
FDH	Forward 5′-TCGGGATCCATGAAAAAGTCGTCACG GTTTGCC-3′[b] Reverse 5′-CCGCTCGAGTTACGCCAGTGCCG CTTCG-3′[c]	Genome of *Candida boidinii*

[a] The underlined site is the *Nco*I restriction site
[b] The underlined site is the *Bam*HI restriction site
[c] The underlined sites are the *Xho*I restriction sites

Solarbio (Beijing, China) and L-Leucine was obtained from Sigma (St. Louis, United States). All other chemicals were commercially available and of analytical grade.

3.2.2 Construction of pLeuDH and pFDH

DNA synthesis by PCR was performed with a DNA Thermal Cycler (Perkin-Elmer) in 25 μL of a mixture containing deoxynucleoside triphosphate at a concentration of 1 μL, 1 μL primers, 1 μL template DNA, 2.5 μL reaction buffer (Takara), and 2.5 μL PfuDNA polymerase (Takara). The PCR program consisted of predenaturation at 95 °C for 8 min, denaturation at 95 °C for 30 s, annealing at 57 °C for 1 min, and extension at 72 °C for 10 min for a total of 32 cycles. The genome of *B. cereus* was carried out with a DNA extraction kit from CWBIO (Beijing, China). The genome of *C. boidinii* was obtained as described by Manuel et al. [7]. All the primers used are shown in Table 3.1.

3.2.3 Construction of pLeuDHFDH

Plasmid for the simultaneous expression of LeuDH and FDH (pLeuDHFDH) was constructed as shown in Fig. 3.2. Plasmids pLeuDH and pFDH encoding the genes for LeuDH [8] and FDH [9], respectively, were prepared as described previously and used as template DNAs for PCR (Table 3.2). The LeuDH gene was cloned by PCR by using pLeuDH as template and was introduced into pET-28a at the *Bam*HI and *Sac*I sites, and then the FDH gene was cloned by PCR by using pFDH as template and was introduced into the plasmid at the *Sal*I and *Xho*I sites to produce plasmid pLeuDHFDH (Fig. 3.2).

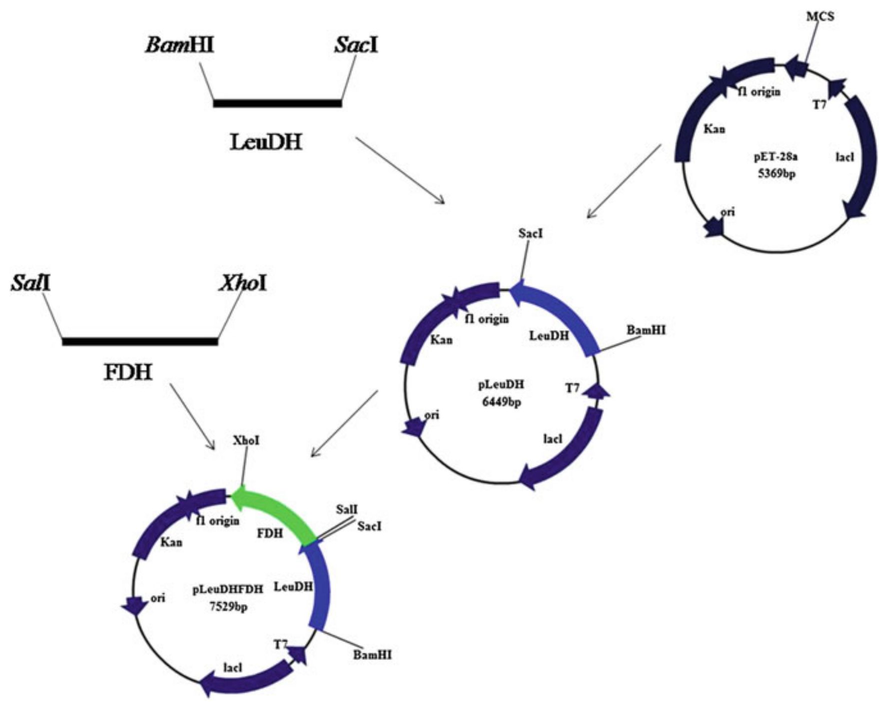

Fig. 3.2 Construction of the plasmid pLeuDHFDH used for production of L-*tert*-Leucine by expression in *Escherichia coli* cells

Table 3.2 Primers and template DNAs used for construction of pLeuDHFDH

Gener	Primer	Template
LeuDH	Forward 5′-GCGGATCCATGGCATTAGAAATCTTCGAATA-3′[a] Reverse 5′-GGCGAGCTCTTAGCGACGGCTAATAATGTCA TG-3′[b]	pLeuDH
FHD	Forward 5′-GCGTCGACAAGGAGATATACCATGAAGATCGTTTT AGTCTTATACGA-3′[c] Reverse 5′-CCGCTCGAGTTATTTCTTATCGTGCTT ACCATAA-3′[d]	pFDH

[a] The underlined site is the *Bam*HI restriction site
[b] The underlined sites are the *Xho*I restriction sites
[c] The underlined sites are the *Sac*I restriction sites
[d] The underlined sites are the *Sal*I restriction sites

3.2.4 *Cultivation of Recombinant E. coli Strains and Enzyme Assays*

Plasmid pLeuDH, pFDH, or pLeuDHFDH was introduced into *E. coli* BL21 (DE3) and the resulting transformant was cultivated in 5 mL Luria-Bertani medium [10] supplemented with 50 μg/mL kanamycin, 34 μg/mL chloramphenicol, and 1 mM isopropyl-β-D-thiogalactopyranoside in a test tube of 12 mL volume, shaking at 37 °C with 220 rpm. The volume of 5 mL cells were collected at the beginning of the stationary phase of the culture when the cells OD_{600} reached 2.5, and then suspended in 5 mL lysis buffer (100 mM Tris/HCl, pH 7.5). Cell extracts were prepared by sonication. The enzyme activity of FDH and LeuDH were assayed with a MAPADA UV-3200 spectrophotometer by determining the NADH at 340 nm using the methods described previously [11–14]. One unit of the enzyme was defined as the amount of enzyme that catalyzes the production (or consumption) of 1 μmol of NADH per min under the standard assay conditions.

3.2.5 Production of L-tert-Leucine

The clone cells were cultured and collected as described above and suspended in lysis buffer (100 mM Tris/HCl, pH 7.5). Cell extracts were prepared by sonication. The standard reaction mixture for L-*tert*-Leucine synthesis contained 200 mM trimethylpyruvate, 200 mM ammonium formate, 0.4 g/L NAD supplemented with water in a final volume of 30 mL and initiated by the addition of 2 mL washed cells or cell extracts treated as described above shaking at 30 °C for 24 h. The reaction mixture without NAD was also used for leucine synthesis and the other components were as the same as the standard reaction mixture.

3.2.6 Identification of Reaction Products

The product was derivatived with OPA/BOCCys and analyzed by HPLC using an LC-18DB column (5 μm, 4.6 × 250 mm, Agilent). The gradient elution profile, at 1 mL/min, was as follows: 95 % A and 5 % B at 0 min, 5 % A and 95 % B at 30 min (A: 20 % 0.02 M sodium acetate, and 1 % acetic acid, pH 7.2; B: acetonitrile/MeOH (1:1 by vol). Ultraviolet detector was used to determine the product at 340 nm. LC-MASS was used to identification molecular weight of the production.

3.2.7 GenBank Accession Numbers at NCBI

The obtained sequences of LeuDH and FDH were performed at the website of NCBI. The GenBank accession number of *leudh* is KM454878, and the number of *fdh* is KM454879.

3.3 Result

3.3.1 Construction of LeuDH and FDH Expression Strains

Strain containing pLeuDH used for expressing LeuDH was constructed. The specific activity for LeuDH of the cell extract was 0.183 U/mL. Strains containing FDH used for expressing FDH was constructed and the activity for FDH of the cell extract was 0.084 U/mL. Recombinant strain containing pLeuDHFDH used for

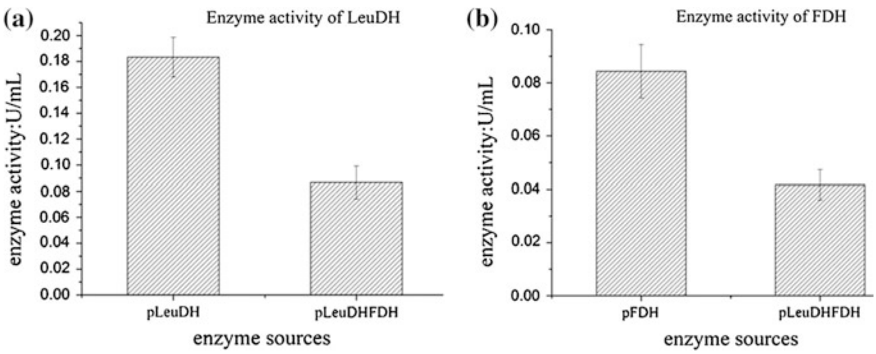

Fig. 3.3 The enzyme activity of LeuDH (**a**) and FDH (**b**) of recombinant strains of *E. coli* BL21 (DE3)

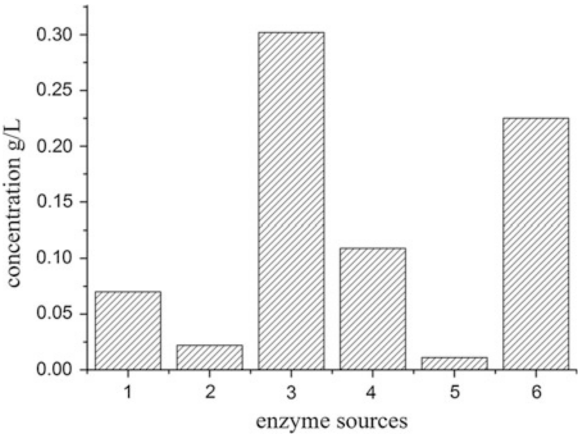

Fig. 3.4 Concentration of the L-*tert*-Leucine in the reaction system using different recombinant strains and conditions. *1* Whole cells of the stains containing pLeuDH and pFDH with NAD; *2* whole cells of the strains containing pLeuDH and pFDH without NAD; *3* cell extraction of the strains containing pLeuDH and pFDH with NAD; *4* whole cells of the strains containing pLeuDHFDH with NAD; *5* whole cells of the strain containing pLeuDHFDH without NAD; *6* cell extraction of the strains containing pLeuDHFDH with NAD

simultaneous expression of LeuDH and FDH was also constructed. LeuDH and FDH were tandem expressed using the T7 promoter of pET28a. The activity for LeuDH of the cell extract of the strain was 0.087 U/mL, which reached 47.5 % of the strain containing pLeuDH. The activity for FDH of the cell extract of the strain was 0.042 U/mL, which reached 50 % of the strain containing pFDH (Fig. 3.3).

3.3.2 Production of L-tert-Leucine

L-*tert*-Leucine synthesized by the constructed strains in different conditions was compared. Figure 3.4 showed the L-*tert*-Leucine concentration of the 30 mL reaction systems after 24 h reaction using 2 mL whole cell or cell extraction as enzyme source. The production of L-*tert*-Leucine was the highest when cell extraction of strains containing pLeuDH and pFDH was used together as the enzyme source and NAD was added into the system. At this condition, 1 mL cells extract could produce 4.5 mg L-*tert*-Leucine (Figs. 3.3 and 3.4), while 1 mL whole cells could only produce 1.05 mg L-*tert*-Leucine. The yield of L-*tert*-Leucine was 3.375 mg/mL cell extraction of the strain containing pLeuDHFDH when NAD was added, while the yield fell to 1.635 mg/mL when the whole cell was used. What is more, the result concluded that the yield of L-*tert*-Leucine was dramatically low when the reaction system without NAD was used.

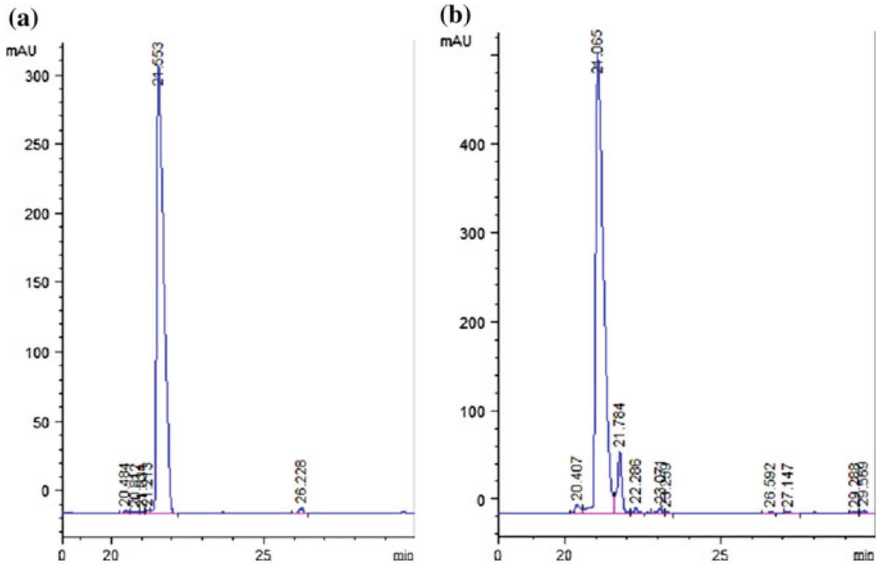

Fig. 3.5 HPLC result of the standard L-*tert*-Leucine (**a**) and product of the reaction system (**b**)

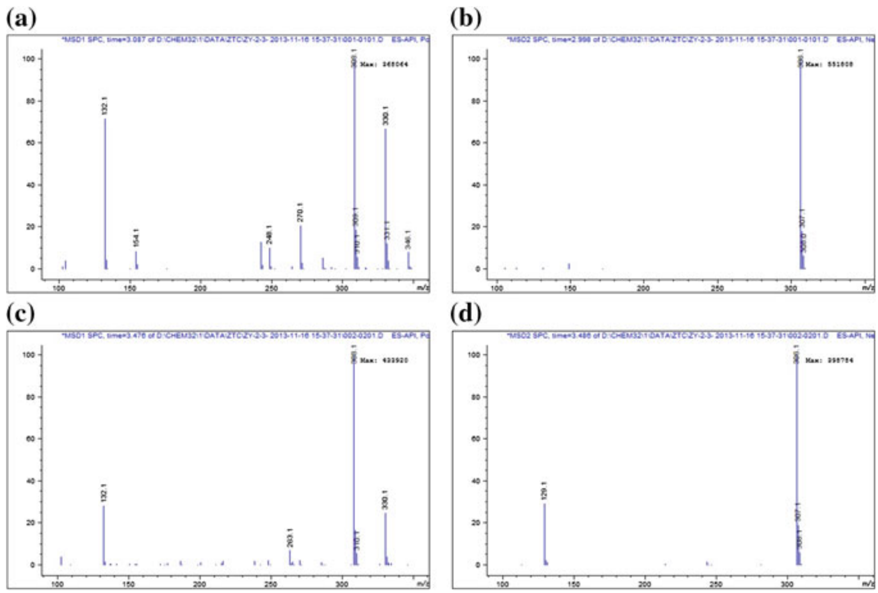

Fig. 3.6 LC-MASS of the L-*tert*-Leucine and product of the reaction system: **a** standard substance (+); **b** standard substance (−); **c** product of reaction system (+); **d** product of reaction system (−)

3.3.3 Identification of L-tert-Leucine

The reaction liquid was detected by HPLC (Fig. 3.5) and LC-MASS (Fig. 3.6). The results show that the appearance time of product was the same as the standard substance at 21 min (Fig. 3.5). The molecular weight of product was 131.1 (+), 130.1 (−) and was identical to the standard substance.

3.4 Discussion

In this study, we successfully constructed L-*tert*-Leucine producing strains by introducing *leudh* from *B. cereus* and *fdh* from *C. boidinii* into *E. coli*. Strains expressing LeuDH and FDH, respectively, were constructed first. As substrate, trimethylpyruvate can be transformed into L-*tert*-Leucine using the cell extract of the two strains together but cannot be transformed using the whole cells [4, 5]. It suggested that the trimethylpyruvate could not overcome the barrier of the cell membrane and get into the cells freely.

Meanwhile, the strain co-expressing LeuDH and FDH was constructed, the LeuDH and FDH activity of the crude enzyme can reach about half the strains expressing the two enzymes, respectively, and the yield of L-*tert*-Leucine could reach about 75 % of it [15]. It concluded that we have successfully constructed

L-*tert*-Leucine producing strain by simultaneously expressing two heterologous genes in *E. coli*, however, the product yield was lower than using two strains expressing LeuDH and FDH separately. In further study, we will attempt to optimize the codon of genes and change different inducible promoters to enhance the expression of the two enzymes and optimize their ratio in order to improve the yield of L-*tert*-Leucine.

The addition of NAD could remarkably enhance the product yield, which suggested that the coenzyme produced by cells itself could not satisfy the reaction system and NAD/NADH could successfully achieve mutual conversion in this system. In addition, this reaction system is also suitable for the synthesis of other natural or unnatural amino acids which contain different side chains and can be transformed by LeuDH.

References

1. Bea HS, Park HJ, Lee SH, Yun H (2011) Kinetic resolution of aromatic β-amino acids by-transaminase. Chem Commun 47:5894–5896
2. Allenmark S, Lamm B (2001) A useful route to (R)—and (S)-tert-leucine. Chirality 13:43–47
3. Bommarius AS, Schwarm M, Drauz K (1998) Biocatalysisto amino acid-based chiral pharmaceuticals—examples and perspectives. J Mol Catal B Enzym 5:1–11
4. Wandrey C, Bossow B (1986) Continuous cofactor regeneration-utilisation of polymer bound NAD (H) for the production of optically active acids. Biotechnol Bioind 3:813
5. Ohshima T, Soda K (1989) Thermostable amino acid dehydrogenases: applications and gene cloning. Trends Biotechnul 7:210–214
6. Bommarius AS, Schwarm M, Sfingl K, Kottenhahn M, Huthmacher K, Drauz K (1995) Synthesis and use of enantiomerically pure tert-leucine. Tetrahedron Asymmetry 6:2851–2888
7. Manuel RK, Luis ES, Ericka PF, Anne G (2011) Strategy for the extraction of yeast DNA from artisan agave must for quantitative PCR analysis. Biosci Bioeng 112:518–521
8. Ohshima T, Nishida N, Bakthavatsalam S, Kataoka K, Takada H, Yoshimura T, Esaki N, Soda K (1994) The purification, characterization, cloning and sequencing of the gene for a halo stable and thermo stable leucine dehydrogenase from Thermo actionmyces intermedius. Eur J Biochem 222:305–312
9. Galkin A, Kulakova L, Tishkov V, Esaki N, Soda K (1995) Cloning of formate dehydrogenase gene from a methanol-utilizing bacterium Mycobacteriumvaccae N10. Appl Microbiol Biotechnol 44:479–483
10. Maniatis T, Fritsch EF, Sambrook J (1982) Molecular cloning: a laboratory manual. Cold Spring Harbor Laboratory Press, Cold Spring Harbor
11. Kuroda S, Tanizawa K, Sakamoto Y, Tanaka H, Soda K (1990) Alanine dehydrogenase from two Bacillus species with distinct thermo stabilities: molecular cloning, DNA and protein sequence determination, and structural comparison with other NAD (P)-dependent dehydrogenases. Biochemistry 29:1009–1015
12. Ohshima T, Nishida N, Bakthavatsalam S, Kataoka K, Takada H, Yoshimura T, Esaki N, Soda K (1994) The purification, characterization, cloning and sequencing of the gene for a halo stable and thermo stable leucine dehydrogenase from Thermo actinomyces intermedius. Eur J Biochem 222:305–312
13. Takada H, Yoshimura T, Ohshima T, Esaki N, Soda K (1991) Thermostable phenylalanine dehydrogenase of Thermo actinomyces intermedius: cloning, expression, and sequencing of its gene. J Biochem 109:371–376

14. Tishkov VI, Galkin AG, Gladyshev VN, Karzanov VV, Egorov AM (1992) Analysis of gene structure, optimization of expression in E. coli and properties of recombinant formate dehydrogenase of bacterium Pseudomonassp. 101. Biotechnology (Russia) 5:52–59
15. Mädje K, Schmölzer K, Nidetzky B, Kratzer R (2012) Host cell and expression engineering for development of an E. coli ketoreductase catalyst: enhancement of formate dehydrogenase activity for regeneration of NADH. Microb Cell Fact 11:1–7

Chapter 4
The Distribution Characteristics of *Microcystis novacekii* Based on 16S rDNA Sequence

Da Huo, Yang Luo, Yunsi Nie, Jing Sun, Yanan Wang and Zhiyi Qiao

Abstract *Microcystis* has been regarded as the most common cause of water bloom. The spatial and temporal distribution of *Microcystis* provides a method of bloom warning. *Microcystis novacekii* was the dominant cyanobacteria species in Yuqiao reservoir in recent years. Seven sampling stations were set and the phytoplankton were collected in both July and October. Comparing morphological observation with the molecular biological method, which is based on 16S rDNA sequencing, the recognizing research of *M. novacekii was conducted*. The results showed that the average biomass of *M. novacekii* was 0.92 ± 0.23 mg/L; cell density was $1833.48 \pm 457.70 \times 10^4$/L affected by light, temperature, nutrients, and other environmental factors. In July, the maximum biomass was 2.21 mg/L at Center station and the minimum was 0.83 mg/L at the same site; in October, the maximum was 0.18 mg/L at intake site, the minimum was 0.09 mg/L at Center West. The significant seasonal fluctuation meant that *M. novacekii* favored high temperature, which is the same habit with universal *Microcystis* algae. 30 clones of *M. novacekii* were collected and amplified the 16S rDNA fragments. Results proved that the molecular identification of *Microcystis*, which is based on the conservative fragment of 16S rDNA, was consistent with the traditional morphology judgement, we confirmed that environmental factors have a huge impact on the distribution of *Microcystis* and the molecular biology techniques based on 16S rDNA sequencing were reliable for *Microcystis* identification.

Keywords *Microcystis novacekii* · Distribution · 16S rDNA · Molecular identification

D. Huo · Y. Nie · J. Sun · Y. Wang · Z. Qiao (✉)
Tianjin Key Lab of Aqua-Ecology and Aquaculture, Tianjin Agricultural University, Tianjin 300384, People's Republic of China
e-mail: qiaozhiyi7070@163.com

Y. Luo
Haihe River Water Resources Protection Bureau, 15 Longtan Road, Hedong District, Tianjin 300170, People's Republic of China

T.-C. Zhang and M. Nakajima (eds.), *Advances in Applied Biotechnology*,
Lecture Notes in Electrical Engineering 333, DOI 10.1007/978-3-662-46318-5_4

4.1 Introduction

China has suffered from the most serious and widely distributed cyanobacteria bloom. In recent years, cyanobacteria bloom frequent caused local water quality deterioration, ecological disasters happened frequently [1], after the outbreak of algal blooms, the accumulated death cells would released a lot of cyanobacterial toxins, odor, toxic and harmful substances threats to the water security [3]. The main toxic substance released by *Microcystis* was microcystin (MC), which partly cyanobacteria produced, and the molecular producing mechanism has been figured out clearly. It was produced through non ribosome ways by Giant enzyme complex include peptide synthetase, polyketide synthases (PKSs) and other modification enzyme [8, 18].

Hence the researches of the toxigenic identification and temporal, and spatial distribution of the *Microcystis* was imminent and important.

Cyanobacteria species have traditionally been identified on the basis of their microscopic morphology, physiology, and staining characteristics, which are inadequate and inaccurate, leading to misidentification due to their similarities [22]. *Microcystis* strains usually form scum [13], and thus *Microcystis* spp. to *Aphanocapsa* spp. is often misidentified in the same way. *C. raciborskii* has similar morphology with other cyanobacteria, such as *Anabaenopsis* and *Raphidiopsis*, making their quantification more difficult [5].

The lack of a simple and rapid method to detect the composition of algae in water bodies was a barrier of *Microcystis* identification. DNA barcode technology can directly detect the distribution of algal species and analyze the composition of algae, making the algae research toward a higher level. Using barcode technology to identify algae species of algae can make people exempt tedious microscopy analysis steps to determine if the species occurred.

Yuqiao reservoir—the drinking water source of Tianjin has usually appeared the water bloom in small scale, which caused the potential risk on the safety of drinking water [9, 16]. According to the reports, *Microcystis novacekii* is one of the dominant species of cyanobacteria in recent years. The laws of spatial and temporal distribution of *M. novacekii* may allow us to understand the algae growth causation better. These consequences combined with the rapid identification using molecular technology may provide a basis for early warning and ecological control in the future.

The purpose of this study was to analyze the regular water bloom in the Yuqiao reservoir. We investigated the distribution patterns of *Microcystis* algae in Yuqiao reservoir and established a set of standard operation process to distinguish it, in the hope of giving a prewarning of *Microcystis* bloom.

4.2 Materials and Methods

4.2.1 Sampling

Yuqiao reservoir located in Ji county in Tianjin, covers a flow area of 2,060 km^2 with a total storage capacity of $1.559 \times 106\ m^3$. It is an important adjusting reservoir and functions as the water resource for the drinking water, industry, and agriculture of Tianjin. The dam is located in the west of the reservoir; there is a water intake site in the south, this water drains into the culvert in Tianjin (Fig. 4.1).

The sites for sampling are shown in Fig. 4.1 and the GPS coordinates in Table 4.1. There are three important rivers—Sha River, Lin River, and Guo River in the east. The dam is located in the west of the reservoir (site 1, outlet of Yuqiao). There is a water intake site in the south (site 7), and the water drains into the culvert in Tianjin.

Seven sampling sites were studied at reservoir in July and October 2012 at 9:30–10:00 a.m. A 1-L sample of surface (50 cm) water was collected with a stainless steel Kitahara's sampling apparatus for the quantity of phytoplankton at each site. Another 1-L water sample was taken with a sampling tube and directly transported

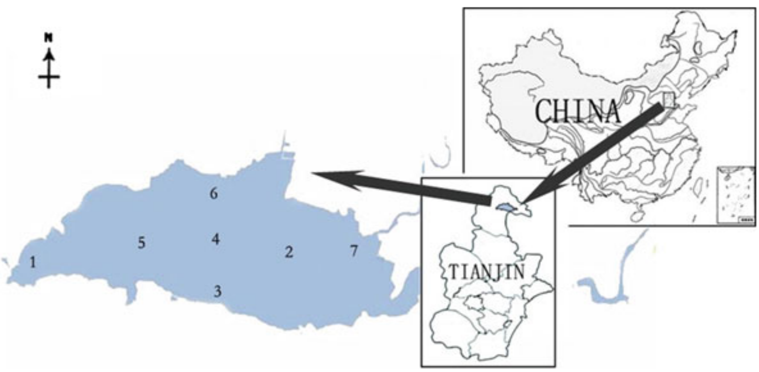

Fig. 4.1 Map showing the sampling sites of Yuqiao reservoir

Table 4.1 The coordinate of sampling sites

	Sites	Latitude (N)	Longitude (E)
1	Intake	40°01.624′	117°26.593′
2	Center east	40°01.967′	117°33.178′
3	Center south	40°01.583′	117°34.967′
4	Center	40°02.533′	117°31.255′
5	Center west	40°02.172′	117°29.493′
6	Center north	40°03.167′	117°31.017′
7	Feng hill	40°01.647′	117°31.255′

to the laboratory for molecular identification. The other samples were collected with phytoplankton net for qualitative research and fixed with Lugol's iodine solution.

4.2.2 The Qualitative and Quantitative Analyses

The phytoplankton samples were preserved with 1.5 % Lugol's iodine solution and were concentrated to 30 mL after sedimentation for 48 h. After mixing, 0.1 mL concentrated samples were estimated by using a Sedgwick–Rafter counting chamber under an Olympus optical microscope at 800×. Classification and identification of phytoplankton species and genera were based on Hu et al. [6]. The phytoplankton biomass was estimated from the approximate geometric volume of each taxon, assuming that the biomass per μm^3 equal 1–6 μg fresh weight. The geometric dimensions were measured on 10–30 individuals of each phytoplankton species in each sample. The cell numbers of individual species were quantified. Phytoplankton abundance was expressed as the number of cells or the total algal biomass per liter sample.

4.2.3 Molecular Identification

30 monoclonal *M. novacekii* were transformed to 0.5 mL PCR tubes after washing with pure water. DNA extracting method based on patent (CN201410177188.7). Specific primers used in this study was

27F: 5′TGGCGGCGTGCCTAACACATGCAAG-3′
1494RC: 5′AGGAATGACTTCGGGCGTGACCAG-3′ [11],

which is conserved sequence of 16S rDNA 3′ end and the 5′ end of 23S rDNA.

The 25 μL PCR contained 1 μL of DNA template, 4 mol/L dNTPs mix (25 mM), 1× PCR Buffer, 1 μL $MgCl_2$ (50 mM), 0.5 μL forward primer (10 mM), 0.5 μL reverse primer (10 mM), and 5 U *EasyTaq*® *DNA Polymerase* (TransGen Biotech, Beijing, P.R. China) then add molecular biology grade H_2O in a total volume of 25 μL. PCR was performed using the following conditions: 94 °C for 10 min followed by 30 cycles of 94 °C for 1 min, 54 °C for 2 min, 72 °C for 1 min, then 1 cycle of 72 °C for 10 min; PCR was performed on Eppendorf amplification instrument.

The PCR products were checked by electrophoresis in a 1 % agarose gel. Gels were stained with ethidium bromide and visualized under UV in a transilluminator. PCR products were sent for sequencing (Genewiz, Beijing, China).

4.2.4 Alignment and Phylogenetic Analysis

Sequences were assembled by Software ContigExpress and aligned with Clustal X 1.81. All sequences were confirmed by doing a BLAST search against the GenBank nr database (http://blast.ncbi.nlm.nih.gov/Blast.cgi). Neighbor-joining tree computed using MEGA 5.05 and the Kimura 2-parameter distance nucleotide model. The tree was evaluated by 1,000 bootstrap replications.

Statistical analysis was performed with SPSS 14.0 for Windows. The results were expressed as means and standard deviations (±SD).

4.3 Results

4.3.1 Spatial and Temporal Distribution of *Microcystis novacekii*

The average biomass of *M. novacekii* was 1.70 ± 0.45 mg/L (average cell density 3396.85 ± 909.88 × 10^4 ind/L) in July and 0.14 ± 0.06 mg/L (average cell density 278.28 ± 114.55 × 10^4 ind/L) in October, Fig. 4.2 shows the maximum of biomass was 1.74 mg/L (average cell density 3470.02 × 10^4 ind/L) at intake site and the minimum of 0.09 mg/L (average cell density 186.03 × 10^4 ind/L) at Center West.

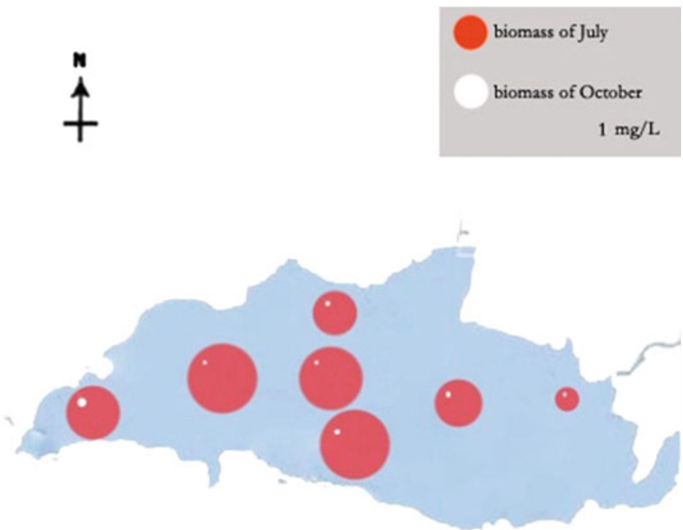

Fig. 4.2 The biomass of *Microcystis novacekii* in Yuqiao reservoir (1 mg/L)

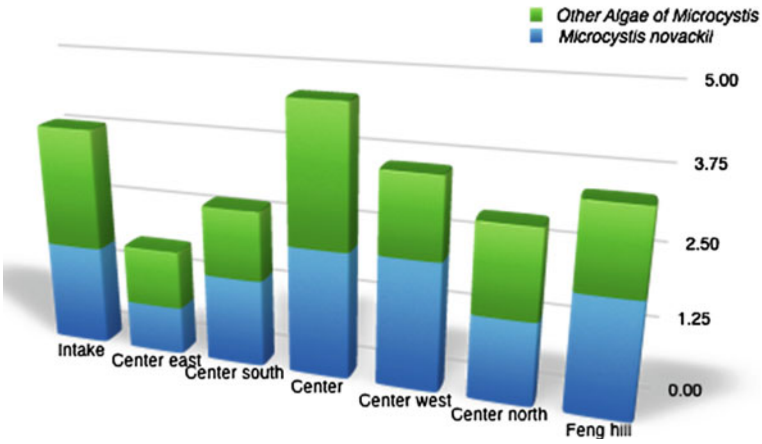

Fig. 4.3 *Microcystis novacekii* biomass proportion in July (1 mg/L)

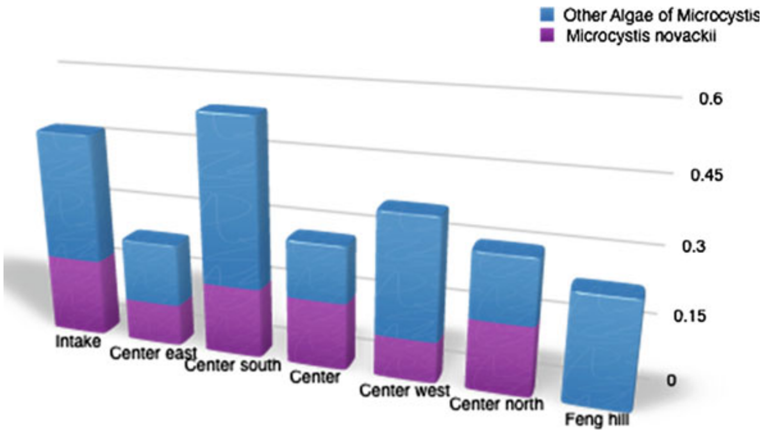

Fig. 4.4 *Microcystis novacekii* biomass proportion in October (1 mg/L)

The rapid growth of *M. novacekii* was related to the high temperature and intense illumination in summer. Two-month biomass of *M. novacekii* had significant difference ($P < 0.01$). In July, *M. novacekii* grown to dominant populations, the average biomass takes part of 52 % in *Microcystin* algae. The peak value appeared at Center point, which was 58 % (Fig.4.3). In October, it changes to another situation. *M. novacekii* is no longer a dominant species in *Microcystis*. The special circumstance appears at Feng hill site, no *M. novacekii* was detected at that site (Fig. 4.4).

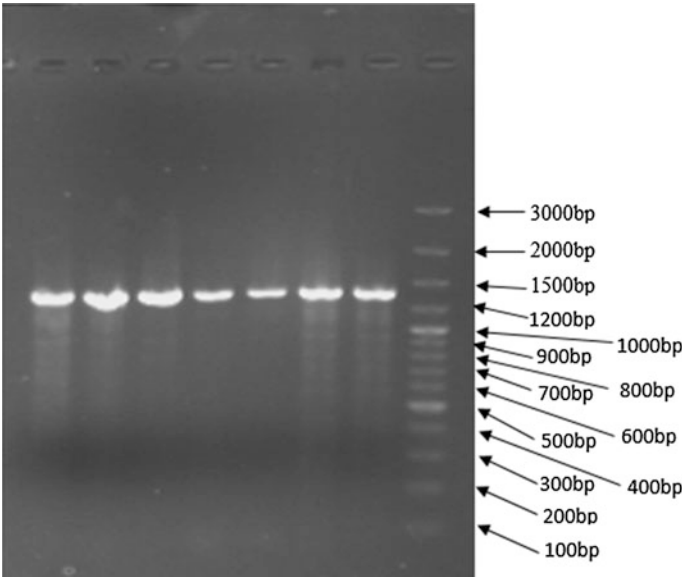

Fig. 4.5 *Microcystis novacekii* 16S rDNA fragments amplified result

4.3.2 Molecular Identification

The 30 PCR productions were confirmed by electrophoresis and sequencing, the size of fragments was in the range of 1,257–1,276 bp, and the homology of *M. novacekii* 16S rDNA fragment was between 95 and 99 % (Figs. 4.5 and 4.6).

The average content of A, T, G, C four bases are 25.4, 19.2, 32.2, 23.3 %. A+T: 44.6 %, G+C: 55.4 %. Bases composition was similar between individual clones. Using MEGA to aggregate difference sequence and evaluate Base transversion rate. Table 4.2 shows the base substitution of *M. novacekii* 16S rDNA.

Monoclonal 16S rDNA gene in sample 30, according to Table 4.2, the frequency of transitions and transversions were all 0, except A–G transition which was 1. We divided the samples and GenBank downloaded results into two groups; the group genetic distance of the first group was 0.00086, the second group was 0.00074; the genetic distance between the two groups was 0.00082 (Fig. 4.6).

4.4 Discussion

4.4.1 Seasonal Distribution of Microcystis novacekii

The rainy season of Yu Qiao is from June to September, and the normal river flow period appears in May [23]. The biomass distribution of *M. novacekii* in summer

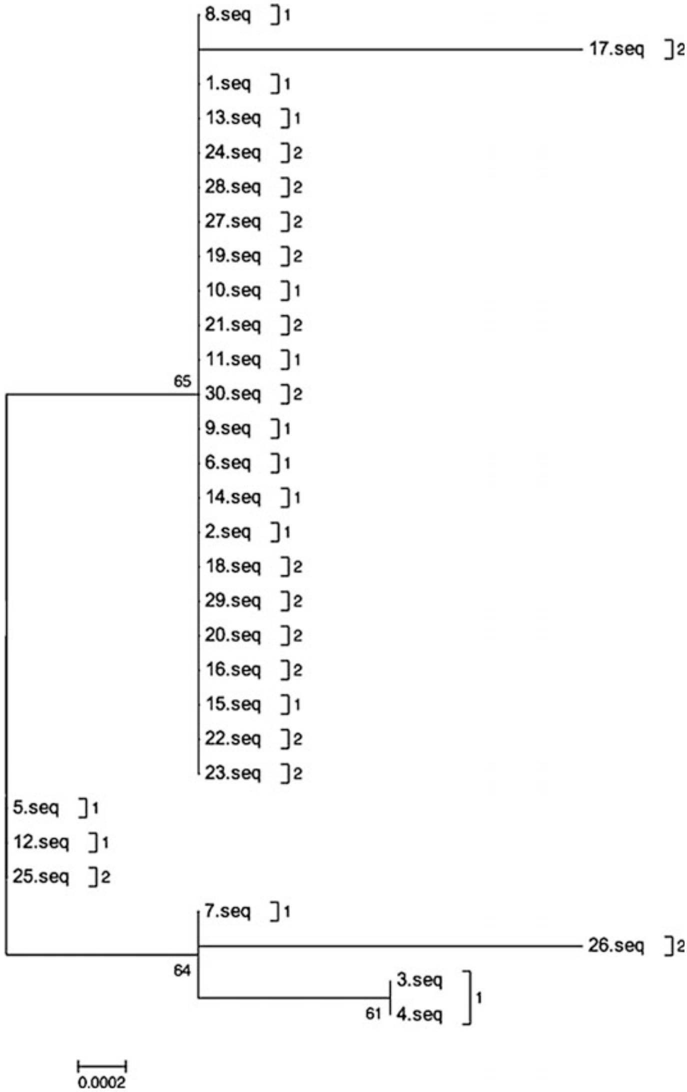

Fig. 4.6 Neighbor-joining bootstrap consensus tree. Numbers on branches represent the bootstrap support for each node in 1,000 replicates

Table 4.2 Base substitution of *Microcystis novacekii* 16S rDNA

	ii	si	sv	R	TT	TC	TA	TG	CC	CA	CG	AA	AG	GG	Total
Average	1,259	1	0	4.1	241	0	0	0	293	0	0	320	1	405	1260.8

was significantly higher than in autumn ($P < 0.01$). *M. novacekii* shows growth advantage in flood season. Enough water, high temperature of water, and high pH value are suitable for algae growth [21]. In recent years, the dominant bloom algae were *Microcystis* [10]. According to the results from analysis of water samples, compared with other researches, we concluded that the distribution of *M. novacekii* shows seasonal changes.

We did a comparison between each station. The biomass of *M. novacekii* shows a significant difference in July ($P < 0.05$). In this study, Intake was a special position where the highest biomass (2.21 mg/L) appears at this position. Wind and temperature have a significant impact on the distribution of *Microcystis* [15]. After verification, there was high temperature and precipitation in July 2013. Strong northwest wind leads to the high biomass of *Microcystis* at intake.

4.4.2 Monoclonal DNA Extracting Methods of Microcystis

Normal DNA extracting methods of *Microcystis* was DPS purification [2], extraction–centrifugation method [17], Bio kit method, and even execute PCR directly without DNA extraction [12, 20]. These methods cannot extract *Microcystin* monoclonal DNA, and the operation is cumbersome and prone to errors. In this study, repeated freezing and thawing methods were used to extract monoclonal DNA of *Microcystis*. The whole progress of extraction is less than 1 h, no need for purification, and the production of extraction was effective for accurate analysis of monoclonal DNA. The study provided a new high-throughput method of DNA analysis.

4.4.3 DNA Barcoding Fragment of Microcystis novacekii

In 30 samples, the base is almost no transitions and transversions, only one base transition appears between A and G, and the genetic distance was very small. This proves the interspecific conservation of *M. novacekii* 16S rDNA. 16S rDNA fragment has a higher mutation rate, the intergeneric difference is very large, but the interspecific difference is small [19, 14]. 16S rDNA gene cannot have high genetic diversity [7]. However, there are significant differences in the primary structure of interspecific *Microcystis* [4]. Classification and identification of species herein may be based on the similarity between the values of 16S rRNA nucleotide sequence, which can be used between the morphologically similar algae.

According to the NJ tree, there were several samples of this study that were not in the same branch, it may be the cryptic species that existed in samples we collected. There was system isolation between *Microcystis* in Taihu Lake [15].

It shows that the wind may change the phenotype of *Microcystis* and lead to the same phenotype with different genotypes. Nevertheless, most of the samples belonging to the same branch proves that this area has a large conservation among species. DNA barcode technology was a powerful tool for *Microcystis* identification.

Acknowledgments This work was supported by The International Science & Technology Cooperation Program of China (Grant No. 2013DFA71340) and Major National Science & Technology Project of Water Pollution Control and Management of China (Grant No. 012ZX07203-002).

References

1. An J, Carmichael WW (1994) Use of a colorimetric protein phosphatase inhibition assay and enzyme linked immunosorbent assay for the study of microcystins and nodularins. Toxicon 32 (12):1495–1507
2. Chen YQ, Zhuang JY, Zhuang L, Zeng LM, Qu LH (1999) Sequence analysis of rDNA 16-23S intergenic spacer from Microcystis aeruginosa ana Microcystis wesenbergii in Donghu Lake, China. Acta Hydrobiol Sin 23(1):41–45
3. Codd GA, Morrison LF, Metcalf JS (2005) Cyanobacterial toxins: risk management for health protection. Toxicol Appl Pharmacol 203(3):264–272
4. Davis TW, Berry DL, Boyer GL, Gobler CJ (2009) The effects of temperature and nutrients on the growth and dynamics of toxic and non-toxic strains of Microcystis during cyanobacteria blooms. Harmful Algae 8(5):715–725
5. Hawkins PR, Chandrasena NR, Jones GJ, Humpage AR, Falconer IR (1997) Isolation and toxicity of cylindrospermopsis raciborskii from an ornamental lake. Toxicon 35(3):341–346
6. Hu HI, Li YY, Wei YX, Zhu HZ, Chen JY, Shi ZX (1980) Freshwater algae in China. Science Press, Peking
7. Humbert JF, Duris-Latour D, Le Berre B, Giraudet H, Salençon MJ (2005) Genetic diversity in Microcystis populations of a French storage reservoir assessed by sequencing of the 16S-23S rRNA intergenic spacer. Microb Ecol 49(2):308–314
8. Jaiswal P, Singh PK, Prasanna R (2008) Cyanobacterial bioactive molecules—an overview of their toxic properties. Can J Microbiol 54(9):701–717
9. Li JR, Chen LD, Fu BJ, Zhang SR, Li GQ (2002) Temporal and spatial characteristics of non-point source N in surface water of yuqiao reservoir watershed. Sci Geogr Sin/Dili Kexue 22(2):242
10. Liu XB, Peng WQ, He GJ, Liu JL, Wang YC (2008) A coupled model of hydrodynamics and water quality for Yuqiao reservoir in Haihe river basin. J Hydrodyn Ser B 20(5):574–582
11. Neilan BA, Jacobs D, DelDot T, Blackall LL, Hawkins PR et al (1997) rRNA sequences and evolutionary relationships among toxic and nontoxic cyanobacteria of the genus Microcystis. Int J Syst Bacteriol 47:693–697. doi:10.1099/00207713-47-3-693
12. Nonneman D, Zimba PV (2002) A PCR-based test to assess the potential for microcystin occurrence in channel catfish production ponds 1, 2. J Phycol 38(1):230–233
13. Oh KH, Shin SH (2012) Simultaneous quantification of cyanobacteria and *Microcystis* spp. using real-time PCR. J Microbiol Biotechnol 22(2):248–255
14. Otsuka S, Suda S, Li R, Watanabe M, Oyaizu H, Matsumoto S, Watanabe MM (1999) Phylogenetic relationships between toxic and non-toxic strains of the genus *Microcystis* based on 16S to 23S internal transcribed spacer sequence. FEMS Microbiol Lett 172(1):15–21

15. Otten TG, Paerl HW (2011) Phylogenetic inference of colony isolates comprising seasonal *Microcystis* blooms in Lake Taihu, China. Microb Ecol 62(4):907–918
16. Peitong LFWHL (1988) The quantitative identification of nonpoint source pollution and its application in the yuqiao reservoir watershed. Acta Geogr Sin 4:004
17. Qian KC, Chen D, Lin SJ, Yuan ZQ, Hu R, Han BP (2005) The analysis of PC-IGS sequences from four freshwater *Microcystis* sp. Ecol Sci 24(2):150–153
18. Rouhiainen L, Vakkilainen T, Siemer BL, Buikema W, Haselkorn R, Sivonen K (2004) Genes coding for hepatotoxic heptapeptides (microcystins) in the cyanobacterium Anabaena strain 90. Appl Environ Microbiol 70(2):686–692
19. Tillett D, Parker DL, Neilan BA (2001) Detection of toxigenicity by a probe for the microcystin synthetase A gene (mcyA) of the cyanobacterial genus Microcystis: comparison of toxicities with 16S rRNA and phycocyanin operon (phycocyanin intergenic spacer) phylogenies. Appl Environ Microbiol 67(6):2810–2818
20. Wang J, Xie SL, Wang ZJ, Xu Y, Li RH (2011) Molecular diversity and microcystin production of Microcystis in Fenhe River of Taiyuan. J Lake Sci 23(4):505–512
21. Zhang SR, Chen LD, Fu BJ, Li J (2003) The risk assessment of nonpoint pollution of phosphorus from agricultural lands: a case study of Yuqiao reservoir watershed. Quat Sci 23(3):262–269
22. Zhang W, Lou I, Ung WK, Kong Y, Mok KM (2014) Application of PCR and real-time PCR for monitoring cyanobacteria, Microcystis spp. and Cylindrospermopsis raciborskii in Macau freshwater reservoir. Front Earth Sci 8(2):291–301
23. Zhao Y, Nan J, Cui FY, Guo L (2007) Water quality forecast through application of BP neural network at Yuqiao reservoir. J Zhejiang Univ Sci A 8(9):1482–1487

Chapter 5
The Distribution and Molecular Identification of the *Microcystis aeruginosa* in Yuqiao Reservoir

Zhiyi Qiao, Da Huo, Jun Zhang, Jing Sun, Yunsi Nie and Yanan Wang

Abstract Yuqiao reservoir, the only drinking water source of Tianjin in the downstream of Luan river basin, has occurrence of water bloom, at a small scale, annually. Hence the research in *Microcystis* distribution spatially and temporally has been conducted. In this study, we focus on *Microcystis aeruginosa*, which is one of the most contributing causes of the bloom. Samples are collected from seven sites in July and October 2012 and molecular techniques conducted to identify the selected clone from the samples by 16S rDNA sequencing. According to the results, *M. aeruginosa* has grown vigorously in July with the average biomass of 1.59 ± 0.39 mg/L and the cell density of $3191.25 \pm 768.04 \times 10^4$/L. The maximum value occurs in the site of the northern reservoir (the average biomass and the cell density were 1.37 ± 1.07 mg/L and $2723.33 \pm 2131.13 \times 10^4$/L respectively). By analyzing the sequencing results and comparing with the morphological characters, the accuracy of molecular identification based on the 16S rDNA region is confirmed. From the BLAST alignments in NCBI, we find that the homology of 30 clones of *M. aeruginosa* is between 97 and 99 %; A+T (56.6 %), which is higher than C+G (43.4 %). The samples almost match the same branch of phylogenetic tree.

Keywords *Microcystis aeruginosa* · Distribution · Molecular identification · 16S rDNA

Z. Qiao (✉) · D. Huo · J. Sun · Y. Nie · Y. Wang
Tianjin Key Lab of Aqua-Ecology and Aquaculture, Tianjin Agricultural University, Tianjin 300384, People's Republic of China
e-mail: qiaozhiyi7070@163.com

J. Zhang
Haihe River Water Environmental Monitoring Center, 15 Longtan Road, Hedong District, Tianjin 300170, People's Republic of China

T.-C. Zhang and M. Nakajima (eds.), *Advances in Applied Biotechnology*,
Lecture Notes in Electrical Engineering 333, DOI 10.1007/978-3-662-46318-5_5

5.1 Introduction

Cyanobacterial dominance in phytoplankton has become a common feature of eutrophic freshwaters worldwide [8]. Considerable concern has arisen over the temporal and spatial distribution of the water bloom in ecological research [4, 7, 9, 12].

Cyanobacterial or *Cyanophyt*—the oldest and the most primitive algae reproduces rapidly and blooms often arise in many lakes and reservoirs in China during spring through autumn [1]. The influencing factors of *Cyanophyta* bloom have been widely investigated [10]. Recently, Yuqiao reservoir—the drinking water source of Tianjin discovered the water bloom regularly in small scale, which risks potentially the safety of drinking water. In the last 9 years, six dominants (*Microcystis aeruginosa, Microcystis viridis, Microcystis novacekii, Microcystis wesenbergii, Microcystis flos-aquae* (Wittr). Kirchner, *and Microcystis incerta* Lemm.) occurred successively with abrupt succession every 2–3 years [11]. *M. aeruginosa* is one of the dominants that occurred the most in the last 2 years. *M. aeruginosa* cells usually aggregate to the visible mass and form the cooper green/odour/toxic in most cases [13] of algal bloom.

The distribution regular of dominant provides data for controlling and early-warning of bloom. Usually, the taxonomy of the species is time-consuming. The accuracy and consistency can be ensures by professional researchers only, which greatly impedes the expanded monitoring and research of algal bloom. In this study, the DNA of *M. aeruginosa* of 30 clones directly selected from the wild samples was extracted (the national patent number of the method of the DNA extract in this research is 201410177188.7); 16S ribosomal RNA genes (16S rDNAs) are amplified by PCR. By analyzing sequencing data, we explore the possibility of a simple-quick method to identify the taxonomic status accurately.

5.2 Materials and Methods

5.2.1 Sampling and Counting

Yuqiao Reservoir is located in Ji county of Tianjin, about 30 km west to east. The reservoir has a surface area of 86.8 km^2 and a mean depth of 16 m. The drainage basin is 2,060 km^2 with a total water circulation of 155,900,000 m^3 per year, when the yearly mean rainfall value is 750 mm. Yuqiao Reservoir is the main water resource for the supply of Tianjin from 1961. There are three import rivers—Sha River, Lin River, and Guo River in the east. The dam is located in the west of the reservoir; there is a water intake site in the south (site 1, outlet of Yuqiao), then the water drains to the culvert to Tianjin (Fig. 5.1).

Water samples were taken below the surface (50 cm) on seven sites of the reservoir in July and October 2012 at 9:30–10:00 a.m (Table 5.1). The phytoplankton samples

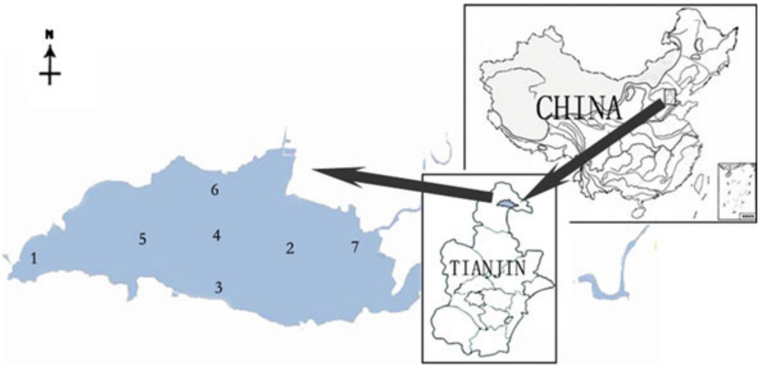

Fig. 5.1 Map showing the sampling sites of Yuqiao reservoir

were preserved with 4 % formalin solution and concentrated to 30 mL after sedimentation for 48 h. After mixing, 0.1 mL concentrated samples were counted directly using an Olympus optical microscope at 800×. Classification and identification of phytoplankton species and genera were based on Hu et al. [5].

The phytoplankton biomass was estimated from the approximate geometric volume of each taxon, assuming that the biomass per μm^3 equals 1–6 μg fresh weight. The geometric dimensions were measured on 10–30 individuals of each phytoplankton species in each sample. The cell numbers of individual species were quantified. Phytoplankton abundance was expressed as the number of cells or the total algal biomass per liter sample. Statistic analysis was performed with SPSS 14.0 for Windows. The results were expressed as means and standard deviations (±SD) (Table 5.2).

5.2.2 *Molecular Identification*

30 monoclonals of *M. aeruginosa* algae were transferred to 0.2 mL EP tubes by micropipette after washing with ultrapure H_2O. The DNA extracting method used national patent (CN201410177188.7). Specific primers used in this study were

Table 5.1 The coordinate of sampling sites

	Sites	Latitude (N)	Longitude (E)
1	Intake	40°01.624′	117°26.593′
2	Center east	40°01.967′	117°33.178′
3	Center south	40°01.583′	117°34.967′
4	Center	40°02.533′	117°31.255′
5	Center west	40°02.172′	117°29.493′
6	Center north	40°03.167′	117°31.017′
7	Feng hill	40°01.647′	117°31.255′

27F: 5′TGGCGGCGTGCCTAACACATGCAAG-3′ and 1494RC: 5′AGGAATGA CTTCGGGCGTGACCAG-3′ [10] which is the sequence of 16S rDNA with the length of about 1,300 bp.

The 25 μL PCR contained 1 μL of DNA template, 4 mol/L dNTPs mix (25 mM), 1× PCR Buffer, 1 μL $MgCl_2$ (50 mM), 0.5 μL forward primer (10 mM), 0.5 μL reverse primer (10 mM), and 5 U EasyTaq® DNA Polymerase (TransGen Biotech, Beijing, P.R. China), then ultrapure H_2O was added in a total volume of 25 μL. PCR was performed using the following conditions: 94 °C for 10 min followed by 30 cycles of 94 °C for 1 min, 54 °C for 2 min, 72 °C for 1 min, then 1 cycle of 72 °C for 10 min; PCR was performed on Eppendorf amplification instrument.

PCR product was checked by electrophoresis in 1 % agarose gel (1× TAE buffer) under the electric voltage of 90 mV/cm^2. Gels were stained with ethidium bromide (0.5 μg/mL) and visualized under UV in a transilluminator. Then purification and sequencing were done (Genewiz, Beijing, China).

5.2.3 Alignment and Phylogenetic Analysis

Sequences were assembled by Contig Express and aligned with Clustal X 1.81. All sequences were confirmed by doing a BLAST search against the GenBank database (http://blast.ncbi.nlm.nih.gov/Blast.cgi). Neighbor-joining tree was computed using MEGA 5.05 and the Kimura 2-parameter distance nucleotide model. The tree was evaluated by 1,000 bootstrap replications.

Statistical analysis was performed with SPSS 14.0 for Windows. The results were expressed as means and standard deviations (±SD).

5.3 Results and Discussion

5.3.1 The Distribution of the Microcystis aeruginosa

Microcystis aeruginosa is a typical high temperature pond species whose average cell density ($3191.25 \pm 768.04 \times 10^4$ ind/L) and biomass (1.59 ± 0.39 mg/L) in July is significantly higher than that in October ($331.31 \pm 74.99 \times 10^4$ ind/L, 0.17 ± 0.04 mg/L) ($P < 0.01$). Owing to the effect of the southeast wind in summer and autumn, *M. aeruginosa* spreads more rapidly in the center north (Fig. 5.2, site 6).

By comprehensive analysis from the biomass of seven sites, the northwest of the reservoir (site 5 and 6) had distributed more *M. aeruginosa* cell than other regions. The result is mainly contributed by the data of July (Table 5.2). Because the competitive inhibition of vascular plants, *M. aeruginosa* cannot grow fast in feng hill (site 7). The encouraging result is that the biomass of the outlet of Yuqiao (site 1) is relatively low.

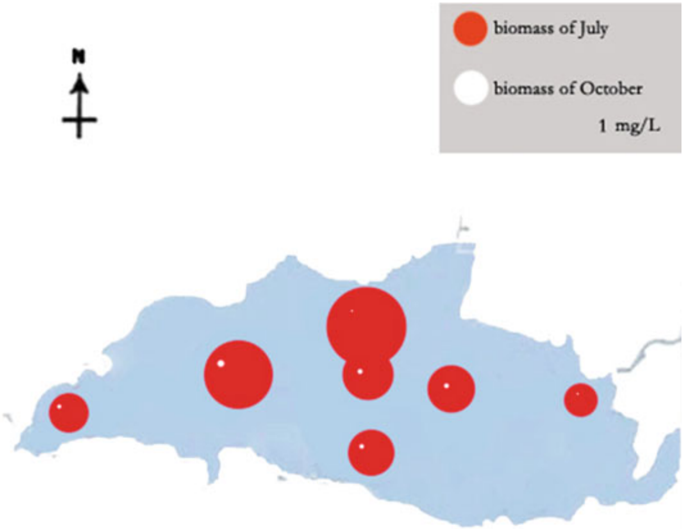

Fig. 5.2 The biomass of *Microcystis aeruginosa* in Yuqiao reservoir (mg/L)

Table 5.2 The spatial changes in *Microcystis aeruginosa* (mg/L)

Sites	July	October	Average	Standard deviations
1	1.21	0.12	0.67	±0.55
2	1.44	0.15	0.80	±0.65
3	1.39	0.14	0.77	±0.63
4	1.53	0.17	0.85	±0.68
5	2.11	0.18	1.15	±0.97
6	2.43	0.30	1.37	±1.07
7	1.02	0.11	0.57	±0.46

Similarly, the speared trend of *M. aeruginosa* for 2 months is that the cell biomass accumulated more in the western and northern regions than in other regions of the lake.

5.3.2 Molecular Identification

30 PCR products were confirmed by electrophoresis and sequencing; fragments were in the range of 1,200–1,500 bp, and the homology of *M. aeruginosa* 16S rDNA fragment was between 95 and 99 % (Fig. 5.3).

After the DNA sequence assembly, BLAST analysis was conducted by NCBI, which showed that the sequences of 30 nomoclones had high homology (about 98–99 %) with the reported sequences of *M. aeruginosa* in GENBANK, respectively.

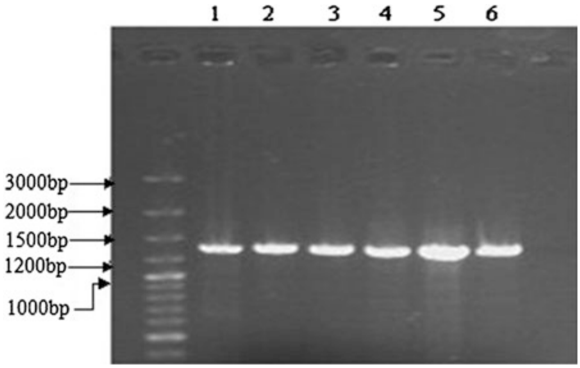

Fig. 5.3 The electrophoretic confirming of 16S rDNA of *M. aeruginosa*

From these results, we can identify the species of 30 nomoclones which have been selected randomly from field water, they are all *M. aeruginosa.*

After the integrating and comparing of 30 sequences used by Clustal, continued analysis was done by MEGA 4.1. Results show that the average contents of A, T, G, C were 25.0, 31.6, 19.6, 23.8 %, respectively. A+T: 44.6 %, G+C: 55.4 %. The genetic distance was between 0.000 and 0.001.

At the same time, the high homology sequences were downloading from GENEBANK for the construction of phylogenetic tree with our sequences.

5.4 Discussions

5.4.1 The Regularities of Algal Distribution Can Provide Reference to the Monitoring and Early-Warning

The bloom of *M. aeruginosa* would usually release microcystin (a toxics protein) which has raised concern for many years. At the same time, it is a typical high temperature pond species. From the results of this experiment, the management should pay extra attention during summer. According to the study, the optimum temperature of *M. aeruginosa* is 28.8–30 °C. The high light intensity also helps in the growth of the cyanobacteria. The average cell density of July was $3191.25 \pm 768.04 \times 10^4$ ind/L when it was $331.31 \pm 74.99 \times 10^4$ ind/L in October in the same year. Research has proved that the outbreak of water bloom was controlled by many external factors: lake depth, station morphometric, substratum, and hydraulic regime [2]. This partly coincides with this investigation, where the results clearly demonstrate that wind can entrain the *M. aeruginosa* downward, wind-driven horizontal *M. aeruginosa* drift. The data indicate that the highest *M. aeruginosa* biomass values were in the north-west portions of the reservoir. The biomass in the north region has a dramatic season change, with the maximum value in July but relatively lower than other regions in October. These may be caused by the southeast monsoon in summer and the northwest monsoon in winter.

The same pattern was approved by satellite images acquired in the past 20 years, also showing that the cyanobacterial bloom appeared predominantly in the western and northern portions of the lake [3]. Thus, during the growth season, *M. aeruginosa* biomass is distributed downwind along the dominant wind direction, and wind-driven drift is a major factor involved in the downwind accumulation.

Above all, we should pay more attention to the north-west region in summer in Yuqiao reservoir, especially after a windy day.

5.4.2 A Simple Fast Method to Identified Algal Is Necessary

Limited by the cell size of *Microcystis* (diameter usually at 2–6 μm), most molecular research has to expand the culture of monoclones before DNA extracting which is time-consuming, easy polluting, or extracting the total DNA from the samples directly that cannot analyze accurate sequencing. The procedure of extracts of the total DNA in this research (National invention patent CN201410177188.7) can solve this problem. The DNA of the monoclone *Microcystis* cells which are selected from the wild samples directly can be instantly guaranteed for PCR and sequencing. The procedure makes the larger scale and genetic analysis of prokaryotic algae possible and also provides the convenient identification of cyanobacteria for laypeople (Fig. 5.4).

5.4.3 The Genetic Relationship of Microcystis aeruginosa

The high (98–99 %) homology of 30 clones explains the conservative evolution of *M. aeruginosa*, and confirms the consistence of the identification from morphology and molecular biology. By the analysis of MEGA and comparison with the sequences downloaded from Gene Bank, the 30 clones belong to the same branch-*M. aeruginosa*. 16S rDNA region was a widely used DNA barcoding fragment [6, 13] with compatible length (1,100–1,600 bp) and amount of information, consisting of the coding region that is highly conserved and the moderate and high variation region. So the identical procedure based on DNA barcoding of *M. aeruginosa* is reliable.

Fig. 5.4 The phylogenetic tree of *M. aeruginosa*

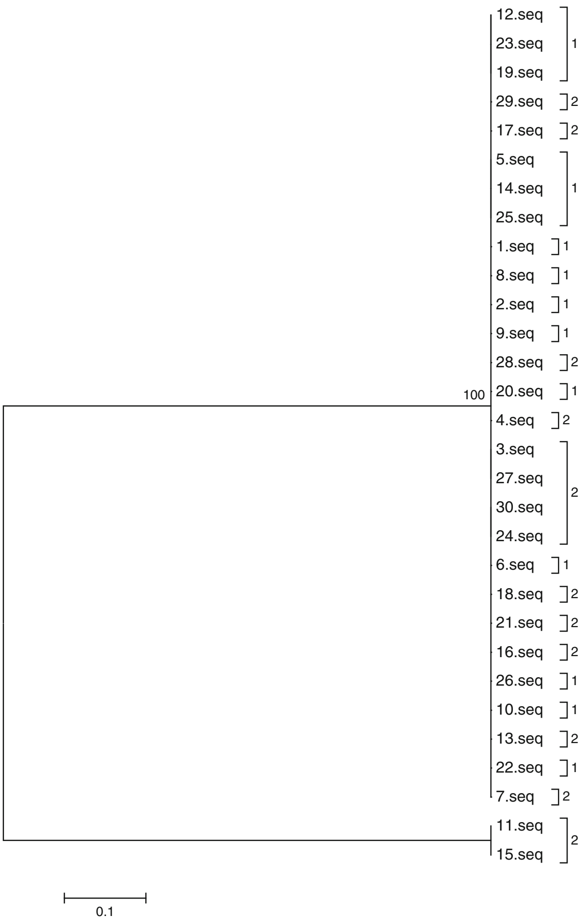

Acknowledgments This work was supported by International Science & Technology Cooperation Program of China (Grant No. 2013DFA71340) and Major National Science & Technology project of Water Pollution Control and Management of China (Grant No. 012ZX07203-002).

References

1. Chen ZD, Chen DH, Zhang ZS et al (2000) The dynamics of *Microcystis aeruginosa* Kütz and *Scenedesmus obliquus* (Turp.) Kütz Competition for resources—I. Growth dynamics and half-saturated constant of phosphorus-limited and irradiance of light-limited. J Acta Scientiae Circumstantiae 3:349–354
2. Delphine L, Hervé G (2004) Factors influencing the spatio-temporal distribution of benthic *Microcystis aeruginosa* colonies (Cyanobacteria) in the hypertrophic Grangent Reservoir (Loire, France). Original Res Art Competes Rendus Biol 327(8):753–761

3. Duan HT, Ma RH, Xu XF et al (2009) Two decade reconstruction of algal blooms in China's Lake Taihu. J Environ Sci Technol 43:3522–3528
4. Figueredo C, Giani A (2001) Seasonal variation in the diversity and species richness of phytoplankton in a tropical eutrophic reservoir. J Hydrobiologia 445:165–174
5. Hu HJ, Li YU, Wei YX et al (1980) Freshwater algae in China. Press of Science, Beijing
6. Jean-BP MJ, Benedicte W et al (2010) Variations of bacterial 16S rDNA phylotypes prior to and after chlorination for drinking water production from two surface water treatment plants. J Microbiol Biotechnol. doi:10.1007/s10295-009-0653-5
7. Kamenir Y, Dubinsky Z, Zohary T (2004) Phytoplankton size structure stability in a mesa-eutrophic subtropical lake. J Hydrobiologia 520:89–104
8. Moustaka GM, Vardaka E, Tryfon E (2007) Phytoplankton species succession in a shallow Mediterranean. J Hydrobiologia 575:129–140
9. Negro AI, Hoyos CD, Vega J (2000) Phytoplankton structure and dynamics in Lake Sanabria and Valparaiso reservoir (NW Spain). J Hydrobiologia 424:25–37
10. Neilan BA, Jacobs D, DelDot T et al (1997) rRNA sequences and evolutionary relationships among toxic and nontoxic cyanobacteria of the genus Microcystis. Int J Syst Bacteriol 47: 693–697. doi:10.1099/00207713-47-3-693
11. Qiao ZY, Sun JH, Zhang K (unpublished) The population succession of *Microcystis* in Yuqiao reservoir
12. Reynolds CS (1998) What factors influences the species composition of phytoplankton in lakes of different trophic status. J Hydrobiologia 369(370):11–26
13. Shigeto O, Shoichiro S, Renhui L et al (1998) 16S rDNA sequences and phylogenetic analyses of *Microcystis* strains with and without phycoerythrin. J FEMS Microbiol Lett 164:119–124

Chapter 6
The Improved Stress Tolerance of *Escherichia coli* by Directed Evolution of IrrE

Jianmei Luo, Jiajia Liu, Yuanyuan Zheng and Min Wang

Abstract IrrE, a global regulator of *Deinococcus radiodurans*, has proven to be effective in enhancing microbial stress tolerance. In this paper, IrrE from *D. radiodurans* R1, was introduced into *Escherichia coli* and directed evolved by error-prone PCR. The influence of mutation of IrrE on the cell growth and tolerance to various stresses was further investigated. First, one of the mutations, designated M4 with higher ethanol tolerance was obtained by error-prone PCR using the pET-28a(+)-*irrE*(W) as a template. The OD_{600} value of M4 reached 1.6 after 28 h cultivation under 8 % ethanol, while no obvious cell growth was observed in the recombinant strain harboring plasmid pET-28a(+)-*irrE*(W) and the control strain harboring plasmid pET-28a(+). The cell viability of M4 under different stress shock conditions (such as pH = 5.0, pH = 10.0, 3 mmol/L sorbitol and 15 % methanol), the cell growth rate, and the final biomass were improved obviously. The sequence comparison of *irrE* revealed that there were two sense substitutions (C24T and G530A). The substitution of G530A caused one amino acid change Gly177Glu. The homology modeling of IrrE was built according to the known structure of IrrE protein from *D. deserti*, which showed that the amino acid mutation located in HTH motif of IrrE. The work laid a foundation for further research on the relationship of IrrE structure and host cell tolerance to stress.

Keywords IrrE · *Escherichia coli* · *Deinoeoccus radiodurans* · Stress tolerance · Error-prone PCR

J. Luo (✉) · J. Liu · Y. Zheng · M. Wang
Key Laboratory of Industrial Fermentation Microbiology, Ministry of Education,
National Engineering Laboratory for Industrial Enzymes, The College of Biotechnology,
Tianjin University of Science & Technology, Tianjin 300457, People's Republic of China
e-mail: luojianmei@tust.edu.cn

T.-C. Zhang and M. Nakajima (eds.), *Advances in Applied Biotechnology*,
Lecture Notes in Electrical Engineering 333, DOI 10.1007/978-3-662-46318-5_6

6.1 Introduction

Recently, global transcriptional machinery engineering (gTME) has been widely explored to improve strain phenotypes by engineering transcription factors or RNA polymerase subunits, thereby altering transcriptional profiles of target strains; various degrees of success have been achieved [1–3]. The genus *Deinococcus* is known for its ability to survive extreme stress conditions, conferred by a unique pool of genes.

Deinococcus radiodurans is one of the most radio-resistant organisms known. This bacterium can survive extreme cold and dehydration as well as exposure to vacuum and acidic conditions [4]. Genetic analysis of a DNA damage-sensitive strain of *D. radiodurans* R1 led to the discovery of a novel regulatory protein, IrrE (GeneID: 7738927) [5, 6]. IrrE, a newly identified gene switch responsible for extreme radio-resistance of *D. radiodurans*, plays a central regulatory role in multiple DNA damage repair and protection pathways in response to radiation stress [6]. Interestingly, the heterologous expression of *irrE* could enhance the tolerance to osmotic pressure in *Escherichia coli* [7], salt tolerance in *E. coli* and *Brassica napus* [8], the anti-oxidation and anti-ultraviolet irradiation in *Bacillus subtilis* [9].

Escherichia coli is one representative strain of prokaryotes and model microorganism, which has been widely used for the production of bio-fuels and other chemicals. But the strain always faces various abiotic stresses in the industrial application, such as organic solvents, extreme pH, osmotic pressure, and so on, which seriously restricts its application efficiency.

In our previous work, the wild *irrE* gene from *D. radiodurans* R1 has been heterologously expressed in *E. coli* BL21(DE3). The results showed that the growth rate and the final biomass of recombinant strain containing pET-28a(+)-*irrE*(W) under stress were significantly higher than the control strain (harboring the empty vector pET-28a(+)). In order to obtain the mutants with higher tolerance to stress, IrrE was further directed evolved by error-prone PCR using pET-28a(+)-*irrE*(W) as a template in this paper. The cell growth performance and tolerance to stress of the evolved strain were investigated. The sequence comparison between the wild and evolved IrrE, and homologous modeling analysis by SWISS MODEL were further studied. The results could better understand the relationship of IrrE structure and host cell tolerance to stress.

6.2 Materials and Methods

6.2.1 Materials

Restriction enzymes, DNA-modifying enzymes, DNA markers, and T4 Ligases were purchased from TaKaRa (Dalian, China). The kits for DNA purification, gel recovery, and plasmid mini-prep were purchased from Omega Bio-Tek (USA).

Protein Marker II was purchased from Biomed (Beijing, China). Taq DNA polymerase, dNTPs was purchased from Sangon (Shanghai, China). The kit for protein purification was purchased from ComWin (Beijing, China). Sequence analysis was performed by BGI (Beijing, China). All cloning steps were performed in *E. coli* DH5α or BL21(DE3). The plasmid pET-28a(+) was stored in Key Laboratory of Industrial Fermentation Microbiology (Tianjin University of Science & Technology).

6.2.2 Strains

Escherichia coli BL21(DE3)/pET-28a(+) and *E. coli* BL21(DE3)/pET-28a(+)-*irrE* (W) have been successfully constructed in our previous work, which were grown in Luria-Bertani (LB) medium containing 50 μg/mL kanamycin at 37 °C. When required, 2 mmol/L IPTG was added to the medium to induce the expression of IrrE.

6.2.3 Library Construction and Selection

Using the plasmid pET-28a(+)-*irrE*(W) as a template, error-prone PCR method was employed to construct the library. The mutation ratio was controlled by adjusting the concentration of manganese ions and magnesium ions.

A total volume of 100 μL of reaction mixture contained 10 μL 10 × Taq DNA polymerase buffer, 0.2 mmol/L dATP and dGTP, 1 mmol/L dCTP and dTTP, 10 ng of template, 0.05–0.25 mmol/L $MnCl_2$, 1–7 mmol/L $MgCl_2$ and 5 units (U) of Taq DNA polymerase. A pair of primers used was F1 (5′-CCCATGGCTGCAGAAAT-GCCCAGTGC-3′) and R1 (5′-CATGCCATGGTCTAGATGTGCAGCG-3′). PCR was carried out at 94 °C for 30 s, 63 °C for 30 s, and 72 °C for 1 min for a total of 30 cycles. The products of error-prone PCR were purified, digested, and inserted into *Nco*I and *Eco*RI sites of plasmid pET-28a(+)-*irrE*(W) replacing the wild-type *irrE* gene. The ligation products were transformed into *E. coli* BL21(DE3) competent cells. Cells were plated on LB-agar plates containing 50 mg/mL kanamycin, incubated at 37 °C overnight, and scraped off to create a liquid library. The library size was approximately 10^6.

The liquid library was inoculated into the challenging medium. After cultivation at 37 °C on a rotary shaker (180 r/min) to the late logarithmic phase, the cultures were transferred into the fresh challenging medium to cultivate for 2–3 times under the same conditions. The unique difference was that the ethanol concentration in the challenging medium was gradually increased until the final concentration reached 8 %. Finally, the cultures were spread onto LB agar plates containing 50 mg/mL kanamycin. After incubation at 37 °C overnight, the grown colonies were preliminary considered as mutants with ethanol tolerance, which should be further screened.

The single colony on the LB-agar plates was, respectively, inoculated into LB liquid medium containing 50 μg/mL kanamycin. After incubation overnight at 37 °C on a rotary shaker (180 r/min), the OD_{600} value of culture was adjusted to the same level and transferred into the fresh challenging medium (LB medium containing 50 μg/mL kanamycin, 2 mmol/L IPTG and different concentration of ethanol (4, 8, 12 % (v/v)) using 0.5 % (v/v) of the seed culture. The cell was grown at 37 °C on a rotary shaker (180 r/min). The culture was withdrawn during growth and OD_{600} value was detected. The higher ethanol tolerance mutants were selected by comparison of cell growth rate and the final biomass.

During the above selection process, the plasmid of the mutant with higher ethanol tolerance was verified by PCR and enzyme digest methods, and then retransformed into fresh *E. coli* DH5a cells. The mutant growth in challenging media was retested to separate the effects of the mutated irrE gene from any possible spontaneous chromosomal mutations acquired during the selection process.

6.2.4 Cell Growth Assay

To test the influence of *irrE* mumants on the cell growth, strains were inoculated into LB liquid medium containing 50 μg/mL kanamycin. After cultivation overnight at 37 °C on a rotary shaker at 180 r/min, the OD_{600} value of cultures were adjusted to the same level and transferred into the fresh challenging medium (LB medium containing 50 μg/mL kanamycin and 2 mmol/L IPTG using 0.5 % (v/v) of the seed culture. The cells were grown at 37 °C on a rotary shaker at 180 r/min. The culture was withdrawn during growth and OD_{600} value was detected to obtain the growth curve.

6.2.5 Shock Experiments and Cell Growth Under Different Stress Conditions

To test the tolerance of strain toward extremely stresses, strains were grown overnight at 37 °C on a rotary shaker at 180 r/min in LB medium containing 50 mg/mL kanamycin. The cultures were transferred into the fresh LB medium containing 50 mg/mL kanamycin using 1 % (v/v) of the seed culture and grown at 37 °C on a rotary shaker at 180 r/min. When reaching an OD_{600} value of 0.6, the cultures were added 2 mmol/L IPTG and inoculated for 6 h to induce the expression of IrrE. Then 1 mL of culture was withdrawn and the cells were harvested by centrifugation at 6,000 r/min for 10 min. The same mass cells were transferred to 50 mL challenging

Table 6.1 Shock experiment conditions of the control strain (*E. coli* BL21(DE3) harboring plasmid pET-28a(+)), the recombinant strain harboring pET-28a(+)-*irrE*(W) and the mutant harboring pET-28a(+)-*irrE*(M)

Stresses	Sorbitol (mol/L)	pH	Methanol (%, v/v)	Ethanol (%, v/v)	H_2O_2 (%, v/v)
Condition	3.0	pH = 2; pH = 12	10	12	1
Time (min)	30	30	30	30	30

medium containing 50 μg/mL kanamycin and different kinds of stresses (Table 6.1). During incubation, optical density at 600 nm was used to measure cell growth.

To test the cell growth performance in challenging medium, strains were grown overnight at 37 °C on a rotary shaker at 180 r/min in LB medium containing 50 mg/mL kanamycin, respectively. The OD_{600} values of culture were adjusted to the same level and transferred to the fresh challenging medium (LB medium containing 50 μg/mL kanamycin, 2 mmol/L IPTG and different challenging substances (4 % ethanol, 5 % methanol and 1 M sorbitol)) using 0.5 % (v/v) of the seed culture. During incubation, optical density at 600 nm was used to measure cell growth.

6.2.6 Mutational Sites Analysis of IrrE

The mutated *irrE* gene was sequenced and then translated into the amino acids by software DNAMAN. To analyze the influence of the mutant sites on the function and structure of IrrE, the homology modeling was built based on the solved structure of IrrE protein from *Deinoeoccus deserti* by SWISS-MODEL.

6.3 Results and Discussion

6.3.1 Library Construction and Selection of Ethanol-Tolerant Mutants

6.3.1.1 The Development of Error-Prone PCR Conditions

Low concentration of Mg^{2+} is required for Taq DNA polymerase while high level can promote the stability and the complementarity of base pairs. Mn^{2+} can reduce the specificity of the polymerase to the template, which is advantageous for mutation. Therefore, error-prone PCR conditions were optimized by adjusting the concentration of Mg^{2+} (1–7 mmol/L) and Mn^{2+}(0.05–0.25 mmol/L). When the concentration of Mg^{2+} was set at 3 mmol/L, all stripes were clear and bright, and no

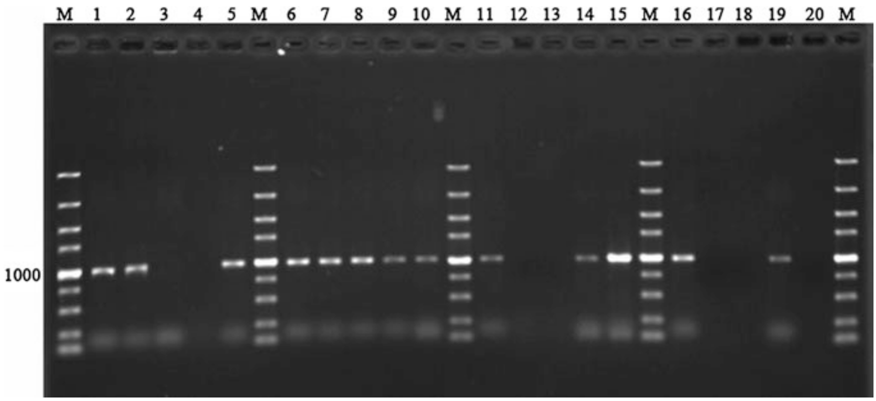

Fig. 6.1 Error-prone PCR conducted with different concentrations of Mn^{2+} and Mg^{2+}. *M* DL5000 DNA Marker. *1–5* The concentration of Mn^{2+} is 0.05, 0.1, 0.15, 0.2, 0.25 mmol/L, respectively, at Mg^{2+} is 1 mmol/L. *6–10* The concentration of Mn^{2+} is 0.05, 0.1, 0.15, 0.2, 0.25 mmol/L, respectively, at Mg^{2+} is 3 mmol/L. *11–15* The concentration of Mn^{2+} is 0.05, 0.1, 0.15, 0.2, 0.25 mmol/L, respectively, at Mg^{2+} is 5 mmol/L. *15–20* The concentration of Mn^{2+} is 0.05, 0.1, 0.15, 0.2, 0.25 mmol/L, respectively, at Mg^{2+} is 7 mmol/L

obvious dispersion was observed under different concentrations of Mn^{2+} (Fig. 6.1). So 3 mmol/L of Mg^{2+} was used for the error-prone PCR.

6.3.1.2 Library Construction

Error-prone PCR was employed to construct the library using the plasmid pET-28a (+)-*irrE*(W) as a template. PCR was carried out under different Mn^{2+} concentrations (0.05–0.25 mmol/L) and 3 mmol/L Mg^{2+}. As presented in Fig. 6.2, the target band was clear and bright. The size of *irrE* was about 1,000 bp [8]. Therefore, IrrE library (about 10^6) was constructed by using the above PCR conditions and the detailed procedures are described in Sect. 6.2.3.

6.3.1.3 Selection of Ethanol-Tolerant Mutants

The liquid library was screened according to the detailed procedures described in Sect. 6.2.3. After incubation in the challenging medium (LB medium containing 50 μg/mL kanamycin, 2 mmol/L IPTG and 8 % ethanol), the cultures were spread onto LB agar plates containing 50 mg/mL kanamycin. After incubation at 37 °C overnight, 24 single colonies (named M1-M24) were grown and preliminary considered as mutants with higher ethanol tolerance.

24 single colonies were respectively inoculated into LB medium and the cell growth curves under different ethanol stresses were determined according to the detailed procedure shown in Sect. 6.2.3. By comparison of cell growth rate and the

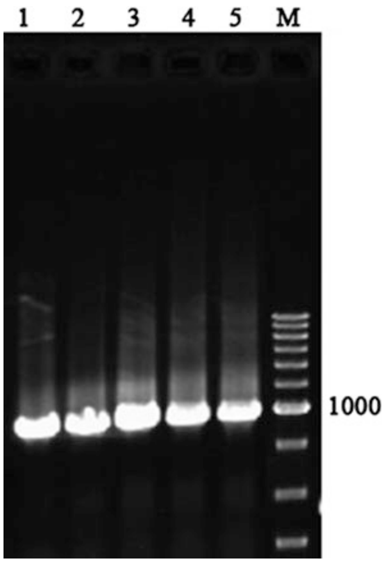

Fig. 6.2 Error-prone PCR conducted with different Mn^{2+} concentrations. *M* DL500 DNA marker. *1–5* The concentration of Mn^{2+} is 0.05, 0.1, 0.15, 0.2, 0.25 mmol/L, respectively, at Mg^{2+} is 3 mmol/L

final biomass, four mutants named M1-M4 were screened and grown well in the presence of 4 % ethanol (Fig. 6.3a). When the ethanol concentration was increased to 8 %, one mutant (M4) showed good growth performance and a maximum OD_{600} of 1.6 was reached after 28 h (Fig. 6.3b). Further increase in ethanol concentration (12 %) and no obvious cell growth was observed in all mutants. So mutant M4 was considered as the better ethanol-tolerant strain.

The cell growth performance of the control strain (*E. coli* BL21(DE3) harboring plasmid pET-28a(+)), the recombinant strain harboring pET-28a(+)-*irrE*(W), and the mutant M4 harboring pET-28a(+)-*irrE*(M4) were compared in LB medium containing 8 % ethanol. As shown in Fig. 6.4, the cell growth of the control strain harboring plasmid pET-28a(+) and recombinant strain harboring pET-28a(+)-*irrE* (W) were completely inhibited, while the *irrE* mutant M4 strain showed rapid growth after a 20 h lag phase. The maximum OD_{600} reached 1.6 after 28 h cultivation.

6.3.2 The Influence of Expression of IrrE on Cell Growth Under No Stress

As shown in Fig. 6.5, the lag phase of the control strain (*E. coli* BL21(DE3) harboring plasmid pET-28a(+)) and the recombinant strain harboring pET-28a(+)-*irrE*(W) under no stress condition were 0–8 h, while the lag phase of the *irrE* mutant M4 was 2 h shorter than the other two strains. After 14 h cultivation, the

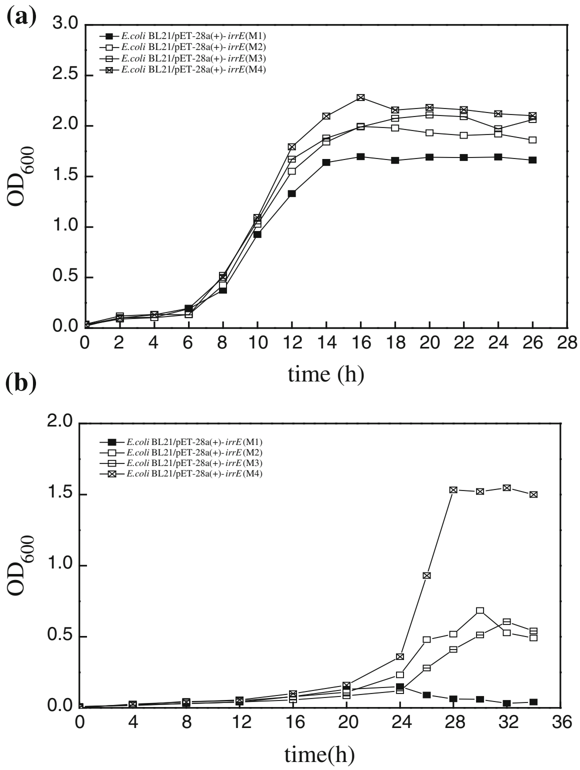

Fig. 6.3 The growth curves of *E. coli* BL21/pET-28a(+)-*irrE*(M1-M4) under various concentrations of ethanol. **a** 4 % ethanol. **b** 8 % ethanol

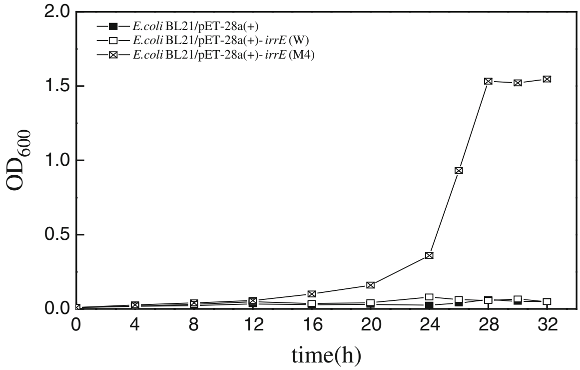

Fig. 6.4 The growth curves of *E. coli* BL21/pET-28a(+)-*irrE*(M4), *E. coli* BL21/pET-28a(+)-*irrE*(W) and the control strain under 8 % ethanol

final biomass of the recombinant strain harboring pET-28a(+)-*irrE*(W) and the *irrE* mutant M4 was silimilar and 10 % more than the control strain harboring plasmid pET-28a(+). This indicated that the expression of *irrE* shortened the cell lag phase and increased the final biomass.

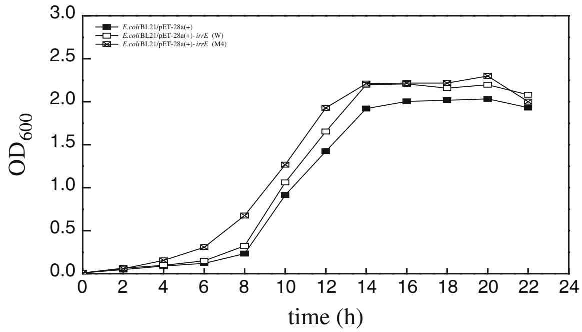

Fig. 6.5 The growth curves of *E. coli* BL21/pET-28a(+)-*irrE*(M4), *E. coli* BL21/pET-28a(+)-*irrE* (W) and the control strain under no stress condition

6.3.3 The Influence of Expression of IrrE on Cell Viability and Growth Performance Under Different Stress Conditions

6.3.3.1 The Influence of Expression of IrrE on Cell Viability Under Stress Shock

After shocked with 1 % H_2O_2 and 10 % ethanol for 30 min, the cell viability of the mutant M4 was less than 15 %, which was higher than those of the control strain and wild type strain. For other shock conditions (pH = 5, pH = 10, 15 % methanol and 3 M sorbitol), the cell viabilities of mutant M4 were 56.9, 70, 55, 51.6 %, respectively, which increased by 25.0, 30.4, 17.5, and 6.7 %, respectively, compared with the wild type strain and increased by 36.4, 45.4, 35.0, and 16.0 % compared with the control strain (shown in Fig. 6.6). These results indicate that the expression of mutant *irrE* could remarkably enhance the tolerance of *E. coli* to stresses of 3 M sorbitol, pH = 5, pH = 10, and 15 % methanol.

6.3.3.2 The Influence of Expression of IrrE on Cell Growth Performance Under Different Stress Conditions

In the presence of 4 % ethanol, the lag phase of the control strain and the wild-type stain was 10 h, while the lag phase of the *irrE* mutant M4 was shortened to 6 h and its cell growth rate and final biomass were obviously increased, indicating that the IrrE mutation enhanced the strain tolerance to 4 % ethanol (Fig. 6.7a). Under the other stress conditions (5 % methanol and 1 M sorbitol), the control strain, the wild-type stain and the *irrE* mutant M4 showed the similar growth tendency. However, the *irrE* mutant M4 showed higher growth rate and final biomass. In the presence of 5 % methanol, the *irrE* mutant M4 reached a maximum OD_{600} of 2.2 after 18 h

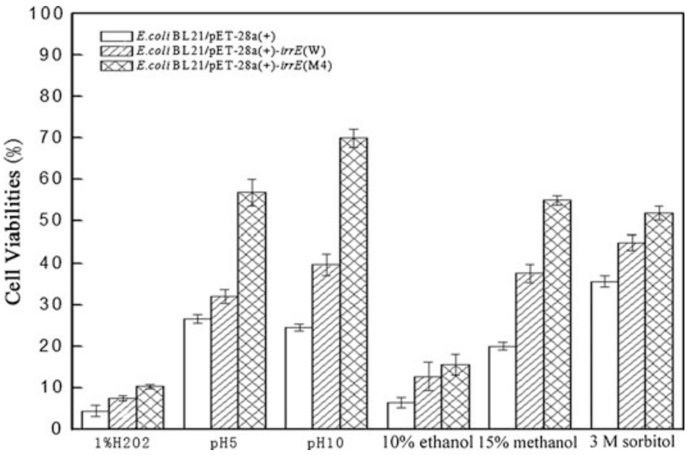

Fig. 6.6 The cell viability of *E. coli* BL21/pET-28a(+)-*irrE*(M4), *E. coli* BL21/pET-28a(+)-*irrE* (W) and the control strain under various kinds of shock conditions

cultivation, which was 18 and 25 % higher than the control strain and wild-type strain, respectively (Fig. 6.7b). In the presence of 1 M sorbitol, the *irrE* mutant M4 reached a maximum OD_{600} of 2.0 after 16 h cultivation, which was 17 and 42 % higher than the control strain and wild-type strain, respectively (Fig. 6.7c). These results indicate that the expression of the mutated IrrE could promote host cell tolerance to organic solvents and osmotic pressure.

6.3.4 The Mutation Site Analysis of IrrE

The *irrE* sequence of mutant M4 was analyzed. The whole length of *irrE* was 987 bp, encoding 328 amino acids. The comparison result between the wild-type and mutated *irrE* showed that there were two sense substitutions (C24T and G530A). The substitution of G530A caused one amino acid change Gly177Glu.

The IrrE protein structure of *D. deserti* has been solved, which shows 64 % homology with the IrrE protein from *D. radiodurans*. Therefore the homology structural model of IrrE from mutant M4 was built using SWISS-MODEL according to the known structure of IrrE protein from *D. deserti.* The domain boundary of IrrE from *D. radiodurans* was as follows: the N-terminal domain (residues 1–161); the middle domain (residues 162–203); and the C-terminal domain (residues 204–328) (Fig. 6.8a). The results show that the mutational amino acid was located in helix-turn-helix (HTH) motif of IrrE, which was considered to be involved in DNA binding and recognition [10] (Fig. 6.8b).

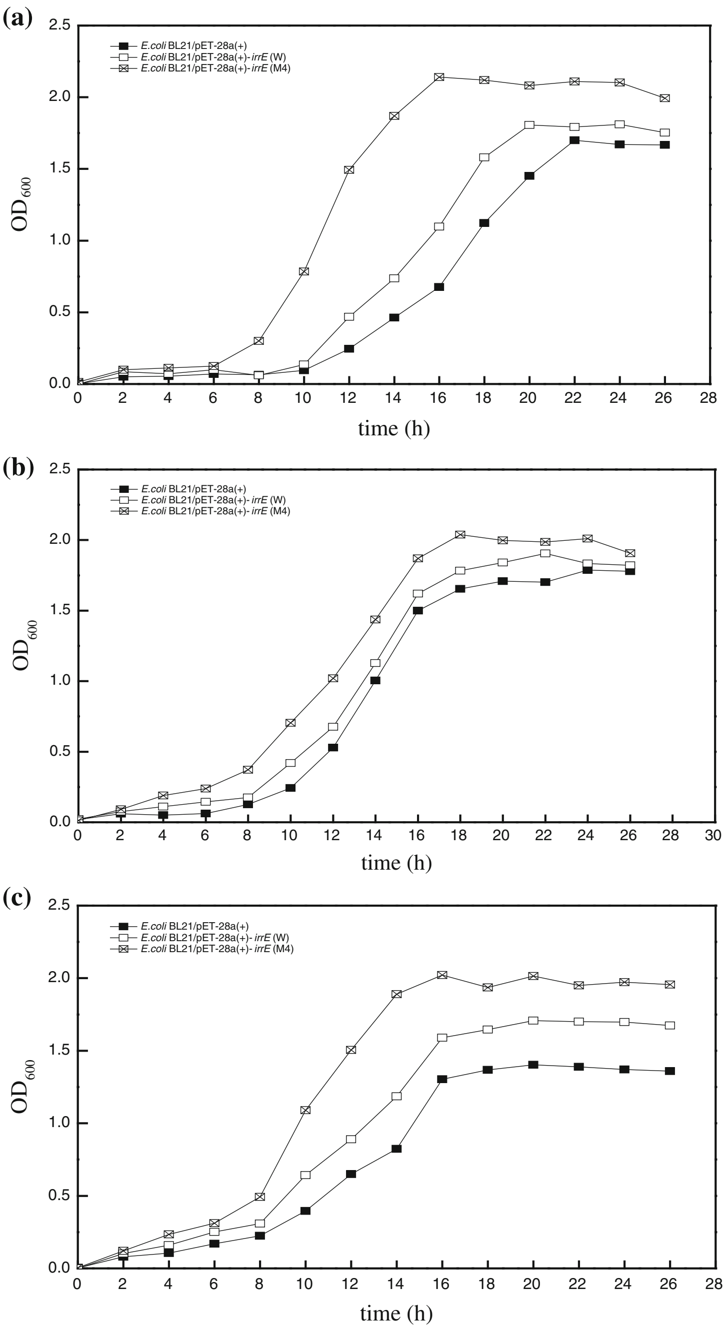

Fig. 6.7 The growth curves of *E. coli* BL21/pET-28a(+)-*irrE*(M4), *E. coli* BL21/pET-28a(+)-*irrE* (W) and the control strain under certain concentration of stress conditions. **a** 4 % ethanol. **b** 5 % methanol. **c** 1 M sorbitol

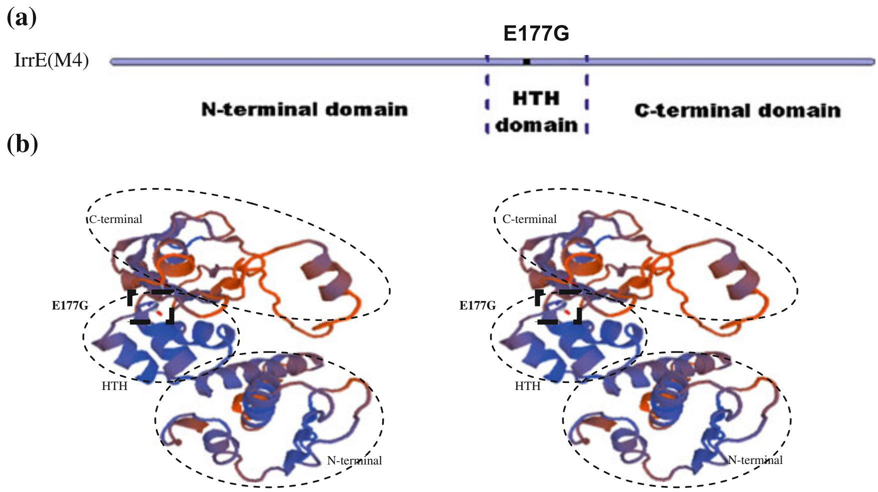

Fig. 6.8 Summary and location of mutation sites of IrrE. **a** Summary of mutation site in the amino acid sequence of the mutant M4, the full sequence is divided into three parts by two *dashed lines*. Each part represents a separate domain of *irrE* (from *left* to *right* N-terminal domain, HTH domain, C-terminal domain). **b** Location of mutation sites of the mutant M4 in a modeled structure of *irrE* from *D. radiodurans*

6.4 Conclusions

The *irrE* gene from *D. radiodurans* R1 was directed evolved by error-prone PCR method and was introduced into *E. coli*. One mutant M4 with better stress tolerance was obtained, which showed good cell growth performance in the presence of 8 % ethanol. Also, the cell viabilities of mutant M4 were promoted under extremely stress shock conditions (pH = 5, pH = 10, 15 % methanol and 3 M sorbitol). On the other hand, mutant M4 exhibited higher growth rate and final biomass in the presence of challenging medium (4 % ethanol, 5 % methanol and 1 M sorbitol) compared with the control and wild type strains. These results indicate that the expression of mutational IrrE could further improve the tolerance of *E. coli* to various stresses.

The comparison result between the wild-type and mutated *irrE* showed that there were two sense substitutions (C24T and G530A). The substitution of G530A caused one amino acid change, Gly177Glu. The homology modeling of IrrE was constructed using the known IrrE from *D. desertias* as a template, indicating the mutational amino acid was located in HTH motif of IrrE, which was thought to be involved in DNA binding and recognition [10].

Acknowledgments This work is supported by the National Natural Science Foundation of China (No. 21306138) and the Natural Science Foundation of Tianjin (No. 13JCYBJC20600).

References

1. Alper H, Moxley J, Nevoigt E et al (2006) Engineering yeast transcription machinery for improved ethanol tolerance and production. Science 314:1565–1568
2. Alper H, Stephanopoulos G (2007) Global transcription machinery engineering: a new approach for improving cellular phenotype. Metab Eng 9:258–267
3. Klein-Marcuschamer D, Santos CNS, Yu HM et al (2009) Mutagenesis of the bacterial RNA polymerase alpha subunit for improvement of complex phenotypes. Appl Environ Microbiol 75:2705–2711
4. Makarova KS, Omelchenko MV, Gaidamakova EK et al (2007) *Deinococcus geothermalis*: the pool of extreme radiation resistance genes shrinks. PLoS ONE 2:e955
5. Earl AM, Mohundro MM, Mian IS et al (2002) The IrrE protein of *Deinococcus radiodurans* R1 is a novel regulator of recA expression. J Bacteriol 184:6216–6224
6. Hua YJ, Narumi Issay, Gao GJ et al (2003) IrrE: a general switch responsible for extreme radioresistance of *Deinococcus radiodurans*. Biochem Biophys Res Commun 306:354–360
7. Ma R, Zhang Y, Hong HZ et al (2011) Improved osmotic tolerance and ethanol production of ethanologenic *Escherichia coli* by IrrE, a global regulator of radiation-resistance of *Deinococcus radiodurans*. Curr Microbiol 62:659–664
8. Pan J, Wang J, Zhou ZF et al (2009) IrrE, a global regulator of extreme radiation resistance in *Deinococcus radiodurans*, enhances salt tolerance in *Escherichia coli* and *Brassica napus*. PLoS ONE 4(2):e4422
9. Gao JW, Xie SB, Tang ZP et al (2010) Study on enhances of the resistance in *Bacillus subtilis* by *Deinococcus radiodurans pprI*. J Univ South China 24(1):78–82
10. Chen TJ, Wang JQ, Yang R et al (2011) Laboratory-evolved mutants of an exogenous global regulator, IrrE from *Deinococcus radiodurans*, enhance stress tolerances of *Escherichia coli*. PLoS ONE 6(1):e16228

Chapter 7
Cloning and Characterization of the *TMEPAI* Gene Promoter

Ailong Guo, Ping Qin, Weiwei Shi, Yuyin Li and Aipo Diao

Abstract *TMEPAI* was originally identified as a highly androgen-induced gene by serial analysis of gene expression in androgen-treated prostate cancer cell. *TMEPAI* is highly expressed in many tumor cells. However, little is known about the transcriptional mechanism regulating *TMEPAI* gene expression, and its promoter has not yet been characterized. In this study, the 5′ regulatory region of the *TMEPAI* gene was characterized, the 5′ flanking sequence of *TMEPAI* gene was successfully amplified by PCR, and the 925 bp fragment of *TMEPAI* gene promoter was inserted into pGL4-Basic vector to measure its activity. Furthermore, the transcriptional regulators in *TMEPAI* promoter region were analyzed by bioinformatics. Taken together, these results will help to understand the expression regulation of *TMEPAI* and its role in tumorigenesis.

Keywords *TMEPAI* · Promoter · Bioinformatics

7.1 Introduction

The gene encoded transmembrane prostate androgen-induced protein (*TMEPAI*) is located on the chromosome 20q13.31-q13.33, which was discovered during systematic search for androgen-induced genes [1]. TMEPAI protein is highly expressed in many tumor including prostate, breast, and colon cancers [2–4]. TMEPAI protein is predominantly expressed in the prostate gland and is directly regulated by androgen receptor [5]. *TMEPAI* gene encodes a protein of 287 amino acids with a

A. Guo · P. Qin · W. Shi · Y. Li (✉) · A. Diao (✉)
Key Lab of Industrial Fermentation Microbiology of the Ministry of Education, Tianjin, College of Bioengineering, Tianjin University of Science and Technology, Tianjin 300457, China
e-mail: liyuyin@tust.edu.cn

A. Diao
e-mail: diaoaipo@tust.edu.cn

T.-C. Zhang and M. Nakajima (eds.), *Advances in Applied Biotechnology*, Lecture Notes in Electrical Engineering 333, DOI 10.1007/978-3-662-46318-5_7

trans-membrane Ib domain, and two PY motifs that can interact with the WW domain of the E3 ubiquitin ligase Nedd4 [6]. Structural analysis of the *TMEPAI* protein indicates similarities to the Nedd4 ubiquitin ligase binding protein coded by the N4wbp4 gene suggesting a role for *TMEPAI* in the ubiquitin-proteasomal pathway. Assessment of *TMEPAI* functions suggests specific interaction between *TMEPAI* and Nedd4 uniquitin E3 ligase [7–10]. *TMEPAI* has been reported highly expressed in many cancers, overexpression of *TMEPAI* promoted cell proliferation of prostate cell, and knockdown of *TMEPAI* expression decreased the growth of lung cancer cell Calu3 [11–14].

In this article, in order to analyze the transcriptional regulation of *TMEPAI* expression, the promoter of the *TMEPAI* gene was cloned and analyzed. This study provides the basis to understand the transcription regulation of *TMEPAI* gene, and further considers the regulatory mechanism will help to develop therapeutic reagents for human cancers using *TMEPAI* as the target.

7.2 Materials and Methods

7.2.1 Genomic DNA Isolation and Cloning of the TMEPAI Promoter

Genomic DNA was extracted from human blood using a genomic DNA extraction kit (Promega, Madison, WI). Primers were designed based on the sequence of the 5′ untranslated region of *TMEPAI* (Gen Bank ID: 56937). Primers for amplification of promoter were: forward primer 5′-CGGGGTACCAAGGCGACACACTAAATTTT TAAGAG-3′ and reverse primer 5′-CCGCTCGAGCGCTCCGAGACCGCGGT-3′. The isolated genomic DNA was used as the template to amplify the *TMEPAI* promoter region. *Kpn*I and *Xho*I restriction sites were introduced into the forward and reverse primers, respectively. The PCR product was purified using a gel purification kit and cloned into the T/A cloning vector pUCm-T (Shanghai Sangon Biological Engineering Technology, Shanghai, China). *TMEPAI* promoter fragment was cloned into the pGL4 basic vector (Shanghai Sangon Biological Engineering Technology, Shanghai, China). The 925 bp 5′ blank region of *TMEPAI* gene was generated by digesting the plasmid pT/A-925 with *Kpn*I and *Xho*I, and subcloned the released fragment into the *Kpn*I/*Xho*I site of pGL4 basic vector to obtain plasmid pGL4-925. The positive clones of pT/A-925 were isolated and sequenced.

7.2.2 Cell Culture and Transfection

Human hepatic carcinoma cell line (HepG2), human alveolar epithelial lung cell line (A549), human breast cancer cell line (MDA-MB231), Hela cells, human gastric cancer cell line (MGC-803), and human prostate cancer cell line (DU145) were cultured in Dulbecco's modified Eagle' medium (DMEM) containing 10 % fetal bovine serum (FBS), 2 mM glutamine, 1,000 U/mL penicillin, and 0.01 mg/mL streptomycin at 37 °C in a humidified incubator with 5 % carbon dioxide. Cells were transfected using Turbofect (Thermo Scientific) according to manufacturer's recommendations. 10^5 cells were seeded in each well of 12-well plate and cultured for 24 h before transfection. The cells were transfected with 1 μg of *TMEPAI* promoter construct or pGL4 basic vector.

7.2.3 Analysis of Luciferase Activity

Luciferase activity was measured 48 h after transfection. Cells were harvested and washed twice with PBS, then lysed in cold lysis buffer (25 mmol/L glycylglycine, pH 7.8; 1 % Triton X-100; 15 mmol/L $MgSO_4$; 4 mmol/L EGTA, and 1 mmol/L dithothreitol). For luciferase assay, 100 μL 25 mmol/L luciferin and 5 μL assay cocktail (1 mol/L adenosine triphosphate; 15 mmol/L KH2PO4, pH 7.8; 15 mmol/L $MgCl_2$) were added to 45 μL cell lysate, and the luiferase activities were measured using a FLUOstar OPTIMA fluorescence reader.

7.2.4 Bioinformatics Analysis of TMEPAI Promoter Region

The putative binding sites for transcription factors with 5′-regulatory region of *TMEPAI* gene were analyzed with the following software packages: Match 1.0 public (http://www.gene-regulation.com), and TRANSFAC database (http://www.gene-regulation.com/pub/databases.html). Transcription start sites were identified by using DBTSS (http://www.biomedsearch.com/sci/Dbtss.com) and BDGP (http://www.Fruitfly.org/seq-tools/promoter.html).

7.2.5 Statistical Analysis

Experiments were repeated at least thrice, with two replicates per sample for each experiment. The data were analysis of variance using the Student's *t*-test. Values of $p < 0.05$ were considered to indicate statistical significance.

7.3 Results

7.3.1 Identification of the Upstream Promoter Region of TMEPAI Gene

To better understand the mechanism involved in *TMEPAI* gene expression, the promoter region of *TMEPAI* was cloned and analyzed. A blast search using *TMEPAI* (Gene ID: 56937) as query was performed online (basic local alignment search tool: BLAST; http://blast.ncbi.nlm.nih.gov/Blast.cgi) and revealed the 5′-upstream sequence of the *TMEPAI* gene.

A genomic DNA fragment that spans positions −761 to +164 relative to the transcriptional initiation site about 925 bp (Fig. 7.1) was amplified by PCR. The fragment was then cloned into the T/A cloning vector pUCm-T, and sequenced.

7.3.2 Construction of TMEPAI Promoter Plasmids

The pUCm-T-925 plasmid was digested with *Kpn*I and *Xho*I, and then the promoter region of *TMEPAI* was subcloned into pGL4-Basic vector, which was digested with the same restriction enzymes. The reporter plasmid was named pGL4-925. The recombinant plasmid was identified by enzymes digestion and PCR (Fig. 7.2).

7.3.3 Analysis of TMEPAI Promoter Activities

In order to analyze *TMEPAI* gene promoter activities, pGL4-925 and pGL4-Basic were transfected into six cell lines including HepG2, A549, MDA-MB231, HeLa, MGC-803, and DU145. We observed that the highest *TMEPAI* promoter activity was found in HeLa cells (Fig. 7.3). Other cells showed lower promoter activity, and

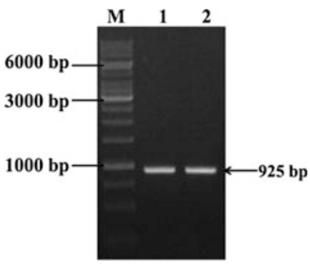

Fig. 7.1 PCR was performed to amplify *TMEPAI* gene promoter. PCR product was separated on 0.8 % agarose gel. *M* 1 kb ladder DNA marker. *1–2 TMEPAI* gene promoter

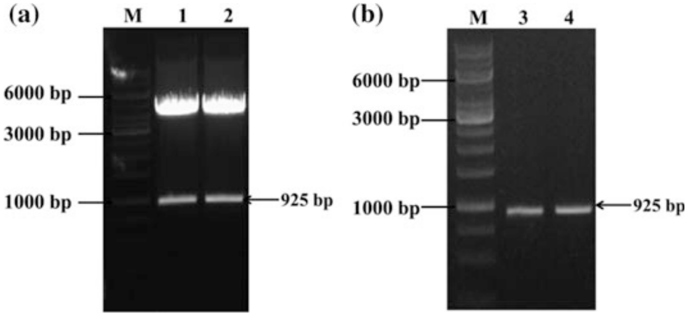

Fig. 7.2 Identification of the recombinant plasmids with *Kpn*I and *Xho*I digestion (**a**) and PCR (**b**) *M* 1 kb ladder DNA marker. *1–4 TMEPAI* gene promoter

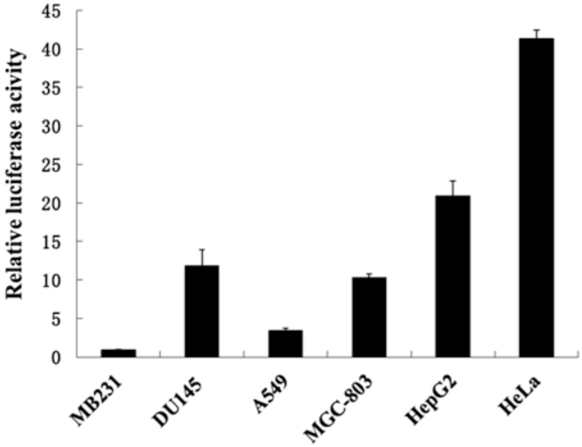

Fig. 7.3 Determination of the *TMEPAI* promoter activity in different cell *lines* by luciferase assay pGL4-925 and pGL4-Basic were transiently transfected into six different cell *lines*. After 48 h transfection, cell lysates were prepared and assayed for luciferase activity. Relative pGL4-Basic activity of representative experiment is shown

the MDA-MB-231 cells showed the lowest promoter activity. Therefore, pGL4-925 can be used to screen anticancer reagents with the *TMEPAI* promoter as the target.

7.3.4 Bioinformatic Analysis of TMEPAI Promoter Region

TFSEARCH database was used to analysis the binding sites for transcriptional regulators in *TMEPAI* promoter. The promoter does not contain a TATA box, however, a CAAT box and a GC box were identified, which are both often encountered in TATA-less promoters and they contribute to the correct RNA polymerase positioning. In addition, the sequence search in *TMEPAI* promoter

```
-161  TGCGGCTGGC  ACCGAGTTCG  GCTCCCCGGC  CCCGGGCGTG  CGCCGGGCAG  GCGTTCCAAG
                                                                   HSF
-101  CTGACCGCCG  TTGGGGAGAG  GGCACAGCGC  CCCTCCTCCG  TTGCGCGGGT  GCCGGGTCTA
                  ADR1
-41   CGTGGGCCGC  CTAGCTCTGG  CCCTTTAAGA  GCCCGCCCCG  TTTCCCGTCA  CCCCGCCCCC
            Sp1                                 Sp1       +1TSS(transcriptional start site)
+20   CGGCTCGGGG  AGGGGGTGCG  GGGGAACCTC  GGCGGGGATT  GCGCAGCGCG  CGCCCCCTC

+81   CCCGGCCCCC  GCGCGGTGGG  AACCGGCAGC  CCCGTCTAGC  GCTGACGTCA  GACCGTCTGC
                                                            CREB
```

Fig. 7.4 Nucleotide sequence of the *TMEPAI* gene promoter region. The numbering of the sequence is relative to the TSS. Putative binding sites for the transcriptional factors are *underline* and *labeled* below. Transcriptional start site was predicted with DBTSS database analysis

region revealed several regulatory elements such as the binding sites for transcriptional factors Sp1, CREB, ADR1, HSF, and AP-2 (Fig. 7.4).

7.4 Discussion

TMEPAI was identified originally as a highly androgen-inducible gene with prostate-abundant expression that was restricted to prostatic epithelial cells [15]. Studies of *TMEPAI* have suggested its role in regulating cell growth as noted by the androgen induction of *TMEPAI* expression, elevated *TMEPAI* expression in nontumorigentic revertants of tumor cell lines, and the *TMEPAI* expression alterations (up- or down-regulation) in human tumors [1, 16]. Functional analysis indicates that *TMEPAI* is a Nedd4 E3 ligase binding protein and plays a role in down-regulation of androgen receptor through a negative feedback loop between androgen receptor and *TMEPAI* [15]. Studies also suggest that *TMEPAI* is involved in other cancers through regulation of TGF-β, PI3K and WNT pathway [17, 18].

A 925 bp fragment of *TMEPAI* promoter region was amplified from human genomic DNA by PCR (Fig. 7.1). Transcriptional regulation is the result of the balance between chromatin remodeling and RNA polymerase activity on accessible regulatory regions [19], the consensus recognition sequences for several transcription factors in *TMEPAI* promoter were analyzed by the TRANSFAC database (http://www.gene-regulation.com/pub/databases.html), and some of them are transcription factors including Sp1, CREB, ADR1, HSF, and AP-2 (Fig. 7.4). These results serve as a basis for future studies to understand the regulation of *TMEPAI* expression at transcriptional level.

Acknowledgments This research is supported by the program for Changjiang Scholars and Innovative Research Team in University (IRT1166), National Natural Science Foundation of China grant (31471335) and scientific research fund project of Tianjin University of Science and Technology (20130106).

References

1. Xu LL, Shanmugam N et al (2000) A novel androgen-regulated gene, *PMEPA1*, located on chromosome 20q13 exhibits high level expression in prostate. Genomics 66:257–263
2. Ishkanian AS, Mallof CA et al (2009) High-resolution array CGH identifies novel regions of genomic alteration in intermediate-risk prostate cancer. Prostate 69:1091–1100
3. Tanner MM, Tirkkonen M et al (1994) Increased copy number at 20q13 in breast cancer: defining the critical region and exclusion of candidate genes. Cancer Res 54:4257–4260
4. Hidaka S, Yasutake T, Takeshita H et al (2000) Differences in 20q13.2 copy number between colorectal cancers with and without livermetastasis. Clin Cancer Res 6:2712–2717
5. Masuda K, Werner T, Maheshwari S, Frisch M, Oh S, Petrovics G, May K, Srikantan V, Srivastava S, Dobi A (2005) Androgen receptor binding sites identified by a GREF-GACA model. J Mol Biol 353:763–771
6. Jolliffe CN, Harvey KF, Haines BP, Parasivam G, Kumar S (2000) Identification of multiple proteins expressed in murine embryos as binding partners for the WW domains of the ubiquitin-protein ligase Nedd4. Biochem J 351:557–565
7. Kumar S, Tomooka Y, Noda M (1992) Identification of a set of genes with developmentally down-regulated expression in the mouse brain. Biochem Biophys Res Commun 185:1155–1161
8. Kumar S, Harvey KF, Kinoshita M (1997) A cDNA cloning, expression analysis, and mapping of the mouse Nedd4 gene. Genomics 40:435–443
9. Anan T, Nagata Y, Koga H, Honda Y, Yabuki N, Miyamoto C, Kuwano A, Matsuda I, Endo F (1998) Human ubiquitin-protein ligase Nedd4: expression, subcellular localization and selective interaction with ubiquitin conjugating enzymes. Genet Cells 3:751–763
10. Harvey KF, Kumar S (1999) Nedd4-like proteins: an emerging family of ubiquitin protein ligases implicated in diverse cellular functions. Trends Cell Biol 9:166–169
11. Hicke L (2001) A new ticket for entry into budding vesicles-ubiquitin. Cell 106:527–530
12. Goulet CC, Volk KA, Adams CM, Prince LS, Stokes JB, Snyder PM (1998) Inhibition of the epithelial Na channel by interaction of Nedd4 with a PY motif deleted in Liddle's syndrome. J Biol Chem 273:30012–30017
13. Pham N, Rotin D (2001) Nedd4 regulates ubiquitination and stability of the guaninenucleotide exchange factor CNrasGEF. J Biol Chem 276:46995–47003
14. Konstas AA, Shearwin-Whyatt LM, Fotia AB, Degger B, Riccardi D, Cook DI, Korbmacher C (2002) Regulation of the epithelial sodium channel by N4WBP5A, a novel Nedd4/Nedd4–2-interacting protein. J Biol Chem 277:29406–29416
15. Xu LL, Shi Y, Petrovics G et al (2003) *PMEPA1*, an androgen-regulated NEDD4-binding protein, exhibits cell growth inhibitory function and decreased expression during prostate cancer progression. Cancer Res 63:4299–4304
16. Xu L, Su Y, LaBiche R, Segawa T, Shanmugam N, McLeod DG, Moul JW, Srivastava S (2001) Quantitative expression profile of androgen regulated genes (ARGs) in prostate cancer cells and identification of prostate specific genes. Int J Cancer 92:322–328
17. Watanabe Y, Itoh S, Goto T et al (2010) *TMEPAI*, a transmembrane TGF-betainducible protein, sequesters Smad proteins from active participation in TGF-beta signaling. Mol Cell 37:123–134
18. Carver BS, Chapinski C et al (2011) Reciprocal feedback regulation of PI3K and androgen receptor signaling in PTEN-deficient prostate cancer. Cancer Cell 19:575–586
19. Stirzaker C, Song JZ, Davidson B, Clark SJ (2004) Transcriptional gene silencing promotes DNA hypermethylation through a sequential change in chromatin modifications in cancer cells. Cancer Res 64:3871–3877

Chapter 8
Cloning and Expression of a Novel Xylanase Xyn11-1 from Alkaline Soil

Kun Li, Zhongyuan Li, Xuegang Luo, Cuixia Feng, Cuiqiong Wang, Minghui Zhang and Tongcun Zhang

Abstract A novel xylanase of family 11 (*Xyn11-1*) was obtained from the metagenomic DNA of alkaline soil by touchdown-PCR and thermal asymmetric interlaced (TAIL) PCR methods. *Xyn11-1* is composed of 645 nucleotides, which encodes a signal peptide of 19 amino acids and a mature protein of 196 amino acids. It is a novel GH11 xylanase sharing the highest identity (79 %) with the reported GH11 xylanase (XP_008721536) in GenBank database. In order to detect its biological activity, the recombinant plasmid *xyn11-1*-pET28a(+) was constructed and recombinant protein was successfully expressed in heterologous hosts *Escherichia coli* BL21 (DE3) induced by isopropy-beta-D-thiogalactopyranoside (IPTG). Using the 3,5-dinitrosalicylic acid (DNS) method, the xylanase activity of crude intracellular protein is 11.32 U/mL. The optimal inducing IPTG concentration and inducing temperature was examined at 0.2 mM and 15 °C, respectively.

Keywords Xylanase · Alkaline soil · Gene cloning · Recombinant expression · Optimization

8.1 Introduction

Hemicelluloses are the second most abundant plant polysaccharides in nature. Due to their potential role as sustainable energy sources, hemicelluloses are increasingly becoming an important concern [1]. Xylan is the major carbohydrate of hemicelluloses, its complete degradation requires the synergistic action of a variety of

K. Li and Z. Li—Co-first author.

K. Li · Z. Li · X. Luo · C. Feng · C. Wang · M. Zhang · T. Zhang (✉)
Key Laboratory of Industrial Fermentation Microbiology, Ministry of Education and Tianjin City, College of Biotechnology, Tianjin University of Science and Technology, Tianjin 300457, People's Republic of China
e-mail: tony@tust.edu.en

T.-C. Zhang and M. Nakajima (eds.), *Advances in Applied Biotechnology*,
Lecture Notes in Electrical Engineering 333, DOI 10.1007/978-3-662-46318-5_8

enzymes, including xylanase, β-xylosidase, α-glucuronidase, α-arabinofuranosidase, and acetylxylan esterase [2]. Among them, xylanase plays a crucial role in the hydrolysis of the xylan backbone [3], in which xylanase cleaves the β-1,4-glycosidic bond between xylose residues to release xylooligosaccharides. For some biotechnological applications, xylanase is useful, especially in the papermaking, bioconversion, and food industry [4]. Due to the increasing demand for xylanase production, exploring new enzyme sources has been a hot topic in recent years [5]. Therefore, we try to explore some novel alkaline xylanase from alkaline soil, in this study, a novel xylanase of family 11 (*Xyn11-1*) was obtained from the metagenomic DNA of alkaline soil, and it was heterologously expressed in *Escherichia coli* BL21 (DE3).

8.2 Materials and Methods

8.2.1 Strains, Plasmids, and Culture Conditions

Escherichia coli DH5α and the vector PMD-19T (TaKaRa, Dalian, China) were used for gene cloning. *E. coli* BL21(DE3) and vector pET28a(+) obtained from Invitrogen (Carlsbad, CA, USA) were used for gene expression. *E. coli DH5α* and *E. coli BL21(DE3)* was grown in LB medium (10 g/L tryptone, 5 g/L yeast extract, and 10 g/L NaCl) supplemented with 50 mg/L ampicillin or kanamycin, respectively, at 37 °C with shaking at 220 rpm.

8.2.2 Alkaline Soil Sampling and Metagenomic DNA Extraction

Alkine soil was obtained from the coastal saline area in Tianjin (China) and stored in −20 °C. The pH was measured by pH meter (SevenEasy, Shanghai). About 1 g soil sample was first grinded by liquid nitrogen, and the metagenomic DNA was extracted by CTAB-SDS method [6]. The crude DNA was purified by DNA purification kit (Solarbio, Beijing, China), and was detected by electric.

8.2.3 Cloning and Sequence Analysis of Xylanase Gene Xyn11-1

The xylanase gene *xyn11-1* was obtained by touchdown-PCR and TAIL-PCR methods. First, the conserved sequence of *xyn11-1* was amplificated by Touchdown-PCR with the conserved primer GH11F and GH11R according to Wang et al. [7].

Table 8.1 Primers used in this work

Primers	Primer sequence (5′–3′)
X11-F	AACTGCTACCTGKCNITNTAYGGNTGG
X11-R	CCGCACGGACCAGTAYTGNKIRAANGT
11-1sp1D	TACCATCGATCGAGGGCTGGTTGGTGC
11-1sp1U	CCTCGTCGAGTACTACGTGATTGAATCGTACG
11-1sp2D	ACGTAGATGTTGTAGGTTCCGCCGTCGG
11-1sp2U	GTCGAGTACTACGTGATTGAATCGTACGGCAC
11-1sp3D	CGTACGATTCAATCACGTAGTACTCGACGAGG
11-1sp3U	CACCAACCAGCCCTCGATCGATGGTAC
11-1-28-F	ATGCgaattcCGCCCATTCGACTTCCTCGACGATATCG
11-2-28-R	GGGctcgagaGTGGGTTTGCACGTACACTTCGGACTCG

The letters in lowercase were the endonuclease site

The nucleotide fragment was sequenced by GENEWIZ, Beijing, China. The full gene sequence was amplificated and the six specific primers designed based on the conserved sequence using Tail-PCR method. The primers used in the study are shown in Table 8.1. The sequence was assembled by Vector IN7.0 (Invitrogen), and was blasted by BLASTX (http://blast.ncbi.nlm.nih.gov/Blast.cgi). The accessory number of the protein sequence of Xyn11-1 on NCBI was KM893863.

8.2.4 Heterologous Expression of Xyn11-1

The full-length gene sequence of *xyn*11-1 was digested with *Eco*RI and *Xho*I, ligased with pET28a(+) vector, and transformed into *E. coli* DH5α competent cells. The correct recombinant plasmid *xyn*11-1-pET28a(+) was transformed into *E. coli* BL21(DE3) competent cells. The clone was incubated in LB medium for OD_{600} reach to 0.6, and then the clone was induced at 25 °C using 1 mM IPTG for 20 h. The cells was collected by centrifugation at 7,000 g, 4 °C for 10 min, and then dissolved by sonication in phosphate buffer (8 g/L NaCl, 3.58 g/L $Na_2HPO_4 \cdot 12H_2O$, 0.2 g/L KCl, 0.27 g/L KH_2PO_4). Cell debris and supernatant was collected to SDS–PAGE analysis, respectively.

8.2.5 Enzyme Activity Assays

The 3,5-dinitrosalicylic acid (DNS) method was used to assay xylanase activity [8]. One unit of xylanase activity was defined as the amount of enzyme that released 1 μmol of reducing sugar from the substrate equivalent to xylose per minute under the assay conditions.

8.3 Results

8.3.1 Cloning and Sequence Analysis of the Xylanse Gene Xyn11-1

With the degenerate primers by touchdown PCR, about 250 bp DNA fragment was amplificated as shown in Fig. 8.1. The conserved sequence of *xyn11-1* was sequenced and show 87 % identity with the reported GH11 xylanase (XP_008721536). The flanking sequences were amplicated by Tail-PCR. After sequence assembling, the ORF of xylanase *Xyn11-1* was obtained which contains 645 bp in length and 19 amino acid signal peptide and 196 aa mature protein. The protein sequence of *Xyn11-1* shared 79 % identity with endo-1,4-beta-xylanase from *Cyphellophora europaea* CBS 101466 (ETN36718).

8.3.2 Expression of Recombinant Enzyme

The structure of recombinant plasmid *xyn*11-1-pET28a(+) is shown in Fig. 8.2. *Xyn11-1* was successfully expressed in *E. coli*, and its activities in cellular and extracellular fractions were compared. Major portions of the total activity were detected in the intracellular, because there were no signal peptides in the expression vector or in the recombinant protein sequence. The recombinant enzymes showed the apparent molecular masses of approximately 30.0 kDa for *Xyn11-1* in SDS–PAGE gel (Fig. 8.3), which was consistent with their calculated molecular masses. Using the DNS method, the xylanase activity of crude intracellular protein is 11.32 U/mL.

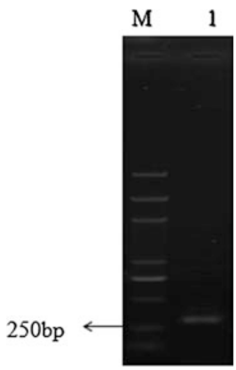

Fig. 8.1 Conserved region of Xyn11-1 by touchdown PCR. *M* DM2000 marker; *1* GH11 xylanase conserved region from the metagenomic DNA of alkaline soil

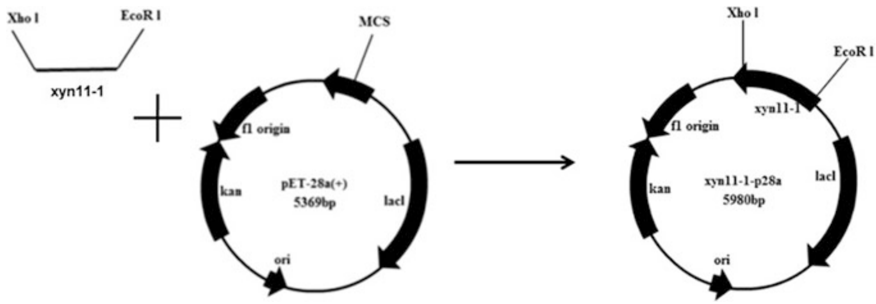

Fig. 8.2 The structure of recombinant plasmid *xyn*11-1-pET28a(+)

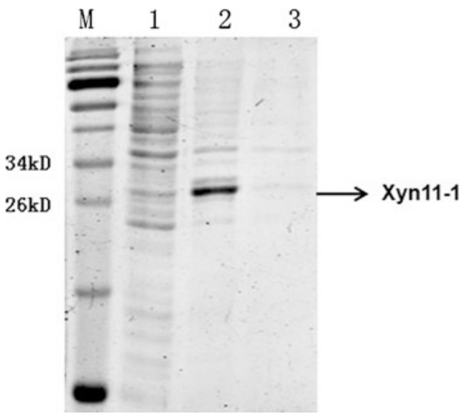

Fig. 8.3 SDS–PAGE analysis for the expression of *Xyn11-1*. *M* protein marker; *1* cell sonication debris; *2* cell sonication supernatant; *3* LB culture medium

8.3.3 Optimization of IPTG Concentration

IPTG is an expensive chemical for industrial production. Using excess IPTG will cause unnecessary waste and, meanwhile, it is poisonous to cells. So the IPTG concentration is also very crucial for the expression level of fusion protein *Xyn11-1*. 0.2, 0.4, 0.6, 0.8, 1 mM were used in this study, and the results suggest that the optimal IPTG concentration for the expression of the fusion protein was 0.8 mM (Fig. 8.4).

8.3.4 Optimization of Inducing Temperature

Escherichia coli usually grows better at temperatures of 37–39 °C, but this temperature is not suitable for the recombinant enzyme, because it might form inclusion bodies under these temperatures. In order to find the optimal temperature for the

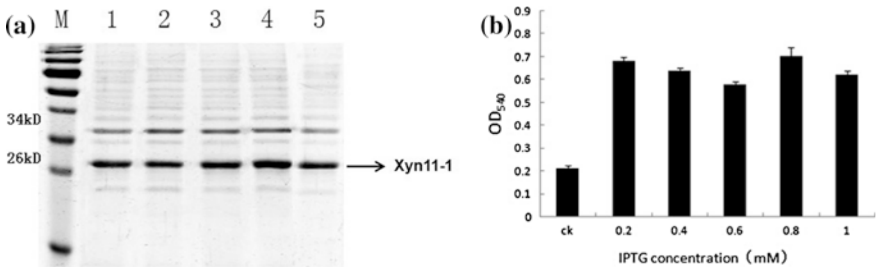

Fig. 8.4 Optimization of IPTG concentration for the expression of Xyn11-1. **a** SDS–PAGE analysis with different IPTG concentrations: (*M*) protein marker, (*1*) 0.2 mM, (*2*) 0.4 mM, (*3*) 0.6 mM, (*4*) 0.8 mM, (*5*) 1 mM. **b** Enzyme activity asays with different IPTG concentrations

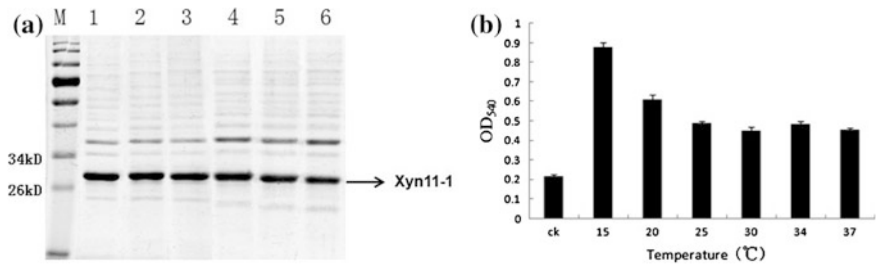

Fig. 8.5 Optimization of temperature for the expression of *Xyn11-1*. **a** SDS–PAGE analysis with different inducing temperature: (*M*) protein marker, (*1*) 15 °C, (*2*) 20 °C, (*3*) 25 °C, (*4*) 30 °C, (*5*) 34 °C, (*6*) 37 °C. **b** Enzyme activity assays under different inducing temperature

soluble expression protein, several different temperature grades were under experiment, including 15, 20, 25, 30, 34, 37 °C. The results under different temperature conditions are shown in Fig. 8.5 and implies that 15 °C was the most suitable temperature for *Xyn11-1*.

8.4 Discussion

Xylanase is the most critical xylan degrading glycoside hydrolase, xylan could be degraded into oligosaccharides, which could be further degraded to xylose by glucosidase and other side-chain hydrolase. In this study, a novel GH11 xylanase *Xyn11-1* was obtained, and the recombinant plasmid *Xyn11-1*-pET28a(+) was successfully constructed and expressed in *E. coli*. Meanwhile, we carried out the work to optimize the inducing conditions for the soluble expression of *Xyn11-1*. The results showed that the optimal IPTG concentration and inducing temperature was examined at 0.2 mM and 15 °C. The xylanase activity of crude intracellular protein is 11.32 U/mL.

As the data showed, the enzyme activity of *Xyn11-1* in the prokaryotic expression system was not as satisfactory as expected. This is mostly because the novel xylanase *Xyn11-1* was from fungal genome. And as is shown in many studies [9], GH11 xylanases are usually expressed better in *Pichia methanolica* Expression System. In view of the work we have done, now we are structuring *P. methanolica* Expression System and characterizing the recombinant protein.

References

1. Saha BC (2003) Hemicellulose bioconversion. J Ind Microbiol Biotechnol 30:279–291
2. Chávez R, Bull P, Eyzaguirre J (2006) The xylanolytic enzyme system from the genus Penicillium. J Biotechnol 123:413–433
3. Kambourova M, Mandeva R, Fiume I, Maurelli L, Rossi M, Morana A (2007) Hydrolysis of xylan at high temperature by coaction of the xylanase from Anoxybacillus flavithermus BC and the β-xylosidase/α-rabinosidase from Sulfolobus solfataricus Oalpha. J Appl Microbiol 102:1586–1593
4. Jordan DB, Wagschal K (2010) Properties and applications of microbialβ-D-xylosidases featuring the catalytically efficient enzyme from Selenomonas ruminantium. Appl Microbiol Biotechnol 86:1647–1658
5. Denise Naomi Xavier SALMON, Michele Rigon SPIER, Carlos Ricardo (2014) Analysis of inducers of xylanase and cellulose activities production by Ganoderma applanatum LPBMR-56. Fungal Biol 118:655–662
6. Brady SF (2007) Construction of soil environmental DNA cosmid libraries and screening for clones that produce biologically active small molecules. Nat Protoc 2:1297–1305
7. Wang G, Meng K, Luo H et al (2012) Phylogenetic diversity and environment-specific distributions of glycosyl hydrolase family 10 xylanases in geographically distant soils. PLoS ONE 7(8):e43480
8. Miller GL, Blum R, Glennon WE et al (1960) Measurement of carboxymethylcellulase activity. Anal Biochem 1:127–132
9. Yang Xinzhuo, Shi Pengjun, Huang Huoqing et al (2014) Two xylose-tolerant GH43 bifunctional β-xylosidase/α-arabinosidases and one GH11 xylanase from Humicola insolensand their synergy in the degradation of xylan. Food Chem 148:381–387

Chapter 9
To Establish the Regeneration System of Sweet Sorghum Immature Embryos

Xiaomu Chen, Oujing Li, Lili Shi, Xianhua Wu, Boxian Xia and Zhongyou Pei

Abstract Sweet sorghum is an important forage and energy crop. In this experiment, sweet sorghum immature embryos were taken to be explants, through inducting and regenerating for sweet sorghum callus of different genotypes, to obtain the best culture medium formula and create appropriate conditions for establishing efficient regeneration system. The result showed that, for callus induction, the response of immature embryos varied with the genotype, but the medium is not. Of these, Xinliang 52 showed the highest frequency of callus induction under appropriate culture conditions. As regards regenerable callus formation, the response of callus varied with the genotype and medium. 07-27 regeneration occurred at high frequencies when MSR and MBR were added in the regeneration medium. And there is nothing on NBI medium for the whole genotypes. So NBI is not suitable for callus regeneration culture.

Keywords Sweet sorghum · Immature embryo · Tissue culture · Medium · Genotype

9.1 Introduction

Sweet sorghum is a variant of ordinary sorghum. It has affluent stem juice, high sugar content, and efficient ethanol conversion frequency. It was used to make silage and process sugar and ethanol. At the same time, sweet sorghums are a kind of green energy crops, which have such attractive prospects in the field of renewable energy that it has been closely highlighted by experts and scholars

X. Chen · O. Li · L. Shi · X. Wu · B. Xia · Z. Pei (✉)
Agriculture Resource and Environment College, Tianjin Agricultural University, Tianjin, China
e-mail: zhongyoupei@yahoo.com.cn

X. Chen
e-mail: 1164110289@qq.com

T.-C. Zhang and M. Nakajima (eds.), *Advances in Applied Biotechnology*, Lecture Notes in Electrical Engineering 333, DOI 10.1007/978-3-662-46318-5_9

worldwide [21]. But sweet sorghum seed resource is deficient, traditional breeding application is limited, and as a result, the process of variety improvement and new variety breeding is slow [23]. Therefore, the biological technology assisted breeding is taken seriously, of which the most important is tissue culture. Plant tissue culture technology is not restricted by the growth season. The genetic transformation of sweet sorghum could be achieved in a relatively short period of time, so as to enrich seed resource. However, sweet sorghum is considered to a plant that has difficulty with plant tissue culture, and is yet to establish efficient regeneration system in vitro.

Sorghum immature embryos [4–6, 12, 16], stem tips [18, 22], anther [8, 14, 19], spikes [1, 17, 20], mature embryos, mature seeds and mature seeds germination buds [2, 3, 9, 11, 24] in vitro have all obtained regeneration plants. In addition, sorghum immature embryos were considered to be the best explants for tissue culture. Gamborg et al. [6] were the earliest researchers to study sorghum immature embryo tissue cultivation. They used immature sorghum embryos, which are harvested 12–18 days after pollinating and are cultured in vitro. They obtained the regeneration shoots, and finally the mature regeneration plants. Dunstan et al. [4], Elkonin [5], Ma and Liang [12], Shi et al. [16], Wang et al. [20] obtained regeneration plants and Fuguang Han obtained callus by using the sorghum immature embryos. What is more, Liu et al. [10] achieved the transgenic plants of sorghum immature embryos during the genetic transformation study.

In this experiment, we regarded immature embryos of ten sweet sorghum varieties as explants, studying different mediums and different genotypes and whether they had effect on sweet sorghum callus induction and regeneration or not, so that we can establish a highly efficient regeneration system of sweet sorghum.

9.2 Materials and Methods

9.2.1 Materials

The varieties were sweet sorghum materials with good agronomic traits. Xinliang 52, BJ-285, 07-27, BJ-299, Rome, M81-E, Cowley, Tianza2, Liaotian3, and Sanrio were provided by the Agronomy department of Tianjin Agricultural University, and were planted in the Crop Arboretum of East Campus of Tianjin Agricultural University.

Constant temperature and humidity box were bought from MMM Group; plant growth chamber were bought from BINDER company; tissue culture box were bought from PERCIVAL company.

9.2.2 Medium

9.2.2.1 Induction Medium

$$\text{MSI} = \text{MS medium} + 0.5\,[\text{g/L}]\text{CH} + 1.0\,[\text{g/L}]\text{Pro} + 30\,[\text{g/L}]\text{Sur} + 2.0\,[\text{mg/L}]\text{2,4-D}.$$

$$\text{MBI} = \text{MS majority} + \text{MS minority} + \text{B}_5 \text{ organic} + 0.5\,[\text{g/L}]\text{CH} + 1.0\,[\text{g/L}]\text{Pro} + 30[\text{g/L}]\text{Sur} + 2.0\,[\text{mg/L}]\text{2,4-D}.$$

$$\text{NBI} = \text{N}_6 \text{ majority} + \text{B}_5 \text{ minority} + \text{B}_5 \text{ organic} + 0.5\,[\text{g/L}]\text{CH} + 1.0\,[\text{g/L}]\text{Pro} + 30[\text{g/L}]\text{Sur} + 2.0\,[\text{mg/L}]\text{2,4-D}.$$

9.2.2.2 Subculture Medium

$$\text{MSS} = \text{MS medium} + 0.5\,[\text{g/L}]\text{CH} + 1.0\,[\text{g/L}]\text{Pro} + 30[\text{g/L}]\text{Sur} + 2.0\,[\text{mg/L}]\text{2,4-D}.$$

9.2.2.3 Regeneration Medium

$$\text{MSR} = \text{MS medium} + 8.0\,[\text{g/L}]\text{D-sor} + 0.8\,[\text{g/L}]\text{CH} + 0.5\,[\text{g/L}]\text{Vc} + 30[\text{g/L}]\text{Sur} + 2.0\,[\text{mg/L}]\text{KT} + 0.5[\text{mg/L}]\text{6-BA} + 0.2\,[\text{mg/L}]\text{IAA}.$$

$$\text{MBR} = \text{MS majority} + \text{MS minority} + \text{B}_5\text{organic} + 8.0\,[\text{g/L}]\text{D-sor} + 0.8\,[\text{g/L}]\text{CH} + 0.5\,[\text{g/L}]\text{Vc} + 30[\text{g/L}]\text{Sur} + 2.0\,[\text{mg/L}]\text{KT} + 0.5\,[\text{mg/L}]\text{6-BA} + 0.2\,[\text{mg/L}]\text{IAA}.$$

$$\text{NBR} = \text{N}_6 \text{ majority} + \text{B}_5\text{minority} + \text{B}_5\text{organic} + 8.0\,[\text{g/L}]\text{D-sor} + 0.8\,[\text{g/L}]\text{CH} + 0.5\,[\text{g/L}]\text{Vc} + 30[\text{g/L}]\text{Sur} + 2.0\,[\text{mg/L}]\text{KT} + 0.5\,[\text{mg/L}]\text{6-BA} + 0.2\,[\text{mg/L}]\text{IAA}.$$

9.2.2.4 Rooting Medium

$$\text{MSRt} = 1/2 \text{ MS majority} + \text{MS minority} + \text{MS organic} + 30[\text{g/L}]\text{Sur} + 0.2\,[\text{mg/L}]\text{IAA}.$$

In the above medium, the PH is adjusted to 5.8 before adding 6.8 g agar; all the mediums are autoclaved for 20 min at 113 °C.

9.2.3 Immature Embryos Callus Induction

Panicles were covered with pollination bags before flowering to ensure self-fertilization. 20–25 days after flowering, immature seeds were collected from these plants. The seed surfaces were wiped with 70 % alcohol and then placed in the refrigerator at 4 °C for pretreatment for about 24 h. Immature seeds were immersed in 70 % ethanol for 1 min, and then immersed in 0.1 % mercuric chloride for 10 min. After this treatment, finally the seeds were rinsed six times in sterile distilled water. Then the seeds were placed on sterilized Whatman filter papers to dry. Immature embryos (IEs) were aseptically removed and placed (scutellum-side up) on induction medium in a plastic Petri dish (90 × 15 mm), and maintained for 3–4 weeks in dark at 28 °C. Then the embryos were transferred to the subculture medium and cultured for 3–4 weeks. The percentage of embryos producing callus was calculated.

9.2.4 Immature Embryo Callus Regeneration

The callus that grew well was selected from subculture medium and transferred to the regeneration medium, and kept for 3–4 weeks at 28 °C with a photoperiod of 16/8 h in light/dark. Then the number of explants forming shoots were counted and the percentage of embryos forming shoots was calculated.

9.2.5 Rooting Culture and Transplantation

The shoots of buds growing up to 3–5 cm were transferred to the rooting medium for 2 weeks. The bottle vents were opened, when there were around 3–4 roots. To adapt for 1–2 days, the medium were washed from roots, and the shoots were transplanted to pots that contained vermiculite and nutrient soil for 2–3 weeks, and then grown to maturity in a greenhouse. When transplanting shoots, the roots are protected from damage, and the nutrition soil is kept moist.

9.2.6 Data Analysis

$$\text{The callus induction rate} = (\text{No. callus/No. inoculated embryos}) \times 100\,\%$$

$$\text{The regeneration rate} = (\text{No. regenerated callus/No. inoculated callus}) \times 100\,\%$$

The data were analyzed using SPSS statistical software. Significance was determined by analysis of variance (ANOVA) and the differences between the means were compared by Duncan's new multiple range test.

9.3 Results

9.3.1 Immature Embryos Callus Induction

After culturing for 3–4 weeks, all the ten materials on different induction mediums could induce callus (Fig. 9.1a), but the morphological character and callus induction rate of these ten materials are distinct. The callus of 07-27, Cowley, Sanrio, Rome, Tianza2 and BJ299 were light yellow granular. The callus of Liaotian3, Xinliang 52, BJ-285, M81-E were white granular. 07-27, Xinliang 52, Sanrio, Rome and BJ299 secreted mucilage. Liaotian3, Cowley, Xinliang 52, M81-E, Rome and Tianza2 secreted brown substance. 07-27, BJ-285, Sanrio, Rome, Tianza2, BJ299, Liaotian3 and Cowley had close texture. Xinliang 52 and M81-E were opposite.

9.3.1.1 Effect of Genotype on the Callus Induction Rate

After culturing for about 3–4 weeks, immature embryos had come into being callus. As a result, callus induction rate of different genotypes has a significant difference. Of which Xinliang 52 showed the highest frequency, followed by Cowley, Tianza2, and BJ-299; BJ-285 induction rate is the worst (Table 9.1).

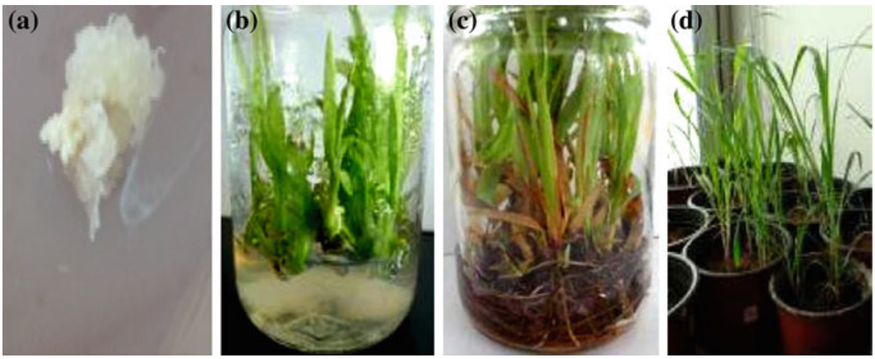

Fig. 9.1 **a** Induction of 07-27; **b** regeneration of 07-27; **c** rooting of 07-27; **d** transplantation of 07-27

Table 9.1 Genotype as the main effect to analyze significance

Varieties	Percentage of callus formation (%)[a]
Xinliang 52	90.8 ± 4.9 a
Cowley	71.9 ± 3.5 b
Tianza2	66.5 ± 3.7 bc
BJ-299	64.1 ± 7.2 bc
Sanrio	61.2 ± 9.9 c
07-27	57.8 ± 15.3 cd
Rome	51.4 ± 3.6 de
Liaotian3	50.4 ± 7.9 de
M81-e	45.7 ± 7.5 e
BJ-285	27.4 ± 8.4 f

[a] Each value is the mean percentage of three experiments. Numbers (mean ± standard deviation) followed by the same letter are not significantly different at the 5 % level by Duncan's new multiple range test

9.3.1.2 Effect of Medium on Callus Induction Rate

According to the data which have been counted, Callus induction rate of different mediums has no significant difference (Table 9.2). This indicates that MSI, NBI, and MBI could all be used for callus induction.

9.3.2 Immature Embryo Callus Regeneration

After regenerating culture for 3–4 weeks, callus appeared green based on different regeneration mediums. After 4 weeks' culturing, there were visible buds, and buds grow into shoots for 5 weeks (Fig. 9.1b). Then it was transferred to the rooting medium (Fig. 9.1c). In the process of regeneration, Liaotian3, Cowley, Xinliang 52, BJ-285, Sanrio, Cowley and Rome secreted brown substance. Tianza2 secreted little brown substance. M81-E and 07-27 do not secrete colored substance.

Table 9.2 Medium as main effect to analyze significance

Medium	Percentage of callus formation (%)[a]
MSI	58.3 ± 18.3 a
NBI	60.9 ± 17.4 a
MBI	58.1 ± 19.3 a

[a] Each value is the mean percentage of three experiments. Numbers (mean ± standard deviation) followed by the same letter are not significantly different at the 5 % level by Duncan's new multiple range test

Table 9.3 Callus regeneration results of different genotypes on different mediums

Varieties	Medium	No. of calli tested	No. of green dots	Percentage of regeneration (%)
Xinliang 52	MBR	105	2	1.90
BJ-285	MSR	78	2	2.57
07-27	MSR	77	31	40.26
	MBR	91	37	40.66
M81-E	MBR	61	3	4.92
Tianza2	MSR	54	1	1.85
	MBR	92	1	1.09
Liaotian3	MSR	117	18	15.39
	MBR	141	24	17.02
Cowley	MSR	158	7	4.43

9.3.2.1 Effect of Genotype on the Regeneration Rate of Immature Embryo Callus

After regenerating for about 3–4 weeks, some callus had grown into shoots, and it is easily found that not all the genotypes can differentiate for callus regeneration. Callus regeneration rate for 07-27 is the highest, followed by Liaotian3; the regeneration rate of other genotypes is between 1 and 5 % (Table 9.3).

9.3.2.2 Effect of Medium on the Regeneration Rate of Immature Embryo Callus

The result was achieved based on statistical data. 07-27, Liaotian3, and Tianza2 can all regenerate shoots both on MSI and MBI; Xinliang 52 and M81-E only regenerate shoots on MBI, Cowley and BJ-285 only regenerate shoots on MSI. But there is nothing on NBI. So it is clear that MSI and MBI are suitable for callus regeneration (Table 9.3).

9.4 Discussions

The experiment demonstrated that genotypes not only had significant effect on callus induction culture, but also had great influence on callus regeneration culture. Thus selecting excellent genotype is very important. This agrees with Shi et al. [16]. In addition, we found that the induction rate and regeneration rate of other genotypes were low. In contrast, 07-27 showed the high frequency of callus induction and regeneration. What is more, the culture process is not brown, and finally obtained regeneration plants. Therefore, we thought that 07-27 was an ideal material for tissue culture and genetic improvement of sweet sorghum. Besides, Zhao et al. [24] thought that the M81-E was very good genotype, but the M81-E in this experiment, the callus induction rate, and regeneration rate were very low, and not suitable for tissue culture of sorghum immature embryos.

For callus induction culture, MSI, MBI, and NBI have no significant difference. But the result was the opposite for callus regeneration culture. Both MSR and MBR regenerated shoots, NBR had nothing. Therefore, in comprehensive consideration of sweet sorghum tissue culture, MS is a suitable basic medium. In the experiment, the regeneration rate is very low for a majority of genotypes, which reveals that it is difficult to develop the sorghum tissue culture and find an appropriate medium for sweet sorghum tissue culture. Hagio [7] thought that adding cytokinins (BA or Kin) into callus inducing medium will increase the regeneration rate, when using MS basic medium. What is more, adding PVP and Pro into regeneration medium can also increase the cell regeneration rate. But there is no use of adding cytomin into regeneration medium. However, Oldach and Morgenstern [13] considered that L_3 medium was more suitable for sorghum callus induction and regeneration, but also the medium supplemented with $AgNO_3$ can significantly increase the regeneration rate. Robert et al. [15] found that the regeneration medium mM11 supplemented with 3 mg/l BAP and 1 mg/l TDZ and removing 2,4-D with light treatments for 2 weeks can increase the regeneration rate.

Acknowledgments This work was supported by the innovative talents training plan of the young and middle-aged backbone of Tianjin and the innovation team project of genetic improvement of the crop quality and resistance of Tianjin, for which the authors are thankful.

References

1. Brettell R et al (1980) Embryogenesis from cultured immature inflorescences of sorghumbicolor. Protoplasma 104:141–148
2. Bhaskaran S et al (1983) Sorghum plant regeneration from aluminum selection media. Plant Cell Rep 2:129–132
3. Cai TS et al (1987) Callus induction and plant regeneration from shoot portions of mature embryos of high tannin sorghum. Plant Cell, Tissue Organ Cult 9:245–252
4. Dunstan DI et al (1978) The anatomy of and secondary morphogenesis in cultured scutellum tissues of sorghum bicolor. Protoplasma 97:251–260
5. Elkonin LA (1996) The beginning and maintain of amino acids induce sorghum embryogenesis callus. Rain Fed Crops 2:20–22
6. Gamborg OL et al (1977) Morphogenesis and plant regeneration callus of immature embryos of sorghum. Plant Sci Lett 10(1):67–74
7. Hagio T (2002) Adventitious shoot regeneration from immature embryos of sorghum. Plant Cell, Tissue Organ Cult 68:65–72
8. Kumaravadivel N, Rangsamy SR (1994) Plant regeneration from sorghum anther culture and field evaluation of progeny. Plant Cell Rep 13:286–290
9. Liu XY et al (2010) To establish sweet sorghum of high frequency, high efficiency regeneration system. Agric Sci China 43(23):4963–4969
10. Liu GQ et al (2012) Highly efficient sorghum transformation. Plant Cell Rep 31:100–999

11. Masteller VJ, Holden DJ (1970) The growth of and organ formation from callus tissue of sorghum. Plant Physiol 45:362–364
12. Ma HT, Liang GH (1985) Research on immature embryo culture and plant variation of sorghum. J Genet Genomics 12(5):350–357
13. Oldach KH, Morgenstern A (2001) Efficient in vitro plant regeneration from immature zygotic embryos of pearl millet and sorghum. Plant Cell Rep 20:416–421
14. Rose JB, Dunwell JM (1986) Anther culture of sorghum bicolor. Plant Cell, Tissue Organ Cult 6:15–22
15. Robert G et al (2010) Genetic transformation of sweet sorghum. Plant Cell Rep 29:997–1005
16. Shi TY et al (1995) Response of different genotypes and explants response during sorghum somatic cell culture. Rain Fed Crops 6:26–28
17. Shi TY, Yang LG (1995) The effects of medium and genotype on sorghum immature embryo culture in vitro. Rain Fed Crops 4:27–29
18. Shi YS et al (2004) The effects of antibiotics on sorghum stem tip regeneration and establishment of regeneration system. Rain Fed Crops 24(2):78–79
19. Wen FS et al (1991) Callus induction and plant regeneration from anther and inflorescence culture of sorghum. Euphytica 52:177–181
20. Wang LQ et al (2004) Screen and application of sorghum restorers somaclonal variants. Acta Agriculturae Boreali-Sinica 19(1):8–9
21. Zhu CY (1999) Sweet sorghum—a promising crop. Rain Fed Crops 19(2):29–32
22. Zhang MZ et al (2006) Research on regeneration system and factors of genetic transformation of sorghum stem apex. J Nucl Agric Sci 20(1):23–26
23. Zou JQ, Wang YQ (2007) Direction and efficient breeding technology of sweet sorghum breeding in china. Rain Fed Crops 27(6):403–404
24. Zhao LM et al (2008) Establishment of sweet sorghum regeneration system. Bot Bull 25(4):465–468

Chapter 10
Cloning and Sequence Analysis of a Novel ACC Oxidase Gene from Peanut (*Arachis hypogaea* L.)

Quanxi Sun, Xiuzhen Wang, Yueyi Tang, Qi Wu, Yunyun Wang, Qingyun Zhang, Guangying Cao, Shuo Meng and Chuantang Wang

Abstract Ethylene plays important roles in seed dormancy. As a key enzyme in ethylene biosynthesis, ACC oxidase gene (*ACCO*) converts 1-aminocyclopropane-1-carboxylic acid (ACC) into ethylene. To study the mechanism underlying peanut seed dormancy, cDNA sequence of the candidate gene was isolated from peanut using RACE technique. As in the situation in *Arabidopsis*, the *ACCO* from peanut (*AhACCO* gene) contained four exons and three introns. Homology comparison analysis showed 68–87 % sequence similarity between *AhACCO* and *ACCO* genes of other selected plants.

Keywords Peanut · ACC oxidase · RACE · Homology comparison

10.1 Introduction

Peanut (*Arachis hypogaea* L.) is one of the five most important oilseed crops worldwide. The duration of seed dormancy is of great importance to peanut. Seeds without dormancy or short dormancy duration would germinate before they are harvested, leading to reduced seed oil, poor seed quality, and high risk for aflatoxin contamination [1].

A complex network of plant hormones, including abscisic acid (ABA), gibberellin (GA), ethylene, auxin, brassinosteroids, and jasmonates, control seed dormancy, and germination [2]. In our previous study, ethylene could break the dormancy of peanut seed [3], but its mechanism is still unclear. In the past decades, ethylene signaling had been shown to play roles in mediating plant response to

Q. Sun · X. Wang · Y. Tang · Q. Wu · Y. Wang · Q. Zhang · G. Cao · C. Wang (✉)
Shandong Peanut Research Institute, Qingdao, People's Republic of China
e-mail: chinapeanut@126.com

S. Meng
Hebei Agricultural University, Baoding, People's Republic of China

T.-C. Zhang and M. Nakajima (eds.), *Advances in Applied Biotechnology*,
Lecture Notes in Electrical Engineering 333, DOI 10.1007/978-3-662-46318-5_10

biotic and abiotic stresses [4–7]. In recent years, ethylene biosynthesis has proved to be necessary for several physiology functions. For example, in a maize ACC synthase mutant where the first step in ethylene biosynthesis was affected, drought tolerance was enhanced and drought-induced leaf senescence was inhibited [8]. ACC oxidase gene (*ACCO*) catalyzes the final step of ethylene biosynthesis, converting 1-aminocyclopropane-1-carboxylic acid (ACC) to ethylene [9]. The genes have been isolated from several organisms including white clover [10], alfalfa [11], pear [12], and tomato [13]; however, the *ACCO* gene from peanut has not been isolated yet, and its function in seed dormancy remains largely unknown.

Here we report the isolation and analysis of a full-length cDNA encoding an ACC oxidase from peanut.

10.2 Materials and Methods

10.2.1 Plant Material

Huayu 33, a peanut cultivar from Shandong Peanut Research Institute, was grown in a temperature-controlled chamber at 20 °C with a photoperiod of 16 h light and 8 h dark. After about 1 month, the leaves were collected and immediately frozen in liquid nitrogen and stored at −80 °C.

10.2.2 Nucleic Acid Manipulation and PCR-Based Cloning

Total RNAs were isolated from leaves of Huayu 33 using Trizol reagent (Invitrogen) according to the manufacturer's protocol. The first-strand cDNA was synthesized by M-MLV reverse transcriptase following SMARTer™ RACE cDNA Amplication Kit Use Manual (Clontech). We performed PCR using Phusion (Thermo) according to its protocol. The PCR products were separated by electrophoresis though a 1.5 % agarose gel, and purified using a Gel Extraction Kit (TransGen). All purified PCR products were cloned into pEASY-blunt simple vector (TransGen) and sequenced.

10.2.3 DNA and Protein Sequence Analysis

The DNA sequences were sequenced in Sangon (Shanghai, China). The open reading frame and deduced amino acid sequence were analyzed using ORF Finder (http://www.ncbi.nlm.nih.gov/projects/gorf/). Homology comparison and phylogenetic analysis of *ACCO* genes were performed by DNAMAN Sequence Analysis Software (Lynnon Biosoft).

10.3 Results and Discussion

10.3.1 Bioinformatics Analysis and Degenerate Primers Design

Seven *ACCO* homolog genes from different organisms were obtained using NCBI blast. These sequences were aligned with DNAMAN Software (Fig. 10.1). Two degenerate primers (AhACCO-F1 and AhACCO-R1) (Table 10.1) were designed based on the conserved sequences underlined in Fig. 10.1.

10.3.2 Isolation of AhACCO Gene from Peanut

An about 600-bp fragment (*AhACCO* middle fragment) was obtained by conventional PCR using primers: AhACCO-F1 and AhACCO-R1 (Fig. 10.2). The fragment was purified from gel, and ligated to pEASY-blunt simple vector (TransGen). The selected clones were sequenced using M13-47 primer. The sequences showed high homology to *ACCO* genes from other sources (data not shown). Gene-specific primers (AhACCO-R2 and AhACCO-F2) were designed based on the sequence information (Table 10.1) to amplify the 3′- and 5′-regions.

To amplify the 3′-region of the cDNA, the gene-specific antisense primer AhACCO-F2 was used with the universal primer UPM provided in the kit. A ~500 bp PCR product was cloned and sequenced. The 5′-region of the cDNA was PCR-amplified using sense primer AhACCO-R2 combined with UPM. A ~300 bp PCR product was obtained and sequenced (Fig. 10.2). The middle fragment was

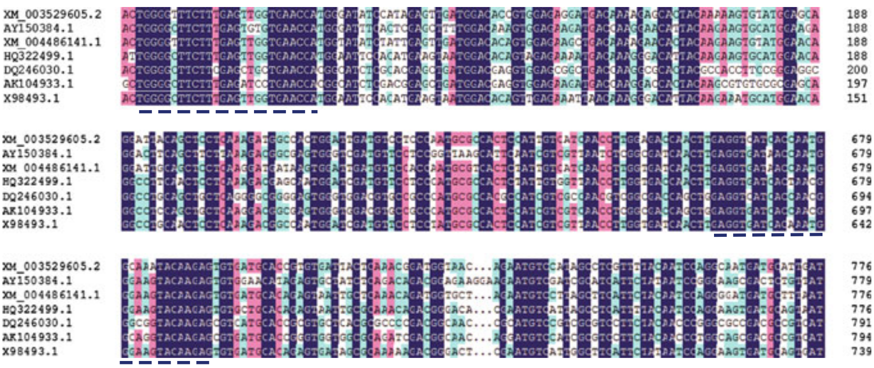

Fig. 10.1 Alignment of the *ACCO* mRNA sequences from different organisms. Note two conserved sequences (a and b) were *underlined* and used to design degenerate primers. XM_003529605.2: *Glycine max*, AY150384.1: *Arabidopsis thaliana*, XM_004486141.1: *Cicer arietinum*, HQ322499.1: *Solanum lycopersicum*, DQ246030.1: *Zea mays*, AK104933.1: *Oryza sativa*, X98493.1: *Nicotiana tabacum*

Table 10.1 Primers use in this study

Primer	Sequence
AhACCO-F1	TGGGGYTTCTTYGAGHKBSTGAAC
AhACCO-R1	CTCTTGTAYYKSCCRTTDGTKATSACCTC
AhACCO-F2	GAAGGTGTTTCATGGGTC
AhACCO-R2	ACTCCAAGCCTTTGCTTGCCAC
AhACCO-F3	ACTTGTAGTGAGAGACCAAAC
AhACCO-R3	GCTTTCATAATCCATATTGCTTAA

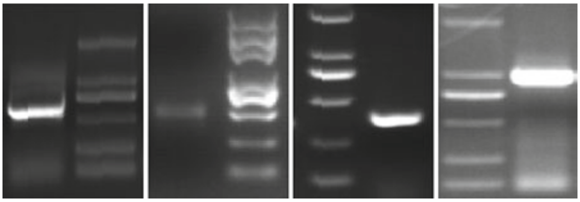

Fig. 10.2 Isolation of peanut *ACCO* cDNA. *1* PCR amplified middle fragment of *AhACCO*, *2* 3′-RACE product, *3* 5′-RACE product, *4* full-length cDNA of *AhACCO*. *M1* Trans2K DNA marker (TransGen), *M2* Trans2K plus II DNA Marker (TransGen)

overlapped with 5′/3′-PCR product sequence by about 150 and 250 bp, respectively, confirming that they were ultimately derived from a single gene. The full-length cDNA of *AhACCO* was isolated using primers AhACCO-F3 and AhACCO-R3 (Table 10.1) and its deduced amino acids sequence were predicted with ORF Finder.

The *AhACCO* genomic DNA sequence was downloaded from PeanutBase and the Peanut Genomics Initiative (http://www.peanutbase.org/). The *AhACCO* gene was found to contain four exons and three introns, similar to *AtACCO* from *Arabidopsis* (Table 10.2). This indicated that the *AhACCO* in this study was an *ACCO* gene. The exons of the gene from Arabidopsis and peanut were much of a size, while the introns varied widely.

10.3.3 Homology Comparison and Phylogenetic Analysis

AhACCO was predicted to encode a protein of 321 amino acids with a molecular mass of 36.3 kDa. The deduced amino acid sequence of AhACCO aligned with other ACCO proteins is shown in Fig. 10.3. To examine the relationships among different

Table 10.2 The exon and intron structures of *ACCO* genes from *Arabidopsis* and peanut

Gene	Accession number	ORF size (bp)	Exon 1 (bp)	Intron 1 (bp)	Exon 2 (bp)	Intron 2 (bp)	Exon 3 (bp)	Intron 3 (bp)	Exon 4 (bp)	Protein (aa)
AtACCO	CP002684.1	960	114	174	227	88	334	172	285	320
AhACCO	–[a]	963	108	85	227	156	334	508	294	321

[a] No accession number is available for this gene

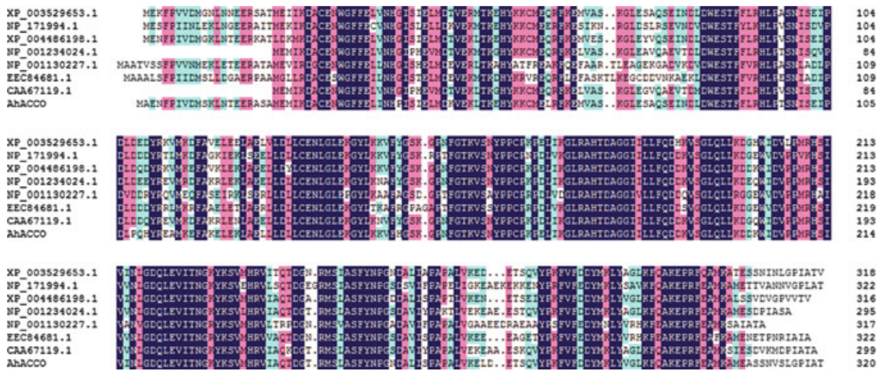

Fig. 10.3 Alignment of the predicted protein sequence of *AhACCO* with sequence predicted from other known *ACCO* genes. XP_003529653.1: *G. max*, NP_171994.1: *A. thaliana*, XP_004486198.1: *C. arietinum*, NP_001234024.1: *S. lycopersicum*, NP_001130227.1: *Z. mays*, EEC84681.1: *O. sativa*, CAA67119.1: *N. tabacum*

sources of ACCO genes, sequences from representative plants were selected to construct the phylogenetic tree by the DNAMAN software (Fig. 10.4). The amino acid sequence of AhACCO exhibited 87 % identity to ACCO from *Glycine max* (XP_003529653.1) and *Cicer arietinum* (XP_004486198.1), 81 % identity to *Solanum lycopersicum* (NP_001234024.1) and *Nicotiana tabacum* (CAA67119.1), and 72, 72 and 68 % identity, respectively, to *Arabidopsis thaliana* (NP_171994.1), *Oryza sativa* (EEC84681.1) and *Zea mays* (NP_001130227.1) (Fig. 10.3).

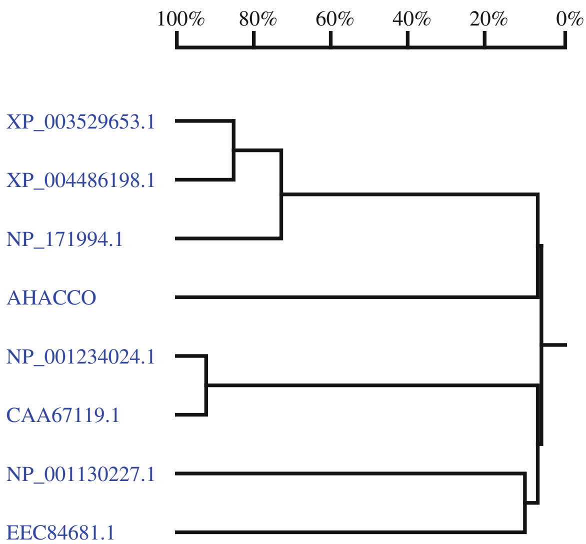

Fig. 10.4 Phylogenetic analysis of ACCO genes. The tree shown was constructed using the amino acid sequences by DNAMAN software. XP_003529653.1: *G. max*, NP_171994.1: *A. thaliana*, XP_004486198.1: *C. arietinum*, NP_001234024.1: *S. lycopersicum*, NP_001130227.1: *Z. mays*, EEC84681.1: *O. sativa*, CAA67119.1: *N. tabacum*

10.4 Conclusion

In this study, a novel cDNA, *AhACCO*, was isolated from peanut cultivar Huayu 33 using RACE technique. Homology comparison and phylogenetic analysis indicated that it encoded an ACC oxidase. Its detailed function in peanut seed dormancy, however, is yet to be studied in the future work.

Acknowledgments We would like to thank China Agricultural Research System (Grant No. CARS-14) and SAAS (Shandong Academy of Agricultural Sciences) Key Science & Technology Achievements Incubation Project (2014CPGY09) for providing financial support to this study.

References

1. Wang CT, Zhang JC (2013) Peanut genetic improvement. Shanghai Science and Technology Press, Shanghai
2. Finkelstein R, Reeves W, Ariizumi T, Steber C (2008) Molecular aspects of seed dormancy. Annu Rev Plant Biol 59:387–415
3. Qu B, Guan SY, Wang XZ, Wu Q, Sun QX, Zhang JC, Tang YY, Wang PW (2014) Screening and identification of seed dormancy in 34 peanut germplasm lines. J Peanut Sci 43(2):50–54
4. Johnson PR, Ecker JR (1998) The ethylene gas signal transduction pathway: a molecular perspective. Annu Rev Genet 32:227–254
5. Wang F, Cui X, Sun Y, Dong CH (2013) Ethylene signaling and regulation in plant growth and stress responses. Plant Cell Rep 32:1099–1108
6. Achard P, Cheng H, De Grauwe L, Decat J, Schoutteten H, Moritz T, Peng J, Harberd NP (2006) Integration of plant responses to environmentally activated phytohormonal signals. Science 311:91–94
7. Cao WH, Liu J, He XJ, Mu RL, Zhou HL, Chen SY, Zhang JS (2007) Modulation of ethylene responses affects plant salt-stress responses. Plant Physiol 143:707–719
8. Young TE, Meeley RB, Gallie DR (2004) ACC synthase expression regulates leaf performance and drought tolerance in maize. Plant J 40:813–825
9. Yang SF, Hoffman NE (1984) Ethylene biosynthesis and its regulation in higher plants. Annu Rev Plant Physiol 35:155–189
10. Du Z, Leung S, Dorling S, McManus M (2011) ACC oxidase (*ACO*) genes in *Trifolium occidentale* (L.) and their relationship to *ACO* genes in white clover (*T. repens* L.) and *T. pallescens* (L.). Plant Physiol Biochem 49(4):420–426
11. Feng B, Wu B, Zhang C, Huang X, Chen Y, Huang X (2012) Cloning and expression of 1-aminocyclopropane-1-carboxylate oxidase cDNA induced by thidiazuron during somatic embryogenesis of alfalfa (*Medicago sativa*). J Plant Physiol 169(2):176–182
12. Shi H, Zhang Y (2012) Pear *ACO* genes encoding putative 1-aminocyclopropane-1-carboxylate oxidase homologs are functionally expressed during fruit ripening and involved in response to salicylic acid. Mol Biol Rep 39(10):9509–9519
13. Zohreh J, Raheem H, Ramin H, Ghasemali G (2013) Cloning, identification and expression analysis of ACC oxidase gene involved in ethylene production pathway. Mol Biol Rep 40 (2):1341–1350

Chapter 11
Genetic Diversity Among the Microorganisms in Daqu Used for Beidacang Liquor as Revealed by RAPD Analyses

Shi-Wei Wang, Qing-Hui Wang, Li-Ping Zhai, Jun Liu, Zhi-Dan Yu, Mao-Mao Zheng and Fang Wang

Abstract To assess the genetic diversity among five microorganisms (namely, DSL(CS)-01, DSL(CS)-02, DSL(PDA)-C, DSL(PDA)-E, DSL(PDA)-F), RAPD (random amplified polymorphic DNA) analysis was performed. Seven primers with stable polymorphisms were screened from 64 primers. PCR was carried out with the seven primers. The data indicated that the molecular markers gave different levels of polymorphism. 94 RAPD bands were obtained and out of them 64 were polymorphic bands (68.09 %) and the best primer screened was b8. The primer b8 was considered as the most effective RAPD marker for the five microorganisms above. The dendrogram built on the basis of data from RAPD analysis represented the genetic distances among the five microorganisms. Understanding the genetic variability among the microorganisms opens up a possibility for developing a molecular genetic map that will lead to the application of marker-assisted selection tools in genetic improvement of the microorganisms.

Keywords Genetic · Diversity · Microbial · Strain · Daqu

11.1 Introduction

The development and advancement of liquor-making industry in China is dependent on scientific development and technical innovation [2]. Heilongjiang Beidacang Group Co. Ltd. was founded in 1914, when the name "Juyuan permanent pot", is one

S.-W. Wang (✉) · Q.-H. Wang · L.-P. Zhai · J. Liu · Z.-D. Yu ·
M.-M. Zheng · F. Wang
The College of Life Sciences and Engineering, Qiqihar University,
No. 42, Wenhua Street, Qiqihar, Heilongjiang, China
e-mail: wsw888535@sohu.com

T.-C. Zhang and M. Nakajima (eds.), *Advances in Applied Biotechnology*,
Lecture Notes in Electrical Engineering 333, DOI 10.1007/978-3-662-46318-5_11

of the eight distilleries. Beidacang spirit was the earliest popular liquor in Northeast China. As a saccharifying ferment, Daqu is made from “Snake Eyes” sorghum as raw material. The raw material is made into Daqu billets first through crushing and water pressed at a certain temperature and humidity. The microorganisms in Daqu mainly are mold, less yeast, and bacteria [5]. The bacteria mainly included lactic acid bacteria, acetic acid bacteria, bacillus, etc. [4]. Knowledge of the microbial diversity in Daqu provides the basis for dominant microflora analysis and understanding of the role of microbes in the Daqu production process. Daqu is a multistrain mixed starter. Bacteria such as butyric acid bacteria and caproic acid bacteria are *Clostridium prazmowski*, which are the functional bacteria in pit mud and create a long aftertaste in liquor [9]. The utilization of molecular biology and genomics in the production of liquor is important [3, 12, 14]. In our earlier work, 11 microbial strains were isolated from “Beidacang” Daqu using different culture media (Czapek’s medium, PAD medium and LB medium) and temperatures (37 and 60 °C). By morphological preliminary evaluation, these strains consisted of *Aspergillus*, *Rhizopus*, *Saccharomyces* as well as several strains like *Bacillus* sp. But for the five strains like *Bacillus* (DSL(CS)-01 (37 °C), DSL(CS)-02 (55 °C), DSL(PDA)-C (37 °C), DSL (PDA)-E (55 °C) DSL(PDA)-F) (55 °C), it is difficult to analyze and differentiate them only from the morphology. In this paper, we will study the five strains using RAPD molecular marker.

As a type of PCR, the DNA segments amplified are random. Several arbitrary, short primers (10 nucleotide length) are created, then PCR proceeds. RAPD markers are able to differentiate between genetically distinct individuals. It can also analyze genetic diversity. RAPD has been used to characterize and trace the phylogeny of diverse microbial species. The analysis of genetic variation and relatedness in microbial strains of Daqu are of great value for genetic resources conservation and application. The objectives of this investigation were to determine the genetic variability among five microorganisms (namely, DSL(CS)-01, DSL (CS)-02, DSL(PDA)-C, DSL(PDA)-E, DSL(PDA)-F) at the molecular levels using RAPD markers and to use the data to construct a phylogenetic tree. The genotype-specific markers were also determined.

11.2 Materials and Methods

11.2.1 Microbial Materials

Materials Five microorganisms (namely, DSL(CS)-01, DSL(CS)-02, DSL(PDA)-C, DSL(PDA)-E DSL(PDA)-F) were separated from Daqu used in Heilongjiang Beidacang Group Co. Ltd. China.

Now they are reserved in the molecular laboratory of Qiqihar University.

Microbial culture The five microbial materials were activated and cultured in different media and at different temperatures. The two strains (DSL(CS)-01, DSL(CS)-02) were cultured in Czapek's solid media at 37 °C, the three strains (DSL(PDA)-C, DSL(PDA)-E DSL(PDA)-F) were in PDA solid media at 37 °C. After 24 h, the different plate colonies were observed.

11.2.2 RAPD Analysis

DNA extraction The colonies in different solid plates were transferred to the corresponding liquid media (Czapek and potato dextrose). They were cultivated under 37 °C at 200 rpm for 2 days in a shaking incubator. DNA was extracted from the mycelium by the method reported [13]. Purity extracted genomic DNA was examined by UV spectrophotometer and the gel with 1 % agarose.

Primers screened and used Seven stable primers were screened from 64 primers. They were d2, b17, b18, b1, b3, b8, c9, respectively. These primers were found to be very stable and had good polymorphism in our previous work. So, the nine primers will be used for RAPD. The primer sequences are shown in Table 11.1.

PCR analysis PCR was performed in a total volume of 20 μL containing 10 ng DNA, 200 μM dNTPs, 1 μM of 6 arbitrary 10-mer primers (Sangon Biotech (Shanghai) Co. Ltd, China), 1 unit of *Taq* polymerase (Beijing TransGen Biotech Co., Ltd., China) and 10× *Taq* polymerase buffer (Beijing TransGen Biotech Co., Ltd., China). For DNA amplification thermal cycler (MG96G/Y, Hangzhou Longgene Scientific Instruments Co., Ltd., China) was programmed as follows: 94 °C for 5 min followed by 40 cycles, 94 °C for 1 min, 36 °C for 1 min, 72 °C for 1 min, and 72 °C for 7 min. The amplification products were analyzed by electrophoresis in 1 % agarose in TBE buffer, stained by ethidium bromide, and photographed under UV light.

Polymorphism and cluster analysis The RAPD gel images were scanned using AlphaImager EP gel imaging systems (USA) and analyzed with Alpha Viewer Software (USA). The bands were sized and then binary coded by "1" or "0" for their presence or absence in each genotype. The genetic diversity of strains was analyzed by DNA fingerprints. Resembled indexes were calculated by the reported method [10]. Cluster analysis was based on similarity matrices obtained with Statistical Product and Service Solutions (SPSS) V19.0 Software to estimate the dendrogram.

Table 11.1 Names and sequences of RAPD primer used to assess the genetic variability among the five microorganisms

Primer name	Sequence	Primer name	Sequence	Primer name	Sequence
b1	GTTTCGCTCC	b17	AGGGAACGAG	d2	TGCCGAGCTG
b3	CATCCCCCTG	b18	CCACAGCAGT		
b8	GGTGACGCAG	c9	TGGACCGGTG		

11.3 Result and Discussion

11.3.1 Petri Dishes of Five Microorganisms

Bacillus is a genus of Gram-positive, rod-shaped bacteria and a member of the phylum *Firmicutes*. *Bacillus* sp. can be obligate aerobes, or facultative anaerobes. Under stressful environmental conditions, the bacteria can produce oval endospores. These characteristics originally defined the genus, but not all such species are closely related, and many have been moved to other genera of *Firmicutes*.

As shown in Fig. 11.1, the five microorganisms were identified preliminarily as genus Bacillus, according to their colonial and cellular morphologies as well as their spore staining in earlier work (Note: The results are not shown here).

11.3.2 Extraction of DNA from Five Microorganisms

Breaking the cells open is commonly referred to as cell lysis, to expose the DNA within. This is commonly achieved by grinding the sample. The membrane lipids were removed by adding SDS.

DNA ladder (λ-*Hin*dIII digest DNA Marker) is in lane 1; the DNA in other lanes (2, 3, 4, 5, 6) one by one is the DNA from DSL(CS)-01, DSL(CS)-02, DSL(PDA)-C, DSL(PDA)-E, DSL(PDA)-F.

As shown in Fig. 11.2, DNA of all strains were extracted and purified by analysis of agarose gel electrophoresis (1 % agarose). The results showed that the DNA purified can be used as the template for RAPD.

11.3.3 Screening of Primers and RAPD Analysis

RAPD markers are easier and quicker to use and preferred in applications where relationships between closely related breeding lines are of interest.

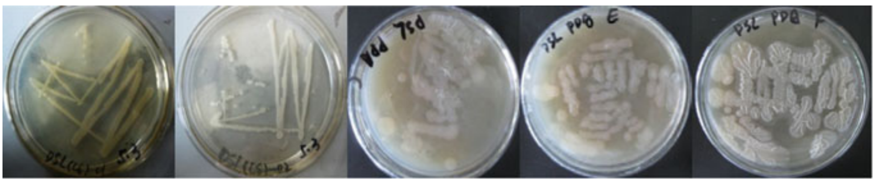

Fig. 11.1 Colonial morphology of microorganism on the petri dishes (they are DSL(CS)-01, DSL (CS)-02, DSL(PDF)-C, DSL(PDF)-E, DSL(PDF)-F, respectively, from the *left* to the *right*)

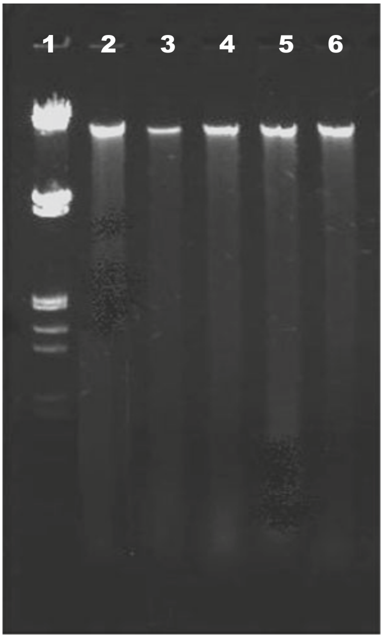

Fig. 11.2 The DNA purified from five microbe strains using agarose electrophoresis (agarose 1 %)

As shown in Fig. 11.3a, there are obvious polymorphisms in five RAPD fingerprinting obtained with DSL(CS)-01 strain DNA as a template using five primers (b1, b8, c9, b18, d2) except for primer b3. But in Fig. 11.3b, for DNA template from strain DSL(CS)-02, only four better RAPD finger printings were obtained (b18, b8, c9, b1). No RAPD finger printing occurred with the primer b3 or the primer b17. So we can find that some primers (such as b1, b8, c9, b18, d2,) are better than the primers like b3 and b17.

As shown in Fig. 11.4a–c stand for the RAPD fingerprinting from strains DSL (PDA)-C, DSL(PDA)-E, and DSL(PDA)-F, respectively. There are obvious polymorphisms in RAPD fingerprinting obtained (like Fig. 11.4b, except for primer b3).

In Fig. 11.4a, it is seen that three primers (b8, b18, and d2) obtained good polymorphisms, but the other three primers (b1, b3, c9) had almost no polymorphisms. However, the other primers did not make polymorphisms in Fig. 11.4c except for primers b8 and c9. Among all, primer b8 was the best primer chosen for RAPD experiment below. According to Figs. 11.3 and 11.4, the total bands are 94 and the genetic special DNA bands are 64. The results show that five strains have a high level of genetic diversity and the percentage of DNA polymorphic was 68.09.

Recently, the identification of microorganisms is dependent on the application of RAPD markers. DNA sequences are independent of environmental conditions, identification can be determined at any stage of microbial growth [1]. RAPD markers are easier and quicker to use and preferred in applications where relationships between closely related breeding lines are of interest.

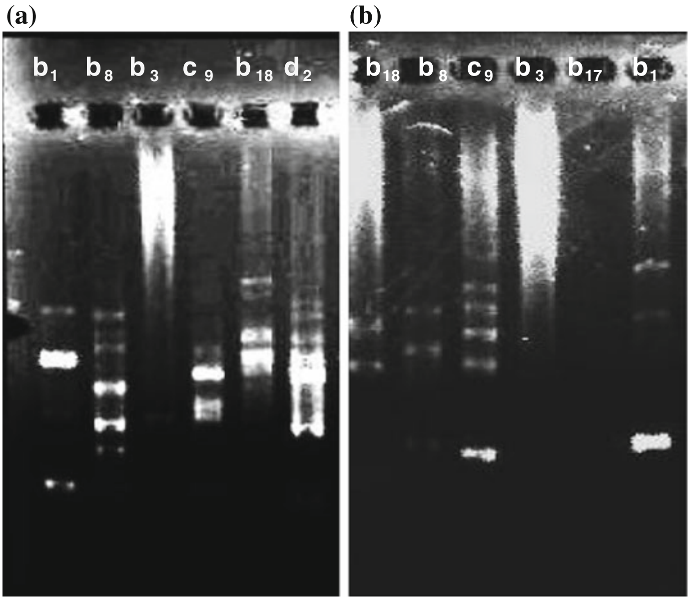

Fig. 11.3 RAPD finger printings obtained with DSL(CS)-01 strain (**a**) and DSL(CS)-02 strains (**b**) with different primers using agarose electrophoresis (agarose 1 %)

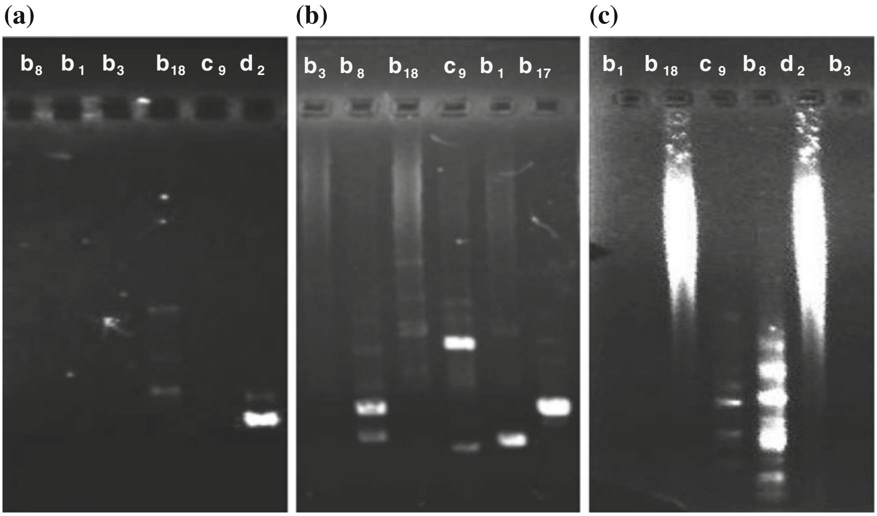

Fig. 11.4 RAPD finger printings obtained with DSL(PDA)-C strain (**a**), DSL(PDA)-E strain (**b**), and DSL(PDA)-F strain (**c**) using different primers (agarose 1 %)

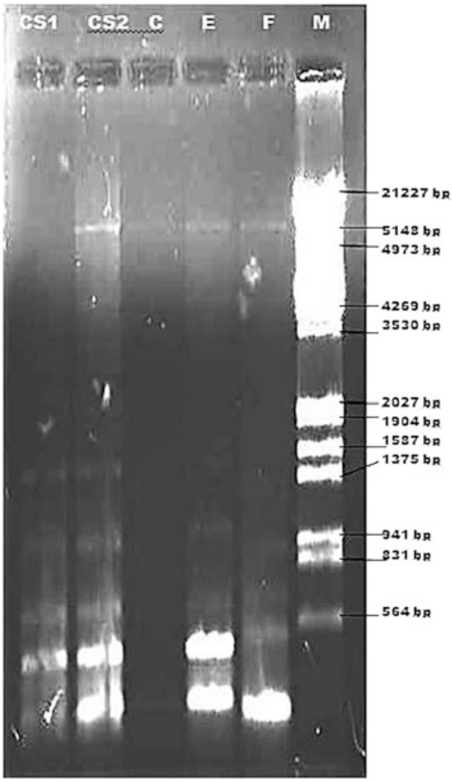

Fig. 11.5 RAPD finger printings from five different strains using primer b8 (1.5 % agarose). *M* DNA marker (λDNA/*Hin*dIII+*Eco*RI) (125, 564, 831, 941, 1375, 1584, 1904, 2027, 3530, 4268, 4973, 5148, 21227 bp)

As shown in Fig. 11.5, the obvious RAPD finer printings were obtained with DNA from the five strains (DSL(CS)-01, DSL(CS)-02, DSL(PDA)-C, DSL)PDA)-E, DSL(PDA)-F) as templates, respectively, using primer 8.

Obviously, in Fig. 11.5 there is no band for DNA template from strain DSL(CS)-01 in size 5,000 bp, but other DNA templates from the other four strains can make the same band in the same size. Many bands are located in a range in size between 5,000 and 564 bp. These bands are dim. For the five strains (DSL(CS)-01, DSL (CS)-02, DSL(PDA)-C, DSL)PDA)-E, DSL(PDA)-F), there are at least 3, 8, 1, 5, and 4 dim bands, respectively, in this size range. However, at a range below 564 bp, there are very obvious different bright bands for four strains (DSL(CS)-01, DSL (CS)-02, DSL(PDA)-E, DSL(PDA)-F).

A comparison between seven random primers on PCR showed that every strain had its special DNA fingerprints (see Figs. 11.3 and 11.4).

Fingerprints of primer b8 showed that the strain DSL(CS)-01 had five bands; DSL(CS)-02 had nine bands (including two bright bands). For the strain DSL(PDF) had only two dim bands. But for DSL(PDA)-E and DSL(PDA)-F, they had at least 6–8 bands, the former have more bands than the latter.

11.3.4 Genetic Similarity Index

DNA bands of RAPD-PCR from seven primers were grouped by cluster analysis. The genetic similarity index for nine strains was from 0.9091 to 0.2324. The average genetic similarity index was 0.5282 (Table 11.2).

As shown in Table 11.2, the highest genetic similarity was found between the strain DSL-CS(01) and the strain DSL-CS(02), and the lowest genetic similarity was found between the strain DSL-CS(01) and the strain DSL(PDA)-C.

11.3.5 Genetic Relation and Clustering Analysis

The RAPD-based dendrogram group investigated microorganisms in two main clusters. The first cluster included DSL(PDA)-F and DSL(PDF)-C, the second cluster was divided into two subclusters. The first cluster contains the strain DSL (CS)-01 and DSL(CS)-02 and the second has only DSL(PDA)-E (Fig. 11.6).

As shown in Fig. 11.6, the genetic relation and clustering analysis showed that there was closest genetic relationship between the strains DSL(CS)-01 and DSL (CS)-02, they may be different specials which came from the same genus. Because of gene mutation, the latter was more thermophile than the former. The strain DSL (CS)-02 can grow well at 55 °C unlike DSL(CS)-02 (its most suitable growth

Table 11.2 Matrix of genetic similar index of five strains separated from "Beidacang" Daqu

	DSL(CS)-01	DSL(CS)-02	DSL(PDA)-E	DSL(PDA)-F	DSL(PDA)-C
DSL(CS)-01	1.0000				
DSL(CS)-02	0.9091	1.0000			
DSL(PDA)-E	0.8000	0.7273	1.0000		
DSL(PDA)-F	0.6000	0.7273	0.3333	1.0000	
DSL(PDA)-C	0.2324	0.2857	0.3333	0.3333	1.0000

In the table there are five microorganisms compared to each other

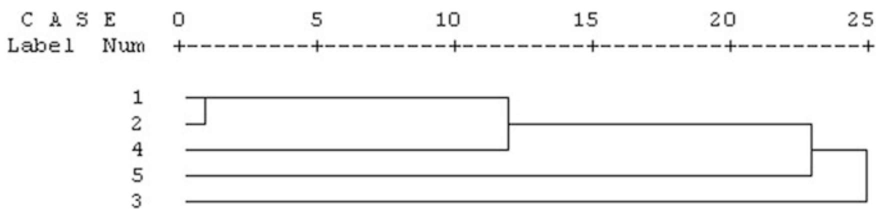

Fig. 11.6 Phylogenetic tree constructed with UPMGA of five strains of "Beidacang" Daqu. "*1*, *2*, *3*, *4*, *5*" stands for strain DSL(CS)-01, DSL(CS)-02, DSL(PDA)-C, DSL(PDA)-E, DSL(PDA)-F, respectively

temperature is 37 °C). The clustering analysis also showed that there was a closer genetic relationship between the strains DSL(CS)-01 and DSL(PDA)-E. The two strains clustered into one category between 10 and 15 in the rescaled distance cluster combine. However, the strain DSL(PDA)-F had farther genetic relative relationship with strains such as DSL(CS)-02, DSL(CS)-01 and DSL(PDA)-E (between 20 and 25 in the rescaled distance cluster combine). The strain DSL (PDA)-F is close to the strain DSL(PDA)-C in genetic relationship. But the strain DSL(PDA)-C had the lowest genetic similarity with the other four strains.

RAPD markers are easier and quicker to use and are preferred in applications where relationships between closely related breeding lines are of interest. It was reported that more than 200 colonies were isolated and characterized. The isolates were discriminated by phenotypic and conventional biochemical taxonomic methods [11]. The results revealed the presence of bacteria, molds, and yeasts. Bacteria consist of bacillus, *Acetobacter*, Lactobacillus, and Clostridium, among which Bacillus strains were found to be predominant. So, Bacillus strains are very important microbes in the process of liquor production. Maotai flavor substances were mainly from functional bacteria in high temperature Daqu. These functional microorganisms are of great importance. Some hemophilic bacteria were isolated from high temperature Daqu of Maotai flavor liquor [15]. The result showed that the strain B3 was functional bacteria of Maotai. The strains from high temperature Maotai Daqu had a close relationship with the quality, production, and flavor liquor. The brewing microorganisms were the basis of Maotai unique flavor [6]. Maotai microorganism has obvious diversities [7]. The thermophiles Bacillus is the effective strain of Maotai liquor [2]. The furan, aromatic, and pyrazine compounds were characteristic components of Maotai flavor [16]. The future development direction of liquor will be from the research of functional bacteria to the development on microbial community [2, 8].

11.4 Conclusion

The results of this study indicate that DNA markers represent efficient tools for estimating the genetic variability and the genetic relationships among the microorganisms. The markers generated are enough to distinguish between the different genotypes used. The genotype-specific molecular markers were determined and these markers can be considered as useful markers for the other microorganisms in Daqu used for Beidacang liquor. This opens up a possibility for developing a molecular genetic map that will lead to the study of other microorganisms in Daqu used for Beidacang liquor.

Acknowledgments This work was supported by the Foundation of Hei longjiang Educational Committee (No. 12541855).

References

1. Ahmad N, Munir I, Khan I et al (2007) PCR-based genetic diversity of rape seed germplasm using RAPD markers. Biotechnology 6(3):334–338
2. Chao J, Zhang X (2005) Technical progress and development in liquor-making industry in China. Liquor-Making Sci Technol 5:10–16
3. Chen Y (2013) Analysis of technical development trend in liquor-making industry. Liquor-Making Sci Technol 3:11–13
4. Du L, Rao J, Tang C et al (2010) Application of cellar functional microbes in Luzhou flavour liquor production. Liquor Making 37(6):43–44
5. Du L, Wang Y, Rao J et al (2009) Studies on the culture and application of cellar mud complex functional microorganism. Liquor Making 36(5):35–36
6. Guo K (2002) Investigation on value of research and the reasons of microbial biodiversity of Mao-tai liquor. Liquor Making 29(2):36–38
7. Jiang H (2003) Research and prospect of the brewing microbial diversity of Mao-tai-favour liquor in the ecological environment. Liquor Making 30(4):22–24
8. Li X (2004) Review of development and trend of Chinese liquor. Liquor Making 1:9–10
9. Li Z, Wang D, Ma M et al (2010) Comparison of enzymes species and fermentation performance of different liquor starter. Liquor-Making Sci Technol 1:17–22
10. Nei M (1972) Genetic distance between populations. American. Nature 106:183–292
11. Wang C, Shi D, Gong G (2008) Microorganisms in Daqu: a starter culture of Chinese Mao-tai-flavour liquor. World J Microbiol Biotechnol 24(10):2183–2190
12. Wang R, Guan F, Yu H et al (2001) The research for application of dried active pit mud function microbe in production of heavy fragrant Chinese spirits. Liquor Making 28(6):35–36
13. Wang S, Dong Y, Li T et al (2006) The method of DNA effective and quick means for DNA extraction of taxol producing fungi. J Sci Teach Coll Univ 26(1):60–64
14. Wang W, Jiang F, Zhao T et al (2014) Technical progress of liquors of the main flavour types. Liquor-Making Sci Technol 3:88–89
15. Zhuang M, Wang Z (2003) Separation, breeding selection and taxonomic determination of functional bacteria strain B3-1 from high temperature Daqu starter for Mao-tai-flavour liquors. Liquor Making 30(5):26–28
16. Zeng Z (2002) On the relationship favour components in liquor and quality style. Liquor Making 29(1):8–10

Chapter 12
Stenotrophomonas maltophilia Having Decolorization Capability of Azo Dye Isolated from Anaerobic Sludge

Wei Feng, Peng Song, Yang Zhang and Zixing Dong

Abstract Strain 5-8 was isolated from anaerobic sludge which was collected from a sewage treatment plant located at Shandong Province. Strain 5-8 has efficient ability to decolorize Fast Yellow2G. Fast Yellow2G was decolorized by more than 80 % in 48 h, and completely decolorized in 60 h. Strain 5-8 was observed to form yellow colored, smooth, circular, convex colonies of 5 mm diameter with entire margins on LB medium. Cells of strain 5-8 were observed to be gram-negative, aerobic, motile with a single polar flagellum and rod-shaped with dimensions of 0.3–0.4 × 0.6–1.5 μm. Growth was observed at 18–40 °C (optimum 35–37 °C), pH 6.0–9.0 (optimum pH 7.0–8.0) and with 0.5–5 % (w/v) NaCl (optimum 1 %). Neighbor-joining phylogenetic tree based on 16S rRNA gene sequences showed that strain 5-8 belongs to the genus *Stenotrophomonas*, clustering coherently with the type strain of *Stenotrophomonas maltophilia* showing sequence similarity value of 99 %.

Keyword Decolorization azo dye phylogenetic analyses *Stenotrophomonas*

12.1 Introduction

Azo dyes are synthetic organic colorants, which are characterized by the presence of one or more azo groups. The largest class of dyes in industrial use is known as azo dyes in number and amount produced [1]. Dyes are usually released into the environment as industrial effluents from textile and dye manufacturing. Release of such colored compounds into the environment is undesirable not only because of

W. Feng · Y. Zhang
School of Life Science, Liaocheng University, Shandong 252059, China

P. Song · Z. Dong (✉)
College of Bioengineering, Tianjin University of Science and Technology,
Tianjin 300457, China
e-mail: star1987.com@163.com

T.-C. Zhang and M. Nakajima (eds.), *Advances in Applied Biotechnology*,
Lecture Notes in Electrical Engineering 333, DOI 10.1007/978-3-662-46318-5_12

their aesthetic appearance, which may drastically affect photosynthesis in the aquatic ecosystem, but also because many of the dyes and/or their breakdown products are toxic and mutagenic to life [2]. The presence of dyes or their degradation products in water even at very low concentrations can be toxic and sometimes carcinogenic, mutagenic, or teratogenic to various organisms, including humans [3]. Therefore, azo dyes are of significant concern as pollutants of the environment, and removal of dyes from environment using different methods has become a focus for environmental scientists.

Physical and chemical methods are not suitable to treat dye effluent due to their operational costs or secondary sludge disposal problems [4]. Biological methods represent a more proper way of textile azo dye removal. Several microorganisms such as algae, yeast, filamentous fungi, and bacteria individually or in consortium are shown to degrade azo dyes in the presence of nutrients [5]. Various wood-rotting fungi were able to decolorize azo dyes using peroxidases or laccases. But fungal treatment of effluents is usually time-consuming. Under static or anaerobic conditions, bacterial decolorization generally demonstrates good color removal effects. However, aerobic treatment of azo dyes with bacteria usually achieved low efficiencies because oxygen is a more efficient electron acceptor than azo dyes [6]. Bacteria studied for biodegradation include *Pseudomonas* NBAR, *Rhodopseudomonas palustris,* etc. [7]. Use of microbial consortium for biodegradation of dyes has also been reported [8]. Therefore, the isolation of effective strains to decolorize azo dyes is a key point. During the course of our research, we have isolated a bacterial strain that highly decolorized the toxic azo dye Xylene Fast Yellow2G from anaerobic sludge samples by an enrichment culture.

12.2 Materials and Methods

12.2.1 Dyes and Chemicals

All chemicals including azo dyes (Xylene Fast Yellow2G) (Fig. 12.1) used in this study were provided by Shanghai Sangon Biological Engineering Technology & Services Co., Ltd.

12.2.2 Bacterial Strains and Culture Conditions

Anaerobic sludge was collected from a sewage treatment plant located at Shandong Province, eastern China and used as a source for the isolation of bacterial strains.

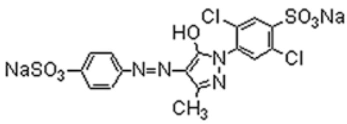

Fig. 12.1 The chemical structure of Xylene Fast Yellow2G

Strain 5-8 was isolated by the standard dilution plating technique at 30 °C on the medium including azo dye (0.5 % glucose, 0.2 % ammonium sulfate, 0.05 % polypepton, 0.05 % yeast extract, 0.03 % K_2HPO_4, 0.02 % KH_2PO_4, 0.01 % $MgSO_4 \cdot 7H_2O$, and 0.005 % azo dye, pH 6.8) and cultivated routinely at 37 °C in LB medium (containing 0.005 % azo dye). Strain 5-8 was maintained on LB media at 4 °C for short-term preservation and as a glycerol suspension (20 %, w/v in distilled water) at −80 °C for long-term preservation.

Cellular biomass required for DNA extraction was obtained from cultures grown in LB media at 37 °C for 2 days. The decolorization experiments were also performed in LB medium (containing 0.005 % azo dye) at 37 °C.

12.2.3 Morphological, Physiological and Biochemical Characterization

Colony morphology was examined after 3 days of incubation at 35 °C on LB medium. Cell morphology was investigated by light microscopy and Gram reaction was observed by staining using a Gram staining kit according to the manufacturer's protocol. Motility was assessed under phase contrast microscopy.

Strain 5-8 was cultured over the temperature range of 5–50 °C (at intervals of 5 °C) and the pH range of 5.0–10.0 (at intervals of 1 pH unit) in LB. Growth at various NaCl concentrations was tested over the range of 0.5–10 % (w/v) NaCl [0.5 % (w/v) and 1–10 % (w/v) at intervals of 1 %] by incubating under conditions of 35 °C and pH 7.0.

Oxygen requirement, activities of catalase, urease and oxidase, hydrolysis of casein, starch, Tweens 20, 40 and 80, aesculin, nitrate reduction, Voges–Proskauer test, indole and H_2S production were performed according to the conventional methods described by Cowan and Steel [9] and Smibert and Krieg [10]. The utilization of sole carbon and nitrogen sources was determined according to the method described by Gao et al. [11].

12.2.4 16S rRNA Gene Sequencing and Phylogenetic Analyses

Extraction of genomic DNA was performed according to the method of Sambrook and Russell [12]. PCR amplification of the 16S rRNA gene was performed using the following two primers: 27F(50-AGA-GTTTGATCMTGGCTCAG-30) and 1492R(50-GGTTACCTTGTTACGACTT-30) [13].

The purified gene fragment was sequenced by Shanghai Sangon Biological Engineering Technology & Services Co., Ltd. Phylogenetic neighbors were identified using GenBank (http://www.ncbi.nlm.nih.gov/blast/), and multiple alignments were generated using CLUSTAL X [14]. A phylogenetic tree was constructed from the evolutionary distance data with the neighbor-joining [15], maximum likelihood PHYLIP (phylogeny inference package), version 3.5c. Department of Genetics, University of Washington, Seattle) and maximum parsimony [16] methods using MEGA 5.0, and bootstrap values were calculated based on 1,000 replicates.

12.3 Results

12.3.1 Decoloriation of Azo Dyes by Growing Cells

Xylene Fast Yellow2G decolorizing bacteria were isolated by the enrichment culture containing Xylene Fast Yellow2G in the medium. Among isolated bacteria, 15 strains showed the decolorization of Xylene Fast Yellow2G with different rates in the liquid medium. Of these, an isolate 5-8 was selected as having the most efficient ability to decolorize Fast Yellow2G. Fast Yellow2G were decolorized more than 80 % (Fig. 12.2) in 48 h, and almost completely decolorized in 60 h.

12.3.2 Morphological, Physiological, and Biochemical Characterization

Strain 5-8 was observed to form yellow colored, smooth, circular, convex colonies of 5 mm diameter with entire margins on LB.

Cells of strain 5-8 were observed to be gram-negative, aerobic, motile with a single polar flagellum and rod-shaped with dimensions of 0.3–0.4 × 0.6–1.5 μm. Growth was observed at 18–40 °C (optimum 35–37 °C), pH 6.0–9.0 (optimum pH 7.0–8.0) and with 0.5–5 % (w/v) NaCl (optimum 1 %) (Table 12.1).

Fig. 12.2 The color contrast of two culture disposed by centrifugation with one culture bacteria (*right*) and the other blank (*left*), after 48 h

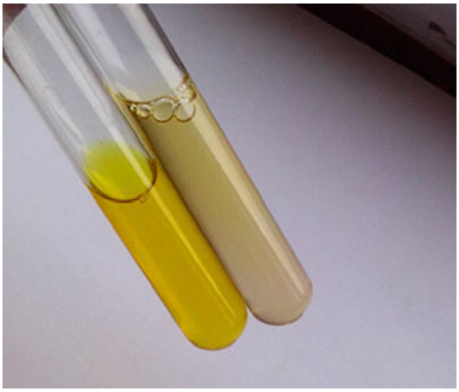

Table 12.1 Part of the physiological and biochemical characteristics of strain 5-8

Characteristic	Strain 5-8
Cell size (μm)	0.3~0.4 × 0.6~1.5
Temperature growth range (°C)	18–40
Optimum temperature	35
pH range	6.0–9.0
NaCl range (%, w/v)	0.5–5
Nitrate reduction to nitrite	+
Tween 80	+
Carbon source utilisation Lactose	+
Xylose	−
Maltose	+
Sucrose	+
Mannose	+
Inulin	−
Salicin	+
Galactose	−
L-Arabinose	−
Mannitol	−
Cellobiose	+
D-Arabinose	−
Raffinose	−
Trehalose	−
Melibiose	−
Hydrolysis of Gelatin	+
Hydrolysis of Starch	−

All data are obtained from this study unless indicated otherwise. +, positive; −, negative. All strains could use Lactose, Maltose, Sucrose, Mannose, Salicin, Cellobiose as Carbon source; none of strains could use Xylose, Inulin, D-Arabinose, Raffinose, Trehalose, Melibiose; hydrolysis of Gelatin positive and Starch hydrolysis was negative

12.3.3 16S rRNA Gene Sequencing and Phylogenetic Analysis

Comparison of the almost complete 16S rRNA gene sequence (1,440 bp, Fig. 12.3) of strain 5-8 showed that it is most closely affiliated to the genus *Stenotrophomonas*. The highest 16S rRNA gene sequence similarity was found with *Stenotrophomonas maltophilia* (99 %). The neighbor-joining phylogenetic tree showed that 58 clustered with *S. maltophilia* 6B2-1 (bootstrap value of 90 %). The relationship between these two strains was maintained using maximum likelihood and maximum parsimony (Fig. 12.4).

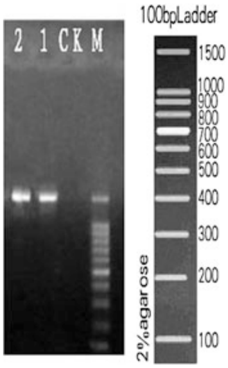

Fig. 12.3 Electrophoretogram of PCR amplified 16S rRNA gene. *Marker* 100 bp ladder; 1, 2 amplified 16S rRNA gene of strain 5-8 by primer 27F and 1492R

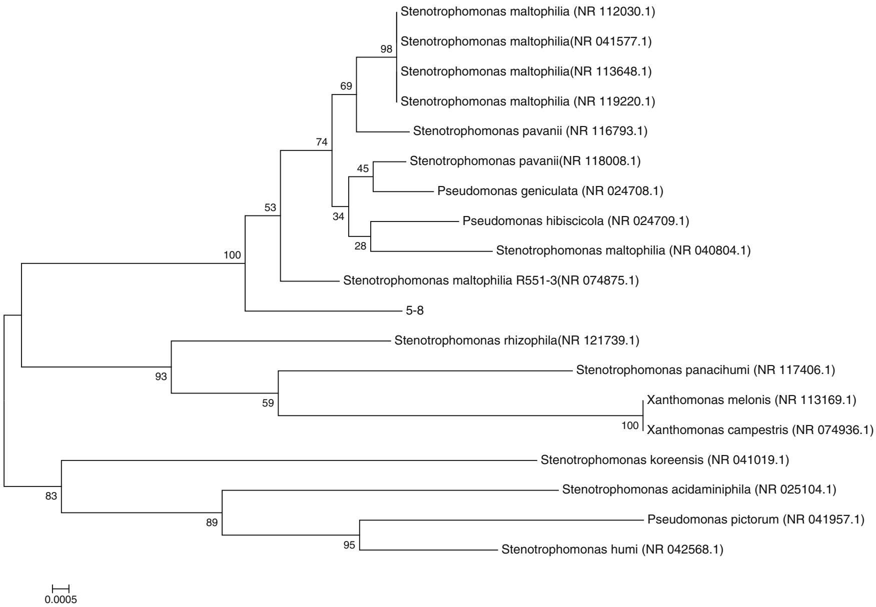

Fig. 12.4 Neighbor-joining phylogenetic tree based on 16S rRNA gene sequences showing the positions of strain 5-8 and related taxa. Bootstrap values (expressed as percentages of 1,000 replications) are shown at branching points. *Bar* 0.0005 substitutions per site

12.4 Discussion

16S rRNA gene sequence analysis indicated strain 5-8 to be most closely related to *S. maltophilia* R551-3 (99 % sequence similarity). Generally accepted criteria for delineating bacterial species state that strains showing less than 97 % of 16S rRNA gene sequence similarity or lower than 70 % of DNA–DNA relatedness in current bacteriology are considered to belong to different species [17].

Goodfellow et al. [18] reported that the DNA–DNA relatedness provides a reliable way of distinguishing between representatives of species that share high 16S rRNA gene sequence similarity.

Xylene Fast Yellow2G was used as the experimental dye in cell's decolorization rate. The culture condition for the highest decolorization rate of Xylene Fast Yellow2G by the strain was at 37 °C, pH 6–9. Most wastewaters from textile industries have a neutral to alkaline pH (around 7–11). The strain 5-8 used in the present study was able to degrade the dye efficiently in the range of pH 6–9 similar to earlier report.

Citrobacter sp. CK3 exhibited decolorization of Reactive Red 180 at pH 6.0 and 7.0, with 96 % decolorization in 48 h, while at pH 10 and 11, the decolorization of dye was completely inhibited [19] In view of this, the strain 5-8 seems to be better candidate for bioremediation with low pH.

Stenotrophomonas maltophilia sp. was able to degrade wide variety of textile dyes and consistent with earlier reports of the bacterial species [20, 21]. In this study, strain 5-8 also showed ability to decolorize the structurally different textile dyes in plain distilled water. This approach can provide more practical and cost-effective way of bioremediation.

Acknowledgments This work was supported by The Scientific Research Foundation of Liaocheng University, China (Project No. X10023).

References

1. Griffiths J (1984) Developments in the light absorption properties of dyes-color and photochemical degradation reactions. In: Griffiths J (ed) Developments in the chemistry and technology of organic dyes. Blackwell, Oxford, pp 1–30
2. Chung KT, Cerniglia CE (1992) Mutagenicity of azo dyes: structure-activity relationships. Mutat Res 277:201–220
3. Novotny C, Dias N, Kapanen A, Malachova K, Vandrovcova M, Itavaara M (2006) Comparative use of bacterial, algal and protozoan tests to study toxicity of azo and anthraquinone dyes. Chemosphere 63:1436–1442
4. Kaushik P, Malik A (2009) Fungal dye decolourization: recent advances and future potential. Environ Int 35:127–141
5. Asgher M, Bhatti HN, Ashraf M, Legge R (2008) Recent developments in biodegradation of industrial pollutants by white rot fungi and their enzymes. Biodegradation 19:771–783
6. Stolz A (2001) Basic and applied aspects in the microbial degradation of azo dyes. Appl Microbiol Biotechnol 56:69–80

7. Liu G, Zhou J, Wang J, Song Z, Qv Y (2006) Bacterial decolorization of azo dyes by Rhodopseudomonas palustris. J Microbiol Biotechnol 22:1069–1074. doi:10.1159/000093241
8. He F, Hu W, Li Y (2004) Biodegradation mechanisms and kinetics of azo dye 4BS by a microbial consortium. Chemosphere 57:293–301
9. Cowan ST, Steel KJ (1965) Manual for the identification of medical bacteria. Cambridge University Press, London
10. Smibert RM, Krieg NR (1994) Phenotypic characterization. In: Gerhardt P, Murray RGE, Wood WA, Krieg NR (eds) Methods forgenera land molecular bacteriology. American Society for Microbiology, Washington, pp 607–655
11. Gao JL, Sun JG, Li Y, Wang ET, Chen WX (1994) Numerical taxonomy and DNA relatedness of tropical rhizobia isolated from Hainan Province, China. Int J Syst Bacteriol 44:151–158
12. Sambrook J, Russell DW (2001) Molecular cloning: a laboratory manual. Cold Spring Harbor Laboratory, New York
13. Weisburg WG, Barns SM, Pelletier DA, Lane DJ (1991) 16S ribosomal DNA amplification for phylogenetic study. J Bacteriol 173:697–703
14. Thompson JD, Gibson TJ, Plewniak F, Jeanmougin F, Higgins DG (1997) The CLUSTAL_X windows interface: flexible strategies for multiple sequence alignment aided by quality analysis tools. Nucleic Acids Res 25:4876–4882
15. Saitou N, Nei M (1987) The neighbor-joining method: a new method for reconstructing phylogenetic trees. Mol Biol Evol 4:406–425
16. Fitch WM (1971) Toward defining the course of evolution: minimum change for a specific tree topology. Syst Zool 20:406–416
17. Stackebrandt E, Goebel BM (1994) Taxonomic note: a place for DNA–DNA reassociation and 16S rRNA sequence analysis in the present species definition in bacteriology. Int J Syst Bacteriol l44:846–849
18. Goodfellow M, Stainsby FM, Davenport R, Chun J, Curtis T (1998) Activated sludge foaming: the true extent of actinomycete diversity. Water Sci Technol 37:511–519
19. Wang H, Su JQ, Zheng XW, Tian Y, Xiong XJ, Zheng TL (2009) Bacterial decolorization and degradation of the reactive dye reactive red 180 by Citrobacter sp. CK3. Int Biodeter Biodegr 63:395–399
20. Sandrine R,Alain H,Guy S (2001) Isolation and characterisation of flew gram-negative and gram-positive atrazine degrading bacteri a from different French soils. FEMS Microbiol Ecol 36:211–222
21. Shinjiro T, Naoko K, Fusako K, Masaaki Y et al (2003) Involvement of a quinoprotein (PQQ-containing) alcohol dehydrogenase in the degradation of polypropylene glycols by the bacterium Stenotrophomonas mahophilia. FEMS Microbiol Lett 218:345–349

Chapter 13
In Silico Cloning and Sequence Analysis of F3H Gene in *Raphanus sativus* L.

Guang Ma and Jiping Guo

Abstract Flavanone 3-hydroxylase is a key enzyme in the biosynthetic pathway of plant flavonoids. The complete cDNA sequence of *Raphanus sativus* L. F3H gene was in silico cloned using *Brassica napus* F3H-2 gene cDNA sequence (DQ513329.1) as a probe. Then the hydrophilicity, secondary structure, and advanced structure of F3H protein in *R. sativus* L. were analyzed using bioinformatics methods. The results showed that the cDNA was 1,437 bp, contains an open reading frame of 1,077 bp, encoding 358 amino acids. The protein coded by *R. sativus* L. F3H gene cDNA showed 98 % similarity to *B. napus* F3H-2. Its secondary structure contains 38.55 % alpha helix, 41.9 % random coil and 4.93 % beta turn. The homology analysis of 3D structure showed that the three-dimensional structure of the protein is a compact globular structure.

Keywords Flavanone 3-hydroxylase · 3D structure · *Raphanus sativus* L. · Cloning · Bioinformatics

13.1 Introduction

Flavanone 3-hydroxylase (F3H; EC 1.14.11.9) is a key enzyme of flavonoid biosynthesis in plant. It catalyzes hydroxylation of C-ring third position hydroxyl catalytic at flavanone to form two hydrogen flavanols [1–3]. It was first found in the crude extracts of violet, and the properties studied by parsley cell culture [4]. Subsequently, F3H gene was cloned from the petunia and showed high activity by functional expression in *Escherichia coli* [5]. Later, more characteristics of F3H gene in different species were reported such as barley, begonia, alfalfa, maize, *Arabidopsis thaliana* and perilla. In different species, expression characteristics of F3H are different. In petunia and snapdragon, regulation of flavonoid biosynthesis pathway of the preliminary steps and late stage is different. In petunia F3H gene belongs to the early gene, but it belongs to the late genes in antirrhinum. In maize, the flavonoid biosynthesis pathway is through

G. Ma (✉) · J. Guo
Department of Life Sciences, Hengshui College, Hengshui 053000, China
e-mail: maaohan@163.com

T.-C. Zhang and M. Nakajima (eds.), *Advances in Applied Biotechnology*,
Lecture Notes in Electrical Engineering 333, DOI 10.1007/978-3-662-46318-5_13

co-regulation to produce anthocyanin in organizations, but flavonol F3H gene expression is only consistent with accumulation of flavonol in anthers [6]. In the study of alfalfa, F3H is also expressed in the roots and nodules, but its role is not clear.

Flavonoids have very high application value in medical and health care. As an important flavonoid biosynthesis gene, F3H gene of *Brassica napus* had been cloned, however, it was little reported in other *Brassica* plants. There is no report on *Raphanus sativus* L. In this study, with the *B. napus* F3H gene cDNA as probe, the F3H gene of *R. sativus* L. was in silico cloned. We obtained the F3H cDNA coding sequence. The sequence and coding protein characteristics are studied, and the three-dimensional structure was constructed homology. The study has laid a solid basis for further research on F3H function.

13.2 Materials and Methods

13.2.1 BLAST Searching of Raphanus sativus L. EST Databases

The cDNA sequence of *B. napus* flavanone 3-hydroxylase 2 (F3H-2) mRNA (GenBank: DQ513329.1) was used as a probe to search the *R. sativus* L. expressed sequence tag (EST) database (http://www.ncbi.nlm.nih.gov/dbEST/) for a homologous clone, using the BLAST program. The EST sequence of score ≥100 and length ≥100 bps selected from the blast result, were generated contigs (http://pbil.univ-lyon1.fr/cap3.php). The longer contig was used as the second probe. The above step was not repeated until the newly generated probe could not be elongated. This approach led to a sequence as a putative *R. sativus* L. F3H gene cDNA.

13.2.2 Bioinformatics Analysis of the Raphanus sativus L. F3H Gene

The putative *R. sativus* L. F3H gene cDNA was analyzed by bioinformatics software. The cDNA sequence was submitted to open reading frame software (http://www.ncbi.nlm.nih.gov/gorf/gorf.html), to find the start codon and termination codon positions. The protein sequence of F3H gene of *R. sativus* L. and *B. napus* were aligned by multiple sequence alignment software clustalw2.1 (http://www.ebi.ac.uk/Tools/msa/clustalw2/) to compare their protein similarity. Primary structure characteristics of *R. sativus* L. F3H protein was analyzed using online server (http://www.expasy.org/tools/protparam.html). Its secondary protein structure was analyzed in online server (http://npsa-pbil.ibcp.fr/cgi-bin/npsa_automat.pl?Page=/NPSA/npsa_sopma.html). Hydrophobicity analysis used ProtScale program (http://www.expasy.org/cgi-bin/protscale.pl). The neighbor-joining phylogenetic tree was constructed by Mega 5.05 software.

13.2.3 The Prediction of F3H Protein Three-Dimensional Structure

The three-dimensional structure of the protein was predicted using Swiss-Model online server (http://swissmodel.expasy.org/workspace/index.php?func=modelling_simple1). The three-stage structure model is shown by the CN3D software.

13.3 Results

13.3.1 In Silico Cloning of *Raphanus sativus* L. F3H Gene

With the cds of *B. napus* F3H-2 mRNA (GenBank: DQ513329.1) as probe, 24 EST sequences (score ≥100 and length ≥100) were found by Blastn searching the *R. sativus* L. EST database, in NCBI (Fig. 13.1).

The selected sequences were saved in a file in FASTA format. The file was submitted to online CAP software. One contig was obtained by assembling EST sequences. It was putative *R. sativus* L. F3H cDNA (Fig. 13.2). Searching the cDNA sequence for potential coding regions by ORF finder, an entire open reading frame (ORF) of 358 amino acids was detected with a potential start codon at the 196th site and a stop codon at the 1,272th site (Fig. 13.2).

13.3.2 Gene Comparison Between *Raphanus sativus* L. F3H and *Brassica napus* F3H-2 cDNA

The alignment of *R. sativus* L. and *B. napus* F3H-2 amino acid sequences, constructed using ClustalW program, suggest that *R. sativus* L. F3H amino acid sequences are similar to *B. napus* F3H-2. There are only 7 different amino acids of a total of 358 amino acids (Fig. 13.3).

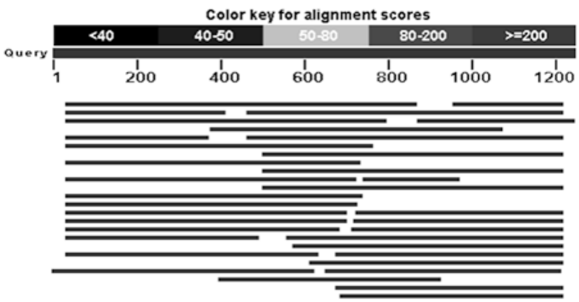

Fig. 13.1 BLAST result of F3H cDNA in the *Raphanus sativus* L. EST databank

```
   1 gggtcttctagaaagagaggagatagaagcaccgtggtaggtagctaacgatctcctcattcgtcagtcatcacaagctttgaaaggttttcc
  94 cagctaccacgcactctctttctcttcttatatattcattacatactctctctcattttcttgttcatgcattctttttaccgttttgtaatttaattataa
 196 atggctccaggaactctaaccgagcttgccggagagactaagctcaactctaagttcgtccgggacgaggatgaacgtcccaaggttgcc
      M  A  P  G  T  L  T  E  L  A  G  E  T  K  L  N  S  K  F  V  R  D  E  D  E  R  P  K  V  A
 286 tacaatgagttcagcacggagatccccgtaatctctcttgccggaatcgacgatgttggtgggaaaagaggagagatctgtcgtcagatc
      Y  N  E  F  S  T  E  I  P  V  I  S  L  A  G  I  D  D  V  G  G  K  R  G  E  I  C  R  Q  I
 376 gttgaagcttgtgagaactggggtgtttttcaggtggtcgatcatggagtggatactagtttggtggcggatatgactcgtctggctcgt
      V  E  A  C  E  N  W  G  V  F  Q  V  V  D  H  G  V  D  T  S  L  V  A  D  M  T  R  L  A  R
 466 gacttcttcgctttagctcctgaggagaaactgaagttcgacatgtccggtggtaaaaagggaggatttattgtctctagtcatcttcag
      D  F  F  A  L  A  P  E  E  K  L  K  F  D  M  S  G  G  K  K  G  G  F  I  V  S  S  H  L  Q
 556 ggagagtctgttcaagattggagagagatcgtgacgtatttctcgtacccggtgagaaacagagactactcacggtggccgactaagccg
      G  E  S  V  Q  D  W  R  E  I  V  T  Y  F  S  Y  P  V  R  N  R  D  Y  S  R  W  P  T  K  P
 646 gaagggtgggtgaaagtgacggaggagtacagcgagaagctgatgagtttggcttgtaaacttcttgaggttttgtctgaagctatgggg
      E  G  W  V  K  V  T  E  E  Y  S  E  K  L  M  S  L  A  C  K  L  L  E  V  L  S  E  A  M  G
 736 cttgagaaagaggcacttaccaatgcatgcgtcgatatggaccaaaaaatagttgttaactattacccaaaatgccctcagcctgatcta
      L  E  K  E  A  L  T  N  A  C  V  D  M  D  Q  K  I  V  V  N  Y  Y  P  K  C  P  Q  P  D  L
 826 accctcggactcaagcgtcacaccgaccccggaaccatcactttgctgctccaagaccaagtcggtggtttacaagccacacgagacgat
      T  L  G  L  K  R  H  T  D  P  G  T  I  T  L  L  L  Q  D  Q  V  G  G  L  Q  A  T  R  D  D
 916 gggaagacatggattacggttcagcctgttgaaggagcttttgtcgttaatctcggcgaccatggccactatctgagcaatgggaggttc
      G  K  T  W  I  T  V  Q  P  V  E  G  A  F  V  V  N  L  G  D  H  G  H  Y  L  S  N  G  R  F
1006 aagaacgctgaccaccaggcggtggtgaattccaactcgagcagattatcaatagccacgttccagaatccggcgccggaagcaaccgtg
      K  N  A  D  H  Q  A  V  V  N  S  N  S  S  R  L  S  I  A  T  F  Q  N  P  A  P  E  A  T  V
1096 tatcctcttaaagtgagagaaggagagaagccgatcctggaggagcctattacgtttgcggagatgtataagagaaagatgagtagagat
      Y  P  L  K  V  R  E  G  E  K  P  I  L  E  E  P  I  T  F  A  E  M  Y  K  R  K  M  S  R  D
1186 attgagctggctcgcctcaagaagctggcgaaagaagaacatgaccacaaggaagctggcaagcctctcgaccaaatcatcgcttag
      I  E  L  A  R  L  K  K  L  A  K  E  E  H  D  H  K  E  A  G  K  P  L  D  Q  I  I  A  *
1273 actactccttgtgttggccccttgctattgtgttggttcggttgtgtaagttggtactgaaattaagttatgtcatgttgggtgaaattgtgttgt
     atctcttttctatcatatagaaataatgataataatgtctatgacgcaaaaaaaaaaaaaaaaaaaaa 1437
```

Fig. 13.2 Nucleotide sequence and deduced amino acid sequence of *R. sativus* L. F3H gene

```
R. sativus L.  MAPGTLTELAGETKLNSKFVRDEDERPKVAYNEFSTEIPVISLAGIDDVGGKRGEICRQI 60
B. napus       MAPGTLNELAGETKLNSKFVRDEDERPKVAYNEFSTEIPVISLAGIDDVGEKRGEICRQI 60
               ******.****************************************** **********

R. sativus L.  VEACENWGVFQVVDHGVDTSLVADMTRLARDFFALAPEEKLKFDMSGGKKGGFIVSSHLQ 120
B. napus       VEACENWGVFQVVDHGVDTSLVADMTRLARDFFALPPEEKLKFDMSGGKKGGFIVSSHLQ 120
               ***********************************.************************

R. sativus L.  GESVQDWREIVTYFSYPVRNRDYSRWPTKPEGWVKVTEEYSEKLMSLACKLLEVLSEAMG 180
B. napus       GESVQDWREIVTYFSYPVRNRDYSRWPTKPEGWVKVTEEYSERLMGLACKLLEVLSEAMG 180
               ******************************************:**.**************

R. sativus L.  LEKEALTNACVDMDQKIVVNYYPKCPQPDLTLGLKRHTDPGTITLLLQDQVGGLQATRDD 240
B. napus       LEKEALTNACVDMDQKIVVNYYPKCPQPDLTLGLKRHTDPGTITLLLQDQVGGLQATRDD 240
               ************************************************************

R. sativus L.  GKTWITVQPVEGAFVVNLGDHGHYLSNGRFKNADHQAVVNSNSSRLSIATFQNPAPEATV 300
B. napus       GKTWITVQPVEGAFVVNLGDHGHYLSNGRFKNADHQAVVNSNSSRLSIATFQNPAPEATV 300
               ************************************************************

R. sativus L.  YPLKVREGEKPILEEPITFAEMYKRKMSRDIELARLKKLAKEEHDHKEAGKPLDQIIA 358
B. napus       YPLKVREGEKPILEEPITFAEMYKRKMSRDLELARLKKLAKEEHDHKEAAKPLDQIIA 358
               ******************************:*****************.*********
```

Fig. 13.3 Homology of *R. sativus* L. and *Brassica napus* F3H

13.3.3 Secondary Structure of Raphanus sativus L. F3H Protein

The secondary structure of *R. sativus* L. F3H protein was predicted utilizing online service (http://npsa-pbil.ibcp.fr/cgi-bin/npsa_automat.pl?page=/NPSA/npsa_sopma.html). The results showed that *R. sativus* L. F3H protein have 38.55 % alpha helix, 15.36 % extended strand, 41.9 % random coil, and 4.19 % beta turn.

13.3.4 Hydrophilicity Prediction of Raphanus sativus L. F3H Protein

Hydrophilicity of *R. sativus* L. F3H protein was predicted utilizing Program of ProtScale (Kyte and Doolittle). The results showed that most sites of *R. sativus* L. F3H protein is in the hydrophilic region (Score: 2.278 to −2.293) (Fig. 13.4). It was concluded that the *R. sativus* L. F3H protein is a hydrophilic protein.

13.3.5 Analysis of Raphanus sativus L. F3H Phylogenetic Tree

F3H cDNA sequence of *R. sativus*, *Brassica rapa naringenin, B. napus* (F3H-1), *B. napus* (F3H-2), *B. rapa* subsp. *campestris* (F3H-1), *A. thaliana, Arabidopsis lyrata, Eutrema salsugineum, Parrya nudicaulis, M. incana, Capsella rubella, Cardamine resedifolia* were downloaded from genebank database. These sequences were stored in a FASTA file including F3H cDNA sequence of *R. sativus* L. The neighbor-joining phylogenetic tree was constructed with the FASTA file by software MEGA 5.05 (Fig. 13.5). The phylogenetic tree analysis showed *B. napus, B. rapa, R. sativus* L. clustered into one branch. *R. sativus* L. F3H cDNA is close to *B. napus* and *B. rapa*. The genetic relationship between the F3H cDNA is consistent with the phylogenetic tree.

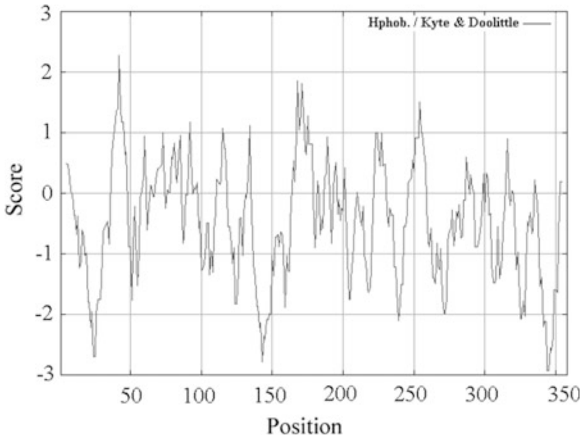

Fig. 13.4 Hydrophilicity profile of *R. sativus* L. F3H protein

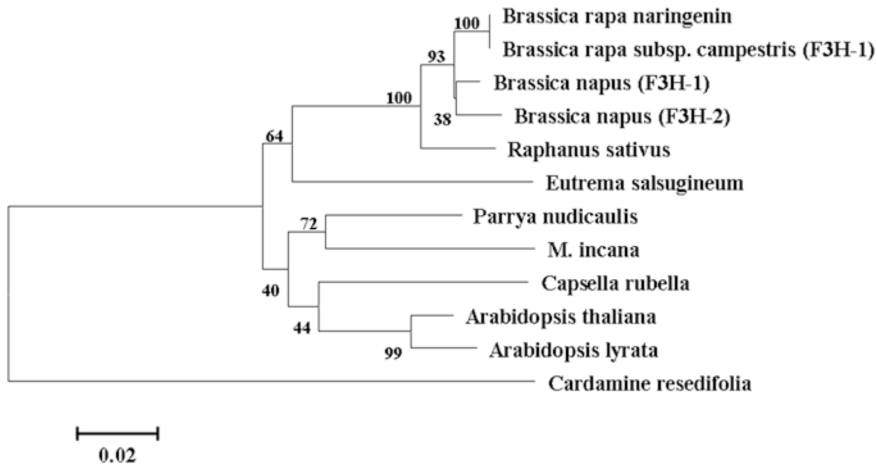

Fig. 13.5 Analysis of *R. sativus* L. F3H protein phylogenetic tree

13.3.6 Advanced Structure of Raphanus sativus L. F3H Protein

The structure prediction from primary to advanced structure is an important task in the field of protein research. The three-dimensional structure model of *R. sativus* L. F3H protein was predicted by the Swiss-Model server, by homology modeling, based on the available structures. The homologous sequence of pdb1gp6A and pdb1w9yA with high homology and three-dimensional structure were two models. Because the C terminal of *R. sativus* L. F3H is poor homology to *B. napus*, and less than 10 amino acids, the template of pdb1w9yA matching 2-332 to *R. sativus* L. F3H was selected for homology modeling (Fig. 13.6). The results were close to the protease real space conformation.

Fig. 13.6 The predicted three-dimensional structure of *R. sativus* L. F3H protein

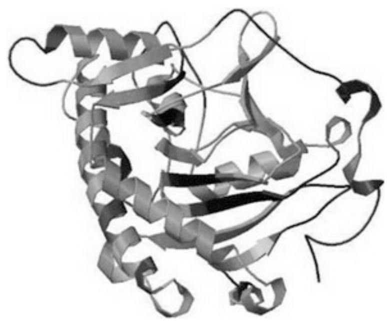

13.4 Discussion

In silico cloning is a method developed in recent years for functional gene identification using genome and EST database. Compared to traditional methods, such as molecular hybridization, screening of genomic or cDNA library, it is advanced for low cost, high efficiency, easy operation, etc. With more and more EST and genome sequencing data being reported, it would become possible and feasible to isolate and identify the functional genes by in silico cloning. Many successful examples strongly support the fact that in silico cloning is an absolutely feasible tool for gene cloning and presents some advantages compared to the traditional methods.

In this study, we present in silico cloning and characterization of one flavonoid biosynthetic genes, flavanone-3 hydroxylase of *R. sativus* L. The F3H transcripts are abundant in seed of *R. sativus* L. In addition, a sequence similar to the Myb-like box A/CACC T/AAA/CC found in several genes of the flavonoid pathway. It was thought to be involved in the regulation of the flavonoid biosynthesis pathway and is present in inverse orientation between −1,024 and −1,016 upstream from the start codon of the *R. sativus* L. F3H gene. Future analysis of *R. sativus* L. plants transformed with the F3H promoter-GUS fusions may demonstrate the involvement of the Myb-like sequence in the expression of this gene. The structure and function of *R. sativus* L. F3H were analyzed and predicted using bioinformatics methods successfully. The results revealed that it is a convenient technique for cloning novel gene by searching EST database with homologous gene of model living things. To our knowledge, it was the first report on cloning of *R. sativus* L. F3H cDNA with in silico cloning. This research achievement will provide the theory and reference for flavonoid biosynthesis research in *R. sativus* L.

Acknowledgments This work was supported by the Hebei Higher School Science and Technology Research Youth Fund Project (No. QN2014328) and Hebei province Science and Technology Research and Development Program (No. 12212702).

References

1. Hichri I, Barrieu F, Bogs J et al (2011) Recent advances in the transcriptional regulation of the flavonoid biosynthetic pathway. J Exp Bot 62:2465–2483
2. Lepiniec L, Debeaujon I, Routaboul JM et al (2006) Genetics and biochemistry of seed flavonoids. Annu Rev Plant Biol 57:405–430
3. Halbwirth H (2010) The creation and physiological relevance of divergent hydroxylation patterns in the flavonoid pathway. Int J Mol Sci 11:595–621
4. Falginella L, Castellarin SD, Testolin R et al (2010) Expansion and subfunctionalisation of flavonoid 3′,5′-hydroxylases in the grapevine lineage. BMC Genom 11:562–579

5. Han Y, Vimolmangkang S, Soria-Guerra RE et al (2010) Ectopic expression of apple F3′H genes contributes to anthocyanin accumulation in the Arabidopsis tt7 mutant grown under nitrogen stress. Plant Physiol 153:806–820
6. Takahashi R, Dubouzet JG, Matsumura H et al (2010) A new allele of flower color gene W1 encoding flavonoid 3′5′-hydroxylase is responsible for light purple flowers in wild soybean Glycine soja. BMC Plant Biol 10:155–164

Chapter 14
The Comparative Study of Fermentation Capability of Wheat Beer Yeast

Jinxu Sun, Yue Wang and Cuicui Wang

Abstract In this study, the wheat beer fermentation performances of three beer yeasts S-15, S-16 and S-17 were comparatively studied. Here the best strain was selected for fermentation of wheat beer. Comparison of three strains had been experimented at fermentation capability, such as sugar-reducing rate, higher ethanol concentration, fermentation degree, agglutinating, and alcohol yield. Among these three yeasts, sugar-reducing rate of S-17 was the quickest and up to 0.1452 Brix/h. The data showed that S-17 could rapidly utilize sugar to ferment and was better in the brewing process to initiate fermentation. After 96 h of fermentation, alcohol yield of S-17 was slightly higher than other yeasts in agreement with sugar-reducing rate and up to 3.55 % (v/v). The real fermentation degree and the apparent fermentation degree of S-17 were also higher than the other two yeasts. Three beer yeasts belong to weak yeast coherency and the sequence of yeast coherency was S-17 > S-16 > S-15. The total content of high alcohol for S-17 was 126.39 mg/L, in which, the main ingredient is isopentanol and up to 56.48 %. The content of the high alcohol produced by S-17 during beer fermentation is in the normal range. Under the same conditions, strain S-17 showed faster fermentation speed, shorter fermentation period, higher alcohol degree, and stronger cohesion property. So S-17 was selected for wheat beer fermentation.

Keywords Wheat beer · Fermentation degree · High alcohol · Alcohol

14.1 Introduction

In recent years, world barley production had slumped because of dry climate, so barley price was higher than beforehand. A lot of beer companies were looking for some sort of magic bullet that would solve this problem. Based on this, wheat came

J. Sun (✉) · Y. Wang · C. Wang
Department of Life Sciences, Hengshui University, Hengshui 053000, Hebei, China
e-mail: bdsunjinxu@163.com

T.-C. Zhang and M. Nakajima (eds.), *Advances in Applied Biotechnology*,
Lecture Notes in Electrical Engineering 333, DOI 10.1007/978-3-662-46318-5_14

into view. Wheat can be used in place of barley and has long been known as the main raw materials for beer production. Wheat beer was also taking off rapidly in the emerging economies such as China. The first wheat beer in China was made and used in Shandong province.

Wheat beer was popular among consumers because of its wide source of raw materials, cheap price, mellow taste, and unique flavor. However, there are still many problems with respect to wheat beer fermentation technology, of which the most important is the strain selection for wheat beer fermentation. The content of ethanol and high alcohols produced by strain fermentation greatly affect the quality and flavor of wheat beer [1]. In this study, we determined the fermentation parameters of beer yeast strain S-15, S-16 and S-17, including the fermentation degree, high alcohol content, and alcohol content index, in different culture medium in order to select superior strains suitable for wheat beer fermentation.

14.2 Materials and Methods

14.2.1 Material and Equipment

Beer yeast strains, S-15, S-16 and S-17, were stored in Department of Life Sciences Laboratory of Hengshui University; P-type Pipette was purchased from Jia'an Analytical Instrument Company in Shanghai); gas chromatograph (7890A) was purchased from Agilent Technologies Instrument Co. Ltd.; isobutanol, *n*-butanol and isoamyl alcohol were obtained from Ji'nan Aohui Chemical Co. Ltd.

14.2.2 Medium

Yeast culture medium (YEPD) (w/v): natural pH, 121 °C, 0.1 MPa sterilized for 20 min.

Malt extract medium: the amount ratio of crushed malt to distilled water is 1:4, the medium was mashed according to certain route.

14.2.3 Standard Solution of High Alcohol

0.1 mL chromatography grade of *N*-propanol, isobutanol, isopentanol, *n*-butanol was accurately mixed with 60 % ethanol solution up to 10 mL to yield the 1 % mixed standard solution, and stored at 4 °C.

14.2.4 Determination of Alcohol Content by Rapid Oxidation Method

As described in the literature [2, 3], distilled alcohol may be oxidized by excess potassium dichromate to glycolic acids under acidic conditions:

$$2C_2H_5OH + 2{Cr_2O_7}^{2-} + 16H^+ \rightarrow 4Cr^{3+} + 3CH_3COOH + 11H_2O$$

The remaining potassium dichromate was reduced by potassium iodide:

$${Cr_2O_7}^{2-} + 6I^- + 14H^+ \rightarrow 2Cr^{3+} + 3I_2 + 7H_2O$$

Precipitated iodine was titrated by standard sodium hyposulfite $I_2 + 2{S_2O_3}^{2-} \rightarrow 2I^- + {S_4O_6}^{2-}$.

Alcohol concentration was calculated by dose of sodium hyposulfite.

14.2.5 Determination of the Fermentation Degree

(1) Determination of the appearance fermentation degree

1 g yeast mud is added in an Erlenmeyer flask filled with 150 mL wort, and the flask was delivered to the incubator for fermentation. The temperature was set at 25 °C. The flask was shaken once every 8 h and removed after being incubated for 3–4 days. The yeasts were removed by filtration and the proportion of fermentation broth measured, then the residual extract concentration was calculated.

(2) Determination of real fermentation degree

After fermentation, the yeasts were removed from the wort by filtration and the filtrate was heated to evaporate the ethanol by a simmer until the filtrate accounted for 1/3 of the original volume. The original volume was restored by adding distilled water, then the specific gravity was determined and the residual extract concentration calculated.

14.2.6 Determination of Cohesion Property

1 g of processed yeast sample was added and suspended in a centrifuge tube supplemented with 10 mL acetate buffer. The yeast suspension was heated in a water bath at 20 °C for 20 min. The tubes were gently shaken for 5 min to make the yeasts resuspended, and then left to stand. At 20-min intervals, the volume of

precipitated yeasts was recorded once at 1 min. The accumulated deposition amount of the yeasts up to 10 min was defined as Burns Value [4]. This experiment is known as the Burns Test [5]. The volume of yeast sedimentation >1.0 mL is defined as strong agglutination, while the volume <0.5 mL, weak agglutination.

14.2.7 Beer Fermentation Experiment

Wort concentration: 10 Brix; yeast inoculum: 10 %; fermentation temperature: 20 °C; fermentation period: 4 days; main fermentation period: the first 2 days. Timing sampling was performed to measure the fermentation performance.

14.2.8 CO_2 Weightlessness Experiment [6]

The flask supplemented was weighed with distilled water and fermented liquid each 12 h and calculated the weight loss of CO_2.

14.2.9 Determination of Fermentation Speed

135 mL of 10 Brix wort was added into a 250 mL sterilized erlenmeyer flask. The seed liquid was inoculated at a ratio of 10 %, and fermented at 20 °C. The concentration of the fermentation liquid was determined everyday and records made for consecutive comparison.

14.3 Results and Analysis

14.3.1 Fermentation Performance Comparison of Different Strains

Wheat beer fermentation yeasts S-15, S-16 and S-17 were selected for this study. Fermentation speed, alcohol content, fermentation degree, and high alcohol content of the three yeasts were compared to select the best strain for beer fermentation.

14.3.1.1 Fermentation Speed

After expanding culture, the selected strains of beer yeasts S-15, S-16, and S-17 underwent fermentation culture (10 % inoculation, fermentation temperature 20 °C,

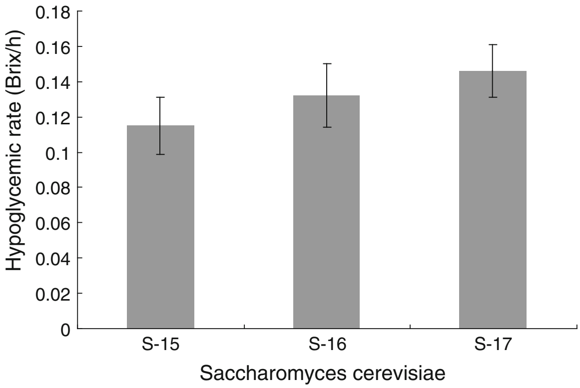

Fig. 14.1 The hypoglycemic rate comparing of three brewer yeast for reducing sugar in 48 h

liquid volume 75 %) for 48 h. Then sugar content of the fermentation liquid was determined and hypoglycemic rate was simultaneously calculated. The results are shown in Fig. 14.1.

Figure 14.1 showed that of the three strains of beer yeast cultured for 48 h, strain S-17 exhibited maximum hypoglycemic rate of 0.1452 Brix/h. The results indicate that strain S-17 can quickly utilize sugar for fermentation.

Quick fermentation initiation and rapid fermentation mediated by the strain S-17 is beneficial for beer fermentation. So, compared to strains S-15 and S-16, strain S-17 is more advantageous for wheat beer fermentation.

After expanding culture, the selected strains S-15, S-16 and S-17 were inoculated in the wheat beer fermentation medium and incubated for 96 h. The sugar content was determined at each 8 h, and the result is shown in Fig. 14.2.

The results show that the three strains were at a main fermentation stage within the first 48 h. Strain S-17 exhibited the fastest hypoglycemic speed, followed by strains S-16 and S-15. After 48 h fermentation, the three strains entered the post fermentation period, during which period, all of the three strains showed slow hypoglycemic speed with little change. After 96 h, reducing sugar of strain S-17 fell to 2.68 Brix. In the

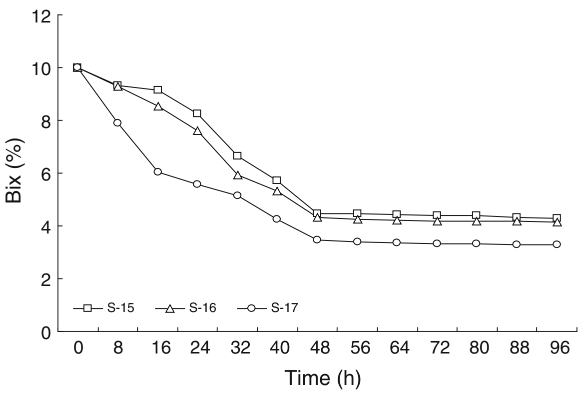

Fig. 14.2 The reducing sugar curve of three brewer yeasts

fermentation process, all beer yeasts showed an adaptation period after being inoculated in wort, thus, strain with fast fermentation initiation and short adaptation period will soon become the dominant bacteria. No bacteria contamination is conducive to fermentation. Comparison of hypoglycemic correlation curves of the three strains revealed that strain S-17 was suitable for the fermentation production.

14.3.1.2 Alcohol Comparison

After expanding culture, the selected strains of beer yeasts S-15, S-16 and S-17 underwent fermentation culture (10 % inoculation, fermentation temperature 20 °C, liquid volume 75 %) for 96 h. Then the alcohol content was determined and the result is shown in Fig. 14.3.

The data revealed that the alcohol content produced by the three strains showed minor differences. Relatively, the alcohol content of strain S-17, was more than that of the other two strains and reached 3.55 % (v/v), which is consistent with the hypoglycemic results.

14.3.1.3 Comparison of Fermentation Degree

After fermentation for 96 h, the real fermentation degree and the apparent fermentation degree of the three strains were determined. The results are shown in Fig. 14.4. The data showed that the apparent and real fermentation degree of strain S-17 is higher than the other two strains, which indicates that strain S-17 showed better fermentation performance.

14.3.1.4 Cohesion Comparison

Cohesion phenomenon, which is one of the main physiological characteristics of yeast, has been found and applied for a long time. Different yeast strains exhibited

Fig. 14.3 The alcohol content comparing of three brewer yeast

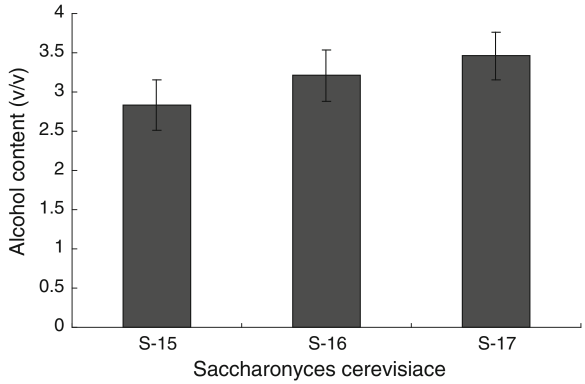

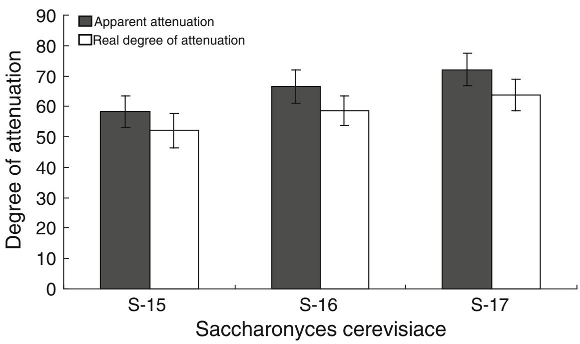

Fig. 14.4 The fermenting degree comparing three brewer yeasts

large differences in cohesion property. The sedimentation speed is quick for the yeast with strong cohesion, and this kind of yeast is easily separated from fermented liquid, and vice versa. Thus, when selecting fermentative strains, yeast with moderate cohesion performance should be recommended. The best strain could not only achieve a high fermentation degree but shows high sedimentation speed, which is easy to separate [7]. The cohesion property of the three yeasts after fermentation was determined by Burns Test as shown in Fig. 14.5. The test showed that the selected three yeast strains all exhibited weak cohesion, wherein strain S-17 showed slight stronger coherency, and strain S-15 was the weakest. Through artificial evaluation, the order of the cohesion effect of the three strains after fermentation was S-17 > S-16 > S-15.

14.3.1.5 Overall Fermentation Characteristics Comparison of the Three Yeast Strains

After fermentation for 96 h, overall fermentation index comparison of the three yeasts is shown in Table 14.1.

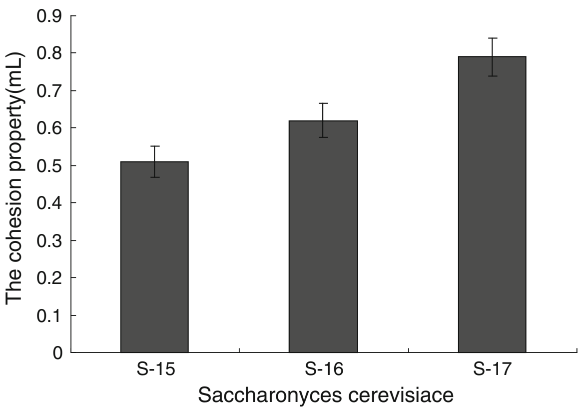

Fig. 14.5 The cohesion comparing of three brewer yeasts

Table 14.1 The fermentability comparing of three brewer yeasts

Strain	Brix (v/v, %)	Apparent attenuation (%)	Real degree of attenuation (%)	Cohesion (mL)
S-17	3.55	72.35	66.80	0.8
S-16	3.15	66.40	58.25	0.6
S-15	2.89	57.12	50.21	0.5

Table 14.1 shows that strain S-17 exhibited faster fermentation speed, shorter fermentation cycle, higher alcohol content, higher fermentation degree, and stronger coherence, compared to the other two strains. Therefore, strain S-17 was selected as the starting strain for subsequent experiments.

14.3.2 *Determination of High Alcohol Content of Strains S-17 During Fermentation*

As one of the main sources of beer aroma, high alcohols endow beer rich taste and make the wine full-bodied. But excessive high alcohols will affect the taste of beer. The content of senior alcohols was generally 50–150 mg/L in the common beer of low temperature fermentation. The content of senior alcohols exceeded 100 mg/L will make the beer smelly. Therefore, in the beer production process, higher alcohol content must be controlled at a proper level by a series of measures, including yeast screening, raw materials selection and match, and fermentation conditions control, etc., among which, the yeast strain is the main factor affecting the formation of high alcohol content. Thus, selection of beer yeast suitable for fermentation is of vital importance.

After the fermentation of strain S-17, the content of high alcohols was determined. As can be seen from Fig. 14.6, the high alcohols content of strain S-17 after

Fig. 14.6 The fusel oil content of S-17 after fermenting

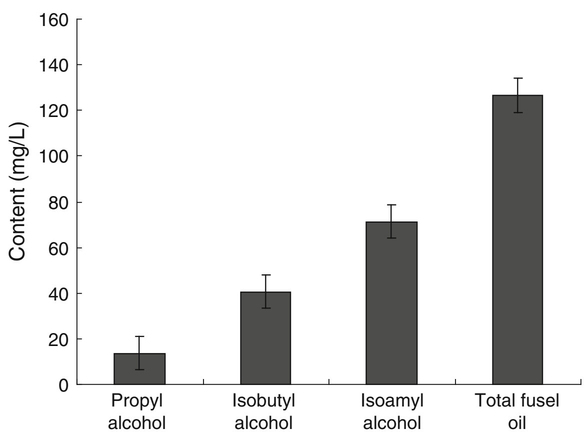

fermentation was 126.39 mg/L, wherein the isopentanol content was most abundant, accounting for 56.48 % of the total amount. The high alcohol content was within the normal range of beer, but slightly higher. High senior alcohol content is disadvantageous to human health and affects the beer flavor. Thus, to make the strain suitable for industrialized application, the content of high alcohols should be reduced.

14.4 Conclusion

In this study, the fermentation performance of three strains of wheat beer fermentation yeast S-15, S-16, and S-17 were compared. Of the three strains, S-17 exhibited fast fermentation speed, short fermentation cycle, high alcohol content, high fermentation degree, and strongest cohesion under the same conditions. High alcohols content produced by the strain S-17 reached a total amount of 126.39 mg/L, wherein the content of isoamyl alcohol was most abundant. The high alcohol content was within the normal range of beer, though a little higher. High content of senior alcohols would bring about unhealthy impacts on the human body and influence the beer flavor. Therefore, in order to make industrialized application of the yeast strain, the content of high alcohols should be decreased.

Acknowledgments This work was supported by the Science and Technology Research Project for Hebei Higher Education (Z2013091).

References

1. Yuan Z, Zhang BS, Ma QY et al (2010) Mutation breeding of yeast with high pressure technology for whole wheat beer and it sapplication. China Brew 12:33–37
2. Wang YN, Xiao DG (2002) A rapid determination method of alcohol and real fermentation degree in beer. Liquor Making 29(6):84–86
3. Jiao J, Ge XX, Zhou SM et al (2012) Comparison of the fermentation properties of top-fermented wheat beer yeasts. China Brew 1:147–150
4. Cai Y, Mu Q, Wang ZY et al (2008) Construction of self-cloning industrial brewing yeast with high-glutathione production and low-ADH II enzyme activity. Microbiology 8:1171–1175
5. Wu YM, Wang DL (2007) Screening of the medium flocculablity by Laser-LiCl cooperative mutagenesis. Liquor Making 2:81–83
6. Peter B, Ding HY (2011) Extracts and constituents of rubus chingii with 1,1-Diphenyl-2-picr ylhydrazyl (DPPH) free radical scavenging activity. Food Eng 12:12–15
7. Yi QP, Li JN (2013) Bear yeast and high concentrated to screen of fusion strains with Qingdao yeast for high concentration brewing yeast and 100 L fermentation analysis. Sci Technol Food Ind 2:95–98

Chapter 15
Screening of Dual Defects Strain and Effects on L-Isoleucine Production in *Escherichia coli* NML

Linan Yu, Huiyan Liu, Haitian Fang and Qing Wu

Abstract Original strain *Escherichia coli* N12 with lifting the repression of L-isoleucine was mutated mutagenesis by diethylsulfate (DES), then L-isoleucine producing strain named *E. coli* NML were obtained. The effects of *E. coli* K12, N12, and NML in fermentation process on biomass, yield of L-isoleucine and glucose consumption rate were studied by carrying out fed-batch fermentation by analyzing the metabolic sysnthesis process. At 48 h, L-isoleucine production in the fermentation medium of N12 and NML was 2.25 and 4.64 g/L, respectively, and it was not detected in *E. coli* K12. Results show that mutant strains with dual genetic markers (Met^{-} + Leu^{-}) can help with the synthesis of L-isoleucine, which also provide some frame of reference for the production of other amino acids.

Keyword *Escherichia coli* NML · Screening · L-Isoleucine · Production

15.1 Introduction

L-Isoleucine (L-Ile), one of the eight essential amino acids and one of the three branched-chain aliphatic amino acids (BCAAs) that are essential substrates for protein synthesis in all organisms, holds an important place in the amino acid market share [1, 2]. However, productive capacity of L-isoleucine cannot meet the huge market of China. Traditionally, strain improvement was achieved mainly by multiple rounds of random mutagenesis and selection, which are still very useful nowadays [3–5]. In *E. coli*, Ile is synthesised from aspartate by a 10-step reaction (Fig. 15.1) [6, 7]. The first 5 reactions convert L-aspartate to L-threonine, and the second 5 reactions convert L-threonine to L-Ile (Fig. 15.1). Several enzymes in the pathway are regulated by feedback inhibition. Aspartate kinase (AK), homoserine dehydrogenase (HD), and homoserine kinase (HK) are inhibited by L-threonine,

L. Yu · H. Liu · H. Fang (✉) · Q. Wu
Bioengineering Laboratory, Agricultural College of Ningxia University,
Yinchuan 750021, China
e-mail: fanght2014@163.com

T.-C. Zhang and M. Nakajima (eds.), *Advances in Applied Biotechnology*,
Lecture Notes in Electrical Engineering 333, DOI 10.1007/978-3-662-46318-5_15

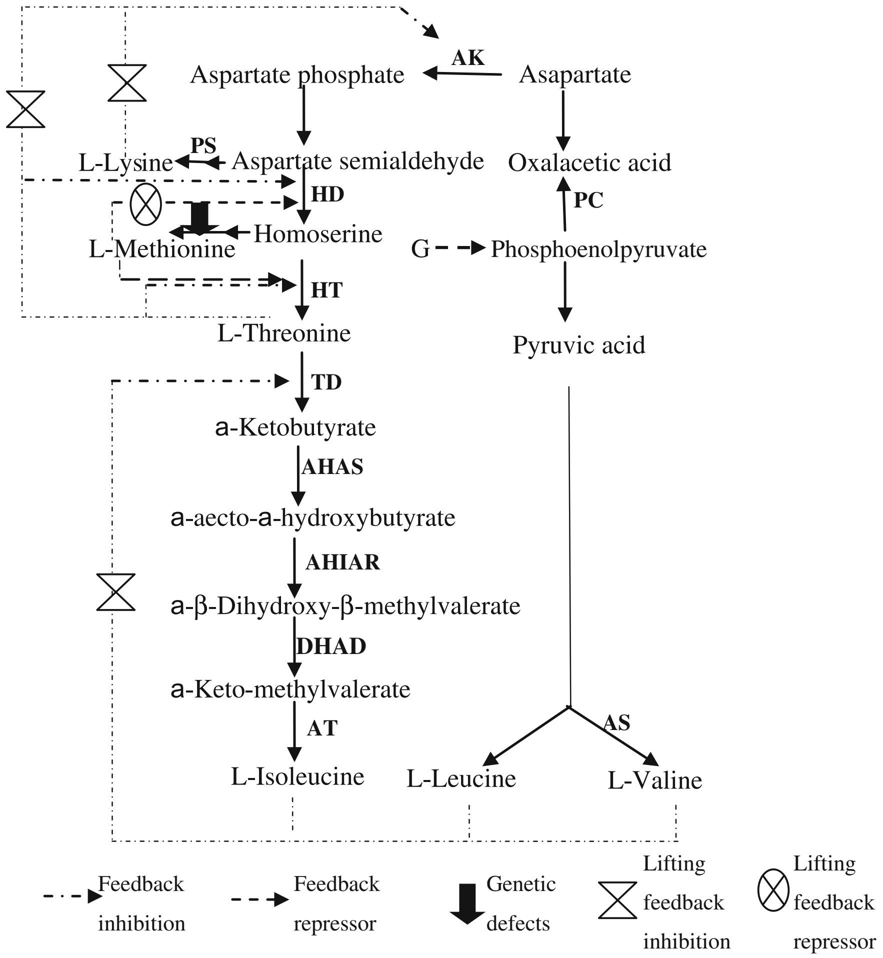

Fig. 15.1 Biosynthesis pathway of L-isoleucine in *Escherichia coli*. *G* Glucose; *AK* aspartate kinase; *ASD* aspartyl semialdehyde dehydrogenase; *HD* homoserine dehydrogenase; *HK* homoserine kinase; *TS* threonine synthase; *TD* threonine dehydratase; *AHAS* acetohydroxy acid synthase; *AHIAR* acetohydroxy acid isomeroreductase; *DHAD* dihydroxy acid dehydratase; *AT* branched chain acid aminotransferase

threonine dehydrogenase (TD) is inhibited by L-Ile, and acetohydroxy acid synthase (AHAS) is inhibited by all three branched-chain amino acids (Fig. 15.1). Because of its longer biosynthesis pathway and tighter regulation, bacterial strains for L-Ile production have not been developed as well as those for the production of amino acids which have a simpler biosynthesis pathway, such as L-lysine [8–10]. Therefore, to improve the efficiency of Ile production, rational metabolic engineering strategies should be implemented.

To accumulate more L-isoleucine, cutting off certain metabolic pathways of other amino acids is important. In this paper, we obtained NML that the synthesis route of methionine and leucine were cutted by mutating by diethylsulfate (DES) with *E. coli* N12 with analog resistance and studied the changes of biomass, glucose consumption rate, and production of L-isoleucine in the fermentation process. We obtained *E. coli* NML by mutation screening for defects of methionine, lysine, and leucine in *E. coli* N12 with diethylsulfate (DES) by analyzing the pathway and regulation of L-isoleucine biosynthesis. The strategies and researchers for developing L-isoleucine over-producer by metabolic engineering way are proposed and reviewed [11].

15.2 Materials and Methods

Escherichia coli K12 and N12 were preserved in Bioengineering Laboratory of Ningxia University. Methionine (Met) and leucine (Leu) were from Sigma.

The complete medium (CM) contained glucose (5 g/L), tryptone (10 g/L), sodium chloride (5 g/L), and agar (25 g/L). The minimal medium (MM) contained glucose (10 g/L), $(NH_4)_2SO_4$ (1.5 g/L), $KH_2PO_4{\cdot}3H_2O$ (1.5 g/L), $MgSO_4{\cdot}7H_2O$ (0.5 g/L), vitamin H (50 μg/L), $MnSO_4{\cdot}H_2O$ (0.01 g/L), $FeSO_4{\cdot}7H_2O$ (0.01 g/L), and agar (20 g/L) and then mixed methionine and/or leucine (0.1 g/L) in MM to be supplemental medium (SM). The production medium contained glucose (10 g/L), $(NH_4)_2SO_4$ (3.5 g/L), $MgSO_4{\cdot}7H_2O$ (0.05 g/L), $KH_2PO_4{\cdot}3H_2O$ (0.1 g/L), and corn steep liquor (15 ml/L).

The Ile production experiments pick out a single point of access to the colonies corresponding basic medium and selective medium after handling 30 min by 1 % diethyl sulfate (DES) and then verify that the amino acid-deficient strain through filter paper method [12]. *E. coli* cells were precultured in seed medium at 36 °C and 200 rpm for 18–24 h and measured OD_{600}. The preculture was inoculated into 50 ml fermentation medium to a final optical density (OD_{600}) of 1.0 and shaken at 200 rpm for 48 h at 36 °C [13, 14]. Samples were taken every 4 h to determine residual glucose with a biosensor (Institute of Biology, Shandong Academy of Science, China). The biomass was calculated by measuring the OD of the fermentation broth using a spectrophotometer at 600 nm and one unit OD 600 nm was equal to 0.3 g in 1 L of dry cell weight (DCW) [15, 16]. The amino acid concentration was determined using reversed-phase high-pressure liquid chromatography [11, 17].

15.3 Results and Analysis

15.3.1 Screening of Genetic Defects on L-Isoleucine Producing Strain

A was determined as the deficient strain when the cells grown around the filter paper containing the amino acid A and did not grow around B [18]. Figure 15.2

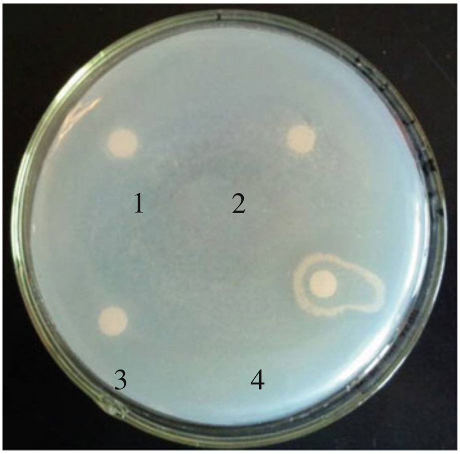

Fig. 15.2 The result of auxotrophic test. NML (Met^{-} + Leu^{-}). *1* methionine; *2* leucine; *3* lysine; *4* mixing of three amino acid

shows that the strain grown around the sterile filter that contained methionine, leucine, and mixture of methionine, leucine, and lysine did not grow surrounding the sterile filter paper involves lysine, then it was NML (Met^{-} + Leu^{-}).

15.3.2 Comparison of Growth and Yield of L-Isoleucine in Different Mutants

To study the effect of genetic defects on L-Ile biosynthesis, N12 and NML, the strains selection by mutation were generated, analyzed, and compared to the initial *E. coli* K12.

The growth of these strains in fermentation medium revealed that the K12, N12, and NML strains exhibited similar growth rates (Fig. 15.3a). After 48 h cultivation,

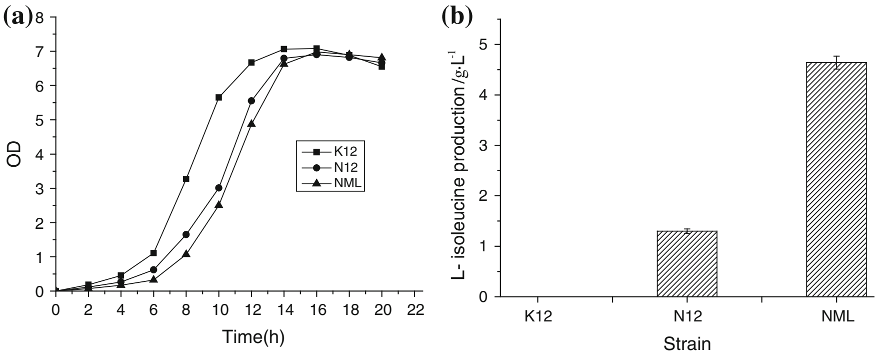

Fig. 15.3 Fermentation of *E. coli* K12, N12 and NML. **a** Growth of different mutant strains; **b** production of L-isoleucine in different mutant strains

the production of L-Ile in these *E. coli* strains was determined (Fig. 15.3b). L-Ile production in the fermentation medium of N12 and NML was 2.25 and 4.64 g/L, respectively, which was higher than the production of the initial strain K12 (Not detected), which indicated that auxotrophic mutants contributed to the synthesis of Ile and also provided a reference for the production of other amino acids.

15.3.3 Fermentation Processing Control of L-Isoleucine in Mutant Strain E. coli NML

The production of L-isoleucine is associated with growth status [14]. As shown in Fig. 15.4, 0–28 h, the rate of glucose consumption, biomass, and L-isoleucine production showed an increasing trend. 28–36 h, the rate of increase of biomass and L-isoleucine production slowed with the rate of consumption of sugar into the stationary phase. After 36 h, biomass and L-isoleucine production entered into the stationary phase with the rate of consumption of sugar declining rapidly.

15.4 Conclusion and Discussion

To improve the efficiency of Ile production, rational metabolic engineering strategies should be implemented. Breeding of auxotrophic and structural analogues resistant mutants is conductive to accumulate L-Ile by changing the biosynthesis of

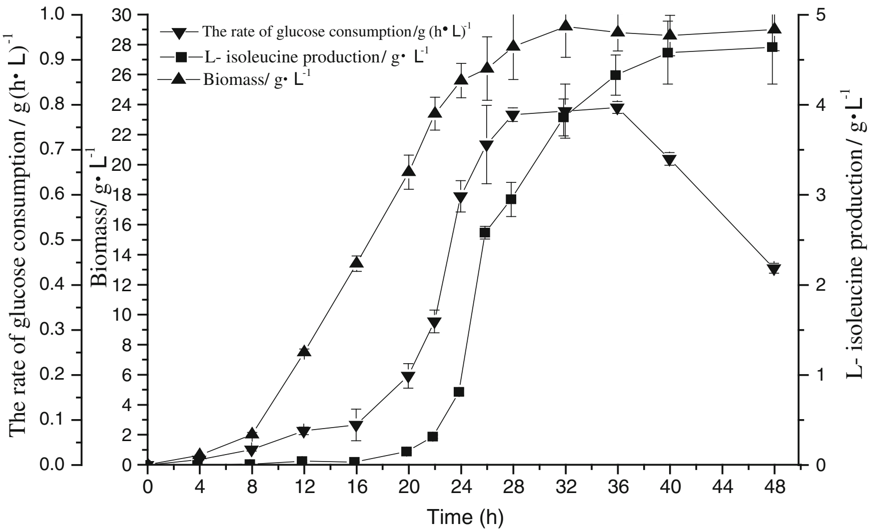

Fig. 15.4 The curve of L-isoleucine fermentation processing in *E. coli* NML

L-Ile [19, 20]. It accumulated more L-Ile by filtering strains with auxotrophic and structural analogs resistant mutants [18, 21]. In this study, L-Ile production in the fermentation medium of NML was higher than *E. coli* N12 and *E. coli* N12 was higher than the wild type K12. At 48 h, production of L-Ile in the fermentation medium of *E. coli* N12 and NML was 2.25 and 4.64 g/L, respectively, and it was not detected in *E. coli* K12.

In *E. coli* N12, lifting of the feedback repression of L-isoleucine was conducted to accumulate more L-isoleucine than the wild type K12. In *E. coli* NML, the biosynthesis of methionine and leucine was done by mutating in *E. coli* N12, which led to increase in L-isoleucine production. These results suggest that breeding of auxotrophic strain is a useful metabolic engineering strategy to improve L-isoleucine biosynthesis and also provide some reference for other amino acids.

Acknowledgments We thank colleagues for critical reading of the manuscript and providing valuable suggestions. This work was supported by the Key Technology R&D Program of Ningxia (2012).

References

1. Moorthi PP, Gunasekaran S, Ramkumaar GR et al (2014) Vibrational spectroscopic studies of isoleucine by quantum chemical calculations. Spectrochim Acta Part A Mol Biomol Spectrosc 124:365–374
2. Yin LH, Hu XQ, Xu DQ et al (2012) Co-expression of feedback-resistant threonine dehydratase and acetohydroxy acid synthase increase L-isoleucine production in Corynebacterium glutamicum. Metab Eng 14:542–550
3. Chen XZ, Zhou L, Tian KM et al (2013) Metabolic engineering of *Escherichia coli*: a sustainable industrial platform for bio-based chemical production. Biotechnol Adv 31:1200–1223
4. Portnoy VA, Bezdan D, Zengler K (2011) Adaptive laboratory evolution-harnessing the power of biology for metabolic engineering. Curr Opin Biotechnol 22:590–594
5. Sonderegger M, Sauer U (2003) Evolutionary engineering of Saccharomyces cerevisiae for anaerobic growth on xylose. Appl Environ Microbiol 69:1990–1998
6. Chen N, Zhang KX, Zhang B et al (2007) Metabolic control fermentation. China Light Ind. Press 7(1):288–292
7. Park JH, Lee SY (2010) Metabolic pathways and fermentative production of L-aspartate family amino acids. J Biotechnol 5:560–577
8. Schrumpf B, Eggeling L, Sahm H (1992) Isolation and prominent characteristics of an L-lysine hyperproducing strain of *Corynebacterium glutamicum*. App Microbiol Biotechnol 37:566–571
9. Vrljic M, Kronemeyer W, Sahm H, Eggeling L (1995) Unbalance of L-lysine flux in *Corynebacterium glutamicum* and its use for the isolation of excretion-defective mutants. J Bacteriol 177:4021–4027
10. Georgi T, Rittmann D, Wendish VF (2005) Lysine and glutamate production by Corynebacterium glutamicum on glucose, fructose and sucrose: roles of malic enzyme and fructose-1, 6-bisphosphatase. Metab Eng 7:291–301
11. Shi F, Huan XJ, Wang XY et al (2012) Overexpression of NAD kinases improves the L-isoleucine biosynthesis in *Corynebacterium glutamicum ssp. Lactofermentum*. Enzym Microb Technol 51:73–80

12. Javed S, Asgher M, Sheikh MA et al (2010) Strain improvement through UV and chemical mutagenesis for enhanced citric acid production in molasses-based solid state fermentation. Food Biotechnol 24(2):165–179
13. Xie XX, Xu LL, Shi JM (2012) Effect of transport proteins on L-isoleucine production with the L-isoleucine-producing strain *Corynebacterium glutamicum* YILW. J Ind Microbiol Biotechnol 39:1549–1556
14. Lorenz E, Klatte S, Wendisch VF (2013) Reductive amination by recombinant *Escherichia coli*: whole cell biotransformation of 2-keto-3-methylvalerate to L-isoleucine. J Biotechnol 168:289–294
15. Peters-Wendisch PG, Wendisch VF, Paul S, Eikmanns BJ, Sahm H (1997) Microbiol 143:1095–1103
16. Wang J, Wen B, Wang J et al (2013) Enhancing L-isoleucine production by *thrABC* overexpression combined with alaT deletion in *Corynebacterium glutamicum*. Appl Biochem Biotechnol 171:20–30
17. Blombach B, Schreiner ME, Holatko J, Bartek T, Oldiges M, Eikmanns BJ (2007) L-valine production with pyruvate dehydrogenase complex-deficient *Corynebacterium glutamicum*. Appl Environ Microbiol 73:2079–2084
18. Ikeda S, Fujita I, Yoshinaga F (1976) Screening of L-isoleucine produces among Methionine resistant mutants of L-threonine producing bacterium. Agric Biol Chem 40:511–516
19. Herman T et al (1996) Mechanism and regulation of Ile in CG. Appl Environ Microbiol 9:3238–3244
20. Boles E, Ebbighausen H et al (1993) Unusual regulation of the uptake system for branched-chain amino acid in *Cornebacterium glutamicum*. Arch Microbiol 159:147–152
21. Hermann T (2003) Industrial production of amino acid by coryneform bacteria. J Biotechnol 104(1–3):155–172

Chapter 16
Effect of *MIG1* Gene Deletion on Lactose Utilization in Lac$^+$ *Saccharomyces cerevisiae* Engineering Strains

Jing Zou, Xuewu Guo, Jian Dong, Cuiying Zhang and Dongguang Xiao

Abstract A lactose-consuming *Saccharomyces cerevisiae* strain EY-510 was constructed by expressing *LAC4* and *LAC12* gene of *Kluyveromyces marxianus* in the host strain AY-5. *Mig1* is a zinc finger DNA-binding protein that plays a critical role on glucose repression in *S. cerevisiae*. In order to study in anaerobic condition the degree of glucose repressing galactose metabolism, a deletion fragment *MIGIA-KanMX-MIG1B* was transformed into AY-5, resulting a Δ*mig1* strain DY-510. In order to study whether the presence of glucose inhibits the consumption of lactose, a Lac$^+$ Δ*mig1* strain RY-510 was constructed by transforming the deletion fragment into EY-510. Galactose consumption was initiated at higher glucose concentrations in the *MIG1* deletion strain RY-510 and DY-510 than in the corresponding wild-type strain AY-5 and EY-510, wherein galactose was consumed until glucose was completely depleted in the mixture. On lactose medium, the duration of fermentation for RY-510 was 168 h, whereas the duration for EY-510 was 252 h. The lactose uptake rate was 0.357 g/L/h for RY-510 and that was 0.238 g/L/h for EY-510. The ethanol productivity of RY-510 was 0.127 g/L/h and that was 0.085 g/L/h for EY-510. And in cheese whey powder solution medium, RY-510 was able to produce 30.25 g/L ethanol from 76.8 g/L initial lactose in 190 h, during which EY-510 was able to consume 70.8 % of the initial lactose and produced 24.14 g/L ethanol. Therefore, relieving glucose control provides an approach for constructing lactose-consuming *S. cerevisiae*.

Keywords *MIG1* · Lac$^+$ *S. cerevisiae* · Glucose repression · Whey cheese

---

J. Zou · X. Guo · J. Dong · C. Zhang · D. Xiao (✉)
Key Laboratory of Industrial Fermentation Microbiology, Ministry of Education,
Tianjin Industrial Microbiology Key Laboratory, College of Biotechnology,
Tianjin University of Science and Technology, Tianjin 300457
People's Republic of China
e-mail: xdg@tust.edu.cn

J. Zou
e-mail: zoujing520315@126.com

J. Zou
College of Food Science and Technology, Hebei Normal University of Science
and Technology, Qinhuangdao 066000, People's Republic of China

T.-C. Zhang and M. Nakajima (eds.), *Advances in Applied Biotechnology*,
Lecture Notes in Electrical Engineering 333, DOI 10.1007/978-3-662-46318-5_16

16.1 Introduction

Fuel ethanol fermentations from different renewable resource have received high attention due to increasing petroleum shortage. Whey is a by-product of milk industry and the annual world production is 160 million tons. Whey contains 5 % lactose, which means 8 million tons of lactose needs disposal each year. There are much research on using whey to produce single cell protein or bioethanol because of its high carbohydrate content and availability [1, 2].

Only a few yeast strains are able to ferment lactose to produce ethanol, including, e.g., *Kluyveromyces lactis*, *Kluyveromyces marxianus*, and *Candida pseudotropicalis* [3]. The most common distillers yeast *Saccharomyces cerevisiae*, however, cannot ferment lactose since it lacks both lactose permease and β-galactosidase, which are responsible to transport the lactose into cytoplasm and hydrolyze lactose to monsaccharides. These characteristics prevent *S. cerevisiae* from fermenting cheese whey to ethanol. Most of *the Kluyveromyces* genus is able to ferment lactose which is present in cheese whey. However, *S. cerevisiae* is more excellent on ethanol production than that of *Kluyveromyces*. Alternatives have been sought, such as hydrolyzed lactose by β-galactosidase from another microorganism and subsequent fermentation by *S. cerevisiae*, protoplast fusion between *Saccharomyces* and *Kluyveromyces*, or expression of heterologous genes in *S. cerevisiae*, which are responsible for hydrolyzing lactose.

A Lac^+ strain EY-510 was constructed which expressed two key genes *LAC4* and *LAC12* of *K. marxianus* on wild-type *S. cerevisiae* strain AY-5. As lactose was first hydrolyzed into glucose and galactose, the presence of glucose can inhibit the transcription of *GAL* genes which encode the enzymes needed by galactose metabolic pathway, i.e., glucose repression. *Mig1*, a zinc finger class of DNA-binding protein, plays a critical role in glucose repression on galactose metabolism. In this work, the *MIG1* gene of the Lac^+ strain EY-510 was deleted, resulting RY-510. The ability of the two lactose-consuming strains to utilize lactose was examined using anaerobic shake flasks. In addition, the degree of glucose repression was studied in anaerobic batch cultivations on glucose–galactose mixture medium.

16.2 Materials and Methods

16.2.1 Strains, Media, and Growth Conditions

The yeast strains used in this study are listed in Table 16.1. Yeast strain AY-5 and TY-3 and *Escherichia coli* strain DH5α used in this study were obtained from the Yeast Collection Center of Tianjin Industrial Microbiology Key Laboratory of Tianjin University of Science and Technology, P.R. China. *Escherichia coli* strain DH5α was grown in LB broth with ampicillin for plasmid maintenance. *S. cerevisiae* and *K. marxianus* strains were incubated in YPD medium at 30 °C. The

Table 16.1 Yeast strains used in this study

Strains	Genotype	Source
AY-5		Guo et al. [5]
TY-5		Guo et al. [5]
EY-510	*ath1(1678, 2355): PGK-LAC12 nth1(1215, 1664): PGK-LAC4*	This study
RY-510	*ath1(1678, 2355): PGK-LAC12 nth1 (1215, 1664): PGK-LAC4 mig1 (499, 1123): KanMX*	This study
DY-510	*mig1(499, 1123): KanMX*	This study

recombination strains were screened on YPD medium supplemented with 1,000 μg/mL G418 and 250 μg/mL zeocin. Lactose fermentation media (containing 5 g/L $(NH_4)_2SO_4$, 1 g/L KH_2PO_4, 0.5 g/L $MgSO_4 \cdot 7H_2O$, 10 mL/L trace element solution, 1 mL/L vitamin solution, and 60 g/L lactose) was prepared according to the method by Verduyn [4] with slight modifications. The galactose and glucose media were prepared similar to lactose fermentation media, replacing lactose with the corresponding sugar. The sugar mixture media (containing 30 g/L glucose, 30 g/L galactose, 5 g/L $(NH_4)_2SO_4$, 1 g/L KH_2PO_4, 0.5 g/L $MgSO_4 \cdot 7H_2O$, 10 mL/L trace element solution, and 1 mL/L vitamin solution) was used to analyze the glucose repression exerted on galactose metabolism.

16.2.2 Plasmid and Strain Construction

The genomic DNA used as templates for DNA amplification was isolated from strains AY-5 and TY-3. The recombinant plasmid pUC-MABK used for *MIG1* deletion provided by Zhang et al. [6]. The construction of integrative plasmids pPNLZ and pPALK, which were constructed to express *LAC4* and *LAC12* genes of *K. marxianus* was described by Ref. [7]. The pPNLZ and pPALK plasmid were transformed into the AY-5 a/α, respectively, selecting for zeocin$^+$ and G418$^+$ mutant strains on resistance plates. Then, the G418 resistance gene was deleted through transforming the plasmid pGAPza expressing the Cre recombinase. Finally, the expected phenotypes of AY-5 a/α were selected and mated to obtain the hybrid EY-510. In order to study the effect of glucose repression on galactose–lactose metabolism, a recombinant cassette *MIG1A-Kan-MIG1B* fragment that was amplified from plasmid pUC-MABK was transformed into AY-5 a/α and EY-510 a/α, resulting DY-510 and RY-510, respectively. The purpose of construction of DY-510 was mainly to verify whether deletion of the *MIG1* gene could eliminate glucose repression on galactose metabolism. The recombination of the three plasmids was verified by PCR [8], and primers for verifying the recombination of plasmids, pPNLZ, pPALK, and pUC-MABK were listed in Table 16.2.

Table 16.2 Primers for verifying the recombination of plasmid pPNLZ, pPALK, and pUC-MABK

Plasmid name	Primer name	Sequence
pPNLZ	N up1	AGGTATGGTGGAGCATTTTATT
	N down1	TTTCGGTTAGAGCGGATGT
	N up2	GCTGTAGGTATCTCAGTTCGGT
	N down2	AACTTGGGTAGTGCTTTCTCC
pUC-MABK	R1-U	TACAAACTCCCACCCTCG
	R1-D	TCATTGGCAACGCTACCT
	R2-U	GCTGTAGGTATCTCAGTTCGGT
	R2-D	TGAAT CCGACTGAGAAATGG
pPALK	A up1	ATCGTCCCTATTCCATTTACTA
	A down1	CAAACCGTTATTCATTCGTG
	A up2	GCTGTAGGTATCTCAGTTCGGT
	A down2	AGTTTCTAATAGCGATACCACCA

16.2.3 Standard Solutions for the Medium Used

The trace element solution and the vitamin solution had the following compositions: Trace element solution: 3 g/L EDTA; 0.09 g/L $CaCl_2 \cdot 2H_2O$; 0.90 g/L $ZnSO_4 \cdot 7H_2O$; 0.60 g/L $FeSO_4 \cdot 7H_2O$; 200 mg/L H_3BO_3; 156 mg/L $MgCl_2 \cdot 2H_2O$; 80 mg/L $Na_2MoO_4 \cdot 2H_2O$; 60 mg/L $CoCl_2 \cdot 2H_2O$; 60 mg/L $CuSO_4 \cdot 5H_2O$; and 20 mg/L KI. The pH of the trace element solution was adjusted to 4.00 with NaOH, and autoclaved afterward.

Vitamin solution: 50 mg/L D-biotin; 200 mg/L *para*-amino-benzoic acid; 1 g/L nicotinic acid; 1 g/L Capantothenate; 1 g/L pyridoxine·HCl; 1 g/L thiamine·HCl; and 25 g/L *m*-inositol. The pH was adjusted to 6.5 and stored at 4 °C after sterile filtration.

16.3 Result and Discussion

16.3.1 Construction of MIG1 Deletion Mutant

The linearized pPNLZ, pPALK were transformed into AY-5, resulting a Lac^+ strain EY-510. Chromosomal DNA of EY-510 was prepared and used as a template for the PCR. A 1.7 kb fragment was amplified when using the forward primer (N-up1) upstream of *NTH1* together with the backward primer (N-down1) in the plasmid pPNLZ, which verified the existence of the linearized pPNLZ in the *NTH1* locus (Fig. 16.1a). In the same way, a 2,600 bp fragment was amplified using the forward primer N-up2 in the pPNLZ together with a down primer N-down2 in *NTH1* downstream (Fig. 16.1c). The recombination of the pPALK plasmids was verified

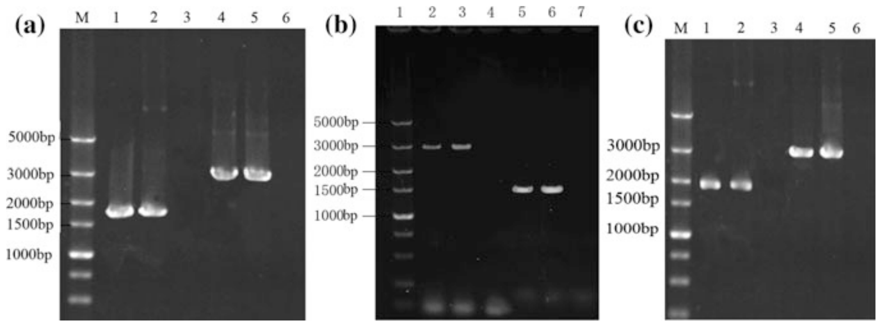

Fig. 16.1 Verification of the transformants of pPNLZ (**a**), pUC-MABK (**b**), and pPALK (**c**). **a** *M* is DL5000 marker; *1–2* a 1,700-bp fragment amplified from the EY-510 genome with N-up1 and N-down1 as primers; *3* no fragment amplified from the AY-5 genome with N-up1 and N-down1 as primers; *4–5* a 2,600 bp fragment amplified from the EY-510 genome with N-up2 and N-down2 as primers; *6* no fragment amplified from the AY-5 genome with N-up2 and N-down2 as primers. **b** *1* DL5000 maker; *2–3* a 1.5-kb fragment amplified from the mutant RY-510 with R2-U and R2-D as primers; *4* no PCR product amplified from the Lac$^+$ strain EY-510 with R2-U and R2-D as primers; *5–6* a 3-kb fragment amplified from the mutant RY-510 with R1-U and R1-D as primers; *7* no PCR product amplified from the Lac$^+$ strain EY-510 with R1-U and R1-D as primers. **c** M is DL5000 marker; *1–2* a 1,900-bp fragment amplified from the EY-510 genome with A-up1 and A-down1 as primers; *3* no fragment amplified from the AY-5 genome with A-up1 and A-down1 as primers; *4–5* a 2,900-bp fragment amplified from the EY-510 genome with A-up2 and A-down2 as primers; *6* no fragment amplified from the AY-5 genome with A-up2 and A-down2 as primers

through the same way and the verification fragment was shown in Fig. 16.1c. The verification of the recombinant cassette *MIG1A-Kan-MIG1B* fragment that was amplified from pUC-MABK by PCR and the result was shown in Fig. 16.1b.

16.3.2 Cultivation on Mixed Glucose–Galactose

In *S. cerevisiae*, glucose was exhausted before galactose. EY-510, RY-510, DY-510, and AY-5 were cultivated on the mixture of 30 g/L glucose and galactose to analyze the influence of glucose control on galactose metabolism in the anaerobic shake flask fermentations.

The sugar consumption can be divided into two phases for AY-5 (Fig. 16.2a). In the first phase, while glucose was present in the medium, the galactose consumption was inhibited. Until glucose in the mixture was completely consumed, the galactose just began to be utilized. The duration of cultivation for the AY-5 strain lasted about 114 h. The same phenomenon was also observed in strain EY-510, in which glucose was consumed before galactose (Fig. 16.2c). Although there was glucose repression in the two strains AY-5 and EY-510, the fermentation time was significantly different. The difference might be caused by the heterologous *LAC12* gene expressed in EY-510 which could help to transport galactose in *S. cerevisiae*

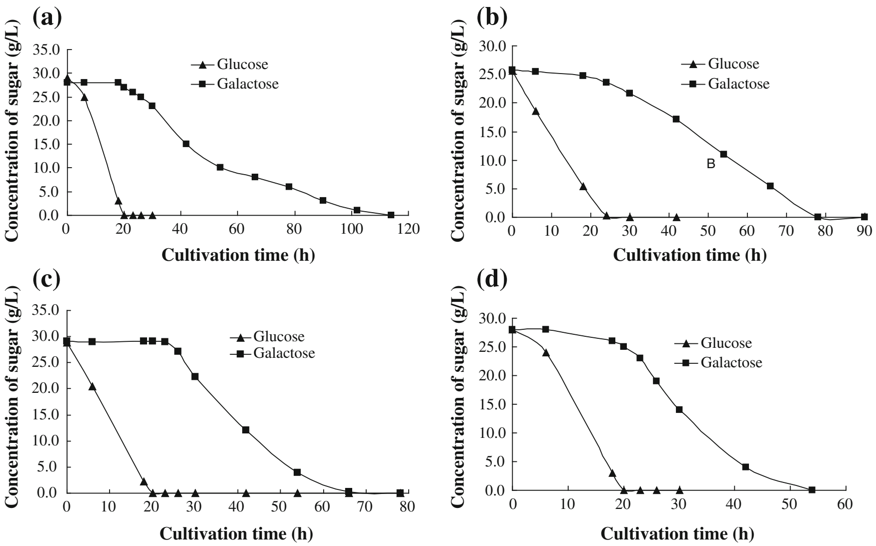

Fig. 16.2 Concentrations of glucose (*filled triangles*) and galactose (*filled squares*) during the anaerobic cultivation of strains **a** AY-5, **b** DY-510, **c** EY-510, and **d** RY-510 on a galactose–glucose mixture. After inoculation with 10 % fresh yeast cells was added into 150 mL galactose–glucose mixture medium, the residual concentration of glucose and galactose in the mixture medium was analyzed every 12 h until the total sugar was completely depleted. Glucose and galactose were detected by HPLC using an Aminex HPX-87H column (Bio-Rad) at 65 °C for separation, using 5 mM H_2SO_4 as the mobile phase at a flow rate of 0.6 mL/min, and were detected by a refractive index detector (Waters 410)

[6]. In strains DY-510, galactose metabolism was initiated despite the high glucose concentration, and the cultivation duration was 78 h, reduced by 34 % compared with the wild-type AY-5 (Fig. 16.2b). In RY-510, the same phenomenon was also observed that glucose and galactose were simultaneously utilized (Fig. 16.2d). As the exogenous *LAC12* gene expressed in RY-510, the fermentation duration of it was significantly shorter than that of DY-510 strain, reduced about 24 h. The data demonstrated that the deletion of *MIG1* gene had partly relieved glucose repression of galactose metabolism.

16.3.3 Characterization of Fermentation on Lactose

In the same culture condition, the two Lac$^+$ strains EY-510, RY-510 were cultured on lactose medium. The lactose utilized ability, fermentation period, and ethanol productivity were compared (Fig. 16.3). EY-510 was able to grow on lactose medium but the growth was slow. After 252 h of cultivation on 60 g/L lactose, the residual lactose was 0.24 g/L and the ethanol was 21.38 g/L. The lactose uptake rate

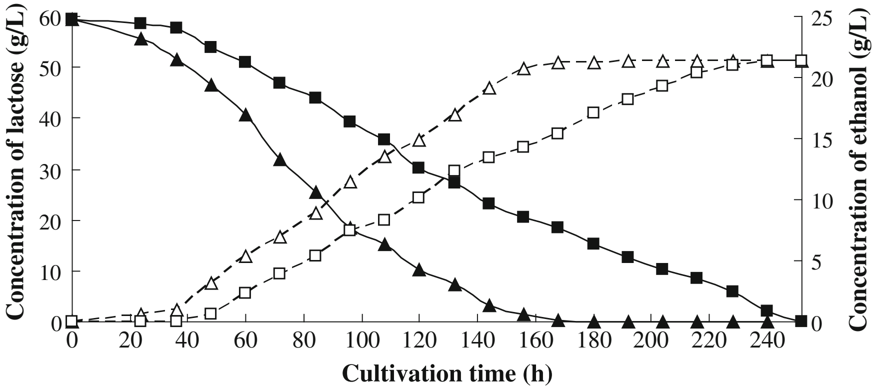

Fig. 16.3 Profiles of Lactose consumption (*solid symbols*, *solid line*) and ethanol production (*open symbols*, *dashed line*) in EY-510 (*solid* and *open squares*) and RY-510 (*solid* and *open triangles*). The duration of fermentation for the *MIG1* deletion strain was 168 h. The residual lactose was 0.15 g/L and the final concentration of ethanol was 21.34 g/L. However, the duration of fermentation for EY-510 was 252 h, the residual lactose was 0.24 g/L, and the concentration of ethanol was 21.38 g/L

of EY-510 was 0.238 g/L/h and the ethanol productivity was 0.085 g/L/h. The performance of RY-510, in which the *MIG1* gene was deleted, differed from that of EY-510 and the lactose was able to be depleted in 168 h. The residual lactose of RY-510 was 0.15 g/L and the final ethanol concentration was 21.34 g/L, which the ethanol productivity was 0.127 g/L/h and the lactose uptake rate was 0.357 g/L/h. The differing performance of RY-510 from EY-510 in utilizing lactose might be due to glucose repression. In EY-510, as glucose and galactose were liberated from lactose, glucose repressed galactose consumption, thereby affecting lactose consumption. The deletion of the *MIG1* gene in RY-510 removed the associated mechanism, accelerating the lactose consumption.

16.3.4 Characterization of Fermentation on Concentrated Cheese Whey Powder Solution (CWPS)

Two transformants were cultivated on CWPS which corresponds to 76.8 g/L initial lactose in the anaerobic shake flask fermentations. During the fermentation of RY-510, the lactose was nearly depleted after about 190 h, resulting in the production of 30.25 g/L ethanol, with a corresponding productivity of 0.159 g/L/h. The EY-510 was able to utilize lactose to produce ethanol in CWPS. During the fermentation, only 70.8 % lactose was utilized in 190 h and 24.14 g/L ethanol was produced. The ethanol productivity was 0.127 g/L/h. Therefore, RY-510 enables utilization of lactose in whey more efficiently to produce more ethanol than EY-510 (Fig. 16.4).

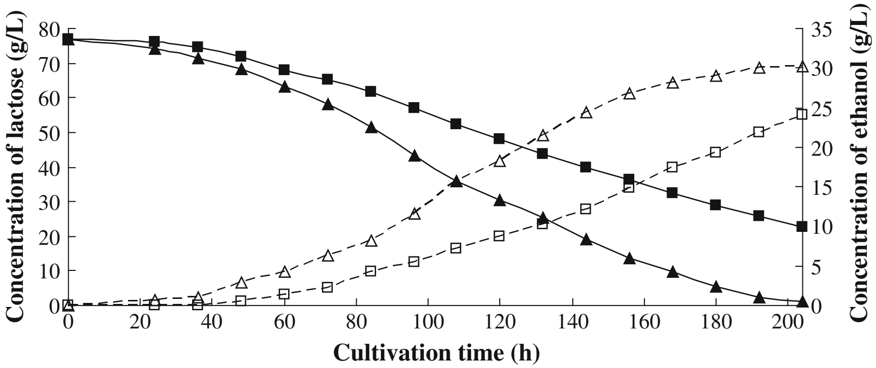

Fig. 16.4 Profiles of lactose consumption (*solid symbols*, *solid lines*) and ethanol production (*open symbols*, *dashed lines*) in RY-510 (*open* and *solid triangles*) and EY-510 (*solid* and *open squares*) during fermentation in CWPS. The duration of fermentation for the RY-510 was 190 h. The residual lactose was 1.98 g/L and the final concentration of ethanol was 30.25 g/L. However, in this duration for EY-510, the residual lactose was 22.45 g/L and the concentration of ethanol was 24.14 g/L

16.4 Conclusion

In *S. cerevisiae*, the presence of glucose affects the galactose metabolism. For the Lac$^+$ *S. cerevisiae*, the repression could not only inhibit the galactose utilization on the galactose–glucose mixture, but also affect the lactose consumption as equivalence glucose and galactose were liberated from lactose. While the *MIG1* gene was disrupted, this glucose repression was relieved and the lactose utilization was accelerated. Therefore, the fermentation period on lactose was reduced and the ethanol productive rate was increased. Thus, eliminating glucose repression provides a method for constructing a lactose-consuming *S. cerevisiae* strain.

References

1. Mawson AJ (1994) Bioconversions for whey utilization and waste abatement. Bioresour Technol 47(3):195–203
2. Guimaraes PMR, Teixeira JA, Domingues L (2010) Fermentation of lactose to bio-ethanol by yeasts as part of integrated solutions for the valorisation of cheese whey. Biotechnol Adv 28 (3):375–384
3. Fukuhara H (2006) Kluyveromyces lactis—a retrospective. FEMS Yeast Res 6(3):323–324
4. Verduyn C, Postma E, Scheffers WA, van Dijken JP (1990) Physiology of Saccharomyces cerevisiae in anaerobic glucose-limited chemostat cultures. J Gen Microbiol 136(3):395–403
5. Guo X, Zhou J, Xiao D (2010) Improved ethanol production by mixed immobilized cells of Kluyveromyces marxianus and Saccharomyces cerevisiae from cheese whey powder solution fermentation. Appl Biochem Biotechnol 160(2):532–538

6. Zhang Y, Xiao DG, Zhang CY, Sun X, Wu MY (2012) Effect of MIG1 gene deletion on glucose repression in baker's yeast. Adv Mater Res 396:1531–1535
7. Zou J, Guo XW, Shen T, Dong J, Zhang CY, Xiao DG (2013) Construction of lactose-consuming Saccharomyces cerevisiae for lactose fermentation into ethanol fuel. J Ind Microbiol Biotechnol 40:353–363
8. Ostergaard S, Olsson L, Johnston M, Nielsen J (2000) Increasing galactose consumption by Saccharomyces cerevisiae through metabolic engineering of the GAL gene regulatory network. Nat Biotechnol 18(12):1283–1286

Chapter 17
Enzyme Activity Analysis of Protease Produced by Marine Bacteria

Qi Zhang, Xihong He and Hao Liu

Abstract Proteolytic enzymes are ubiquitous in nature, found in all living organisms, and have been applied to many aspects of industry. In this study, 19 strains hydrolyzing protein were screened from deep-sea sediments, of which No. 9 strain has the largest protease activity. Based on morphological characterization and 16S rDNA gene sequences analysis, the strain was identified to be *Bacillus subtilis*. The optimum medium for producing protease was determined through orthogonal test as follows: 2.5 % xylose, 3.5 % peptone, 1.6 % yeast extract and 1 % NaCl, the highest protease activity reached 215.95 U/mL, and increased by 128.06 % than the origin.

Keywords Marine microorganisms · 16S rDNA · Protease · Enzyme activity

17.1 Introduction

Proteases are one of the most important industrial enzymes, accounting for nearly 60 % of all enzyme sales [1], and have been used in various industrial processes, such as pharmaceutical, food, leather, silver recovery, and textiles [2, 3]. However, the use of protease in industrial application is limited by the low activity and instability of the enzymes [4]. In order to improve the stability of the enzyme, the technique of random mutagenesis and site-directed mutagenesis emerged. Pantoliano et al. [5] reported that the rate of inactivation of the combination variant was 300 times slower than that of wild-type subtilisin by six individual amino acid substitution at separate positions. Narhi et al. [6] reported the stabilization of subtilisin from *Bacillus subtilis* by modification of two Asn-Gly sequences. However, this approach is dependent on the number of structural and biochemical data, so the number of variants is rare. While, the microorganisms from exotic

Q. Zhang · X. He · H. Liu (✉)
MOE Key Laboratory of Industrial Fermentation Microbiology, College of Biotechnology, Tianjin University of Science & Technology, Tianjin 300457, China
e-mail: liuhao@tust.edu.cn

T.-C. Zhang and M. Nakajima (eds.), *Advances in Applied Biotechnology*, Lecture Notes in Electrical Engineering 333, DOI 10.1007/978-3-662-46318-5_17

environment are considered to be an important source of enzymes, and they remain catalytically active at the extremes of salinity, pH, and pressure [7, 8]. Therefore, screening of producing stable protease strains and studying the optimum medium for protease production are becoming increasingly important.

In this study, we screened the strains producing protease from deep-sea sediment, and studied the factors on enzyme production to improve the protease activity, so as to provide theoretical support for the screening strains producing stable protease.

17.2 Materials and Methods

17.2.1 Materials and Reagents

Sterile taken deep-sea sediments, R2A Agar (Oxoid) [containing protease peptone 0.5 g, starch 0.5 g, glucose 0.5 g, yeast extract 0.5 g, casein hydrolysate 0.5 g, potassium hydrogen phosphate 0.3 g, sodium pyruvate 0.3 g, magnesium sulfate anhydrous 0.024 g, bacteriological agar 15 g, 1 L distilled seawater], 2216 marine agar [9] (Difco Laboratories), artificial seawater (sodium chloride 24 g, magnesium chloride 10.88 g, sodium sulfate 4 g, calcium chloride 146 g, potassium chloride 0.7 g, sodium bicarbonate 0.2 g, potassium bromide 0.1 g, boric acid 0.027 g, strontium chloride 0.04 g, sodium fluoride 0.003 g, 1 L distilled water) [10].

17.2.2 Isolation and Screening [11]

The strains producing protease were isolated from deep-sea sediments through plate screening. In detail, 1 g of sediments sample was added to 9 mL of sterile artificial seawater, and inoculated, respectively, on R2A and 2216 marine agar plate containing sterile skimmed milk with final concentration of 1 % after gradient dilution (10^{-2}–10^{-5}), then cultured for 2 days at 28 °C. Finally, the single colonies that grew well, and obviously formed proteolytic circles were retained for subsequent screening.

The strains with big proteolytic circles were inoculated in fermentation medium, respectively, and cultured in shaken flasks with rotational speed of 200 r/min for 48 h at 28 °C. The enzyme activity was measured by Folin-phenol method [12], and the strain with the highest enzyme activity was as candidate strain.

17.2.3 Bacterial Cultivation and Identification

The candidate strains were cultured in 2216 marine agar plates at 28 °C, and separated single colonies were selected for PCR amplification. The 16S rDNA gene was amplified by the forward primer 27F (5′-AGAGTTTGATCCTGGCTCAG-3′) and the reverse primer 1492R (5′-TACGGCTACCTTGTTACGACTT-3′). The amplification procedure included 5 min at 95 °C, 50 s at 95 °C, 50 s at 52 °C, followed by 30 cycles of 2 min at 72 °C and extend for 10 min at 72 °C. The PCR products were purified and linked with pMD18-T and sequenced with both the forward and reverse primers. The initial nearest neighbor sequences were made by the online BLAST program to the NCBI GenBank database. Sequences were aligned using the CLUS-X program, and phylogenetic tree was constructed with MEGA program.

17.2.4 Protease Activity Analysis

The protease activity was determined by the method of Kembhavi et al. [13]. One unit of protease activity was defined as the amount of enzyme that liberated 1 μmol of tyrosine in 1 min.

17.2.5 Effects of Different Factors on the Ability of Candidate Strain Producing Protease

Only one factor was changed in each experiment keeping all others constant. The salt content, different carbon and nitrogen sources, and their different concentrations were initially studied at single factor test.

17.3 Result

17.3.1 Screening of Strains Producing Protease and Preliminary Identification of the Ability of Enzyme Production

As shown in Fig. 17.1, four stains displayed relatively larger zone of proteolytic activity when grown on skimmed milk agar medium. Then, by using Folin-phenol method, the ability of enzyme production was measured to screen the candidate strain. The result revealed that the ability of enzyme production of No. 9 is the highest (94.69 U/mL), so No. 9 strain was the candidate strain.

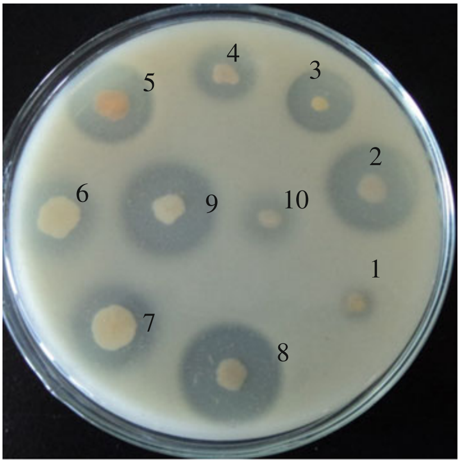

Fig. 17.1 Different strains were inoculated on skimmed milk plate. Different numbers represent different strains, Nos. *2*, *5*, *8*, and *9* strains displayed relatively larger proteolytic *circles* and defined as primarily screening strains

17.3.2 Analysis of 16S rDNA and Physiological and Biochemical Characterization of Candidate Strain

A maximum-likelihood phylogenetic tree (Figs. 17.2 and 17.3) showed that candidate strain (No. 9) had quite high sequence identity to the *B. subtilis* strain Acj 115, and further the result of Gram's method showed that No. 9 strain was a Gram-positive bacterium (Fig. 17.4). Identification of physiological and biochemical characterization of candidate strain revealed that V.P. test was positive, while methyl red test was negative, and most of the carbon source could be used. So the candidate strain was identified to be *B. subtilis.*

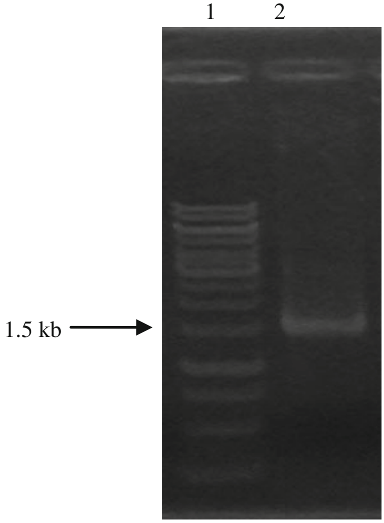

Fig. 17.2 The amplification of 16S rDNA. *Lane 1* 1 kb DNA ladder, *Lane 2* PCR product of 16S rDNA fragment of 1,465 bp

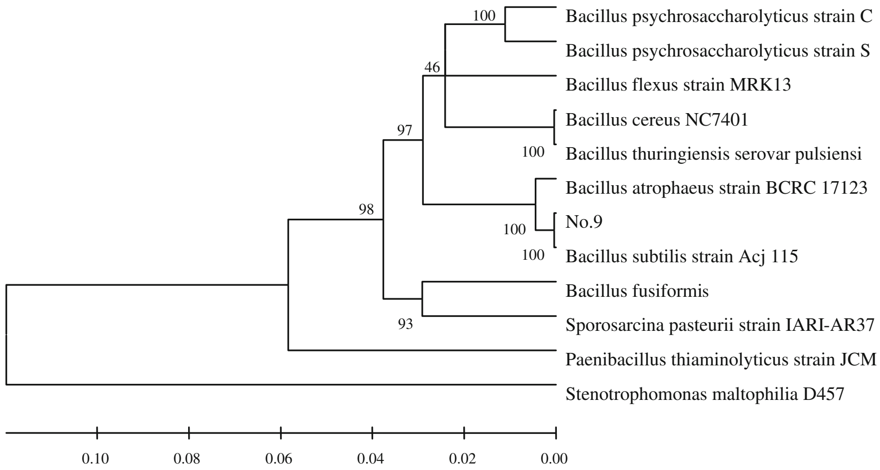

Fig. 17.3 The phylogenetic tree resulting from analysis of the 16S rDNA sequences of candidate strain (No. 9). The tree was created using maximum-likelihood distance clustered by the neighbor-joining method and with MEGA program

Fig. 17.4 The result of Gram's dye of bacterium. The strain cultured in the 2216 E medium for 2 days, then Gram's staining and oil microscopy observation, the result showed that the candidate strain is a Gram-positive bacterium

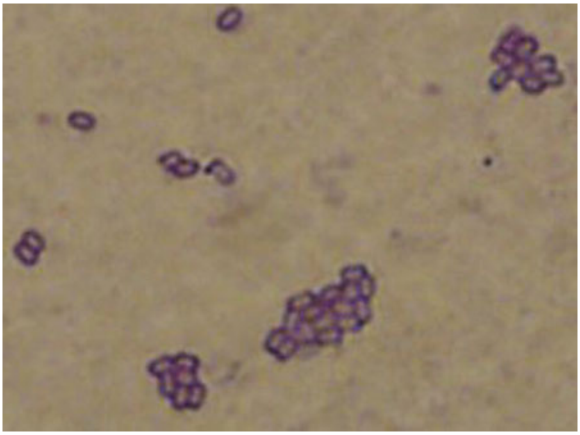

17.3.3 Effect of Different Factors on the Ability of Candidate Strain Producing Protease

17.3.3.1 Carbon Sources

After carbon sources were added to the fermentation medium, compared with the control containing 2 % glucose, the ability of candidate strain producing protease increased by 1.37 fold with xylose (Fig. 17.5). In addition, xylose was added with

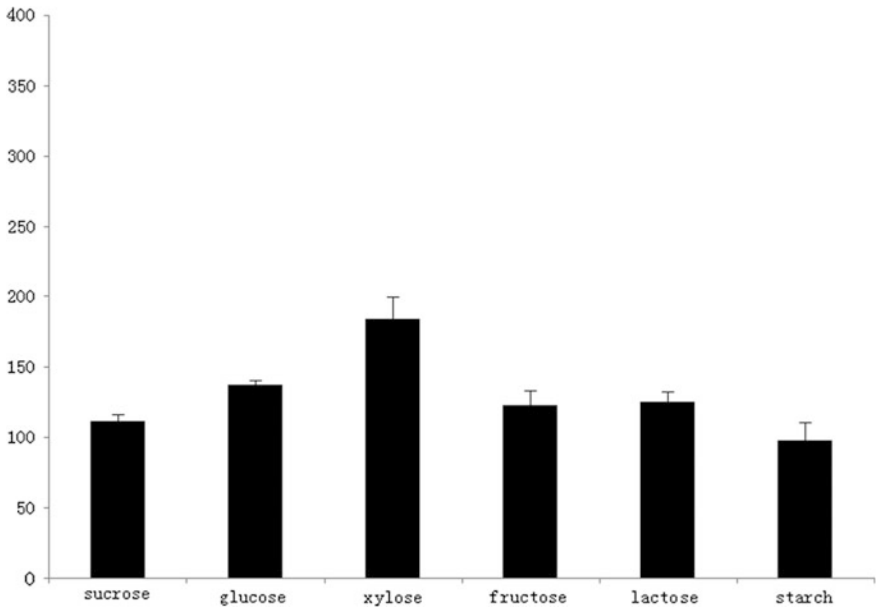

Fig. 17.5 Effects of carbon sources on protease activity. The candidate strain was grown on 2216 E medium at 28 °C and 200 rpm. The protease activity was detected by Folin-phenol method. The highest enzyme activity was 185.78 U/mL, when the carbon source was xylose

concentration of range from 1 to 5 % respectively, and the result showed that the protease activity improved obviously with 2 % of xylose in the medium (185.78 U/mL).

17.3.3.2 Nitrogen Sources

After nitrogen sources were added to the fermentation medium, the result (Figs. 17.6 and 17.7) shows that the protease activity is higher with organic nitrogen sources than inorganic nitrogen sources, and the control has the highest protease activity (123.15 U/mL). Moreover, the supplementation of yeast extract (1.6 %) and peptone (3 %), respectively, resulted in maximal protease activity.

17.3.3.3 NaCl Concentration

Different concentrations of NaCl were added to the fermentation medium, the result showed that the ability of candidate strain producing protease reduced compared with the control containing 2 % NaCl (125.81 U/mL).

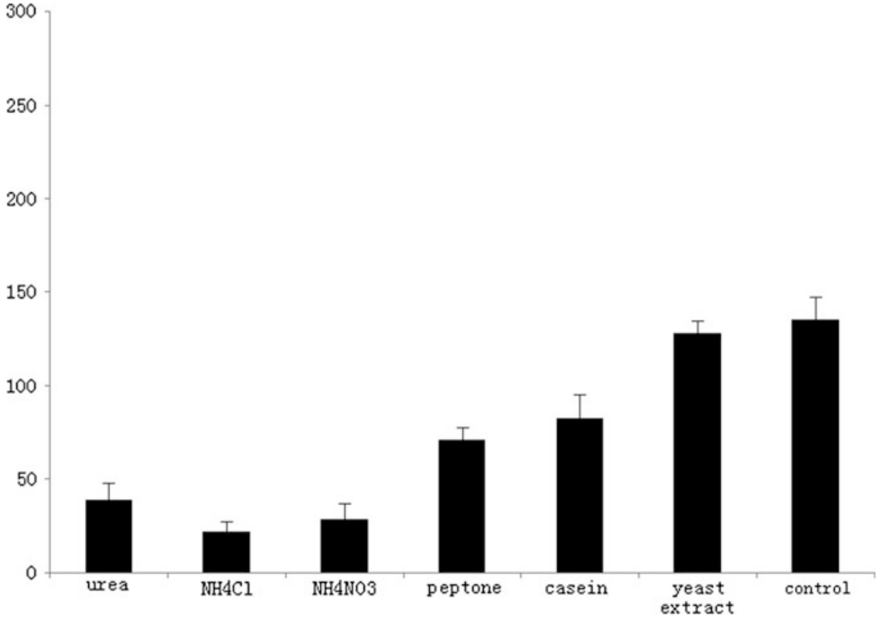

Fig. 17.6 Effects of nitrogen sources on protease activity. The strain grown on 2216 E medium at 28 °C and 200 rpm with 2 % glucose. The protease activity reached the maximum (123.15 U/mL), when peptone and yeast extract are the complex nitrogen sources

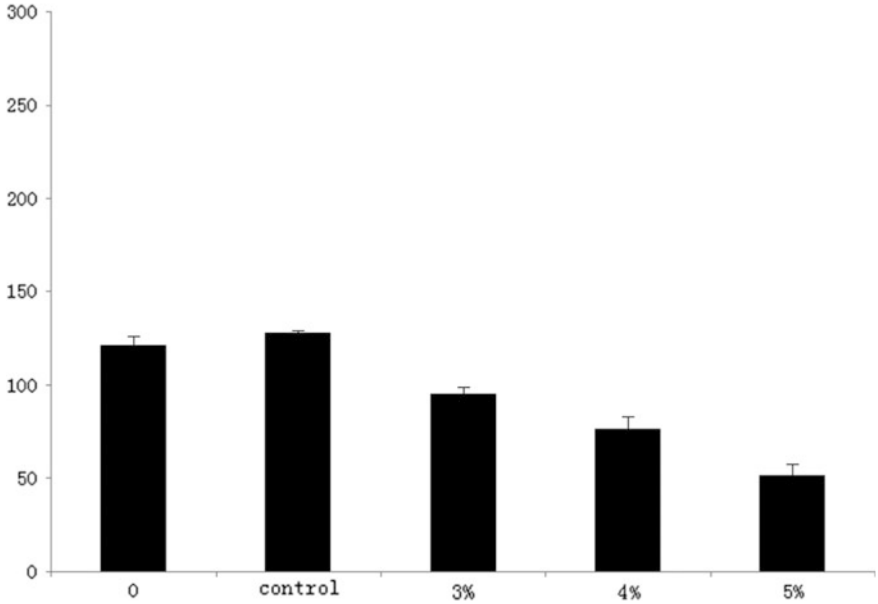

Fig. 17.7 Effects of different concentrations of NaCl on protease activity. The strain grown on 2216 E medium at 28 °C with 2 % glucose, 1 % peptone and 0.5 % yeast extract

Table 17.1 The result of orthogonal test

Group number	Xylose (%)	Peptone (%)	Yeast extract (%)	NaCl (%)	Enzyme activity (U/mL)
1	1.5	2.5	1.2	1	174.13
2	1.5	3	1.6	2	190.35
3	1.5	3.5	2	3	192.87
4	2	2.5	1.6	3	174.13
5	2	3	2	1	212.07
6	2	3.5	1.2	2	184.87
7	2.5	2.5	2	2	200.87
8	2.5	3	1.2	3	164.98
9	2.5	3.5	1.6	1	215.95
K_1	557.35	523.98	523.98	602.15	
K_2	571.06	567.41	580.43	576.09	
K_3	581.81	620.89	605.81	531.98	
F	1.00	23.49	11.68	8.37	

F stands for analysis of variance values

17.3.3.4 Orthogonal Test

Orthogonal test with four factors and three levels was performed to analyze the optimal medium for producing protease. The result (Table 17.1) showed that the order of importance that influenced protease activity was found to be peptone > yeast extract > NaCl > xylose, and the optimal combination parameters were 2.5 % xylose, 3.5 % peptone, 1.6 % yeast extract, and 1 % NaCl. Under the optimal culture medium, the activity of protease increased by 128.06 % than the previous culture medium.

17.4 Discussion

By plate screening and enzyme activity determination, No. 9 strain was screened as the experimental strain, followed by construct phylogenetic tree and identification of physiological and biochemical characteristics showed that experimental strain was *B. subtilis*.

Further, through orthogonal test, the best culture medium was determined as: xylose 2.5 %, peptone 3.5 %, yeast extract 1.6 %, NaCl 1 %, and artificial seawater without NaCl. The activity of protease increased by 128.06 % compared to the origin, and peptone was the most important factor. The results of single factor experiment and orthogonal test were different may be due to the interaction between the factors. This paper has studied the conditions for improving the activity of protease, but the stability of protease needs further analysis.

Acknowledgments The authors gratefully acknowledge the support of the National Nature Science Foundation of China (No. 31201282) and the 863 project (No. 2012AA020403).

References

1. Orhan E, Omay D, Gvüenilir Y (2005) Partial purification and characterization of protease enzyme from Bacillus subtilis and Bacillus cereus. Appl Biochem Biotechnol 121(1–3):183–194
2. Basu SK, Govardhan CP, Jung CW (2004) Protein crystals for the delivery of biopharmaceuticals. Expert Opin Biol Ther 4(3):301–317
3. Kumar S, Sharma NS, Saharan MR (2005) Extracellular acid protease from Rhizopus oryzae: purification and characterization. Process Biochem 40(5):1701–1705
4. Gupta R, Beg QK, Lorenz P (2002) Bacterial alkaline proteases: molecular approaches and industrial applications. Appl Microbiol Biotechnol 59(1):15–32
5. Pantoliano MW, Whitlow M, Wood JF et al (1989) Large increases in general stability for subtilisin BPN' through incremental changes in the free energy of unfolding. Biochemistry 28 (18):7205–7213
6. Narhi LO, Stabinsky Y, Levitt M et al (1991) Enhanced stability of subtilisin by three point mutations. Biotechnol Appl Biochem 13(1):12–24
7. Holmes ML, Scopes RK, Moritz RL et al (1997) Purification and analysis of an extremely halophilic β-galactosidase from Haloferax alicantei. Bba-Protein Struct M 1337(2):276–286
8. Synowiecki Z, Grzybowska B, Zdzieblo A (2006) Sources, properties and suitability of new thermostable enzymes in food processing. Crit Rev Food Sci 46(3):197–205
9. ZoBell CE (1941) Studies on marine bacteria. I. The cultural requirements of heterotrophic aerobes. J Mar Res 4:42–75
10. Lyman J, Fleming RH (1940) Composition of sea water. J Mar Res 3(2):134–146
11. Zhou Y, He W, Fu S, Tian J, Ma T (2011) Screening of Strains Producing Alkaline Protease from Soil and Study on the Conditions for Enzyme Production. Meteo Envl Res 08:82–85
12. Folin O, Denis W (1915) A colorimetric method for the determination of phenols (and phenol derivatives) in urine. J Biol Chem 22(2):305–308
13. Kembhavi AA, Kulkarni A, Pant A (1993) Salt-tolerant and thermostable alkaline protease from Bacillus subtilis NCIM No. 64. Appl Biochem Biotechnol 38(1–2):83–92

Chapter 18
Expression of Gene *uvrA* from *Acetobacter pasteurianus* and Its Tolerance to Acetic Acid in *Escherichia coli*

Yu Zheng, Xingjing Chen, Jing Wang, Haisong Yin, Liqing Wang and Min Wang

Abstract The *uvrA* gene of *Acetobacter pasteurianus* AC2005 coding for subunit A of the excinuclease ABC complex involved in the nucleotide excision repair mechanism was identified. Gene *uvrA* was amplified using *A. pasteurianus* AC2005 genomic DNA as a template. Then the pMV24 plasmid, an expression vector of *Acetobacter*, was used for constructing the recombinant plasmid pMV24-*uvrA*. UvrA was expressed in *Escherichia coli* JM109, and its molecular weight was about 91.1 kDa. With 0.5 % acetic acid shock for 20 and 40 min, the survival rates of recombinant strain *E. coli* JM109/pMV24-*uvrA* were 0.48 and 0.056 %, which increased by 17.5 and 10.2 times, respectively, compared with those of *E. coli* JM109/pMV24. All these demonstrate that the expression of repair excinuclease UvrA could increase the acetic acid tolerance of the strain.

Keywords *E. coli* · *uvrA* · Acetic acid · Gene expression

18.1 Introduction

Acetate ion in the microorganism is toxic mainly to itself, and acetobacter can improve its resistance to a high concentration of acetic acid with a unique mechanism. Studies suggest that there are two main mechanisms that confer high acetic acid concentration to the bacteria. One is to maintain the intracellular pH relatively constant, like the proton pump, overoxidation of acetic acid, changes in fatty acid

Y. Zheng · X. Chen · J. Wang · H. Yin · L. Wang · M. Wang (✉)
Key Laboratory of Industrial Fermentation Microbiology (Tianjin University of Science & Technology), Ministry of Education, Tianjin Key Lab of Industrial Microbiology, College of Biotechnology, Tianjin University of Science and Technology, Tianjin 300457, People's Republic of China
e-mail: minw@tust.edu.cn

T.-C. Zhang and M. Nakajima (eds.), *Advances in Applied Biotechnology*,
Lecture Notes in Electrical Engineering 333, DOI 10.1007/978-3-662-46318-5_18

composition in membrane, etc.; all these could affect the permeability of the proton [1, 2]. Another is to repair the damage of cellular components caused by high concentrations of acetic acid, like improvement of the stability of enzyme under high concentrations of acetic acid, correct folding of the protein involved by molecular chaperone, and so on [3–5].

Nucleotide excision repair (NER) is a mechanism commonly used to maintain the integrity of DNA and the proteins involved in this mechanism are mainly UvrA, UvrB, and UvrC [6]. UvrA is the initial induced protein in bacteria that test various structurally unrelated DNA lesions and excise and repair them. In prokaryotic microorganism, repair excinuclease UvrA involves in the excision and repair of DNA, and this repair mechanism is applicable to repair of many DNA damages [7]. According to the literature, in *Thermus thermophilus*, UvrA was overexpressed induced by IPTG and it makes the strain resist high temperature at neutral pH and resist low pH at room temperature. In *Lactobacillus helveticus*, UvrA was activated by exposure to UV radiation and oxidative stress, and the expression of *uvrA* was inducible by pH; UvrA contributes to acid and oxidative tolerance in *L. helveticus* [8].

Acetobacter pasteurianus is an important acid-producing bacterium during solid-state fermentation of vinegar, and is one of the bacteria commonly used in pure liquid fermentation worldwide. As its important application value, the whole-genome of *A. pasteurianus* has been sequenced completely [9, 10]. This research is focused on the repair excinuclease UvrA from *A. pasteurianus* AC2005. Using genetic engineering technology, we study the effects of UvrA on the acetic acid tolerance of *Escherichia coli*, which would lay the foundation for further clarifying the function of repair excinuclease.

18.2 Materials and Methods

18.2.1 Bacterial Strains, Plasmids, and Growth Conditions

Acetobacter pasteurianus AC2005, stored in the laboratory, was cultured in GYE media (2 % glucose, 1.5 % yeast extract, 3.5 % ethanol) at 30 °C. *E. coli* JM109 were used as hosts for the cloning experiments and *E. coli* was grown at 37 °C on Luria–Bertani (LB) broth supplemented with or without 100 μg/ml ampicillin. The pMD19-T simple vector (TaKaRa) was used for both cloning and sequencing analysis. The pMV24 plasmid (Ap^r, lacZ), gifted by Mizkan Group Corporation, Japan, was used for expression of the gene in *E. coli*.

18.2.2 Construction of the Recombinant Plasmid and Expression of the Target Protein

We used expression vector pMV24 (Ap^r, 3,854 bp) and selected two restriction sites (*Eco*RI and *Xba*I) to construct recombinant plasmid. As pMV24 had a lactose promoter, the target protein was expressed induced by IPTG.

18.2.3 Shock Experiments

To test the tolerance of the strains toward extremely high acetate stresses, shock experiments were performed with much higher concentrations of acetic acid. Strains were grown overnight at 37 °C in LB medium containing 100 mg/mL ampicillin, then diluted at a ratio of 1:100 into fresh LB medium containing 100 mg/mL ampicillin, and grown at 37 °C to logarithmic phase reaching an OD_{600} value of 0.6, then added 1 mM IPTG and inoculated for 4–5 h to induce the expression of UvrA. After that acetic acid was added to final concentrations of 0.5 % (v/v). With 40 min incubation at 37 °C, samples were removed and the number of viable bacteria was determined by spread plating serial dilutions onto LB agar containing 100 mg/mL ampicillin. The plates were incubated at 37 °C for about 16 h before enumeration of the colonies. At the same time, the cultures shocked for 20 and 40 min were serially diluted, plated onto LB/agar plates with the Oxford Cup, and incubated at 37 °C for 16 h and then photographed.

18.3 Results

18.3.1 Sequence Analysis of the uvrA in A. pasteurianus AC2005

The *uvrA* gene of *A. pasteurianus* AC2005 was cloned and its nucleotide sequence was determined. Analysis of the sequence revealed a gene of 2,514 nt that encoded a protein with 837 amino acids (aa) and a predicted molecular mass of 91.1 kDa. In this study, UvrA was expressed in *E. coli* JM109 induced by 1 mM IPTG. By SDS-PAGE, as shown in Fig. 18.1, a significant band of the protein induced appeared at about 91.1 kDa, and its molecular weight was in line with expectation.

The result of comparison indicates that the protein has high homology with the genus *Acetobacter* and *Gluconobacter*. The protein sequence contains a conserved region of NER enzymes.

The sequence obtained was compared with the *uvrA* gene sequence (GenBank: 8435212) of *A. pasteurianus* IFO3283-01 in GenBank. The result showed that the coding sequence from *A. pasteurianus* AC2005 has a similarity of 93.2 % with the

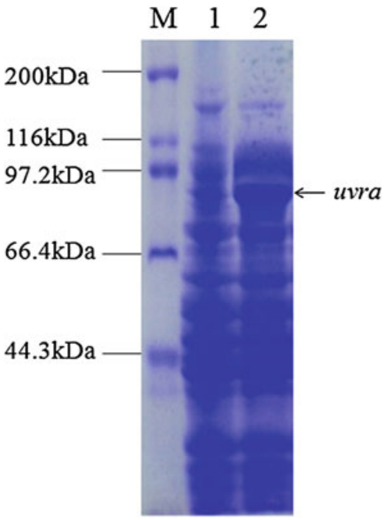

Fig. 18.1 Expression of pMV24-*uvrA* induced by IPTG *M* Marker; *1 E. coli* JM109/pMV24; *2 E. coli* JM109/pMV24-*uvrA*

corresponding region from *A. pasteurianus* IFO3283-01. Compared with the protein UvrA from *A. pasteurianus* AC2005 speculated by the coding region with UvrA from Acetobacter IFO3283-01, the amino acid sequence has a similarity of 98.6 %. Therefore, we can determine the amplified bands for *uvrA* gene of *A. pasteurianus*.

18.3.2 Effect of uvrA Expression on the Growth of E. coli Under Acidic Conditions

To determine the effect on cell growth caused by the expression of UvrA, the experiment studies the growth curves of the strains with the same initial amount of bacteria cells in LB medium. As acetic acid treatment could significantly reduce the final biomass of different strains, *E. coli* JM109/pMV24 and *E. coli* JM109/pMV24-*uvrA* were grown in LB broth supplemented with or without 0.05 % (vol/vol) acetic acid and their growth curves were determined. As shown in Fig. 18.2, in the presence of acetic acid, the growth of control strain *E. coli* JM109/pMV24 in early logarithmic phase and steady growth was suppressed obviously. However, the growth of recombinant strain *E. coli* JM109/pMV24-*uvrA* in the presence or absence of acetic acid is similar. It showed that the expression of UvrA increased the acetic acid tolerance of recombinant strain, and it initially proved that UvrA was related to the acetic acid tolerance.

As we all know acetic acid is highly toxic to *E. coli* cells, and the concentration of acetic acid for use in *E. coli* is often under 0.1 %. Then acetic acid shock experiments were subsequently performed to test the tolerance of *uvrA* expression strain toward acetic acid at higher concentration. The final concentrations of acid required to adjust cultures of *E. coli* to 0.5 % acetic acid were pH 3. After shocking

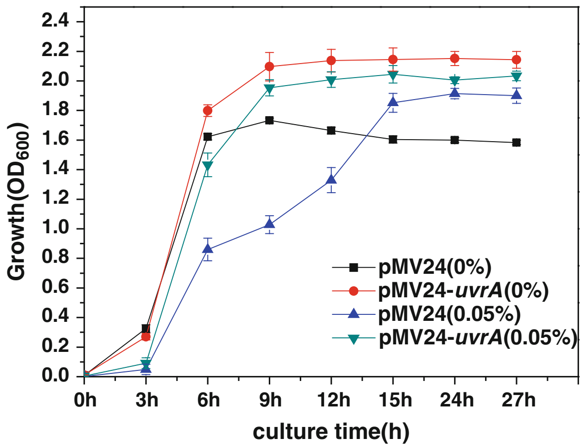

Fig. 18.2 Growth curves of *E. coli* JM109/pMV24 and *E. coli* JM109/pMV24-*uvrA* induced by IPTG with or without 0.05 % acetic acid, respectively

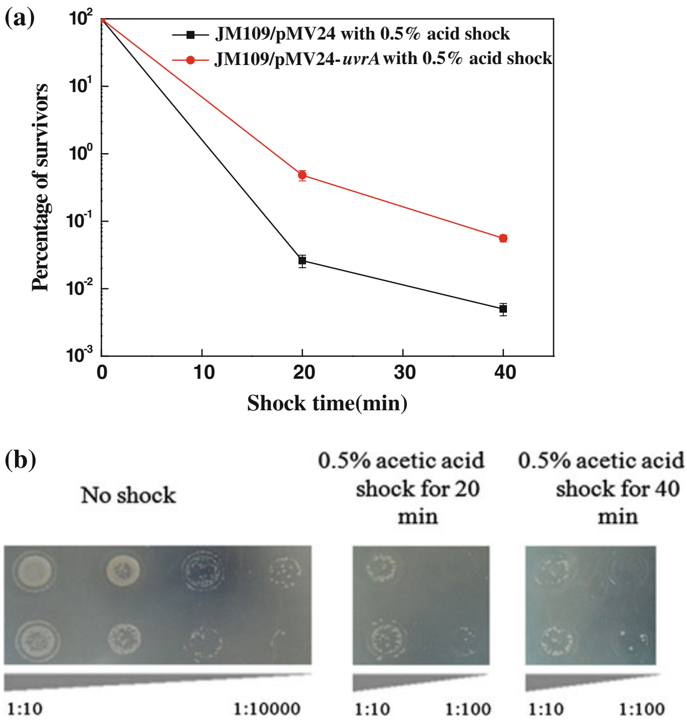

Fig. 18.3 Survival of *E. coli* JM109/pMV24 and *E. coli* JM109/pMV24-*uvrA* under acid-shock conditions, **a** bacterial survival rate at different times treated with 0.5 % acetic acid, **b** colony morphology shocked with 0.5 % acetic acid for 40 min

with 0.5 % acetic acid for different times, the survival curves for the control strain *E. coli* JM109/pMV24 and the recombinant strain *E. coli* JM109/pMV24-*uvrA* are as shown in Fig. 18.3. The changeable survival rate after the acetic acid treatment reflected that the expression of UvrA affects acetic acid tolerance of *E. coli*. With increasing shock time, the recombinant strain showed a clearly increased tolerance to acetic acid as compared to the control strain exposed to 0.5 % acetic acid. With 0.5 % acetic acid shock for 20 and 40 min, the survival rates of recombinant strain *E. coli* JM109/pMV24-*uvrA* were 0.48 and 0.056 %, which increased by 17.5 and 10.2 times, respectively, compared with those of control strain *E. coli* JM109/pMV24. And with 0.5 % acetic acid shock for 40 min, the plaques of two strains on solid plate were observed. Although the number of colonies of control strain under normal culture condition was slightly higher than the recombinant strain, the number was 10 times higher than control strain after acetic acid shock. All these demonstrate that the expression of repair excinuclease UvrA could increase the acetic acid tolerance of the strain.

18.4 Discussion

We have constructed a recombinant strain of *E. coli* with the help of the pMV24 plasmid which is an expression vector of *Acetobacter*. UvrA was expressed in *E. coli* JM109, and its molecular weight was about 91.1 kDa. Homology analysis of the *A. pasteurianus uvrA* gene product revealed high level homology to the *Acetobacter* and *Gluconobacter* UvrA proteins. The protein sequence contained a conserved region of NER enzymes was found. Comparison of the *A. pasteurianus* AC2005 and *A. pasteurianus* IFO3283-01 UvrA protein demonstrated 98.3 % identity and 98.6 % similarity.

With 0.5 % acetic acid shock for 20 and 40 min, the survival rates of recombinant strain *E. coli* JM109/pMV24-*uvrA* increased by 17.5 and 10.2 times, respectively, compared with those of *E. coli* JM109/pMV24. These demonstrate that the expression of repair excinuclease UvrA could increase the acetic acid tolerance of the strain.

Acknowledgments This work was supported by the National High Technology Research and Development Program of China (2012AA022108, 2013AA102106), the National Natural Science Foundation of China (31201406), the Natural Science Foundation of Tianjin, China, (13JCQNJC10000).

References

1. Hanna MN, Ferguson RJ, Li YH et al (2001) *uvrA* is an acid-inducible gene involved in the adaptive response to low pH in *Streptococcus mutans*. J Bacteriol 183(20):5964–5973
2. Mullins EA, Francois JA, Kappock TJ (2008) A specialized citric acid cycle requiring succinyl-coenzyme A (CoA): acetate CoA-transferase (AarC) confers acetic acid resistance on the acidophile *Acetobacter aceti*. J Bacteriol 190(14):4933–4940

3. Matsushita K, Inoue T, Adachi O, Toyama H (2005) *Acetobacter aceti* possesses a proton motive force-dependent efflux system for acetic acid. J Bacteriol 187(13):4346–4352
4. Nakano S, Fukaya M, Horinouchi S (2006) Putative ABC transporter responsible for acetic acid resistance in *Acetobacter aceti*. Appl Environ Microbiol 72(1):497–505
5. Trcek J, Toyama H, Czuba, Misiewicz A, Matsushita K (2006) Correlation between acetic acid resistance and characteristics of PQQ-dependent ADH in acetic acid bacteria. Appl Microbiol Biotechnol 70(3):366–373
6. Van Houten B, Croteau DL, DellaVecchia MJ, Wang H, Kisker C (2005) 'Close-fitting sleeves': DNA damage recognition by the UvrABC nuclease system. Mutat Res 577:92–117
7. Kuper J, Kisker C (2012) Damage recognition in nucleotide excision DNA repair. Sciverse Sci Direct 22:88–93
8. Cappa F, Cattivelli D (2005) Pier Sandro Cocconcelli. The *uvrA* gene is involved in oxidative and acid stress responses in *Lactobacillus helveticus* CNBL1156. Res Microbiol 156:1039–1047
9. Azuma Y, Hosoyama A, Matsutani M et al (2009) Whole-genome analyses reveal genetic instability of *Acetobacter pasteurianus*. Nucleic Acids Res 37(17):5768–5783
10. Matsutani M, Hirakawa H, Saichana N et al (2012) Genome-wide phylogenetic analysis of differences in thermotolerance among closely related *Acetobacter pasteurianus* strains. Microbiology 158(1):229–239

Chapter 19
Construction of *Eschericha coli-Staphylococcus* Shuttle Vector for EGFP Expression and Potential Secretion via Tat Pathway

Bao-yin Xu, Yi-bing Cheng, Lin Wang, Hao Zhou, Lin Huang, Xiao-yan Tang and Qiang Gao

Abstract In this study, the potential for heterologous protein expression and secretion via twin-arginine translocation (Tat) pathway was investigated in *Escherichia coli* DH5α host using enhanced green fluorescent protein (EGFP) as model protein reporter. To construct the shuttle vector pBT2-ET-5X-EGFP, 17 kinds of PCR-amplified *5x-egfp* fragments were, respectively, cloned into plasmid pBT2-Peftu-Tat-EGFP and transformed into *E. coli* DH5α host. By SDS-PAGE, fluorescence microscope observation and flow cytometry analyzation, EGFP was expressed in an active form in the cells of *E. coli* DH5α, but failed to translocate to the culture medium.

Keywords *E. coli* DH5α · Enhanced green fluorescent protein (EGFP) · Twin-arginine translocation pathway · Plasmid pBT2

B. Xu and Y. Cheng—Co-first authors.

B. Xu · Y. Cheng · H. Zhou · L. Huang · X. Tang · Q. Gao (✉)
Key Laboratory of Industrial Fermentation Microbiology, Ministry of Education,
College of Biotechnology, Tianjin University of Science & Technology,
Tianjin 300457, People's Republic of China
e-mail: gaoqiang@tust.edu.cn

L. Wang
School of Computer Science and Information Engineering,
Tianjin University of Science & Technology,
Tianjin 300457, People's Republic of China
e-mail: linwang@tust.edu.cn

T.-C. Zhang and M. Nakajima (eds.), *Advances in Applied Biotechnology*,
Lecture Notes in Electrical Engineering 333, DOI 10.1007/978-3-662-46318-5_19

19.1 Introduction

Compared to the general protein secretion (Sec) system [1], the twin-arginine translocation (Tat) system can deliver the properly folded proteins to the extracellular environment [2]. Thus, the Tat system can be used in gene engineering to secrete exogenous protein which cannot utilize the Sec system [3].

Green fluorescent protein (GFP) can be expressed in *Escherichia coli* as an ideal reporter [4], but whether it is correctly folded and transported across the plasma membrane depends on the choice of the Tat signal peptide sequence [2]. The wild-type GFP is sensitive to temperature, sometimes less expressed and weakly fluorescent in some cells [5], thus researchers have optimized GFP through site-directed mutagenesis. The enhanced green fluorescent protein (EGFP) is now a widely used GFP mutant with two independent substitutions (F64L, S65T), which has improved the fluorescence intensity as well as stability to be detectable for 16–24 h after excitation [6]. In this study, N-terminal modified EGFP was used as model reporter to study the Tat-dependent secretion pathway in *E. coli* DH5α host.

Shuttle vector has two different replication origins of two microbial plasmids, selection marker gene and a multicloning site, which can be replicated in two different organisms, and is usually used for cloning the amplified cloned gene. In this study, pBT2-ET-5X-EGFP, a shuttle vector of *E. coli* and *Staphylococcus* derived from a shuttle vector pBT2 [7], was constructed to study the expression and secretion of EGFP via Tat-pathway.

19.2 Materials and Methods

19.2.1 Bacterial Strain, Plasmids, and Growth Medium

The bacterial strain and plasmids used in this study are listed in Table 19.1, and all the recombinant DNA manipulations were carried out in *E. coli* DH5α host. *E. coli* DH5α was cultured at 37 °C in LB broth (0.5 % yeast extract, 1 % tryptone, and 1 % NaCl) supplemented with 100 μg/mL ampicillin for plasmid selection.

19.2.2 Preparation of the 5x-egfp Fragment

Based on our previous experiments, a linker consisting of five identical amino acids was designed and inserted between the Tat signal peptide and the N-terminal of *egfp* gene to generate a *5x-egfp* fusion gene fragment, where *x* here stands for a certain amino acid codon. Such *5x-egfp* fragment is found to be helpful for secretion from the bacterial host (data not shown). Since 5N-, 5Q- and 5R-EGFP were previously expressed in *E. coli* DH5α host, in order to construct the other 17

Table 19.1 Strain and plasmids used in this work

Bacterial strain and plasmids	Relevant properties	References
E. coli DH5α	–	Laboratory storage
pMD19-T simple vector	Amp^r	TaKaRa Biotechnology (Dalian) Co., Ltd.
pBT2	Amp^r Cm^r	A gift from University of Tuebingen, Germany
pBT2-Peftu-Tat-EGFP [8] (pBT2-ET-EGFP)	Amp^r Cm^r	Laboratory storage

kinds of *5x-egfp* fragment, the primers (Table 19.2) were correspondingly designed according to the sequence of *egfp* gene (No. AF302837).

The primers above were used to, respectively, amplificate the *5x-egfp* fragment using plasmid pBT2-ET-EGFP as PCR template. The following reaction mixture was set up as: 17.5 μL ddH_2O, 2.5 μL parent plasmid, 2.5 μL each primer, 25 μL 2× Taq PCR Master Mix. The cycling parameters for the PCR were as follows: 30 cycles of 95 °C for 5 min, 95 °C for 50 s, 70 °C for 30 s, 72 °C for 1 min followed by a single cycle of 72 °C for 10 min. The PCR products were purified by GeneJET Gel Extraction Kit (Thermo, Germany) after 1 % agarose gel electrophoresis.

19.2.3 Transformation of E. coli DH5α

The *E. coli* DH5α competent cells were thawed in ice for 5 min, then a 10-μL ligation product was added to the cells, and the mixture was incubated in ice for 30 min, heat-shocked for 90 s in a 42 °C water bath, immediately transferred to an ice bath for 1–2 min, followed by the addition of 1 mL sterile LB broth and constant shaking at 37 °C and 200 r/min for 1.5 h; a 100-μL culture broth was spread on LB agar plates containing 100 μg/mL chloramphenicol, and incubated at 37 °C for 12 h [9].

19.2.4 Preparation of Plasmid pBT2-ET-5X-EGFP

The resulting PCR products were, respectively, cloned into pMD19-T Simple Vector after overnight ligation at 16 °C and transformed into *E. coli* DH5α host. Plasmid pMD19-T-5X-EGFP prepared from *E. coli* was purified using the TIANprep Mini Plasmid Kit (TIANGEN, Beijing, China). The constructed *5x-egfp* fragment was first digested by double digestion of *Hin*dIII and *Nhe*I (Fermentas, Lietuvos) from plasmid pMD19-T-5X-EGFP, then inserted into the synonymous sites in pBT2-Peftu-Tat-EGFP, a shuttle vector of *E. coli* and *Staphylococcus*, by T4 ligase (Fermentas, Lietuvos). After overnight ligation at 16 °C, the linked products were transformed into *E. coli* DH5α to create the recombinant plasmid

Table 19.2 Primers used in this work

Primer	Sequence	Underline sequence
5A-egfp-F	CAAGCTTGCAGCAGCTGCAGCAGTGAGCAAGGGCGAG	*Hin*dIII
5D-egfp-F	CAAGCTTGATGATGATGATGATGTGAGCAAGGGCGAGGAGCTGTTCACC	*Hin*dIII
5I-egfp-F	CAAGCTTATTATAATTATTATTGTGAGCAAGGGCGAGGAGCTGTTCACCGGGG	*Hin*dIII
5G-egfp-F	CAAGCTTGGCGGAGGAGGAGGAGTGAGCAAGGGCGAG	*Hin*dIII
5N-egfp-F	CAAGCTTAATAACAATAATAACGTGAGCAAGGGCGAGGAGCTGTTCACCGGGG	*Hin*dIII
5L-egfp-F	CAAGCTTCTTCTGTTACTTCTTGTGAGCAAGGGCGAGGAGCTGTTCACC	*Hin*dIII
5F-egfp-F	CAAGCTTTTTTTTTTCTTTTTTGTGAGCAAGGGCGAGGAGCTGTTCACCGGGG	*Hin*dIII
5P-egfp-F	CAAGCTTCCTCCTCCGCCTCCTGTGAGCAAGGGCGAG	*Hin*dIII
5S-egfp-F	CAAGCTTTCATCAAGTTCATCAGTGAGCAAGGGCGAGGAGCTGTTCACC	*Hin*dIII
5T-egfp-F	CAAGCTTACAACAACAACAACAGTGAGCAAGGGCGAGGAGCTGTTCACC	*Hin*dIII
5W-egfp-F	CAAGCTTTGGTGGTGGTGGTGGGTGAGCAAGGGCGAG	*Hin*dIII
5Y-egfp-F	CAAGCTTTATTATTATTATTATGTGAGCAAGGGCGAGGAGCTGTTCACCGGGG	*Hin*dIII
5V-egfp-F	CAAGCTTGTAGTAGTGGTAGTAGTGAGCAAGGGCGAGGAGCTGTTCACC	*Hin*dIII
5H-egfp-F	CAAGCTTCATCATCATCATCATGTGAGCAAGGGCGAGGAGCTGTTCAC	*Hin*dIII
5M-egfp-F	CAAGCTTATGATGATGATGATGGTGAGCAAGGGCGAGGAGCTGTTCAC	*Hin*dIII
5C-egfp-F	CAAGCTTTGTTGTTGTTGTTGTGTGAGCAAGGGCGAGGAGCTGTTCAC	*Hin*dIII
5K-egfp-F	CAAGCTTAAGAAAAAAAAGAAGGTGAGCAAGGGCGAGGAGCTGTTCACCGGGGT	*Hin*dIII
5X-egfp-R	GGCTAGCGAATTCATTACTTGTACAGCTCGTCCATGCCGAGAGTGATCC	*Nhe*I

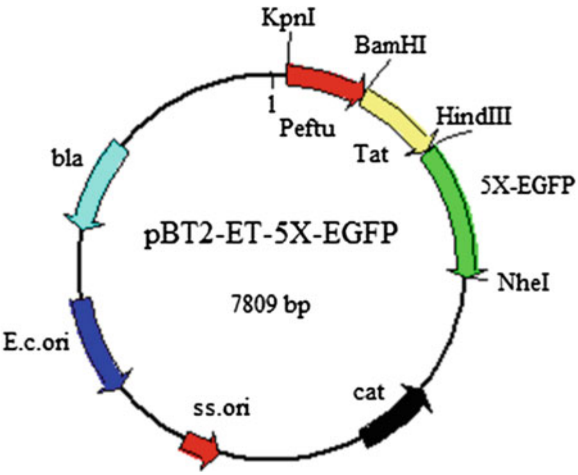

Fig. 19.1 Diagram of plasmid pBT2-ET-5X-EGFP. 5X-EGFP, EGFP with a 5 identical amino acids linker at its N-terminal (X represents for an amino acid of A, C, D, F, G, H, I, K, L, M, N, P, S, T, V, W and Y, respectively); *Tat* a twin-arginine translocation signal peptide of *efeB* gene in *S. carnosus* TM300; *Peftu* a strong promoter of *tufA* gene in *S. carnosus* TM300; *bla* ampicillin resistance gene; *cat* chloramphenicol resistance gene; *E.c.ori* origin of replication in *E. coli*; *ss.ori* origin of replication in *Staphylococcus*

pBT2-ET-5X-EGFP (Fig. 19.1). All plasmid constructions were verified by double restriction enzyme digestion and DNA sequence analysis.

19.2.5 Extraction of EGFP

Single colonies of *E. coli* DH5α/pBT2-ET-5X-EGFP and *E. coli* DH5α were, respectively, grown in 50 mL LB broth at 37 °C and 180 r/min for 16 h. The cell pellets were harvested by centrifugation at 12,000 r/min and 4 °C for 15 min. Proteins present in the culture medium were treated with 10 % trichloroacetic acid (TCA) for 12 h at 4 °C. The cells were resuspended in 2 mL PBS buffer, disrupted by sonication, and centrifuged to separate the supernatant from cell fragment. The supernatant was carefully transferred to a new vial and then precipitated by adding 10 % TCA for 12 h at 4 °C. The precipitated proteins were washed successively in 100 and 80 % acetone and dried at room temperature.

19.2.6 Detection of EGFP

After fermentation culture, the expression of the modified 5X-EGFP in *E. coli* DH5α host was observed by fluorescence microscopy (Olympus (China) Co., Ltd., China), the number of fluorescent cells per 10,000 was counted by flow cytometry

(Accuri C6, BD, America), and the expression of EGFP in cells and culture medium of *E. coli* DH5α/pBT2-ET-5X-EGFP was also analyzed by SDS-PAGE.

19.3 Result

19.3.1 Construction of 5x-egfp Fragment

The 17 kinds of *5x-egfp* fragment obtained from PCR were examined by agarose gel electrophoresis (Fig. 19.2a, b) and purified with GeneJET Gel Extraction Kit (Fig. 19.2c). Double restriction digestion and sequence alignment of plasmid pMD19-T-5X-EGFP (Fig. 19.2d) showed the same result with the target gene.

19.3.2 Verification of pBT2-ET-5X-EGFP

Recombinant plasmid pBT2-ET-5X-EGFP extracted from recombinant strain was examined by 1 % agarose gel electrophoresis (Fig. 19.3). Their molecular weights were expected as 8,000 bp for pBT2-ET-5X-EGFP and 800 bp for 5X-EGFP.

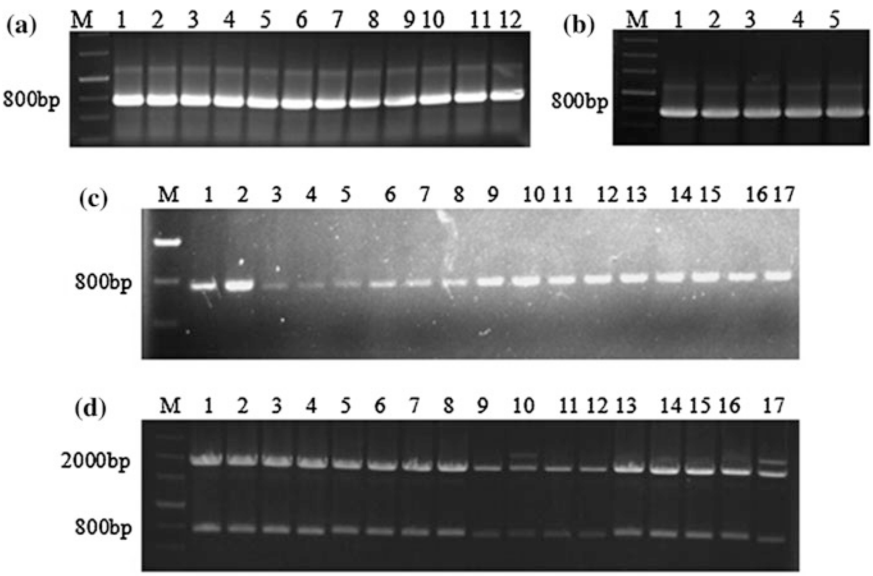

Fig. 19.2 Agarose gel electrophoresis of the PCR product of *5x-egfp* fragment. *M* DNA Marker; *a1–a12* PCR product of *5x-egfp* (x = codon for A, C, D, F, G, H, I, K, L, M, N or P); *b1–b5* PCR product of *5x-egfp* (x = codon for S, T, V, W and Y); *c1–c17* purified product of *5x-egfp* (x = codon for A, C, D, F, G, H, I, K, L, M, N, P, S, T, V, W or Y); *d1–d17* pMD19-T-5X-EGFP digested by *Hin*dIII and *Nhe*I (X = A, C, D, F, G, H, I, K, L, M, N, P, R, S, T, V, W or Y)

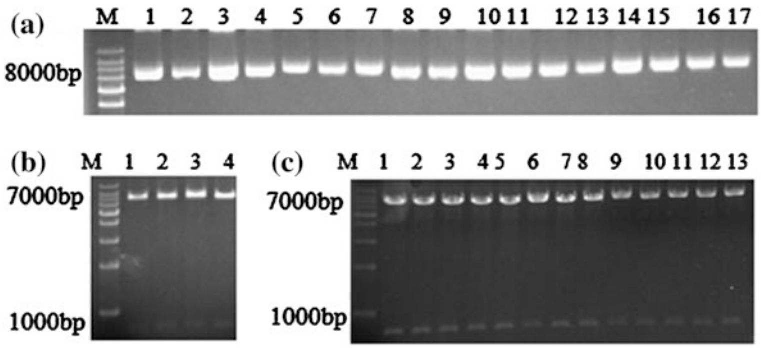

Fig. 19.3 Agarose gel electrophoresis of pBT2-Peftu-Tat-5X-EGFP. *M* DNA Marker. *a1–a17* pBT2-ET-5X-EGFP (X = A, C, D, F, G, H, I, K, L, M, N, P, S, T, V, W or Y); *b1–b4* pBT2-ET-5X-EGFP digested by *Hin*dIII and *Nhe*I (X = A, C, D or F); *c1–c13* pBT2-ET-5X-EGFP restricted with *Hin*dIII and *Nhe*I (X = F, G, H, I, K, L, M, N, P, R, S, T, V, W or Y)

19.3.3 Florescence Detection of EGFP in E. coli DH5α

A 10 μL culture broth of *E. coli* DH5α/pBT2-ET-5X-EGFP was used for florescence microscope observation. The *E. coli* DH5α host strain bearing pBT2-ET-5X-EGFP exhibited strong fluorescence, while the control strain showed no fluorescence (Fig. 19.4).

19.3.4 Detection of EGFP in E. coli DH5α by SDS-PAGE

Dried precipitated proteins in the culture medium and the supernatant were resuspended in 50 μL PBS. After adding 12.5 μL loading buffer, the 30 μL samples were

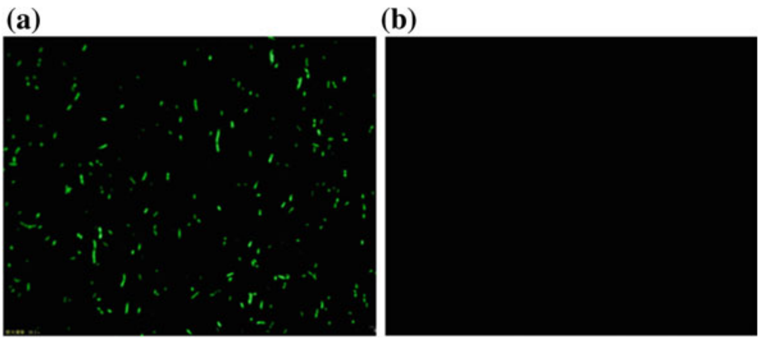

Fig. 19.4 Observation of *E. coli* DH5α/pBT2-ET-5X-EGFP and *E. coli* DH5α by fluorescence microscope. **a** *E. coli* DH5α/pBT2-ET-5X-EGFP; **b** *E. coli* DH5α

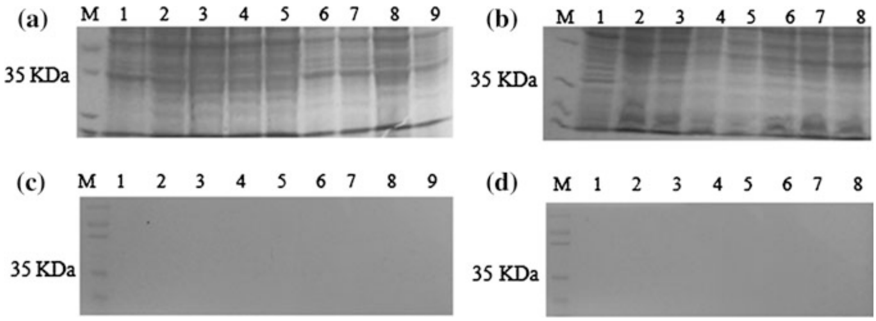

Fig. 19.5 Expression of 5X-EGFP in *E. coli* DH5α validated by SDS-PAGE. *M* Protein Marker (Fermentas, Lietuvos); *a1–a9* 5X-EGFP extracted from the cytoplasm of *E. coli* DH5α/pBT2-ET-5X-EGFP (X = A, C, D, F, G, H, I, K or L); *b1–b8* 5X-EGFP extracted from the cytoplasm of *E. coli* DH5α/pBT2-ET-5X-EGFP (X = M, N, P, S, T, V, W or Y); *c1–c9* 5X-EGFP extracted from the culture medium of *E. coli* DH5α/pBT2-ET-5X-EGFP (X = A, C, D, F, G, H, I, K or L); *d1–d8* 5X-EGFP extracted from the culture medium of *E. coli* DH5α/pBT2-ET-5X-EGFP (X = M, N, P, R, S, T, V, W or Y)

applied for SDS-PAGE analysis. The molecular weights of the 17 homologous target proteins were expected at about 35 kDa for 5X-EGFP. The results proved that 5X-EGFP were properly expressed in a soluble form in *E. coli*, but could not be translocated outside the cell wall (Fig. 19.5).

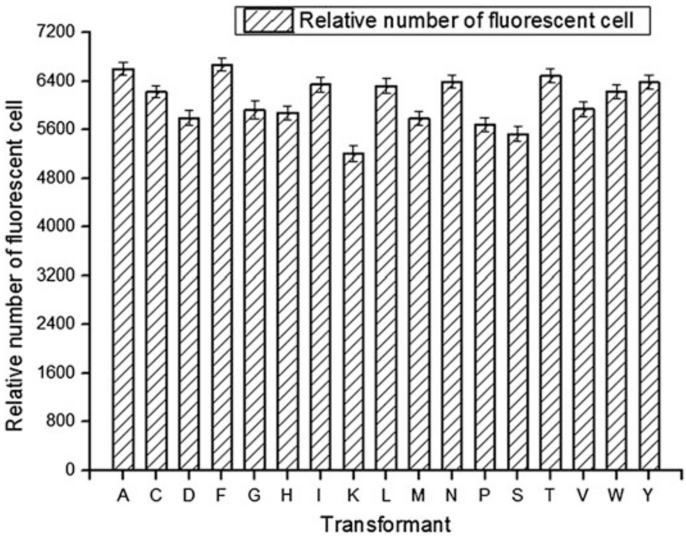

Fig. 19.6 Fluorescence of *E. coli* DH5α/pBT2-ET-5X-EGFP measured by flow cytometry. *X axis* transformants *A* to *Y* strand for *E. coli* DH5α/pBT2-ET-5X-EGFP; *Y axis* number of fluorescent cell per 10,000 cells

19.3.5 Expression of EGFP in E. coli DH5α Detected by Flow Cytometry

A 1-mL suspension of *E. coli* DH5α/pBT2-ET-5X-EGFP was analyzed by flow cytometry. An average of fluorescent cell number indicated that more than half of the cells expressed active 5X-EGFP in *E. coli* DH5α cells (Fig. 19.6).

19.4 Discussion

Tat pathway first found in *E. coli* was now a focus of protein transportation research around the world due to its feature to help translocate fully folded proteins across the bacterial plasma membrane. Bolhuis et al. [10] found that two integral cytoplasmic membrane proteins TatB and TatC make up a structural and functional unit of the twin-arginine translocases in *E. coli.* Tat-dependent heterologous protein secretion was analyzed in the three different Gram-positive bacteria *Staphylococcus carnosus*, *Bacillus subtilis,* and *Corynebacterium glutamicum* using GFP as reporter [11]. Differences about the final localization and the folding status of the exported GFP proved that the choice of potential bacteria host and suitable microorganism is essential in GFP secretion via Tat pathway.

In this study, the constructed 5X-EGFP was used as a model protein reporter to study the possibility of Tat-dependent heterologous protein secretion in *E. coli* DH5α. By means of SDS-PAGE, fluorescence microscope observation and flow analyzation, all the 17 kinds of 5X-EGFP were successfully expressed in a soluble and active form in *E. coli* DH5α cytoplasm, but failed to be translocated out of the cell wall. One possible explanation is the lack of a series of cofactor-binding-proficient proteins which plays an important role in protein transportation [12], the existence of Gram-negative *E. coli* outer membrane is another reason for this failure.

This research constructed an *E. coli-Staphylococcus* shuttle vector to study the function of Tat-pathway upon exogenous protein secretion. In the future research, the recombinant plasmid pBT2-ET-5X-EGFP is to be transformed into *Staphylococcus carnosus* TM300, a valuable genetic engineering strain in food industry [13] with low extracellular proteolytic activity and no by-products like toxin, hemolysin, coagulase [14], and thereby lays the preliminary experimental basis for further insight into heterologous protein secretion via twin-arginine translocation pathway.

Acknowledgments We are very grateful to Prof. Dr. Friedrich Goetz of University of Tuebingen, Germany, for kindly providing plasmid pBT2, we also thank Ms. Lin Huang and Mr. Hao Zhou for excellent technical assistance and instrument support. This work was sponsored by the Natural Science Foundation of China (31370075 & 31471725), the National 973 Program of China (2013CB734004), and the National 863 Program of China (2012AA021302).

References

1. Driessen AJM, Fekkes P, van der Wolk JPW (1998) The Sec system[J]. Curr Opin Microbiol 1(2):216–222
2. Tjalsma H, Bolhuis A, Jongbloed JDH et al (2000) Signal peptide-dependent protein transport in *Bacillus subtilis*: a genome-based survey of the secretome. Microbiol Mol Biol Rev 64: 515–547
3. Wu LF, Bérengère I, Angélique C et al (2000) Bacterial twin-Arginine signal peptide-dependent protein translocation pathway: evolution and Mechanism. J Mol Microbiol Biotechnol 2(2):179–189
4. Chalife M, Tu Y, Euskirchen G et al (1994) Green fluorescent protein as a maker for gene expression. Science 263(5148):802–805
5. Pédelacq JD, Cabantous S, Tran T et al (2006) Engineering and characterization of a superfolder green fluorescent protein. Nat Biotechnol 24(9):79–88
6. Cormack BP, Valdivia RH, Falkow S (1996) FACS-optimized mutants of the green fluorescent protein (GFP). Gene 173(1):33–38
7. Brückner R (1997) Gene replacement in *Staphylococcus carnosus* and *Staphylococcus xylosus*. FEMS Microbiol Lett 151(1):1–8
8. Gao Q, Wang MX, Yu CY et al (2012) Optimization of the electroporation conditions for DNA transformation of *Staphylococcus carnosus.* In: Zhang TC, Ouyang PK, Kaplan S et al (eds) Proceedings of the 2012 international conference on applied biotechnology. Lecture Notes in Electrical Engineering, vol 251. Springer, Heidelberg, pp 1699–1707
9. Yu C, Zheng X, Zhu Y et al (2011) Construction and expression of *tat-gfp* fusion vector. Biotechnol Bull 08:203–207
10. Bolhuis A, Mathers JE, Thomas JD et al (2001) TatB and TatC form a functional and structural unit of the twin-arginine translocase from *Escherichia coli*. J Biol Chem 276 (23):20213–20219
11. Meissner D, Vollstedt A, van Dijl JM et al (2007) Comparative analysis of twin-arginine (Tat)-dependent protein secretion of a heterologous model protein (GFP) in three different Gram-positive bacteria. Appl Genet Mol Biotechnol 76:633–642
12. Blaudeck N, Springer GA, Freudl R, Wiegert T (2001) Specificity of signal peptide recognition in Tat-dependent bacterial protein translocation. J Bacteriol 183:604–610
13. Papamanoli E, Kotzekidou P (2002) Characterization of Micrococcaceae isolated from dry fermented sausage. Food Microbiol 19:441–449
14. Götz F (1990) *Staphylococcus carnosus*: a new host organism for gene cloning and protein production. Soc Appl Microbiol Symp Ser 19:49–53

Chapter 20
SNP Affects the Mobility of Breast Cancer Cells and the Expression of Metastasis-Related Genes

Juan Hu, Hongpeng He, Hao Zhou, Dandan Wang, Yijie Wang, Xuena Liu, Yongwei Lai and Tongcun Zhang

Abstract Protein S-nitrosylation is a type of posttranslational modification that changes protein stability, intracellular localization, and biological activity. In mammalian cells, NO is synthesized by NOS which is highly expressed in many solid tumors, including breast cancer. NOS is involved in the progress of carcinogenesis by generating NO to modify various tumor-related proteins to enhance or suppress their function. However, the effect of NO on tumor metastasis is less studied. Herein, breast cancer cells MCF-7 and MDA-MB-231 were treated with NO donor SNP, which resulted in altered cell mobility. Meanwhile the expression of several metastasis-related genes was regulated. These results suggest a novel mechanism by which NO promotes the metastasis of breast cancer.

Keywords Breast cancer · Cell migration · SNP · NO

20.1 Introduction

Nitric oxide (NO) is originally identified as a biologic mediator molecule functioning in several processes, including neurotransmission, antimicrobial, and antitumoral activities. Recently, it has been found that NO is able to chemically modify proteins at cysteine or tyrosine residues, which is termed S-nitrosylation or tyrosine nitrosation respectively. Quite a few proteins in mammalian cells were found to be

---

J. Hu and H. He—Co-first authors.

J. Hu · H. He · H. Zhou · D. Wang · Y. Wang · X. Liu · Y. Lai · T. Zhang (✉)
Key Laboratory of Industrial Microbiology, Ministry of Education and Tianjin City,
College of Biotechnology, Tianjin University of Science and Technology,
Tianjin 300457, People's Republic of China
e-mail: tony@tust.edu.en

T.-C. Zhang and M. Nakajima (eds.), *Advances in Applied Biotechnology*,
Lecture Notes in Electrical Engineering 333, DOI 10.1007/978-3-662-46318-5_20

S-nitrosylated, including HIF, c-Fos, c-Myc, Src, Bcl-2, etc. [1–3]. S-nitrosylation alters the stability or the activity of the modified protein and thereby regulates cell apoptosis, proliferation, angiogenesis, and other biological processes [2].

In mammalian cells, NO is synthesized by nitric oxide synthase (NOS) from L-arginine. There are three types of NOS, namely iNOS (inducible NOS), eNOS (endothelial NOS), and nNOS (neuronal NOS). iNOS was observed to be highly expressed in some tumors such as colon, gastric, prostate, cervical, ovarian, and lung cancers [3–6]. In breast cancer patients, increased expression of iNOS was reported to be associated with a basal-like transcription pattern which is frequently observed in poor survival, ER-negative patients [7]. For ER-positive breast cancer cell, such as MCF7, the disruption of S-nitrosothiol homeostasis altered MCF-7 cell proliferation in a dose-dependent manner [8]. However, the effect of NO on the mobility of breast cancer cell is less studied.

Several NO donors which are able to release NO into cell culture medium have been identified, such as GSNO, DETA/NO, SNAP, and sodium nitroprusside (SNP). To further explore the effects of NO stress on the proliferation and mobility of breast cancer cells, herein, MCF-7 and MDA-MB-231 cells were treated with SNP at different concentrations, the mobility and the proliferation of breast cancer cells were investigated, and the expression of metastasis-related genes was measured.

20.2 Materials and Methods

20.2.1 Cell Culture and Reagents

MCF-7 and MDA-MB-231 human breast cancer cells were cultured in Dulbecco's modified Eagle's medium with L-Glutamine (DMEM; Gibico) supplemented with 10 % fetal bovine serum (Sijiqing, Hangzhou China) and 1 % Antibiotic/Anti-mycotic (Solarbio, China) at 37 °C in a 5 % CO_2 incubator. SNP was purchased from Beyotime, China.

20.2.2 Wound Healing Assay

Breast cancer cells were seeded in 6-well plates and cultured to confluence, then cells were serum-starved for 24 h. Wound was introduced by scratching the monolayer of cells with a micropipette tip. Cells in 6-well plates were washed with PBS to remove floating cells and cultured in serum-free media containing SNP at different concentrations. The healing of the wound was investigated every 12 h and pictures were taken with a microscope.

Table 20.1 Primer sequences used in this study

Primer	Sequence (5′ → 3′)
18S-F	CACGGG AAACCTCACCCGGC
18S-R	CGGGTGGCTGAACGCCACTT
CYR61-F	GTCGTCACCCTTCTCCACTT
CYR61-R	CTTGGCGCAGACCTTACAG
MYL9-F	GAGCCCAAGCGCCTTCT
MYL9-R	GTCAATGAAGCCATCACGGT
MYH9-F	AGCGTTACTACTCAGGGCTCATC
MYH9-R	TCATACTCCTGTAGGCGGTGTCT

20.2.3 MTT Assay

Breast cancer cells were seeded in 96-well culture plates and cultured overnight before being treated with SNP at different concentrations. Twenty-four hours after SNP treatment, 20 μL of MTT (5 mg/mL, Solarbio, China) was added to each well and incubated in an incubator for 4 h, then the medium was removed and formazan crystals were dissolved with 100 μL of DMSO. Cell viability was analyzed by measuring the absorbance at 590 nm using an ELISA reader (BioTek, USA).

20.2.4 Isolation of Total RNA and RT-PCR

Total RNA was extracted with Trizol reagent (Invitrogen). Reverse transcription was performed with M-MLV reverse transcriptase (Promega). Complementary DNA was quantified by semi-quantitative PCR using EasyTaq DNA Polymerase kit (TransGen Biotech). PCR primers were designed with NCBI online software Primer-BLAST and synthesized by Dingguo Biotech. Sequences of the primers were listed in Table 20.1. Thirty cycles of PCR were carried out and PCR products were visualized by electrophoresis using 2 % agarose gels.

20.3 Results

20.3.1 SNP Promoted the Migration of Breast Cancer Cells

To examine the effect of SNP on the migration of breast cancer cells, wound healing assay was performed for both low mobility breast cancer cell line MCF7 and high mobility breast cancer cell line MDA-MB-231. Pictures were taken with microscopy at different time points. The results of wound-healing assay showed that the breast cancer cells scrambled from both sides of the scratch toward the middle (Fig. 20.1a, b). MCF7 cells treated with SNP at low concentrations, in particular 0.1

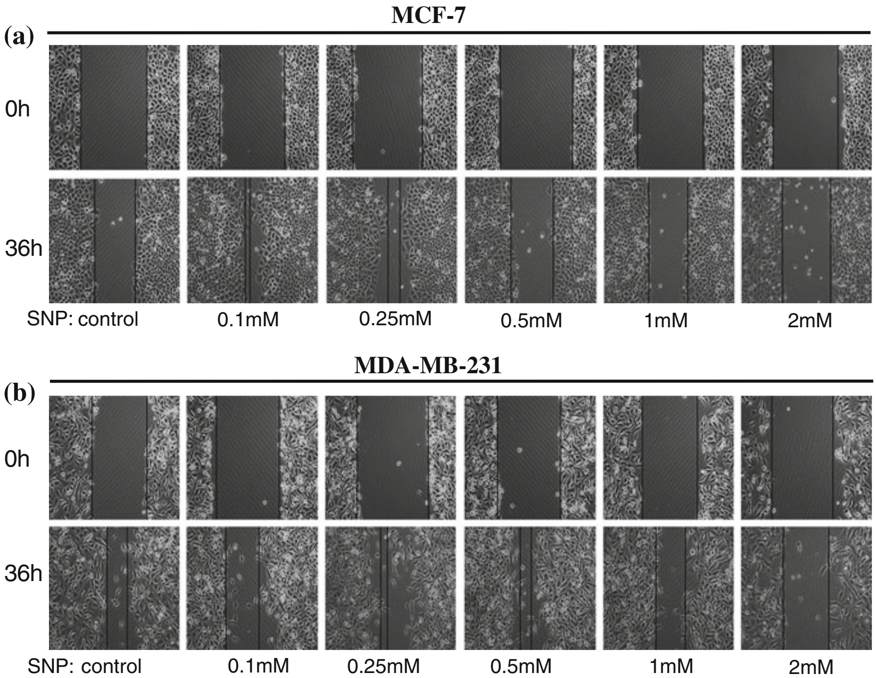

Fig. 20.1 SNP promoted the migration of breast cancer cells. Pictures were taken at different time points after scratch and treatment with SNP. For control group, cells were treated with H_2O, the dissolvent of SNP

and 0.25 mM, moved faster than untreated cells or cells treated with SNP at high concentrations (Fig. 20.1a, compares columns 2 and 3 with other columns in the lower panel). These results suggest that SNP at lower concentration promotes the migration of MCF7 cells.

MDA-MB-231 is another breast cancer cell line with higher mobility. From results of wound healing assay, MDA-MB-231 cell indeed moved faster than MCF-7 (Fig. 20.1a, b). MDA-MB-231 cells treated with SNP at 0.25 and 0.5 mM concentrations moved faster than control group, whereas cells treated with 0.1 and 2 mM of SNP moved slower than control group (Fig. 20.1b). These results suggest that the migration of MDA-MB-231 cells were promoted by SNP at modest concentrations.

20.3.2 SNP Inhibited the Proliferation of Breast Cancer Cells

NO was previously reported to display different biological effects dependent on its concentration [3]. To exclude the possibility that the faster wound healing after SNP

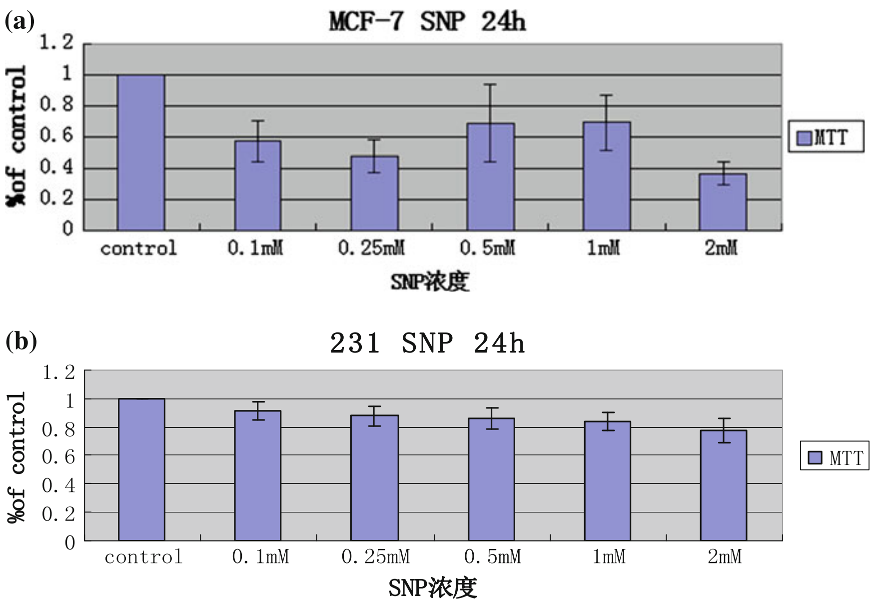

Fig. 20.2 SNP inhibited the proliferation of breast cancer cells

treatment observed for MCF-7 and MDA-MB-231 cells is due to the increased cell proliferation, cell growth was measured with MTT method.

As shown in Fig. 20.2a, SNP inhibited the growth of MCF7 in a dose-dependent manner. For MDA-MB-231, cell growth was inhibited by SNP as well, but the effect was more modest compared to that of MCF-7 (Fig. 20.2b). These results suggest that the faster wound healing observed for MCF-7 and MDA-MB-231 cells was resulted from higher cell mobility but not from cell proliferation. The inhibition of cell growth by SNP at high concentrations is in agreement with a previous report that NO induces apoptosis of MCF-7 cells at high concentration [9].

20.3.3 SNP Affected the Expression of Metastasis-Related Genes in a Dose-Dependent Manner

Metastasis is a common phenomenon of malignant tumors and is correlated with the increased mobility of tumor cells. To explore the mechanism by which SNP affects the mobility of breast cancer cells, the expression of a series of genes, such as MYL9, MYH9, CYR61, and MMP9 which are known to be metastasis-related [10, 11], were determined by RT-PCR. As shown in Fig. 20.3a, the expression of the metastasis-related genes in MCF-7 was stimulated by NO at 0.1 or 0.25 mM concentrations (Fig. 20.3a, lane 2 and lane 3), which is in line with the increased

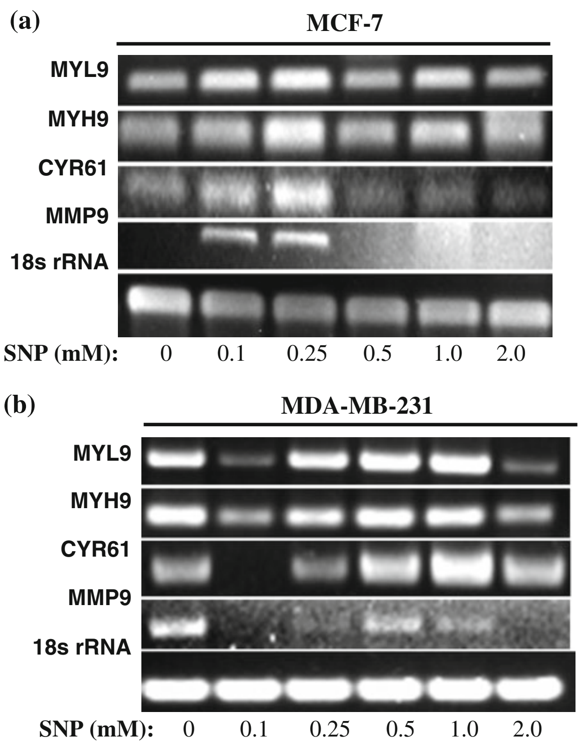

Fig. 20.3 SNP altered the expression of metastasis-related genes in breast cancer cell lines. **a** MCF-7 cells were treated with SNP, total RNA was extracted 24 h later. Products of RT-PCR were analyzed with 2 % agarose gel. **b** MDA-MB-231 cells were treated for 4 h before being harvested and analyzed

mobility of SNP-treated MCF-7 (Fig. 20.1a). In MDA-MB-231 cells, the expression of these metastasis-related genes was stimulated by SNP at 0.25–1.0 mM concentrations, but suppressed by SNP at 0.1 or 2.0 mM concentrations (Fig. 20.3b), which is also in agreement with the effects of SNP on MDA-MB-231 mobility (Fig. 20.1b). Taken together, these results indicate that SNP, at proper concentrations, stimulates the expression of metastasis-related genes and increased the mobility of breast cancer cells simultaneously.

20.4 Discussion

In malignant solid tumor, NO is released by macrophage and tumor cells to generate a microenvironment inducing angiogenesis which is correlated with the S-nitrosylation of a transcription factor HIF [1]. In addition to the effect on angiogenesis, low level NO was also found to stimulate cell proliferation and high level NO was shown to induce apoptosis. In this study, breast cancer cells were treated with serial diluted NO donor SNP and the results reveal that low mobility breast cancer cell MCF-7 and high mobility breast cancer cell line MDA-MB-293 respond differently to SNP. For MCF-7 cell, SNP obviously inhibited cell proliferation, meanwhile, at low concentration, SNP promoted MCF-7 cell migration which is coincident with the upregulation of metastasis-related genes. At high concentration, SNP has little effect on both MCF-7 cell migration and metastasis-gene expression. However, for MDA-MB-231 cell, the growth was not significantly affected by SNP. At low or high concentration, SNP inhibited MDA-MB-231 cell migration and the expression of metastasis-related genes. At modest level, SNP promoted cell migration and the expression of metastasis-related genes. These results indicate that SNP stimulates breast cancer cell migration by inducing the expression of metastasis-related genes.

A common property of the genes examined in this study is that they carry CarG-box elements in their promoter regions and were previously shown to be regulated by myocardin-related transcription factors (MRTFs) [11]. MRTFs control cell mobility, cell invasion, and also other cell skeleton-related processes via activating the expression of target genes. The activity of MRTFs is regulated by posttranslational modifications, such as phosphorylation. MRTFs contain cytidine residues in their amino acid sequences. Therefore, it is possible that MRTFs in breast cancer cells were modified by NO released from SNP and this modification stimulates MRTFs transactivity to activate the expression of metastasis-related genes, and in the end, promote breast cancer cell migration. This hypothesis is worth of further study in the future.

Acknowledgments We thank Professor Zhonghua Pang from the Institute of Hematology & Blood Diseases Hospital, Chinese Academy of Medical Sciences & Peking Union Medical College for providing MDA-MB-231 cell line. This work was supported by the National Natural Science Foundation of China (31301073) and Applied Basic Science and Frontier Technology Program of Tianjin (13JCYBJC38000).

References

1. Dimova EY, Kietzmann T (2010) Hypoxia-inducible factors: post-translational crosstalk of signaling pathways. Methods Mol Biol 647:215–236
2. Wang Z (2012) Protein S-nitrosylation and cancer. Cancer Lett 320:123–129
3. Switzer CH et al (2011) Nitric oxide and protein phosphatase 2A provide novel therapeutic opportunities in ER-negative breast cancer. Trends Pharmacol Sci 32:644–651
4. Anttila MA et al (2007) Prognostic significance of iNOS in epithelial ovarian cancer. Gynecol Oncol 105:97–103
5. Puhakka A et al (2003) High expression of nitric oxide synthases is a favorable prognostic sign in non-small cell lung carcinoma. APMIS 111:1137–1146
6. Lopez-Sanchez LM et al (2008) Alteration of S-nitrosothiol homeostasis and targets for protein S-nitrosation in human hepatocytes. Proteomics 8:4709–4720
7. Glynn SA et al (2010) Increased NOS2 predicts poor survival in estrogen receptor-negative breast cancer patients. J Clin Invest 120:3843–3854
8. Canas A et al (2012) Maintenance of S-nitrosothiol homeostasis plays an important role in growth suppression of estrogen receptor-positive breast tumors. Breast Cancer Res 14:R153
9. Feng X et al (2013) S-nitrosylation of ERK inhibits ERK phosphorylation and induces apoptosis. Sci Rep 3:1814

10. Liao XH et al (2014) MRTF-A and STAT3 synergistically promote breast cancer cell migration. Cell Signal 26:2370–2380
11. Medjkane S et al (2009) Myocardin-related transcription factors and SRF are required for cytoskeletal dynamics and experimental metastasis. Nat Cell Biol 11:257–268

Chapter 21
Molecular Cloning and Characterization of Glycerol Dehydrogenase from *Klebsiella pneumoniae*

Yanhua Liu, Li Zhao, Jianguo Zhang and Yu Zheng

Abstract Glycerol dehydrogenase (GDH) was a key enzyme for 1,3-propanediol fermentation from glycerol. In this report, gene *gdh*, encoding GDH of *Klebsiella pneumoniae* KG1 was gained by PCR with genomic DNA as template. The open reading frame (ORF) of *gdh* consisted of 1,143 bp and encoded 380 amino acids with a deduced molecular mass of 42 kDa. The gene *gdh* was overexpressed in *E. coli* BL21 (DE3) and produced 886-fold higher activity of GDH than that of KG1. The optimum temperature of recombinant GDH was 37 °C and glycerol was the optimum substrate.

Keywords 1,3-Propanediol · 1,3-Propanediol oxidoreductase · Glycerol dehydratase · Glycerol dehydrogenase · *Klebsiella pneumonia*

21.1 Introduction

It is known that certain enteric bacteria are capable of fermenting glycerol to 1,3-propanediol (1,3-PD) as the main product. Fermentation was carried out in two parallel pathways: oxidative and reductive. Through the oxidative pathway, glycerol

Y. Liu
College of Science, Tianjin University of Science and Technology, Tianjin 300457, People's Republic of China
e-mail: liu_yanhua@tust.edu.cn

Y. Zheng (✉)
Key Laboratory of Industrial Fermentation Microbiology, Ministry of Education, Tianjin 300457, People's Republic of China
e-mail: yuzheng@tust.edu.cn

L. Zhao
State Key Laboratory of Bioreactor Engineering, East China University of Science and Technology, Shanghai 200237, People's Republic of China

J. Zhang
School of Medical Instrument and Food Engineering, University of Shanghai for Science and Technology, Shanghai 200093, People's Republic of China

T.-C. Zhang and M. Nakajima (eds.), *Advances in Applied Biotechnology*, Lecture Notes in Electrical Engineering 333, DOI 10.1007/978-3-662-46318-5_21

was dehydrogenated by a NAD^+-linked enzyme, glycerol dehydrogenase (GDH), to dihydroxyacetone (DHA), and then to dihydroxyacetone phosphate (DHAP). The reductive pathway, a coenzyme B_{12}-dependent glycerol dehydratase (GDHt) removed a water molecule from glycerol to form 3-hydroxypropionaldehyde (3-HPA) which was then reduced to 1,3-PD by an NADH-linked 1,3-PD oxidoreductase (1,3-PDOR) [1, 2]. The GDHt or 1,3-PDOR of *Klebsiella pneumoniae* was sequenced and expressed in *Escherichia coli* successfully [3, 4]. In recent years some messages of construction and characterization of *dha* operon of *K. pneumoniae* were reported, and much more information it contained was available [5–8].

Although many studies on the 1,3-PDOR or GDHt of *K. pneumoniae* and properties of GDH are available on many other organisms, there are few reports on the GDH of *K. pneumoniae* and the corresponding gene. In order to investigate the metabolism of *K. pneumoniae* and improve the productivity of 1,3-PD, we cloned and sequenced the *gdh* gene from *K. pneumoniae*, and then overexpression and characterization was performed in *E. coli*.

21.2 Materials and Methods

21.2.1 Bacterial Strains and Plasmids

Bacterium, *K. pneumoniae* KG1 (kindly provided by Prof. Gong Heng), was used as a *gdh* donor strain. *E. coli* DH5α was used as host for plasmid construction. *E. coli* BL21(DE3) was used as a host strain for expression of pET-*gdh*, which was constructed in this study. pGEM-T (Promega Madison, U.S.A.) a cloning vector and pET-28a(+) were used. *E. coli* was grown aerobically at 37 °C in LB medium supplemented, when necessary, with 25 mg/L kanamycin.

21.2.2 Construction of the Recombinant Vector

Two primers, Pgdh-1 and Pgdh-2, were prepared for PCR to obtain the open reading frame (ORF) of the gene *gdh* according to the sequence of *gdh* of *E. coli* K-12 from Genbank (accession no. NC_000913). Primer Pgdh-1, 5′-ccggaattcatgccgcatttggcactactc-3′, consisted of an *Eco*RI site. Primer Pgdh-2, 5′-ccgctcgagTTATTCCCACTCTTGCAGG-3′, consisted of an *Xho*I site. PCR was done with the chromosomal DNA of *K. pneumoniae* KG1 as template, and Pfu-DNA polymerase was used (Dingguo Beijing, China). The 1.2 kb product was ligated to pGEM-T to achieve the plasmid pGEM-*gdh* and then Plasmid pGEM-*gdh* was sequenced. Plasmid pGEM-*gdh* was digested with *Eco*RI and *Xho*I (Takara Dalian, China). The resultant was purified and ligated to pET-28a(+) already digested with the same restriction enzymes. The recombinant plasmid pET-*gdh* was obtained.

Other DNA manipulations were carried out according to standard methods. DNA sequencing was done by Invitrogen Co. Ltd. (Shanghai, China).

21.2.3 Preparation of Cell Extract

The cells were harvested by centrifugation (6,000×*g*, 4 °C, 10 min). The cell pellet was washed twice with cold kalium phosphate buffer (pH 7.0), then it was suspended in the same buffer, 0.2 (g wet cell)/mL, and dithiothreitol (DTT) was added to 0.1 mmol/L. The cells were treated by sonication with ice bath for 3 s at 200 W, followed by a 5 s pause. This cycle was repeated 60 times. The cell debris was removed by centrifugation (13,000×*g*, 4 °C, 20 min) and GDH activity of the supernatant was determined. The protein in supernatant was examined by SDS-PAGE (15 %).

21.2.4 GDH Activity Assay

The activity of GDH was determined spectrophotometrically at 340 nm at different temperatures according to Ahrens et al. [1]. One unit of enzyme activity was defined as the amount of enzyme that consumed 1 μmol glycerol per minute.

21.3 Results

21.3.1 Expression of gdh Gene in E. coli

The gene *gdh* from KG1 was gained by PCR with genomic DNA of *K. pneumoniae* KG1 as template. DNA sequence showed that the open reading frame of *gdh* was 1,143 bp, corresponding 380 amino acid residues.

The expression plasmid, pET-*gdh*, was transformed into *E. coli* BL21 (DE3) competent cells to express recombinant his-tagged GDH. Expression of the GDH was carried out at different temperatures and IPTG concentrations. The optimum condition for expressing GDH was 1 mmol/L IPTG and at 37 °C (data not shown). Examined by SDS-PAGE, a band corresponding to about 42 kDa protein was observed which was identical to the deduced molecular weight (Fig. 21.1). The SDS-PAGE also revealed that the GDH was soluble in *E. coli* BL21 (DE3), which was important for the high enzyme activity.

Fig. 21.1 SDS-PAGE analysis of GDH protein. *Lane M* Protein Marker (Takara Dalian, China), *Lane 1* KG1, *Lane 2* BL21/pET-28, *Lane 3* BL21/pET-*gdh*, *Lane 4* the sample of Lane 3 diluted to 10-1 with water

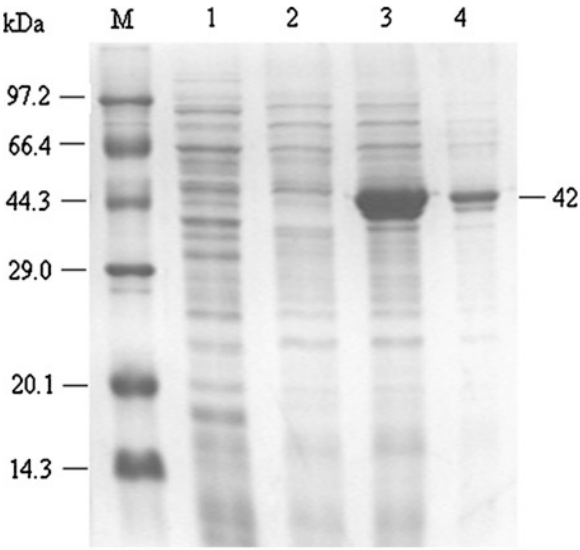

21.3.2 Characteristics of GDH

As depicted in Fig. 21.2, the activity of GDH of *E. coli* BL21/pET28-*gdh* increased as the temperature increased until 37 °C, and then decreased. So 37 °C was its optimum reactive temperature. Hereafter, the enzyme reaction was performed at 37 °C.

Strains of *E. coli* BL21/pET-gdh and *E. coli* BL21/pET-28 were cultured, respectively, at 37 °C to OD600 about 0.5 and then induced for 4 h with 1 mM IPTG. KG1 was cultured at 37 °C. The kinetics of the GDH was compared (Table 21.1).

Surprisingly, the recombinant GDH showed very high dehydrogenate activity, with 774 times and 886 times more than that of *E. coli* BL21/pET-28 and KG1, respectively (Table 21.1). It was reported that exposure to O_2 of cells growing

Fig. 21.2 Effect of temperature on activity of GDH

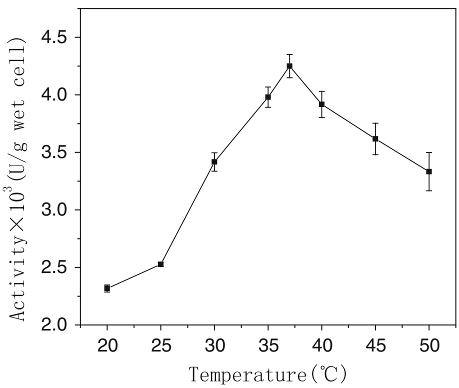

Table 21.1 Activity of GDH in different strains

GDH	Specific activity (U/(g wet cell))
BL21/pET-*gdh*	$4.17 \pm 0.88 \times 10^3$
BL21/pET-28	5.38 ± 0.64
KG1	4.7 ± 0.42

Table 21.2 Substrate specificity of GDH from *E. coli* BL21/pET-*gdh*

Substrates	Relative activity (%)
Glycerol	100
Glycol	30.7 ± 2.2
1,2-Propanediol	6.7 ± 1.2
2,3-Butanediol	2.3 ± 0.34
1,3-Propanediol	0.6 ± 0.1
1,3-Butanediol	0.3 ± 0.1
1,4-Butanediol	<0.1
Propanol	<0.1
Iso-propanol	<0.1
Butanediol	<0.1

anaerobically resulted in irreversible inactivation of GDH from *K. pneumoniae* or *Klebsiella aerogenes* [9]. But both *E. coli* BL21/pET-*gdh* and KG1 cultured anaerobically or aerobically showed good activity of GDH in the present of O_2 in this study (data not shown). Therefore, its character to O_2 was different from the GDH of *K. pneumoniae* reported before [9].

Enzyme activities of GDH with different substrates are summarized in Table 21.2. It revealed that GDH exhibited the most activity with its physiological substrate (glycerol). Moreover, it showed some activity on several diols with adjacent hydroxyls, especially glycol.

21.4 Discussion

By blasting the sequence *gdh* of *K. pneumoniae* KG1 in Genbank (accession no. DQ985161), we found that it had significant similarity to that of bacteria such as *E. coli*, *Salmonella*, *Shigella*, *Klebsiella* and *Citrobacter*. Strains of *E. coli* that were able to convert glycerol to 1,3-PD have been constructed by expressing genes of GDHt (*dhaB*) and 1,3-PDOR (*dhaT*) from *K. pneumoniae* or those from *C. freundii* [10–12]. However, there were at least three enzymes (GDHt, PDOR, and GDH) that composed the key enzyme system of glycerol metabolism for producing 1,3-PD [11]. The GDH from *E. coli* was so similar to that from *K. pneumoniae* (99.7 % similarity) that it could compose the key enzyme system to produce 1,3-PD with GDHt and 1,3-PDOR in recombinant strain containing the gene of *dhaB* and *dhaT*.

GDHt and PDOR were overexpressed both or either in *K. pneumoniae*, however, the recombinant strains did not produce much more 1,3-PD than the wild-type strain

[12]. It was postulated that the accumulation and toxicity of the intermediate 3-HPA was responsible for it [11, 12]. 3-HPA could be reduced to 1,3-PD by 1,3-PDOR, which needed NADH as coenzyme. Moreover, the production of 1,3-PD of *E. coli* expressing genes of GDHt and 1,3-PDOR was relatively low even after optimizing [12]. The physiological role of 1,3-PD formation was to regenerate the reducing equivalent that was released from the formation of DHA by GDH [13], so NADH was essential for keeping the glycerol reductive pathway active to form 1,3-PD. Considering the high activity of recombinant GDHt and 1,3-PDOR in engineering strains of *K. pneumoniae* or *E. coli*, a large amount of NADH would be needed for the balance of glycerol metabolism. Therefore, the relatively low yield of 1,3-PD in engineering strains was possibly due to the lack of NADH. It was reported that fermentation with glucose as co-substrate could improve the conversion ratio of glycerol to 1,3-PD [14]. A large amount of reducing equivalent and energy contributed from the oxidation of glucose was probably the reason for it. GDH could regenerate NADH by oxidating glycerol [15]. Thus the conversion ratio of glycerol to 1,3-PD would increase if enough reducing equivalents could be regenerated by high activity recombinant GDH or glucose dehydrogenase when glucose was used as co-substrate.

Acknowledgments This project supported by the Foundation of Key Laboratory of Industrial Fermentation Microbiology of Ministry of Education and Tianjin Key Lab of Industrial Microbiology (Tianjin University of Science & Technology) (No. 2013IM002).

References

1. Ahrens K, Menzel K, Zeng AP et al (1998) Kinetic, dynamic, and pathway studies of glycerol metabolism by *Klebsiella pneumoniae* in anaerobic continuous culture: III. Enzymes and fluxes of glycerol dissimilation and 1,3-Propanediol formation. Biotechnol Bioeng 59:544–552
2. Biebl H, Marten S (1995) Fermentation of glycerol to 1,3-propanediol: use of cosubstrates. Appl Microbiol Biotechnol 44:15–19
3. Zhang XM, Li Y, Zhuge B (2006) Technical note optimization of 1,3-propanediol production by novel recombinant *Escherichia coli* using response surface methodology. J Chem Technol Biotechnol 81:1075–1078
4. Zhu MM, Lawman PD, Cameron DC (2002) Improving 1,3-propanediol production from glycerol in a metabolically engineered *Escherichia coli* by reducing accumulation of sn-glycerol-3-phosphate. Biotechnol Prog 18:694–699
5. Tobimatsu T, Azuma M, Matsubara H (1996) Cloning, sequencing, and high level expression of the genes encoding adenosylcobalamin-dependent glycerol dehydrase of *Klebsiella pneumoniae*. J Biol Chem 271:22352–22357
6. Céline R, Patricia S, Isabelle MS et al (2003) Molecular characterization of the 1,3-propanediol (1,3-PD) operon of *Clostridium butyricum*. PNAS 100:5010–5015
7. Zheng YY, Cao Y, Fang BS (2004) Cloning and sequence analysis of the *dhaT* gene of the 1,3-propanediol regulon from *Klebsiella pneumoniae*. Biotechnol Lett 26:251–255
8. Seo MY, Seo JW, Heo SY et al (2009) Elimination of by-product formation during production of 1,3-propanediol in *Klebsiella pneumoniae* by inactivation of glycerol oxidative pathway. Appl Microbiol Biotechnol 84(3):527–534

9. Johnson EA, Levine RL, Lin ECC (1985) Inactivation of glycerol dehydrogenase of *Klebsiella pneumoniae* and the role of divalent cations. J Bacteriol 164:479–483
10. Zheng Y, Zhao L, Zhang JG et al (2008) Production of glycerol from glucose by co-expressing glycerol-3-phosphate dehydrogenase and glycerol-3-phosphatase in *Klebsiella pneumoniae*. J Biosci Bioeng 105(5):508–512
11. Sun JB, Heuvel JVD, Soucaille P et al (2003) Comparative genomic analysis of *dha* regulon and related genes for anaerobic glycerol metabolism in bacteria. Biotechnol Prog 19:263–272
12. Zheng P, Wereath K, Sun JB (2006) Overexpression of genes of the *dha* regulon and its effects on cell growth, glycerol fermentation to 1,3-propanediol and plasmid stability in *Klebsiella pneumoniae*. Process Biochem 41:2160–2169
13. Oh BR, Hong WK, Heo SY et al (2013) The production of 1,3-propanediol from mixtures of glycerol and glucose by a *Klebsiella pneumonia* mutant deficient in carbon catabolite repression. Bioresour Technol 130:719–724
14. Petrov K, Stoyanov A (2012) Accelerated production of 1,3-propanediol from glycerol by *Klebsiella pneumoniae* using the method of forced pH fluctuations. Bioprocess Biosyst Eng 35 (3):317–321
15. Oh BR, Seo JW, Heo SY et al (2012) Fermentation strategies for 1,3-propanediol production from glycerol using a genetically engineered *Klebsiella pneumoniae* strain to eliminate by-product formation. Bioprocess Biosyst Eng 35(1–2):159–165

Chapter 22
Expression of Glucose-6-Phosphate Dehydrogenase and 6-Phosphogluconate Dehydrogenase Improve L-Citrulline Biosynthesis in *argG*-Deleted *Corynebacterium glutamicum*

Zhaoxing Liu, Luping Chen, Ning Hao, Lin Xu, Yan Li, Ming Yan and Pingkai Ouyang

Abstract *Corynebacterium glutamicum*, a well-known producer in the amino acids industry, has become a potential platform organism for synthetic biology in industrial biotechnology. During L-citrulline biosynthesis, NADPH is required as a crucial cofactor. Production of L-citrulline requires 2 mol of NADPH per mole of L-citrulline. The strategy focused on engineering of the pentose phosphate pathway (PPP) flux by different genetic modifications. In this study, two NADPH-supplying strategies based on glucose-6-phosphate dehydrogenase and 6-phosphogluconate dehydrogenase was compared, and their influences on L-citrulline biosynthesis were examined. The *zwf* and *gnd* genes were overexpressed in the L-citrulline-producing strain CgΔargG. The expression of both genes greatly enhanced intracellular NADPH concentration and L-citrulline production. The concentration of intracellular NADPH was increased by 287 and 363 %, and the production of L-citrulline was increased by 30.8 and 20.5 % in CgΔargG/pXMJ19-zwf and CgΔargG/pXMJ19-gnd, respectively, compared with CgΔargG. The concentration of NADPH in a *zwf*- and *gnd*-expressing strain was increased by 287 and 363 %, respectively. These results are helpful for improving L-citrulline biosynthesis and other biosynthetic processes.

Keywords *Corynebacterium glutamicum* · L-Citrulline · L-Ornithine · Glucose-6-phosphate dehydrogenase · 6-Phosphogluconate dehydrogenase

Z. Liu · L. Chen · N. Hao (✉) · L. Xu · Y. Li · M. Yan · P. Ouyang
College of Biotechnology and Pharmaceutical Engineering, Nanjing Tech University, Nanjing 211816, China
e-mail: haoning@njtech.edu.cn

T.-C. Zhang and M. Nakajima (eds.), *Advances in Applied Biotechnology*,
Lecture Notes in Electrical Engineering 333, DOI 10.1007/978-3-662-46318-5_22

22.1 Introduction

Corynebacterium glutamicum is the workhorse for the production of amino acids, such as L-glutamate, L-lysine, L-arginine, and L-ornithine [1]. L-Citrulline is also an important amino acid for our health since it is a source of endogenous L-arginine in the body. It is an amino acid of commercial interest that can be used as a food and feed additive and as an intravenous infusion agent. In *C. glutamicum*, L-citrulline is the precursor of L-arginine biosynthesis [2]. The biosynthesis of L-arginine can be improved through overexpressing biosynthetic pathway genes, blocking competing metabolic pathways, improving export systems, and increasing the precursor availability, as researched in recombinant *C. glutamicum* [3–5]. However, cofactor regulation is also important for the biosynthesis of L-arginine and L-citrulline. The most important cofactor for biosynthesis of L-arginine and L-citrulline is NADPH. Two molecules of NADPH are required for generation of one molecule of L-citrulline from ketoglutarate by the enzymes glutamate dehydrogenase (GDH) and *N*-Acetylglutamate 5-semialdehyde dehydrogenase (ArgC, Fig. 22.1). Thus, a sufficient supply of NADPH may be crucial for L-citrulline biosynthesis.

NADPH can be generated through two types of reactions. One is the reductive regeneration of NADPH from $NADP^+$ through various $NADP^+$-dependent dehydrogenases. The important $NADP^+$-dependent dehydrogenases in *C. glutamicum* include glucose-6-phosphate dehydrogenase (Zwf) and 6-phosphogluconate dehydrogenase (Gnd) in the pentose phosphate pathway (PPP) [6, 7] and malic enzyme (MalE) [8]. The overexpression of genes encoding these enzymes or the enhancement of PPP [9] would increase the supply of NADPH. Another reaction for generating NADPH is the phosphorylation of NADH through NADH kinase [10].

To understand the differential influences of Zwf and Gnd on NADPH supply and L-citrulline biosynthesis and to reveal the optimal NADPH-supplying strategy, Zwf expression and Gnd expression were researched in this study.

22.2 Materials and Methods

22.2.1 Strains and Cultivation Conditions

Escherichia coli strains DH5α was used as the hosts for cloning. *E. coli* was grown in Luria-Bertani (LB) medium (tryptone 10 g/L, yeast extract 5 g/L, and NaCl 10 g/L, pH 7.2) at 200 rpm and 37 °C. ArgG-deleted *C. glutamicum* was used for the production of L-citrulline. *C. glutamicum* was grown in LBG medium (LB supplemented with 5 g/L glucose) at 200 rpm and 30 °C. The concentration of chloromycetin was 20 μg/mL for *E. coli* and 10 μg/mL for *C. glutamicum*.

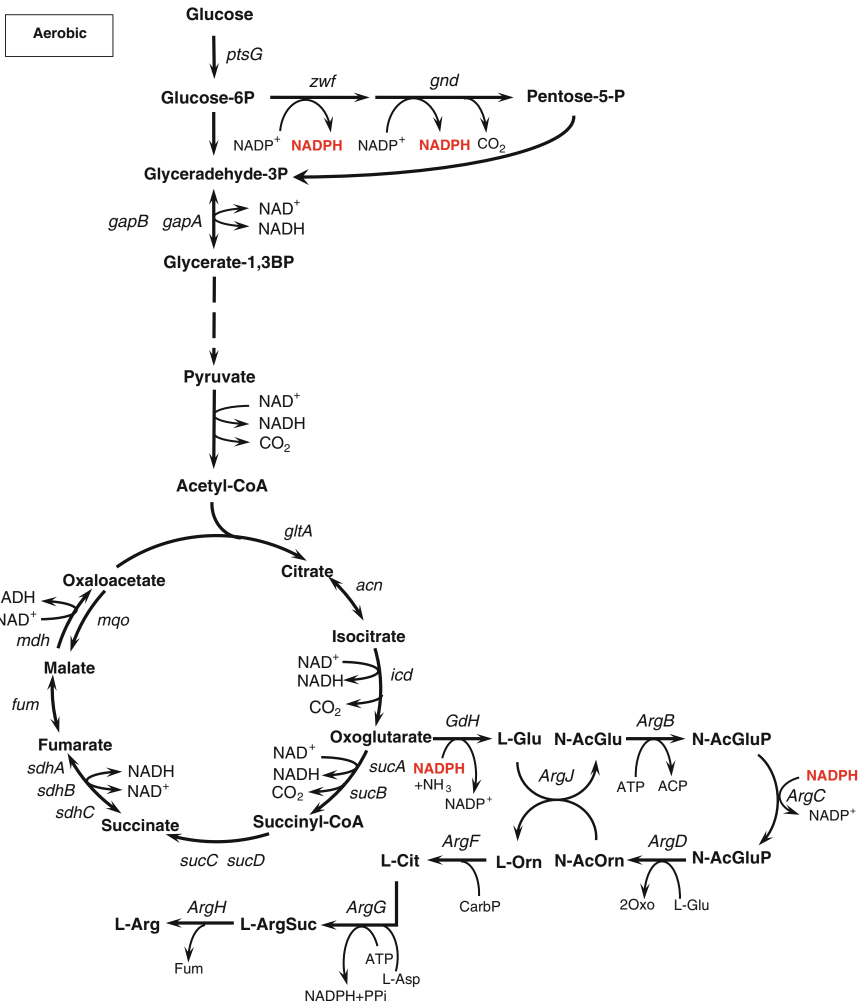

Fig. 22.1 L-Arginine biosynthetic pathway and NADPH metabolism in *Corynebacterium glutamicum*

22.2.2 *Construction of ppnK and zwf Expression Plasmids and Strains*

For the expression of *zwf* or *gnd* genes in *C. glutamicum*, the *zwf* gene (1,545 bp) was amplified at first from the genomic DNA of ATCC 13032 using the primers zwf-F and zwf-R and then ligated into vectors pXMJ19 to generate the plasmid, pXMJ19-zwf. Secondly, the *gnd* gene (1,455 bp) was amplified from the genomic DNA of ATCC 13032 using the primers gnd-F and gnd-R and then ligated into

Table 22.1 Plasmids and strains used in this study

Plasmid or strain	Relevant characteristics	Source
Plasmids		
pXMJ19	Shuttle plasmid	Stored in lab
pXMJ19-zwf	Shuttle plasmid carrying 1545-bp DNA fragment	This study
pXMJ19-gnd	Shuttle plasmid carrying 1455-bp DNA fragment	This study
Strains		
CgΔargG	Wild type ATCC 13032 + deletion of *argG*, encoding argininosuccinate synthase	Tang et al. [12]
CgΔargG/pXMJ19-zwf	CgΔargG harborring pXMJ19-zwf	This study
CgΔargG/pXMJ19-gnd	CgΔargG harborring pXMJ19-gnd	This study

vectors pXMJ19 to generate the plasmid, pXMJ19-gnd. Finally, *argG*-deleted *C. glutamicum* was transformed with the plasmids pXMJ19-zwf and pXMJ19-gnd to generate two strains, CgΔargG/pXMJ19-zwf and CgΔargG/pXMJ19-gnd (Table 22.1).

22.2.3 Determination of L-Citrulline Production

For the L-citrulline production experiments, *C. glutamicum* cells were precultured in seed medium (LB medium) at 30 °C and 200 rpm for 12 h. The preculture was inoculated into 50 mL of fermentation medium (glucose 100 g/L, $(NH_4)_2SO_4$ 20 g/L, urea 5 g/L, $K_2HPO_4{\cdot}3H_2O$ 1 g/L, KH_2PO_4 1 g/L, $MgSO_4$ 0.25 g/L, Mn^{2+}, Fe^{2+} 0.01 g/L, $ZnSO_4$ 1 mg/L, $CuSO_4$ 0.2 mg/L, $CaCl_2$ 10 mg/L, biotin 0.1 mg/L, pH 7.0) to a final optical density (OD_{600}) of 2.0 and shaken at 30 °C and 200 rpm for 36 h. For the inducible strains of CgΔargG/pXMJ19-zwf and CgΔargG/pXMJ19-gnd, IPTG was added to a final concentration of 1 mM after 12 h of fermentation to induce the expression of the target genes. The amino acid concentration in the fermented broth was measured using high-pressure liquid chromatography (HPLC, DIONEX, UltiMate 3000, USA) after pre-column derivatization with PITC [11]. HPLC separation was performed at 40 °C using a DIONEX C18 column (250 × 4.6 mm). The elution buffer consisted of an aqueous phase (0.1 M sodium acetate, pH 6.5) and an organic phase (80 % acetonitrile). The amino acids were detected at 254 nm, and the spectra were recorded online. The residual glucose concentration in the fermented broth was determined with a biosensor (Institute of Biology, Shandong Academy of Science, China). The cell concentration of fermented broth was determined by measuring the OD_{600} value after dilution with 1 M HCl. The dry cell weight (DCW, grams per liter) was calculated according to an experimentally determined formula: $DCW = 0.25 \times OD_{600}$.

22.2.4 Determination of Intracellular NAD(H) and NADP(H) Concentrations

The intracellular $NAD(P)^+$ and NAD(P)H of *C. glutamicum* cells were extracted using HCl and NaOH, respectively, and the amounts of NAD^+, NADH, $NADP^+$, and NADPH in each extract were quantified using a spectrophotometric enzymatic cycling method as described previously [10].

22.3 Results and Discussion

CgΔargG is a strain used for L-citrulline production. It can accumulate approximately 13–15 mM L-citrulline after fermentation in a shake flask for 36 h. Because NADPH is an important coenzyme in the L-citrulline biosynthetic pathway, NADPH supply would be crucial. Therefore, in this study, the glucose-6-phosphate dehydrogenase gene (*zwf*) and 6-phosphogluconate dehydrogenase gene (*gnd*) from *C. glutamicum* were cloned and expressed in CgΔargG, and their influence on L-citrulline biosynthesis was investigated.

To elucidate the influence of glucose-6-phosphate dehydrogenase and 6-phosphogluconate dehydrogenase on NADPH supply and L-citrulline biosynthesis, strains expressing *zwf* and *gnd* of *C. glutamicum* by an inducible expression vector pXMJ19 were generated, analyzed, and compared to the initial non-recombinant strain CgΔargG and the control strain carrying the empty vector pXMJ19. Expression of these genes was induced by 1 mM IPTG at 6 h of fermentation. Growth of these strains in fermentation medium revealed that CgΔargG/pXMJ19-zwf and CgΔargG/pXMJ19-gnd exhibited similar growth rates as CgΔargG. After fermentation for 36 h, the dry cell weight of the fermented broth from CgΔargG, CgΔargG/pXMJ19-zwf, and CgΔargG/pXMJ19-gnd cultures was 10.4 ± 0.2, 9.4 ± 0.6, and 11.0 ± 0.2 g/L, respectively. In addition, glucose was consumed in a similar pattern for all the strains. After fermentation for 36 h, approximately 30.2–38.1 g/L (75.5–95.3 %) of the glucose was consumed in these strains (Fig. 22.2).

Next, the intracellular NAD^+, NADH, $NADP^+$, and NADPH concentrations of these strains after fermentation at 30 °C for 24 h were assayed (Table 22.2). The intracellular NADPH concentration in CgΔargG/pXMJ19-zwf and CgΔargG/pXMJ19-gnd increased by 86 μM (287 %) and 109 μM (363 %), respectively. Accordingly, the ratio of NADP(H) to NAD(H) increased in *zwf*- and *gnd*-expression strains.

Finally, the production of L-citrulline in these *C. glutamicum* strains was determined. L-Citrulline production in the fermentation medium of CgΔargG/pXMJ19-zwf and CgΔargG/pXMJ19-gnd increased by 75.6 and 43.6 %, respectively, compared with JHI/pDXW8 and increased by 30.8 and 20.5 %, respectively, compared with CgΔargG. This result indicates that the increase of glucose-6-phosphate

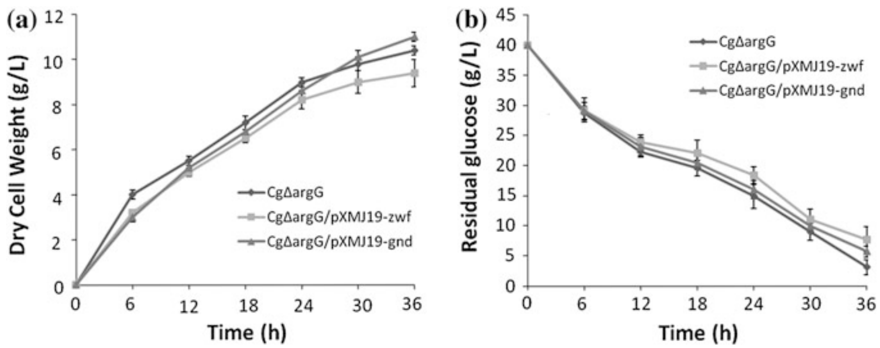

Fig. 22.2 L-Citrulline fermentation of *zwf*- and *gnd*-expressing *C. glutamicum* strains. **a** Cell growth; **b** residual glucose

Table 22.2 L-Citrulline production in *argG*-deleted *C. glutamicum* control stains and *zwf*- and *gnd*-expressing strains

Strains[a]	CgΔargG	CgΔargG/pXMJ19-zwf	CgΔargG/pXMJ19-gnd
NAD^+ (μM)	323 ± 37	343 ± 24	357 ± 15
NADH (μM)	44 ± 4	93 ± 23	81 ± 24
$NADP^+$ (μM)	110 ± 7	68 ± 15	84 ± 12
NADPH (μM)	30 ± 8	116 ± 19	139 ± 17
($NADP^+$ + NADPH)/ (NAD^+ + NADH)	0.38	0.42	0.50
(NADH + NADPH)/ (NAD^+ + $NADP^+$)	0.17	0.51	0.50

[a] The averages of three independent experiments are shown

dehydrogenase and 6-phosphogluconate dehydrogenase activity contributes to Ile biosynthesis, with the effect of glucose-6-phosphate dehydrogenase (Zwf) better than that of 6-phosphogluconate dehydrogenase (Gnd). In addition, the L-citrulline yield on glucose as well as the specific L-citrulline yield by CgΔargG/pXMJ19-zwf and CgΔargG/pXMJ19-gnd improved obviously compared with the control strain CgΔargG (Table 22.3).

Corynebacterium glutamicum is the most widely used bacterium for the production of amino acids, including L-citrulline. During the biosynthesis of these amino acids, NADPH is required as an important cofactor, and thus sufficient supply of NADPH may be helpful for the biosynthesis of amino acids. NADPH can be supplied by reductive regeneration of $NADP^+$ through various $NADP^+$-dependent dehydrogenases or by phosphorylation of NADH through NADH kinase. Several important $NADP^+$-dependent dehydrogenases of *C. glutamicum* had been examined previously, such as Zwf and Gnd of the PPP pathway. Conversion of the carbon flux from glycolytic pathway to PPP pathway had also been demonstrated to improve the NADPH regeneration and amino acid biosynthesis, such as the expression of the

Table 22.3 L-Citrulline production in *argG*-deleted *C. glutamicum* control stains and *zwf*- and *gnd*-expressing strains

Strains[a]	CgΔargG	CgΔargG/pXMJ19-zwf	CgΔargG/pXMJ19-gnd
OD_{600}	41.6 ± 0.8	37.5 ± 2.4	44.0 ± 0.8
Glucose consumed (g/L)	36.9 ± 1.2	32.3 ± 2.1	34.3 ± 0.9
Glucose consumed (mM)	204.6 ± 6.7	179.5 ± 11.7	190.2 ± 5.0
Glucose uptake rate (mmol g^{-1} (cdw) h^{-1})	0.55 ± 0.09	0.53 ± 0.05	0.48 ± 0.07
Glutamate titer (mM)	72.7 ± 3.9	1.2 ± 0.06	1.5 ± 0.08
Citrulline titer (mM)	14.6 ± 0.9	19.1 ± 1.2	17.6 ± 1.1
Arginine titer (mM)	1.55 ± 0.09	0.53 ± 0.03	0.49 ± 0.03
Ornithine titer (mM)	17.1 ± 3.4	24.7 ± 4.9	24.3 ± 4.8
Yield citrulline/glucose (mol/mol)	0.07 ± 0.01	0.11 ± 0.01	0.09 ± 0.01
Citrulline production rate (mmol g^{-1} (cdw) h^{-1})	0.039 ± 0.005	0.057 ± 0.005	0.044 ± 0.012

[a] The averages of three independent experiments are shown

fructose 1,6-bisphosphatase gene (*fbp*) and deletion of the phosphoglucoisomerase gene (*pgi*).

Among the inducible expression strains, the mere expression of *zwf* and *gnd* gene did not obviously influence the cell growth and glucose consumption. Such results demonstrate coenzyme regulation and NADP(H) supply as a useful metabolic engineering strategy for improving L-citrulline biosynthesis. However, the effect of these NADPH-supplying strategies on other biosynthetic pathways, as well as the systematic metabolic engineering of CgΔargG based on such NADPH-supplying strategies and other crucial metabolic engineering strategies shall be researched in the future.

Acknowledgments This study was supported by the National Basic Research Program of China (973 Program, No. 2011CBA00807), National High Technology Research and Development Program of China (863 Project, No. 2012AA022101), National Natural Science Foundation of China (NSFC, No. 21406113), Natural Science Foundation of the Higher Education Institutions of Jiangsu Province (No. 13KJB530008), and Scientific Research Innovation Projects of Jiangsu Province for University Graduate Students (No. KYLX_0777).

References

1. Becker J, Wittmann C (2012) Systems and synthetic metabolic engineering for amino acid production—the heartbeat of industrial strain development. Curr Opin Biotechnol 23 (5):718–726
2. Ikeda M, Mitsuhashi S, Tanaka K et al (2009) Reengineering of a Corynebacterium glutamicum L-arginine and L-citrulline producer. Appl Environ Microbiol 75(6):1635–1641
3. Park SH, Kim HU, Kim TY et al (2014) Metabolic engineering of Corynebacterium glutamicum for L-arginine production. Nat Commun. doi:10.1038/ncomms5618

4. Xu M, Rao Z, Dou W et al (2012) Site-directed mutagenesis and feedback-resistant N-acetyl-L-glutamate kinase (NAGK) increase Corynebacterium crenatum L-arginine production. Amino Acids 43(1):255–266
5. Xu M, Rao Z, Yang J et al (2012) Heterologous and homologous expression of the arginine biosynthetic argC~ H cluster from Corynebacterium crenatum for improvement of L-arginine production. J Ind Microbiol Biotechnol 39(3):495–502
6. Moritz B, Striegel K, de Graaf AA et al (2000) Kinetic properties of the glucose-6-phosphate and 6 phosphogluconate dehydrogenases from Corynebacterium glutamicum and their application for predicting pentose phosphate pathway flux in vivo. Eur J Biochem 267 (12):3442–3452
7. Becker J, Klopprogge C, Herold A et al (2007) Metabolic flux engineering of l-lysine production in Corynebacterium glutamicum—over expression and modification of G6P dehydrogenase. J Biotechnol 132(2):99–109
8. Georgi T, Rittmann D, Wendisch VF (2005) Lysine and glutamate production by Corynebacterium glutamicum on glucose, fructose and sucrose: roles of malic enzyme and fructose-1, 6-bisphosphatase. Metab Eng 7(4):291–301
9. Bartek T, Blombach B, Lang S et al (2011) Comparative 13C metabolic flux analysis of pyruvate dehydrogenase complex-deficient, L-valine-producing Corynebacterium glutamicum. Appl Environ Microbiol 77(18):6644–6652
10. Shi F, Li K, Huan X et al (2013) Expression of NAD (H) Kinase and glucose-6-phosphate dehydrogenase improve NADPH supply and l-isoleucine biosynthesis in corynebacterium glutamicum ssp. lactofermentum. Appl Biochem Biotechnol 171(2):504–521
11. Zhou H, Hao N, Yan M et al (2009) Determination of l-citrulline and l-ornithine by high performance liquid chromatography with precolumn derivation. J Nanjing Univ Technol (Natural Science Edition) 31(2):77–79
12. Tang J, Hao N, Xu S et al (2013) Construction of Corynebacterium glutamicum mutant with knockout of argG gene. J Nanjing Univ Technol (Natural Science Edition) 35(6):86–90

Part II
Optimization and Control of Biological Process

Chapter 23
Production of Amino Acids by Mixed Bacterial Strains-Mediated Solid State Fermentation of Feathers and Dynamic Changes to the Fermentation System

Yu Li, Dunji Hu, Sheng Chen, Xiangnan Lei, Xiangjin Zhang, Xiaoguang Liu and Fuping Lu

Abstract Bioprocessing of chicken feather wastes for production of free amino acids was investigated by solid-state fermentation (SSF) with (1) single strain, (2) double strains, (3) triple strains of *B. licheniformis* TCCC 11593, *B. alcalophilus* TCCC 11004 and *B. subtilis* TCCC 11279. The maximum production of total amino acids amounting to 161.35 mg/g was obtained under optimal SSF conditions: feather concentrations 1.0 g/250 mL, moisture contents 1:9 (w/v), inocula ratios (v/v) of 5:5:3 for *B. licheniformis*: *B. alcalophilus*: *B. subtilis respectively*, 60 h fermentation. Monitoring of mixed bacterial populations in the SSF process by real-time PCR indicated that *B. alcalophilus* was the dominant microorganism present in the SSF cultures. Moreover, measurements of dynamic changes in multienzyme activities in the SSF process suggested that, in terms of amino acid production, keratinase might play an important role in the initial hydrolysis of keratin and the further hydrolysis was most likely to be accomplished by elastase, collagenase, alkaline protease, and neutral protease elaborated by the three mixed bacterial strains. The above results indicated that mixed-strain SSF could serve as a cost-effective method to utilize chicken feather wastes to produce value-added feed additives or organic fertilizers.

Keywords Feathers waste · Solid-state fermentation · Total amino acids products · Dominant microorganism · Multienzyme activities

---

Y. Li · D. Hu · S. Chen · X. Lei · X. Zhang · X. Liu · F. Lu
Key Laboratory of Industrial Fermentation Microbiology, Ministry of Education, National Engineering Laboratory for Industrial Enzymes, The College of Biotechnology, Tianjin University of Science & Technology, Tianjin 300457, People's Republic of China

F. Lu (✉)
Industrial Microbiology Laboratory, College of Biotechnology, Tianjin University of Science & Technology, Tianjin 300457, People's Republic of China
e-mail: lfp@tust.edu.cn

T.-C. Zhang and M. Nakajima (eds.), *Advances in Applied Biotechnology*,
Lecture Notes in Electrical Engineering 333, DOI 10.1007/978-3-662-46318-5_23

23.1 Introduction

Though chicken feathers contain 90 % keratins, they have found limited use because keratins are resistant to degradation by common proteolytic enzymes such as pepsin, trypsin, and papain [1]. Worldwide, millions of tons of feather wastes are generated annually by poultry-processing industries and has become a solid waste management problem [2]. However, feather wastes are a rich source of natural protein and degradation of keratinous substrates represents a potential cost-effective means to produce amino acids that can be used as food additives for animals or a source of nitrogen for plants [3]. Traditional ways of hydrolyzing feathers such as alkali hydrolysis and steam pressure cooking to produce feather meal as animal feed supplement may destroy certain types of valuable amino acids, not to mention that such processes consume large amounts of energy [4] Biodegradation by microorganisms possessing keratinolytic activity represents an alternative attractive method of improving the nutritional value of keratin wastes, as it offers a cheap approach to the production of value-added products [5].

Keratins are easily degraded by keratinases [6] but single keratinase could not efficiently degrade feather even after prolonged incubation. It was shown that complete feather degradation occurred only when bacteria cells were used [7]. However, utilization of substrates by a single strain in pure-culture-based processes has been limited to a narrow range of biomaterials [8]. Mixed cultures are structured by highly diverse microbes and constructed from natural inocula, which facilitate biological processes under nonsterile conditions without altering strain stability. Furthermore, high microbial diversity enables such cultures to utilize complex substrates with complex compositions [9].

Effective use of mixed culture fermentation requires a better understanding of dynamics of microbial communities participating in a specific fermentation process, thus allowing the creation of optimal conditions for desirable population composition of the mixed culture. In recent years, real-time polymerase chain reaction (PCR) approach has been an effective means for analyzing the structure and species composition of complex microbial communities in a wide range of samples from soil [10], compost [11], and solid-state fermentation (SSF) [12].

In this study, a feather-degrading system comprising *Bacillus licheniformis*, *Bacillus alcalophilus*, and *Bacillus subtilis* was employed for SSF of chicken feather meal. Isolates of *B. licheniformis* and *B. subtilis* have shown previously to be capable of effective degradation of feathers, including *B. licheniformis* PWD-1 [13], *B. subtilis* RM-1 [14].

The aim of this study was to improve production of amino acids from chicken feather meal using mixed-culture SSF. Mixed-culture SSF conditions for maximum production of amino acids were determined. Dynamics of bacterial populations and multienzyme activities during SSF were monitored by real-time PCR and specific enzymatic activity assays, respectively, and plausible connections among bacterial population composition, multienzyme activities, and amino acid contents were examined.

23.2 Materials and Methods

23.2.1 Microorganism and Inoculums

The three bacterial strains used throughout this work, *B. licheniformis* TCCC 11593, *B. alcalophilus* TCCC 11004, and *B. subtilis* TCCC 11279 were previously isolated from chicken manure from a chicken farm in Tianjin and identified by the lab. These three strains were maintained on a medium containing (%) yeast extract 0.5, peptone 1.0, NaCl 1.0, agar 2.0 %, pH 7.5.

23.2.2 Solid Substrate Fermentation Process

At the beginning, chicken feathers including barbs, calamuses, and rachises were chopped into 5 mm segments with a grinder. Then, 1 g finely cut feather power and 9 mL culture solution containing (g/L) maltose 1, NH_4Cl 1.5, K_2HPO_4 1, KH_2PO_4 0.4, NaCl 0.4, $MgSO_4$ 0.3 were added into 250 mL Erlenmeyer flasks and mixed thoroughly. After that, the three bacteria strains with a colony concentration of about 1×10^9 CFU/mL were inoculated into the 250 mL Erlenmeyer according to a proportion 1:1:1. Finally, inoculated flasks were incubated in relative humidity of 87 %, at 37 °C for 60 h.

23.2.3 Real-Time PCR

The genomic DNA was extracted from SSF samples by the method previously described with slight modifications [15] and stored at −20 °C. The three pairs of primers used and the predicted sizes of amplicons are shown in Table 23.1.

Real-time PCR amplification of specific sequences from the three bacterial genomes was used to estimate the total number of cells of individual strains. Real-time PCR amplification was conducted on a 7,500 Fast Real-Time PCR System (Applied Biosystems) using the SYBR ®Premix Ex Taq™ (Perfect Real Time) kit (Takara).

Table 23.1 Three pairs of primers used and the sizes of predicted amplicons of *B. licheniformis*, *B. alcalophilus* and *B. subtilis*

Bacillus sp.	Primer: F	Primer: R	Amplicons (bp)
B. licheniformis	ATTATCAGGAA	GAAACTTTTC	646
	TTTGAACGTGG	AAGCGCTTCT	
B. alcalophilus	GGCACTAC	TCTCCACCTG	678
	GGGCATCG	GAGAGAGGG	
B. subtilis	AATCCCCG	GACCATGTAC	433
	TTTCGTCCA	TCTTGCCATG	

23.2.4 Assay of Enzymatic Activity in Solid-State Fermentation

Keratinase activity was determined using 1 % feather powder in Tris/HCl (50 mM, pH 8.0) as a substrate. One unit (U/mL) of keratinolytic production was defined as an increase in the absorbance at 280 nm (A280) [16] of 0.01 per hour under the conditions described above.

Elastolytic activity was assayed by the colorimetric method of Sacher [17]. One unit of elastase activity was defined as the amount of enzyme required to solubilize 20 mg of elastin-Congo red under the tested conditions.

The activity of collagenolytic protease was assayed by the method of Kang [18] with modifications. One unit (U) of collagenase activity was expressed as 1 mmol of glycine equivalent released per mL per minute.

The Anson–Hagihara method was employed for alkaline protease assay [19] using casein as the substrate. The protocol was previously described [20]. One unit of alkaline protease activity (U) was defined as the amount of enzyme that produces 1 μg of tyrosine/min under the assay conditions.

Neutral protease activity was assayed by the method of Chandran Sandhya [21]. One unit of enzyme activity was defined as the amount of enzyme that produced 1 mM tyrosine/min under the assay conditions.

23.2.5 Estimation of Free Amino Acids by HPLC

The quantities of amino acids released during feather degradation by mixed bacterial strains under SSF were estimated by an HPLC method described by Sieberr [22].

23.3 Results and Discussion

23.3.1 Determination of Optimal Parameters for Production of Amino Acids by SSF

As shown in Fig. 23.1, SSF of feather meal by mixed-culture of the three bacterial strains resulted in higher levels of total amino acids compared with that of SSF by either mixed-culture of two bacterial strains or a single bacterial strain. The highest amino acid yield was 96.61 mg/g.

The optimal combination of variables for the highest yield of total amino acids was determined to be: the inoculation volume for *B. licheniformis*, *B. alcalophilus*, and *B. subtilis* was 5 mL (5.03×10^9 CFU/mL), 5 mL (4.95×10^9 CFU/mL) and

Fig. 23.1 Effect of mode of SSF on total amino acid yield (D: *B. licheniformis*, S: *B. alcalophilus*, K: *B. subtilis*)

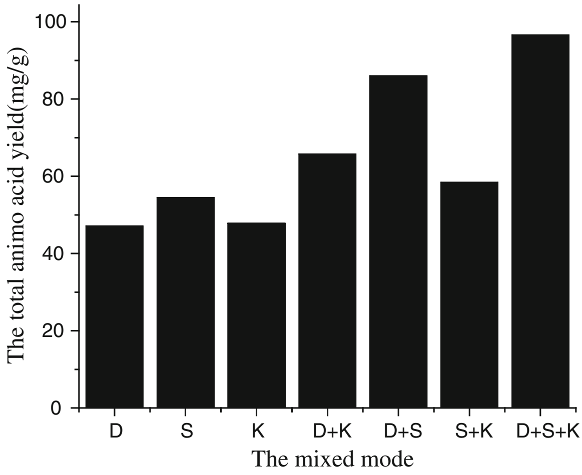

3 mL (2.6×10^9 CFU/mL), respectively. The maximum production of total amino acids amounting to 161.35 mg/g was obtained.

Through optimization of mixed-strain SSF conditions, as shown in Fig. 23.2. the highest yield of total amino acids (161.35 mg/g) was obtained when medium feather concentration was 1.0 g/250 mL, moisture content 1:9 (W/V), and fermentation time 60 h. Decreased production of total amino acids was observed at 72 h (114.21 mg/g) and reached the lowest level at 84 h (89.64 mg/g) (Fig. 23.2), which could be explained by the utilization of available free amino acids by the three bacterial strains as carbon and nitrogen sources. However, further fermentation resulted in improved yields of total amino acids (131.47 mg/g) at 96 h (Fig. 23.2).

When the feather concentrations were increased to more than 1 g/250 mL (1.5–3 %), the total amino acid contents started to decline, most likely due to the substrate inhibition effect caused by the high concentration of feather [23]. Among several important factors affecting microbial growth and enzyme yields under SSF using a particular substrate, moisture level is considered as one of the most critical [24]. SSF processes differ from submerged fermentation culture, since microbial growth and product formation occur at or near the surface of the solid substrate particle [24]. As shown in Fig. 23.2, increases in medium moisture contents resulted in increased levels of total amino acid production and near linearity between moisture content and the total amino acids yield was observed from 1:1 to 1:9 (w/v). Maximum total amino acid yields were achieved at a moisture content of 1:9 (w/v). Thereafter, further increases in moisture level in the fermentation medium resulted in reduced levels of total amino acids (Fig. 23.2). Under solid-state fermentation, levels of moisture higher than the optimum caused a decrease in porosity, an alteration in substrate particle structure, and a lower oxygen transfer, which had a negative effect on *Bacillus* sp. growth and metabolism [25]. On the other hand, at the lowest and the highest moisture levels, the decomposition rate of the total organic matter decreased [26].

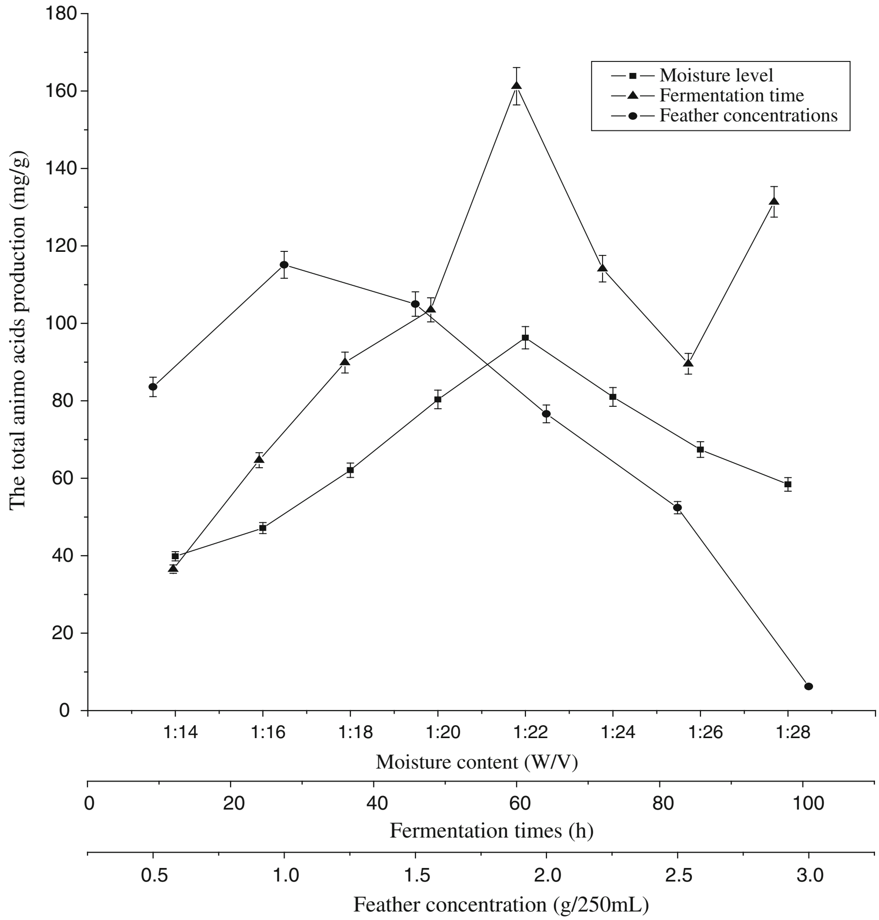

Fig. 23.2 Effect of moisture level (w/v), fermentation time (h) and feather concentrations (g/250 mL) on total amino acid yield

23.3.2 The Dynamic Change in the Populations of the Three Bacillus Species

The three *Bacillus* strains used for SSF of chicken feathers are highly similar in terms of colony morphology. Thus, changes in the bacterial populations of the individual strains during SSF were enumerated by real-time PCR. The standard curves used to quantify the genome copies of the three bacterial strains in SSF were generated by plotting threshold cycles against the logarithm of the initial copy

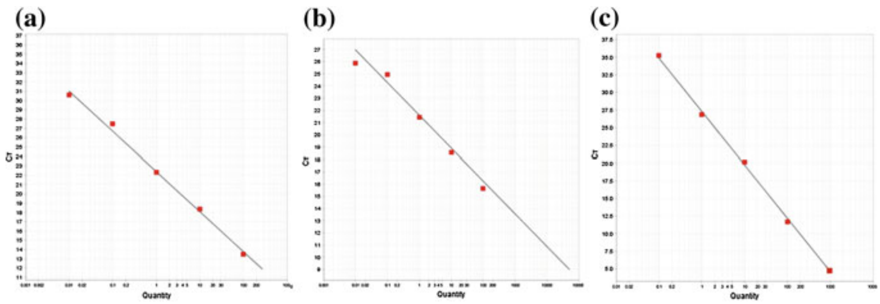

Fig. 23.3 **a**, **b**, **c** The standard curves of *B. licheniformis* (R^2 = 0.994), *B. subtilis* (R^2 = 0.991), and *B. alcalophilus* (R^2 = 0.998)

Table 23.2 The total amino acid yield (mg/g) produced by solid-state fermentation and the numbers of genome template copies of the three *Bacillus* sp. (copies per gram of sample) in the SYBR green real-time PCR assay

Sample (h)	Total amino acids yield (mg/g)	Copy numbers (copies/g sample)		
		B. alcalophilus	*B. licheniformis*	*B. subtilis*
12	36.59	2.203E+10 ±3.325E+08	2.515E+10 ±1.056E+08	7.813E+09 ±3.325E+08
24	64.74	2.226E+10 ±2.822E+08	2.526E+10 ±1.161E+08	7.836E+09 ±6.302E+07
36	89.97	2.545E+10 ±2.834E+08	2.645E+10 ±1.854E+08	7.945E+09 ±8.854E+07
48	103.59	2.977E+10 ±6.519E+08	2.927E+10 ±5.319E+08	8.227E+09 ±6.519E+07
60	161.35	3.704E+10 ±3.367E+08	3.502E+10 ±3.372E+08	8.802E+09 ±3.367E+07
72	114.21	3.714E+10 ±1.421E+08	3.634E+10 ±1.431E+08	8.914E+09 ±1.421E+08
84	89.64	3.727E+10 ±1.140E+09	3.687E+10 ±1.140E+08	8.997E+09 ±1.140E+08
96	131.47	3.798E+10 ±4.680E+08	3.703E+10 ±4.680E+08	9.043E+09 ±4.680E+07

number of the target DNA molecules. The known concentrations of PCR products of *B. licheniformis* and *B. subtilis* were diluted from 10^7 copies/μL to 10^3 copies/μL and of *B. alcalophilus* diluted from 10^8 copies/μL to 10^4 copies/μL. A high reproducibility between three independent standard dilutions was obtained. The curves showed good linear relationship between the amounts of PCR products and C_T of the target gene (Fig. 23.3a–c). In the range of the detection concentration, the real-time PCR efficiency was calculated as 1.13 based on the equation amplification efficiency = $10^{-1/\text{slope}} - 1$ [27]. In the standard samples, melting curve with a single melting peak was detected at 86.1 °C, and no primer dimers or other unspecific PCR products were amplified, indicating the presence of a single amplicon for each strain. Table 23.2 shows the dynamic change of three strains in gene copies during SSF.

As shown in Table 23.2, it was apparent that the number of *B. alcalophilus* cells was much greater than that of either *B. licheniformis* or *B. subtilis* during 24–60 h. Therefore, it can be concluded that *B. alcalophilus* played a dominant role in the mixed culture SSF using feather meal as a substrate.

In our previous work, *B. licheniformis* TCCC11593 showed a strong ability to degrade feathers, with a maximum keratinase activity of 98.0 U/mL after 48 h of submerged fermentation. The results shown in Table 23.2 indicate that the number of *B. licheniformis* cells was second only to that of *B. alcalophilus* and was closely related to the total amino acid yield. In the meantime, the increase of *B. subtilis* cells number also had a role in promoting production of amino acids. After 60 h, with the consumption of amino acids and the accumulation of harmful metabolites, the total population of the three *Bacillus* strains began to level off.

23.3.3 Dynamic Changes of Multiple Enzyme Activities

A combination of different enzymes could effectively hydrolyze complex substrates of feed stuff [28]. To investigate the relationship between changes in activities of multiple enzymes and the total amino acid contents during feather meal SSF, we measured the respective activities of keratinase, elastase, collagenase, alkaline protease, and neutral protease at indicated time points.

As shown in Fig. 23.4a, during 0–24 h, increased levels of keratinase activity were detected and the highest value reached at 24 h. However, after 24 h, keratinase activity exhibited a dramatic decline and was undetectable at about 60 h, while elastase, collagenase, alkaline protease, and neutral protease activities displayed significant increases in feather meal SSF during 0–60 h. As shown in Fig. 23.4b–d, the keratinase activity was mainly elaborated by *B. licheniformis* and *B. alcalophilus*, while the collagenase was produced by *B. licheniformis* and *B. subtilis*, and all three *Bacillus* species produced high levels of elastase activities.

The fact that total amino acid contents peaked at 60 h, while the levels of keratinase activity started to decline after 24 h and other multiple proteases activities continued to increase until 60 h, suggest that keratinase played an important role during the first 24 h fermentation process for amino acid production, and elastase, collagenase, alkaline protease, and neutral protease used denatured keratins as substrates to produce more amino acids through further hydrolysis during the period of 24–60 h in SSF process.

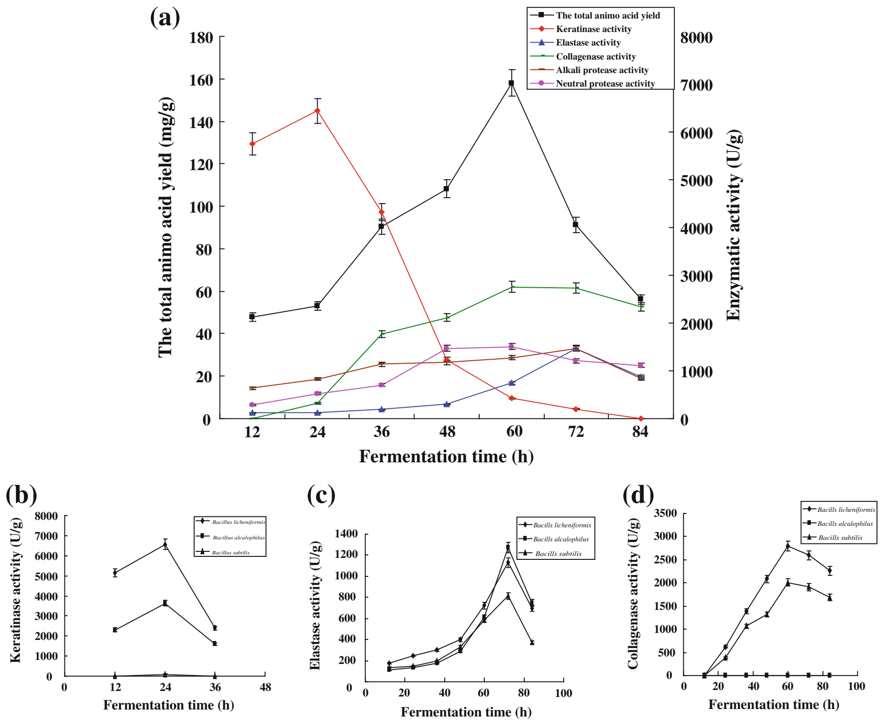

Fig. 23.4 **a–d** Relation between the dynamic changes in activities of enzymes and the total amino acid yield in SSF

23.3.4 Analysis of Composition of the Total Amino Acids

HPLC method was used to determine the major composition of the hydrolysates of the feather meal mixed-culture SSF. As shown in Table 23.3, under the optimum fermentation conditions, the free amino acids detected in the SSF culture included serine, arginine, tyrosine, valine, cystine, isoleucine, norleucine, and lysine. Interestingly, isoleucine was the most abundant amino acid, reaching 28.01 mg/g, which may be due to the high disulfide content of feather keratin [29]. Previous work showed that the major free amino acids of degradation of feathers by *B. licheniformis* PWD-1 are leucine, tryptophan, valine, isoleucine, phenylalanine, and alanine [13]. The differences could be due to the use of different microorganisms [30].

Table 23.3 Free amino acid analyses in SSF by mixed bacterial strains at 37 °C with a feather concentration of 1.0 g/250 mL, a moisture content of 1:9 (w/v) in 60 h

Amino acids	Serine	Arginine	Tyrosine	Valine	Cystine	Isoleucine	Norleucine	Lysine
The yield (mg/g)	3.33 ± 0.02	8.05 ± 0.03	6.05 ± 0.04	9.41 ± 0.05	22.09 ± 0.07	28.01 ± 0.06	7.76 ± 0.01	2.52 ± 0.01

23.4 Conclusion

In this work, mixed three-strain SSF of chicken feathers was shown to be superior to either single strain or double-strain SSF for optimal production of free amino acids, which can be used either as a low cost ingredient in animal feed formulation or as an organic fertilizer. Monitoring of the dynamics of the mixed bacterial populations, multienzyme activities, and contents of total amino acids during the course of SSF has provided valuable insights for further designing a cost-effective process to produce amino acids from chicken feather wastes.

Acknowledgments This work was supported by the National High-Tech Research and Development Plan (“ 863” Plan), No. 2011AA100905-4 and 2012AA021502, National Natural Science Foundation of China (NSFC), No. 21076159 and Program for Changjiang Scholars and innovative Research Team in University (PSCIRT), No. IRT1166.

References

1. Riffel A, Brandelli A (2006) Keratinolytic bacteria isolated from feather waste. Braz J Microbiol 37:395–399
2. Prakash P, Jayalakshmi SK, Sreeramulu K (2010) Production of keratinase by free and immobilized cells of Bacillus halodurans strain PPKS-2: partial characterization and its application in feather degradation and dehairing of the goat skin. Appl Biochem Biotechnol 160:1909–1920
3. Awad GEA, Esawy MA, Salam WA et al (2011) Keratinase production by Bacillus pumilus GHD in solid-state fermentation using sugar cane bagasse: optimization of culture conditions using a Box-Behnken experimental design. Ann Microbiol 61:663–672
4. Cai CG, Lou BG, Zheng XD (2008) Keratinase production and Keratin degradation by a mutant strain of Bacillus subtilis. J Zhejiang Univ Sci B 9:60–67
5. Kim JM, Lim WJ, Suh HJ (2001) Feather degrading Bacillus species From poultry waste. Process Biochem 37:287–291
6. Ramnani P, Singh R, Gupta R (2005) Keratinolytic potential of Bacillus licheniformis RG1: structural and biochemical mechanism of feather degradation. Can J Microbiol 51(3):191–196
7. Riffel A, Lucas F, Heeb P et al (2003) Characterization of a new keratinolytic bacterium that completely degrades native feather keratin. Arch Microbiol 179:258–265
8. Kalogo Y, Habibi S, Malclean HL et al (2007) Environmental implications of municipal solid waste-derived ethanol. Environ Sci Technol 41:35–41
9. Lin CW, Wu CH, Tran DT et al (2011) Mixed culture fermentation from lignocellulosic materials using thermophilic lignocellulose-degrading anaerobes. Process Biochem 46:489–493
10. Innerebner G, Knapp B, Vasara T, Romantschuk M, Insam H (2006) Traceability of ammonia-oxidizing bacteria in compost-treated soils. Soil Biol Biochem 38(5):1092–1100
11. Danon M, Franke-Whittle IH, Insam H et al (2008) Molecular analysis of bacterial community succession during prolonged compost curing. FEMS Microbiol Ecol 65(1):133–144
12. Yong XY, Cui YQ, Chen LH et al (2011) Dynamics of bacterial communities during solid-state fermentation using agro-industrial wastes to produce poly-γ-glutamic acid, revealed by real-time PCR and denaturing gradient gel electrophoresis (DGGE). Appl Microbiol Biotechnol 92:717–725
13. Williams CM, Richter CS, Mackenzie JM et al (1990) Isolation, identification and characterization of a feather-degrading bacterium. Appl Environ Microbiol 56:1509–1515

14. Rai SK, Konwarh R, Mukherjee AK (2009) Purification, characterization and biotechnological application of an alkaline β-keratinase produced by Bacillus subtilis RM-01 in solid-state fermentation using chicken-feather as substrate. Biochem Eng J 45:218–225
15. Williams CM, Richter CS, Mackenzie JM et al (1990) Isolation, identification and characterization of a feather-degrading bacterium. Appl Environ Microbiol 56:1509–1515
16. Friedrich J, Gradisar H, Vrecl M et al (2005) In vitro degradation of porcine skin epidermis by a fungal keratinase of Doratomyces microsporus. Enzyme Microb Technol 36:455–460
17. Mehrotra S, Pandey PK, Gaur R et al (1999) The production of alkaline protease by a Bacillus sp. isolate. Biores Technol 67:201–203
18. Kang SI, Jang YB, Choi YJ (2005) Purification and properties of a collagenolytic protease produced by marine bacterium Vibrio vulnificus CYK279H. Biotechnol Bioprocess Eng 10:593–598
19. Hagihara B, Matsubara H, Nakai M (1958) Crystalline bacterial proteinase of Bacillus subtilis. J Biochem 45:185–194
20. Sachar LA, Winter KK, Sicher N (1955) Photometric method for estimation of elastase activity. Proc Soc Exp Biol Med 90:323–326
21. Sandhya C, Sumantha A, Szakacs G et al (2005) Comparative evaluation of neutral protease production by Aspergillus oryzae in submerged and solid-state fermentation. Process Biochem 40:2689–2694
22. Sieberr J, Palmer RJ, Hirsch P (1991) Analyse of free amino acids in microbially colonized sandstone by precolumn phenyl isothiocyanate derivatization and high-performance liquid chromatography. Appl Environ Microbiol 59:879–881
23. Cortezi M, Monti R, Contiero J (2005) Temperature effect on dextransucrase production by Leuconostoc mesenteroides FT 045 B isolated from alcohol and sugar mill plant. Afr J Biotechnol 4(3):279–285
24. Pandey A, Soccol CR, Mitchell D (2000) New developments in solid state fermentation: I-bioprocesses and products. Process Biochem 35:1153–1169
25. Archana A, Satyanarayana T (1997) Xylanase production by thermophilic Bacillus licheniformis A99 in solid state ermentation. Enzyme Microb Technol 21:12–17
26. Gautam P, Sabu A, Pandey A (2002) Microbial production of extra-cellular phytase using polystyrene as inert support. Bioresour Technol 83:229–233
27. Bustin SA, Benes V, Garson JA (2009) The MIQE guidelines: minimum information for publication of quantitative real-time PCR experiments. Clin Chem 55:611–622
28. Silversides FG, Scott TA, Korver DR (2006) A study on the interaction of xylanase and phytase enzymes in wheat-based diets fed to commercial white and brown egg laying hens. Poult Sci 85(2):297–305
29. Jeong JH, Jeon YD, Lee OM et al (2010) Characterization of a multifunctional feather-degrading Bacillus subtilis isolated from forest soil. Biodegradation 21(6):1029–1040
30. Yamamura S, Morita Y, Hasan Q (2002) Keratin degradation: a cooperative action of two enzymes from Stenotrophomonas sp. Biochem Biophys Res Commun 294(5):1138–1143

Chapter 24
Effects of Culture Medium on PUFAs Production by *Mortierella isabellinas*

Dengyue Sun, Cuixia Zhou, Chuanhe Zhu and Yanru Sun

Abstract In the paper, in order to improve the polyunsaturated fatty acids (PUFAs) by *Mortierella isabellina*, the effects of carbon source, nitrogen source, carbon to nitrogen (C/N) ratio, and metal ions on PUFAs production were investigated. The results of the research showed that different kinds of carbon source and nitrogen source had obviously effect on PUFAs production, the glucose and mixture nitrogen (yeast extract: peanut meal at 3:1 (w/w)) were greatly suitable for PUFAs production and cell growth. The glucose concentration and C/N ratios have significant effect on PUFAs production. Meanwhile, the results indicate the metal ions have profound effects on fungus growth and PUFAs production. Ca^{2+} and Mg^{2+} could promote PUFAs production. Almost all the improvement of PUFAs was obtained through increasing thallus biomass, though there were some influences on the metabolism. Under the optimal culture media composition, the yields of cell dry weight, linoleic acid (LA), gama-linolenic acid (GLA), and total PUFAs were 32.48, 2.90, 2.83, and 7.36 g/L, respectively.

Keywords *Mortierella isabellina* · Polyunsaturated fatty acids · Carbon source · Nitrogen source · C/N ratio · Metal ions

24.1 Introduction

Polyunsaturated fatty acids (PUFAs) present a potential industrial value and economic value owning to their specific characteristics [1]. In recent years, there has been an increased interest in nutrient and medical application, especially the ω-3

D. Sun and C. Zhou contributed equally to this work.

D. Sun · C. Zhou · C. Zhu (✉) · Y. Sun
College of Food Science and Engineering, Shandong Agricultural University, No. 61, Daizong Road, Tai'an 271018, Shandong, People's Republic of China
e-mail: chhzhu@sdau.edu.cn

T.-C. Zhang and M. Nakajima (eds.), *Advances in Applied Biotechnology*,
Lecture Notes in Electrical Engineering 333, DOI 10.1007/978-3-662-46318-5_24

and ω-6 series of PUFAs are supposed to be potential food additives and pharmaceuticals for their biological activities [2]. As we all know, the PUFAs could be used to treat heart and circulatory disorders, cancer, or inhibit the inflammatory reaction effectively [13].

Up-to-date, a variety of microorganisms has been found to yield exceptionally large amount of PUFAs under some special conditions. The PUFAs production of microorganisms could be manipulated and changed substantially just by simply changing their growth conditions instead of having to depend on genetic manipulation or extensive breeding efforts [3]. In this study, one of the typically realistic commercial fungal alternatives called *Mortierella isabellina* was chosen as the target microorganism.

Over the past several years, many researchers have put much effort to develop the more economical bioprocesses for PUFAs production. In particular, the production of PUFAs using the fungus *Mortierella* in liquid culture has been extensively studied [4, 5]. But, the cost of PUFAs production was still higher. The mutant gained mutagenesis screening has its own requirement of special conditions for maximum objective product production [6]. In the present study, the effects of the key medium nutrient such as carbon source, nitrogen source, C/N ratio, and metal ions on the LA, GLA, and total PUFAs production of *M. isabellina* were investigated.

24.2 Materials and Methods

24.2.1 Microorganism and Culture Mediums

Microorganism: *M. isabellina* NTG_{1-121} was a mutant of *M. isabellina* As 3.3410 obtained through mutagenesis screening in our lab and was kept on potato dextrose agar (PDA) at 4 °C.

Culture mediums: Seed medium contained (g/L): $(NH_4)_2SO_4$, 2; yeast extract, 2; glucose, 100; KH_2PO_4, 1 and $MgSO_4$, 0.3. Basal submerged culture medium: The carbon source was glucose (100 g/L); nitrogen source was yeast extract (2 g/L); KH_2PO_4 was at 2 g/L; $MgSO_4$ was at 0.3 g/L; and sodium citrate was at 2 g/L. The initial pH of all mediums was adjusted to 6.0 before autoclaving and all cultures were sterilized at 121 °C for 20 min.

24.2.2 Cultivate Methods

All the slants were incubated at 28 ± 1 °C for 6 days. And all research experiments were performed in 500 mL conical flasks, containing 100 mL of liquid medium. The seed medium was added with 1 mL of spore suspension (1.0×10^5–10^6 cfu/mL) before being incubated in an orbital shaker (TENSUC, Shanghai, China) at 28 ± 1 °C for 2 days at 160 rpm. And the fermentation medium was inoculated with 10 mL seed culture solution, shaken at 160 rpm and incubated at 28 ± 1 °C for 7 days.

24.2.3 Cell Dry Weight Determination and Lipid Extraction

Cell dry weight determination: After 7 days, the mycelia were harvested from the fermentation culture by suction filtration through Whatman-1440-110. Cell dry weight was determined. The dried mycelia were transferred to a 50 mL centrifuge tube after being grinded.

Lipid extraction: Extraction of lipids from mycelia was carried out according to the modified procedure of Bligh and Dyer [7].

24.2.4 Fatty Acid Analysis

Fatty acid methyl ester (FAME) was prepared by the process of boron trifluoride (GB/T 17376-2008) [8]. The fatty acids composition and content were analyzed by using Gas Chromatography–Mass Spectrometer (GC–MS), and the chromatographic column was Stabilwax-DA (30 m × 0.32 mm × 0.25 μm). The initial column temperature (200 °C) was maintained for 8 min, increased to 230 °C with the increasing rate of 5 °C min^{-1}, and the temperature was maintained at 230 °C for 10 min. Helium was used as the carrier gas, and the flow rate was 2.0 mL min^{-1}, with one 10:1 of splitting ratio. Electron impact (EI) mode with a mass scan range of 45–450 amu was applied in the mass spectrum, and the ionization voltage was set at 70 eV. Both the injector port and ion source temperature were maintained at 200 °C. Methyl esters of different fatty acids such as linoleic acid, gama-linolenic acid, palmitic acid, palmitoleic acid, stearic acid, oleic acid, linoleic acid, and so on were used as standard for fatty acid identification and quantitation [9]. There is a linear correlation between the concentration of fatty acids (X) and the peak area (Y) at a specific retention time. In the concentrations between 0 and 4,000 mg/L, the equation and correlation coefficient (r) were $Y = 11692x + 80378$ and 0.9965, $Y = 106803x + 108407$ and 0.9995 for gama-linolenic acid and linoleic acid, respectively.

24.2.5 Effects of Carbon and Nitrogen Source, C/N Ratio, and Metal Ions on PUFAs Production

Effect of carbon source on PUFAs production: In the experiment, glucose in the basal fermentation medium was replaced by sucrose (100 g/L), maltose (100 g/L), molasses (100 g/L), and soluble starch (100 g/L) and incubated at 28 °C for 7 days.

For carbon source concentration experiments, the range of carbon source concentrations was from 0 to 140 g/L.

Effect of nitrogen source and C/N ratios on PUFAs production: Yeast extract as the sole nitrogen source in the basal medium was replaced by 2 g/L of beef extract, peptone, urea, $(NH_4)_2SO_4$, KNO_3, peanut meal, and soybean cake powder. Based on the screening results of nitrogen source, the effect of different ratios of yeast extract and peanut meal (w/w) on PUFAs production was evaluated. The effect of C/N ratio was studied with 100 g/L of carbon source, adjusting the ratio of the mixture of peanut meal and yeast extract at 1:3 (w/w) from 10 to 50.

Effect of metal ions on PUFAs production: Magnesium (Mg^{2+}), manganese (Mn^{2+}), iron (Fe^{2+}), and copper (Cu^{2+}) ions were in the form of sulfates ($MgSO_4 \cdot 7H_2O$ 99.0 %, $MnSO_4 \cdot H_2O$ 99.0 %, $FeSO_4 \cdot 7H_2O$ 99.0 %, $CuSO_4 \cdot 5H_2O$ 99.0 %); while zinc (Zn^{2+}) and calcium (Ca^{2+}) ions in the form of iron II chloride, which are anhydrous and the purity were 98.0 and 96.0 %, respectively. Fe^{2+}, Cu^{2+}, Zn^{2+}, and Ca^{2+} were added into basal fermentation medium containing the optimal carbon and nitrogen source and the concentrations were all 5, 50, and 100 mg/L (concentrations referred to the effective metal ion content), respectively. And the concentration of Mg^{2+} was 50, 100 and 500 mg/L, while the concentration of Mn^{2+} was 2, 10, and 100 mg/L.

24.2.6 Statistical Analysis

All treatments were carried out in triplicate, and the experimental data was analyzed by analysis of variance and Duncan's multiple range tests using the Statistical Analysis System (SAS 8.0) [10].

24.3 Results and Discussions

24.3.1 Effect of Carbon Source on PUFAs Production

The effect of carbon source on PUFAs production was showed in Table 24.1. A high value of cell dry weight was obtained when glucose and maltose were used as carbon source, while molasses proved to be the poorest growth carbon source for the strain and yielded very small detectable biomasses of PUFAs followed by sucrose. Soluble starch was not the poorest carbon source for cell growth, but it was not suitable for LA, GLA, and total PUFAs production. In the study, the results indicated the glucose be the best carbon source for LA, GLA, and total PUFAs production.

According to the above research results, the effect of the different glucose concentrations on PUFAs production was investigated, and the results were

Table 24.1 Effect of carbon source on biomass and PUFAs production of NTG_{1-121}

Carbon source	Cell dry weight (g L^{-1})	LA (g L^{-1})	GLA (g L^{-1})	Total PUFAs (g L^{-1})
Glucose	9.14 ± 0.37 a	0.80 ± 0.07 a	0.79 ± 0.13 a	1.62 ± 0.14 a
Sucrose	4.38 ± 0.15 b	0.16 ± 0.04 b	0.16 ± 0.06 b	0.33 ± 0.05 b
Maltose	6.63 ± 0.29 c	0.41 ± 0.11 c	0.40 ± 0.09 c	0.82 ± 0.09 c
Molasses	1.24 ± 0.07 d	NF	NF	0.0046 ± 0.0005 d
Soluble starch	5.87 ± 0.24 e	0.14 ± 0.08 d	0.13 ± 0.02 d	0.27 ± 0.01 e

Data are expressed as means ± standard deviations of triplicate assays. The different alphabetic superscripts in the same column are significantly different ($p < 0.05$) according to Duncan's multiple range test. *NF* no found

represented in Fig. 24.1. As presented in Fig. 24.1, cell dry weight, GLA, LA, and total PUFAs production gradually increased with increasing glucose concentration, and then decreased when the concentration was higher than 120 g/L. When the concentrations of glucose were at 100 and 120 g/L, there was maximum yield of cell dry weight, GLA, LA, and total PUFAs. The results of statistical analysis showed there are no significant difference at the two concentrations ($p > 0.05$). The results were similar to those obtained by Papanikolaou et al. [11] who found that the cell dry weight and lipids achieved were remarkably high when the initial glucose concentration was manipulated at 101.9 g/L, though the fermentation conditions were nonoptimized. The detailed explanation of Fig. 24.1 was that at 100 g/L of glucose, the total PUFAs reached to 1.82 g/L including 0.87 g/L of GLA and 0.85 g/L of LA. In the case of 120 g/L of glucose, 1.79 g/L of the total PUFAs containing 0.88 g/L of GLA and 0.82 g/L of LA could be obtained. While the growth condition of fungus was worse when the glucose content was 0 g/L (data not shown in Fig. 24.1) in the fermentation medium. Similarly, the result was also reported by Xain et al. [12]. The relatively optimum concentration of glucose (100 g/L) was used in the following experiments.

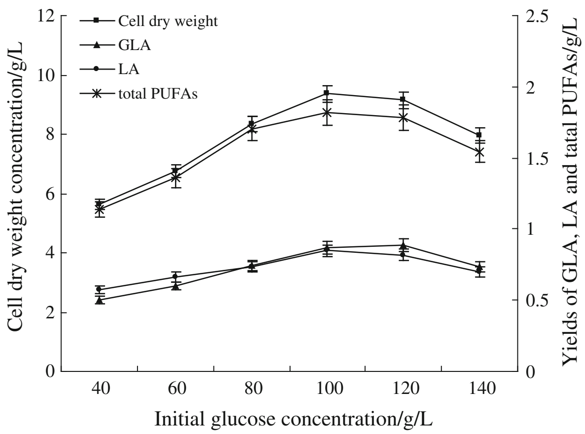

Fig. 24.1 The effect of glucose concentration on PUFAs production

24.3.2 Effects of Nitrogen Source and C/N Ratio on PUFAs Production

The effect of nitrogen source on PUFAs production was presented in Table 24.2. Peanut meal gave the highest cell biomass and PUFAs yields including LA, GLA and total PUFAs production, which were 13.59, 1.10, 1.06 and 2.21 g/L, respectively. Peptone, beef extract, and soybean cake powder were the second best nitrogen for cell dry weight, however, the lipids content were obviously lower than yeast extract when they were used as nitrogen source. As we all know, yeast extract is one of the typical nitrogen sources for the cultivation of microorganisms. In the study, although the dry biomass just achieved 10.03 g/L, the yields of LA, GLA, and total PUFAs production all were significantly higher than the case that peptone, beef extract, and soybean cake powder. KNO_3 as one kind of nitrate used as nitrogen source should show an obviously high cell growth and better PUFAs production than $(NH_4)_2SO_4$. However, in the study the difference of cell dry weight and PUFAs production between KNO_3 and $(NH_4)_2SO_4$ were not significant. There was almost no cell growth obtained with the urea source as well as with the 0 g/L nitrogen source control. It was not surprising since both glucose and urea does not contain metal ions and other vital micronutrients for cell growth or since one would not expect in the absence of one nitrogen source. Thus, the effect of different ratios of a mixture of yeast extract and peanut meal (w/w) on PUFAs production was carried out and the results were shown in Fig. 24.2.

From Fig. 24.2, the mixtures of yeast extract and peanut meal (3:1, w/w) had higher cell biomass and yields of GLA, LA, and total PUFAs than that of other mixture ratios. And the yield of GLA, LA, and PUFAs gradually declined along with the increase of peanut meal except the cell dry weight had slight rise. In view of the same aim, many other literatures have also investigated the effect of different ratios of various nitrogen sources on one certain PUFA or PUFAs production [13, 14].

Table 24.2 Effect of nitrogen source on biomass and PUFAs production of NTG_{1-121}

Nitrogen source	Cell dry weight ($g\ L^{-1}$)	LA ($g\ L^{-1}$)	GLA ($g\ L^{-1}$)	Total PUFAs ($g\ L^{-1}$)
Yeast extract	10.03 ± 0.31 a	0.79 ± 0.06 a	0.78 ± 0.07 a	1.59 ± 0.11 a
Beef extract	11.45 ± 0.44 b	0.78 ± 0.13 a	0.73 ± 0.09 b	1.53 ± 0.07 a
Peptone	11.59 ± 0.27 b	0.74 ± 0.05 b	0.71 ± 0.11 c	1.47 ± 0.06 a
Urea	4.48 ± 0.16 c	0.20 ± 0.02 c	0.24 ± 0.03 d	0.45 ± 0.09 b
$(NH_4)_2SO_4$	7.87 ± 0.23 d	0.34 ± 0.05 d	0.36 ± 0.04 e	0.71 ± 0.12 c
KNO_3	7.81 ± 0.26 d	0.38 ± 0.08 e	0.36 ± 0.06 e	0.76 ± 0.13 d
Peanut meal	13.59 ± 0.57 e	1.10 ± 0.13 f	1.06 ± 0.17 f	2.21 ± 0.18 e
Soybean meal	11.64 ± 0.49 b	0.77 ± 0.11 a	0.74 ± 0.08 b	1.53 ± 0.08 f

Data are expressed as means ± standard deviations of triplicate assays
The different alphabetic superscripts in the same column are significantly different ($p < 0.05$) based on Duncan's multiple range test

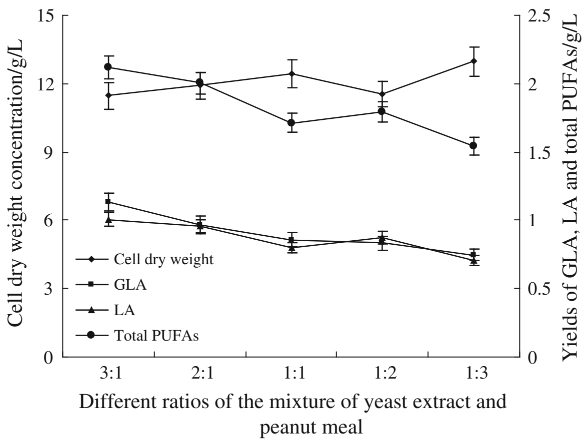

Fig. 24.2 The effects of different ratios of the mixture of yeast extract and peanut meal on PUFAs production

As can be seen in Fig. 24.3, the cell dry weight sharply increased from the ratio of 50/1–50/3, then increased slightly with reducing the C/N ratio, and the difference among ratios of 50/3, 50/4, and 50/5 were not significant. While, the total PUFAs presented the maximum yield (up to 4.83 g/L) at the ratio of 50/3, and the yield of GLA and LA nearly had the same trend showing a peak at the ratio of 50/3. The results are consistent with the result reported by Kioke (2001). A number of researchers have found that the medium with higher carbon source and lower nitrogen source are relatively suitable for lipids accumulation [15]. Some eukaryotic oleaginous species like yeast and mold are able to accumulate a mass of oil taking up more than 70 % of the biomass [16]. And the accumulative process of acetyl CoA in eukaryotic oleaginous organisms will be activated when the assimilable nitrogen source is exhausted and the assimilable carbon source is abundant. As a result, it promotes the synthesis of PUFAs in fungus [11]. The test results obtained

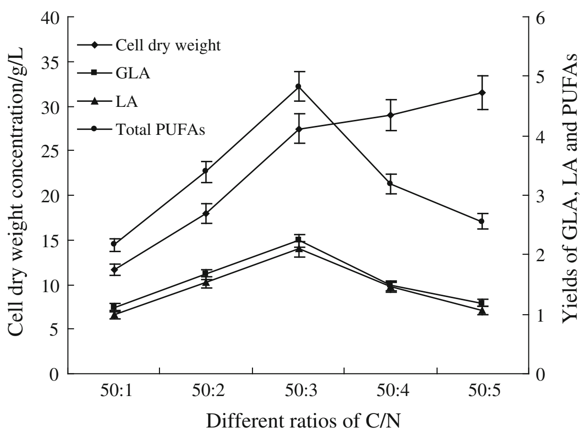

Fig. 24.3 The effects of different C/N ratios on PUFAs production

in the experiment were also corresponded to the theory, so the C/N ratio at 50/3 was selected for the following research.

24.3.3 Effects of Metal Ions on PUFAs Production

The effects of some metallic ions on the PUFAs production were shown in the following Table 24.3. The metal ions containing Mn^{2+}, Fe^{2+}, Cu^{2+}, and Zn^{2+} had strong inhibitory effect (data not shown) on the cell growth and PUFAs production. As illustrated in Table 24.3, in the case of Ca^{2+}, each investigation index increased to the maximum and then decreased with the concentration increasing (had maximal values at 50 mg/L). Similarly, Mg^{2+} in the medium appeared to be the same condition and the concentration of 100 mg/L had the maximum. Compared with the controlled test metal ion, a certain amount of Ca^{2+} and Mg^{2+} were capable of promoting fungi growth and lipid synthesis. In order to improve one or more PUFAs yields, many experts examined the effects of metallic ions on PUFAs production and gained some achievements [17, 18]. The growth and lipid production of the *M. isabellina* NTG_{1-121} were also strongly influenced by metal ions (50 mg/L Ca^{2+} and 100 mg/L Mg^{2+}).

24.3.4 Production of PUFAs Under the Optimal Medium

On the basis of the above results, the main culture medium composition was optimized by central composite design, and an optimal cultivation was given as follows: carbon source 116 g/L, nitrogen source 10.8 g/L, Ca^{2+} 30.8 mg/L, and Mg^{2+}

Table 24.3 Effects of metal ions on biomass and PUFAs production of NTG_{1-121}

Metal ions	Concentration (mg L^{-1})	Cell dry weight (g L^{-1})	GLA (g L^{-1})	LA (g L^{-1})	Total PUFAs (g L^{-1})
Ca^{2+}	5	26.87 ± 0.14 a	1.96 ± 0.06 a	1.90 ± 0.10 a	4.03 ± 0.16 a
	50	28.24 ± 0.27 b	2.35 ± 0.11 b	2.27 ± 0.13 b	4.70 ± 0.12 b
	100	27.64 ± 0.19 c	1.93 ± 0.09 a	1.89 ± 0.07 a	3.94 ± 0.32 a
Control	0	26.06 ± 0.17 d	2.24 ± 0.12 b	2.21 ± 0.11 b	4.51 ± 0.24 b
	50	26.42 ± 0.26 a	1.74 ± 0.15 a	1.69 ± 0.09 a	3.5 ± 0.19 a
Mg^{2+}	100	27.70 ± 0.31 b	2.48 ± 0.20 b	2.240 ± 0.17 b	4.80 ± 0.30 b
	500	25.43 ± 0.21 c	1.87 ± 0.08 c	1.71 ± 0.14 a	3.64 ± 0.18 a
Control	0	26.06 ± 0.17 a	2.24 ± 0.12 b	2.21 ± 0.11 b	4.51 ± 0.24 b

Data are expressed as means ± standard deviations of triplicate assays
The different alphabetic superscripts in the same column are significantly different ($p < 0.05$) based on Duncan's multiple range test

96.8 mg/L. Meanwhile, the fermentation conditions were optimized and the results will be discussed in another article.

In conclusion, the optimum medium composition for PUFAs production with the mutant NTG_{1-121} of *M. isabellina* AS3.3410 were 2 g/L of KH_2PO_4 and sodium citrate, 116 g/L of glucose as carbon source, 10.8 g/L of the mixture of yeast extract and peanut meal at 3:1 (w/w) as nitrogen source at C/N ratio of 50/3, supplements with Ca^{2+} 30.8 mg/L and Mg^{2+} 96.8 mg/L, respectively. Under the optimum medium condition, the yields of cell dry weight, GLA, LA, and total PUFAs were 32.48, 2.90, 2.83 and 7.36 g/L, respectively. And the changes of PUFAs yields were almost by improving the biomass, though the factors had some effect on the metabolism.

References

1. Virginie TA, Kari LK, Maoa JQ et al (2012) Supercritical carbon dioxide extraction of polyunsaturated fatty acids from Northern shrimp (Pandalus borealis Kreyer) processing by-products. Food Chem 130:853–858
2. Eiji S, Akinori A, Sakayu S et al (2013) B Metabolic engineering for the production of polyunsaturated fatty acids by oleaginous fungus Mortierella alpina 1S-4. J Biosci Bioeng http://dx.doi.org/10.1016/j.jbiosc.2013.04.008
3. Subramaniam R, Dufreche S, Zappi M et al (2010) Microbial lipids from renewable resources: production and characterization. J Ind Microbiol Biot 37(12):1271–1287
4. Fakas S, Certik M, Papanikolaou S et al (2008) Gamma-Linolenic acid production by Cunninghamella echinulata growing on complex organic nitrogen sources. Bioresour Technol 99:5986–5990
5. Muammer D, Irfan T, Ahmet K (2013) Oil production by Mortierella isabellina from whey treated with lactase. Bioresour Technol 128(2013):365–369
6. Zhu CH, Lu FP, He YN et al (2007) Statistical optimization of medium components for avilamycin production by Streptomyces viridochromogenes Tü57-1 using response surface methodology. J Ind Microbiol Biotechnol 34:271–278
7. Bligh EC, Dyer WJ (1959) A rapid method of total lipid extraction and purification. Can J Biochem Physiol 37:911–917
8. Ministry of Health of the People's Republic of China. Standards for making fatty acid methyl ester, GB/T 17376-2008
9. Jang HD, Lin YY, Yang SS (2000) Polyunsaturated fatty acid production with Mortierella alpina by solid state fermentation. Bot Bull Acad Sinicia 41:41–48
10. SAS Institute (2002) SAS user's guide statistics. SAS Institute Inc., Cary
11. Papanikolaou S, Sarantou S, Komaitis M (2004) Repression of reserve lipid turnover in Cunninghamella echinulata and Mortierella isbellina cultivated in multiple-limited media. Appl Microbiol 97:867–875
12. Xian M, Bi YL, Zhen KJ (2002) Production of linolenic acid by Mortierella isabellina Grown on Octadecanol. Current Microbiol 44:141–144
13. Jing HD, Lin YY, Yang SS (2005) Effect of culture media and conditions on polyunsaturated fatty acids production by Mortierella alpina. Bioresour Technol 96:1633–1644
14. Enoch Y, Park L, Yasuhisa K et al (1999) Effect of nitrogen source on mycelial morphology and arachidonic acid production in cultures of mortierella alpine. J Biosci Bioeng 88(1):61–67
15. Liu B, Sun Y, Zhao ZB (2005) Research progress of lipids biosynthesis and metabolic regulation with oleaginous organisms. J Acta Microbiolaogica Sinica 45(1):153–155

16. Evans CT, Scragg AH, Ratledge C (1983) Regulation of citrate efflux from mitochondria of oleaginous and non-oleaginous yeasts by adenine nucleotides. J Biochem 132:609–615
17. Weete JD, Kim H, Gandhi SR (1997) Lipids and ultrastructure of Thraustochytrium sp ATCC 26185. Lipids 8:839–845
18. Wang AQ, Dai CC, Chen JX (2005) Study of the effect of six metal ions on the growth and ARA production. Food Chem 26(9):67–71

Chapter 25
A Simple Mechanochemical Cycle Model for Dynein

Xiaoyang Zhao, Wei Sun, Junping Zhang, Tala Lei and Weisheng Guo

Abstract Dynein is the largest and most morphologically complex of biological molecular motors. By analyzing and summarizing the structure and experimental parameters, we develop a mechanochemical cycle model for dynein hydrolyzing ATP. Based on the model, we discuss the relationship between the load and the step size of the dynein, the result derived fit well with the experimental results.

Keywords Dynein · Mechanochemical cycle · Load · Power stroke · Step size

25.1 Introduction

Dynein is a kind of motor protein that uses the energy from an ATP hydrolysis to make work [1, 2]. Dyneins are subdivided into two major groups: axonemal and cytoplasmic dyneins [3]. The cytoplasmic dynein is responsible for intracellular transport including nuclear migration, organization of the mitotic spindle, chromosome separation during mitosis, and the positioning and function of many intracellular organelles [4]. The axonemal dyneins are anchored in linear arrays along microtubules inside cilia and flagella. These dyneins coordinate their motion to cause the rhythmic beating of the cilia and flagella [5, 6].

X. Zhao · W. Sun · J. Zhang · T. Lei · W. Guo (✉)
School of Physical Science and Technology, Inner Mongolia University, 235 West Street, Hohhot 010021, Inner Mongolia, China
e-mail: pygws@imu.edu.cn

X. Zhao
Inner Mongolia Vocational College of Chemical Engineering, Higher Vocational Technology Park, Hohhot 010070, Inner Mongolia, China

W. Sun
Department of Information and Automation, Ordos Vocational College, Yikezhao Street, Kangbashi New District, Ordos 017000, Inner Mongolia, China

T.-C. Zhang and M. Nakajima (eds.), *Advances in Applied Biotechnology*,
Lecture Notes in Electrical Engineering 333, DOI 10.1007/978-3-662-46318-5_25

Every axonemal dynein has 1–3 heavy chains, where each heavy chain consists of three major parts: the AAA ring head, the stalk, and the tail. The head serving as the catalytic engine of the motor contains six AAA modules (AAA1–AAA6) tandemly arranged in a ring, which is structurally related to hexameric ATPases in the AAA + superfamily. The first four AAA modules (AAA1–4) contain nucleotide-binding and hydrolysis Walker A motifs. The stalk emerging from between AAA4 and AAA5 is a ~ 15 nm anti-paralled coiled-coil. A globular microtubule-binding domain is located at its tip [7]. Linker, which has been proposed to serve as a mechanical element, is a structure connecting AAA1 and the main part of the tail.

In axonemes, the tail of dynein is fixed on the A-tubule of a doublet microtubule; the stalk interacts cyclically with the B-tubule of a neighboring doublet microtubule [8]. In the mechanochemical cycle of dynein hydrolyzing ATP, the hydrolyzing ATP in the head causes conformational change of the head; the change is transmitted through the stalk and the tail to the neighboring doublet microtubules leading to a translocation of the adjacent doublet. The mechanism of the relative motion is not clear.

The electron micrographs of a single dynein molecular show that in different biochemical states dynein has distinct conformations. In the absence of nucleotide (apo-dynein) the stem and stalk are closer together than in the ADP·Pi molecule state. In either state, the stalk is always perpendicular to the head [9]. Between the tail and the head is the linker docked onto the head, which swings relative to the head ring to make the motion between the tail and the head [9, 10].

Some models for dynein assumed that the stalk acted as a lever arm, in apo-nucleotide state the stalk bind to B-tubule and tilted toward the minus end of the microtubule, and then rotated toward the plus end of the microtubule to make the relative motion of the adjacent doublet. However, these models had some contradictions with recent experiments [9–16]. (1) By analyzing the electron micrographs Ueno et al. [11] found that the stalk angles relative to microtubules did not change significantly either in the ADP·Pi or the apo-nucleotide states. The stalk always tilted towards the plus end of the microtubule. They thought that dynein pulled microtubules without rotating its stalk; the stalk was used as a tether rather than as a lever arm, and the dynein moved by shortening the distance between its head/stalk and the tail-micrtubule attachment. (2) By calculating the stiffness of the tail and stalk, Linderman et al. [1] found that if the head was supported only by the tail, the stalk and the tail were in series in transmitting the force generated by dynein to the microtubule. The maximum stiffness of the stalk was 0.47 and 0.1 pN/nm for the tail, the flexibility of the tail limited the force that can be transferred by the entire dynein heavy chain to 0.6 pN. The force was much smaller than experimental value 5 pN. And in the following experiment, dynein could generate force even without the tail. This implies that the head and the stalk are the functional bridge for force production, and that there is a second anchoring mechanism to hold the head. It is that the head anchors on the A-tubule. (3) Kon et al. [13] found in experiment that the tail had undergone twice ATP-induced motions relative to the head domain during the mechanochemical cycle of dynein. When ATP binds to the head, the tail rotates relative to the head immediately. The release of the hydrolysis products induced the second rotation of the tail relative to the head; this rotation corresponded to the power stroke.

Based on the researches above, we proposed a simple mechanochemical cycle for dynein hydrolyzing ATP. Based on the model, we discussed the relationship between the load and the step size of the dynein; the result we derived fits well with the experimental results.

25.2 The Mechanochemical Cycle for Dynein Hydrolyzing ATP

Based on the researches above we developed a simple mechanochemical cycle for a dynein single head hydrolyzing ATP, as shown in Fig. 25.1

In the model, in the dynein exist two states while binding to B-tubule and a state while dissociating from the B-tubule, as shown in Fig. 25.1. The transition between these states includes three steps: (1), (2), (3). (1) ATP binding to AAA1 of the head causes the stalk to dissociate from the B-tubule, the head moves laterally relative to the microtubule. ATP bound to the dynein forming dynein·ATP complex. (2) ATP hydrolysis to ADP and Pi. The hydrolysis products bind to dynein. In this process the conformational of the dynein changes, dynein binds tightly to B-tubule again. (3) ADP and Pi are released and the rotation of the linker relative to the head makes

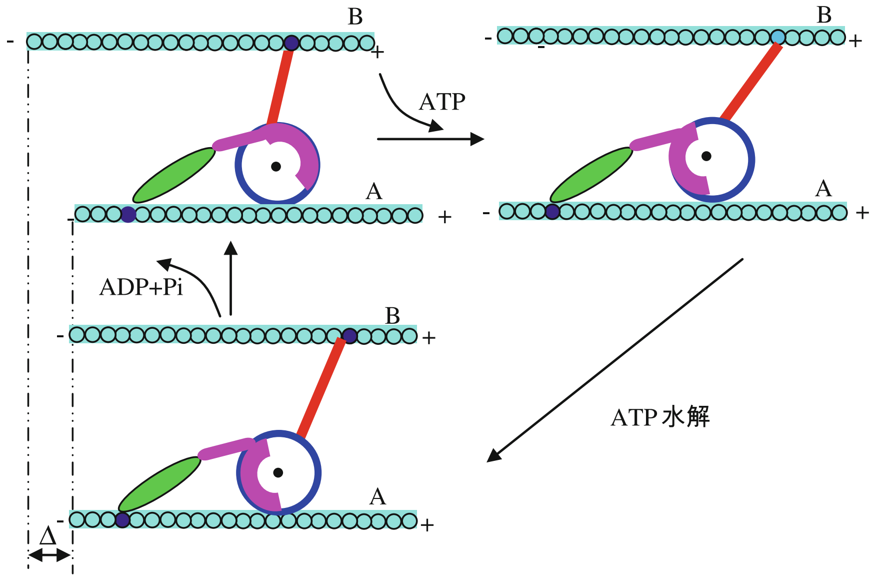

Fig. 25.1 The mechanochemical cycle for dynein hydrolyzing ATP. The *blue bars* represent the doublet microtubules. + and − represent the minus and plus end of the microtubule respectively

the tail rotate relative to the head and the stalk. The rotation leads a relative displacement Δ, which is regarded as the value of the power stroke.

Considering the size of the dynein, the stalk is about 25 nm long, the diameter of the head is about 13 nm, the tail is about 10 nm long, and the linker is about 10 nm long. The overall length of the dynein is 45–50 nm, and the distance between the A-tubule and B-tubule of a relaxed axoneme is 20–25 nm [9]. The cross-bridge formed by dynein in the inner of the neighbor doublet microtubule should be like the illustration in Fig. 25.1.

In the model, the power stroke is caused by the relative rotation between the tail and the head, this fit well with the experimental results of Hironori Ueno et al. When ATP binds to the head, the tail rotates relative to the head, and when the hydrolysis products release, the tail rotates again relative to the head; this fit well with the experimental researches of Takahide Kon et al.

25.3 The Step Size of the Dynein Responds to Load

Assume that in ADP·Pi state, the position of the binding site for dynein to the microtubule is x, in apo-state the position is x_p, $x - x_p$ is the value of the step size. But in this process there exist a displacement between the doublet microtubules, and the value of the displacement is d. So dynein moves $x - x_p - d$ along the microtubule in completing one power stroke. The relative position of the dynein and the microtubules is shown in Fig. 25.2.

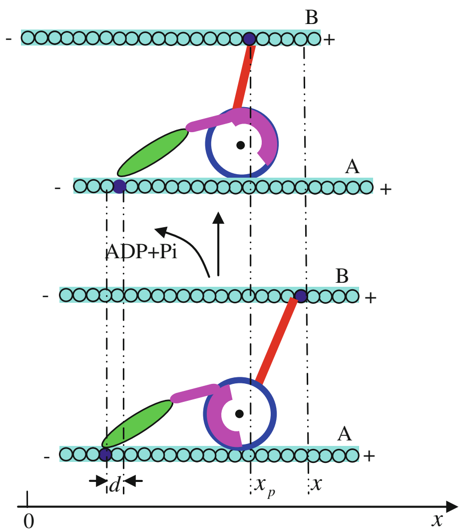

Fig. 25.2 The schematic illustration for power stroke of the dynein

So, the length change between the ADP·Pi state and apo-state is $k(x - x_p - d)$, k is proportional constant. The energy stored in dynein is

$$E = \frac{1}{2} K_{ps} \left[k \left(x - x_p - d \right) \right]^2 \tag{25.1}$$

K_{ps} is the elastic coefficient of the dynein. On the load F_{ext}, the work did by dynein is

$$E = \frac{1}{2} K_{ps} \left[k \left(x - x_p - d \right) \right]^2 + F_{ext} x \tag{25.2}$$

When the energy is smallest, x is also the smallest. Deformation Eq. (25.2),

$$E = \frac{1}{2} K_{ps} k^2 x^2 - \left(K_{ps} k^2 x_p + K_{ps} k^2 d - F_{ext} \right) x + \left(\frac{1}{2} K_{ps} k^2 x_p^2 + K_{ps} k^2 x_p d \right) \tag{25.3}$$

When the energy is the smallest,

$$x_{min} = \frac{K_{ps} k^2 x_p + K_{ps} k^2 d - F_{ext}}{K_{ps} k^2} \tag{25.4}$$

So in this situation the average value of the step size of dynein is

$$x_{min} - x_p = d - \frac{F_{ext}}{K_{ps} k^2} \tag{25.5}$$

When $F_{ext} = 0$, the step size of the dynein is 32 nm, the value of the d is 32 nm. The elastic coefficient, K_{ps}, is not a constant. According to the WLC model for worm-like polymer, the elastic force between two heads of dynein can be expressed as

$$F = \frac{K_B T}{A} \left[\frac{1}{4} \left(1 - \frac{z}{L} \right)^{-2} - \frac{1}{4} + \frac{z}{L} \right] \tag{25.6}$$

where F is the elastic force, K_B is the Boltzman's constant, T is absolute temperature (300 K in our model), A is the persistence length, L is the chain's contour length, and z is the elongation value. Note that $\frac{z}{L}$ denotes the fractional extension of the chain.

From Eq. (25.6), we can get

$$K_{ps} = \frac{dF}{dz} = \frac{K_B T}{AL} \left[1 + \frac{1}{2} \left(1 - \frac{z}{L} \right) - 3 \right] \tag{25.7}$$

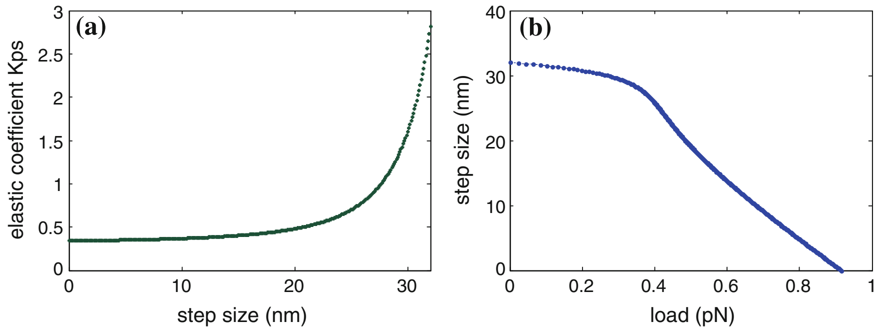

Fig. 25.3 **a** The change in K_{ps} with the step size. **b** The step size of dynein calculated using Eq. (25.11)

When $z = 0$, the value of K_{ps} is about 0.48 pN/nm, therefore,

$$K_{ps} = 0.32\left[1 + 0.5\left(1 - \frac{z}{L}\right)^{-3}\right] \tag{25.8}$$

Because z is equal to

$$z = x_{\min} - x_{p} - L \tag{25.9}$$

Then Eq. (25.7) can be written as

$$K_{ps} = 0.32\left[1 + 0.5\left(2 - \frac{x_{\min} - x_{p}}{L}\right)^{-3}\right] \tag{25.10}$$

Substituting Eq. (25.10) into Eq. (25.5), we can derive the step size-force relation, shown as

$$F_{ext} = 0.32k^2\left[d - \left(x_{\min} - x_{p}\right)\right] \cdot \left[1 + 0.5\left(2 - \frac{x_{\min} - x_{p}}{L}\right)^{-3}\right] \tag{25.11}$$

in which the term $x_{\min} - x_{p}$ represents the step size of dynein. Based on the literature [9], the value of 20 nm is used for L. Since the step size is 32 nm at $F_{ext} = 0$, the value of d is 32 nm too. Taking $k = 0.29$, we obtained the change in K_{ps} with step size and the relationship between the step size and load, see Fig. 25.3

25.4 Discussion

Based on the structure and the kinetic theory of dynein, we proposed a simple mechanochemical cycle for dynein hydrolyzing ATP. Based on the model, we calculate the step size of the dynein response to load. The relationship between the step size and the load fits well with the experimental results; this implies that our model is credible.

In the calculation, we note that the relationship between the external load and the step size is related to the elastic coefficient of the dynein; we considered the nonlinear effect of the dynein on the step size, this point was always ignored in the previous model. From Fig. 25.3a we note that the larger the step size the bigger the value of K_{ps}. Thus, the nonlinear effect of the dynein cannot be ignored when the step size is bigger.

But in our model we assume the proportional constant between the length of the entire dynein and the step size of the dynein. This factor has not been justified by experiments and needs to be tested in the future.

Acknowledgments This work was supported by Natural Science Foundation of Inner Mongolia Autonomous Region of China (2011ZD01), Natural Science Foundation of Inner Mongolia Autonomous Region of China (2014MS0355), Research Program of Science and Technology at Universities of Inner Mongolia Autonomous Region (NJZY14012) and Research Program of Science and Technology of Inner Mongolia Vocational College of Chemical Engineering (HYZR1202).

References

1. Lindemann CB, Hunt AJ (2003) Does axonemal dynein push, pull, or oscillate? Cell Motil Cytoskelet 56:237–244
2. Oiwa K, Sakakibara H (2005) Recent progress in dynein structure and mechanism. Curr Opin Cell Biol 17:98–103
3. Gibbons IR (1995) Dynein family of motor proteins: present status and future questions. Cell Motil Cytoskelet 32:136–144
4. Cho C, Vale RD (2012) The mechanism of dynein motility: insight from crystal structures of the motor domain. Biochimica Et Biophysica Acta-Molecular Cell Research 1823:182–191
5. DiBella LM, King SM (2001) Dynein motors of the Chlamydomonas flagellum. In: Jeon KW (ed) International review of cytology, vol 210. International review of cytology, The United States of America, pp 227–268
6. Gibbons IR (1981) Cilia and flagella of eukaryotes. J Cell Biol 91:107S–124S
7. Gee MA, Heuser JE, Vallee RB (1997) An extended microtubule-binding structure within the dynein motor domain. Nature (London) 390:636–639
8. Gibbons IR, Garbarino JE, Tan CE, Reck-Peterson SL, Vale RD, Carter AP (2005) The affinity of the dynein microtubule-binding domain is modulated by the conformation of its coiled-coil stalk. J Biol Chem 280:23960–23965
9. Burgess SA, Walker ML, Sakakibara H, Knight PJ, Oiwa K (2003) Dynein structure and power stroke. Nature 421:715–718
10. Burgess SA, Knight PJ (2004) Is the dynein motor a winch? Curr Opin Struct Biol 14:138–146
11. Burgess SA (1995) Rigor and relaxed outer dynein arms in replicas of cryofixed motile flagella. J Mol Biol 250:52–63
12. Burgess SA, Dover SD, Woolley DM (1991) Architecture of the outer arm dynein atpase in an avian sperm flagellum with further evidence for the b-link. J Cell Sci 98:17–26
13. Kon T, Mogami T, Ohkura R, Nishiura M, Sutoh K (2005) ATP hydrolysis cycle-dependent tail motions in cytoplasmic dynein. Nat Struct Mol Biol 12:513–519

14. Sakakibara H, Oiwa K (2011) Molecular organization and force-generating mechanism of dynein. FEBS J 278:2964–2979
15. Sale WS, Goodenough UW, Heuser JE (1985) The substructure of isolated and in-situ outer dynein arms of sea-urchin strongylocentrotus-purpuratus sperm flagella. J Cell Biol 101:1400–1412
16. Ueno H, Yasunaga T, Shingyoji C, Hirose K (2008) Dynein pulls microtubules without rotating its stalk. Proc Natl Acad Sci USA 105:19702–19707

Chapter 26
The Research on Biotransformation Pathway of Digitoxin by *Aspergillus ochraceus* and the Analysis of Products Activity

Jianmei Luo, Ting Song, Fangfang Cui, Yanbing Shen and Min Wang

Abstract In order to analyze the biotransformation pathway of digitoxin by *Aspergillus ochraceus* Rn405, a product—digitoxigenin was used as the substrate to biotransform. The substrate consumption and product synthesis were monitored by HPLC during the bioconversion process. The preliminary results were as follows: Firstly, hydrolysis reaction happened and digitoxin was converted into digitoxigenin; then, with extension of the reaction time, the hydroxyl group was introduced to the C-11 of digitoxigenin by the role of hydroxylase and another product named 11α-hydroxydigitoxigenin was generated in a large amount. The influences of these two products on myocardial apoptosis and their antineoplastic activities were further analyzed. It was found that compared with the substrate digitoxin and reference substance digoxin, the apoptosis effects of digitoxigenin and 11α-hydroxydigitoxigenin on rat myocardial cells remarkably decreased; but no obvious antineoplastic activities on the four tumor cells, including human breast cancer cell MCF-7, rat breast cancer cell 4T1, human cervical cancer cell Hela, and rat melanoma cell B-16 were observed.

Keywords *Aspergillus ochraceus* · Digitoxin · Bioconversion · Biotransformation pathway · Activity analysis

Digitaloid drug is an exogenous cardiac glycoside compound, which has a good effect on the treatment of congestive heart failure diseases [1, 2] and antitumor activities [3–6]. However, its clinical application is seriously limited by defects like slow metabolism and therapeutic dose approximates to toxic dose. In order to solve these problems, lead compounds with new structures would be developed continuously,

J. Luo (✉) · T. Song · F. Cui · Y. Shen · M. Wang
Key Laboratory of Industrial Fermentation Microbiology (Tianjin University of Science & Technology), Ministry of Education, Tianjin Key Lab of Industrial Microbiology, College of Biotechnology, Tianjin University of Science and Technology, Tianjin 300457, People's Republic of China
e-mail: luojianmei@tust.edu.cn

T.-C. Zhang and M. Nakajima (eds.), *Advances in Applied Biotechnology*,
Lecture Notes in Electrical Engineering 333, DOI 10.1007/978-3-662-46318-5_26

and the structure of the existing cardiac glycoside drugs would be further modified. Cardiac glycosides have quite complicated structures and contain multiple chiral centers. When chemical approach is used for structural modification, poor selectivity, side reactions like oxidization, cyclization, and polymerization, and the complex steps are easy to happen. Besides, it is hard to reform the structure of some special loci [7]. Bioconversion is another effective way to modify and reform the structure of native compound. It is equipped with advantages of strong stereoselectivity, mild reaction condition, few by-products, low cost, and environmentally friendly nature. What is more, this method can conduct chemical reactions that traditional chemical synthesis cannot or can hardly achieve. At present, bioconversion has become an important method to gain a large number of new-type lead compounds [8].

In our previous research work, two converted products (digitoxigenin and 11α-hydroxydigitoxigenin) have been separated, purified, and identified from the bioconversion liquid of digitoxin by *Aspergillus ochraceus* [9]. In order to discuss the biotransformation pathway, the bioconversion reaction was conducted by using digitoxigenin as the substrate. Meanwhile, the influences of converted products on rat myocardial apoptosis ratio and their antineoplastic activities were preliminarily studied. This work would lay a foundation for the development of lead compounds of efficient antineoplastic drugs with low toxicity.

26.1 Materials and Methods

26.1.1 Experimental Materials

26.1.1.1 Experimental Strain

Aspergillus ochraceus Rn405 was kept by Microbial Pharmaceutical Laboratory, College of Biotechnology, Tianjin University of Science & Technology.

26.1.1.2 Culture Medium

The strain was kept with potato juice slant medium. The culture medium consisted of 20 g/L glucose, 20 g/L yeast cream, and 20 g/L peptone; pH was adjusted to 4.5 before autoclaving. 50 mL culture medium was loaded in 250-mL shake flasks and sterilized at 115 °C for 20 min.

26.1.1.3 Cell Lines

Human breast cancer cell MCF-7, rat breast cancer cell 4T1, human cervical cancer cell Hela, and rat melanoma cell B-16 were kept by Tianjin International Joint Academy of Biomedicine. Rat myocardial cell H9c2 was kept by College of Biotechnology, Tianjin University of Science & Technology.

26.1.1.4 Main Reagents and Instruments

Digitoxin (99.0 % purity, Dr Company, Germany); digoxin (99.0 % purity, National Institutes for Food and Drug Control); acetonitrile (chromatographical purity, Real & Lead Chemical Co., Ltd., China); other reagents (analytical purity, Real & Lead Chemical Co., Ltd., China); ESI-MS mass spectrometer (Bruker Daltonics Inc., USA); AV400 nuclear magnetic resonance analysis meter (Bruker Optics, USA); the preparative liquid phase analysis meter (Agilent Technologies, USA).

26.1.2 Experimental Methods

26.1.2.1 Strain Culture

The strain was inoculated on the slant medium and cultured under 28 °C for 5–7 days. When the slant bottom turned into maroon and a large number of golden yellow spores appeared on the surface, it could be applied to bioconversion reaction.

26.1.2.2 Bioconversion Process

The spore suspension of *A. ochraceus* Rn405 was inoculated into 250-mL shake flask containing 50 mL culture medium to make its final concentration of 10^6 cells/mL. After cultivation at 28 °C for 28 h on a rotary shaker (180 r/min), the digitoxin, which was previously dissolved in DMF (0.1 mL) was added into each flask at the final concentration of 200 mg/L. The bioconversion was carried out under the same cultivation conditions for 96 h.

26.1.2.3 Separation and Purification of Products

The culture supernatant and mycelium were separated by filtration with suction. The filter liquor was extracted with ethyl acetate in 3 volumes for 3 times. The organic phase was collected and further concentrated by the rotary evaporator. Then silica gel column chromatography was used for separation and purification according to the literature [9].

26.1.2.4 Analysis of Bioconversion Pathway

Digitoxigenin (compound **2**) was used as the substrate for bioconversion according to the bioconversion conditions described in Sect. 26.1.2.2. The samples were taken every 24 h and the substrate conversion ratio and product formation ratio were monitored by HPLC. One flask culture of organism without exogenous substrate (for the identification of endogenous metabolites) was also performed as a control. HPLC analysis conditions were as follows: A Kromasil C18 (4.6 mm × 250 mm, 5 μm particle size) was used and acetonitrile–water (40:60, v/v) was employed as the mobile phase at 1.0 mL/min. The system was operated at 30 °C and the detection wavelength was set as 220 nm; the injection volume was 10 μL.

26.1.2.5 Analysis of Pharmacological Activities of Products

Influences of Converted Products on Myocardial Apoptosis

Rat myocardial cell H9c2 was cultivated on the 16-well microplate and high-glucose DMEM culture solution was added. After incubation on 5 % CO_2 incubator at 37 °C for 24 h, a certain amount of digitoxin and various converted products were, respectively, dissolved in DMSO to prepare the mother liquor. Six concentration gradients of 10^{-9}, 10^{-8}, 10^{-7}, 10^{-6}, 10^{-5}, and 10^{-4} mol/L were set for each compound, and three parallel samples were used for each concentration. After the induction of 24 h, 4 % paraformaldehyde was used to fix the cell at 4 °C for 20 min. Then PBS buffer solution was applied to wash for 2 times (3 min for each time). After washing with PBS buffer solution by shaking hands for several times, the cells were dyed with Hoechst 33258 staining solution at a final concentration of 10 μg/mL on incubator at 37 °C for 30 min and then washed with PBS buffer solution for 2 times (3 min for each time). Finally, 200 cells were randomly selected for observing under fluorescence microscope and 340 nm exciting light conditions. The apoptosis ratio was calculated by the percentage of apoptotic cells in total cells. During the experiment, one group only adding DMSO was set as the blank control, and staurosporine with a final concentration of 5 μmol/L was used as positive control (the induction time of positive control group was 40 min).

Antineoplastic Activities of Converted Products

The in vitro inhibitory activities of digitoxin and its converted products on human breast cancer cell MCF-7, rat breast cancer cell 4T1, human cervical cancer cell Hela, and rat melanoma cell B-16 were detected via MTT method.

(1) Tumor cell culture

The tumor cell freezing tube was taken out from the liquid nitrogen container, and put at 37 °C on water bath until the cell suspension in freezing tube was thawed. The cell suspension was put into 25-mL culture flask and 5 mL of DMEM culture medium with 10 % serum was added. It was cultivated on 5 % CO_2 incubator at 37 °C until it filled the culture flask.

(2) Cytotoxicity screening

The cultivated tumor cells were spread out onto a 96-well microplate at the concentration of 1×10^6 CFU and 100 μL of diluted compound solution was added. At the same time, 100 μL of blood serum medium was added into the well as a blank control group. After cultivation on 5 % CO_2 incubator at 37 °C for 48 h, MTT solution was added. After incubation at 37 °C for 2 h, the purple crystal appeared and the supernatant was then taken out. DMSO was added to dissolve purple crystal and the microplate was vibrated at room temperature for 15 min. OD value was detected at the wavelength of 570 nm with microplate reader.

The tumor cell suppression ratio was calculated according to the following formula:

$$\text{Suppression ratio}\,(\%) = \frac{\text{Average OD value of blank control group} - \text{Average of OD value of test group}}{\text{Average OD value of blank control group}} \times 100\,\%$$

26.2 Results and Analysis

26.2.1 Analysis of Biotransformation Pathway

According to the structures of two products (Fig. 26.2), 11α-hydroxydigitoxigenin (compound **3**) had a hydroxyl group at the C-11 when compared with digitoxigenin. Therefore, it was speculated that during the bioconversion of digitoxin by *A. ochraceus*, hydrolysis reaction firstly occurred and the substrate digitoxin (compound **1**) was converted into digitoxigenin (compound **2**). After that, with extension of the reaction time, the hydroxyl group was introduced to the C-11 of digitoxigenin by the role of hydroxylase. Another product named 11α-hydroxydigitoxigenin (compound **3**) was then generated in a large amount. In order to verify the above conjecture, the product named digitoxigenin (compound **2**) which was obtained by separation and purification from the broth of *A. ochraceus* Rn405 was used as substrate to carry out bioconversion. The conversion process was monitored by HPLC.

According to Fig. 26.1, when digitoxigenin (compound **2**) was set as the substrate, a retention peak 3 with the retention time of 5.676 min appeared in the reaction liquid after conversion for 48 h. It was almost the same with the retention time of the standard substance of 11α-hydroxydigitoxigenin [9]. It was speculated that 11α-hydroxydigitoxigenin was generated during the bioconversion process. Thereby, it was preliminarily suggested that the biotransformation pathway on bioconversion of digitoxin by *A. ochraceus* 405 was presented in Fig. 26.2.

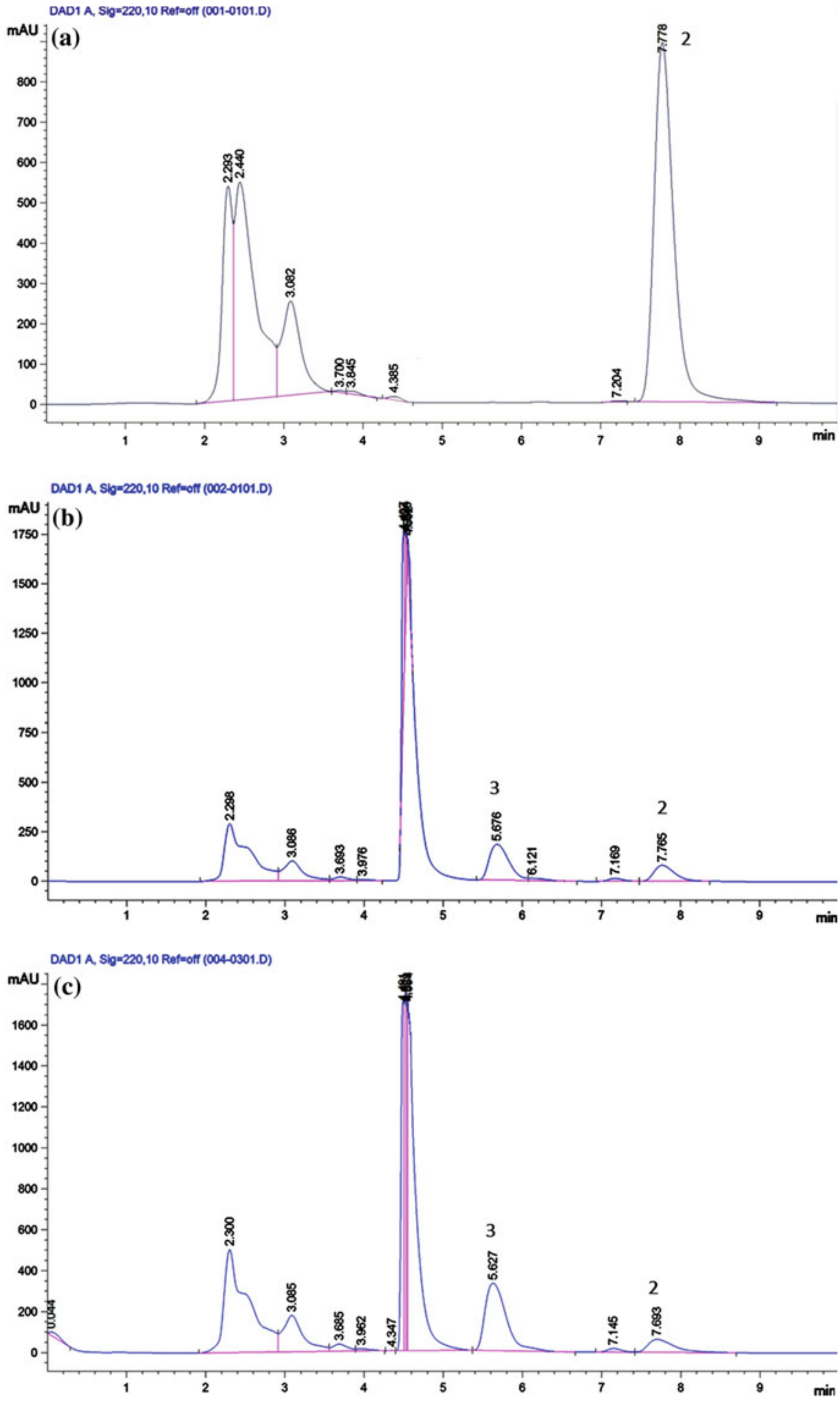

DAD1 A, Sig=220,10 Ref=off (001-0101.D)
mAU
(a)
2.293
2.440
3.082
3.700
3.845
4.385
7.204
7.778
2
min
DAD1 A, Sig=220,10 Ref=off (002-0101.D)
mAU
(b)
2.298
3.086
3.693
3.976
5.676
6.121
7.169
7.765
3
2
min
DAD1 A, Sig=220,10 Ref=off (004-0301.D)
mAU
(c)
0.044
2.300
3.085
3.685
3.962
4.347
5.627
7.145
7.693
3
2
min

◀**Fig. 26.1** HPLC diagram of bioconversion of digitoxigenin (compound **2**) by *Aspergillus ochraceus* 405, **a** conversion for 0 h; **b** conversion for 48 h; **c** conversion for 96 h, *1* digitoxin (compound **1**); *2* digitoxigenin (compound **2**); *3* 11α-hydroxydigitoxigenin (compound **3**)

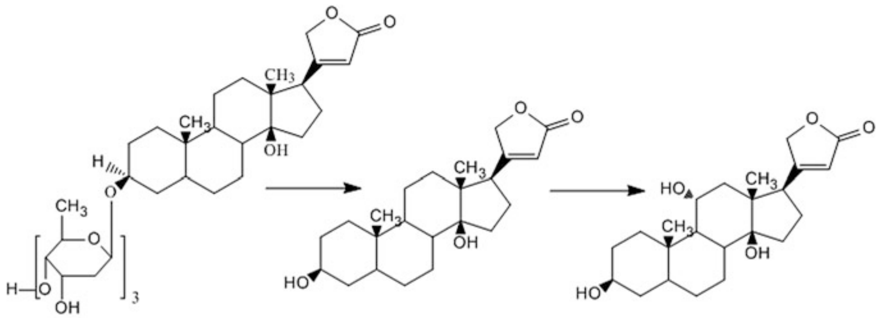

1 2 3

Fig. 26.2 Reaction formula of bioconversion of digitoxin (compound **1**) by *A. ochraceus* 405, *1* digitoxin (compound **1**); *2* digitoxigenin (compound **2**); *3* 11α-hydroxydigitoxigenin (compound **3**)

26.2.2 Influences of Digitoxin and Relevant Products on Cell Apoptosis

Digitoxin (compound **1**), digitoxigenin (compound **2**), 11α-hydroxydigitoxigenin (compound **3**), the reference substance digoxin, and the positive control group of staurosporine were used as reaction medicines to induce apoptosis of rat myocardial cell H9c2, respectively. As shown in Fig. 26.3, similar impacts on myocardial apoptosis ratio were observed among the reference substance digoxin, digitoxin (compound **1**), digitoxigenin (compound **2**), and 11α-hydroxydigitoxigenin (compound **3**). The apoptosis ratio of rat myocardial cell H9c2 declined with the decreasing concentration of the four compounds from 10^{-4} to 10^{-9} mol/L. When the concentration of the two converted products decreased from 10^{-4} to 10^{-5} mol/L, the apoptosis ratio of myocardial cell H9c2 fluctuated between 99 and 100 %. When the concentration of the two converted products decreased to 10^{-6} mol/L, the apoptosis ratio declined slightly and reached 98.7 and 96.3 %, respectively. The concentration of the two converted products further reduced from 10^{-7} to 10^{-9} mol/L, the apoptosis ratio reduced from 33.8 and 29.1 % to 13.4 and 11.5 %, respectively, which was obviously lower than those of digitoxin (compound **1**) and the reference substance digoxin (Fig. 26.3). It was preliminarily concluded that the removal of carbohydrate chain from digitoxin (compound **1**) or the insertion of the hydroxyl group at C-11 position would weaken the apoptosis ratio of rat myocardial cell H9c2.

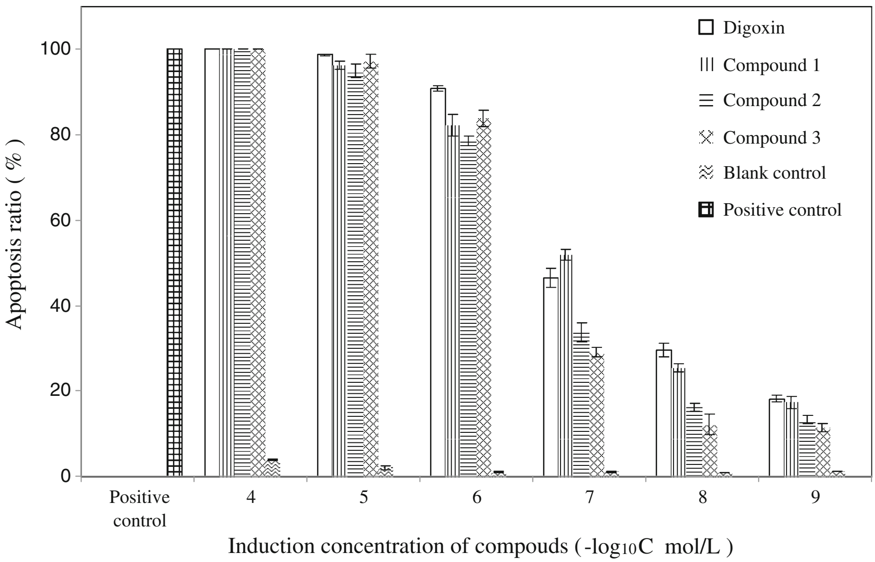

Fig. 26.3 Influences of four compounds on apoptosis ratio of rat myocardial cell H9c2. Digoxin was the control group of pharmacological activity; compound **1**, **2**, and **3** were test groups of digitoxin, digitoxigenin, and 11α-hydroxydigitoxigenin, respectively; the group only with DMSO was set as the blank control; staurosporine at the final concentration of 5 μmol/L was the positive control

26.2.3 Suppression Effects of Digitoxin and Relevant Products on Tumor Cells

The suppression effects of digitoxin (compound **1**), digitoxigenin (compound **2**), 11α-hydroxydigitoxigenin (compound **3**) and the reference substance digoxin on human breast cancer cell MCF-7, rat breast cancer cell 4T1, human cervical cancer cell Hela, and rat melanoma cell B-16 were analyzed by MTT experiment.

As shown in Fig. 26.4, a certain suppression effect of the reference substance digoxin on all the four tumor cells were detected. Digitoxin (compound **1**) at 0.1 μmol/L promoted the proliferation of rat breast cancer cell 4T1 and human cervical cancer cell Hela while no suppression effects on human breast cancer cell MCF-7 and rat melanoma cell B-16 were observed. When the concentration of Digitoxin (compound **1**) increased to 1 μmol/L, no suppression effects on the four tumor cells were observed. Almost no suppression effects of Digitoxigenin (compound **2**) at the concentration of 0.1 and 1 μmol/L on human breast cancer cell MCF-7 and rat melanoma cell B-16 were detected but the facilitation effects on the proliferation of rat breast cancer cell 4T1 and human cervical cancer cell Hela were observed. The proliferative effects of 11α-hydroxydigitoxigenin (compound **3**) at the concentration of 0.1 μmol/L on human breast cancer cell MCF-7, rat breast cancer cell 4T1, and human cervical cancer cell Hela were observed while neither

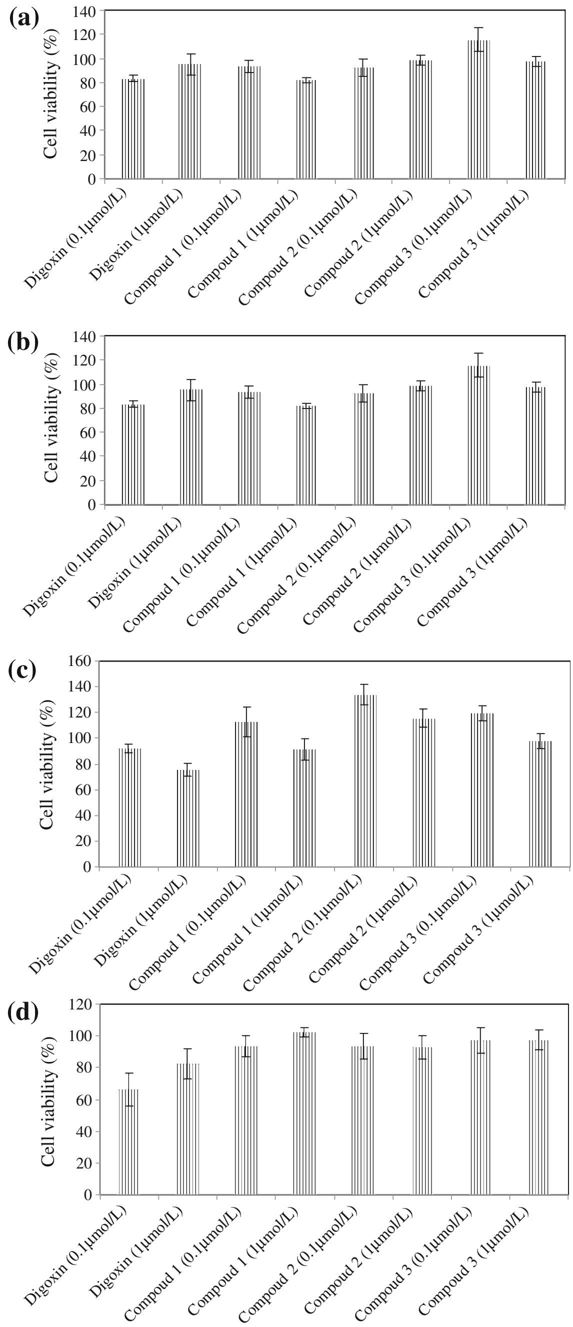

Fig. 26.4 Inhibitory activities of four compounds on tumor cells. Digoxin was the control group of pharmacological activity; compound **1**, **2**, and **3** were test groups of digitoxin, digitoxigenin, and 11α-hydroxydigitoxigenin, respectively. **a** Human breast cancer cell MCF-7; **b** rat breast cancer cell 4T1; **c** human cervical cancer cell Hela; **d** rat melanoma cell B-16

suppression effects nor proliferative effects on rat melanoma cell B-16 was presented. When the concentration of 11α-hydroxydigitoxigenin (compound **3**) increased to 1 μmol/L, neither suppression effects nor proliferative effects on the four tumor cells were observed. In conclusion, no inhibitory activities of digitoxigenin (compound **2**) and 11α-hydroxydigitoxigenin (compound **3**) at the concentration of 0.1 and 1 μmol/L on all the four tumor cells were observed.

26.3 Conclusion

(1) The biotransformation pathway of digitoxin by *A. ochraceus* 405 was preliminarily speculated by the bioconversion experiment using one product named digitoxigenin (compound **2**) as the substrate. It was suggested that hydrolysis reaction happened first and the substrate digitoxin (compound **1**) was converted into digitoxigenin (compound **2**); After that, with extension of the reaction time, the hydroxyl group was introduced to the C-11 of digitoxigenin by the role of hydroxylase, and another product named 11α-hydroxydigitoxigenin (compound **3**) was generated in a large amount.
(2) The influences of digitoxigenin (compound **2**) and 11α-hydroxydigitoxigenin (compound **3**) on apoptosis ratio of myocardial cells and their antineoplastic activities were analyzed with Hoechst dyeing and MTT methods, respectively. The results showed that when concentration of digitoxigenin (compound **2**) was ranged from 10^{-7} to 10^{-9} mol/L, the apoptosis ratio of rat myocardial cells was obviously lower than those of digitoxin (compound **1**) and the reference substance digoxin while no suppression effects on human breast cancer cell MCF-7, rat breast cancer cell 4T1, human cervical cancer cell Hela, and rat melanoma cell B-16 were observed at the concentration of 0.1 and 1 μmol/L. When the concentration of 11α-hydroxydigitoxigenin (compound **3**) was ranged from 10^{-7} to 10^{-9} mol/L, the apoptosis ratio of rat myocardial cells was obviously lower than those of the reference substance digoxin and digitoxin (compound **1**) while no suppression effects on the above four tumor cells were presented at the concentration of 0.1 and 1 μmol/L. In conclusion, the apoptosis ratio of rat myocardial cells could be reduced by the hydrolysis of digitoxin carbohydrate chain, but no suppression effects on the above four tumor cells were observed. The apoptosis ratio of rat myocardial cells could be decreased by C-11 hydroxylation, but no suppression effects on the above four tumor cells were detected.

Acknowledgments This work is supported by the Natural Science Foundation of Tianjin (No. 13JCYBJC20600).

References

1. Newman RA, Yang P, Pawlus AD et al (2008) Cardiac glycosides as novel cancer therapeutic agents. Mol Interv 8:36–49
2. Hood WB, Dans AL, Guyatt GH et al (2005) Digitalis for treatment of congestive heart failure in patients in sinus rhythm. The Cochrane Database of Systematic Reviews 2005 Issue 2
3. Mijatovic T, Roland I, Van QE (2007) The alpha 1 subunit of the sodium pump could represent a novel target to combat non-small cell lung cancers. Am J Pathol 212(2):170–179
4. Zhang H (2008) Digoxin and other cardiac glycosides inhibit HIF-1 alpha synthesis and block tumor growth. Proc Natl Acad Sci USA 105:19579–19586
5. Sreenivasan Y, Raghavendra RB, Manna SK (2006) Oleandrin-mediated expression of Fas potentiates apoptosis in tumor cells. J Clin Immunol 26(4):308–322
6. Svensson A, Azarbayjani R, Backman U (2005) Digoxin inhibits neuroblastoma tumor growth in mice. Anticancer Res 25(1A):207–212
7. Hu XY, Cui L, Feng K (2012) Optimization of fermentation medium for 11α-hydroxylation of steroid catalyzed by Rhizopus nigricans RN-M246. Chem Biochem Eng 29(6):77–79
8. Giri A, Dhingra V, Giri CC et al (2001) Biotransformationsusingplantcells, organ cultures and enzyme systems: current trends and futureprospects. Biotechnol Adv 19(3):175
9. Fu YW, Sun H, Shen YB et al (2012) Biotransformation of digitoxin by *Aspergillus ochraceus*. Adv Mater Res 343–344:1281–1284

Chapter 27
Astragalus membranaceus Polysaccharide-Enhanced Lymphocytes Proliferation of Yellow Drum *Nibea albiflora* In Vitro

Huilai Shi, Fangping Yu and Qingkui Wang

Abstract To quickly evaluate the immunostimulatory effect of *Astragalus membranaceus* polysaccharide (AMP) on yellow drum *Nibea albiflora*, the head kidney lymphocytes proliferation was tested with/without concanavalin A (Con A) or lipopolysaccharide (LPS) in vitro. The lymphocytes were incubated within 0, 25, 50, 100, 200, 400, and 800 μg/mL AMP for 48 h, with/without Con A (2.3 μg/mL) or LPS (18.2 μg/mL). Results showed that there was a dose-dependent relationship between lymphocytes proliferation and the AMP concentration ($P < 0.05$). The AMP-enhanced lymphocytes proliferation at 50–200 μg/mL significantly ($P < 0.05$), with peak value at 100 μg/mL. Low dose (0–25 μg/mL) and high dose (400–800 μg/mL) of AMP did not stimulate lymphocytes proliferation significantly ($P < 0.05$). Synergetic effects were observed between AMP and Con A/LPS on lymphocytes proliferation. Data in this chapter implied that the AMP might contribute to both cellular and humoral immunity of *N. albiflora* in a dose-dependent manner.

Keywords *Astragalus membranaceus* · Polysaccharide · Lymphocytes proliferation · *Nibea albiflora*

27.1 Introduction

The yellow drum *Nibea albiflora*, which belongs to Perciformes, Sciaenidae, and Nibea, is naturally distributed in the coastal waters of China, Korea, and south Japan. Yellow drum is a well-known fishing species in China and loved for its

H. Shi · F. Yu
Zhejiang Province Key Lab of Enhancement and Mariculture, Marine Fisheries Research Institute of Zhejiang, Zhoushan 316100, People's Republic of China

Q. Wang (✉)
Tianjin Key Laboratory of Aqua-Ecology and Aquaculture, College of Fisheries, Tianjin Agricultural University, Tianjin 300384, People's Republic of China
e-mail: wqkmail@qq.com

T.-C. Zhang and M. Nakajima (eds.), *Advances in Applied Biotechnology*,
Lecture Notes in Electrical Engineering 333, DOI 10.1007/978-3-662-46318-5_27

delicious taste and trophic value. In the recent decades, because of overfishing and environmental deterioration, the wild population of yellow drum declined rapidly. The culture of yellow drum developed rapidly these years [1]. With the increase of culture scale and density, yellow drum diseases have become more and more serious [2].

More and more antibiotics and chemotherapeutics that previously widely used to control fish diseases have been banned because of their unwanted residues in fish and environmental pollution. A large number of studies showed that plant extracts are a promising alternative to chemotherapy in fish aquaculture [3]. The *Radix Astragali*, which is the dry root of *Astragalus membranaceus* var. *mongholicus* and *A. membranaceus* var. *membranaeceus*, is a commonly used Chinese herbal medicine for its tonic effects [4]. The *A. membranaceus* polysaccharide (AMP), which is extracted from the root of *A. membranaceus*, showed multiple pharmacological effects on livestock and poultry, such as antivirus, antiradiation, antistress, antioxidation, and immunostimulatory activity [5, 6]. The AMP also showed promising application prospects in aquaculture, such as its immunostimulation [7], growth promotion [8], antivirus [9], and hepatocyte protection [10] efficacy.

To date, the main means to study the immunomodulatory mechanism of immunostimulants on fish is via dietary administration, which needs long-term culture period. The in vitro test means, which have the advantages of easy controllability, well repeatability, less material requirement, and short time consumption, have been widely employed in the research and development of veterinary and human immunostimulants. But in vitro test means were rarely employed in fish species. This paper evaluated the immunostimulatory effect of AMP on *N. albiflora* by means of testing its lymphocytes proliferation capacity in vitro, in order to provide a rapid reference that whether the AMP can be used as an immunostimulant for *N. albiflora* healthy culture.

27.2 Materials and Methods

27.2.1 AMP Purification

The crude AMP (purchased from Shengwang Pharmacy Company in Shandong province) was dissolved in distilled water. Then ethanol was added to the supernatant to reach 80 % content, in order to precipitate crude AMP. The protein in crude AMP was moved out by Sevag method [11]. Then the AMP was obtained by lyophilization. Total sugar, reducing sugar, uronic acid, and protein in the resulting AMP were assayed. Total sugar was measured by phenol-sulfuric acid method [12] with glucose as standard. Reducing sugar was measured as described by Wen et al. [13]. Uronic acid was measured as described by Meseguer [14] and Yu et al. [15]. Protein was measured using Bradford [16] method, using bovine serum albumin as the standard.

27.2.2 Lymphocytes Preparation

The head kidney lymphocytes from healthy *N. albiflora* (80 ± 5 g) were separated according to Wang et al. [17].

27.2.3 Lymphocytes Proliferation

The RPMI-1640 proliferation medium was prepared as following: RPMI-1640 culture medium contained 10 % heat inactive (56 °C water bath for 30 min) FBS, 2 % heat inactive (45 °C water bath for 30 min) *N. albiflora* serum, 100 IU/mL ampicillin, and 0.1 mg/mL streptomycin sulfate. The AMP was dissolved in RPMI-1640 culture medium at 0, 50, 100, 200, 400, 800, and 1,600 μg/mL, and filtered (0.22 μm) for later use.

Lymphocytes proliferation was assayed according to the method described by Wang et al. [17] with some modifications. A 90 μL aliquot of proliferation medium containing 7×10^5 cells was added to wells of a 96-well flat bottom plate. Then the AMP was added as one of the following: (1) 100 μL AMP solution and 10 μL of proliferation medium (four wells each fish); (2) 100 μL AMP solution and 10 μL lipopolysaccharide (LPS, Sigma, 200 μg/mL, four wells each fish); and (3) 100 μL AMP solution and 10 μL concanavalin A (Con A, Sigma, 25 μg/mL, four wells each fish). The final AMP concentration in 96-well plate was 0, 25, 50, 100, 200, 400, and 800 μg/mL, respectively. The 96-well plate was cultured in humidified 5 % CO_2 incubator at 28 °C for 48 h. Then 20 μL of 3-[4,5-dimethylthiazol-2-yl]-2,5-diphenyl tetrazolium bromide (MTT, 1 mg/mL HBSS) was added to each well and incubated for additional 4 h at 28 °C. The plate was centrifuged at 500×g for 10 min at 4 °C. The supernatant was discarded, the formazan crystals in each well were dissolved by adding 200 μL DMSO and 25 μL of glycine buffer (0.1 M glycine, 0.1 M NaCl, pH 10.5). The contents of the wells were then thoroughly mixed, and the O.D. at 550 nm of the resulting suspension was measured using a microplate reader (Varioskan Flash) 10 min later. The stimulation index (SI) was calculated as $OD_{550\ (\text{AMP added group})}/OD_{550\ (\text{control group})}$.

27.2.4 Statistical Analysis

Data were analyzed by one-way analysis of variance (ANOVA), and any significant difference was determined at the $P < 0.05$ level by Duncan's multiple range tests. The analyses were carried out with the SPSS 18.0 software. Data were presented as means ± standard error, $n = 6$.

27.3 Results

Total sugar, reducing sugar, uronic acid, and protein in resulting AMP were 74.63 ± 1.96, 4.94 ± 0.13, 15.38 ± 1.25, and 4.73 ± 0.14 %, respectively.

Data in Table 27.1 indicated that there was a dose-dependent relationship between lymphocytes proliferation and the AMP concentration ($P < 0.05$). A medium dose of AMP (50–200 μg/mL) stimulated lymphocytes proliferation significantly ($P < 0.05$), with peak O.D. value at 100 μg/mL, while low dose (0–25 μg/mL) and high dose (400–800 μg/mL) of AMP did not stimulate lymphocytes proliferation significantly ($P < 0.05$). Synergetic effects were observed between AMP and stimuli (Con A and LPS). The lymphocytes proliferation reached peak value in group AMP and AMP + LPS at 100 μg AMP/mL, and in group AMP + Con A at 200 μg AMP/mL. The SI also showed the same trend in each group.

27.4 Discussion

The thymus-, kidney-, spleen-, and mucosa-associated lymphoid tissues are believed to be the primary immune organs in fish. The thymus degenerates with the growth of fish. In the development of fish kidney, head kidney lost urination function and become the immune and hemopoietic organ. The head kidney develops to be the second immune organ after thymus. Fish spleen is generally smaller in size than head kidney. The mucosa-associated lymphoid tissue is not easy to separate and the immune related cells in it are small in amount. So fish head kidney becomes the most important source of immune cells for in vitro studies [18].

Table 27.1 The effect of AMP on lymphocytes proliferation of *N. albiflora*, with/without the presence of Con A or LPS

AMP (μg/mL)	AMP		AMP + Con A		AMP + LPS	
	$O.D._{570}$	SI	$O.D._{570}$	SI	$O.D._{570}$	SI
0	0.107 ± 0.006 a		0.134 ± 0.006 a		0.123 ± 0.004 a	
25	0.125 ± 0.006 ab	1.17	0.139 ± 0.012 a	1.04	0.120 ± 0.011 a	0.98
50	0.145 ± 0.013 b	1.36	0.144 ± 0.010 a	1.07	0.135 ± 0.011 a	1.10
100	0.171 ± 0.017 c	1.60	0.254 ± 0.036 c	1.90	0.241 ± 0.044 c	1.96
200	0.141 ± 0.016 b	1.21	0.257 ± 0.016 c	1.92	0.185 ± 0.012 b	1.50
400	0.128 ± 0.007 ab	1.20	0.190 ± 0.012 b	1.42	0.147 ± 0.006 a	1.20
800	0.117 ± 0.007 a	1.09	0.125 ± 0.007 a	0.93	0.122 ± 0.012 a	0.99

The optical density data are represented as mean ± standard error; Data within the same column sharing the same letters do not differ significantly ($P > 0.05$), whereas those with different letters differ significantly ($P < 0.05$)

Lymphocytes proliferation is an important indicator of immune defense in aquatic animals. The Con A-responsive lymphocytes belong to the B-cell subpopulation and the LPS-responsive lymphocytes belong to the T-cell subpopulation. The B-cell subpopulation involves cellular immunity while the T-cell subpopulation involves humoral immunity [19]. In this paper, Con A and LPS were used in lymphocytes proliferation assay to examine whether the two mitogens have synergy or antagonism effect with AMP on head kidney lymphocytes, and whether AMP contributes to the humoral or cellular immunity of *N. albiflora*. Results in Table 27.1 showed that Con A and LPS have synergy effect with AMP. Data in AMP + Con A group and AMP + LPS group implied that the AMP might contribute to both cellular and humoral immunity of *N. albiflora* in a dose-dependent manner (Table 27.1). This paper provided a rapid reference that the AMP is a potential immunostimulant for the healthy culture of *N. albiflora*. Further oral administration tests are needed to verify the immunostimulant efficacy of AMP.

Acknowledgments The financial support provided by Science and Technology Agency of Zhejiang province (Grant No. 2012C12907-8) is gratefully acknowledged.

References

1. Xu DD, Li SL, Lou B et al (2010) Research status of biological characteristics and culture ecology of *Nibea albiflora* (Richardson) and its culture prospect. Mod Fish Inform 25(10):23–26
2. Yan MC, Yang JY, Chen SB et al (2010) The investigation of diseases of major marine cultured species and their controlling measure in the southern Zhejiang province. Bull Sci Technol 26(4):550–555
3. Reverter M, Bontemps N, Lecchini D et al (2014) Use of plant extracts in fish aquaculture as an alternative to chemotherapy: Current status and future perspectives. Aquaculture 433:50–61
4. Pharmacopoeia committee (1995) Pharmacopoeia of the people's republic of China. The Ministry of Health of the People's Republic of China Beijing, Chemical Industry Press, p 271
5. Shao BM, Xu W, Dai H (2004) A study on the immune receptors for polysaccharides from the roots of *Astragalus membranaceus*, a Chinese medicinal herb. Biochem Biophys Res Commun 20(4):1103–1111
6. Yao XJ, Wang M, Jiang SX et al (2009) Recent advance in studies on pharmacological activities and application in animal production of astragalus polysaccharides. Feed Ind 30 (18):1–3
7. Liu MZ, Yu H, Yin FQ et al (2014) Researches in effects of Astragalus polysaccharides on immune performance of Fish. Hubei Agric Sci 53(9):1985–1988
8. Xiang X, Chen J, Zhou XH et al (2011) Effect of Astragalus polysaccharides on growth, body composition and immune index in *Schizothorax pernanti*. Acta Hydrobiol Sin 35(2):291–299
9. Hong XP, Lu HD, Zhang QH et al (2014) Effect of Astragalus polysaccharide on the anti-infection of white spot syndrome virus (WSSV) in *Procambarus clarkia*. J Shanghai Ocean Univ 23(3):423–428
10. Jia R, Du JL, Cao LP et al (2014) Inhibition effect of *Astragalus* polysacharin on chemical hepatocyte damage of common carp (*Cyprinus carpio*). J Huazhong Agric Univ 33(2):103–110
11. Staub AM (1965) Removal of proteins (Sevag method). Method Carbohydr Chem 5:5–6
12. Dubois M, Gilles KA, Hamilton JK et al (1956) Colorimetric method for determination of sugars and related substances. Anal Chem 28:350

13. Wen CF, Dong AW, Li GZ et al (2005) Determination of total sugar and reducing sugar in *Viola philippicassp*. Mod Food Sci Technol 21(3):122–123
14. Meseguer I (1988) Extraction and colorimetric quantification of uronic acids of the pectic fraction in fruit and vegetables. J Food Compos Anal 11:285–291
15. Yu D, Ma L, Zhao J et al (2009) Quantitative determination of uronic acid in polysaccharides from *Vitis vinifer* L. J Xinjiang Med Univ 32(5):533–535
16. Bradford MM (1976) A rapid and sensitive method for the quantitation of microgram quantities of protein utilizing the principle of protein-dye binding. Anal Biochem 72:248–254
17. Wang QK, Chen CX, Guo YJ et al (2011) Dietary polysaccharide from Angelica sinensis enhanced cellular defence responses and disease resistance of grouper *Epinephelus malabaricus*. Aquacult Int 19:945–956
18. Zhang YA, Sun BJ, Nie P (2000) Immune tissues and cells of fish: a review. Acta Hydrobiol Sin 24(6):648–654
19. Sizemore RC, Miller NW, Cuchens MA (1984) Phylogeny of lymphocyte heterogeneity: the cellular requirements for in vitro mitogenic responses of channel catfish leucocytes. J Immunol 133:2920–2924

Chapter 28
Aspergillus niger Pellets Absorbed *Bacillus* sp. Isolated from Soybean Wastewater Sludge

Ningning Diao, Xiaowei Wu and Jianguo Zhang

Abstract More efficient soybean wastewater treatment approach is necessary because of the increasing soybean processed in the worldwide. *Aspergillus niger* pellets formed during the wastewater treatment was a promising method from the views of easy harvest, safety authorized by FDA, and lower sludge obtained. For further COD removal on the base of *A. niger* pellets, a bacteria (*Bacillus* sp.) was isolated from sludge of classical soybean wastewater treatment. And then the absorption ratio was tested in different conditions for potential application in wastewater treatment. In this research, 76.24 % of *Bacillus* sp. was absorbed from the 3.0×10^8/mL initial cell concentration at pH 5.0. These results confirmed the possibility of further COD removal by the combination of *A. niger* and bacteria without losing the advantages of fungal pellets.

Keywords Wastewater · Fungal pellet · Absorption

28.1 Introduction

Soybean food is a kind of typical food in Asian area and is nourishable for human body. Soybean food was approved by more and more people in worldwide as the result of more flavors of soybean food provided and cultural communication. Therefore, the requirement of soybean food is huge and increasing. The total soybean processed for soybean foods production was 9,753,000 ton in China in 2010 [1]. Therefore, there is a huge amount of wastewater need to be treated also.

N. Diao · J. Zhang (✉)
School of Medical Instrument and Food Engineering, University of Shanghai for Science and Technology, 334 Jungong Road, Shanghai 200093, People's Republic of China
e-mail: jgzhang@usst.edu.cn

X. Wu
Tianjin LG BOTIAN Chemical Co., Ltd, No.1085, Haihe Road,
Lingang Industrial Area, Tianjin 300452, People's Republic of China
e-mail: 156430160@qq.com

T.-C. Zhang and M. Nakajima (eds.), *Advances in Applied Biotechnology*,
Lecture Notes in Electrical Engineering 333, DOI 10.1007/978-3-662-46318-5_28

One promising method for soybean wastewater treatment was fungal pellet formation [2]. Fungal pellet is one kind of morphologies, which like a ball consisted of entangled fungal mycelium. Fungal pellet was formed well in soybean wastewater because soybean wastewater has high content of organic compounds and varieties of other nutrients [3]. Fungal pellet has the advantages of easy harvest, low fermentation broth viscosity [4], and high yield of some proteins [5]. The diameter of fungal pellet is about 0.5 cm, which is harvested by simple filter with low cost. *Aspergillus niger* is the most used fungal species for pellet formation because *A. niger* was authorized as "Generally Regarded As Safe" by the American Food and Drug Administration (FDA) [6]; and *A. niger* genome was sequenced [7, 8]; *A. niger* has solid foundation of research [9]. Also, *A. niger* has a long history in food industry. *A. niger* hyphae in the form of pellet absorbed Cu^{2+}, Zn^{2+}, Ni^{2+} at pH 4.0–6.0 [10]. *A. niger* pellet was the right condition for citric acid production for food industry [11].

The crystal clear supernatant was obtained after 72 h cultivation after inoculation of *A. niger* spores. However, the chemical oxygen demand (COD) of supernatant was not low enough [2]. Therefore, it is necessary to modify the fungal pellet approach for further low COD. The dominated microbial species in typical soybean wastewater sludge was considered as the major contribution for COD removal. In this research, the *A. niger* pellets cooperated with this major species by absorption as assumpted was a potential method for further COD decreasing. The dominated species in soybean wastewater sludge was isolated and identified as *Bacillus* sp. The absorption of *Bacillus* sp. to *A. niger* pellets at different conditions was tested. The forces of *A. niger* and *Bacillus* sp. absorption were attributed to electrostatic interaction, hydrophobicity, and spatial interaction. Within these forces, electrostatic interaction was the major force. Krull reported that *A. niger* charge increased with the pH value increasing from 2.5 [12]. Wargenau showed the wide range of pH for negative charge [13]. This negative charge came from the carboxyl groups of cell wall. The carboxyl group contents in cell wall changed at different physiological conditions of cell [13]. The cell–cell interaction was also affected by the cation ion concentration based on the Derjaguin-Landau-Verwey-Overbeek mode (DLVO) of colloid science [14]. *Bacillus* had negative charge also [15]. *Bacillus* sp. attached to *A. niger* as that of microalgae cell attached onto fungal hyphae [16]. Different cells with same charge aggregated together because of differen charges at different area of cell surface [17] and the salt bridge affection [18]. Hydrophobins of fungal cell also played an important role during cells getting together. Hydrophobin was a kind of amphiphilic protein comprising 100–150 amino acids. Hydrophobin improved the cell aggregated by decreasing the Gibbs free energy [19]. *A. niger* co-pellets with microbial species provided the new route for bioenergy production [16] and wastewater treatment [20].

28.2 Materials and Methods

28.2.1 Fungal Species

Aspergillus niger spores was stored in lab at −70 °C.

28.2.2 Bacillus sp. Isolation

The soybean sludge came from Shanghai Tramy Green Food Co., Ltd. The sludge was diluted with sterilized water. And the liquid was taken to spread on PDA agar plates. These plates were cultivated at different temperature for microbial growth. After several days of cultivation, colonies were taken for identification.

28.2.3 Bacillus sp. Cultivation

The *Bacillus* sp. was cultivated in PDA (potato 200 g/L, dextrose 20 g/L, agar 15 g/L) medium at 37 °C, and then was harvested by centrifugation (4,000 rpm, 5 min). The cell was washed twice by sterilized water through suspension and centrifugation. Finally, the *Bacillus* sp. cell was added with phosphate buffer solution (PBS) for absorption.

28.2.4 Fungal Pellets Preparation

The *A. niger* spore was inoculated in 250 mL flask with 100 mL Czapek's medium (glucose 25.0 g/L, $NaNO_3$ 3.0 g/L, K_2HPO_4 1.0 g/L, KCl 0.5 g/L, $MgSO_4 \cdot 7H_2O$ 0.5 g/L, $FeSO_4 \cdot 7H_2O$ 0.01 g/L). The final pH was adjusted by 1 mol/L HCl and 1 mol/L NaOH to 5.6. The *A. niger* was cultivated at 30 °C, 200 rpm. The *A. niger* pellets were formed after 48 h cultivation and was harvested at 72 h cultivation.

28.2.5 Aspergillus niger Pellets Absorbed Bacillus sp. Cell

Twenty *A. niger* pellets were mixed with *Bacillus* sp. in PBS buffer (50 mmol/L) with different pH, the sample was taken at interval for *Bacillus* sp. cell number determination.

28.2.6 Cell Number Calculation

The *A. niger* spores and *Bacillus* sp. cell numbers were determined by the method of blood counting chamber. The cell number was calculated by the Eq. 28.1.

$$\text{Cell}\,(\text{per mL}) = C_1/80 \times 400 \times 1,0000 \times N \qquad (28.1)$$

C_1 Cell numbers in 80 small chambers
N dilution ratio

28.2.7 Microbial Photos

Pull 100 mL fermentation broth with *A. niger* pellets in a petri dish. Photos were taken by digital camera (Sony Dsc-t70). The *Bacillus* sp. colonies photos were also taken by the same digital camera.

28.3 Results

28.3.1 Bacillus sp. Isolation from Soybean Sludge

The COD removal by *A. niger* pellets worked in aerobic condition. Therefore, the associated microbial isolation process was carried in aerobic condition. Several microbial species were obtained after cultivation. One bacterium was selected for further research because bacteria were the major contribution in aerobic digestion of wastewater treatment (Fig. 28.1). The selected bacteria was white, bulging, and identified as *Bacillus* sp.

28.3.2 Aspergillus niger Pellets Used for Soybean Wastewater Treatment

After 72 h cultivation, *A. niger* spores grew and became cell pellets in soybean wastewater. And the yellow and cloudy soybean wastewater turned into crystal clear (Fig. 28.2). The COD of soybean wastewater reduced from 32,600 to 4,360 mg/L (Table 28.1). Therefore, 86.66 % of COD was removed by *A. niger* pellets.

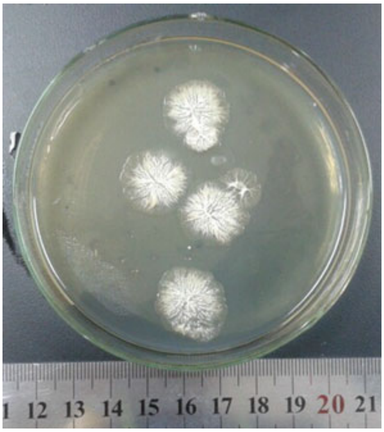

Fig. 28.1 The *Bacillus* sp. colonies from soybean wastewater sludge

Fig. 28.2 *Aspergillus niger* pellets after 72 h cultivation in soybean wastewater

Table 28.1 Chemical oxygen demand of soybean wastewater and wastewater after treatment

	Soybean wastewater	Treated
COD (mg/L)	32,600	4,360

28.3.3 *Aspergillus niger Pellets Preparation in Czapek's Medium*

Figure 28.3 showed the *A. niger* pellets after 72 h cultivation in Czapek's medium. There were about 50 pellets in every 100 mL medium. And the diameter of 90 % pellets was 0.5–1.0 cm, which showed the relatively constant diameter of pellets. The *A. niger* pellets are white, smooth.

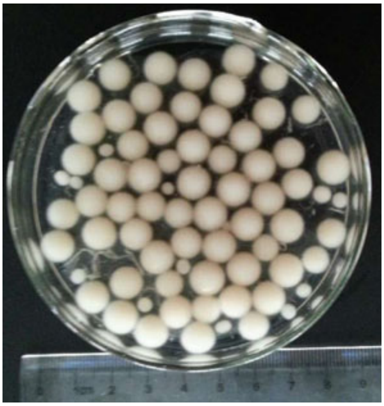

Fig. 28.3 The *A. niger* pellets formed in Czapek's medium

28.3.3.1 Effect of pH on the Bacillus sp. Absorption into Aspergillus niger Pellets

For all the pH values (pH 3.0, 4.0, 5.0, 6.0, 7.0), the *Bacillus* sp. cell number in liquid phase reduced sharply within first 30 min of mixing. And then, *Bacillus* sp. cell number decreased slowly until 150 min except that of pH 6.0. Finally, *Bacillus* sp. cell number increased from 150 to 180 min. The *Bacillus* sp. cell number kept constant from 30 to 180 min (Fig. 28.4). The *A. niger* pellets kept intact during all the process. The minimum *Bacillus* sp. cell in liquid phase was obtained at pH 5.0. Therefore, pH 5.0 was set as the default condition for further research.

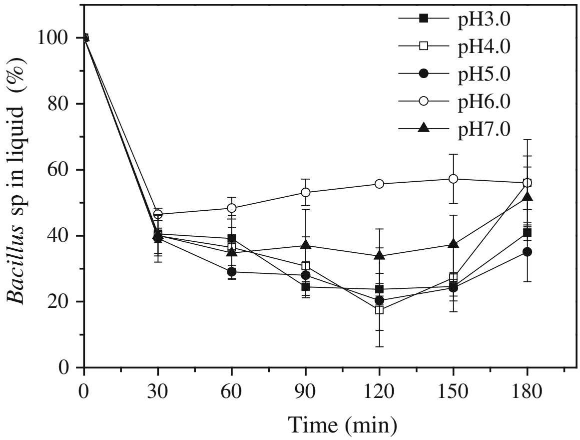

Fig. 28.4 Effects of pH on the *Bacillus* sp. absorption into *A. niger* pellets

28.3.4 *Effect of Ions on the Bacillus sp. Absorption into Aspergillus niger Pellets*

With all different cation ion and different concentrations, the *Bacillus* sp. cell number decreased as time went on (Figs. 28.5, 28.6 and 28.7). The same phenomenon occurred as that in Fig. 28.4. After 30 min, *Bacillus* sp. cell numbers with addition of cation ions had higher values than that of control. *Bacillus* sp. cell number with addition of Na^+ showed an increase during the period from 30 to 60 min. And then *Bacillus* sp. cell number decreased slowly until 180 min. For the Ca^{2+}, the *Bacillus* sp. cell number at 0.1 mol/L was lower than that of 0.25 and 0.5 mol/L. There was no significant difference among 0.1, 0.25, 0.5 mol/L Na^+. The *Bacillus* sp. cell number at different Mg^{2+} concentrations showed difference after 120 min mixing. Finally, the *Bacillus* sp. cell number at 0.1 mol/L was lower than that of 0.25 and 0.5 mol/L with the addition of Mg^{2+}.

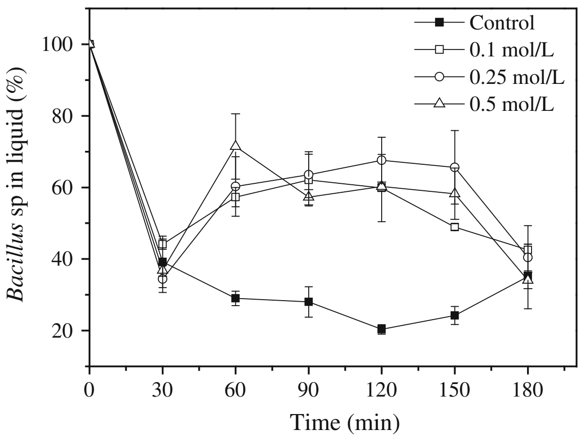

Fig. 28.5 Effects of Na^+ on the *Bacillus* sp. absorption into *A. niger* pellets

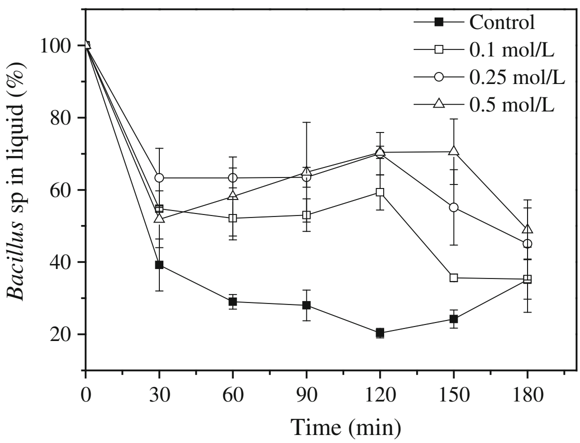

Fig. 28.6 Effects of Ca^{2+} on the *Bacillus* sp. absorption into *A. niger* pellets

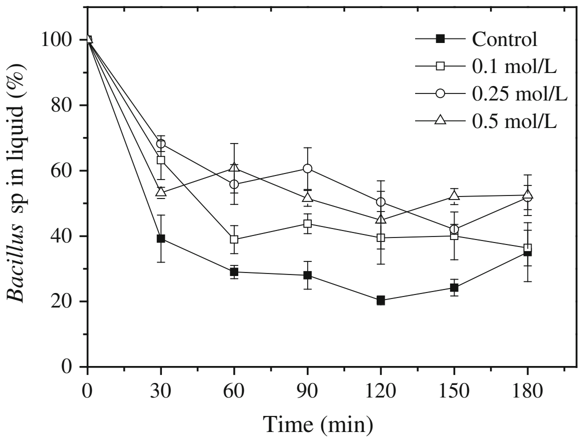

Fig. 28.7 Effects of Mg^{2+} on the *Bacillus* sp. absorption into *A. niger* pellets

28.4 Discussion

The classic approach of soybean wastewater treatment was filtration, anaerobic digestion (Upflow anaerobic sludge blanket, UASB), aerobic reaction (Sequencing Batch Reactor, SBR), and sediment sequencely. This process was contributed by large amount of microbes of different species to enhance the COD removal, fungal pellets formation in soybean wastewater with other microbial species as an association was considered as a potential approach. *Bacillus* sp. was selected because it was an important microbe producing biofilm and enzymes for COD removal in sludge [21, 22]. The *Bacillus* sp. produced biofilm and enzymes which help with organic compounds degradation and attachment to cells.

Bacillus sp., belong to bacteria, grew faster than *A. niger*. Therefore, the *Bacillus* sp. cell number increased significantly, even some of them were absorbed by *A. niger* pellets when these two species were mixed in medium. To test the *Bacillus* sp. absorption into *A. niger*, these two species were mixed in PBS without any nutrients. The Absorption between cells was derived by electrostatic interaction and hydrophobicity mainly [23]. For given filamentous fungi (*A. niger*) in this research, the hydrophobicity was defined because the hydrophobicity was provided by the hydrophobins from filamentous fungi. However, the electrostatic interaction was affected by the ion concentration, and the cation valence [24]. The Na^{+}, Ca^{2+}, and Mg^{2+} were not only major cations for the electrostatic interaction, but also necessary for cell growth as nutrients [13]. The effects of cation concentrations on the absorption between *Bacillus* sp. and *A. niger* showed the same trend of absorption ratio.

The results of this research confirmed that the *Bacillus* sp. cell was absorbed by *A. niger* pellets with the maximal value of 76.24 % absorbed. These two species playing the role of COD removal together provided a further COD reduction compared to the 86.66 % COD removed by *A. niger* pellets only. The *Bacillus* sp. cell number fluctuated during the absorption process especially in Figs. 28.5 and

28.6. This phenomenon was caused by the ion interaction among microbial cell and buffer, which was the same as that of the ion exchange. Therefore, high ion concentration decreased the absorption ratio of *Bacillus* sp. These results gave the clue that ion concentration decreasing from 50 mmol/L was the right direction for *Bacillus* sp. absorption. Further more, immobilization bacteria like *Bacillus* sp. by chemical methods on the base *A. niger* pellets absorption is another method to stabilize the co-pellets for long-time utilization.

Acknowledgments This project supported by the National Natural Science Foundation of China (No. 21306112), Shanghai Municipal Natural Science Foundation (No. 13ZR1429100), Foundation (No. 2013IM002) of Key Laboratory of Industrial Fermentation Microbiology of Ministry of Education and Tianjin Key Lab of Industrial Microbiology (Tianjin University of Science & Technology).

References

1. Wei X (2012) Review and prospect to the development of China’s soybean food industry. Sci Technol Food Ind 33(15):1–4
2. Huang XJ, Zhang JG, Diao NN (2014) Optimization of *Aspergillus niger* pellet formation to treat soybean products wastewater. Ind Microbiol 44(3):41–48
3. Wang J, Li X, Fu W, Wu S, Li C (2012) Treatment of artificial soybean wastewater anaerobic effluent in a continuous aerobic–anaerobic coupled (CAAC) process with excess sludge reduction. Bioresour Technol 126:142–147
4. Hille A, Neu TR, Hempel DC, Horn H (2006) Effect of morphology on transport of matter and conversion in *Aspergillus niger*-Pellets. Chem-Ing-Tech 78(5):627–632
5. Porcel EMR, Lopez JLC, Perez JAS, Sevilla JMF, Chisti Y (2005) Effects of pellet morphology on broth rheology in fermentations of *Aspergillus terreus*. Biochem Eng J 26 (2–3):139–144
6. Schuster E, Dunn-Coleman N, Frisvad J, Van Dijck P (2002) On the safety of *Aspergillus niger*–a review. Appl Microbiol Biotechnol 59(4):426–435
7. Baker SE (2006) *Aspergillus niger* genomics: past, present and into the future. Med Mycol 44 (S1):17–21
8. Andersen MR, Nielsen ML, Nielsen J (2008) Metabolic model integration of the bibliome, genome, metabolome and reactome of *Aspergillus niger*. Mol Syst Biol 4(1):178
9. Guo Y, Zheng P, Sun J (2010) *Aspergillus niger* as a potential cellular factory: prior knowledge and key technology. Chin J Biotechnol 26(10):1410–1418
10. Filipović-Kovačević Ž, Sipos L, Briški F (2008) Biosorption of chromium, copper, nickel and zinc ions onto fungal pellets of *Aspergillus niger* 405 from aqueous solutions. Food Technol Biotechnol 38(3):211–216
11. Papagianni M (2007) Advances in citric acid fermentation by *Aspergillus niger*: Biochemical aspects, membrane transport and modeling. Biotechnol Adv 25(3):244–263
12. Krull R, Cordes C, Horn H, Kampen I, Kwade A, Neu T et al (2010) Morphology of filamentous fungi: linking cellular biology to process engineering using *Aspergillus niger*. Biosyst Eng II:1–21
13. Wargenau A, Kampen I, Kwade A (2013) Linking aggregation of *Aspergillus niger* spores to surface electrostatics: a theoretical approach. Biointerphases 8:7
14. Wargenau A, Fleißner A, Bolten CJ, Rohde M, Kampen I, Kwade A (2011) On the origin of the electrostatic surface potential of *Aspergillus niger* spores in acidic environments. Res Microbiol 162(10):1011–1017

15. Dickson JS, Koohmaraie M (1989) Cell surface charge characteristics and their relationship to bacterial attachment to meat surfaces. Appl Environ Microbiol 55(4):832–836
16. Zhang J, Hu B (2012) A novel method to harvest microalgae via co-culture of filamentous fungi to form cell pellets. Bioresour Technol 114:529–535
17. Prochazkova G, Safarik I, Branyik T (2013) Harvesting microalgae with microwave synthesized magnetic microparticles. Bioresour Technol 130:472–477
18. Mill P (1964) The nature of the interactions between flocculent cells in the flocculation of *Saccharomyces cerevisiae*. J Gen Microbiol 35(1):61–68
19. Ryoo DH, Choi CS (1999) Surface thermodynamics of pellet formation in *Aspergillus niger*. Biotechnol Lett 21(2):97–100
20. Zhou W, Cheng Y, Li Y, Wan Y, Liu Y, Lin X, et al (2012) Novel fungal pelletization-assisted technology for algae harvesting and wastewater treatment. Appl Biochem Biotechnol 167: 214–228
21. Liu WX, Wang XB, Wu LH, Chen MF, Tu C, Luo Y et al (2012) Isolation, identification and characterization of *Bacillus amyloliquefaciens* BZ-6, a bacterial isolate for enhancing oil recovery from oily sludge. Chemosphere 87(10):1105–1110
22. Merrylin J, Kaliappan S, Kumar SA, Yeom IT, Banu JR (2014) Effect of extra polymeric substance removal on sludge reduction potential of *Bacillus licheniformis* at its optimised pH condition. Water Environ J 28(1):95–103
23. Huang X, Diao N, Zhang J (2014) The review of *Aspergillus niger* pellets formation and its application. Food Ferment Ind 11:171–176
24. Wargenau A, Fleissner A, Bolten CJ, Rohde M, Kampen I, Kwade A (2011) On the origin of the electrostatic surface potential of *Aspergillus niger* spores in acidic environments. Res Microbiol 162(10):1011–1017

Chapter 29
Expression, Purification and Characterization of Maltase from "Quick" Baker's Yeast

Cui-Ying Zhang, Hai-Yan Song, Xue Lin, Xiao-Wen Bai and Dong-Guang Xiao

Abstract The "quick" baker's yeasts are capable to rapidly metabolize maltose, thereby improving leavening ability. Given that maltase is the determining factor in maltose fermentation for "quick" baker's yeast, it is hence necessary to research the properties of the maltase independently for the "quick" baker's yeast. In this study, the heterogeneous expression of MAL62 encoding for maltase and purification of maltase were well completed. Furthermore, the enzymatic properties of maltase concentrated on the effects of substrate (maltose) and end product (glucose) were investigated as well as the physic-chemical properties and transglycosylation activity. The substrate maltose did not affect the activity of maltase, while the maltase activity was inhibited by the end product. This study provides guidance for the research of maltose metabolism for "quick" baker's yeast.

Keywords "Quick" baker's yeast · Maltase · Enzymatic properties

29.1 Introduction

Baker's yeast (*Saccharomyces cerevisiae*) is the key biological leaven using in baking industry, and is of crucial importance in dough leavening [1]. Maltose is the most abundant fermentable sugar in lean dough [2–5]. According to the level of utilizing maltose, the baker's yeast could be classified into "quick" and "slow." "Quick" baker's yeasts are capable to rapidly metabolize maltose, thereby improving leavening ability. The ability of a baker's yeast strain to ferment maltose depends on the presence of three gene products; they are maltose permease encoded by MALx1 (where x is locus) gene, maltase encoded by MALx2 gene, and a

C.-Y. Zhang (✉) · H.-Y. Song · X. Lin · X.-W. Bai · D.-G. Xiao
Key Laboratory of Industrial Fermentation Microbiology, Ministry of Education, Tianjin Industrial Microbiology Key Laboratory, College of Biotechnology, Tianjin University of Science and Technology, Tianjin 300457, People's Republic of China
e-mail: cyzhangcy@tust.edu.cn

T.-C. Zhang and M. Nakajima (eds.), *Advances in Applied Biotechnology*,
Lecture Notes in Electrical Engineering 333, DOI 10.1007/978-3-662-46318-5_29

positive regulatory protein activating the two enzymes encoded by MALx3 gene [6–8]. Maltose is transported across the cell membrane via maltose permease and cleaved intracellularly into two units of glucose by maltase. Given that maltase is the determining factor in maltose fermentation for "quick" baker's yeast [5, 9], it is hence necessary to research the properties of the maltase independently for the "quick" baker's yeast.

Maltase (α-D-Glucoside glucohydrolase; EC 3.2.1.20) exists in a large amount of organisms and can be classified into three types (I, II, and III) according to the substrate specificities [10]. The α-glucosidase from Thermoanaerobacter tengcongensis, which belongs to type II, preferentially utilizes maltose and has low specificity toward aryl glucosidase [11]; Type III is similar to type II, except that they hydrolyze di- and oligosaccharides and starch with comparable rates. The enzymes from *Mucor racemosus* and Penicillium species belong to the Type III [12]. The maltase of yeast is classified into type I. Some properties of maltase from different yeasts have been studied [13, 14]. However, the comprehensive properties of maltase for the "quick" baker's yeast are little known, particularly the properties involving in maltose metabolism.

In this study, the MAL62 gene from a "quick" baker's yeast was successfully expressed in *Escherichia coli* BL21 (DE3) and the maltase was well purified. To investigate the enzymatic properties of maltase, we focus on the effects of substrate (maltose) and end product (glucose), in addition to the physic-chemical properties and transglycosylation activity.

29.2 Materials and Methods

29.2.1 Strains and Plasmids

The "quick" industrial baker's strain BY14 was obtained from the Yeast Collection Center of the Tianjin Key Laboratory of Industrial Microbiology. *E. coli* DH5α was stored in our laboratory. The expression vector pET-28a and the strain BL21 (DE3) were provided by Prof. Fu-Ping Lu (Tianjin University of Science and Technology, P.R. China).

29.2.2 Construction of MAL62 Expression System

Yeast genomic DNA was prepared from industrial baker's yeast strain BY14 using a yeast DNA kit (D3370-01, Omega, USA). The MAL62 fragment was amplified via PCR using the genomic DNA of BY14 as template and the primers (CGCGGATCC ATGACTATTTCTGATCATCCAG, the restriction site of BamHI is underlined and CCCAAGCTT GTTATTTGACGAGGTAGATTCT, the restriction site of HindIII is underlined). The PCR product was purified with a Gel Extraction Kit (Sigma, USA) and cloned to the vector pET28a after digestion with BamHI and HindIII (TaKaRa, Japan), thereby generating pET28a-MAL62. DNA sequencing was performed (Beijing Genomic institution, China). For gene expression, the plasmid pET28a-MAL62 was transformed into *E. coli* BL21 (DE3), resulting in the strain BL21-M.

29.2.3 Purification of Maltase

The strain BL21-M carrying the plasmid pET28a-MAL62 was cultured in 50 mL of Luria-Bertani medium (LB medium, 10 g/L tryptone, 5 g/L yeast extract, and 10 g/L NaCl), which was supplemented with kanamycin (60 μg/mL) [11]. When the OD_{600} reached to 1.0, IPTG was added with the final concentration of 0.4 mM, and the cells were continuously cultivated for 12 h at 26 °C. 60 mL of cells were harvested by centrifugation (3,500×g, 4 °C, 20 min) and washed by PBS buffer (0.8 % NaCl, 0.02 % KCl, 0.142 % Na_2HPO_4, 0.027 % KH_2PO_4; pH 7.0) [15]. The cell precipitation was suspended by 7 mL PBS buffer. The suspended cells were disrupted through sonication (power 50 %, on 4 s, off 9 s, total time 40 min) and the crude enzyme was centrifuged at 8,000×g for 20 min. The collected supernatant was loaded onto Ni-NTA affinity column (Kang Wei Company, China) and recombinant protein was eluted with a liner gradient of imidazole (0.1–0.5 M) PBS buffer. The collected enzyme was dialyzed in PBS buffer at 4 °C for 12 h. Protein concentration was determined by the method of Bradford [16], and the bovine albumin was used as standard.

29.2.4 Standard Maltase Activity Assays

Maltase activity was tested using maltose as the substrate. The reaction mixture contained 0.5 mL of 0.4 M maltose, 0.4 mL of PBS buffer (pH 7.0), and 0.1 mL of the maltase. After incubation at 40 °C for 20 min, the reaction was stopped by boiling for 10 min. The freed glucose was assayed with biosensor. When the *p*-nitrophenyl-a-D-glucoside (*p*-NPG) was used as the substrate, maltase activity was measured in a mixture containing 0.9 mL PBS buffer (pH 7.0), 2 mL of 10 mM substrate solution, and 0.1 mL of the maltase. After incubating at 40 °C for 10 min, the reaction was stopped with 2 mL of 1 M Na_2CO_3, and the released *p*-nitrophenol was quantified with spectrophotometer at 410 nm. A unit of maltase activity was defined as the amount of enzyme liberating 1 μmol of glucose or 1 μmol of *p*-nitrophenol in 1 min.

29.2.5 Effects of Maltose and Glucose on Maltase Activity

To investigate the effect of substrate on the enzyme activity, different concentrations (from 40 to 300 mM) of maltose were used. The K_m and V_{max} values were calculated from the Hanes plots relating [s]/v to [s]. The effect of end production was determined using *p*-NPG as the substrate, and the kinetic parameters for the maltase under different concentrations of glucose were obtained from the Lineweaver–Burk plots relating 1/v to 1/s. The K_i value was determined by the graphical method of Dixon. The date was analyzed using Origin Software.

29.2.6 Effects of pH, Temperature, and Chemicals on Maltase Activity and Stability Tests

The optimum temperature of maltase activity was assayed at 20–55 °C for 20 min using 200 mM maltose. After incubation at various temperatures for 2 h, thermal stability was analyzed by assessing residual activity. The optimum pH of maltase activity was tested in PBS buffer with different pH (pH 3.0–9.0) at 40 °C for 20 min. The effect of pH on enzyme stability was analyzed after incubation in PBS buffer with different pH (pH 3.0–9.0) at 4 °C for 24 h. The residual activity was measured under the standard hydrolytic condition.

The effect of metal ions (Cu^{2+}, Fe^{3+}, Co^{2+}, Mn^{2+}, Ni^{2+}, Ca^{2+}, Pb^{2+}, and Mg^{2+}) was examined with a final concentration of 5 mM, and that of the chelating agent EDTA was 5 and 25 mM. All tests were performed in PBS buffer (pH 7.0) and the enzyme activity tested under no ions was defined as 100 %.

29.2.7 Transglycosylation Activity Analysis

The reaction mixture (1 mL), which consists of 0.9 mL of 1 M maltose solution (from pH 7.0 PBS buffer) and 0.1 mL of maltase, was incubated at 30 °C. Every 1 h, sample was taken out and boiled at 100 °C for 10 min for maltase inactivation and filtered through 0.45 μm pore size cellulose acetate filters (Millipore Corp, Danvers, MA, USA). High-performance liquid chromatography (HPLC) with a refractive index detector and Aminex® HPX-87H column (Bio-Rad, Hercules, CA, USA) was utilized at 65 °C with 5 mM H_2SO_4 as the mobile phase at a flow rate of 0.6 mL/min [17] to analyze the sugars.

29.3 Results and Discussion

29.3.1 Purification of Maltase

Maltase from "quick" industrial baker's strain BY14 is an intracellular enzyme, which made us difficult to study the enzymatic properties directly. In this study, the MAL62 gene was successfully expressed in *E. coli* BL21 (DE3). In general, *E. coli* is the preferred host for the property studies of recombinant protein expression due to the easily genetic manipulation, the relatively inexpensive of cultivation, and the rapid target expression, typically producing protein in 1 day. The importance of *E. coli* for heterologous protein production is perhaps best highlighted by the wide variety of commercial products available for the *E. coli* expression system [18]. In the present study, the maltase of "quick" baker's yeast was well purified. A relatively sharp band at 68 kDa was observed on SDS-PAGE (Fig. 29.1). Purification steps are represented in Table 29.1. The final enzyme solution was purified 6.2-fold compared with the crude extract. The molecular mass of the purified enzyme estimated by SDS-PAGE was 68 kDa (Fig. 29.1).

29.3.2 Effect of Different Concentrations of Substrate on Maltase Activity

Different concentrations of maltose were incubated with the same amounts of recombinant enzyme and the maltase activity was represented by the maltose

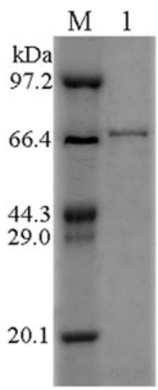

Fig. 29.1 SDS-PAGE of purified recombinant His-tagged maltase. *M* marker; *1* purified protein

Table 29.1 Purification of recombinant enzyme from BL21-M

Step	Protein (mg)	Total activity (μ)	Specific activity (μ/mg)	Purification fold
Crude	43.3	549.4	12.7	
Ni^{2+} affinity	3.0	237.0	79.0	6.2

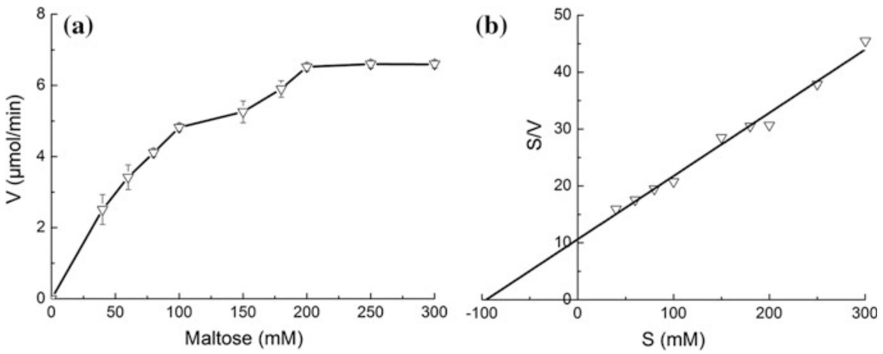

Fig. 29.2 Effect of maltose concentration on maltase activity. **a** 1 mL of reaction mixture consisted of different concentrations of maltose, 0.1 mL of enzyme, and PBS buffer reacted at 40 °C for 5 min; **b** Hans plot of maltase activity was determined using maltose as the substrate. Data were shown as mean ±SD (n = 3)

hydrolysis rate. With the increase of substrate concentration, no decrease trend was found in hydrolysis rate (Fig. 29.2a), which suggested that maltose did not restrain the maltase activity. Furthermore, the apparent K_m (Michaelis constant) value of maltase for maltose calculated from Fig. 29.2b was 95.507 mM. These findings suggested that the enzyme could not be inhibited by substrate (maltose). Simultaneously, the K_m for maltose was 95.507 mM, much higher than that from *Saccharomyces logos* (the K_m for maltase was 7.7 mM) [19], so maltose may not be the optimum substrate for the maltase from the "quick" baker's yeast.

29.3.3 Effect of End Product on Maltase Activity

To investigate the effect of end product on maltase activity, different concentrations of glucose were added to the identical reaction mixtures to test the maltase activity. With the increase of glucose concentration, the maltase activity was gradually decreased (Fig. 29.3a). When the concentration of glucose was increased to 180 mM, 84.6 % of the maltase activity was left. Various substrate (p-NPG) concentrations were used to determine the type of glucose inhibition under different concentrations of glucose. Results were obtained after incubation at 40 °C for 10 min. According to Fig. 29.3b, the K_m and V_{max} were 0.661 mM and 0.018 μmol/min, respectively, without the presence of glucose in reaction mixture. Notably, when the 20 and 180 mM of glucose were added, the K_m and V_{max} increased to 0.901 mM and 0.017 μmol/min, and 1.204 mM and 0.014 μmol/min, respectively. These results indicate that the type of glucose affecting on maltase was linear mixed inhibition (Fig. 29.3c). The graphical method of Dixon was used to determine the K_i, which is the dissociation constant of glucose, and the K_i value for glucose was 139.176 mM. Enzyme activity is inhibited by the end product, which corresponds to the previous

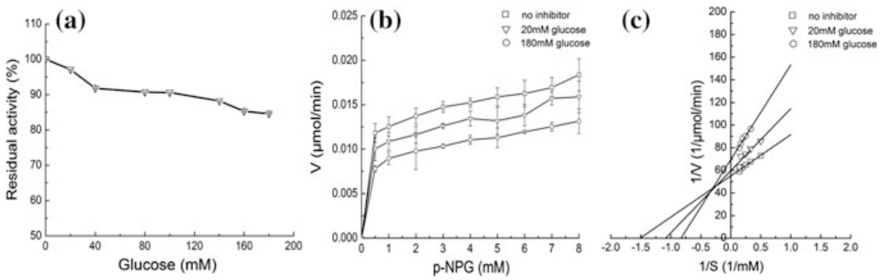

Fig. 29.3 Effect of end product on maltase activity. **a** 3 mL of reaction mixture consisted of different concentrations of glucose, 0.1 mL of enzyme, *p*-NPG and PBS buffer reacted at 40 °C for 20 min; **b** 3 mL of reaction mixture consisted of different concentrations of glucose, 0.1 mL of enzyme, *p*-NPG and PBS buffer reacted at 40 °C for 10 min; 2 mL of 1 M Na_2CO_3 was added to stop the reaction; **c** Lineweaver–Burk plot of *p*-NPG hydrolysis. Data were shown as mean ±SD (n = 3)

studies [20–22]. Compared with the maltase from Saccharomyces italicus exhibiting intense inhibition of end product (glucose) with 1.2 mM of K_i for glucose [23], the effect of end product (glucose) on maltase activity from "quick" baker's yeast was not significant (K_i = 139.176 mM). Furthermore, the glucose liberated from maltose could be rapidly oxidized in "quick" baker's yeast cells. Little or no glucose was accumulated in yeast cells, so that the end product (glucose) inhibition could be neglected. For this reason, "quick" baker's yeast had the capacity of rapidly metabolizing maltose.

29.3.4 Physic-Chemical Properties of Maltase

The physical and chemical factors, which are the basic elements, are also of great importance to influence the enzyme activity. The physic-chemical properties of

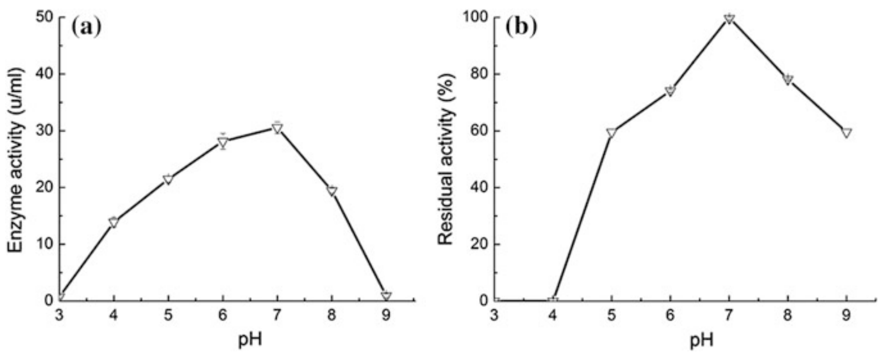

Fig. 29.4 Effect of pH on maltase activity. **a** The maltase activity was measured at various pH. **b** Effect of pH on the stability of maltase. After incubation at different pH at 4 °C for 24 h, the residual activity was measured at standard condition. The highest activity was defined as 100 %. Data were shown as mean ±SD (n = 3)

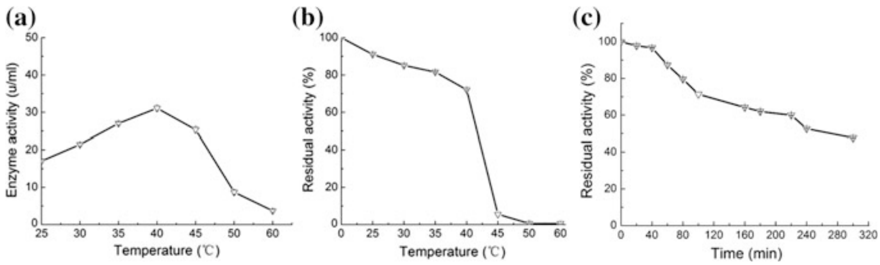

Fig. 29.5 Effect of temperature on maltase activity. **a** The maltase activity was measured at various temperatures at pH 7.0. **b** Thermostability of the recombinant enzyme. After 2-h incubation at different temperature, the residue activity was measured at standard condition. The initial activity was defined as 100 %. **c** Effect of temperature on the stability of maltase. The maltase was incubated at 40 °C for different times and residual activity was assayed at standard condition. Data were shown as mean ±SD (n = 3)

maltase, the effects of pH, temperature, metal ions, and EDTA on maltase activity were assayed. The maximum of maltase activity was shown at pH 7.0 (Fig. 29.4a). More than 60 % of residual maltase activity was observed from pH 5.0 to pH 9.0, while almost no residual activity was found at pH 4.0 or below it (Fig. 29.4b). As shown in Fig. 29.5a, the highest maltase activity was observed at 40 °C. Therefore, the thermotolerance of maltase was determined at 40 °C. The maltase activity significantly decreased by 52.3 % compared with that at the beginning, and the half-life of maltase at 40 °C was 244.6 min (Fig. 29.5c). After 2-h incubation at various temperatures, the maltase displayed different levels of activity decrease. The residual activity of maltase decreases slowly when incubation before 40 °C. However, the residual activity exhibited a much greater decline from 40 to 45 °C, and hardly any maltase activity was found at a higher temperature (50 and 60 °C) (Fig. 29.5b). The presences of Ca^{2+} and Mg^{2+} slightly increased the enzyme activity by 4.3 and 8.3 %, respectively (Table 29.2). By contrast, all the six other metal ions

Table 29.2 Effect of different chemical reagent on activity of the purified maltase

Reagent	Relative activity (%)
Control	100 ± 0.24
Ni^{2+}	11.2 ± 0.12
Co^{2+}	32.6 ± 0.12
Ca^{2+}	104.3 ± 0.31
Mn^{2+}	84.2 ± 0.23
Pb^{2+}	61.4 ± 0.31
Mg^{2+}	108.3 ± 0.20
Cu^{2+}	–
Fe^{3+}	–
EDTA (5 mM)	–100 ± 0.22
EDTA (25 mM)	72.3 ± 0.21

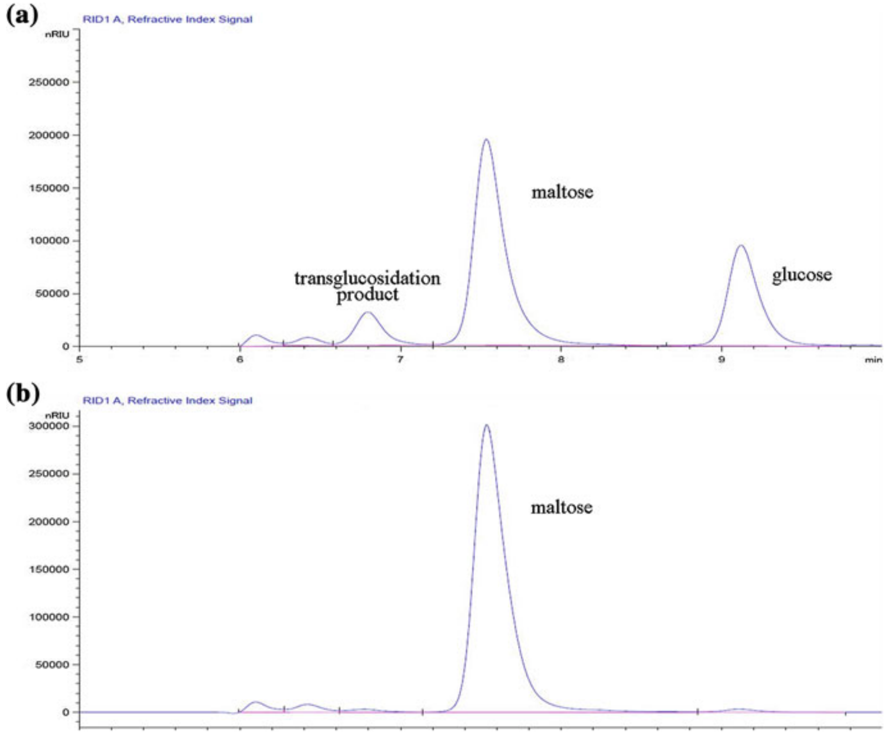

Fig. 29.6 Analysis of transglucosidation products by HPLC. Reaction mixture: 0.9 mL of 1 M maltose, 0.1 mL of maltase. **a** Reaction mixture with enzyme; **b** reaction mixture without enzyme

(Ni^{2+}, Co^{2+}, Mn^{2+}, Pb^{2+}, Cu^{2+}, and Fe^{3+}) decreased the maltase activity at different levels. Evidently, no maltase activity was found at the presence of Cu^{2+} and Fe^{3+} (the final concentration of ions was 5 mM) (Table 29.2). Inaction by Cu^{2+} indicates that the thiol groups, carboxyl groups, or histidine residues, which were important to the function of maltase, existed in the enzyme molecule [24–26]. Addition with 5 mM of EDTA did not evidently affect the maltase activity, but 27.7 % of maltase activity was notably lost when the concentration of EDTA was increased to 25 mM (Table 29.2). The evident inhibition with EDTA, even at 25 mM, indicates that a metal cation is not needed for maltase activity [22].

29.3.5 Transglycosylation Activity of Maltase

The transglycosylation activity of the recombinant maltase was assayed using maltose as the substrate. The reaction mixture incubated with the maltase for 5 h and that without enzyme were comparatively analyzed through HPLC. Compared with the reaction mixture without enzyme, a new transglycosylation substance was detected at 6.7 min in reaction mixture with enzyme (Fig. 29.6). These results reveal that maltase had the capacity of transglycosylation.

29.4 Conclusion

In this study, the maltase was cloned and purified successfully. The enzyme was not inhibited by the substrate (maltose), however, it was inhibited by end product (glucose) and the type of glucose affecting on maltase was linear mixed inhibition. This study also suggested that the maltase had transglycosylation activity, while the physic-chemical properties of enzyme may limit its use in industry.

Acknowledgments The authors are grateful to Professor Fu-Ping Lu (College of Biotechnology, Tianjin University of Science and Technology, P.R. China) for providing the plasmid and the strain used in this study. The current work was financially supported by the National High Technology Research and Development Program of China (2013AA102106), the National Natural Science Foundation of China (31171730; 31000043), and the Program for Changjiang Scholars and Innovative Research Team in University (IRT1166).

References

1. Phaff HJ, Miller MW, Mrak EM (1978) The life of yeasts. Harvard University Press, Cambridge
2. Alves AC, Pacheco A, Almeida MJ et al (2007) Sugar utilization patterns and respiro-fermentative metabolism in the baker's yeast *Torulaspora delbrueckii*. Microbiology 153:898–904
3. Bell PJ, Higgins VJ, Attfield PV (2001) Comparison of fermentative capacities of industrial baking and wild-type yeasts of the species *Saccharomyces cerevisiae* in different sugar media. Lett Appl Microbiol 32:224–229
4. Hazell B, Attfield P (1999) Enhancement of maltose utilisation by *Saccharomyces cerevisiae* in medium containing fermentable hexoses. J Ind Microbiol Biotechnol 22:627–632
5. Jiang T, Xiao D, Gao Q (2008) Characterisation of maltose metabolism in lean dough by lagging and non-lagging baker's yeast strains. Ann Microbiol 58:655–660
6. Cohen JD, Goldenthal MJ, Chow T et al (1985) Organization of the *MAL* loci of *Saccharomyces*. Physical identification and functional characterization of three genes at the *MAL6* locus. Mol Gen Genet 200:1–8
7. Hu Z, Gibson AW, Kim JH et al (1999) Functional domain analysis of the *Saccharomyces MAL*-activator. Curr Genet 36:1–12
8. Wang X, Bali M, Medintz I et al (2002) Intracellular maltose is sufficient to induce *MAL* gene expression in *Saccharomyces cerevisiae*. Eukaryot Cell 1:696–703
9. Sun X, Zhang C, Dong J et al (2012) Enhanced leavening properties of baker's yeast overexpressing *MAL62* with deletion of *MIG1* in lean dough. J Ind Microbiol Biotechnol 39:1533–1539
10. Marín D, Linde D, Lobato M (2006) Purification and biochemical characterization of an α-glucosidase from *Xanthophyllomyces dendrorhous*. Yeast 23:117–125

11. Zhou C, Xue Y, Zhang Y et al (2009) Recombinant expression and characterization of *Thermoanaerobacter tengcongensis* thermostable α-glucosidase with regioselectivity for high-yield isomaltooligosaccharides synthesis. J Microbiol Biotechnol 19:1547–1556
12. Giannesi GC, de Lourdes Teixeira de Moraes Polizeli M, Terenzi HF et al (2006) A novel α-glucosidase from *Chaetomium thermophilum* var. coprophilum that converts maltose into trehalose: Purification and partial characterisation of the enzyme. Process Biochem 41:1729–1735
13. Dušan V, Nenad M, Dejan B et al (2014) The specificity of α-glucosidase from *Saccharomyces cerevisiae* differs depending on the type of reaction: hydrolysis versus transglucosylation. Appl Microbiol Biotechnol 98:6317–6318
14. Wang YF, Ma L, Li Z et al (2004) Synergetic inhibition of metal ions and genistein on α-glucosidase. FEBS Lett 576: 46-50
15. Huang X, Zhao Y, Dai Y, et al (2012) Cloning and biochemical characterization of a glucosidase from a marine bacterium Aeromonas sp. HC11e-3. World J Microbiol Biotechnol 28:3337–3344
16. Bradford MM (1976) A rapid and sensitive method for the quantitation of microgram quantities of protein utilizing the principle of protein-dye binding. Anal Biochem 72:248–254
17. Hauf J, Zimmermann FK, Müller S (2000) Simultaneous genomic overexpression of seven glycolytic enzymes in the yeast *Saccharomyces cerevisiae*. Enzyme Microb Technol 26:688–690
18. Arnau J, Lauritzen C, Petersen GE et al (2006) Current strategies for the use of affinity tags and tag removal for the purification of recombinant proteins. Protein Expers Purif 48:1–13
19. Seiya C, Takeshi S, Tokuji S (1973) Substrate specificity of *Saccharomyces logos* α-glucosidase. Agric Biol Chem 37:1831–1836
20. Elshafei AM, Hassan MM, Morsi NM et al (2014) Purification and some kinetic properties of β-glucosidase from *Aspergillus terreus* NRRL 265. Afr J Biotechnol 10:19556–19569
21. Görts CP (1969) Effect of glucose on the activity and the kinetics of the maltose-uptake system and of α-glucosidase in *Saccharomy cescerevisiae*. Biochim Biophys Acta 184:299–305
22. Guffanti AA, Corpe WA (1976) Partial purification and characterization of alpha-glucosidase from *Pseudomonas fluorescens* W. Arch Microbiol 107:269–276
23. Halvorson H, Ellias L (1958) The purification and properties of an alpha-glucosidase of Saccharomyces italicus Y1225. Biochim Biophys Acta 30:28–40
24. Gupta AK, Gautam SP (1993) Purification and properties of an extracellular α-glucosidase from the thermophilic fungus *Malbranchea sulfurea*. J Gen Microbiol 139:963–967
25. Howard S, Withers SG (1998) Labeling and identification of the postulated acid/base catalyst in the alpha-glucosidase from *Saccharomyces cerevisiae* using a novel bromoketone C-glycoside. Biochemistry 37:3858–3864
26. McCarter JD, Withers SG (1996) Unequivocal identification of Asp-214 as the catalytic nucleophile of *Saccharomyces cerevisiae* alpha-glucosidase using 5-fluoro glycosyl fluorides. J Biol Chem 271:6889–6894

Chapter 30
Evaluation of an Ethanol-Tolerant *Acetobacter pasteurianus* Mutant Generated by a New Atmospheric and Room Temperature Plasma (ARTP)

Xiaoying Wu, Yuqiao Wei, Zeming Xu, Lingpu Liu, Zhilei Tan and Shiru Jia

Abstract A novel atmospheric and room temperature plasma (ARTP) which used helium as the working gas was employed to generate mutants of *Acetobacter pasteurianus* to improve the ethanol tolerance, which is a poorly characterized industrial strain. The best strain U1-1 was selected after mutagenesis. U1-1 could grow in liquid medium with 11 % ethanol. The production of acetic acid reached 32.83 ± 0.75 g/L, 385.7 % higher than that of the parent strain, meanwhile, U1-1 has stable production. Moreover, the cell membrane permeability were measured by PI assay and the results show that the cell membrane permeability of starting strain (AP-1.01) is significantly higher than U1-1. The better ethanol tolerance of strain U1-1 was maybe due to the decreased membrane permeability.

Keywords ARTP · *Acetobacter pasteurianus* · Mutant · Ethanol tolerance · Membrane permeability

30.1 Introduction

Acetic acid bacteria (AAB) are gram-negative strictly aerobic bacteria that are widely used for the production of vinegar, gluconate, bacterial cellulose, and so on. AAB are divided into three species: *Acetobacter*, *Gluconobacter*, and *Gluconacetobacter. Acetobacter pasteurianus*, which belongs to the *Acetobacter* sp. is widely used in the production of vinegar in many countries [1].

X. Wu · Y. Wei · Z. Xu · L. Liu · Z. Tan · S. Jia (✉)
Key Lab of Industrial Fermentation Microbiology of the Ministry of Education,
School of Biotechnology, Tianjin University of Science and Technology,
Tianjin 300457, China
e-mail: jiashiru@tust.edu.cn

T.-C. Zhang and M. Nakajima (eds.), *Advances in Applied Biotechnology*,
Lecture Notes in Electrical Engineering 333, DOI 10.1007/978-3-662-46318-5_30

During the production of vinegar, AAB subjected to many adverse environmental factors, such as high temperature in the solid fermentation, high concentration of acetic acid, and ethanol. There are many researchers who focus on the acetic acid tolerance mechanisms and thermotolerance mechanisms of AAB, and how to improve these tolerances [1–5]. However, few researchers pay attention to the ethanol tolerance. Ethanol is the main carbon source of AAB and the substrate of acetic acid fermentation by AAB. Ethanol has been verified harmful to the growth of microorganism; ethanol would change the permeability of cell membrane, resulting in cell lysis that ultimately leads to cell death [6–8]. The high concentration of ethanol can seriously affect AAB in the fermentation process. Wei et al. [9] used genome shuffling to improve the ethanol tolerance of acetic acid bacterium to 13 %. Yu et al. [10] used continuous ethanol stress adaptation culture succeed in improving the ethanol tolerance of *A. pasteurianus* CGMCC 3089. Atmospheric and room temperature plasma (ARTP) is a novel plasma generating system driven by a radio-frequency (RF) power supply with water-cooled, bare-metallic electrodes which has the advantages of low costs, low plasma temperature, flexible operations, and security and thus shows promising applications in biotechnology [11]. Recently, many researchers used ARTP for their own strain breeding [11–14].

In this paper, the ethanol tolerance of *A. pasteurianus* was obtained by using ARTP generated with helium gas. Specially, we focused on the distinction in the cell membrane permeability between starting strain and mutant strain.

30.2 Materials and Methods

30.2.1 Microorganisms

The acetic acid bacterium strain, *A. pasteurianus* AP-1.01 was used as starting strain.

30.2.2 Culture Medium

The media used in this study were as follows. The compositions of the GY medium were (g/L): glucose 20, yeast extract 10, adding 3 % (v/v) ethanol after sterilization, solid medium with ager power 20 and $CaCO_3$ 10. The composition of $CaCO_3$ selection medium were (g/L): glucose 20, yeast extract 10, $CaCO_3$ 10, agar power 20, adding 11 % (v/v) ethanol after sterilization. The composition of stress medium was the same as GY medium, but the ethanol concentration was 3 % (v/v), 9 % (v/v), 11 % (v/v), 13 % (v/v), respectively. The liquid medium used for shaker screening was GY medium, except the ethanol concentration was 11 % (v/v). The initial pH of the medium mentioned above was adjusted to 6.8.

30.2.3 Culture Conditions

The cells from slant cultures were transferred to 50 mL GY medium in a 250 mL Erlenmeyer flask and shakened with 180 rpm at 30 °C until the optical density (0) of the culture at 600 nm reached 0.8, and then the culture was used as the seed for the following experiment.

5 % (v/v) inoculums were inoculated into the 50 mL medium in a 250 mL Erlenmeyer flask and incubated with shaking at 180 rpm in 30 °C for 96 h. The yield of acetic acid was measured by acid-base titration [2].

30.2.4 Mutation with ARTP

The ARTP mutation breeding system was purchased from Si Qing Yuan Biotechnology Co., Ltd, Beijing, China. It consisted of a plasma generator, a helium gas supply and control subsystem, and a sample plate made of stainless steel which can be moved up and down [11]. The operating parameters of the helium-based ARTP were the following: the helium gas flow rate of Q He = 10.0 L/min and RF power input of 120 W, and the treating time ranged from 0 to 180 s, the treatment distance was 2 mm.

The specific operating steps were according to the methods of Wang [13] with some modifications. The strain *A. pasteurianus* was cultivated at 30 °C and 180 rpm to logarithmic phase (about 24 h). Then 3 mL of culture was moved into sterile tubes and the absorbance of culture was adjusted to $OD_{600} = 0.80 \pm 0.07$ with sterile saline. Then 10 μL of culture was removed and spread on each sterilized steel plate and dried in sterile air for few minutes. This plate was later exposed to the ARTP system's nozzle exit. The working parameters were mentioned above. After mutation, the plate was placed in a new sterile tube containing 1 mL of sterile water, and then the suspension was spread on the GY solid medium. After 48 h of cultivation at 30 °C, colonies that exhibited large transparent zones were selected and then inoculated with sterilized toothpick onto plates of $CaCO_3$ selection medium. After cultivation at 30 °C, colonies that grown fast and exhibited large transparent zones were selected for further shaker screening.

30.2.5 Calculation of Lethality Rate and Shaker Screening

The lethality rate of the bacterial strain was evaluated based on the following equation:

$$\text{Lethality rate } (\%) = \frac{U - T}{U} \times 100$$

where U is the total colony count of the sample without treatment, and T is the total colony count after treatment by the plasma. All the colony numbers were obtained by the CFU (Colony-Forming Units) method on the solid medium.

For shaker screening, the cells isolated from $CaCO_3$ selection medium were transferred to 50 mL GY medium in a 250 mL Erlenmeyer flask at 30 °C and 180 rpm for 24 h, and then with 5 % (v/v) inoculums were inoculated into the 50 mL medium containing 11 % (v/v) ethanol in a 250 mL Erlenmeyer at 30 °C and 180 rpm for 96 h. After cultivation, the acetic acid yield was measured as above. The strain with high acetic acid at high ethanol concentration (11 % (v/v)) was used for further research.

30.2.6 Genetic Stability of the Mutant Strain

The stability of the mutant was evaluated by the serial subcultivation. The mutant strain was incubated on the solid medium with 3 % (v/v) ethanol for 48 h (the first subculture). Then the cell from the plate was incubated on the same medium for further subculture. The cells from the first to sixth subculture were transferred to 50 mL GY medium containing 11 % (v/v) ethanol in a 250 mL Erlenmeyer flask at 30 °C and 180 rpm for 96 h. The yield of acetic acid was measured with the method mentioned above.

30.2.7 Determination of Membrane-Disrupting Activity of Starting Strain and Mutant Strain Under Different Concentration of Ethanol

The membrane-disrupting activity of starting strain and mutant strain was determined by measuring the fluorescence enhancement of PI (Sigma Corp., USA) in different concentration of ethanol-treated cells according to the modified method of Bo et al. [15]. Cells incubated under different ethanol concentration were harvested by centrifugation at 12,000 rpm for 2 min and washed twice with phosphate buffer saline (PBS). Cells were then resuspended in PBS, and the final cell density was adjusted to $OD_{600} = 0.15 - 0.25$. 100 μL of the cell suspension was mixed with 100 μL of PI (initial concentration was 12 μg/mL) and was then incubated at room temperature for 10 min. The fluorescence intensity was measured at excitation and emission wavelengths of 535 and 617 nm, respectively, by a SYNERGY4 multi-functional enzyme mark instrument (Bioteck). Each experiment was conducted in triplicate.

$$\text{Membrane-disrupting activity} = \frac{\text{fluorescence}}{\mathrm{OD}_{600}}$$

30.3 Results and Discussions

30.3.1 Lethality Rate Curve and Choice of Treatment Time

The effect of various plasma treatment times on the lethality rate is shown in Fig. 30.1. There is a clear dose–response relationship between the plasma treatment time and the *A. pasteurianus* lethality rate. As shown in Fig. 30.1, treatment with ARTP for 75 s resulted in a lethality rate of 82.01 %. According to the breeding strategies, we selected treatment time 75, 90, 105 s, so that the lethality rate was from 80 to 90 %. Thus, we could get more positive mutation.

30.3.2 Screening for Ethanol-Tolerant Strains

In this study, more than 90 colonies grown on the $CaCO_3$ selection petri dishes after ARTP treatments were selected randomly based on growth rate and transparent ring diameter. These colonies were further selected based on the production of acetic acid under the high concentration (11 % (v/v)) of ethanol. Part of the screening date was shown in Fig. 30.2. As shown in Fig. 30.2, the production of starting strain was 6.760 g/L, comparing with the starting strain, there are 25 colonies that have higher yield. Among them, we selected 14 colonies for rescreening. The rescreening results were shown in Table 30.1.

As shown in Table 30.1, the production of some colonies decreased comparing with preliminary screening. The instability of production resulted from the instability of mutagenesis. But we could see from Table 30.1, colonies A1-10, A1-9, A2-11, U1-1, 7-26, 7-40 still have high yield. Comparing with starting strain, production was increased by 347.3, 321.8, 289.8, 331.4, 92.67, 216.3 %,

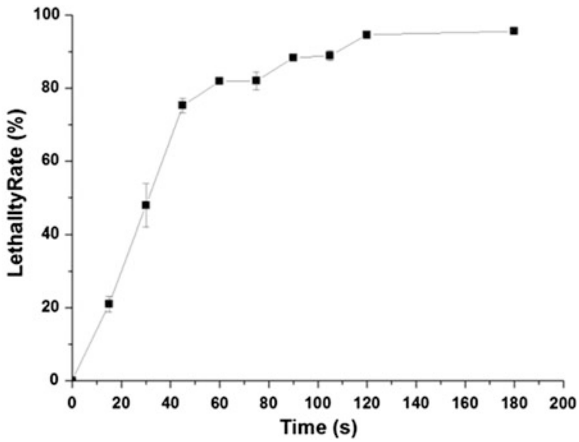

Fig. 30.1 Effect of various plasma treatment times on the lethality rate. Each value is the mean of three replicates ±SD

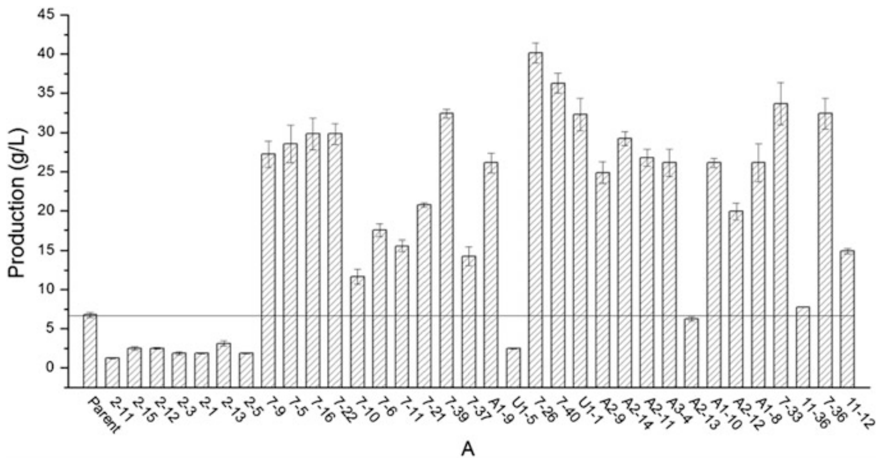

Fig. 30.2 Part of the screening data

Table 30.1 Rescreening results

Strain	Production (g/L)	Improving percentage (%)	Strain number	Production (g/L)	Improving percentage (%)
U1-1	29.16 ± 1.44	331.4	A1-8	14.69 ± 2.70	117.3
A2-11	26.35 ± 1.50	289.8	A2-14	25.92 ± 3.89	283.4
A1-10	30.24 ± 1.50	347.3	A1-9	28.51 ± 1.30	321.8
7-5	3.080 ± 0.71	−54.44	7-33	2.590 ± 0.92	−61.66
7-9	8.600 ± 1.92	27.22	7-39	4.540 ± 0.92	−32.90
7-22	11.66 ± 4.49	72.49	7-40	21.38 ± 0.92	216.3
7-16	7.340 ± 1.50	8.580	7-26	13.02 ± 1.30	92.67

respectively. These six colonies were selected for further screening. The screening result was presented in Table 30.2.

As shown in Table 30.2, the production of A1-10, A1-9, A2-11, 7-26, 7-40 decreased. However, the production of colony U1-1 remained the same compared with former. So U1-1 was selected as the ethanol-tolerant strain.

30.3.3 Stability of the Mutant

Mutant phenotype may occur in delays in the passage, which would lead to recession of production traits of high-yielding strains. So it is necessary to evaluate the stability of the mutant. The genetic stability of U1-1 was confirmed by sub-cultivation. The genetic stability of U1-1 was shown in Table 30.3. As shown in

Table 30.2 The second rescreening results

Strain number	Production (g/L)	Improving percentage (%)	Strain number	Production (g/L)	Improving percentage (%)
A1-10	8.750 ± 0.46	29.41	U1-1	33.70 ± 1.83	398.5
A1-9	10.37 ± 0.37	53.37	7-26	3.890 ± 0	−42.49
A2-11	19.67 ± 3.20	190.8	7-40	4.540 ± 0.92	−32.90

Table 30.3 Genetic stability results

Passage number	Production (g/L)	Improving percentage (%)
The first generation	31.10 ± 1.30	360.1
The second generation	33.26 ± 1.98	392.0
The third generation	32.83 ± 0.75	385.7
The fourth generation	30.67 ± 1.50	353.7
The firth generation	29.81 ± 1.30	341.0
The sixth generation	32.24 ± 1.41	376.9

Table 30.3, the first to sixth generation, the production was 31.10 ± 1.30, 33.26 ± 1.98, 32.83 ± 0.75, 30.67 ± 1.50, 29.81 ± 1.30, 32.24 ± 1.41 g/L, respectively. It was shown that U1-1 has stable property and could be used for the following study.

30.3.4 Membrane-Disrupting Activity of Starting Strain and Mutant Strain Under Different Concentration of Ethanol

The membrane-permeabilizing activity was investigated by using the PI assay (Fig. 30.3). It was based on the principle that the PI enters only membrane-compromised cells, after which the fluorescence of this probe is enhanced by 20–30-fold due to its binding to nucleic acids. A significant increase in fluorescence intensity was observed in the ethanol-treated groups. The fluorescence intensity increased significantly as the ethanol concentration gradually added, simultaneously the fluorescence intensity increased as the treatment time extended.

The membrane-permeabilizing activity of starting strain and mutant strain were compared under different concentration of ethanol. As shown in Fig. 30.4, no matter what the ethanol concentration is, the membrane-permeabilizing activity of starting strain is significantly higher than the mutant strain. Shafiei et al. [16] found ethanol and acetic acid could affect the cell envelope integrity of *Acetobacter senegalensis* by fluorescence staining. Therefore, the ethanol tolerance of U1-1 may be partly

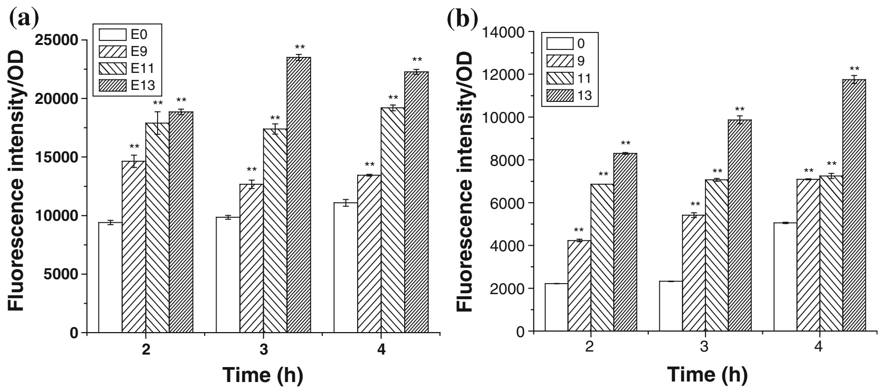

Fig. 30.3 Membrane-disrupting activity as determined in the PI assay. **a** Starting strain; **b** mutant strain. Each value is the mean of three replicates ±SD. The *asterisk* (∗) indicates significant difference from equivalent control point (t test, $P < 0.05$)

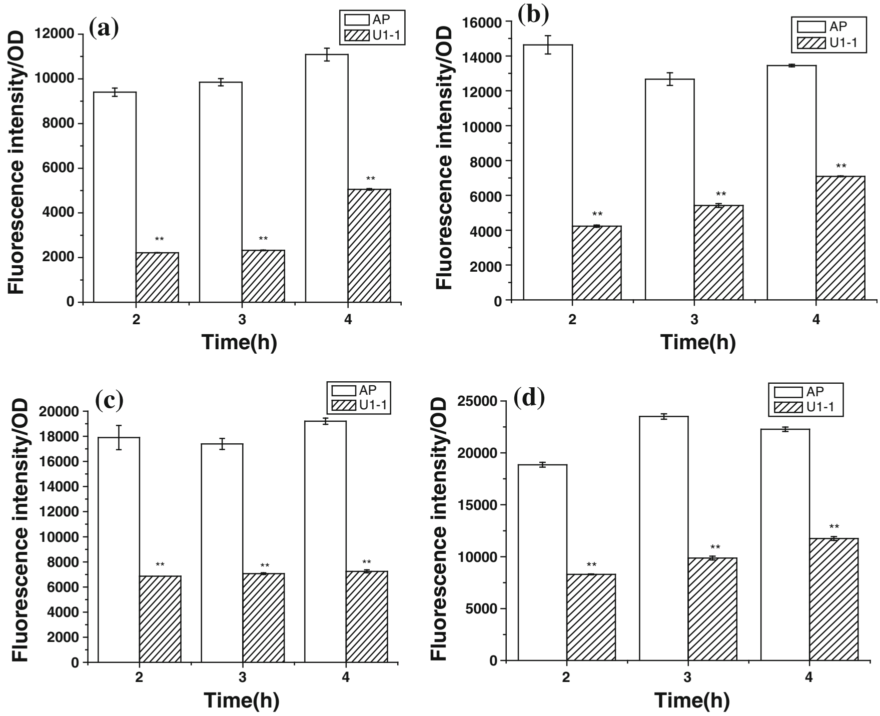

Fig. 30.4 Membrane-disrupting activity difference between starting strain and mutant strain under different concentration of ethanol. **a** Without addition of ethanol; **b** addition of 9 % (v/v) ethanol; **c** addition of 11 % (v/v) ethanol; **d** addition of 13 % (v/v) ethanol. Each value is the mean of three replicates ±SD. The *asterisk* (∗) indicates significant difference from equivalent control point (t test, $P < 0.05$)

because of the change of membrane-permeabilizing activity, so that high concentration of ethanol will not make membrane permeability increased, leading to cell death.

30.4 Conclusion

The present study has revealed that the helium-based ARTP altered certain biochemical characteristics of *A. pasteurianus* parent type strain. As a result, a mutant strain named U1-1 with ethanol tolerance and high yield was isolated due to mutagenesis. The yield of acetic acid reached 32.83 ± 0.75 g/L, 385.7 % higher than that of the starting strain. Furthermore, the membrane permeability of mutant strain is less than the starting strain by PI assay, which may be the reason why U1-1 has ethanol tolerance. In order to confirm this inference more research is needed, for instance, lipidomics and metabonomics.

Acknowledgments This research is supported by the National High Technology Research and Development Program ("863"Program) of China (2012AA022108).

References

1. Qi Z, Wang W, Yang H, Xia X, Yu X (2014) Mutation of *Acetobacter pasteurianus* by UV irradiation under acidic stress for high-acidity vinegar fermentation. Int J Food Sci Tech 49 (2):468–476
2. Matsutani M, Nishikura M, Saichana N, Hatano T, Masud-Tippayasak U, Theergool G et al (2013) Adaptive mutation of *Acetobacter pasteurianus* SKU1108 enhances acetic acid fermentation ability at high temperature. J Biotechnol 165(2):109–119
3. Kanchanarach W, Theeragool G, Yakushi T, Toyama H, Adachi O, Matsushita K (2010) Characterization of thermotolerant *Acetobacter pasteurianus* strains and their quinoprotein alcohol dehydrogenases. Appl Microbiol Biotechnol 85(3):741–751
4. Perumpuli PA, Watanabe T, Toyama H (2014) Pellicle of thermotolerant *Acetobacter pasteurianus* strains: characterization of the polysaccharides and of the induction patterns. J Biosci Bioeng 118(2):134–138
5. Nakano S, Fukaya M, Horinouchi S (2006) Putative ABC transporter responsible for acetic acid resistance in *Acetobacter aceti*. Appl Environ Microbiol 72(1):497–505
6. Salgueiro SP, Sa-Correia I, Novais JM (1988) Ethanol-induced leakage in *Saccharomyces cerevisiae*: kinetics and relationship to yeast ethanol tolerance and alcohol fermentation productivity. Appl Environ Microbiol 54(4):903–909
7. Sreenivasulu Y, Amritphale D (1999) Membrane fluidity changes during ethanol-induced transition from dormancy to germination in cucumber seeds. J Plant Physiol 155(2):159–164
8. Aguilera F, Peinado RA, Millan C, Ortega JM, Mauricio JC (2006) Relationship between ethanol tolerance, H+-ATPase activity and the lipid composition of the plasma membrane in different wine yeast strains. Int J Food Microbiol 110(1):34–42
9. Wei K, Cao X, Li X, Wang C, Hou L (2012) Genome shuffling to improve fermentation properties of acetic acid bacterium by the improvement of ethanol tolerance. Int J Food Sci Tech 47(10):2184–2189

10. Yu Z, Qi H, Keping Z, Min W (2012) Characterization of *Acetobacter pasteurianus* CGMCC 3089 during evolutionary adaptation to ethanol. http://www.papereducn
11. Qiang W, Ling-Ran F, Luo W, Han-Guang L, Lin W, Ya Z et al (2014) Mutation breeding of lycopene-producing strain *Blakeslea Trispora* by a novel atmospheric and room temperature plasma (ARTP). Appl Biochem Biotechnol 174:452–460
12. Lu Y, Wang L, Ma K, Li G, Zhang C, Zhao H et al (2011) Characteristics of hydrogen production of an *Enterobacter aerogenes* mutant generated by a new atmospheric and room temperature plasma (ARTP). Biochem Eng J 55(1):17–22
13. Wang X, Lu M, Wang S, Fang Y, Wang D, Ren W et al (2014) The atmospheric and room-temperature plasma (ARTP) method on the dextranase activity and structure. Int J Biol Macromol 70:284–291
14. Bao H, Liu R, Liang L, Jiang Y, Jiang M, Ma J et al (2014) Succinic acid production from hemicellulose hydrolysate by an *Escherichia coli* mutant obtained by atmospheric and room temperature plasma and adaptive evolution. Enzyme Microb Tech 66:10–15
15. Bo T, Liu M, Zhong C, Zhang Q, Su QZ, Tan ZL et al (2014) Metabolomic analysis of antimicrobial mechanisms of epsilon-Poly-l-lysine on *Saccharomyces cerevisiae*. J Agric Food Chem 62(19):4454–4465
16. Shafiei R, Delvigne F, Babanezhad M, Thonart P (2013) Evaluation of viability and growth of *Acetobacter senegalensis* under different stress conditions. Int J Food Microbiol 163(2–3):204–213

Chapter 31
A Thermotolerant *Acetobacter pasteurianus* T24 Achieving Acetic Acid Fermentation at High Temperature in Self-Adaption Experiment

Yuqiao Wei, Xiaoying Wu, Zeming Xu, Zhilei Tan and Shiru Jia

Abstract The aim of the present work was to improve the thermotolerance of acetic acid bacteria. In this study, a thermotolerant *Acetobacter pasteurianus* T24 was obtained through adaptive experiments. The strain T24 exhibited better growth at 40 °C in solid medium. The strain T24 exhibited rapid growth and the wild stain HN101 exhibited a longer lag phase at 40 °C in acetic acid fermentation than strain T24. Under the condition of low ethanol concentration, the highest acetic acid concentration produced by T24 at 40 °C increased by 18.05 % over the wild stain HN101. These results indicated that the adapted strain had acquired thermotolerance over the course of adaptation. Thus, this strain was used for acetic acid fermentation at high temperature. This work reveals the potential value for improvement in industrial vinegar production.

Keywords *Acetobacter pasteurianus* · Thermotolerance · Acetic acid fermentation

31.1 Introduction

Acetic acid bacteria (AAB) comprise a group of gram-negative or gram-variable, ellipsoidal to rod-shaped cells that have an obligate aerobic metabolism with oxygen as the terminal electron acceptor. In the first classification of AAB, two main genera were determined as *Acetobacter* and *Gluconobacter*, but nowadays 12 genera are recognized and accommodated to the family *Acetobacteraceae*, the *Alphaproteobacteria*: *Acetobacter*, *Gluconobacter*, *Acidomonas*, *Gluconacetobacter*, *Asaia*, *Kozakia*, *Swaminathania*, *Saccharibacter*, Neoasaia, *Granulibacter*,

Y. Wei · X. Wu · Z. Xu · Z. Tan · S. Jia (✉)
Key Lab of Industrial Fermentation Microbiology of the Ministry of Education,
College of Biotechnology, Tianjin University of Science and Technology,
Tianjin 300457, The People's Republic of China
e-mail: jiashiru@tust.edu.cn

T.-C. Zhang and M. Nakajima (eds.), *Advances in Applied Biotechnology*,
Lecture Notes in Electrical Engineering 333, DOI 10.1007/978-3-662-46318-5_31

Tanticharoenia, and *Ameyamaea* [1]. Isolation, purification, identification, and preservation of AAB are very difficult. Since *Acetobacter* prefers to oxidize ethanol more strongly than glucose and *Gluconobacter* prefers glucose more than ethanol, most strains useful in vinegar manufacture belong to *Acetobacter* [2]. *Acetobacter pasteurianus* is a typical example for acetic acid fermentation.

AAB during acetic acid fermentation expose the acetic acid bacteria to various stresses such as high temperature, ethanol, and acetic acid. Temperature is one of the most important environmental factors affecting growth and survival of microbes [3]. Although temperature plays an important role in the fermentation process, large-scale industrial fermentation could not be carried out in strict temperature control. In recent years, temperature in summer has gradually been increasing in many countries. Almost all domestic vinegar manufacturers can produce vinegar for only half a year. Furthermore, the fact that fermentation temperature was improved can reduce cooling costs. Therefore, more thermotolerant microbes will be required to achieve stable fermentation.

Some researches attempted to achieve this goal. Ndoye et al. [4] have isolated a thermotolerant acetic acid bacterium from mango fruit. This strain can survive at 40 °C. Lu et al. [2] have obtained a thermotolerant and high acetic acid producing bacterium *Acetobacter* sp. I14-2. This bacterium is thermotolerant and retained 97 and 68 % of acetic acid producing activity after 3d incubation at 35 and 37 °C, respectively, compared with that when incubated at 30 °C. Akiko et al. [5–7] researched two groups of chaperones GroES/GroEL and dnaK/dnaJ of AAB. After the modification of molecular tools, the strains of two groups of chaperones overexpressed can survive at 42 °C.

In this study, a thermotolerant *A. pasteurianus* T24 was obtained through adaptive experiments. Comparison of growth and acetic acid production between *A. pasteurianus* HN101 and *A. pasteurianus* T24 at high temperature was researched. As a result, *A. pasteurianus* T24 enhanced acetic acid production at 40 °C.

31.2 Materials and Methods

31.2.1 Bacterial Strains

A wild strain *A. pasteurianus* HN101 and a thermotolerant strain *A. pasteurianus* T24 were used in this study. *A. pasteurianus* HN101 was used for a comparison of thermotolerance with this adapted strain.

31.2.2 Culture Media

Two different media were used in this study: GYC solid medium (2 % glucose, 1 % yeast extract, 1 % $CaCO_3$, 3 % ethanol and 2 % agar, pH 6.8) and GY liquid medium (2 % glucose, 1 % yeast extract and 3 % ethanol, pH 6.8). All the chemicals used in this study were purchased from No. 1 Chemical Reagent Factory, Tianjin, China.

31.2.3 Culture Conditions

Shaking-flask fermentation for vinegar production was performed in 250-mL Erlenmeyer flasks. For the preculture, *A. pasteurianus* HN101 was inoculated into the Erlenmeyer flask containing 50 mL GY medium and cultured at 30 °C, 180 rpm for about 24 h, until the OD_{600} reached 0.6–0.8. For the main culture, 2.5 mL seeds were mixed with 47.5 mL fresh GY medium and grown at 180 rpm at different temperatures (30 and 40 °C) for 96 h.

For plate assay, each strain was cultured in GY medium at 30 °C, 180 rpm for 24 h, and then diluted with sterilized 0.9 % NaCl solution (10^{-1}, 10^{-2}, 10^{-3}, 10^{-4} and 10^{-5}). The diluted solutions (5 μL) were spotted onto GYC agar plates. The plates were cultured in an incubator at various temperatures (30 and 40 °C).

31.2.4 Biomass Estimation

Bacterial growth was measured using a spectrophotometer by absorbance maxima (600 nm). Acetic acid concentrations of culture medium at several growth phases were measured by alkali titration with 0.1 M NaOH using 1 % phenolphthalein as a pH indicator.

31.3 Results and Discussions

31.3.1 A Thermotolerant Strain Adaptation to High Temperature

The thermal adaptation was carried out in an unconventional way (Fig. 31.1): one involved repeating the cultivation under fermentation conditions at 40 °C. The cultivation was repeated 12 times. Then, the culture broth was diluted to 10^{-1}, 10^{-2}, 10^{-3}, 10^{-4}, and 10^{-5} using sterilized 0.9 % NaCl solution. The diluted solutions (100 μL) were spread onto GYC agar plates. The plates were cultured in an incubator at 40 °C for 60 h. At last, all single colonies were spotted onto GYC agar plates in the same conditions. As a result, a thermotolerant *A. pasteurianus* T24 was screened (Fig. 31.2). As shown in the Fig. 31.2, the strain T24 exhibited rapid acetic acid fermentation ability under the same cultivation time. Thus, this strain was used

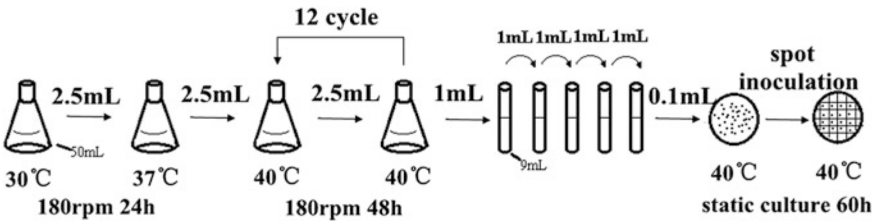

Fig. 31.1 Scheme for self-adaption treatment to high temperature

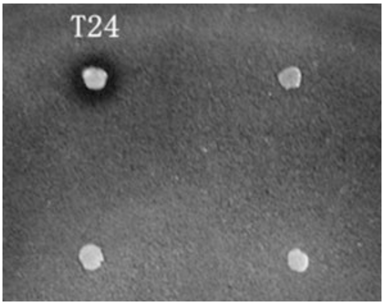

Fig. 31.2 The thermotolerant *A. pasteurianus* T24 has been screened in GYC medium at 40 °C. The clear zone surrounding bacterial colony indicated a hydrolysis of $CaCO_3$ to H_2CO_3 by acetic acid, which is a product obtained from ethanol oxidation

for acetic acid fermentation at high temperature. Yoshinao et al. [8] and Illeghems et al. [9] revealed genetic instability of *A. pasteurianus* through whole-genome analyses. To obtain a thermotolerant stain, this method is available. Qi et al. [10] also used self-adaption under acidic stress to obtain a mutant with higher vinegar production.

31.3.2 Functional Characterization of a Thermoadapted Strain

To confirm the thermotolerance of the mutant, growth comparisons were carried out on a GYC plate (Fig. 31.3). The growth of the strain T24 was not significantly different from wild-type strain HN101 at 30 °C, while the strain T24 exhibited better growth at 40 °C. These results indicate that the strain T24 had acquired thermotolerance over the course of adaptation. Under the same dilution ratio, it is reliable to prove the thermotolerance of the mutant. Hiromi et al. [11] also used this method to confirm the thermotolerance of *Gluconobacter frateurii* CHM43.

To examine the difference in fermentation ability between the wild and adapted strains, the growth was compared in a flask shaking culture with GY medium until

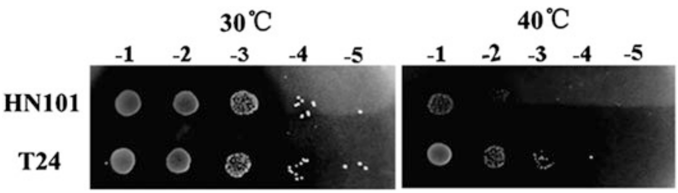

Fig. 31.3 Growth comparison of *A. pasteurianus* HN101 and *A. pasteurianus* T24 strains at 30 and 40 °C

acetic acid was accumulated (Fig. 31.4). As shown in the Fig. 31.4, the growth and acetic acid concentration of the strain T24 were not significantly different from the wild-type strain HN101 at 30 °C. In the acetic acid fermentation, AAB exhibit three growth phases: first growth proceeds by completely oxidizing ethanol to acetic acid (ethanol oxidation phase), then growth stops after consuming the ethanol as the respiratory substrate and the viable cell number gradually decreases in this stationary phase (acetic acid resistance phase). When the viable cell number decreases to some threshold, cell growth starts again by utilizing acetic acid accumulated (acetate overoxidation phase). In the ethanol oxidation phase, cells oxidize ethanol

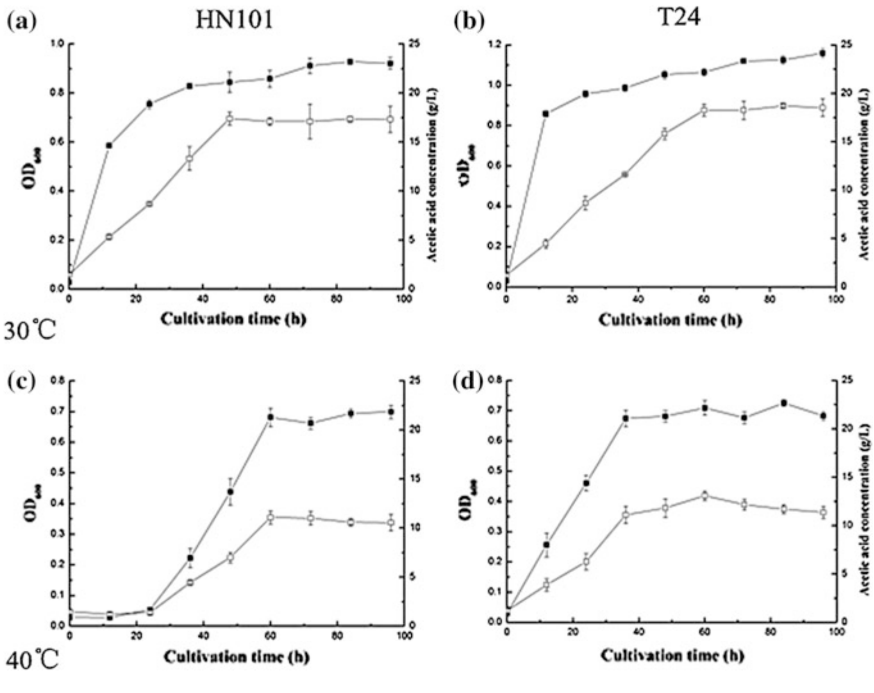

Fig. 31.4 Comparison of growth (■) and acetic acid production (□) between *A. pasteurianus* HN101 and *A. pasteurianus* T24 in flask-shaking cultures at 30 °C (**a**, **b**) and 40 °C (**c**, **d**)

to acetic acid via acetaldehyde, which is carried out by two sequential reactions with membrane-bound alcohol and aldehyde dehydrogenases linked to the respiratory chain [12]. In the acetic acid resistance phase, the cells resist against acetic acid produced themselves by several mechanisms without assimilating the acetic acid, but finally the cells start to assimilate the acetate by oxidizing it to CO_2 via TCA cycle, of which the phase is called as "overoxidation phase" because of this phenomenon is nuisance for acetic acid fermentation [13, 14]. Thus, it was presumed that the substrate ethanol addition influenced the growth and acetic acid production. The next step was to examine the influence of ethanol addition change.

However, the strain T24 exhibited rapid growth and the wild stain exhibited a long lag phase at 40 °C. Besides, the strain T24 achieved the highest acetic acid production at 60 h. The highest acetic acid concentration produced by two strains at 40 °C was 11.08 g/L (HN101, 60 h) and 13.08 g/L (T24, 60 h), respectively. It has been shown that some acetic acid bacteria grew well at 37 °C, but exhibited largely delayed fermentation at 39 °C [15]. The results match with the previous study. The strain T24 will proceed in higher temperature and is suitable for industrial vinegar production without strict temperature control.

31.4 Conclusions

The thermotolerant *A. pasteurianus* T24 was obtained through self-adaption at high temperature. This method is available. The strain T24 exhibited better growth at 40 °C in GYC medium. The strain T24 exhibited rapid growth and the wild stain HN101 exhibited a longer lag phase at 40 °C in acetic acid fermentation than strain T24. The strain T24 had acquired thermotolerance over the course of adaptation. Under the condition of low ethanol concentration, the highest acetic acid concentration produced by T24 at 40 °C increased by 18.05 % over the wild stain HN101. Certainly, further studies on culture conditions and thermotolerant mechanisms of the adapted strain will be taken into consideration in future work.

Acknowledgments This research is supported by the National High Technology Research and Development Program ("863"Program) of China (2012AA022108).

References

1. Ilkin YS, Seniz K (2011) Importance of acetic acid bacteria in food industry. Food Control 22:647–656
2. Lu SF et al (1999) A thermotolerant and high acetic acid-producing bacterium *Acetobacter* sp. I14-2. J App Microbiol 86(1):55–62
3. Minenosuke M et al (2013) Adaptive mutation of *Acetobacter pasteurianus* SKU1108 enhances acetic acid fermentation ability at high temperature. J Biotechnol 165(2):109–119

4. Ndoye B et al (2007) *Acetobacter senegalensis* sp. nov., a thermotolerant aceticacid bacterium isolated in Senegal (sub-Saharan Africa) from mango fruit (Mangifera indica L.). Int J Syst Evol Microbiol 57(7):1576–1581
5. Akiko OK et al (2002) Cloning and Characterization of groESL Operon in *Acetobacter aceti*. J Biosci Bioeng 94(2):140–147
6. Okamoto-Kainuma A et al (2004) Cloning and characterization of the dnaKJ operon in *Acetobacter aceti*. J Biosci Bioeng 97(5):339–342
7. Ishikawa M et al (2010) Cloning and characterization of grpE in *Acetobacter pasteurianus* NBRC 3283. J Biosci Bioeng 109(1):25–31
8. Yoshinao A et al (2009) Whole-genome analyses reveal genetic instability of *Acetobacter pasteurianus*. Nucleic Acids Res 37(17):5768–5783
9. Illeghems K et al (2013) Complete genome sequence and comparative analysis of *Acetobacter pasteurianus* 386B, a strain well-adapted to the cocoa bean fermentation ecosystem. BMC Genom 14:526
10. Qi ZL et al (2014) Mutation of *Acetobacter pasteurianus* by UV irradiation under acidic stress for high-acidity vinegar fermentation. Int J Food Sci Tech 49:468–476
11. Hiromi H et al (2012) High-temperature sorbose fermentation with thermotolerant *Gluconobacter frateurii* CHM43 and its mutant strain adapted to higher temperature. Appl Microbiol Biotechnol 95:1531–1540
12. Matsushita K et al (1994) Respiratory chain and bioenergetics of acetic acid bacteria. Adv Microb Physiol 36:247–301
13. Matsushita, K et al (2005) Acetic acid production in acetic acid bacteria leading to their 'death' and survival. Survival and Death in Bacteria, Research Signpost, Kerala, pp 169–181
14. Kanchanarach W et al (2010) Acetic acid fermentation of *Acetobacter pasteurianus*: relationship between acetic acid resistance and pellicle polysaccharide formation. Biosci Biotech Biochem 74:1591–1597
15. Saeki A et al (1997) Development of thermotolerant acetic acid bacteria useful for vinegar fermentation at higher temperatures. Biosci Biotech Biochem 61:138–145

Chapter 32
Optimization of Cultural Conditions for Extracellular Polymeric Substances (EPS) Production by *Burkholderia* Using Response Surface Methodology

Baojiang Sun, Peipei Han, Ruyu Tao, Qixiu Pang and Shiru Jia

Abstract Extracellular polymeric substances (EPS) are complex biopolymers secreted by a variety of microorganisms. Except for the basic protecting cells from rigorous environment, EPS also influenced the bioflocculation and settleability of sludge. There were reports about the application of EPS in minimizing harbor siltation. On the basis of this point, a series of experiment were proceeded. Based on single factor experiment, the cultural conditions for EPS production were investigated and optimized by response surface methodology (RSM) at the Box–Behnken design. Optimal EPS yield (6.40 g/L) was obtained at a combination of sucrose 21.0 g/L, NH_4Cl 1.1 g/L, $MgSO_4$ 0.2 g/L. And the influence of NH_4Cl for EPS yield was the most significant, as the rest in order was sucrose and $MgSO_4$. A verification experiment confirmed the reliability of the model.

Keywords Optimization · Extracellular Polymeric substances (EPS) · Response surface methodology (RSM)

32.1 Introduction

Extracellular polymeric substances (EPS), a complex high molecular weight mixture of biopolymers, are secreted by a variety of microorganisms during their growth to protect the cells from severe environment, and have been found widely

B. Sun · P. Han · R. Tao · S. Jia (✉)
Key Laboratory of Fermentation Microbiology, Ministry of Education,
College of Biotechnology, Tianjin University of Science and Technology,
Tianjin 300457, People's Republic of China
e-mail: jiashiru@tust.edu.cn

Q. Pang
Tianjin Research Institute of Water Transport Engineering, Key Laboratory of Engineering Sediment of Ministry of Transport, Tianjin, People's Republic of China

T.-C. Zhang and M. Nakajima (eds.), *Advances in Applied Biotechnology*,
Lecture Notes in Electrical Engineering 333, DOI 10.1007/978-3-662-46318-5_32

present in pure cultures, activated sludge, granular sludge, and biofilms [1–3]. EPS are composed of a series of organic materials [4], carbohydrate and protein were the primary constituents in many EPS of activated sludge [5] and pure cultures [6], with nucleic acids, lipids [7] and other polymers being present in lower concentration. EPS have been reported with a significant influence on the physicochemical properties of microbial aggregates and activated sludge, such as the structure, floc size, surface charge, bioflocculation, and settleability [8, 9]. Recently, a new point was brought up that the application of EPS in minimizing harbor siltation [10]. Briefly, EPS secreted by microorganisms from the harbor could interact with the mud. As a result, some characters of the mud changed, sequentially the settleability of the mud was changed. In order to verify whether the EPS produced by isolated microorganism had reduced the settling velocity and finally delayed the settling, and furthermore to find out the mechanism of EPS delaying the settling, amounts of EPS would be needed. In consideration of the truth that there was little available medium and cultural conditions for the new isolated microorganism to produce EPS, it was necessary to find a suitable medium and optimize the cultural conditions for EPS production.

Statistical experimental design methods provide a systematic and efficient means of reaching particular goals and simultaneously studying several control factors [11]. Hence, these methods can be used to examine and optimize the operational variables. Response surface methodology (RSM) was one of applied experimental design frequently. And RSM had been used in broad fields, to optimize the growth and proteolytic activity [12] and production of xanthan gum [13], all acquiring a good job.

In the present study, optimization of EPS production in batch experiments was attempted through RSM, where the effects of three variables (sucrose, NH_4Cl, $MgSO_4$) were investigated.

32.2 Materials and Methods

32.2.1 Bacterial Strain and Cultural Conditions

Burkholderia, used throughout the present study, was previously screened from the mud, Port of Lianyungang China. The organism was grown on seed culture medium [14] at 28 °C for 24 h in 160 r/min, then inoculated to fermentation culture at the inoculum size of 10 %, incubated for 3 days at 28 °C in 160 r/min. The biomass was represented by determining the absorbance of culture at 600 nm.

The seed culture medium (pH 7.2) contained: 5 g/L Glucose, 10 g/L Peptone, 3 g/L Beef extract, 2 g/L $MgSO_4{\cdot}7H_20$.

The composition of basic fermentation medium [15] utilized for the EPS production was as follows: 25 g/L glucose, 1 g/L NH_4Cl, 0.2 g/L $MgSO_4{\cdot}7H_2O$, 2 g/L Na_2HPO_4, 1 g/L KH_2PO_4, and 1.5 g/L $CaCO_3$. The initial pH of media was adjusted to 7.0.

32.2.2 EPS Harvesting

After incubation (3 days), the medium was centrifuged at 4,000 r/min for 15 min after diluted with distilled water to separate the supernatant and cell pellet. The EPS in the supernatant was precipitated with 3 volumes of prechilled ethanol, and further separated by centrifugation. Subsequently, the quantity of EPS was expressed by dry weight [16].

32.2.3 Optimization of Cultural Conditions for EPS Production

32.2.3.1 The Single Factor Experiment

On the basis of basic fermentation medium, carbon source (glucose, sucrose, maltose, lactose), nitrogen source (NH_4Cl, $(NH_4)_2SO_4$, peptone, yeast extract) and $MgSO_4$ on EPS production were determined to acquire the optimum carbon source, nitrogen source and their respective central point concentration. Magnesium used as the activator of lots of enzymes for metabolism in organism was crucial for the synthesis of various products and was the necessary microelement. As a result, $MgSO_4$ was chosen as the mineral salt to optimize for EPS production.

32.2.3.2 Response Surface Methodology Design

Based on above experiments, the variables used for further optimization studies by RSM were sucrose, NH_4Cl, $MgSO_4$, each at three-code levels (−1, 0, 1), as shown in Table 32.1. Design-Expert 8.0 was used to analyze the data of RSM, the treatment schedule for the model is given in Table 32.2.

RSM is an empirical statistical modeling technique employed for multiple regression analysis using quantitative data obtained from properly designed experiments [17]. Box–Behnken statistical design is one type of RSM design that is an independent quadratic design having the treatment combinations at the midpoints of the edges of the process space and at the center [18].

Table 32.1 Factors and levels of Box–Behnken design

Levels	Factors		
	Sucrose	NH_4Cl	$MgSO_4$
	A (g/L)	B (g/L)	C (g/L)
−1	15	1.0	0.15
0	20	1.2	0.20
1	25	1.4	0.25

Table 32.2 Box–Behnken design arrangement and the experimental data

Runs	Sucrose (g/L)	NH_4Cl (g/L)	$MgSO_4$ (g/L)	EPS yield (g/L)
1	0	0	0	6.45
2	0	0	0	5.96
3	0	0	1	5.53
4	−1	−1	0	4.44
5	1	1	−1	5.02
6	−1	1	0	2.44
7	0	0	0	5.76
8	0	0	0	5.42
9	−1	0	1	3.41
10	−1	0	−1	2.93
11	1	0	1	4.55
12	1	−1	0	4.85
13	0	1	−1	2.02
14	0	0	0	6.35
15	0	1	1	2.98
16	0	−1	−1	5.78
17	1	1	0	3.28

32.2.4 Statistical Analysis

All experiments were carried out in triplicate and results represent mean standard ± error.

32.3 Results and Discussions

32.3.1 Single-Factor Experiment

Results of optimal carbon source and nitrogen source were shown in Fig. 32.1. EPS production was not detected while maltose and lactose were used as carbon source, respectively. The same result could be seen while $(NH_4)_2SO_4$, peptone, yeast extract were chosen for nitrogen source, but the biomass was high in each condition indicating that these nitrogen sources just promoted the growth of organisms, not the production of EPS. Some conclusions could be drawn that sucrose and NH_4Cl were the suitable carbon and nitrogen sources, respectively, and the optimal concentration was 20 g/L sucrose, 1.2 g/L NH_4Cl and 0.2 g/L $MgSO_4$ (Fig. 32.1b, d, e).

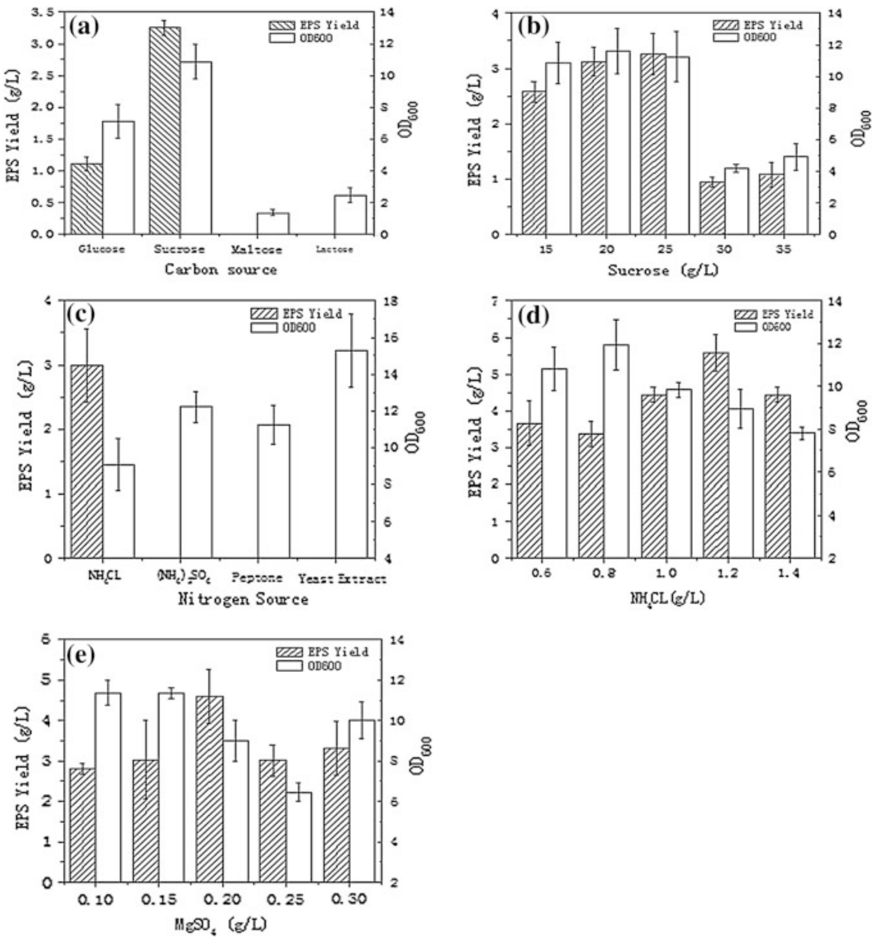

Fig. 32.1 Effect of carbon source, nitrogen source, and $MgSO_4$ for EPS production

32.3.2 Response Surface Methodology Design

The actual yield of EPS (response) obtained was listed in Table 32.2. A second-order polynomial model was fitted for the production of EPS (*Y*), given an equation as follows:

$$
\begin{aligned}
Y = {} & 5.99 + 0.56A - 1.24B + 0.090C + 0.11AB - 0.24AC + 0.29BC \\
& - 1.17A^2 - 1.07B^2 - 0.84C^2
\end{aligned}
$$

The quadratic terms A^2, B^2, C^2 of that model were significant, and the *F*-value was 10.74. All these could be shown obviously in Table 32.3. The significant level *p* of the model was less than 0.005 which indicated that the model was significant.

Table 32.3 Variance analysis of regression model

Source	Sum of squares	DF	Mean square	F-Value	Prob > F	Significance
A	2.51	1	2.51	7.95	0.0258	*
B	12.20	1	12.20	38.65	0.0004	*
C	0.065	1	0.065	0.21	0.6642	
AB	0.046	1	0.046	0.15	0.7133	
AC	0.23	1	0.23	0.71	0.4258	
BC	0.34	1	0.34	1.16	0.3173	
A^2	5.74	1	5.74	18.19	0.0037	*
B^2	4.80	1	4.80	15.21	0.0059	*
C^2	2.99	1	2.99	9.47	0.0179	*
Model	30.50	9	3.39	10.74	0.0025	*
Residual	2.21	7	0.32			
Lack of fit	1.49	3	0.50	2.76	0.1760	
Pure error	0.72	4	0.18			
Total	32.71	16				

In general, the lack of fit represent the conditions that regression model failed to describe experimental point which was out of the regression scope. In this study, lack of fit was not significant, indicating that the equation was well fitting the experiment.

The response surface slope and contour graphically reflected the interaction between various factors. The gentle and steepness of the response surface directly showed the response sensitivity level, for example, the response was slow when the slope was gentle [19]. The point on the corners and center of the contour represented the experimental point, and the contour of ellipse demonstrated the interaction between two factors was significant. Figure 32.2 showed the NH_4Cl has a more negative influence for EPS production than sucrose and $MgSO_4$, inferring that it needs a high ratio between carbon and nitrogen source to produce EPS. When the concentration of sucrose approximately ranged from 19 to 23 g/L (Fig. 32.2b, d), effects of NH_4Cl and $MgSO_4$ for EPS yield was low. The significant level p of C, AB, AC, BC was more than 0.05, which indicate that $MgSO_4$ was not the important factor for EPS production, and there were little interaction between the factors. It may be explained that the magnesium was the microelement which the cells needed. The range of $MgSO_4$ concentration of experiment designed was sufficient for EPS production and the concentration of $MgSO_4$ did not inhibit the EPS production. It could be summarized that the optimum range of sucrose and NH_4Cl were around 20 and 1.1 g/L, respectively, and the influence of $MgSO_4$ would be very low when the other two were in optimum range. In addition, NH_4Cl and sucrose were two significant factors for EPS production, according to Table 32.3.

The optimum levels of the variables were analyzed by Box–Behnken design using the function of “Numerical” in the Design Expert (8.0). The predicted concentration of each factors were sucrose 21.10 g/L, NH_4Cl 1.08 g/L, $MgSO_4$ 0.2 g/L,

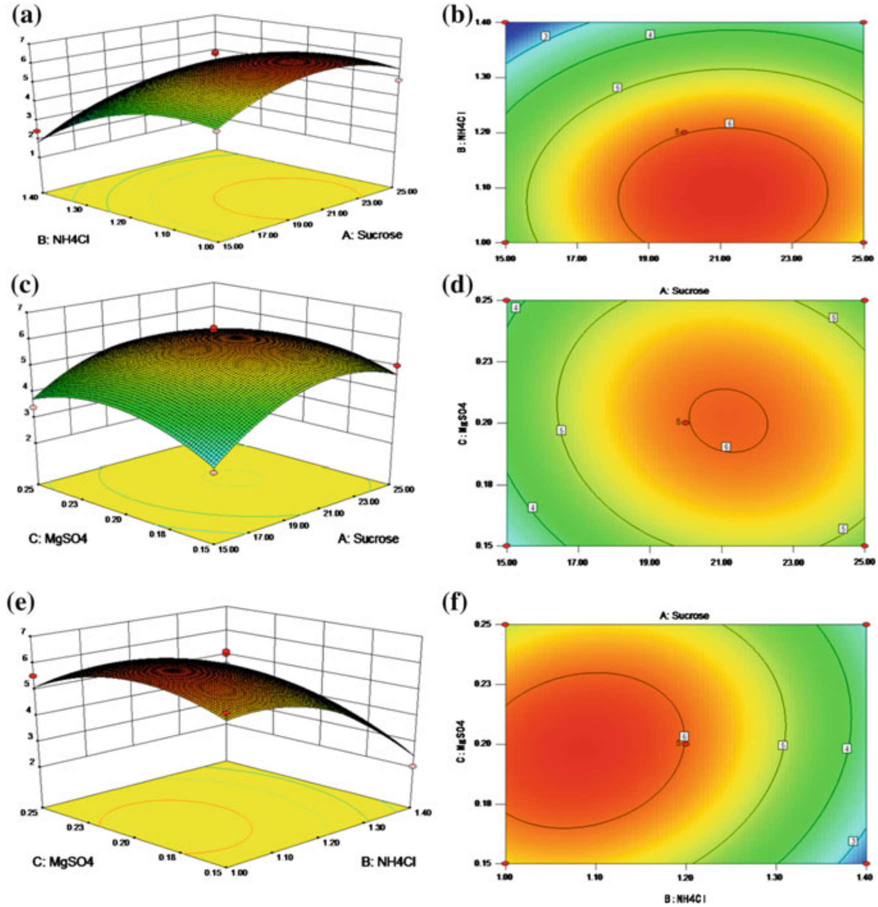

Fig. 32.2 Response surface plots and contour plots

giving a highest EPS yield of 6.40 g/L. A verification experiment was carried out to confirm the reliability of the model under optimal conditions. Maximum EPS yield was 6.26 ± 0.15 g/L, closely agree with the predicted value. To make the actual operation easier, the cultural condition was amended to the condition that were sucrose 21.0 g/L, NH_4Cl 1.1 g/L, $MgSO_4$ 0.2 g/L. The final EPS yield of optimization process increased obviously compared to the initial cultural condition.

32.4 Conclusions

This paper presented a study of optimizing the cultural conditions associated with EPS production by RSM. Results of regression analysis indicated that the influence of NH_4Cl for EPS yield was the most significant, as the rest in order was sucrose and $MgSO_4$. The interaction between any two variables was not significant. The results predicted by Box–Behnken design in RSM analysis showed that a combination of sucrose 21.0 g/L, NH_4Cl 1.1 g/L, $MgSO_4$ 0.2 g/L, gave rise to the maximum EPS yield. Furthermore, this study laid a good foundation for the subsequent mechanism research of reducing the settling velocity of mud by EPS, as well as the study of characteristic of EPS.

Acknowledgments The authors are very grateful for financial support from National Natural Science Foundation of China (Grant No. 31201405) and Central-level Nonprofit Research Institutes Fundamental Research Funds (TKS120101).

References

1. Sheng GP, Yu HQ, Li XY (2010) Extracellular polymeric substances (EPS) of microbial aggregates in biological wastewater treatment systems: a review. Biotechnol Adv 28(6):882–894
2. Ras M, Lefebvre D, Derlon N et al (2011) Extracellular Polymeric Substances diversity of biofilms grown under contrasted environmental conditions. Water Res 45(4):1529–1538
3. Badireddy AR, Chellam S, Gassman PL et al (2010) Role of extracellular polymeric substances in bioflocculation of activated sludge microorganisms under glucose-controlled conditions. Water Res 44(15):4505–4516
4. Frolund BPR, Keiding K, Nielsen P (1996) Extraction of extracellular polymers from activated sludge using a cation ion exchange resin. Water Res 30:1749–1758
5. Liu H, Fang HP (2002) Extraction of extracellular polymeric substances (EPS) sludges. J Biotechnol 95:249–256
6. Jiao Y, Cody GD, Harding AK et al (2010) Characterization of extracellular polymeric substances from acidophilic microbial biofilms. Appl Environ Microbiol 76(9):2916–2922
7. Comte S, Guibaud G, Baudu M (2006) Relations between extraction protocols for activated sludge extracellular polymeric substances (EPS) and EPS complexation properties. Enzyme Microb Technol 38(1–2):237–245
8. Liao BQADG, Droppo IG (2001) Surface properties of sludge and their role in bioflocculation and settleability. Water Res 35(2):339–350
9. Jin B, Wilén B-M, Lant P (2003) A comprehensive insight into floc characteristics and their impact on compressibility and settleability of activated sludge. Chem Eng J 95(1–3):221–234
10. Kirby R (2010) Minimising harbour siltation—findings of PIANC Working Group 43. Ocean Dyn 61(2–3):233–244
11. G-j Ming-yao Chang, Houng Jer-Yiing (2006) Optimization of the medium composition for the submerged culture of Ganoderma lucidum by Taguchi array design and steepest ascent method. Enzyme Microb Technol 38:407–414
12. Lira KG, Pedroza MlV, Rozycki H et al (2010) Response surface analysis on the effect of temperature and pH on growth and proteolytic activity of thermophilic Bacillus sp. Braz Arch Biol Technol 53(5):1067–1072
13. Psomas SK, Liakopoulou-Kyriakides M, Kyriakidis DA (2007) Optimization study of xanthan gum production using response surface methodology. Biochem Eng J 35(3):273–280
14. LianXiang D, FuPing L (eds) (2005) Microbiology laboratory manual. Chinese light industry press, Beijing
15. Bala Subramanian S, Yan S, Tyagi RD et al (2010) Extracellular polymeric substances (EPS) producing bacterial strains of municipal wastewater sludge: isolation, molecular identification,

EPS characterization and performance for sludge settling and dewatering. Water Res 44(7): 2253–2266
16. Badireddy AR, Korpol BR, Chellam S et al (2008) Spectroscopic characterization of extracellular polymeric substance from Escherichia coli and Serratia marcescens: suppression using sub-inhibitory concentrations of bismuth thiols. Biomacromolecules 9(11):3079–3089
17. Rao KJ, Kim CH, Rhee sk (2000) Statistical optimization of medium for the production of recombinant hirudin from Saccharomyces cerevisiae using response surface methodology. Process Biochem 35:639–647
18. Rafigh SM, Yazdi AV, Vossoughi M et al (2014) Optimization of culture medium and modeling of curdlan production from Paenibacillus polymyxa by RSM and ANN. Int J Biol Macromol 70:463–473
19. Zhang H, Liu M, Han S et al (2013) Optimizing the extraction of catechin from peanut red skin using response surface methodology and its antioxidant activity. IERI Procedia 5:312–320

Chapter 33
Effects of pH, Temperature, Storage Time, and Protective Agents on Nisin Antibacterial Stability

Zhilei Tan, Jing Luo, Fang Liu, Qian Zhang and Shiru Jia

Abstract Nisin as a kind of bacteriocin and peptides can inhibit the growth of gram-positive bacteria effectively, which is easily influenced by heat, alkali, and storage time significantly. In this study, it is concluded that adding substances such as chitosan, ascorbic acid, tyrosine, and $FeSO_4$ do well in the enhancement of nisin antibacterial stability. The protective agents have been proposed to improve stability and long-term effectiveness of nisin. Above all chitosan was of great efficiency, followed by $FeSO_4$ and tyrosine, but ascorbic acid was better in acidic conditions. Similar phenomenon occurred when nisin was at elevated pH and high temperature. At pH 6.0, room temperature, nisin titer got rise to 154.7 IU/mL after added chitosan compared to the original 105.6 IU/mL, and even after the 121 °C heating for 20 min, the titer was 2.8 times higher than control.

Keywords Nisin · Titer · Antibacterial stability · Protective agents

33.1 Introduction

Nisin is a 34-amino acid lantibiotic, containing 3.5 kDa polypeptide with antimicrobial activity [1], and has been approved by WHO as a preservative in food [2]. Several studies have reported that the antimicrobial efficacy of nisin was reduced when it was applied in foods. In its free form, nisin can react with reducing sugars through Maillard reaction and can nonspecifically bind with lipids and proteins, and hence decrease its antibacterial activity [3]. In addition, seen from the structure of nisin, it contains unsaturated amino acids Dhb2, Dha5 and Dha33, which make it

Z. Tan · J. Luo · F. Liu · Q. Zhang · S. Jia (✉)
Key Laboratory of Industrial Fermentation Microbiology, Ministry of Education,
College of Biotechnology, Tianjin University of Science and Technology, No. 29,
13th Avenue, Economic-Technological Development Area, Tianjin 300457,
People's Republic of China
e-mail: jiashiru@tust.edu.cn

T.-C. Zhang and M. Nakajima (eds.), *Advances in Applied Biotechnology*,
Lecture Notes in Electrical Engineering 333, DOI 10.1007/978-3-662-46318-5_33

easy to occur intermolecular nucleophilic addition reaction under alkaline pH conditions, making the reductions of solubility and antibacterial activity [4].

In order to overcome these problems, alternative procedures that target the sustained release of nisin have been proposed. Many studies applied liposomes, polymeric capsules, or films to improve nisin biological activity especially for long storage or heat treatment [3, 5]. However, some drawbacks are attributed to liposomes as a nisin carrier including inactivation and fast leakage due to interaction of nisin with liposomes, low stability, and high cost [6, 7]. Our study was aimed to find out a more effective but simple way to solve the poor antibacterial stability of nisin. Chitosan (CS), ascorbic acid (VC), tyrosine (Tyr), and $FeSO_4$ were chosen as protective agents to promote the antibacterial stability of nisin. There exist a strong intra- and intermolecular hydrogen bonds in aqueous media in CS molecular [8], which may result in a solid combination between nisin and CS. And biocompatible organic acids could be interacted with nisin to form hydrogen bond, which may lead to increased solubility and retention of nisin activity at various pH [9]. Besides, Tyr belongs to a phenolic group, and the presence of it accounts for a great binding between surfactant head group and lipid [10], perhaps giving rise to a better antibacterial activity of nisin. In addition, particulate iron has important catalytic effects on reactions that produce reactive oxygen species [11], which may prevent the intermolecular nucleophilic addition reaction of nisin.

33.2 Materials and Methods

33.2.1 Materials and Equipment

Nisin was gifted by New Silver Elephant Biological Engineering Co., Ltd. Tyr, VC, and CS were purchased from Solarbio Science and Technology Co., Ltd. Other drugs were all analytically pure chemical reagents.

33.2.2 Agar Diffusion Method of Nisin Titer Test [12]

Standard nisin is 1,000 IU/mg (dissolved in the sterile 0.02 N HCl, and was diluted to some titers ranging from 5 to 100 IU/mL). Measured 100 μL Nisin standard solution in every Oxford cup, incubated overnight at 33 °C, and then measured the diameters of bacteriostatic rings. Drew the standard curve which takes diameters (mm) of bacteriostatic rings as the abscissa and logarithms of nisin titers as the ordinate ($y = 0.2618x - 1.3979$, $R^2 = 0.9934$). The calculation formula for titer loss rate [13] as formula (33.1) shows:

$$\text{Nisin titer loss rate} = \frac{C_1 - C_2}{C_1} \times 100\,\% \tag{33.1}$$

In the formula, C_1 is for untreated nisin titer, C_2 is for nisin titer measured after processing.

33.2.3 Effects of pH, Temperature, and Storage Time on Nisin Titer

Due to the rare applications of nisin in the alkaline pH condition, the research focused on the pH ranging from 2.0 to 6.0. After nisin solution with different pH (2.0, 4.0 and 6.0, 0.5 g/L) treated at 25, 85, 100 and 121 °C for 20 min, the nisin titers were tested and the titer loss rates were calculated, respectively. Nisin solution (0.5 g/L) with different pH (2.0, 4.0, 6.0) were heated at 121 °C for 20 min and stored in 4 °C for 30 days, then the titers were tested and compared against unheated control solution.

Furthermore, to protect nisin antibacterial stability under different heating (25, 85, 100, and 121 °C) and pH (2.0, 4.0, and 6.0) treatments, VC, Tyr, CS, and $FeSO_4$ were added at the mass ratio of nisin 1:1, 2:1, 1:1, and 2:1 before such treatments, respectively. And then the mixtures were incubated with shaking 200 rpm in 25 °C for 30 min to assure the reaction between them.

33.3 Results and Discussions

33.3.1 Effects of pH, Temperature, and Storage Time on Nisin Titer

33.3.1.1 Effects of pH and Temperature on Nisin Titer

The stability of nisin was studied in the pH range of 2.0–6.0 and at 25, 85, 100 and 121 °C, optimal stability was observed at pH 2.0, 25 °C. As shown in Table 33.1, the antibacterial activity continuously decreased with increasing pH and temperature, showing a greater than 5-fold reduction when the pH was increased from 2.0 to 6.0 at RT (room temperature).

Synergistic effects of temperature and pH on nisin titers were revealed. The titer loss rate was below 40.0 % after nisin solution (pH 2.0) was heated under temperature 100 °C. However, compared to 489.3 IU/mL at RT, the highest titer loss rate was 68.6 % (declined to 153.5 IU/mL) after an elevated temperature (121 °C) heated. The phenomenon is in line with the report of Yun et al. [14]. Besides, pH has greater impact on nisin activity than temperature. The nisin titer loss rate at RT was 29.5 % (pH 4.0) and 78.4 % (pH 6.0) in contrast with control (pH 2.0), respectively. And with the temperature increased from RT to 121 °C, the analogous results were observed that the higher the temperature and pH of nisin, the lower titer

Table 33.1 Increase rates of nisin titers on the condition of different pH and temperatures while adding CS, Tyr, VC, and $FeSO_4$

pH	T (°C)	Nisin		Nisin-VC		Nisin-Tyr		Nisin-CS		Nisin-$FeSO_4$	
2.0	25	489.31 ± 61.05[a]	–	519.88 ± 41.90[a]	0.06[c]	569.68 ± 30.22[a]	0.16[c]	556.49 ± 88.91[a]	0.14[c]	592.48 ± 34.60[a]	0.21[c]
	85	295.25 ± 48.61	39.66[b]	605.70 ± 43.04	1.05	669.45 ± 39.98	1.27	798.73 ± 71.47	1.71	412.57 ± 76.28	0.40
	100	197.15 ± 15.50	59.71	485.49 ± 49.25	1.46	485.49 ± 49.25	1.46	572.26 ± 24.63	1.90	278.82 ± 55.62	0.41
	121	153.51 ± 18.42	68.63	234.05 ± 58.20	0.52	253.43 ± 21.01	0.65	204.83 ± 8.04	0.33	225.72 ± 21.05	0.47
4.0	25	344.94 ± 53.36	29.51	410.09 ± 22.87	0.19	440.85 ± 31.70	0.28	442.92 ± 25.24	0.28	368.92 ± 48.18	0.07
	85	137.15 ± 12.14	71.97	264.57 ± 10.54	0.93	437.41 ± 92.77	2.19	277.55 ±47.14	1.02	136.90 ± 21.28	0.00
	100	99.88 ± 9.26	79.59	235.52 ± 12.91	1.35	317.02 ± 114.51	2.17	128.23 ± 6.02	0.28	141.09 ± 7.65	0.41
	121	35.08 ± 4.12	92.83	72.21 ± 9.83	1.06	136.40 ± 29.44	2.89	152.15 ± 22.10	3.34	96.74 ± 11.22	1.76
6.0	25	105.64 ± 46.10	78.41	168.04 ± 6.38	0.59	140.83 ± 5.51	0.33	154.72 ± 14.42	0.47	211.30 ± 13.17	1.00
	85	42.33 ± 12.82	91.35	85.03 ± 0.51	1.01	110.66 ± 3.37	1.61	113.28 ± 19.39	1.68	106.41 ± 14.49	1.51
	100	35.76 ± 2.058	92.69	50.63 ± 19.66	0.42	77.68 ± 3.97	1.17	89.82 ± 1.70	1.51	87.11 ± 22.07	1.44
	121	15.43 ± 1.01	96.85	20.31 ± 2.76	0.32	17.18 ± 0.80	0.11	58.52 ± 2.00	2.79	80.30 ± 6.94	4.20

[a] Nisin titer (IU/mL), [b] Nisin titer loss rate (%), [c] Increase rates of nisin titer (times)

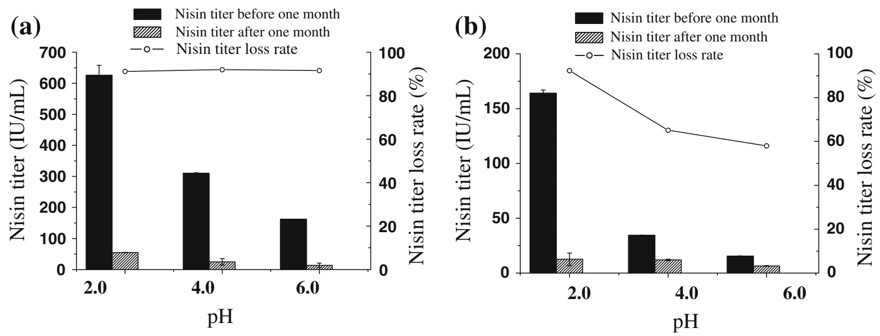

Fig. 33.1 Variation trends of nisin titers before and after a month. **a**, **b** Represent nisin titer and titer loss rate of those stored in 4 °C a month after RT or 121 °C treated for 20 min, respectively

would be. Therefore, the results indicated that in the neutral-to-elevated pH (above 6.0) region as well as high temperature (100–121 °C), the long-term stability of nisin is limited.

33.3.1.2 Effects of Storage Time on Nisin Titer

In addition to temperature and pH, effect of storage time on antibacterial activity of nisin is shown in Fig. 33.1. After nisin solution with different pH (2.0, 4.0, and 6.0) stored at 4 °C for 1 month, all the nisin titer loss rates of different heating treatments (at RT or 121 °C, 20 min) were higher than 90.0 %. Interestingly are the results of Fig. 33.1b that nisin titers decreased below 200 IU/mL after the 121 °C retreating for 20 min before storage, and upon storage for a month at 4 °C, the loss rates were declined to 65.2 and 58.4 % in pH 4.0 and 6.0 conditions, respectively, which were both lower than the 92.3 % loss rate of control (pH 2.0). But seen from the overall titer variation trends, nisin antibacterial activity was seriously decreased to less than 25 IU/mL after a month. In these cases, the storage time could well be a limiting factor with respect to practical applications.

33.3.2 Effects of Different Protective Agents on Nisin Titer

Compared to the control which has not been added any protective agent, those were of great effect on antibacterial stability. Moreover, VC, Tyr, CS, and $FeSO_4$ were all negative on titer-tested plates, suggesting that they do not have evident bactericidal effect under heating and pH treatments.

The results of different treatments are shown in Table 33.1. Considering the four kinds of protective agents, the effect of CS was the best, even after heating at 121 °C for 20 min, the increased titer of nisin remained upon 0.3, 3.3, and 2.8 times

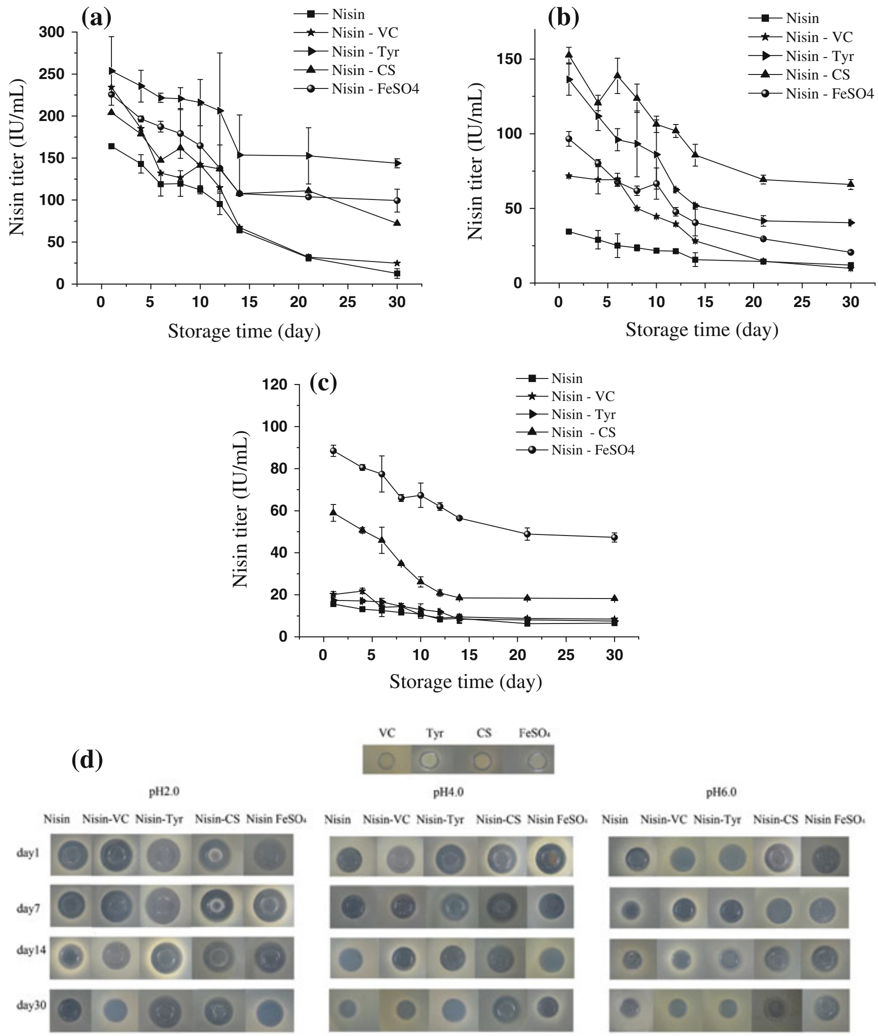

Fig. 33.2 **a**, **b**, and **c** Show nisin titer variation trends of nisin with pH 2.0, 4.0, and 6.0 via heating at 121 °C for 20 min. **d** Evidently represents antimicrobial activity of nisin at pH 2.0, 4.0, and 6.0, 121 °C for 20 min revealed by bacteriostatic rings

of pH 2.0, 4.0 and 6.0, respectively. Besides, the protective effects of VC and Tyr were better in acid conditions, especially in pH 4.0 with a 121 °C 20 min heating, the titers of nisin-VC complex and nisin-Tyr complex were as 1.1 and 2.9 times as nisin, respectively, but in pH 6.0 at the same treatment, they were both without effect. $FeSO_4$ was ideal in neutral environment (pH 6.0), the increased rates of nisin titer was 4.2 times at 121 °C.

As the statistical data shown in Fig. 33.2, after a monthly storage, the titer variation trends of different pH nisin solution via heating or not were both declined, but those with protective agents were higher than controls seen from Fig. 33.2, CS and $FeSO_4$ were always the most effective agents of the four, especially pH 6.0, in which the other two VC and Tyr expressed little effect. The same results were shown in Fig. 33.2d, which evidently revealed the antimicrobial activity of Nisin pretreated in pH 2.0, 4.0 and 6.0 and at 121 °C for 20 min revealed by bacteriostatic rings. Therefore, it becomes evident that the antibacterial stability of nisin, particularly at elevated temperatures, pH and long-term storage, were improved by the protective agents.

33.4 Conclusions

pH and temperature have synergistic effects on nisin titer. In the weak acidic region (pH 6.0 in this paper) and at an elevated pH (pH 9.0), a much lower stability is observed than that at low pH values (pH 2.0 and 4.0). When it was in weak acid and alkaline environments, the influence of temperature on nisin antibacterial stability was significant. Different pH nisin solutions were stored in 4 °C for 1 month, whose titers showed a downward trend and all the loss rates exceeded 90 %. The results implied that nisin has, especially at low pH, a good short-term stability, sufficient to survive in most heat treatments. CS was the most effective agent on nisin antibacterial stability, especially when it was at room temperature that the titer increased from 105.6 IU/mL of control to 154.7 IU/mL, even if the heating temperature was up to 121 °C, still better than other protective agents (except $FeSO_4$ at pH 6.0). Followed by $FeSO_4$ especially on weak acidic condition (pH 6.0) which can stabilize nisin antibacterial stability after heating to 121 °C for 20 min. The protective effects of Tyr and VC to nisin were somehow good, whose titers can be higher than that of the control group especially in acidic region. But with the increase of temperature and pH, the antibacterial activity was still difficult to maintain. What is more, with the increase of storage time, CS, Tyr, VC, and $FeSO_4$ on nisin antibacterial stability were effective all the same.

Acknowledgments The authors are grateful for the financial support from the National Natural Science Foundation of China (Project 21276197).

References

1. Mulders JWM, Boerrigter IJ, Rollema HS, Siezen RJ, Devos WM (1991) Identification and characterization of the lantibioticnisin-z, a natural nisinvariant. Eur J Biochemistr 201 (3):581–584
2. Benech RO, Kheadr EE, Laridi R, Lacroix C, Fliss I (2002) Inhibition of Listeria innocua in cheddar cheese by addition of nisin Z in liposomes or by in situ production in mixed culture. Appl Environ Microbiol 68(8):3683–3690

3. Sant'Anna V, Silva Malheiros P, Brandelli A (2011) Liposome encapsulation protects bacteriocin-like substance P34 against inhibition by Maillard reaction products. Food Res Int 44(1):326–330
4. Pollema HS, Kuipers OP, Both P et al (1995) Improvement of solubility and stability of the antimicrobial peptide nisin by protein engineering. Appl Environ Microbiol 61(8):2873–2878
5. Laridi R, Kheadr EE, Benech RO, Vuillemard JC, Lacroix C, Fliss I (2003) Liposome encapsulated nisin Z: optimization, stability and release during milkfermentation. Int Dairy J 13(4):325–336
6. El Jastimi R, Edwards K, Lafleur M (1999) Characterization of permeability and morphological perturbations induced by nisin on phosphatidylcholine membranes. Biophys J 77(2):842–852
7. Kopermsub P, Mayen V, Warin C (2011) Potential use of niosomes for encapsulation of nisin and EDTA and their antibacterial activity enhancement. Food Res Int 44(2):605–612
8. Prashant A, Gustav JS, Klaas N (2010) Hitosan-based systems for molecular imaging. Adv Drug Deliv Rev 62:42–58
9. Adhikari MD, Das G, Ramesh A (2012) Retention of nisin activity at elevated pH in an organic acid complex and gold nanoparticale composite. Chem Commu 48:8928–8930
10. Joondan N, Jhaumeer-Laulloo S, Caumul P (2014) A study of the antibacterial activity of L-Phenylalanine and L-Tyrosineesters in relation to their CMCs and their interactions with 1,2-dipalmitoyl-sn-glycero-3-phosphocholine, DPPC as model membrane. Microbiol Res 169:675–685
11. Chu B, Hao J, Takekawa H et al (2012) The remarkable effect of FeSO4 seed aerosols on secondary organic aerosol formation from photooxidation of α-pinene/NOx and toluene/NOx. Atmos Environ 55:26–34
12. QB 2394-2007, Food additive-Nisin
13. Qing-qing Zeng, Li-yan Zhang, Qi-lian Liu (2012) Study on the effect of chitosan on antibacterial stability of Nisin. Sci Technol Food Ind 23:114–121
14. Yun J, Feng G, Guanghong Z (2002) Effects of temperature, pH on antibacterial activity of nisin. Food Sci Technol 8:32–34

Chapter 34
Enhanced Solvent-Stable Alpha Glycosidase Production by *Bacillus licheniformis* JXC-1 by Optimization of Feeding Strategies

Jun Fang, Qunfang Tang, Long Liu and Jianghua Li

Abstract In the previous work, we screened a strain (*Bacillus licheniformis* JXC-1) producing solvent-stable (10 % *N*,*N*-Dimethylformamide, short for DMF) α-glucosidase from several different soil samples. In this work, we attempt to improve the α-glucosidase production by optimization of feeding strategies in a 3-L fermenter. Specifically, the key factors of solvent-tolerant α-glycosidase production were investigated first, and the optimal conditions (pH 7.0, the initial maltose concentration 25 g/L, and agitation speed 600 rpm) were obtained; the enzyme activity reached 444.7 U/L under the optimal conditions. Then, four feeding strategies with different feeding rates for 4–8 h to feed maltose or both maltose and tryptone were carried out, and it was found that feeding maltose and tryptone at a rate of 2.25 mL/h (4–5 h), 6.75 mL/h (5–6 h), 9 mL/h (6–7 h), and 15 mL/h (7–8 h) significantly increased the α-glycosidase production, from 444.7 to 872.5 U/L.

Keywords *Bacillus licheniformis* JXC-1 · Alpha glycosidase · Fed-batch fermentation · Solvent-stable enzymes

34.1 Introduction

The α-glucosidase (α-D-glucoside glucohydrolase; EC 3.2.1.20) is an amylase that acts on α-1,4 bonds from nonreducing end [1, 2], preferentially from short saccharides such as α-glucosides, maltooligosaccharides, and α-glucan, releasing α-glucose [3]. In addition, the released α-glucose can be transferred to another glucose, maltose, or maltotriose molecule by α-1,6 linkage [4, 5]. Because of the capacity of transglycosylation, the α-glucosidase has applications in the industrial production of isomalto oligosaccharides (IMO, isomaltose, panose, isomaltotriose,

J. Fang · Q. Tang · L. Liu · J. Li (✉)
Key Laboratory of Carbohydrate Chemistry and Biotechnology,
Ministry of Education, Jiangnan University, Wuxi 214122, China
e-mail: lijianghua@jiangnan.edu.cn

T.-C. Zhang and M. Nakajima (eds.), *Advances in Applied Biotechnology*,
Lecture Notes in Electrical Engineering 333, DOI 10.1007/978-3-662-46318-5_34

and so on) and in the combination of sugars to biologically useful materials [6]. Beyond that, it is also being used as a guide to structure-based design of anti-HIV inhibitors [7].

The solvent-stable enzymes adapt to mediate cellular and metabolic processes in a solvent-rich environment and are stable in the presence of organic solvents [8, 9]. Besides, it is reported that enzyme catalysis in a nonaqueous/low-water media makes it possible to synthesize novel compounds which are difficult to synthesize conventionally and to obtain the biologically active enantiomer for which the racemic resolution is either very complex or difficult [10–12].

As a new type of efficient biological agent, glycosidases can also be used to synthesize oligosaccharides and several important glycosidic derivatives efficiently. Using high concentration of organic solvent system to reduce the concentration and activity of water can significantly reduce the hydrolysis rate of products, and prompt the reaction for the synthesis of glycosidic compounds [13]. As far as we know, the solvent-stable α-glucosidase has potential applications for synthesis of flavonoid glycosides compounds in solvent-water media.

In previous studies, we screened a strain (*Bacillus licheniformis* JXC-1) which can produce solvent-tolerant (10 % DMF) α-glucosidase from several different soil samples [14]. However, the production of α-glucosidase was very low. In this work, we attempt to establish an efficient fermentation process to improve α-glucosidase production. First, the influence of pH (uncontrolled and constant 6.0, 7.0, and 8.0), initial maltose concentration (20, 25, 30, and 35 g/L), and agitation speed (500, 600, 700, and 800 rpm) on α-glycosidase production was investigated in a 3-L fermenter. Based on the optimal fermentation conditions, four different feeding strategies which fed maltose or both maltose and tryptone at different rates for 4–8 h were investigated to improve the production of α-glucosidase.

34.2 Methods

34.2.1 Microorganism and Fermentation

The microorganism used in this work was *B. licheniformis* JXC-1, which was screened from soil in our previous work [14]. The seed culture was prepared by growing cells in 250-mL shaker flasks containing 30 mL Luria-Bertani (LB) medium inoculated with 3 % (v/v) feedstock and then cultivated for 12 h at 37 °C on a shaking flask incubator (200 rpm).

Fermentation medium contained (g/L): maltose 30, tryptone 39, yeast extract 3, $CaCl_2$ 0.4, $FeSO_4{\cdot}7H_2O$ 0.164, NaCl 0.076, and distilled water 1.0 L with natural pH at 7.0–7.5.

Cultivations were done in a 3-L fermentor (LiFlus GM BioTRON, Korea) with a working volume of 1.5 L. The inoculation amount was 3 % (v/v). The temperature in the batch culture was kept at 37 °C. During the whole fermentation process, pH was controlled automatically by a 25 % (v/v) ammonia solution and a 25 % (v/v) hydrochloric acid solution. The agitation speed was set as 500–800 rpm while keeping aeration rate at 1vvm. Samples were taken every 2 h to measure the α-glycosidase production, reducing sugar concentration, and dry cell weight (DCW).

In batch culture, the maximum specific growth and production rate were shown approaching to 4 h while the reducing sugar was 18 g/L (Fig. 34.3). At the same time, the DCW and the production of α-glucosidase raised rapidly for 4–8 h. When the fermentation time was 6 and 8 h, the reducing sugar concentration was 15 and 7 g/L, respectively. To obtain higher production, we designed four feeding strategies at different feeding rates to keep the reducing sugar concentration at 18 g/L and changed the rate using a computer-controlled pump. The feeding rates were set as A 8.25 mL/h (4–8 h), B 4.5 mL/h (4–6 h), and 12 mL/h (6–8 h), C 4.5 mL/h (4–6 h), 9 mL/h (6–7 h), and 15 mL/h (7–8 h), D 2.25 mL/h (4–5 h), 6.75 mL/h (5–6 h), 9 mL/h (6–7 h), and 15 mL/h (7–8 h). Maltose (500 g/L) or maltose (500 g/L) and tryptone (780 g/L, determined by the optimal ratio of carbon and nitrogen sources in the fermentation medium) were fed by different rates according to the four feeding strategies.

34.2.2 Analysis Method

34.2.2.1 DCW Measurement

The fermentation broth was centrifuged at 10,000×*g* and 4 °C for 10 min. The clear supernatant was used for the analysis of reducing sugar. The DCW was determined by drying the pellets at 105 °C in the oven till constant weight. The specific growth rate was determined from the slope of the semi-logarithmic plot of DCW versus culture time.

34.2.2.2 Enzyme Activity Assay

The samples were centrifuged at 10,000×*g* and 4 °C for 10 min, and then the cell pellets were washed with Na_2HPO_4 (0.2 M) and citric acid (0.1 M) buffer solution (pH 6.8) and resuspended in the same buffer. The cell suspension was sonicated to break up the cell walls and centrifuged at 10,000×*g* and 4 °C for 15 min to remove cell debris. The hydrolytic activity of the enzyme was measured basically according to the modified method [15]. Briefly, the reaction mixture in a test tube containing 0.9 mL Na_2HPO_4 (0.2 M) and citric acid (0.1 M) buffer solution (pH 6.8), 0.1 mL of 5 mM *p*-nitrophenyl-α-D-glucopyranoside (α-PNPG, Sigma-Aldrich), 5 min at 37 °C, then adding 1 mL of the cell suspension to them. After 20 min of incubation, the reaction was stopped with 1 mL of 1 M Na_2CO_3, and the *p*-nitrophenolate released was quantified by a spectrophotometer-722 (Third Analytical Instrument Factory, Shanghai, China) at 410 nm. One unit (U) of enzyme activity was defined as the amount of enzyme that releases 1 μmol of p-nitrophenolate per minute per mL reaction mixture at pH 6.8, 37 °C.

34.2.2.3 Reducing Sugar Concentration Determination

The determination of reducing sugar concentration was modified according to what was previously reported [16]. To 1 mL of the sugar solution in a test tube 1 mL of the DNS reagent was added. Tubes were placed in boiling water bath for 15 min, transferred to ice to rapidly cool down to room temperature. Each sample was added with 8 mL of distilled water to stop the reaction. The absorbance was measured at 540 nm, using a spectrophotometer-722. (Third Analytical Instrument Factory, Shanghai, China.)

34.3 Results and Discussion

34.3.1 Influence of pH on α-Glucosidase Production in Batch Culture

The influence of pH (uncontrolled and constant 6.0, 7.0, and 8.0) on α-glucosidase production in batch culture is shown in Fig. 34.1. In our previous shake flask experiments, the initial pH was a key factor influencing the production of α-glucosidase significantly (data not shown). The maximum production of α-glucosidase was

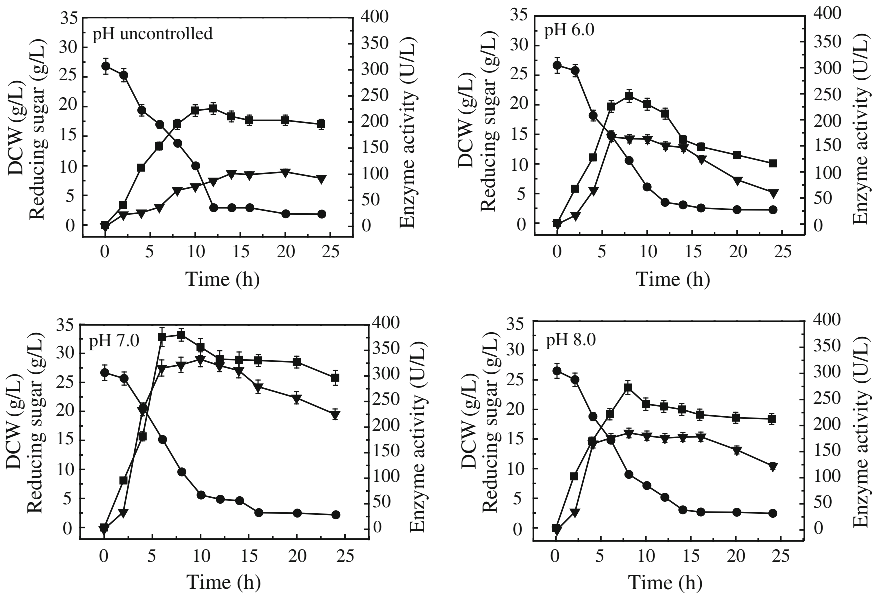

Fig. 34.1 Influence of pH on α-glucosidase production in batch culture. ■: DCW (g/L), ▼: activity of α-glucosidase (U/L), ●: reducing sugar concentration (g/L)

104.6, 167.1, 332.6, and 186.1 U/L with pH was uncontrolled, constant 6.0, 7.0, and 8.0, respectively, and meanwhile, the maximum DCW was 19.7, 21.5, 33.2, and 23.7 g/L, respectively. As shown in Table 34.1, with the pH of constant 7.0, α-glucosidase production per DCW and productivity reached 10.02 U/g and 13.86 U L^{-1} $h^{-1,}$ much higher compared to the other three pH controlled modes. It was concluded that the constant pH at 7.0 was optimal for the production of α-glucosidase.

34.3.2 Influence of Initial Maltose Concentration on α-Glucosidase Production in Batch Culture

The influence of different initial maltose concentrations on cell growth and α-glucosidase production was further examined (Fig. 34.2). The maximum α-glucosidase production was obtained with an initial maltose concentration of 25 g/L with 444.7 U/L while the production was 332.6 U/L with 30 g/L. Though DCW increased with the increase of maltose concentration (the DCW with 30 g/L was higher than that with 25 g/L), increasing maltose concentration in medium did not enhance α-glucosidase production. Thus, feeding maltose in fermentation process may be an efficient approach to obtain higher production. So the initial maltose concentration was set as 25 g/L.

34.3.3 Influence of Agitation Speed on α-Glucosidase Production in Batch Culture

Dissolved oxygen is one of the essential nutrients for aerobic microbial growth as well as a key environmental factor affecting the material production and energy metabolism. In general, under the condition of the air flow normally, agitation speed directly affects the efficiency of oxygen transfer in fermentation liquid, and then affects the cell growth and production of α-glucosidase. We investigated the effect of agitation speed on cell growth and α-glucosidase production in batch culture and the results are shown in Fig. 34.3. Dissolved oxygen has a positive impact on cell growth since the DCW was 44.6 % higher when the agitation speed was increased to 800 rpm (33.2 g/L) from 500 rpm (18.4 g/L). In contrast to that, a good cell growth was not on behalf of a high enzyme production. The maximum α-glucosidase production with 600 rpm (444.7 U/L) was 33.7 % higher than that with 800 rpm (332.6 U/L). At the same time, Table 34.1 shows that 600 rpm had the highest production per DCW (22.1 U/g) as well as the α-glucosidase productivity (18.53 U L^{-1} h^{-1}). Thus, we chose 600 rpm as a condition of further research.

Table 34.1 Comparison of α-glucosidase fermentation parameters on different control conditions by *Bacillus licheniformis* JXC-1 in batch culture

Parameters	pH				Initial maltose concentration (g/L)				Agitation speed (rpm)			
Conditions	Natural	6.0	7.0	8.0	20	25	30	35	500	600	700	800
Fermentation time (h)	24	24	24	24	24	24	24	24	24	24	24	24
Maximum DCW (g/L)	19.7	21.5	33.2	23.7	18.9	23.1	33.2	25.1	18.4	23.1	24.2	33.2
Maximum production (U/L)	104.6	167.1	332.6	186.1	176.1	444.7	332.6	198.9	289.7	444.7	359.2	332.6
Maximum specific growth rate [g/(g h)]	0.95	0.73	6.15	1.88	0.63	0.82	6.15	4.93	9.92	0.82	0.75	6.79
Maximum specific production rate [U/(g h)]	4.56	39.8	17.5	714.3	171.8	135.3	17.5	31.9	13.67	135.3	265.7	17.5
Alpha-glucosidase production per dry cell weight (U/g)	5.9	9.4	10.02	7.85	17.6	22.1	10.7	8.8	16.2	22.1	21.2	10.7
Alpha-glucosidase productivity [U/(L h)]	4.36	6.96	13.86	7.75	7.34	18.53	13.86	8.29	12.1	18.53	15.0	13.9

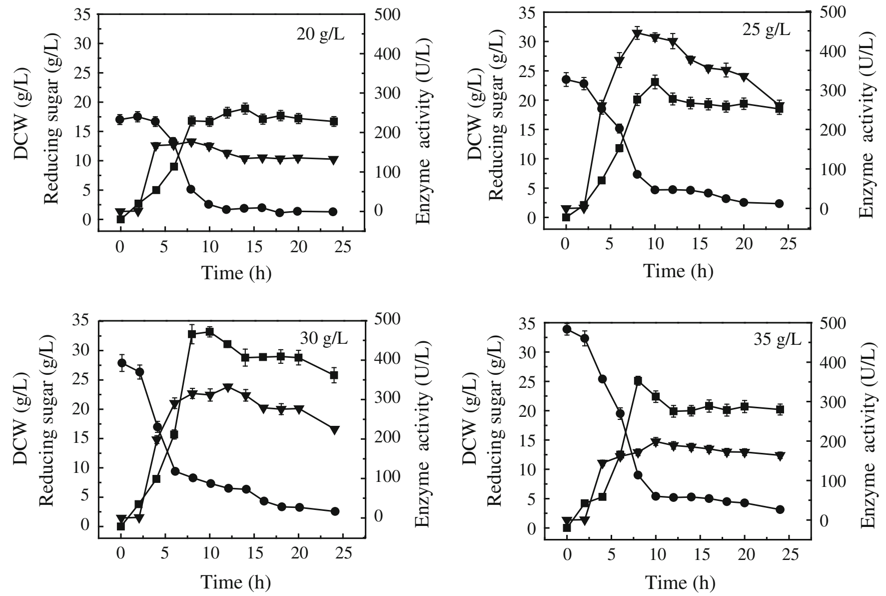

Fig. 34.2 Influence of initial maltose concentration on α-glucosidase production in batch culture. ■: DCW (g/L), ▼: activity of α-glucosidase (U/L), ●: reducing sugar concentration (g/L)

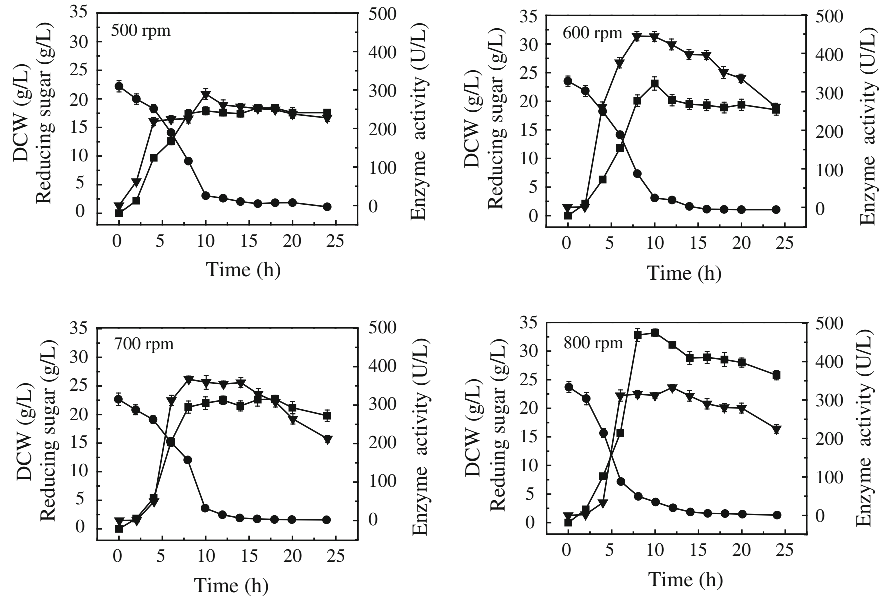

Fig. 34.3 Influence of agitation speed on α-glucosidase production in batch culture. ■: DCW (g/L), ▼: activity of α-glucosidase (U/L), ●: reducing sugar concentration (g/L)

34.3.4 Four Different Strategies of Feeding Maltose for α-Glucosidase Production

In batch culture, the maximum specific growth and production rate were shown approaching to 4 h while the reducing sugar was 18 g/L (data not shown). At the same time, the DCW and the production of α-glucosidase rised rapidly for 4–8 h. Thus, to obtain higher production, we put forward four strategies to feed maltose for 4–8 h at different rates to keep the reducing sugar concentration at 18 g/L. The influence of different fed-batch strategies with the optimal conditions feeding maltose is shown in Fig. 34.4. The maximal DCW in fed-batch fermentation (strategy C) was 45.6 g/L and the maximum α-glucosidase production (strategy D) was 633.8 U/L. Fed-batch fermentation (strategy D) resulted in higher α-glucosi-

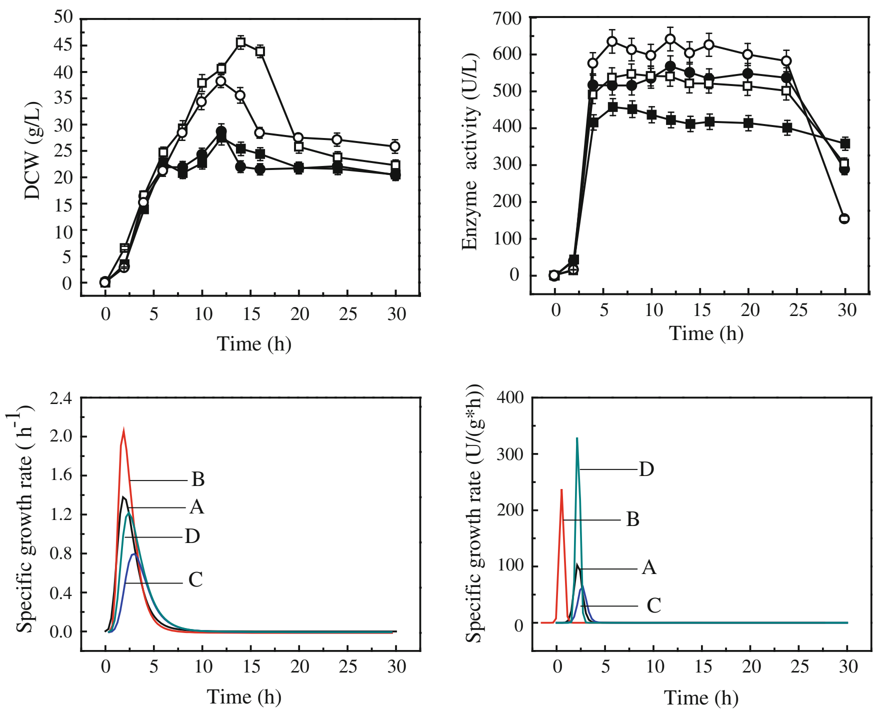

Fig. 34.4 Influence of four fed-batch culture strategies on α-glucosidase production by feeding maltose. ■: strategy A, the feeding rate was set as 8.25 mL/h (4–8 h), ●: strategy B, the feeding rate was set as 4.5 mL/h (4–6 h) and 12 mL/h (6–8 h), □: strategy C, the feeding rate was set as 4.5 mL/h (4–6 h), 9 mL/h (6–7 h), and 15 mL/h (7–8 h), ○: strategy D, the feeding rate was set as 2.25 mL/h (4–5 h), 6.75 mL/h (5–6 h), 9 mL/h (6–7 h), and 15 mL/h (7–8 h)

Table 34.2 Comparison of α-glucosidase fermentation parameters between different carbon and organic nitrogen sources feeding approaches by *B. licheniformis* JXC-1 in fed-batch cultures

Parameters	Feeding maltose				Feeding maltose and tryptone			
Strategy	A	B	C	D	A	B	C	D
Fermentation time (h)	30	30	30	30	30	30	30	30
Maximum DCW (g/L)	27.4	28.5	45.6	38.3	30.7	29.5	35.2	23.5
Maximum production(U/L)	457.3	568.9	545.5	633.8	724.4	616.9	618.2	872.5
Maximum specific growth rate [g/(g h)]	0.76	0.8	0.76	1.23	0.68	0.68	1.3	0.4
Maximum specific production rate [U/(g h)]	201.3	271.6	85.8	429.5	151.2	168.5	272.2	128.8
Alpha-glucosidase production per dry cell weight (U/g)	35.7	20.0	18.6	56.6	31.4	27.1	22.3	43.0
Alpha-glucosidase productivity [U/(L h)]	15.24	18.96	18.18	21.13	24.15	20.56	20.61	29.08

dase production and productivity compared with the other three feeding strategies. With this strategy, the α-glucosidase titer per DCW and productivity reached 56.6 U/g and 21.13 U L^{-1} h^{-1} at 14 h (Fig. 34.4 and Table 34.2). More than that, the production with strategy D increased 42.5 % compared to that in batch culture.

34.3.5 Four Different Strategies Feeding Maltose and Tryptone for α-Glucosidase Production

Nitrogen sources are metabolized to produce amino acids, nucleic acids, proteins, and cell-wall components in bacteria. In order to maintain the maximum cell growth rate, not only sufficient and suitable carbon source should be provided, but the corresponding organic nitrogen source which is beneficial to the growth of cell also should be supplied. With the four feeding strategies, we further investigated the effect of feeding maltose and tryptone at different rates in fed-batch culture, shown in Fig. 34.5. The maximal DCW in fed-batch fermentation (strategy C) was 35.2 g/L and the maximum α-glucosidase production (strategy D) was 872.5 U/L. Though the maximum DCW was lower than 45.6 g/L, it is also worth mentioning that the production of α-glucosidase with feeding maltose and tryptone by four strategies was much higher than that with feeding maltose, the maximum α-glucosidase production increased 37.7 %.

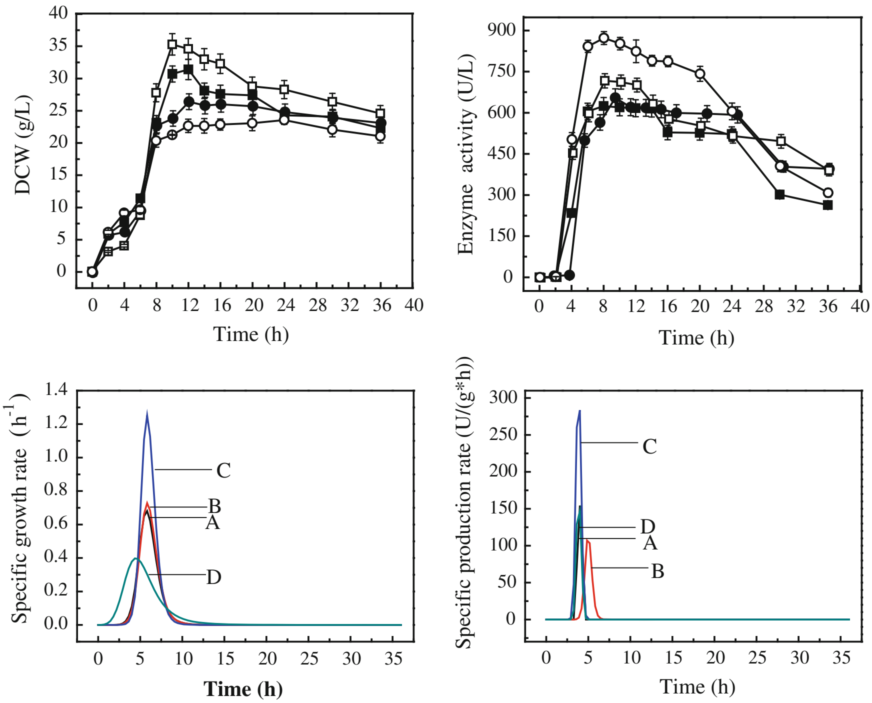

Fig. 34.5 Influence of four fed-batch culture strategies on α-glucosidase production by feeding maltose and tryptone. ■: strategy A, the feeding rate was set as 8.25 mL/h (4–8 h), ●: strategy B, the feeding rate was set as 4.5 mL/h (4–6 h) and 12 mL/h (6–8 h), □: strategy C, the feeding rate was set as 4.5 mL/h (4–6 h), 9 mL/h (6–7 h), and 15 mL/h (7–8 h), ○: strategy D, the feeding rate was set as 2.25 mL/h (4–5 h), 6.75 mL/h (5–6 h), 9 mL/h (6–7 h), and 15 mL/h (7–8 h)

34.4 Conclusions

In this work, the influence of pH, initial maltose concentration, and agitation speed on α-glucosidase production was investigated in a 3-L fermenter. We found that the constant pH 7.0, initial maltose concentration of 25 g/L, and agitation speed of 600 rpm were the better conditions, which raised the production of α-glucosidase 3.25 times from 104.6 to 444.7 U/L. We further proposed four feeding strategies to feed maltose or both maltose and tryptone at different rates for 4–8 h. With the strategy D where the maltose and tryptone feeding rate was as 2.25 mL/h (4–5 h), 6.75 mL/h (5–6 h), 9 mL/h (6–7 h) and 15 mL/h (7–8 h), we finally obtained the highest α-glucosidase production (872.5 U/L) which was 96.2 % higher than that in batch culture. These results indicated that the feeding strategy was effective for the production of α-glucosidase.

References

1. Carvalho AFA, Martin N, Da Silva R et al (2009) Properties of the purified glycosylated alpha-glucosidase produced by thermophilic fungus Thermoascus aurantiacus CBMAI 756 in submerged fermentation. New Biotechnol 25:S48–S48. doi:10.1016/j.nbt.2009.06.254
2. Cihan AC, Ozcan B, Cokmus C (2009) Characterization of thermostable α-glucosidases from newly isolated Geobacillus sp. A333 and thermophilic bacterium A343. World J Microbiol Biotechnol 25:2205–2217. doi:10.1007/s11274-009-0127-y
3. Sato F, Okuyama M, Nakai H et al (2005) Glucoamylase originating from *Schwanniomyces occidentalis* is a typical α-glucosidase. Biosci Biotechnol Biochem 69:1905–1913
4. Shimba N, Shinagawa M, Hoshino W et al (2009) Monitoring the hydrolysis and transglycosylation activity of alpha-glucosidase from Aspergillus niger by nuclear magnetic resonance spectroscopy and mass spectrometry. Anal Biochem 393:23–28. doi:10.1016/j.ab.2009.06.002
5. Carvalho AFA, Boscolo M, Da Silva R et al (2010) Purification and characterization of the alpha-glucosidase produced by thermophilic fungus Thermoascus aurantiacus CBMAI 756. J Microbiol 48:452–459. doi:10.1007/s12275-010-9319-2
6. Da Silva TM et al (2009) Purification and biochemical characterization of a novel alpha-glucosidase from Aspergillus niveus. Antonie Van Leeuwenhoek 96:569–578. doi:10.1007/s10482-009-9372-1
7. Carvalho AFA, Leite RSR, Martins E et al (2007) Partially purified and characterization of the α-glucosidase produced by thermophilic fungus Thermoascus aurantiacus CBMAI 756 in submerged fermentation. J Biotechnol 131:S232. doi:10.1016/j.jbiotec.2007.07.422
8. Tang XY, Pan Y, Li S et al (2008) Screening and isolation of an organic solvent-tolerant bacterium for high-yield production of organic solvent-stable protease. Bioresour Technol 99:7388–7392. doi:10.1016/j.biortech.2008.01.030
9. Gupta A, Khare SK (2009) Enzymes from solvent-tolerant microbes: useful biocatalysts for non-aqueous enzymology. Crit Rev Biotechnol 29:44–54. doi:10.1080/07388550802688797
10. Klibanov AM (2001) Improving enzymes by using them in organic solvents. Nature 409:241–246
11. Karadzic I, Masui A, Zivkovic LI et al (2006) Purification and characterization of an alkaline lipase from Pseudomonas aeruginosa isolated from putrid mineral cutting oil as component of metalworking fluid. J Biosci Bioeng 102:82–89. doi:10.1263/jbb.102.82
12. Gupta A, Khare SK (2007) Enhanced production and characterization of a solvent stable protease from solvent tolerant Pseudomonas aeruginosa PseA. Enzym Microbial Technol 42:11–16. doi:10.1016/j.enzmictec.2007.07.019
13. Chen Z, Xueming W, Bingfang H (2010) Development of glycosidase biocatalysis in non-aqueous phase. Chem Ind Eng Prog 29:1292–1299
14. Zhou L, Li J, Liu L et al (2013) Screening a new α-glucosidase dimethylformamide-tolerant and optimization the transformation conditions of biosynthesising quercetin-d-glucopyranosides Industrial. Microbiology 43:8–13
15. Hung VS et al (2005) Alpha-Glucosidase from a strain of deep-sea Geobacillus: a potential enzyme for the biosynthesis of complex carbohydrates. Appl Microbiol Biotechnol 68:757–765. doi:10.1007/s00253-005-1977-3
16. Saqib AAN, Whitney PJ (2011) Differential behaviour of the dinitrosalicylic acid (DNS) reagent towards mono- and di-saccharide sugars. Biomass Bioenergy 35:4748–4750. doi:10.1016/j.biombioe.2011.09.013

Chapter 35
The Effect of Different Activated Carbon and Bleaching Temperature on Kojic Acid Bleaching

Wu Meng, Cuiying Zhang and Dongguang Xiao

Abstract In this paper, the effects of six different types of activated carbons on decolorization of kojic were studied and two kinds of them were picked out based on the decoloration rate or kojic acid yield, respectively. After mixing in different proportions, the effects of different ratios of the two activated carbons at different bleaching temperature conditions on kojic bleaching were determined by experiments. The results show that the decoloration rate was the highest (79.84 %) at 70 °C when the ratio of 767 was 20 % (total 0.2 g of activated carbon), and it had a higher yield of kojic acid (91.26 %), while the highest kojic acid rate (94.06 %) was obtained at 80 °C when the ratio of 767 was 100 %; the decoloration rate was also better (73.26 %) under these conditions. In contrast, the better bleaching effect with minimum energy consumption was at 50 °C when the ratio of 767 was 40 %, the kojic acid yield reached more than 90 %. These three combined ratios have their own advantages, according to the different needs for various occasions.

Keyword Activated carbon · Kojic · Decoloration rate · Respectively rate

35.1 Introduction

Kojic acid is an organic acid with good antibacterial effect against pathogenic bacterium [1–3], it can also inhibit flies and other pests [4, 5]. Besides its use in the medical field, kojic acid has various applications in several other fields such as food, cosmetics, agriculture field, etc. [6–9]. The primary way to produce kojic acid in the industry was submerge fermentation with glucose as carbon source [10, 11];

W. Meng
Key Laboratory of Shandong Microbial Engineering,
Shandong Polytechnic University, Jinan 250353, China

W. Meng · C. Zhang · D. Xiao (✉)
Key Laboratory of Industrial Fermentation Microbiology, Ministry of Education,
Tianjin University of Science and Technology, TEDA, Tianjin 300457, China
e-mail: xiao99@tuet.edu.cn

T.-C. Zhang and M. Nakajima (eds.), *Advances in Applied Biotechnology*,
Lecture Notes in Electrical Engineering 333, DOI 10.1007/978-3-662-46318-5_35

however, the kojic acid is obtained by fermentation often complexing with ferric ion [12], so the kojic obtained form crude extract must go through bleaching and refining.

Currently, the kojic acid extraction bleaching process in industry still mainly relies on an activated carbon ZX-767 [13]; through optimization experiments, upto 78 % of decoloration rate and 90 % of kojic acid yield can be achieved, but the quality of kojic acid has not been increased significantly and the production cost has not been reduced effectively yet. With the increasing competition of kojic acid production in the domestic market, it is urgent to reduce the cost of kojic acid extraction process and improve the quality of kojic acid's end product. However, bleaching is the most important step in kojic acid extraction process. The decoloration of kojic acid material in industry is mainly activated carbon [14] and the ion-exchange resin [15], both of them have many different types of materials, and between the different types they also have significant differences.

In this paper, we experimented with six different types of activated carbon for decoloration experiments of kojic and used decoloration rate and kojic acid yield as two important indicators to pick out two kinds of activated carbon. Then after combining in different proportions, we studied the effects of different ratios at different carbon bleaching temperature conditions on kojic bleaching.

35.2 Materials and Methods

35.2.1 Activated Carbon

Activated carbons, used in the experiments and shown in Table 35.1, were purchased from Jiangsu Liyang activated carbon plant.

35.2.2 The Choice of Activated Carbon

Different varieties of activated carbon have different effects on bleaching. In this study, Chengdu Jin Kaisheng Ltd. kojic crude material was crystallized as experimental subjects. Six different types of activated carbons (Table 35.1) were used to

Table 35.1 Several main parameters of the selection activated carbon

Name	Species	Particle size (mash)	Moisture (%)	Iron (%)	Specific surface area (m^2/g)
ZX-767	Injection type	200	10	0.02	–
ZXK-AR	Reagents	200	10	0.02	–
ZX-210	Nutshell	φ1.0 mm	5	–	1,100 ± 50
ZX-3011	Sugar class	200	10.0	0.10	~1,300
ZX-720	Medicinal class	200	15	0.10	–
ZX-507	Powdery	200	–	0.02	~1,400

Table 35.2 The experiment scheme of five activated carbons at 50 °C

Name	Species	Subjects	Bleaching temperature (°C)	Bleaching time (min)	Dosage of the activated carbon (g)
ZX-767	Injection type	Crude kojic acid solution mL	50	30	0.200
ZXK-AR	Reagents	Crude kojic acid solution mL	50	30	0.200
ZX-210	Nutshell	Crude kojic acid solution mL	50	30	0.200
ZX-3011	Sugar class	Crude kojic acid solution mL	50	30	0.200
ZX-720	Medicinal class	Crude kojic acid solution mL	50	30	0.200
ZX-507	Powdery	Crude kojic acid solution mL	50	30	0.200

do the experiment. We took 50 g crude kojic acid crystals and dissolved these crystals in 500 mL of distilled water. Then 50 mL of the solution was measured and placed in six 250 mL Erlenmeyer flasks. 0.200 g of the different types of activated carbons was added in the flasks at 50 °C temperature for 30 min for bleaching. The effects of all activated carbon bleaching were compared. The design of the experiments are shown in Table 35.2.

35.2.3 The Ratio of Different Carbon Decoloration Experiments at Different Temperatures

We took 50 g crude kojic acid crystals, dissolved these crystals in 500 mL of distilled water, and stirred and mixed it. Then 50 mL of the solution was measured and placed in six 250 mL Erlenmeyer flasks, adding 0.200 g of the different types of activated carbons in the flasks at 50 °C temperature for 30 min for bleaching. All activated carbon bleaching effects were compared. The design of the experiments are shown in Table 35.3. We selected the highest rate of decoloration activated carbon X and the highest kojic acid yield carbon Y through the different proportions of decoloration experiments. Finally, we obtained the optimal ratio combinations.

Table 35.3 The decolorized experiment scheme of two activated carbons in different proportions at different temperatures

Activated carbon	Subjects	Bleaching temperature (°C)	Dosage of the activated carbon (g)	The proportion of X (%)
X, Y	Crude kojic acid solution of 50 mL	50, 60, 70, 80, 90	0.2	0
X, Y	Crude kojic acid solution of 50 mL	50, 60, 70, 80, 90	0.2	20
X, Y	Crude kojic acid solution of 50 mL	50, 60, 70, 80, 90	0.2	40
X, Y	Crude kojic acid solution of 50 mL	50, 60, 70, 80, 90	0.2	60
X, Y	Crude kojic acid solution of 50 mL	50, 60, 70, 80, 90	0.2	80
X, Y	Crude kojic acid solution of 50 mL	50, 60, 70, 80, 90	0.2	100

35.2.4 Bleaching Methods of the Activated Carbon

Activated carbon is the most commonly used method for decolorizing, which relies on the van der Waals forces to make the pigment adsorb to the surface of the activated carbon. The smaller the particles of the activated carbon are, the greater the surface area and the stronger the adsorption capacity.

There are two important indicators in the kojic acid bleaching process, the decoloration rate, and the kojic acid's final quality.

$$DR = \frac{OD_1 - OD_2}{OD_1} \times 100\,\% \tag{35.1}$$

In the formula:

OD_1 absorption value before bleaching of the solution of kojic acid;
OD_2 absorption value after bleaching of the solution of kojic acid;

Another is kojic acid yield, related to the loss of kojic acid

$$Y = \frac{m_2}{m_1} \times 100\,\% \tag{35.2}$$

In the formula:

m_1 the quality of kojic acid in the solution before bleaching;
m_2 the quality of kojic acid in the solution after bleaching.

35.3 Results and Discussion

35.3.1 Comparison of Different Types of Activated Carbon Decolorization Experiments

Comparison of the experiment can be made from Fig. 35.1: Although the carbon ZX-210's kojic acid yield is up to 98 %, it has almost no bleaching effect on kojic acid, the bleaching rate of ZX-767 activated carbon injection is the highest, it can reach 74 %; the kojic acid rate of medicinal activated carbon ZX-720 is higher, which can reach 92 %. Thus, in order to obtain the optimal ratio combinations we used carbon ZX-767 and ZX-720 in different proportions and at different temperatures to perform the kojic acid decolorization experiments.

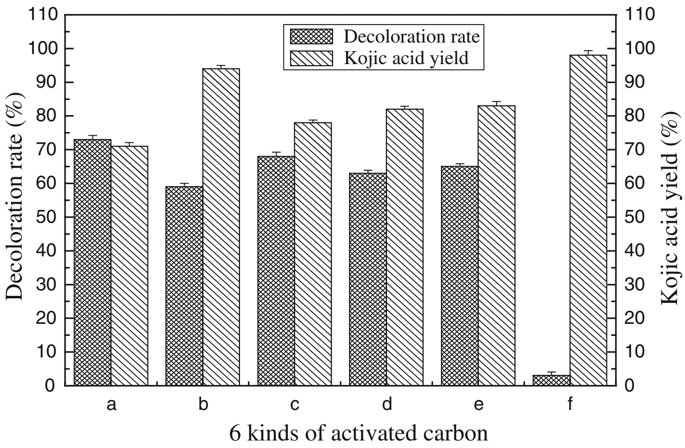

Fig. 35.1 The decolorized result of six kinds of activated carbon. *Note a*, *b*, *c*, *d*, *e*, *g* represent carbon ZX-767, ZX-720, ZXK-AR, ZX-3011, ZX-507, ZX-210

35.3.2 The Combined Ratio of Kojic Acid Bleaching Experiments at Temperature of 50 °C

It can be seen from the experimental results (Fig. 35.2) that at temperature of 50 °C, the combined ratio of: 0.2 g of activated carbon, the 767 is 40 %, the decolorization rate is 74 %, the kojic acid yield is 90.10 %, which is better than any other combination.

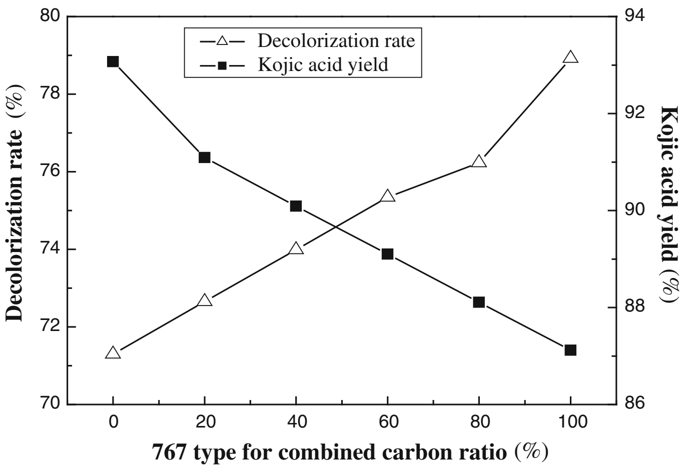

Fig. 35.2 The decolorized result of combined activated carbon at 50 °C

35.3.3 The Combined Ratio of Kojic Acid Bleaching Experiments at Temperature of 60 °C

It can be seen from the experimental results (Fig. 35.3) that at temperature of 60 °C, the combined ratio of: 0.2 g of activated carbon, the 767 is 40 %, the decolorization rate is 75.12 %, the kojic acid yield is 88.04 %, which is better than any other combination.

35.3.4 The Combined Ratio of Kojic Acid Bleaching Experiments at Temperature of 70 °C

It can be seen from the experimental results (Fig. 35.4) that at temperature of 70 °C, the combined ratio of: 0.2 g of activated carbon, the 767 is 20 %, the decolorization rate is 79.84 %, the kojic acid yield is 91.26 %, which is better than any other combination.

35.3.5 The Combined Ratio of Kojic Acid Bleaching Experiments at Temperature of 80 °C

It can be seen from the experimental results (Fig. 35.5) that at temperature of 80 °C, the combined ratio of: 0.2 g of activated carbon, the 767 is 0 %, the decolorization rate is 73.62 %, the kojic acid yield is 94.06 %, which is better than any other combination.

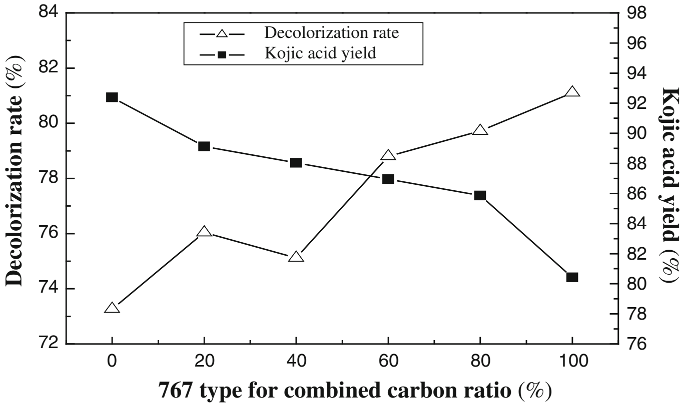

Fig. 35.3 The decolorized result of combined activated carbon at 60 °C

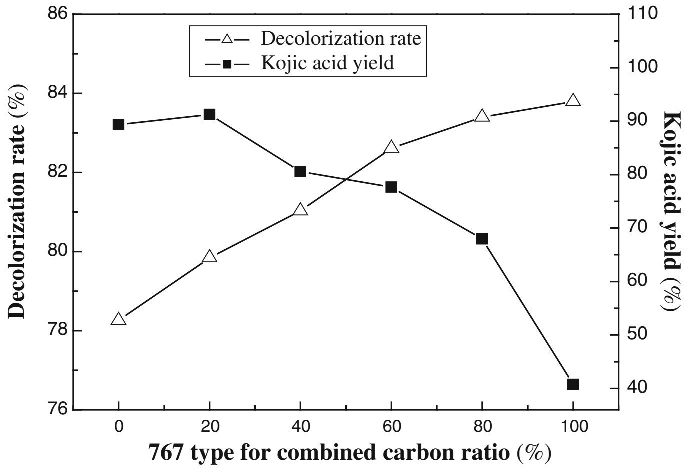

Fig. 35.4 The decolorized result of combined activated carbon at 70 °C

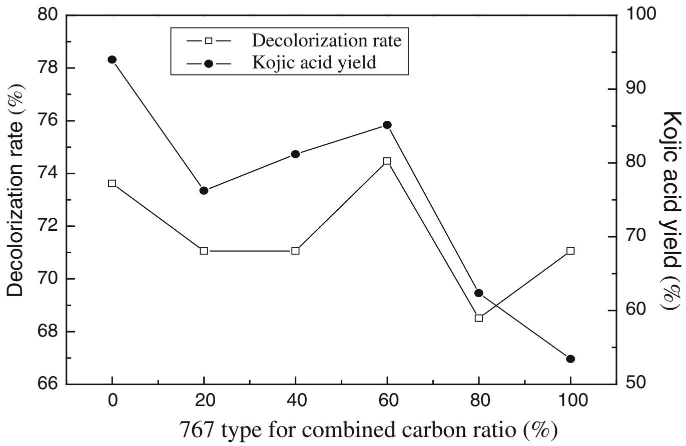

Fig. 35.5 The decolorized result of combined activated carbon at 80 °C

35.3.6 The Combined Ratio of Kojic Acid Bleaching Experiments at Temperature of 90 °C

It can be seen from the experimental results (Fig. 35.6) that at temperature of 90 °C, the combined ratio of: 0.2 g of activated carbon, the 767 is 80 %, the decolorization rate is 79.64 %, the kojic acid yield is 73.16 %, which is better than any other combination.

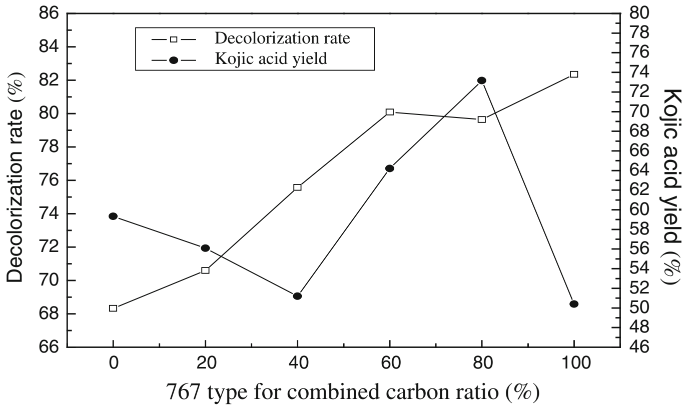

Fig. 35.6 The decolorized result of combined activated carbon at 90 °C

35.4 Conclusion

From the comprehensive comparison of the experimental results, we can see that at temperature of 70 °C, the combined ratio of: 0.2 g of activated carbon, the 767 is 20 %, the decolorization rate is the highest (79.84 %), kojic acid yield is (91.26 %). At temperature of 80 °C, the combined ratio of: 0.2 g of activated carbon, the 720 type activated carbon is (100 %), kojic acid yield is the highest (94.06 %), the decolorization rate is (73.26 %). At temperature of 50 °C, the combined ratio of: 0.2 g of activated carbon, the 767 is 40 %, it required the minimum temperature (low energy consumption), the kojic acid yield is over (90.10 %), the decolorization rate is (74 %) (Table 35.4). Thus, the ratio of the combination of these three have their own advantages. This are the ideal results of the experiments.

Table 35.4 The best proportion of different activated carbons composed at different temperatures

Activated carbon	Temperature (°C)	The amount of activated carbon portfolio (g)	767 The optimum ratio of activated carbon (%)	Decolorization rate (%)	Kojic acid yield (%)
ZX-767, ZX-720	50	0.2	40	74.00	90.10
ZX-767, ZX-720	60	0.2	40	75.12	88.04
ZX-767, ZX-720	70	0.2	20	79.84	91.26
ZX-767, ZX-720	80	0.2	0	73.62	94.06
ZX-767, ZX-720	90	0.2	80	79.64	73.16

Acknowledgment The authors are grateful to Prof. Dongguang Xiao (College of Biotechnology, Tianjin University of Science and Technology) for providing technical assistance.

References

1. Su GC (2005) Study on the inhibition effect of kojic acid on common pollutant bacteria of food. Food Ferment Ind 31(3):47–51
2. Kotani T, Ichimoto I, Tatsumi C et al (1976) Bacteriostatic activities and metal chelation of kojic acid analogs. Agric Biol Chem 40:765–770
3. Lee FH, Boltjes B, William E (1950) Kojic acid as an inhibitor of tubercle bacilli. Am Rev Tuberc 61:38–741
4. Dowd PF (1988) Toxicological and biochemical interactions of the fungal metabolites fusaric acid and kojic acid with xenobiotics in *Heliothis zea* and *Spodoptera frugiperda* (J.E. Smith). Pestic Biochem Physiol 32:123–134
5. Sehgal SS (1976) Effectiveness of kojic acid in inducing sterility in *Trogoderma granarium* everts (*Coleoptera*). Cienc Cultura 28:777–779
6. Huang H (2003) Studies on whitening effect of kojic acid as cosmetic additive. J Xiamen Univ (Nat Sci) 42(5):652–656
7. Zhu XR, Kang JP (2002) Current research and producing of kojic acid and its applying in food and cosmetics industry. Sichuan Food Ferment 38(12):28–31
8. Godfrey A (1998) Production of industrial enzymes and some applications in fermented foods. In: Wood BJB (ed) Microbiology of fermented food, 2nd edn. Springer, New York
9. Burdock GA, Soni MG, Carabin GI (2001) Evaluation of health aspects of kojic acid in food. Reg Toxicol Pharmacol 33:80–101
10. Ariff AB, Rosfarizan M, Herng LS et al (1997) Kinetics and modelling of kojic acid production by *Aspergillus flavus* link in batch fermentation and resuspended cell mycelial. World J Microbiol Biotechnol 13:195–201
11. Rosfarizan M, Ariff AB (2007) Biotransformation of various carbon sources to kojic acid by cell-bound enzyme system of *A. flavus*. Biochem Eng J 35:203–209
12. Buchta K (1982) Organic acids of minor importance. In: Rehm HJ, Reed G, Dellweg HH (eds) Biotechnology: comprehensive treaties, 3rd edn. Federal Republic of Germany, Ingelheim
13. Sun W, Fu YY, Xu ZH (2000) A study of extracting procession of kojic acid. J Wuxi Univ Light Ind 19(5):430–432
14. Zhang YY, Zhang WH, Zhang XJ (1999) Situation of activated carbon research and new product development. Clean Coal Technol 5(3):24–26
15. Liu YN, Shi ZQ, He BL (1993) A study on the decoloring properties of resins. Ion Exch Adsorpt 9(5):429–432

Chapter 36
Effect of Iodine on the Growth and Quality of *Nostoc flagelliforme*

Honglei Fu, Yujie Dai, Yue Han, Lifang Yue, Feng Xia and Shiru Jia

Abstract This study was carried out to evaluate the effect of diverse iodine form-iodide and iodate on the biomass as well as the content of soluble protein, pigment, and iodine in *Nostoc flagelliforme* cells. In our study, tested factors (iodine form-iodide and iodate) significantly influenced the growth and content of soluble protein, pigment, and iodine in *N. flagelliforme* cells. Moreover, results obtained have shown that *N. flagelliforme* cultured with I^- take up greater amounts of iodine than those treated with IO_3^-. Besides, at the initial iodine concentration of 600 mg/L in the form of KI and KIO_3, the biomass of *N. flagelliforme* significantly increased by 2.6 % and decreased by 3.2 %, respectively. In addition, the highest content of soluble protein was, respectively, 2.56 and 2.46 mg/g when the concentration of iodine in the form of iodide and iodate was at a dose of 600 mg/L. With respect to chlorophyll a content, the results of our work have shown that *N. flagelliforme* cells cultured with KI contained higher amounts of chlorophyll a than those treated with KIO_3. All these studies suggest that the introduction of iodine in the form of KI proved to be much more effective in respect to iodine accumulation of *N. flagelliforme* than that of KIO_3.

Keywords Iodine · Bioaccumulation · *Nostoc flagelliforme*

36.1 Introduction

Iodine is an essential micronutrient for humans. It acts as an essential component of thyroid hormones which is of importance for the human metabolism [1]. Iodine deficiency causes many diseases such as endemic goiter, cretinism, fetal

H. Fu · Y. Dai (✉) · Y. Han · L. Yue · F. Xia · S. Jia
Key Laboratory of Industrial Fermentation Microbiology (Tianjin University of Science and Technology), Ministry of Education, College of Bioengineering, Tianjin University of Science and Technology, Tianjin 300457, People's Republic of China
e-mail: yjdai@126.com

T.-C. Zhang and M. Nakajima (eds.), *Advances in Applied Biotechnology*,
Lecture Notes in Electrical Engineering 333, DOI 10.1007/978-3-662-46318-5_36

abnormalities, and Kaschin-Beck disease, the last one being related to simultaneous deficiency of iodine and selenium [2, 3]. Almost 35.2 % of the global population has inadequate iodine nutrition [4] and it has been calculated that 1.6 billion people are at a risk of iodine deficiency [5]. In order to conquer iodine deficiency in the human population, biofortification of microalgae with iodine can be an alternative method of introducing this microelement into the human diet.

Iwamoto and Shiraiwa [6] found that six species of microalgae such as *Bellerochea sp*., *Chlamydomonas reinhardtii*, *Dunaliella tertiolecta*, *Isochrysis galbana*, *Skeletonema costatum*, and *Tetraselmis sp*. exhibited high iodine tolerance. Additionally, *E. huxleyi* was observed to accumulate 10 times more iodine than that found in seawater, indicating that microalgae can be used in iodine-related industries for extracting iodine from seawater and iodine-containing wastewater. The relationship between iodine and microalgae was investigated by some studies. Some researches on iodine in microalgae revealed that microalgae participate in the iodate (IO_3^-)-to-iodide (I^-) speciation and emit iodine as monoiodomethane into the marine environment [7–9]. Moreover, microalgae are supposed to function in the global iodine cycle [10, 11]. All these studies strongly suggest that the physiologic characteristics of microalgae are closely associated with their iodine usage.

Nostoc flagelliforme, an edible terrestrial filamentous cyanobacterium, has been famous for its food and herbal value for more than 400 years [12]. Cultivation of free cells isolated from colonial filaments in liquid medium has also been performed for reasons of low growth rate of *N. flagelliforme* under natural conditions and the great demand from the industry [13, 14]. So the increased cell growth rate in the liquid culture led to a new technique for the culture of *N. flagelliforme*. Some studies found that *N. flagelliforme* was a good candidate for heavy metal ions enrichment [15]. However, very limited information on the iodine-enrichment is available. The aim of this work is to study the effect of iodine on the growth and quality of *N. flagelliforme*, so as to provide basic data for the mechanism of iodine uptake by cabbage and an effective way to reduce iodine deficiency disorders.

36.2 Materials and Methods

36.2.1 Materials and Experimental Design

The *N. flagelliforme* cells used in liquid suspension cultures were obtained from the Tianjin Key Lab of Industrial Microbiology (Tianjin, China). The cells were cultured in BG11 medium with and without iodine in 500-mL shake flasks containing 200 mL medium at 25 °C under continuous illumination of 60 μmol photon/(m^2 s). The solution was formulated by adding iodine in the form of iodide (I^-) or iodate (IO_3^-) at five concentrations (200, 400, 600, 800, 1000 mg/L) to BG11 medium. The formula without iodine served as control.

36.2.2 Sampling and Chemical Analyses

The cell growth was measured by weighing the harvested samples that had been previously dried to a constant weight at 80 °C [16]. The total iodine of the dried samples were quantified by the iodide-starch photometry method [17] following the pretreatment of oxygen flask combustion method [18]. Methanol-soluble pigments (chlorophyll a and carotenoids) were extracted in methanol at 4 °C in the dark and the amount was calculated according to Li et al. [19]. The soluble protein was extracted through the method of ultrasonication and the contents were determined via the Bradford method [20].

36.2.3 Statistical Analysis

Obtained results were statistically verified using ANOVA module of SPSS Statistics 19.0 program for significance level $P < 0.05$. In case of significant changes, homogeneous groups were distinguished on the basis of Duncan test.

36.3 Results and Discussion

36.3.1 Effect of Iodine on the Growth of *N. flagelliforme*

As shown in Fig. 36.1, biomass of *N. flagelliforme* increases with iodine concentration in the culture solution when the concentration remains low, but decreases with the increase in concentration. These results demonstrate that iodine concentrations affect algal growth, including iodine-induced stimulation and inhibition. Moreover, the growth of *N. flagelliforme* was inhibited when the initial potassium iodide in the medium was higher than 600 mg/L (Fig. 36.1a), while the growth of *N. flagelliforme* was inhibited when the initial potassium iodate in the medium was higher than 200 mg/L (Fig. 36.1b), indicating that iodide shows much less toxicity to the *N. flagelliforme* than iodate. Furthermore, at the exogenous iodine level of 200 mg/L, the biomass of *N. flagelliforme* was significantly increased compared with the control group cultivated without additive iodine (Fig. 36.1c, d). Besides, at the initial iodine concentration of 400 and 600 mg/L in the form of KI, the biomass of *N. flagelliforme* significantly increased by 5.1 and 2.6 %, respectively, compared with the control groups cultivated without exogenous iodine addition (Fig. 36.1c). In addition, the biomass of *N. flagelliforme* was correspondingly decreased with the increase in the concentration of iodine in both forms, suggesting that there was a negative correlation between biomass yield and initial iodine addition.

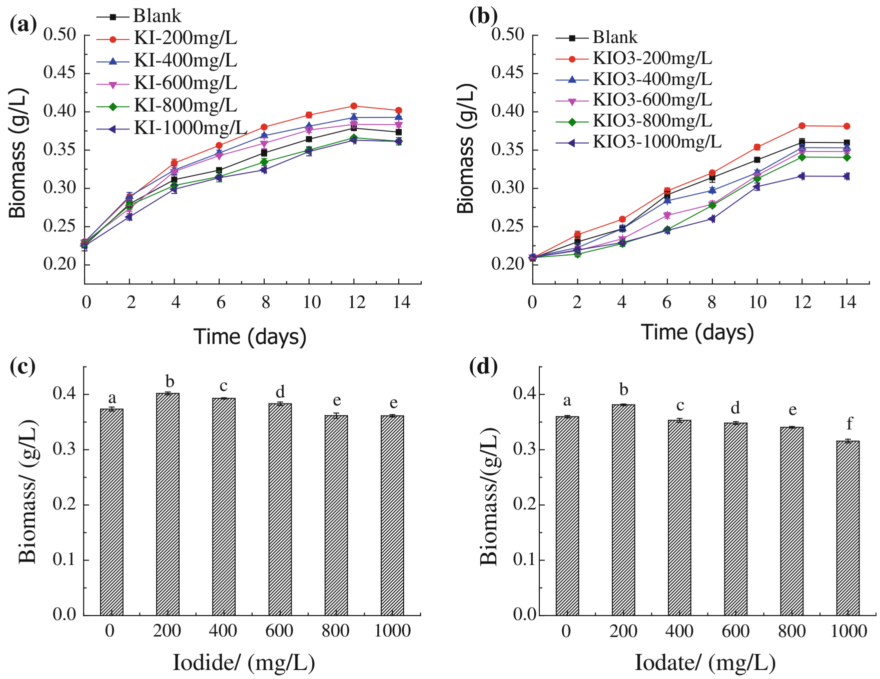

Fig. 36.1 Effect of iodine on the growth of *N. flagelliforme* in the BG11 medium after adding potassium iodide (**a**) or potassium iodate (**b**). Effect of iodine on biomass production (g/L) of *N. flagelliforme* in the BG11 medium after adding potassium iodide (**c**) or potassium iodate (**d**) at the end of the cultivation. Data with the same letters are not significantly different ($P > 0.05$)

36.3.2 Effect of Iodine on the Content of Pigments and Soluble Protein of N. flagelliforme

Particular attention should be given to the fact that a significant increase in the amount of soluble protein was detected in *N. flagelliforme* grown in the presence of KI within the range of 200–1,000 mg/L and KIO_3 within the range of 200–800 mg/L (Table 36.1). Moreover, the content of soluble protein reached the highest point when the iodine concentration was 600 mg/L. The possible explanation for the obtained results could be that some protein synthesis was promoted during the process of iodine accumulation. Fu and Xie [21] hold another view that iodine is the cofactor or activator in the synthesis of some amino acids.

In this study, a higher content of pigment was found in *N. flagelliforme* treated with exogenous iodine (KI and KIO_3) compared with the control groups cultivated without exogenous iodine addition (Table 36.1). It should be mentioned that *N. flagelliforme* cells cultured with KI contained more of chlorophyll a than those treated with KIO_3. However, there was no observed difference in carotenoid after cultivation of *N. flagelliforme* treated with KI and KIO_3.

Table 36.1 Soluble protein and pigment contents of *N. flagelliforme*

Treatments	Iodine concentration in the medium (mg/L)	Soluble protein (mg/g)	Chlorophyll a (mg/L)	Carotenoid (mg/L)	Carotenoid: chlorophyll a
Exogenous iodine in the form of iodide	–	2.22 ± 0.01 a	3.36 ± 0.03 a	0.87 ± 0.01 a	0.259
	200	2.40 ± 0.03 b	3.64 ± 0.02 bc	0.95 ± 0.01 b	0.260
	400	2.41 ± 0.04 b	3.71 ± 0.04 c	0.99 ± 0.03 bc	0.267
	600	2.56 ± 0.01 c	3.81 ± 0.02 d	1.02 ± 0.06 c	0.269
	800	2.47 ± 0.04 d	3.68 ± 0.06 bc	1.02 ± 0.06 bc	0.276
	1,000	2.33 ± 0.03 e	3.61 ± 0.06 b	1.01 ± 0.01 bc	0.279
Exogenous iodine in the form of iodate	–	2.22 ± 0.01 a	3.36 ± 0.03 a	0.87 ± 0.01 a	0.259
	200	2.39 ± 0.01 b	3.55 ± 0.05 bc	0.92 ± 0.02 b	0.260
	400	2.40 ± 0.06 b	3.68 ± 0.06 d	0.99 ± 0.01 c	0.268
	600	2.46 ± 0.04 b	3.76 ± 0.01 e	1.02 ± 0.04 c	0.271
	800	2.42 ± 0.05 b	3.61 ± 0.03 cd	1.00 ± 0.04 c	0.278
	1,000	2.26 ± 0.01 a	3.47 ± 0.05 b	0.97 ± 0.01 c	0.281

Data with the same letters are not significantly different ($P > 0.05$)

The ratio of carotenoid: chlorophyll a has long been considered a valuable parameter for assessing adverse environmental conditions [22]. As shown in Table 36.1, there was a gradual increase in the ratio of carotenoid: chlorophyll a of *N. flagelliforme* exposed to iodine (KI and KIO_3). It should be emphasized that iodine addition might result in higher increase in carotenoid synthesis compared with chlorophyll a. From these observations, the high ratio of carotenoid: chlorophyll a may be related to the reduction of biomass in excess iodine doses.

36.3.3 Accumulation of Iodine in N. flagelliforme Cells

In general, iodine contents in the cells of *N. flagelliforme* increase significantly with the amount of applied iodine in the medium, however, there is a turning point at the concentration of 600 mg/L in the solution (Fig. 36.2); below this point iodine contents in the cells of *N. flagelliforme* increase with the initial iodine concentration, while above this point this phenomenon is the opposite. It is supposed that the toxic effect of the high iodine concentration on the growth of *N. flagelliforme* results in a change in the iodine contents in the cells of *N. flagelliforme* in response to the increase in iodine concentration in the culture solution.

Studies have shown that *Spirulina maxima* cultured with iodine in the form of I^- take up greater amounts of iodine than *S. maxima* treated with IO_3^- [23]. This relation has been already confirmed in our study with cultivation of *N. flagelliforme*, which is another kind of blue-green microalga. Iodine contents of *N. flagelliforme*

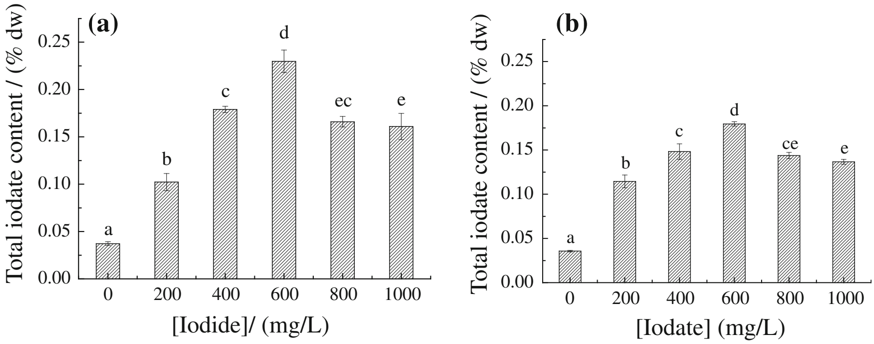

Fig. 36.2 Variation in iodine content in the cells of *N. flagelliforme* as a function of the additive concentration of exogenous potassium iodide (**a**) or potassium iodate (**b**) in the medium. Data with the same letters are not significantly different ($P > 0.05$)

cultured with the initial iodine concentration of 600 mg/L in the form of KI could be increased to 6.18 times as high as that of control (Fig. 36.2a), while the contents of those treated with the initial iodine concentration of 600 mg/L in the form of KIO_3 could be raised to 5.04 times as high as that of control (Fig. 36.2b). It is observed that a higher accumulation of iodine was found after KI application rather than KIO_3. Introduction of iodine in the form of KI proved to be much more effective in respect to iodine accumulation of *N. flagelliforme* than that of KIO_3.

36.4 Conclusions

The results of this study show that low concentration of iodine accelerates the growth of *N. flagelliforme* and raises the content of soluble protein, pigment, and iodine. 600 mg/L is found to be the optimum concentration of iodine in the cultivated medium, while the positive effects turn into toxic effects when the concentration exceeds 800 mg/L. In addition, more iodine was accumulated in *N. flagelliforme* cells grown in KI than in those grown in KIO_3. Data obtained demonstrated that the content of soluble and pigment in *N. flagelliforme* cells cultured with KI contained more than those treated with KIO_3. All these studies reveal that *N. flagelliforme* can be served as an alternative to accumulate this element and the introduction of iodine in the form of KI proved to be much more effective in respect to iodine accumulation of *N. flagelliforme* than that of KIO_3.

Acknowledgments This work was supported by the National Natural Science Foundation of China under Grant number 31271809.

References

1. Rose NR, Bonita R, Burek CL (2002) Iodine: an environmental trigger of thyroiditis. Autoimmun Rev 1:97–103
2. DeLong GR, Leslie PW, Wang SH et al (1997) Effect on infant mortality of iodination of irrigation water in a severely iodine-deficient area of China. Lancet 350:771–773
3. Nian FL, Jie T, Jian MB (2004) Geochemical environment and health problems in China. Environ Geochem Health 26(1):81–88
4. Winger RJ, Konig J, House DA (2008) Technological issues associated with iodine fortification of foods. Trends Food Sci Technol 19:94–101
5. Huang YZ, Zhu YG, Hu Y et al (2003) Iodine in soil–plant systems and prevention of iodine deficiency disorders. Ecol Environ 12:228–231
6. Iwamoto K, Shiraiwa Y (2012) Characterization of intracellular iodine accumulation by iodine-tolerant microalgae. Procedia Environ Sci 15:34–42
7. Butler DCV, Smith JD, Fisher NS (1981) Influence of phytoplankton on iodine speciation in seawater. Limnol Oceanogr 26:382–386
8. Itoh N, Tsujita M, Ando T et al (1996) Formation and emission of monohalomethanes from marine algae. Phytochemistry 45:67–73
9. Wong GTF, Piumsomboon AU, Dunstan WM (2002) The transformation of iodate to iodide in marine phytoplankton cultures. Mar Ecol Prog Ser 237:27–39
10. Moisan TA, Dunstan WM, Udomkit A et al (1994) The uptake of iodate by marine phytoplankton. J Phycol 30:580–587
11. Muramatsu Y, Fehn U, Yoshida S (2001) Recycling of iodine in fore-arc areas: evidence from the iodine brines in Chiba, Japan. Earth Plant Sci Lett 192:583–593
12. Gao KS (1998) Chinese studies on edible blue-green alga, Nostoc flagelliforme: a review. J Appl Phycol 10:37–49
13. Su JY (2006) Study on the photoautotrophic cultivation of Nostoc flagelliforme cells. Dissertation, Tianjin University of Science and Technology, Tianjin, China
14. Jia SR, Su JY, Qiao CS (2005) Nostoc flagelliforme cells cultivation and its products. Chinese patent ZL 03119101
15. Guo JY, Shi MK, Zhao YL et al (2013) Response of Nostoc flagelliforme cell to Cu^{2+}, Cr^{2+} and Pb^{2+} stress. Acta Microbiol Sin 53(6):553–560
16. Su JY, Jia SR, Chen XF et al (2008) Morphology, cell growth, and polysaccharide production of Nostoc flagelliforme in liquid suspension culture at different agitation rates. J Appl Phycol 20:213–217
17. Liu YJ (1997) Spectrophotometric determination of iodine in plant. Yunnan Chem Technol 4:40–43
18. China Pharmacopoeia Committee (2010) Pharmacopoeia of the People's Republic of China, vol II, p 46
19. Li QY, Li AF, Zhang CW (2012) The method of extraction and determination of pigment in Eustigmatophyceae. Ecol Sci 31(3):278–283
20. Bradford MM (1976) A rapid and sensitive method for the quantitation of microgram quantities of protein utilizing the principle of protein dye binding. Anal Biochem 72:248–254
21. Fu JH, Xie JJ (1997) Amino acid contents in the iodine enriched *Ganoderma lucidum*. Mycosystema 16(1):47–51
22. Rai LC, Gaur JP, Kumar HD (1981) Protective effects of certain environmental factors on the toxicity of zinc, mercury and methylmercury to *Chlorella vulgaris*. Environ Res 25:250–259
23. Yang XN (2002) Studies on physiological and biochemical effect of iodine on Spirulina maxima and cultivation of iodine-rich Spirulina. Xiamen University, Xiamen

Chapter 37
The Replacement of Phe28 by Ser Enhances the Stability of the GLP-1 Analog During Fermentation

Peng-Yan Li, Xue-Gang Luo, Qian Li, Wei Zhao, Hao Zhou and Tong-Cun Zhang

Abstract Glucagon-like peptide-1 (GLP-1) is an incretin, which can effectively lower blood glucose levels, increase insulin secretion, and improve insulin sensitivity in patients with diabetes. Therefore, it is a potent endogenous insulin-stimulating hormone. Unfortunately, since GLP-1 can be degraded by the enzyme DPP-IV and NEP 24.11, its therapeutic benefit and fermentation yield are limited by the instability. Previous study has shown that replacement of the Lys34 with Arg could enhance the stability of GLP-1 in the plasma. In this study, to further improve the stability of the GLP-1, an additional mutation, replacement of Phe28 by Ser, was constructed, and then the protein was expressed in the recombinant *Pichia pastoris*, and analyzed by HPLC. The results show that this mutation could improve the stability of GLP-1 during fermentation.

Keywords GLP-1 · Degradation · Gene modification · Stability

P.-Y. Li and X.-G. Luo—Co-first authors.

P.-Y. Li · X.-G. Luo (✉) · Q. Li · H. Zhou · T.-C. Zhang (✉)
Key Laboratory of Industrial Fermentation Microbiology, Ministry of Education and Tianjin City, College of Biotechnology, Tianjin University of Science and Technology, Tianjin 300457, People's Republic of China
e-mail: luoxuegang@tust.edu.cn

T.-C. Zhang
e-mail: tony@tust.edu.cn

W. Zhao
Chia Tai Tianqing Pharmaceutical Group Co., Ltd, Nanjing 210023, People's Republic of China

T.-C. Zhang and M. Nakajima (eds.), *Advances in Applied Biotechnology*, Lecture Notes in Electrical Engineering 333, DOI 10.1007/978-3-662-46318-5_37

37.1 Introduction

Glucagon-like peptide-1 (GLP-1) is a 31 amino-acid polypeptide hormone produced by intestinal L-cells in response to nutrient ingestion [1]. Effects of GLP-1 can promote glucose-mediated insulin secretion, lower plasma glucagon, delay gastric emptying, stimulate β-cell growth, and insulin secretion in a glucose-dependent manner, and therefore help maintain glucose homeostasis [2, 3]. In addition, GLP-1 has also been shown to reduce body weight [4, 5], which is favorable for many people with type 2 diabetes. Hence, GLP-1-based therapies are becoming increasingly attractive for the treatment of type 2 diabetes [6, 7].

However, native GLP-1 is not a viable therapeutic agent because it has a short half-life of <2 min, resulting from rapid degradation by the enzyme dipeptidyl peptidase IV (DPP-IV) and rapid renal elimination [8]. GLP-1(7–36) is rapidly metabolized by DPP-IV to the major metabolite GLP-1(9–36) amide, often thought to be inactive. Besides, the neutral endopeptidase NEP 24.11 (also known as neprilysin, CD10 and CALA antigen [9]) is another endoprotease implicated in GLP-1 degradation. NEP 24.11 cleaves GLP-1 at several internal sites amino-proximal to bulky hydrophobic amino acids such as phenylalanine at residue 28 and leucine at residue 32 (Fig. 37.1) [10]. Therefore, an intracellular form of NEP 24.11, or an endopeptidase with similar specificity, might be responsible for internal

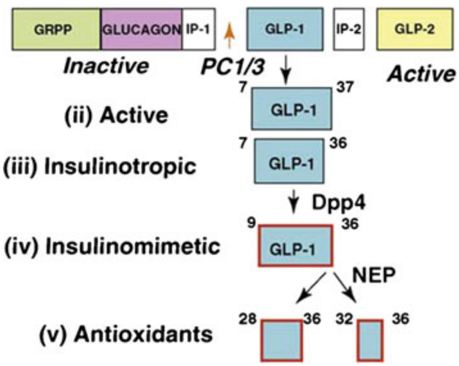

Fig. 37.1 The schematic diagram for the production and degradation of GLP-1. The prohormone convertases PC1/3 selectively cleave proglucagon to produce GLPs. The insulinotropic GLP-1 peptides consist of GLP-1(7–36) amide and a glycine-extended form GLP-1(7–37). They are released from the intestine in response to feeding and stimulate glucose-dependent insulin secretion. After their secretion, these insulinotropic GLP-1s are rapidly converted to insulinomimetic hormones GLP-1(9–36) amide and GLP-1(9–37) by removal of two N-terminal amino acids by Dpp4, and then might be further cleaved by NEP to produce small C-terminal nonapeptide GLP-1(28–36) and pentapeptide GLP-1(32–36), and the corresponding decapeptide GLP-1(28–37) and hexapeptide GLP-1(32–37). It is proposed that these small peptides might target mitochondria and modulate oxidative phosphorylation, glucose and fatty acid metabolism, and energy expenditure, resulting in attenuation of oxidative stress (ROS formation) and promotion of cell survival

cleavage of GLP-1. To solve these problems, some pharmacological mimetics have been developed with improved stability [11, 12], including of the analogs of GLP-1 with extended or truncated N- or C-terminal and analogs with exchanged residues in positions Gly10, Asp15, Val16, Ser17, Ser18, Glu21, Phe27, and Trp31 [13].

Previous study has shown that replacement of the Lys34 with Arg could enhance the stability of GLP-1 in the plasma [14]. In this study, to further improve the stability of GLP-1, an additional mutation, replacement of Phe28 with the Ser, was constructed, and then they were expressed in the recombinant *Pichia pastoris*, and analyzed by HPLC.

37.2 Materials and Methods

37.2.1 Strain and Plasmids

The methylotrophic yeast *P. pastoris* strain GS115 (deficient in histidinol dehydrogenase activity and yps1^{-}, His^{-}) in this study was offered by Shuqing Chen from Zhejiang University. The host strain *E. coli* DH5α and plasmid pPIC9K in this study were maintained in our laboratory.

37.2.2 Enzymes and Reagents

The restriction endonucleases, T4 DNA ligase, Pfu DNA polymerase, Taq DNA polymerase, and agar gel DNA extraction kit were purchased from Takara (Dalian, China). Primer synthesis and DNA sequencing were performed by Invitrogen (Carlsbad, CA, USA). All other reagents were purchased from local companies in Tianjin of China.

37.2.3 Construction of pPIC9K GLP-1 Analog-1 and pPIC9K GLP-1 Analog-2

Plasmid for the expression of GLP-1 analogs (pPIC9K GLP-1 analog-1 and pPIC9K GLP-1 analog-2) were constructed as shown in Fig. 37.2. The GLP-1 analog gene was obtained from the coding DNA of GLP-1 and optimized based on the codon bias of *P. pastoris* GS115. The recombination genes were synthesized with overlapped PCR. First, GLP-1 analog gene fragments were obtained by using primers P1/F, P1/Z, and P1/R (Table 37.1). Second, the product in step was further extended to get the full length of GLP-1 analogs with the primers of P2/F and P2/R.

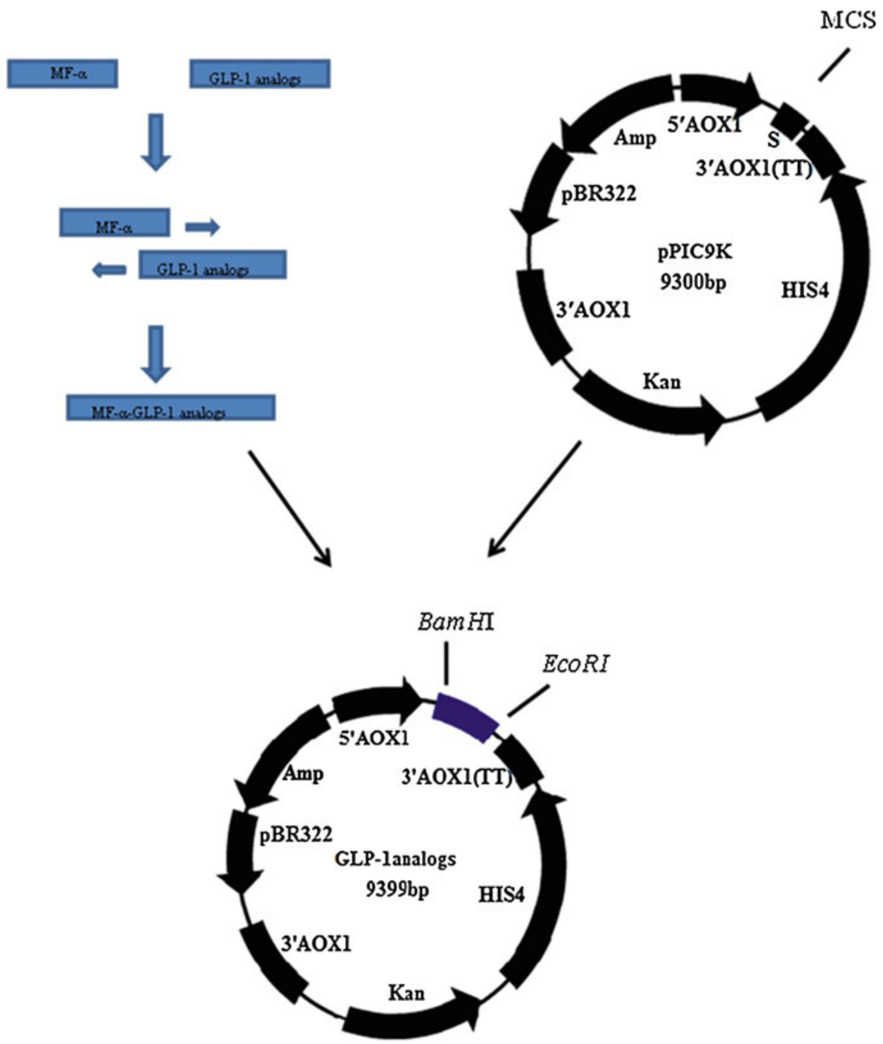

Fig. 37.2 Construction of the plasmid pPIC9K GLP-1 analogs

Third, the α-factor signal sequence was amplified from the pPIC9K plasmid using the primers of P3/F and P3/R. Finally, the α-factor signal sequence was ligated with the GLP-1 analog by PCR using the products of the second and third steps as templates and the primers of P4/F and P4/R. The final PCR products were digested by *Bam*HI and *Eco*RI and then inserted into the pPIC9K vector, generating the recombinant plasmid pPIC9K-GLP-1 analog-1 (K34R) and pPIC9K-GLP-1 analog-2 (K34R/F28S).

Table 37.1 Primers used for construction of pPIC9K GLP-1 analogs

Primer name	Primer sequence (5′–3′)
P1/F	CCGCTCGAGAAAAGACACGCTGAGGGTACTTTCACTTCCGACGTTTCCTCC (*Xho*I)
P1/Z	GCGATGGACTCCTTAGCAGCTTGACCCTCCAAGTAGGAGGAAACGTCGGA
P1/R	CTAGTCTAGATTAACCTCTACCTCTAACCAACCAAGCGAT***GGA***CTCCTTA (*Xba*I)
P2/F	GTATCTCTCGAGAAAAGACACGCTGAGGGTACT
P2/R	GCCGAATTCTTATTAACCTCTACCTCTAAC (*Eco*RI)
P3/F	CGCGGATCCAAACGATGAGATTTCCTTC (*Bam*HI)
P3/R	AGTACCCTCAGCGTGTCTTTTCTCGAGAGATAC
P4/F	AGCGGATCCAAACGATGAGATTTCCTTC (*Bam*HI)
P4/R	GCCGAATTCTTATTAACCTCTACCTCTAACCAACCAAGCGAT***GAA***CTCC (*Eco*RI)

The letters in italic and bold are the mutated gene. GGA was replaced by GAA

37.2.4 Transformation and Screening for Multicopy Transformants by G418 Selection

To obtain the recombinant yeast strain of GLP-1 analogs, *P. pastoris* GS115 was transformed by electroporation at 1.5 kV with *Sal*I-cut fragment of pPIC9K-GLP-1-analogs. The cells were plated on MD His-plates for 3–5 days at 30 °C. Single colonies from the MD plate were carefully removed under sterile conditions and patched to YPD plates containing different concentrations of G418 (0.5, 1.0, 2.0, 3.0 or 4.0 mg/mL) and incubated for 3–5 days at 30 °C in order to select multicopy transformants. The transformant with the fastest growth rate on YPD plates containing the highest concentration of G418 was screened and identified. PCR amplification was performed to confirm whether the gene of GLP-1 was integrated into the *P. pastoris* GS115 genome, according to the specifications of the Multicopy Pichia Expression Kit.

37.2.5 Expression of the Recombinant Protein

The transformant was inoculated into a 250 mL baffled Erlenmeyer flask with 50 mL of buffered minimal glycerol medium (BMGY, 100 mM potassium phosphate, pH 6.0, 1.34 % yeast nitrogen base (YNB), 0.002 % biotin and 1 % glycerol) and was grown at 30 °C overnight with vigorous agitation at 220 rpm. When the optical density (OD_{600}) reached 5.0, the cells were collected by centrifugation at 12,000 rpm for 10 min. The cell pellet was resuspended in BMMY medium

(BMGY with 0.5 % methanol instead of 1 % glycerol) at a starting OD_{600}. Methanol, as an inducer, was added to a final concentration of 0.5 % every 24 h. Samples were collected for analysis after 48 h.

37.2.6 HPLC Analysis

After lyophilization and dissolution of the samples in 1 mL PBS for 10 mL supernatant, analytical HPLC was performed on a Jupiter 5u C18 300A with solvents A (11.5 g ammonium diacid phosphate in 900 mL water and 100 mL acetonitrile, pH 3.7) and B (960 mL acetonitrile in 270 mL water) at a flow rate of 1.0 mL/min. The peptides were eluted with a linear gradient of solvent B from rate of 20–60 % for 30 min and 20 % solvent B eluted for 10 min.

37.3 Results

37.3.1 Construction of the GLP-1 Analogs Recombinant Plasmid

The recombinant yeast *P. pastoris* GS115 strains containing pPIC9K GLP-1 analog-1 and pPIC9K GLP-1 analog-2 used for expressing were constructed. To secretly express the authentic forms of the peptide, the genes of GLP-1 analogs were ligated seamlessly into the downstream of α-factor signal sequence in pPIC9K vector. The results of restriction enzyme digestion and DNA sequencing showed that the expression vectors of two GLP-1 analogs were both constructed successfully (Fig. 37.3).

37.3.2 Establishment of GLP-1 Analogs Recombinant Yeast Strain

Following amplification in the *E. coli* DH5α strain, the recombinant plasmids were linearized with *Sal*I and transformed into *P. pastoris* GS115. After screening, the genomic DNA of the potential positive clones was extracted and PCR was performed to detect the integration of the extraneous gene. As shown in Fig. 37.4, the correct band could be observed in Lane 1, indicating that the target gene has been integrated into the genome of recombinant strains.

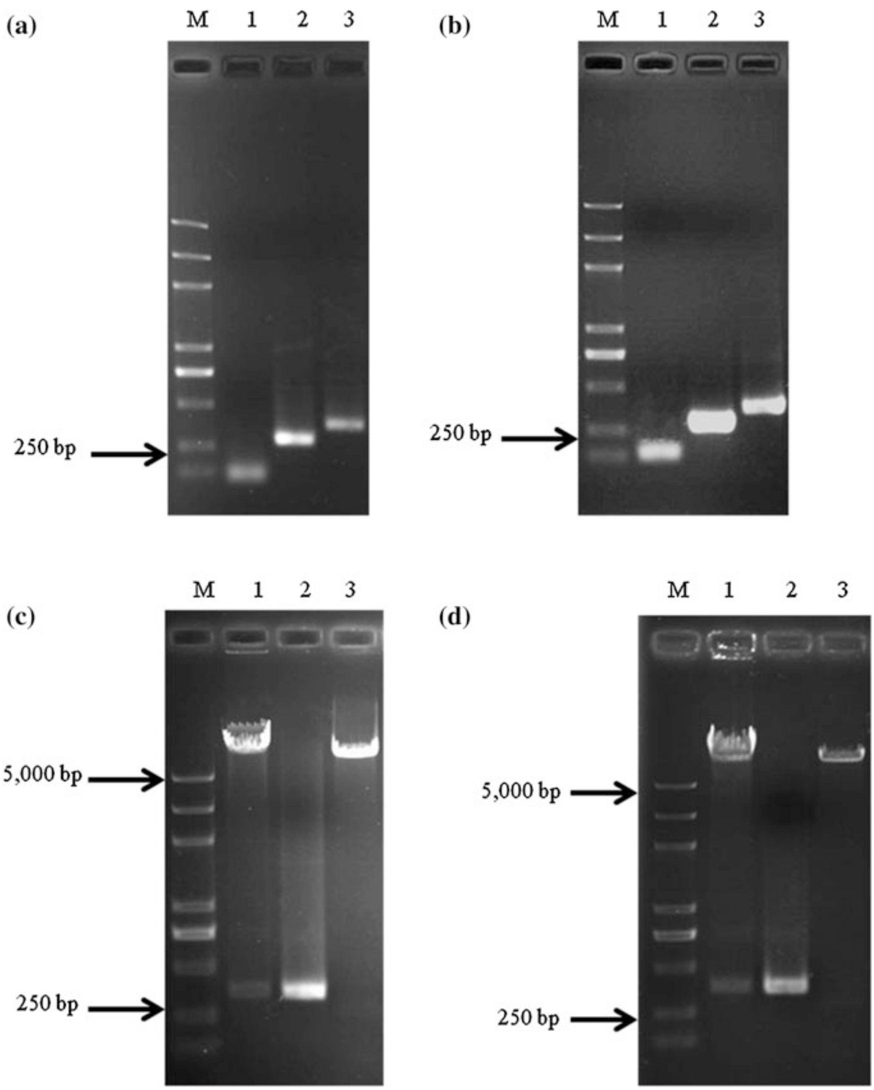

Fig. 37.3 Construction of recombinant plasmid pPIC9K-GLP-1-analogs. **a** The PCR products during the amplification of GLP-1 analog-1. **b** The PCR products during the amplification of GLP-1 analog-2. *Lane M* DNA ladder marker; *Lane 1* the PCR product of GLP-1 analog; *Lane 2* the PCR product of α-factor signal sequence; *Lane 3* the PCR product of α-factor signal sequence fused with GLP-1 analogs. **c** Identification of recombinant plasmid pPIC9K-GLP-1-analog-1. **d** Identification of recombinant plasmids pPIC9K-GLP-1-analog-2. *Lane M* DNA ladder marker; *Lane 1* recombinant plasmid pPIC9K-GLP-1-analogs digested by *Eco*RI and *Bam*HI; *Lane 2* the PCR product; *Lane 3* the vector pPIC9K digested by *Eco*RI and *Bam*HI

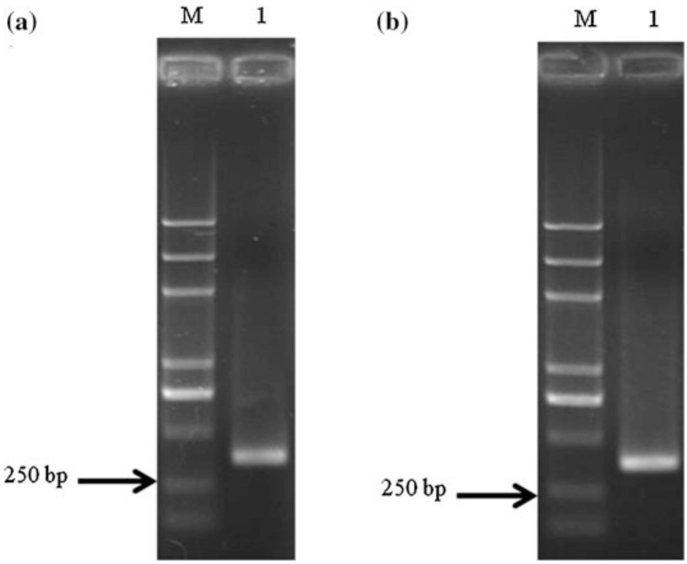

Fig. 37.4 Analysis of integration of GLP-1 analogs in the genome of *Pichia pastoris* GS115. **a** The analysis of the integration of GLP-1 analog-1. **b** The analysis of the integration of GLP-1 analog-2. *Lane M* DNA ladder marker; *Lane 1* the PCR product of GLP-1 analog gene

37.3.3 Analysis of Recombinant GLP-1 Analog-1 and GLP-1 Analog-2 Protein

Expression of the GLP-1 analog gene was induced by the activation of AOX1 promoter with methanol. To confirm GLP-1 analog protein, the purified protein was analyzed by HPLC. As shown in Fig. 37.5, the results showed that the recombinant GLP-1 analog-2 could be detected in the supernatant of fermented broth, whereas

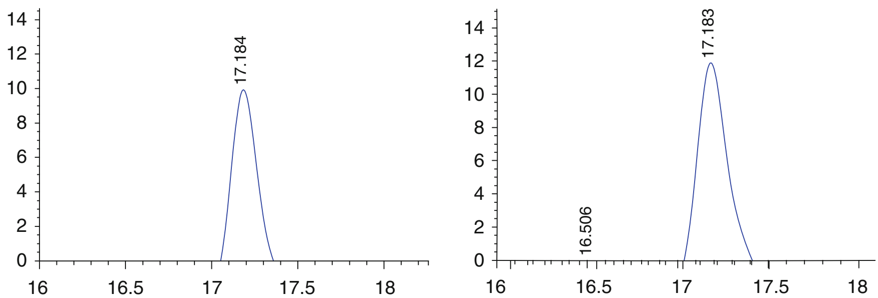

Fig. 37.5 HPLC results of GLP-1 analog proteins. **a** The standard sample; **b** the recombinant GLP-1 analog-2 product

the GLP-1 analog-1 could not be found, indicating that replacement of the 28 amino acid phenylalanine by serine could improve the stability of GLP-1(7–36) amide.

37.4 Conclusion

GLP-1 can be degraded by the action of DPP-IV in vitro and in vivo. In addition, similar to Dpp4, NEP 24.11 is currently considered to function as another degrading enzyme for the destruction and disposal of GLP-1 [10, 15]. Such degradation could not only limit the clinical use of GLP-1, but also hinder the fermented production of this drug. In this study, two mutated GLP-1 analogs which have K34R and K34R/F28S replacements, respectively, were successfully constructed and stably transformed into yeast strains. Using HPLC analysis, we found that compared with K34R mutation, the additional replacement of Phe28 with Ser could significantly further increase the stability of GLP-1.

References

1. Mari A (2007) Effects of the long-acting human glucagon-like peptide-1 analog liraglutide on beta-cell function in normal living conditions. Diab Care 30:2032–2033
2. Russell-Jones D (2009) Molecular, pharmacological and clinical aspects of liraglutide, a once-daily human GLP-1 analogue. Mol Cell Endocrinol 297:137–140
3. Drucker D (2006) The biology of incretin hormones. Cell Metab 3:153–165
4. Nyström T, Gutniak M, Zhang Q, Zhang F, Holst J et al (2004) Effects of glucagon-like peptide-1 on endothelial function in type 2 diabetes patients with stable coronary artery disease. Am J Physiol Endocrinol 287:E1209–E1215
5. Egan JM (2002) Glucagon-like peptide-1 augments insulin mediated glucose uptake in the obese state. J Clin Endocrinol Metab 87:3768–3773
6. Meier JJ (2004) Secretion, degradation, and elimination of glucagon-like peptide 1 and gastric inhibitory polypeptide in patients with chronic renal insufficiency and healthy control subjects. Diabetes 53:654–662
7. Agerso H, Vicini P (2003) Pharmacodynamics of NN2211, a novel long acting GLP-1 derivative. Eur J Pharm Sci 19:141–150
8. Elahi D (2008) Glucagon-like peptide-1 (9-36) amide, cleavage product of glucagon-like peptide-1 (7-36) is a glucoregulatory peptide. Obesity 16:1501–1509
9. Lueking A, Holz C, Gotthold C, Lehrach H, Cahill D (2000) A system for dual protein expression in Pichia pastoris and Escherichia coli. Protein Expr Purif 20:372–378
10. Koganesawa N, Aizawa T, Masaki K, Matsuura A, Nimori T, Bando H, Kawano K, Nitta K (2001) Construction of an expression system of insect lysozyme lacking thermal stability: the effect of selection of signal sequence on level of expression in the Pichia pastoris expression system. Protein Eng 14:705–710
11. Degn KB, Juhl CB, Sturis J et al (2004) One week's treatment with the long-acting glucagon-like peptide 1 derivative NN2211 markedly improves 24-h glycemia and alpha- and beta-cell function and reduces endogenous glucose release in patients with type 2 diabetes. Diabetes 53 (5):1187–1194

12. Niswender K, Pi-Sunyer X, Buse J, Jensen K, Toft A et al (2013) Weight change with liraglutide and comparator therapies: an analysis of seven phase 3 trials from the liraglutide diabetes development programme. Diab Obes Metab 15:42–54
13. Tomas E, Habener JF (2010) Insulin-like actions of glucagon-like peptide-1: a dual receptor hypothesis. Trends Endocrinol Metab 21(2):59–67
14. Cuthbertson D, Irwin A, Gardner C, Daousi C, Purewal T et al (2012) Improved glycaemia correlates with liver fat reduction in obese, type 2 diabetes, patients given glucagon-like peptide-1 (GLP-1) receptor agonists. PLoS ONE 7:e50117
15. Woo JH, Liu YY, Mathias A, Stavrou S, Wang ZR, Thompson J, Neville DM (2002) Gene optimization is necessary to express a bivalent anti-human anti-T cell immunotoxin in Pichia pastoris. Protein Expr Purif 25:270–282

Chapter 38
Optimization of Fermentation Condition of Man-Made Bee-Bread by Response Surface Methodology

Chuanren Duan, Yongfen Feng, Hao Zhou, Xiaohua Xia, Yaning Shang and Yamin Cui

Abstract In research and development for drugs with thrombolytic function, natto kinase is commonly used for the treatment of thrombosis drug. The objective of this research is to use the Box–Behnken design to optimize the four fermentation parameters for activity of nattokinase to create bee-bread by a mixed culture with *Lactobacillus plantarum* MRS3, *Bacillus subtilis natto* ATCC15245, and fresh bee-pollen. The maximum yield of 801.29 IU/mL nattokinase activity was obtained after optimization experiments of culture conditions such as inoculum size 6.6 %, water size 35 %, fermentation temperature 33 °C, culture time 9 days (216 h), and pH stay at the natural range, and incubated the mixture in OMWS Oumai with a solid state cultivation, and finally obtained the new bee-bread products with high nattokinase activity and rich nutrient. The results demonstrated that exploiting functional food of bee-bread as both medicine and food is viable.

Keywords Response surface methodology · Nattokinase · *Lactobacillus plantarum* · *Bacillus subtilis* · Bee-bread · Optimization

C. Duan (✉) · Y. Feng · Y. Shang · Y. Cui
Key Laboratory of Biorheological Science and Technology (Chongqing University), Ministry of Education, Chongqing 400030, People's Republic of China
e-mail: chrduan@cqu.edu.cn

C. Duan · H. Zhou
Key Laboratory of Industrial Fermentation Microbiology (Tianjin University of Science & Technology), Ministry of Education, Tianjin 300457, People's Republic of China

X. Xia
Fungood Meidi Ecological Breeding Limited Company, Chongqing 400043, People's Republic of China

T.-C. Zhang and M. Nakajima (eds.), *Advances in Applied Biotechnology*,
Lecture Notes in Electrical Engineering 333, DOI 10.1007/978-3-662-46318-5_38

38.1 Introduction

In recent years, nattokinase has drawn the increasing attention of investigators because of its important physiological functions in the heart and cerebral vessels. Nattokinase is a potent fibrinolytic enzyme that is considered to be a new promising agent for thrombolytic therapy, while the main drugs of urokinase (UK) and streptokinase (SK) are too expensive and their half-life is short. Compared to the clinical thrombolytic drugs (urokinase and streptokinase), nattokinase have several advantages such as safe, low cost, and easy oral administration [1]. This enzyme has been found in many resources, including Japanese natto [2], Chinese food douchi [3], and doufuru [4]. It is also present in various microorganisms, the most important strain is the genus *Bacillus* [5]. Therefore, many researchers have focused on the healthy food which was fermented by probiotics.

Pollen is the male gamete of seed plant, which plays an important role in sexual reproduction, which is rich in essential nutrients like protein, carbohydrates, vitamins, growth hormone, and other trace elements, and therefore has high nutritional value and special health function. So, bee-pollen is known as the "longevity beauty food", "micro-nutrient library" [6]. Bees do not consume pollen as collected by foragers, the pollen pellets are stored in cells, and honey, nectar, and glandular secretions are added to the mass of stored pollen. Stored pollen generally has a specific bacterial flora associated with it. Pollen stored in this way undergoes lactic acid fermentation and becomes what is called "bee bread". Bee bread is stored in combs and differs from fresh bee-collected pollen, but fermentation may be responsible for increasing stabilization of the product or may lead to chemical changes that increase digestibility and nutritive value for the bee pollen; the worker bees and larvae bees choose the bee-bread as their food but not pollen. Researchers show that at the appropriate period, the nutrient content in bee-bread is higher than pollen [7].

Because the natural output of bee-bread is limited, cannot meet the demand of the market and the price is high. We must pave new roads to make artificial bee-bread. The aim of this study was to maximize nattokinase activity in bee bread, and develop a functional food used as both medicine and food. Optimization was performed as follows: selection of the most significant factors, searching the optimal level using the response surface methodology (RSM), and a confirmation experiment to verify the optimal conditions.

38.2 Materials and Methods

38.2.1 Strains and Incubate Conditions

Lactobacillus plantarum MRS3 was separated and identified from rape bee-bread from Yunyang, Chongqing, China, by Duan et al. [8]. *Bacillus subtilis natto*

ATCC15245 was purchased from American Type Culture Collection. These strains were maintained as a spore suspension in 75 % glycerol and stored at −20 °C.

Nutrient agar medium for *Bacillus subtilis natto* (in g/L distilled water) [9]: peptone, 10; beef extract, 30; NaCl, 5; agar, 15; and pH 7.0.

MRS medium for *L. plantarum* (in g/L distilled water) [10]: peptone, 10; beef extract, 10; yeast extract, 5; citric acid diammonium hydrogen, 2; glucose, 20; K_2HPO_4, 2; sodium acetate, 5; $MgSO_4$, 0.5; $MnSO_4$, 0.25; Tween 80, 1 mL; agar, 15; and pH 6.2–6.4.

The bacteria were maintained on 15 % agar slants, the slants were kept at 4 °C and sub-cultured every 20 days in aforementioned media. The inoculum used in the following fermentation was developed by transferring 1 loop-full of the organism from slant to 100 mL Erlenmeyer flasks with 30 mL of liquid medium (aforementioned media without agar), and the inoculated flasks were incubated at 32 °C in orbital shaker at 180 rpm for 24 h.

38.2.2 Fermentation Conditions

Fermentation experiments were performed with 100 mL Erlenmeyer flask containing 15 g fresh pollen (procured from Yunyang, Chongqing, China), pollen sterilized by autoclaving for 15 min at 90 °C in order not to damage the nutrient, then inoculated the two bacteria successively, controlling the temperature of OMWS Oumai and solid state cultivation mixture for a few days with the normal pH.

38.2.3 Optimization of Culture Conditions for Inoculum Size, Water Size, Fermentation Temperature, Culture Time

RSM is a powerful technique for testing multiple process variables, because fewer experimental trials are required compared with the study of one variable at a time. Also, interactions between variables can be identified and quantified by this technique [11]. RSM helps to explore the optimum concentrations of each variable. RSM has been successfully used for the enhancement of fibrinolytic enzyme production by *Bacillus* sp. strain AS-S20-1 [12], *Bacillus subtilis* [13], and *Bacillus natto* [14].

In this article, the effects of inoculum size, water size, fermentation temperature, and culture time were researched [15]. Primarily, one of these factors changed while the others maintained. Based on these studies, these four independent factors were chosen for the further optimization experiments to obtain maxima nattokinase activity using RSM. The low, middle, and high values were coded as −1, 0, +1, respectively, as present in Table 38.1. The software Design-Expert (Version 8.0.6,

Table 38.1 Factors and levels in the response surface design

Levels	Variables			
	X_1 Inoculum size (%)	X_2 Water size (%)	X_3 Temperature (°C)	X_4 Culture time (day)
−1	3	30	30	8
0	5	35	34	9
1	10	40	37	10

Stat-Ease Inc., Minneapolis, USA) was used for experimental design, the treatment schedule for the model is given in Table 38.2. The response values (Y) in each trial was the average of triples.

38.2.4 Enzyme Separation

At the culture end, the separation of enzyme was according to Wen et al. [16]. About 3 g of sample was dissolved in 45 mL of sterilized normal saline (SS). This mixture stood overnight at 4 °C and was centrifuged at 5,000 rpm for 20 min in a cooling centrifuge at 4 °C. Supernatant was collected as the crude enzyme, and 10 μL of aliquot was prepared on a fibrin plate to assay the fibrinolytic activity.

38.2.5 Enzyme Assay

Fibrinolytic activity of the extracted enzyme was determined by the Fibrin Plate assay [17]. Agarose, fibrinogen, and thrombin were prepared, 15 mL of fibrinogen solution (0.89 mg/mL) was kept in a water bath for 15 min at 46 °C. The heated fibrinogen solution was then mixed with 20 mL of 1 % agarose solution (w/v) and mixed well by shaking, and 20 min later, the resulting media was poured into a dish (9 cm in diameter) with 1 mL of thrombin solution (15 IU thrombin in 10 mmol/L PBS buffer, pH 7.5). The dishes were in static cultivation for an hour to form fibrin clots, and 10 holes (1 mm in diameter) were punched on the dishes.

Aliquots of 10 μL of lumbokinase at 200, 400, 600, 800, 1000, 1200, 1400, 1600, 1800 and 2000 IU/mL were separately added in each hole and incubated at 37 °C for 18 h (each with one test and one control). The diameter of the cleared zone was measured and the thrombolytic circular area was calculated. The standard curve showing the relationship between lumbokinase activity (IU/mL) and thrombolytic circle area (mm^2) was established.

The fibrinolytic activity of samples was determined using the curve through adding 10 μL of sample supernatant prior on each hole of the fibrin plate to incubation for 18 h at 37 °C, and then measuring the lytic area.

Table 38.2 Box–Behnken response surface experimental design and results

Runs	X_1 Inoculum size (%)	X_2 Water size (%)	X_3 Temperature (°C)	X_4 Culture time (day)	Nattokinase activity (IU/mL)
1	0	0	0	0	427.19
2	−1	1	0	0	629.20
3	0	1	0	1	784.74
4	−1	0	0	−1	646.32
5	1	1	0	0	491.43
6	0	0	1	−1	804.37
7	−1	0	−1	0	551.93
8	0	−1	0	1	538.49
9	0	−1	−1	0	601.80
10	0	−1	1	0	526.00
11	0	1	1	0	532.69
12	−1	0	0	1	772.35
13	−1	0	1	0	464.41
14	0	0	−1	1	416.29
15	0	0	0	0	555.89
16	0	0	1	1	506.57
17	1	0	−1	0	574.35
18	0	0	−1	−1	583.92
19	0	0	0	0	618.40
20	0	1	0	−1	590.08
21	1	0	0	−1	796.31
22	1	0	0	1	561.29
23	−1	−1	0	0	573.84
24	1	0	1	0	611.90
25	1	−1	0	0	506.03
26	0	−1	0	−1	531.46
27	0	1	−1	0	432.19
28	0	0	0	0	767.39
29	0	0	0	0	583.06

38.3 Results and Discussion

38.3.1 The Standard Curve of Lumbokinase Activity

The applications of 10 μL lumbokinase, at 200, 400, 600, 800, 1000, 1200, 1400, 1600, 1800, and 2000 IU/mL, all produced clear fibrinolytic zones in the fibrin plates. The lumbokinase activity (IU/mL) and the lytic circle area (mm^2), averaged with triples, the activity and the area (mm^2) were exponentially correlated (R^2 = 0.986, P < 0.001) (Figs. 38.1 and 38.2, Table 38.3).

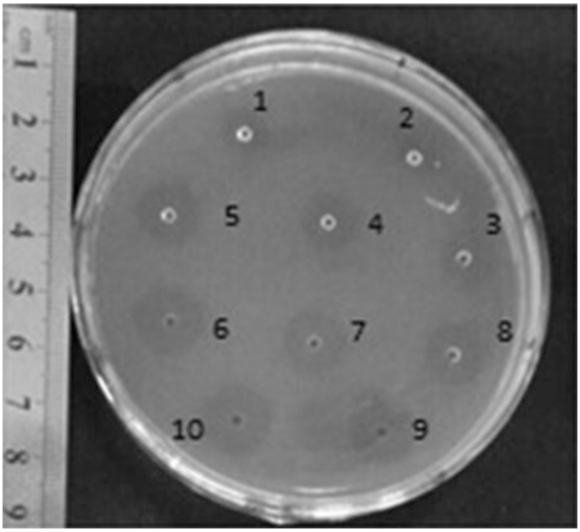

Fig. 38.1 Fibrin plate showing *clear zones* with the lumbokinase 200 IU/mL *1*, 400 IU/mL *2*, 600 IU/mL *3*, 800 IU/mL *4*, 1,000 IU/mL *5*, 1,200 IU/mL *6*, 1,400 IU/mL *7*, 1,600 IU/mL *8*, 1,800 IU/mL *9* and 2,000 IU/mL *10*

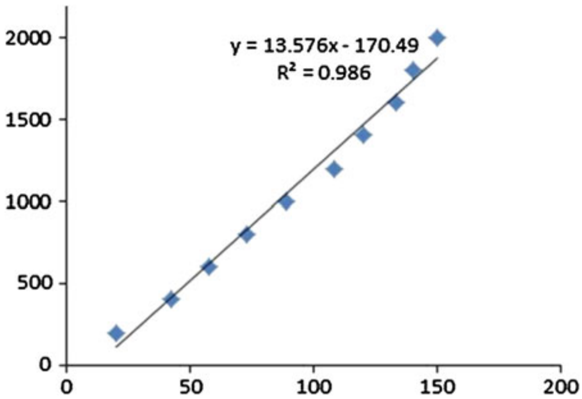

Fig. 38.2 The *standard curve* of the relationship between lumbokinase activity (*Y*) and thrombolytic circle area (*X*) established based on the data of 200, 400, 600, 800, 1000, 1200, 1400, 1600, 1800, and 2000 IU/mL of lumbokinase

38.3.2 Response Surface Methodology

The significant factors (inoculum size, water size, fermentation temperature, and culture time) were examined further by RSM using Box–Behnken design. The nattokinase activity (response) is presented in Table 38.2.

Table 38.3 The actual values of the thrombolytic circle area

Runs	Thrombolytic circle area (mm^2)	Lumbokinase activity (IU/mL)
1	20.5084	200
2	42.4292	400
3	57.5489	600
4	73.1382	800
5	89.2253	1,000
6	108.2495	1,200
7	120.1410	1,400
8	133.5504	1,600
9	140.6054	1,800
10	150.4396	2,000

Based on the ANOVA of the model (Table 38.4), the Model *F*-value of 44.49 implies the model is significant. There is less than 0.01 % chance that the "Model *F*-Value" is not significant. Values of "Prob > *F*" less than 0.0500 indicate model terms are significant. In this model, C, AB, AC, BD, CD, A^2, B^2, C^2, D^2 are

Table 38.4 Analysis of variance table

Source	Sum of squares	df	MeanSquare	*F*-value	*P*-value prob > *F*	
Model	3.279E + 005	14	23422.55	44.49	<0.0001	Significant
A	1665.69	1	1665.69	3.16	0.0970	
B	826.51	1	826.51	1.57	0.2308	
C	9133.39	1	9133.39	17.35	0.0010	
D	1291.48	1	1291.48	2.45	0.1396	
AB	8542.38	1	8542.38	16.23	0.0012	
AC	3888.15	1	3888.15	7.39	0.0167	
AD	566.92	1	566.92	1.08	0.3170	
BC	1483.79	1	1483.79	2.82	0.1154	
BD	32130.56	1	32130.56	61.03	<0.0001	
CD	5323.89	1	5323.89	10.11	0.0067	
A^2	75379.24	1	75379.24	143.17	<0.0001	
B^2	66328.38	1	66328.38	125.98	<0.0001	
C^2	74170.93	1	74170.93	140.88	<0.0001	
D^2	1.794E + 005	1	1.794E + 005	340.78	<0.0001	
Residual	7370.87	14	526.49			
Lack of fit	6397.56	10	639.76	2.63	0.1822	Not significant
Pure error	973.31	4	243.33			
Cor total	3.353E + 005	28				

Table 38.5 Analysis of variance (ANOVA) table for response-surface quadratic model

Parameter	Value
Std. dev.	22.95
Mean	585.51
R-squared	0.9780
Adj *R*-squared	0.9560
Pred *R*-squared	0.8856
Press	383075
Adeq precision	22.769

significant model terms. The equation in terms of the coded factors is given as follows (38.1):

$$\begin{aligned}\text{Nattokinase activity(IU/mL)} = &+785.03 + 11.78 \times A + 8.30 \times B - 27.59 \times C - 10.37 \times D \\ &- 46.21 \times A \times B + 31.18 \times A \times C + 11.90 \times A \times D - 19.26 \times B \times C \\ &+ 89.62 \times B \times D - 36.48 \times C \times D - 107.80 \times A^2 - 101.12 \times B^2 \\ &- 106.93 \times C^2 - 166.31 \times D^2\end{aligned} \tag{38.1}$$

where A is inoculum size, B is water size, C is fermentation temperature, and D is culture time. Values greater than 0.1000 indicate the model terms are not significant. In Table 38.5, the "Lack of Fit F-value" of 2.63 implies that lack of fit is not significant as the pure error. There is a 18.22 % chance that the "Lack of Fit F-value" is nonsignificant. Nonsignificant lack of fit is good—we want the model to fit.

The fit of the model was expressed by the coefficient of regression R^2, which was found to be 0.9780, indicating that the model gives predictions in 97.8 % confidence level. The "Pred R^2" of 0.8856 is in reasonable agreement with the "Adj R^2" of 0.9560. "Adeq Precision" measures the signal to noise ratio. A ratio greater than 4 is desirable. The ratio of 22.769 indicated an adequate signal. In conclusion, this model can be used to navigate the design space.

Accordingly, three-dimensional surface response plots were generated for the pairwise combination of the four factors, while keeping the other two factors at their center point levels. The shape of the contour can reflect the interaction significance, the circular means interaction was not significant, while the oval showed significant interaction. Graphs for the four significant interactions are given here to highlight the roles played by these factors (Fig. 38.3a–d).

As shown in Fig. 38.3a, when keeping the inoculation amount at a certain level, the nattokinase activity increases while the water added increases, but when the water content is greater than 36 %, nattokinase enzyme activity is on the decline. As the water content increases, the quantity of nattokinase activity increases, but when the inoculation amount continues to increase, nattokinase activity is gradually reduced. A similar profile was observed in Fig. 38.3c, d. It is evident from Fig. 38.3b that when the interaction between inoculum size and fermentation temperature was studied while keeping the other parameters such as water size and

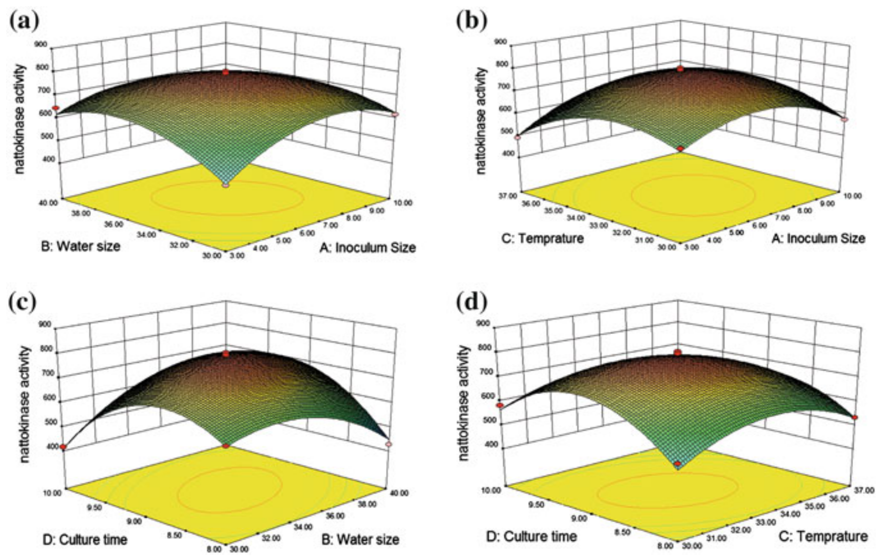

Fig. 38.3 Response surface plot for nattokinase activity, the interaction between inoculum size and water size (**a**), inoculum size and fermentation temperature (**b**), water size and culture time (**c**), and fermentation temperature and culture time (**d**)

culture time at their zero levels, the effect of temperature was significant on the response of nattokinase activity.

From the three-dimensional surface response plots, the optimal process parameters were obtained. It was observed that the fermentation condition of man-made bee-bread was inoculum size 6.59 %, water size 35.23 %, fermentation temperature 33.05 °C, and culture time 9 days. In combination with the results of actual operation convenient and variance analysis, we adjusted the parameters as: inoculum size 6.6 %, water size 35 %, fermentation temperature 33 °C, and culture time 9 days, yielded a maximum nattokinase activity of 801.29 IU/mL which exactly matched the predictions of 787.169 IU/mL.

38.4 Conclusion

From the experiments above, we present a preparation technology for a new nattokinase functional food—bee-bread from several new points as follows. First, a new fermentation substrate of pollen was used; second, we developed a study involving *L. plantarum* MRS3 and *Bacillus subtilis natto* ATCC15245 for production of nattokinase from pollen by the mixed culture; lastly, RSM was adopted to optimize the variables and to study their influence on nattokinase activity. The results showed a combination of concentration of inoculum size 6.59 %, water size 35.23 %, fermentation temperature 33.05 °C, and culture time 9 days, which would yield a maximum nattokinase activity of 801.29 IU/mL, which exactly matched the predicted value of 787.169 IU/mL. Finally the new bee-bread products were obtained with high nattokinase activity and rich nutrient, these data proved that it is possible to create a functional food of bee-bread, which is used as both medicine and food.

Acknowledgments This project was supported by the Foundation (No. 2014IM003) of Key Laboratory of Industrial Fermentation Microbiology of Ministry of Education and Tianjin Key Lab of Industrial Microbiology (Tianjin University of Science & Technology).

References

1. Chitte RR, Dey S (2002) Production of a fibrinolytic enzyme by thermophilic Streptomyces species. World J Microbiol Biotechnol 18:289–294
2. Sumi H, Hamada H, Tsushima H, Mihara H, Muraki H (1987) A novel fibrinolytic enzyme (nattokinase) in the vegetable cheese natto; a typical and popular soybean food in the Japanese diet. Experientia 43:1110–1111
3. Peng Y, Huang Q, Zhang R-H, Zhang Y-Z (2003) Purification and characterization of a fibrinolytic enzyme produced by Bacillus amyloliquefaciens DC-4 screened from douchi, a traditional Chinese soybean food. Comp Biochem Physiol B: Biochem Mol Biol 134:45–52
4. Chen B, Huo J, He Z, He Q, Hao Y, Chen Z (2013) Isolation and identification of an effective fibrinolytic strain Bacillus subtilis FR-33 from the Chinese doufuru and primary analysis of its fibrinolytic enzyme. Afr J Microbiol Res 7:2001–2009
5. Hyun-Kuk K, Gu-Taek K, Dae-Kyung K, Won AC, Sung-Hoon P, Yong-Kee J, In-Soo K (1997) Purification and characterization of a novel fibrinolytic enzyme from Bacillus sp. KA38 originated from fermented fish. J Ferment Bioeng 84:307–312
6. Gao Y, Wang Y, Li SH (2005) The nutrition of maize pollen and its application value. China Food Nutr 11:26–27
7. Herbert EW, Shimanuki H (1978) Chemical composition and nutritive value of bee-collected and bee-stored pollen. Apidologie 9:33–40
8. Duan C, Bao J, Shi Y, Xia X, Feng Y (2014) Isolation and identification of microbe in loquat flower and rape flower bee bread. Sci Technol Food Ind (in press)
9. Du L (1992) Industrial microbiology experiment technology. Tianjin Science and Technology Publishing House, Tianjin
10. Du L (1999) Production technology of lactic acid bacteria and fermentation products. Tianjin Science and Technology Publishing House, Tianjin
11. Myers RH, Montgomery DC, Anderson-Cook CM (2009) Response surface methodology: process and product optimization using designed experiments. Wiley, New York
12. Mukherjee AK, Rai SK (2011) A statistical approach for the enhanced production of alkaline protease showing fibrinolytic activity from a newly isolated Gram-negative Bacillus sp. strain AS-S20-I. New Biotechnol 28:182–189
13. Deepak V, Kalishwaralal K, Ramkumarpandian S, Babu SV, Senthilkumar S, Sangiliyandi G (2008) Optimization of media composition for nattokinase production by Bacillus subtilis using response surface methodology. Bioresour Technol 99:8170–8174
14. Liu J, Xing J, Chang T, Ma Z, Liu H (2005) Optimization of nutritional conditions for nattokinase production by Bacillus natto NLSSE using statistical experimental methods. Process Biochem 40:2757–2762

15. Rasagnya PS, Vangalapati M (2013) Studies on optimization of process parameters for nattokinase production by Bacillus subtilis NCIM 2724 and purification by liquid-liquid extraction. Int J Innov Res Sci Eng Technol 2:4516–4521
16. Wen Y, Li J, Yang F, Zhang W, Li W, Liao C, Chen L (2013) Salting-out assisted liquid–liquid extraction with the aid of experimental design for determination of benzimidazole fungicides in high salinity samples by high-performance liquid chromatography. Talanta 106:119–126
17. Astrup T, Müllertz S (1952) The fibrin plate method for estimating fibrinolytic activity. Arch Biochem Biophys 40:346–351

Chapter 39
Prediction of Lysine Acetylation Sites in *Porcine Pancreas* Lipase Modified by the Ionic Liquids Using Molecular Dynamics Simulations

Yi-Gang Jia, Yang Zhang, Hong-Man Zhang, He Huang, Lu-Jia Zhang and Yi Hu

Abstract The molecular dynamics (MD) simulations method was used to study the lysine acetylation sites of *Porcine Pancreas* lipase (PPL) modified by ionic liquids [HOOCBMIm][Cl] and [HOOCMMIm][Cl]. By analyzing the effects impacting on the difficulty of lysine modifications upon different sites, including the solvent-accessible surface area, hydrogen bonds, and salt-bridges, a prediction model was achieved. The prediction acquired the exact number of modified lysine (4 and 9 respectively) and the specific modification sites in the ionic liquids [HOOCBMIm][Cl] and [HOOCMMIm][Cl] modification systems, respectively, which are consistent with the results of our previous studies.

Keywords *Porcine pancreas* lipase · Molecular dynamics simulation · Ionic liquids modification · Lysine acetylation sites · Solvent-accessible surface area

39.1 Introduction

Lipases (EC3.1.1.3) are a kind of enzymes as important biocatalysts due to their high selectivity, high stability, mild reaction conditions, with no need for coenzyme, and so on. Owing to their ability to catalyze various reactions including hydrolysis, esterification, transesterification, alcoholysis, and aminolysis, lipases are

Y.-G. Jia · Y. Zhang · H.-M. Zhang · H. Huang · Y. Hu (✉)
State Key Laboratory of Material-Oriented Chemical Engineering, Nanjing Tech University, Nanjing 210009, China
e-mail: huyi@njtech.edu.cn

L.-J. Zhang (✉)
New World Biotechnology Institute, State Key Laboratory of Bioreactor Engineering, East China University of Science and Technology, Shanghai 200237, China
e-mail: ljzhang@ecust.edu.cn

T.-C. Zhang and M. Nakajima (eds.), *Advances in Applied Biotechnology*,
Lecture Notes in Electrical Engineering 333, DOI 10.1007/978-3-662-46318-5_39

widely used in pharmaceutical, chemical, food, feed, and energy industries [1–3]. However, lipases still have many shortcomings, especially the vulnerability of being inactive under unnatural conditions such as organic solvent surrounded, high temperature, and extreme pH [4]. Therefore, in order to improve their catalytic properties and make them adapt to further practical applications, quite a number of technological measures can be done to have lipases modified, such as genetic engineering, chemical modification, and immobilization [5, 6].

Recently, as a novel chemical modification reagent, ionic liquids (ILs) have been adopted to improve the properties of immobilized enzyme and modified free enzyme [7–12]. The results showed that the catalytic properties of lipases modified by ILs, such as thermal stability, hydrolytic activity, and enantioselectivity were improved to a different extent. Doumèche's group chose functionalized ionic liquids, e.g., imidazole and pyrrolidine, to modify the formate dehydrogenase (FDH), leading to prolong the half-life ($T_{1/2}$) from 1.5 ± 0.6 days to 4.7–9 days in the carbonate buffer [7]. The significant improvement in the catalytic properties of enzyme was closely related to the excellent properties of ILs and the modification degree upon the lysine in enzymes [10]. However, due to the poor cognitive of the mechanism of how modification improves the catalytic performance of enzymes, it is difficult to offer rational guidance for the modification of various enzymes with different structures.

The identification of the modification sites was essential for uncovering the mysterious veil on the enhancement of catalytic properties after enzyme modification.

With the combination of molecular simulation and experimental methods, Mogharrab et al. attempted to clarify the mechanism regarding traditional chemical modification of the enzymes. AQ-modified HRP was constructed so that carboxylic acid anthraquinone (AQ) was covalently bound to the side-chain ε-nitrogens of these residues (Lys^{174}, Lys^{232} and Lys^{241}); the results revealed the mechanism of structural stabilization and functional improved compared with native Horseradish peroxidase (HRP) [13]. However, ionic liquids, as a novel chemical modification reagent, take great advantages over the traditional modification reagent. Its mechanisms upon improving the catalytic properties of enzymes still remain unclear.

In our previous work, the modification numbers of PPL on two different ionic liquids ([HOOCBMIm] [Cl] and [HOOCMMIm] [Cl]) (3–6 and 7–13, respectively) can be obtained by MALDI-TOF mass spectra experiment [10]. However, the location of modification sites and mechanisms of catalytic properties need to be further elaborated. In this study, molecular dynamics (MD) simulations were performed to investigate the ILs modification sites of PPL in the following three solvents: water (system 1), [HOOCBMIm][Cl] (system 2), and [HOOCMMIm][Cl] (system 3), respectively. The specific modification sites of PPL in the three systems were analyzed and further discussed based on the results of MD simulations. These simulation results will be helpful to understand the mechanism of the enhancement of catalytic properties after enzyme modification and provide a theoretical basis for the design of ILs modifiers and the option of proper modification degrees in enzyme engineering.

39.2 Experimental

39.2.1 Acquisition of Protein Structure

The initial conformation of PPL solved 2.8 Å at resolution was taken from the NMR structure (PDB entry code: 1ETH) [14]. PPL is composed of 448 amino acid residues and 7 disulfide bonds. Ligands and inhibitors in three-dimensional model of PPL were removed prior to MD simulation. 128 bound water molecules in the crystal structure were reserved in the MD simulations.

39.2.2 Structure Determination

The geometric structure of ILs molecules (Fig. 39.1) were derived from Chemoffice (Cambridge Soft Corporation) program and then minimized and the cation charge was +1. The force field parameters of [HOOCBMIm][Cl] and [HOOCMMIm][Cl] were obtained through the Automated force field Topology Builder (ATB) online server [15]. Meanwhile, the coordinate files of those ILs were also derived from online server. Atom partial charges were obtained with the RESP method at the 6-31G(d) level by Gaussian 03 program [16].

39.2.3 Molecular Dynamics Simulations

All MD simulations were performed using GROMACS 4.5.4 package [17–19] at Hp Z800 workstation, employing the GROMOS96 53a6 united atom protein force field [20]. Protonation states of titratable groups Arg, Lys, Asp, His, and Glu were computed by an online server named PROPKA at pH 7.0 [21]. Each model was solvated in a cubic boxes filled with SPC water molecules [22] and neutralized by adding appropriate NA ions. The number of ILs in systems (1, 2 and 3) were 0, 100, and 100, respectively. The 100:1 molar ratio of the modifiers to PPL in systems

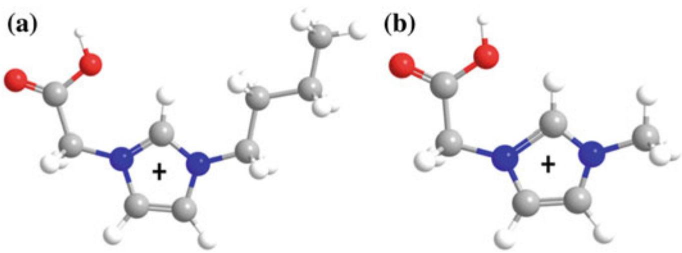

Fig. 39.1 The 2D geometry structural of [HOOCBMIm][Cl] and [HOOCMMIm][Cl], respectively. **a** [HOOCBMIm][Cl]. **b** [HOOCMMIm][Cl]

2 and 3 were in line with the experimental section in previous studies [10]. The LINCS algorithm was used to constrain all bond lengths [23]. The Particle Mesh Ewald (PME) method was used to evaluate the long electrostatic interactions [24, 25]. The temperature of each system was maintained by velocity rescaling method [26]. Similarly, the pressure of each system was maintained by the Parrinello-Rahman method [27]. The cut-offs for short-range nonbonded interactions (van der Waals and electrostatics interactions) were set to 14 Å. The snapshots of each system were saved every 1 ps for data analysis.

Each initial system was subjected to energy minimization (1,000 steepest descents and 1,000 conjugate gradient) and 100 ps equilibration with position restrained. Then the MD simulations were carried out for 10 ns with a timestep of 2 fs at constant temperature (300 K) and pressure (1 atm). The MD trajectories were analyzed and calculated by GROMACS 4.5.4 program including the Cα root mean square deviations (Cα-RMSD) and solvent-accessible surface area (SASA). Visual Molecular Dynamics 1.9.1 program (VMD) was used for the occupy percentages of hydrogen bonds and salt-bridges analysis [28]. The figures of protein structure were carried out by PyMOL program [29].

39.3 Results and Discussion

39.3.1 Structural Investigation

The equilibrium of three systems were evaluated using Cα-RMSD compared to the simulation starting structure (Fig. 39.2). As can be seen from Fig. 39.2, the conformations of protein in systems 1 and 2 maintained stable throughout MD simulations. However, the protein structure in system 2 had larger float compared to systems 1 and 3 (Fig. 39.2). In the last 3 ns of the simulation in systems 1, 2, and 3, the Cα-RMSD values of systems 1, 2, and 3 tended to relatively constant, leveling off around 0.3, 0.35 and 0.2 nm respectively. This is consistent with experimental results that reported the stability of the enzyme in hydrophobic and hydrophilic ILs [30].

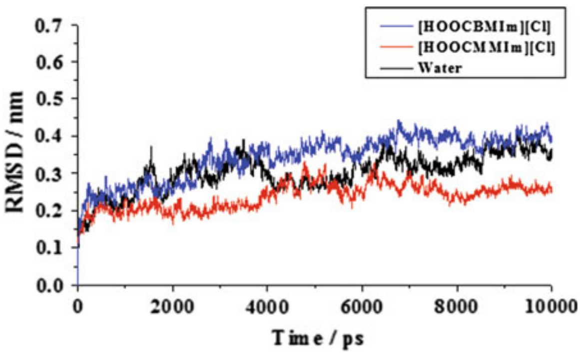

Fig. 39.2 The Cα-RMSD of PPL respectively in systems 1 (*black*), 2 (*blue*) and 3 (*red*) and against time

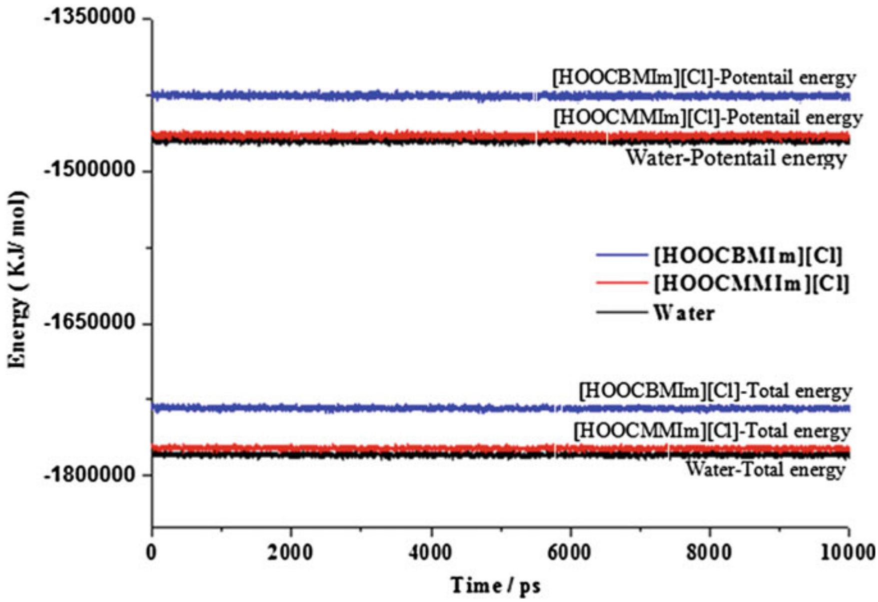

Fig. 39.3 The energy distribution of PPL, respectively, in systems 1 (*black*), 2 (*blue*), and 3 (*red*) and against time

Meanwhile, the overall stability of the total energy and potential energy were examined in three systems over the course of simulation. For all three systems, the total energy and potential energy were conservative and suggested the models in three systems to be well equilibrated (Fig. 39.3).

39.3.2 Calculation of Solvent Accessible Surface Area

SASA is the surface area of a protein molecule that is accessible to a solvent. The greater the degree of the same amino acids exposed to the solution phase, the greater the probability of its reaction with the reagents within the same solution phase. And the main reactive sites of lysine were concentrated in the side chain ε-amino group of lysine. Furthermore, the modification degree of lysine ε-amino groups affected by ILs was mainly determined by the SASA values. Some authors validated this concept for the correlation of residue relative reactivities with the accessibility of lysine residues on the protein surface [31–34].

The main chain structure, surrounding residues and solution phase influenced the variation of exposure rate of lysine residues in PPL. PPL contains 22 lysine residues located on the protein surface (amino acids position 26, 33, 70, 81, 92, 96, 108, 137, 198, 233, 240, 269, 296, 318, 342, 350, 351, 374, 398, 400, 418, and 427) (Fig. 39.4). The SASA values of residues are determined with a sphere of a 1.4 Å

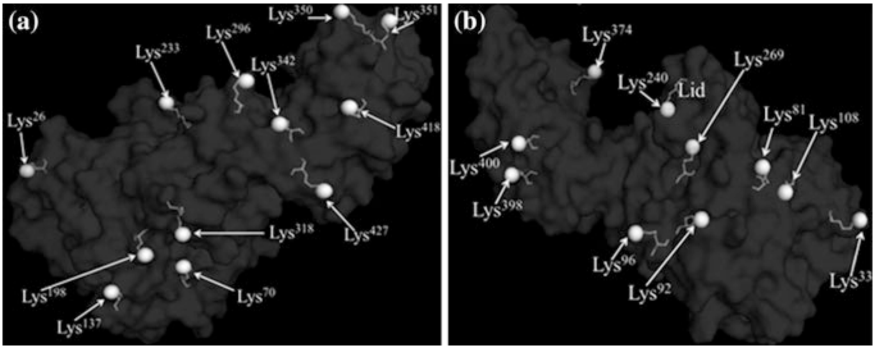

Fig. 39.4 Structure of PPL shown through surface representation. Lysine shown through *white stick* model representation (*Sphere* represents N atom). The *black* of PPL (**b**) is seen by rotating 180 around the *Z*-axis

radius to probe the surface of protein [35]. The SASA values of ε-amino group of lysine residues in PPL are listed in Table 39.1. As seen in Table 39.1, there are large differences in the SASA values of ε-amino group of each lysine residue in these three systems. In addition, it was found that the lysines with larger surface area in system 1 were different from those in systems 2 and 3 throughout MD simulation. This may be partially due to charge redistribution at the protein surface laid in the ILs system, leading to a different unfolding pattern. Although the lysine residues with higher exposure rate could be easily modified in system 1, the same residues could not be achieved in other systems. During the 10 ns simulations, compared with the lysine residues the status of protein structures obtained in system 1 (Fig. 39.5a) deviated substantially from that in systems 2 and 3 (Fig. 39.5b, c, respectively), it could be noted that the lysine residues status of protein structures in systems 1, 2, and 3 showed a significant difference. In order to seek for the precise sites of ILs modification, further studies involving protein structures should be performed with real ILs systems.

To identify the specific sites of ILs modification, the mean accessibility of the side chain ε-amino group of each lysine residue in PPL was analyzed throughout 10 ns MD simulation. There were 11 lysine residues with a SASA over 0.27 nm^2 in system 2, namely: Lys^{26} (0.323 nm^2), Lys^{70} (0.272 nm^2), Lys^{81} (0.316 nm^2), Lys^{96} (0.295 nm^2), Lys^{269} (0.321 nm^2), Lys^{296} (0.290 nm^2), Lys^{350} (0.275 nm^2), Lys^{351} (0.322 nm^2), Lys^{374} (0.290 nm^2), Lys^{400} (0.293 nm^2) and Lys^{418} (0.277 nm^2), and eight residues were with a SASA over 0.2 nm^2 and less than 0.27 nm^2, including Lys^{92}, Lys^{108}, Lys^{137}, Lys^{198}, Lys^{240}, Lys^{318}, Lys^{342} and Lys^{427}. Additionally, three residues were with low SASA, which was Lys^{33}, Lys^{398}, and Lys^{233}, respectively. While in system 3, the highest accessibilities for residues were Lys^{26} (0.287 nm^2), Lys^{33} (0.332 nm^2), Lys^{81} (0.294 nm^2), Lys^{96} (0.315 nm^2), Lys^{198} (0.307 nm^2), Lys^{233} (0.314 nm^2), Lys^{240} (0.317 nm^2), Lys^{269} (0.309 nm^2), Lys^{296} (0.322 nm^2), Lys^{318} (0.304 nm^2), Lys^{350} (0.331 nm^2), Lys^{351} (0.327 nm^2), Lys^{374} (0.309 nm^2), Lys^{400} (0.293 nm^2), Lys^{418} (0.291 nm^2) and Lys^{427} (0.294 nm^2), and

Table 39.1 The SASA of the ε-amino group in lysine residues on the PPL surface in systems 1, 2, and 3, respectively

Residue	Water[a] (nm^2)	[HOOCBMIm][Cl][a] (nm^2)	[HOOCMMIm][Cl][a] (nm^2)
Lys^{26}	0.160	0.323	0.287
Lys^{33}	0.328	0.153	0.332
Lys^{70}	0.285	0.272	0.253
Lys^{81}	0.306	0.316	0.294
Lys^{92}	0.246	0.252	0.224
Lys^{96}	0.307	0.295	0.315
Lys^{108}	0.243	0.263	0.213
Lys^{137}	0.098	0.231	0.247
Lys^{198}	0.304	0.260	0.307
Lys^{233}	0.168	0.045	0.314
Lys^{240}	0.268	0.245	0.317
Lys^{269}	0.306	0.321	0.309
Lys^{296}	0.313	0.290	0.322
Lys^{318}	0.220	0.263	0.304
Lys^{342}	0.223	0.252	0.225
Lys^{350}	0.333	0.275	0.331
Lys^{351}	0.328	0.322	0.327
Lys^{374}	0.210	0.290	0.309
Lys^{398}	0.287	0.193	0.193
Lys^{400}	0.268	0.293	0.293
Lys^{418}	0.289	0.277	0.291
Lys^{427}	0.294	0.261	0.294

[a] The mean SASA values of equilibrium stages (7–10 ns) during 10 ns MD simulations

five residues were with a SASA over 0.2 nm^2 and less than 0.27 nm^2, including Lys^{70}, Lys^{92}, Lys^{108}, Lys^{137} and Lys^{342}. The lowest SASA value lie in the residue Lys^{398} (0.193 nm^2). Accordingly, based on the principle of accessibilities correlation, together with the average modification degrees (systems 2 and 3) which were obtained in preliminary experiments (22.6 ± 1.2 % and 53.4 ± 2.8 % in systems 2 and 3, respectively), we define that lysine with a SASA value over 0.27 nm^2 can be easily modified [10]. Furthermore, we preliminarily supposed the corresponding modification sites to be easily modified by [HOOCBMIm][Cl] were Lys^{26}, Lys^{70}, Lys^{81}, Lys^{96}, Lys^{269}, Lys^{296}, Lys^{350}, Lys^{351}, Lys^{374}, Lys^{400} and Lys^{418}, while that easily modified by [HOOCMMIm][Cl] were Lys^{26}, Lys^{33}, Lys^{81}, Lys^{96}, Lys^{198}, Lys^{233}, Lys^{240}, Lys^{269}, Lys^{296}, Lys^{318}, Lys^{350}, Lys^{351}, Lys^{374}, Lys^{400}, Lys^{418} and Lys^{427}.

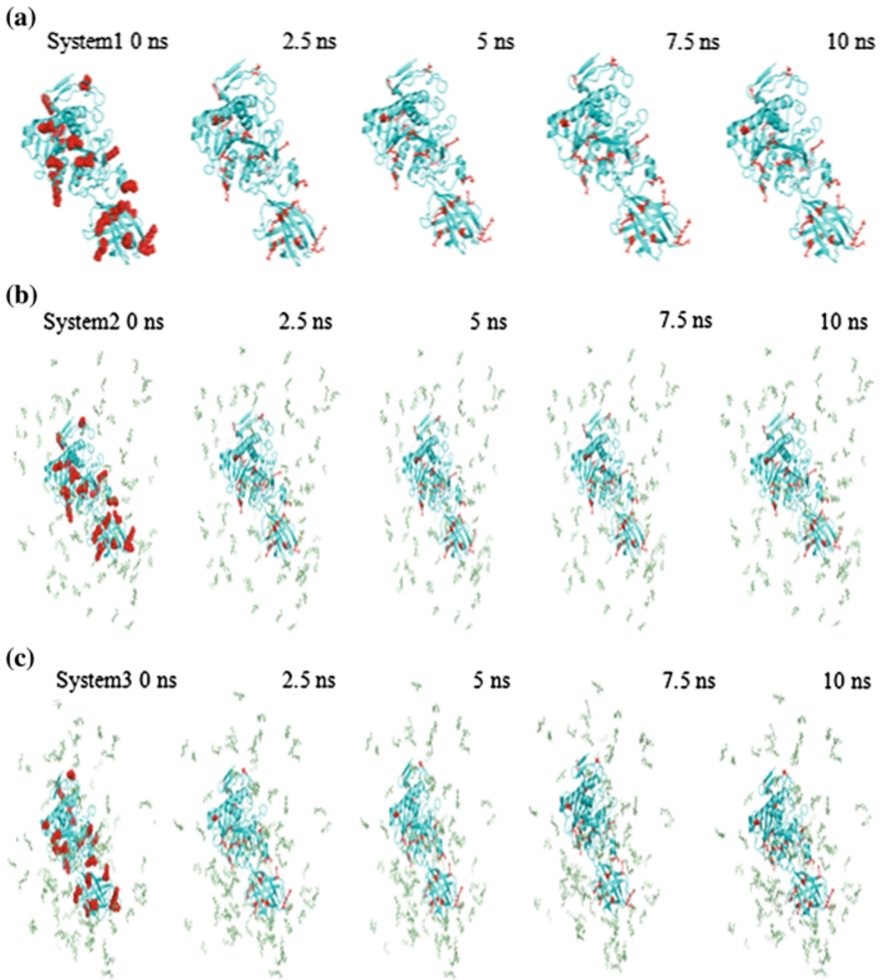

Fig. 39.5 The lysine residues status of PPL obtained in systems 1–3, respectively. **a** Water. **b** [HOOCBMIm][Cl]. **c** [HOOCMMIm][Cl]. All water in solvent was removed in systems 1–3

39.3.3 Effects of Bond Occupancy on the Modification Sites

The other effects impacting on the difficulty of modification of lysine residue at different sites in PPL were examined, respectively, including hydrogen bonds and salt-bridges. Combining the above results with SASA values, the modification sites of modified lysine were ultimately determined.

When Lys on the protein surface is being modified by chemical modifiers, its ε-NH_2 groups can react with other amino acids and cause an occupation of its atomic orbital by other atoms to form a new state, which makes the ε-NH_2 difficult to be modified. We define this as "bond occupancy". The interaction between amino acids on the protein surface is most likely to form two noncovalent strong forces: hydrogen bonds and salt-bridges. Thus, we could partly determine whether Lys can be easily modified by analyzing the bond occupancy (hydrogen bonds and salt-bridges).

In the 10,000 frames of extracted structure from the 10 ns MD simulations, if with over 450 frames of the Lys ε-NH_2 occupied, the Lys was then in low possibility of attack by the modifying agent in the solution. Therefore, we believe the Lys with over 450 frames occupied is difficult to be modified.

39.3.3.1 Effects of Hydrogen Bonds on the Modification Sites

In order to investigate the effects of hydrogen bonds on the modification sites, hydrogen bonds formed between lysine residues and its adjacent residues were analyzed. Based on the experiment results of PEGylation of Hirudin on ion-exchange column, relative reactivities of lysine residues were also concerned with hydrogen bonds [31]. During the equilibrium stages (7–10 ns) of 10 ns MD simulations, the formation of hydrogen bonds in systems 2 and 3 are listed in Tables 39.2 and 39.3, respectively. In system 2 (Table 39.2), the lysine with hydrogen bonds frames over 450 were Lys^{26}, Lys^{70}, Lys^{81}, Lys^{92}, Lys^{137}, Lys^{233}, Lys^{269} and Lys^{400}, and we supposed that the ε-amino group on the side chain of these residues were difficult to be modified. Even though the ε-amino group of lysine residue 26 had accessibility as high as 0.323 nm^2, it was involved in the formation of hydrogen bonds to affect its reactivity. Nevertheless, in system 3, the lysine with strong bond occupancy, i.e., Lys^{26}, Lys^{70}, Lys^{92}, Lys^{108}, Lys^{137}, Lys^{233}, Lys^{342}, Lys^{374}, Lys^{398}, Lys^{400}, Lys^{418} and Lys^{427}, were identified with over 450 occupied frames in the trajectories (Table 39.3). Similarly, Lys^{233}, with accessibility of 0.314 nm^2, whose ε-amino helped in the formation of hydrogen bonds, is difficult to be modified.

39.3.3.2 Effects of Salt-Bridges on the Modification Sites

To explore whether salt-bridges would affect modification sites, salt-bridges between lysines and its adjacent residues in each MD trajectory were analyzed for information about occupied percentages in detail. Shuvaev et al. found that the distance between the N atom of Lys^{75} and carboxyl O atoms of Glu^{79} in apoE may affect glycosylation rate [36]. The distance of salt-bridge between Lys^{75} and Glu^{79} in apoE2 were larger than that identified in apoE2 and apoE3 by molecular simulation methods, thus the 75 lysine residues in apoE2 was more easily glycosylated. Similarly, O'Brien et al. found that the nitrogens of Lys^{65} and Lys^{149} with moderately accessibilities were engaged in salt pairing with carboxylate side chain of Glu^{64} and Asp^{258}, respectively [32]. Therefore, the Lys^{65} and Lys^{149} in HRP had less possibility to react with ethylene glycol bis (succinimidylsuccinate) (EGNHS).

Table 39.2 Hydrogen bonds formed at the side chain ε-amino group of lysine and its around residue in [HOOCBMIm][Cl] system environment

System	Donor	Acceptor	Snapshots occupancy/frame
[HOOCBMIm][Cl][a]	Lys^{26}	Asp^{13}	926
	Lys^{26}	Asp^{14}	1,409
	Lys^{33}	Ser^{31}	201
	Lys^{70}	Ser^{145}	500
	Lys^{70}	Arg^{72}	257
	Lys^{81}	Arg^{112}	738
	Lys^{92}	Ser^{88}	500
	Lys^{96}	Asn^{93}	387
	Lys^{108}	Arg^{112}	423
	Lys^{137}	Ser^{143}	119
	Lys^{137}	Thr^{169}	402
	Lys^{198}	Glu^{171}	210
	Lys^{233}	Tyr^{289}	729
	Lys^{240}	Asn^{241}	50
	Lys^{269}	Phe^{336}	739
	Lys^{269}	Tyr^{268}	208
	Lys^{296}	Ala^{294}	39
	Lys^{318}	Thr^{319}	9
	Lys^{318}	Phe^{199}	90
	Lys^{342}	Phe^{298}	308
	Lys^{351}	Gln^{378}	6
	Lys^{374}	His^{355}	391
	Lys^{398}	Phe^{361}	44
	Lys^{398}	Asn^{446}	26
	Lys^{400}	Thr^{420}	464
	Lys^{418}	Asp^{430}	270
	Lys^{427}	Arg^{423}	34
	Lys^{427}	Tyr^{429}	278

[a] Hydrogen bonds were formed based on three criteria: (1) the distance between hydrogen atom and H-bond receptor ranges from 1.2 to 3.5 Å; (2) an angle constraint (H-bond donor—hydrogen atom—H-bond receptor is equal to or larger than 120°)

In system 2, Lys^{26}, Lys^{33}, Lys^{70}, Lys^{81}, Lys^{108}, Lys^{137}, Lys^{198}, Lys^{240}, Lys^{269}, Lys^{318}, Lys^{342}, Lys^{374}, Lys^{418} and Lys^{427} participated in salt form with acidic amino acids (Asp and Glu) to a different extent (Table 39.4). The relatively high "bond occupancy" were identified as Lys^{26}, Lys^{70}, Lys^{108}, Lys^{342}, Lys^{374}, Lys^{418} and Lys^{427}, which had low reactivities. Thus, while Lys^{70} and Lys^{418}, in system 2 had high accessibilities, the "bond occupancy" analysis of them suggested that these two residues had little chance to react with ILs. In addition, the salt-bridges analysis of lysines in system 3 showed that Lys^{70}, Lys^{198}, Lys^{342} and Lys^{418} had

Table 39.3 Hydrogen bonds formed at the side chain ε-amino group of lysine and around its residue in [HOOCMMIm][Cl] system environment

System	Donor	Acceptor	Snapshots occupancy/frame
[HOOCMMIm][Cl]	Lys^{26}	Asp^{13}	926
	Lys^{26}	Ala^{18}	100
	Lys^{33}	Ser^{31}	201
	Lys^{70}	Asn^{146}	976
	Lys^{70}	Glu^{98}	1,083
	Lys^{81}	Glu^{83}	143
	Lys^{92}	Ser^{88}	1,914
	Lys^{96}	Asn^{93}	413
	Lys^{108}	Asp^{36}	806
	Lys^{137}	Thr^{169}	583
	Lys^{198}	Glu^{137}	210
	Lys^{233}	Tyr^{289}	908
	Lys^{240}	Asn^{241}	12
	Lys^{269}	Tyr^{268}	208
	Lys^{269}	Asp^{258}	83
	Lys^{318}	Asp^{313}	435
	Lys^{342}	Ser^{384}	109
	Lys^{342}	Glu^{422}	1,012
	Lys^{351}	Gln^{378}	122
	Lys^{374}	Glu^{371}	484
	Lys^{398}	Asn^{446}	806
	Lys^{400}	Asn^{366}	842
	Lys^{400}	Phe^{361}	385
	Lys^{418}	Asp^{430}	881
	Lys^{427}	Tyr^{429}	259
	Lys^{427}	Asp^{425}	971

[a] Hydrogen bonds were formed based on three criteria: (1) the distance between hydrogen atom and H-bond receptor ranges from 1.2 to 3.5 Å; (2) an angle constraint (H-bond donor—hydrogen atom—H-bond receptor is equal to or larger than 120°)

formed relatively firm salt-bridges (Table 39.5). Hence, the corresponding ε-amino group of those lysines were difficult to be modified.

By analyzing the "bond occupancy", the ε-amino amino groups of lysine residues easily reacting with the functionalized ionic liquid [HOOCBMIm] [Cl] were Lys^{33}, Lys^{96}, Lys^{198}, Lys^{240}, Lys^{296}, Lys^{318}, Lys^{350}, Lys^{351} and Lys^{398}; while the most likely sites to be modified by [HOOCMMIm] [Cl] were Lys^{33}, Lys^{81}, Lys^{96}, Lys^{240}, Lys^{269}, Lys^{296}, Lys^{318}, Lys^{350} and Lys^{351}. And then, combining SASA with the modification numbers measured in the experiment (3–6 and 7–13, respectively) [10], we thought that the most likely modification sites in systems 2 and 3 were, respectively, (Lys^{96}, Lys^{296}, Lys^{350} and Lys^{351}) (Fig. 39.6a) and (Lys^{33}, Lys^{81}, Lys^{96}, Lys^{240}, Lys^{269}, Lys^{296}, Lys^{318}, Lys^{350}, and Lys^{351}) (Fig. 39.6b).

Table 39.4 Salt bonds formed at the side chain ε-amino group of lysine and its around residue (Asp or Glu) in [HOOCBMIm][Cl] ionic liquid system environment

System	Donor	Acceptor	Snapshots occupancy/frame
[HOOCBMIm][Cl][a]	Lys^{26}	Asp^{13}	876
	Lys^{26}	Asp^{14}	706
	Lys^{33}	Asp^{36}	27
	Lys^{70}	Glu^{98}	1,210
	Lys^{81}	Glu^{83}	76
	Lys^{108}	Asp^{36}	717
	Lys^{137}	Glu^{134}	45
	Lys^{198}	Glu^{171}	107
	Lys^{240}	Asp^{258}	3
	Lys^{269}	Asp^{258}	100
	Lys^{318}	Glu^{171}	43
	Lys^{318}	Asp^{313}	271
	Lys^{342}	Glu^{422}	1,058
	Lys^{374}	Glu^{371}	488
	Lys^{418}	Asp^{430}	942
	Lys^{427}	Asp^{395}	2
	Lys^{427}	Asp^{425}	1,052

[a] Ion pair formed: the distance between acidic amino acid ($RCOO^-$) and a basic amino acid (RNH_3) was less than 4 Å

Table 39.5 Salt bonds formed at the side chain ε-amino group of lysine and its around residue (Asp or Glu) in [HOOCMMIm][Cl] ionic liquid system environment

System	Donor	Acceptor	Snapshots occupancy/frame
[HOOCMMIm][Cl]	Lys^{26}	Asp^{13}	140
	Lys^{33}	Asp^{34}	28
	Lys^{70}	Glu^{98}	1,344
	Lys^{81}	Asp^{106}	34
	Lys^{81}	Glu^{83}	184
	Lys^{108}	Asp^{106}	197
	Lys^{137}	Glu^{134}	12
	Lys^{198}	Glu^{171}	502
	Lys^{240}	Asp^{258}	36
	Lys^{269}	Asp^{258}	5
	Lys^{342}	Glu^{422}	1,625
	Lys^{374}	Glu^{371}	2
	Lys^{418}	Asp^{430}	1,603
	Lys^{427}	Asp^{395}	199
	Lys^{427}	Asp^{425}	131

[a] Ion pair formed: the distance between acidic amino acid ($RCOO^-$) and a basic amino acid (RNH_3) was less than 4 Å

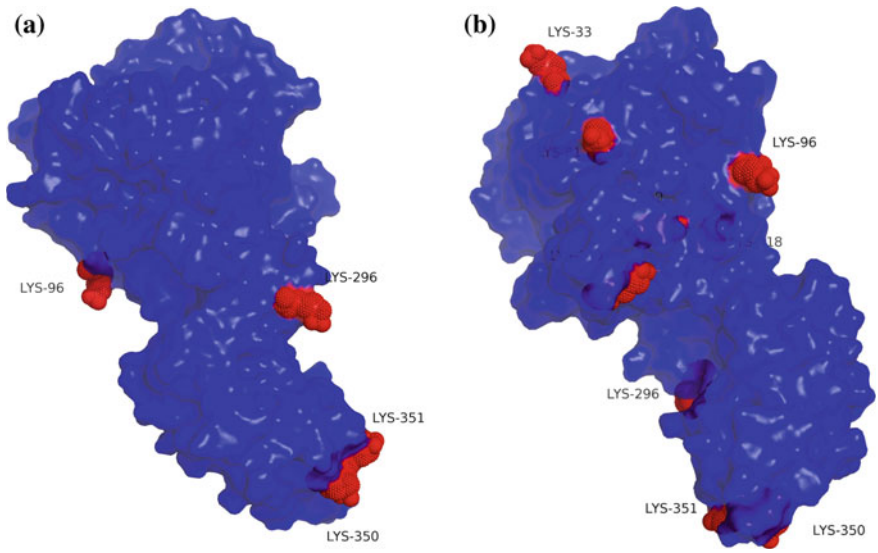

Fig. 39.6 The most likely modification sites of PPL modified by [HOOCBMIm][Cl] (**a**) and [HOOCMMIm][Cl] (**b**), respectively

39.4 Conclusion

Molecular dynamics simulations were performed on ILs modified PPL to investigate the role of structure-function on protein modification sites. In this study, a simple and novel method was established to predict the modification site. First, the number of modified lysine and the modification sites were preliminarily determined by the calculation of SASA. Second, "bond occupancy" including hydrogen bonds and salt-bridges were successfully applied to exclude the low reactivity of lysine residues and further to identify the modification sites. Finally, we found that the most possibly modification sites in systems 2 and 3 were (Lys^{96}, Lys^{296}, Lys^{350} and Lys^{351}) and (Lys^{33}, Lys^{81}, Lys^{96}, Lys^{240}, Lys^{269}, Lys^{296}, Lys^{318}, Lys^{350} and Lys^{351}), respectively. These results of the number of modificated lysine residues are in line with the experimental results reported previously. Further research is underway to develop a more sophisticated method to verify the modification sites and elucidate the modification mechanism.

Acknowledgments This research was supported by the National Science Foundation for Distinguished Young Scholars of China (No. 21225626), the Hi-Tech Research and Development Program of China (863 Program, 2011AA02A209), the National Natural Science Foundation of China for Young Scholars (Grant No. 21106064), the National Basic Research Program of China (2011CB710800).

References

1. Busto E, Gotor-Fernández V, Gotor V (2000) Hydrolases: catalytically promiscuous enzymes for non-conventional reactions in organic synthesis. Chem Soc Rev 39:4504–4523
2. Zheng GW, Xu JH (2011) New opportunities for biocatalysis: driving the synthesis of chiral chemicals. Curr Opin Biotechnol 22:784–792
3. Goswami D, Basu JK, De S (2013) Lipase applications in oil hydrolysis with a case study on castor oil: a review. Crit Rev Biotechnol 33:1–16
4. Bommarius AS, Blum JK, Abrahamson MJ (2011) Status of protein engineering for biocatalysts: how to design an industrially useful biocatalyst. Curr Opin Chem Biol 15:194–200
5. Díaz-Rodríguez A, Davis BG (2011) Chemical modification in the creation of novel biocatalysts. Curr Opin Chem Biol 15:211–219
6. Chalker JM, Bernardes GJ, Lin YA, Davis BG (2009) Chemical modification of proteins at cysteine: opportunities in chemistry and biology. Chem Asian J 4:630–640
7. Bekhouche M, Doumèche B, Blum LJ (2010) Chemical modifications by ionic liquid-inspired cations improve the activity and the stability of formate dehydrogenase in [MMIm][Me_2PO_4]. J Mol Catal B Enzym 65:73–78
8. Bekhouche M, Blum LJ, Doumèche B (2011) Ionic liquid-inspired cations covalently bound to formate dehydrogenase improve its stability and activity in ionic liquids. ChemCatChem 3:875–882
9. Zou B, Hu Y, Jiang L, Jia R, Huang H (2013) Mesoporous material SBA-15 modified by amino acid ionic liquid to immobilize lipase via ionic bonding and cross-linking method. Ind Eng Chem Res 52:2844–2851
10. Jia R, Hu Y, Liu L, Jiang L, Zou B, Huang H (2013) Enhancing catalytic performance of porcine pancreatic lipase by covalent modification using functional ionic liquids. ACS Catal 3:1976–1983
11. Jia R, Hu Y, Liu L, Jiang L, Huang H (2013) Chemical modification for improving activity and stability of lipase B from Candida antarctica with imidazolium-functional ionic liquids. Org Biomol Chem 11:7192–7198
12. Hu Y, Yang Y, Jia R, Ding Y, Li S, Huang H (2014) Chemical modification with functionalized ionic liquids: a novel method to improve the enzymatic properties of *Candida rugosa* lipase. Bioproc Biosyst Eng. doi:10.1007/s0449-014-1134-4
13. Mogharrab N, Ghourchian H, Amininasab M (2007) Structural stabilization and functional improvement of horseradish peroxidase upon modification of accessible lysines: experiments and simulation. Biophys J 92:1192–1203
14. Hermoso J, Pignol D, Kerfelec B, Crenon I, Chapus C, Fontecilla-Camps JC (1996) Lipase activation by nonionic detergents the crystal structure of the porcine lipase-colipase-tetraethylene glycol monooctyl ether complex. J Biol Chem 271:18007–18016
15. Malde AK, Zuo L, Breeze M, Stroet M, Poger D, Nair PC, Oostenbrink C, Mark AE (2011) An automated force field topology builder (ATB) and repository: version 1.0. J Chem Theor Comput 7:4026–4037
16. Frisch MJ, Trucks GW, Schlegel HB, Scuseria GB, Robb MA, Cheeseman JR, Montgomery JA Jr, Vreven T, Kudin KN, Burant JC, Millam JM, Iyengar SS, Tomasi J, Barone V, Mennucci B, Cossi M, Scalmani G, Rega N, Petersson GA, Nakatsuji H, Hada M, Ehara M, Toyota K, Fukuda R, Hasegawa J, Ishida M, Nakajima T, Honda Y, Kitao O, Nakai H, Klene M, Li X, Knox JE, Hratchian HP, Cross JB, Bakken V, Adamo C, Jaramillo J, Gomperts R, Stratmann RE, Yazyev O, Austin AJ, Cammi R, Pomelli C, Ochterski JW, Ayala PY, Morokuma K, Voth GA, Salvador P, Dannenberg JJ, Zakrzewski VG, Dapprich S, Daniels AD, Strain MC, Farkas O, Malick DK, Rabuck AD, Raghavachari K, Foresman JB, Ortiz JV, Cui Q, Baboul AG, Clifford S, Cioslowski J, Stefanov BB, Liu G, Liashenko A, Piskorz P, Komaromi I, Martin RL, Fox DJ, Keith T, Al-Laham MA, Peng CY, Nanayakkara A, Challacombe M, Gill PMW, Johnson B, Chen W, Wong MW, Gonzalez C, Pople JA (2004) Gaussian 03, Revision C. 02. Gaussian Inc., Wallingford

17. Berendsen HJC, van der Spoel D, van Drunen R (1995) GROMACS: a message-passing parallel molecular dynamics implementation. Comput Phys Commun 91:43–56
18. van der Spoel D, Lindahl E, Hess B, Groenhof G, Mark AE, Berendsen HJC (2005) GROMACS: fast, flexible, and free. J Comput Chem 26:1701–1718
19. Hess B, Kutzner C, Van Der Spoel D, Lindahl E (2008) GROMACS 4: algorithms for highly efficient, load-balanced, and scalable molecular simulation. J Chem Theor Comput 4:435–447
20. Oostenbrink C, Soares TA, van der Vegt NF, van Gunsteren WF (2005) Validation of the 53A6 GROMOS force field. Eur Biophys J 34:273–284
21. Li H, Robertson AD, Jensen JH (2005) Very fast empirical prediction and rationalization of protein pKa values. Proteins 61:704–721
22. Berendsen H, Postma J, van Gunsteren W, Hermans J (1981) Interaction models for water in relation to protein hydration. In: Pullman B (ed) Intermolecular forces, vol 11. D. Reidel Publishing Company, Dordrecht, pp 331–342
23. Hess B, Bekker H, Berendsen HJC, Fraaije JGEM (1997) LINCS: a linear constraint solver for molecular simulations. J Comput Chem 18:1463–1472
24. Darden T, York D, Pedersen L (1993) Particle mesh Ewald: an N·log(N) method for Ewald sums in large systems. J Chem Phys 98:10089–10092
25. Essmann U, Perera L, Berkowitz ML, Darden T, Lee H, Pedersen LG (1995) A smooth particle mesh Ewald method. J Chem Phys 103:8577–8593
26. Bussi G, Donadio D, Parrinello M (2007) Canonical sampling through velocity rescaling. J Chem Phys 126:14101–14107
27. Parrinello M, Rahman A (1981) Polymorphic transitions in single crystals: a new molecular dynamics method. J Appl Phys 52:7182–7190
28. Humphrey W, Dalke A, Schulten K (1996) VMD: visual molecular dynamics. J Mol Graph 14:33–38
29. DeLano WL (2002) The PyMOL molecular graphics system, version 1.5.0.4. Schrödinger, LLC, Portland
30. Vidya P, Chadha A (2009) The role of different anions in ionic liquids on Pseudomonas cepacia lipase catalyzed transesterification and hydrolysis. J Mol Catal B Enzym 57:145–148
31. Zhao J, Li XQ, Xiu ZL (2009) Specific-site PEGylation of hirudin on ion-exchange column and theoretical prediction and analysis of modified sites by molecular dynamics simulation. Chem J Chin Univ 7:1410–1416
32. O'Brien AM, Ó'Fágáin C, Nielsen PF, Welinder KG (2011) Location of crosslinks in chemically stabilized horseradish peroxidase: implications for design of crosslinks. Biotechnol Bioeng 76:277–284
33. Rahman RNZA, Tejo BA, Basri M, Rahman MBA, Khan FS, Zain M, Siahaan TJ, Salleh AB (2004) Reductive alkylation of lipase. Appl Biochem Biotech 118:11–20
34. Suckau D, Mak M, Przybylski M (1992) Protein surface topology-probing by selective chemical modification and mass spectrometric peptide mapping. Proc Natl Acad Sci U.S.A. 89:5630–5634
35. Lee B, Richards FM (1971) The interpretation of protein structures: estimation of static accessibility. J Mol Biol 55:379–400
36. Shuvaev VV, Fujii J, Kawasaki Y, Itoh H, Hamaoka R, Barbier A, Zieqler O, Siest G, Taniquchi N (1999) Glycation of apolipoprotein E impairs its binding to heparin: identification of the major glycation site. BBA-Mol Basis Dis 1454:296–308

Chapter 40
Effect of Oxygen on Fermentation Characteristics of Three Non-*Saccharomyces* from Hengshui Laobaigan

Huixia Zhu, Yuhang Zhang, Zexia Li, Yawei Guo, Zongzhi Cheng, Dongguang Xiao and Zhimin Zhang

Abstract In this paper, effects of different oxygen concentrations on the fermentation characteristics of three non-*Saccharomyces* from Hengshui Laobaigan fermented grains were studied. Three non-*Saccharomyces* strains, *Pichia kudriavzevii* (Y3), *Pichia anomala* (Y4), and *Wickerhamomyces anomalus*, were isolated from fermenting grains in previous study. Because it is difficult to control oxygen concentration in solid state fermentation, the amount changes of fluid in containers were utilized to control oxygen. At the initial fermented stage (0 h), the volumes of liquid 50, 100, 150, 200, and 250 mL were corresponding to the oxygen concentrations 6.90, 6.71, 6.25, 4.32, and 4.50 mg/L, respectively. Three strains were separately incubated for 3 % yeast inoculation quantity and cultured in different amounts of sterilized medium for 6 days. The data shows that oxygen had been largely consumed in the stage of rapid yeast reproduction. Significance test concluded that different oxygen concentrations have significant effects on ethyl acetate. Reducing sugar was increased generally with increasing liquid volume; while alcohol yield of Y3 had no significant difference except for 50 mL, but Y4 and Y6 had remarkable differences in every liquid volume. 1-propanol was unaffected by liquid volume while different oxygen concentration has significant effect on isobutanol.

Keywords Hengshui laobaigan · Non-*Saccharomyces* · Fermentation · Oxygen concentration

---

H. Zhu · Y. Zhang · Z. Li · Y. Guo · Z. Cheng · Z. Zhang (✉)
Hengshui Laobaigan Liquor-Making Group, Hengshui, Hebei 053000, China
e-mail: T99998@163.com

H. Zhu
Department of Life Science, Heng Shui University, Hengshui 053000, Hebei, China

H. Zhu · D. Xiao
Key Laboratory of Industrial Microbiology, Ministry of Education,
Tianjin University of Science and Technology, TEDA, Tianjin 300457, China

T.-C. Zhang and M. Nakajima (eds.), *Advances in Applied Biotechnology*,
Lecture Notes in Electrical Engineering 333, DOI 10.1007/978-3-662-46318-5_40

Chinese liquor is produced by solid state fermentation with grains and distilled mainly from fermented cereals. Grains in containers can be quickly fermented by many kinds of microbes in sophisticated biological transformation systems. Yeasts have played a major role in the process of fermentation [1].

In fermented systems, yeasts are divided into two groups: *Saccharomyces cerevisiae* and non-*Saccharomyces*, depending on different functions. The former is mostly completed ethanol fermentation and has better ethanol biosynthetic ability than the latter. But non-*Saccharomyces* can produce multiple enzymes which turn the precursor substance of grains into main flavor components. The flavor components are important for improving full-bodied and well-structured Chinese liquor [2, 3]. For example, the major ingredients of Hengshui Laobaigan-flavor Liquor included ethyl acetate, ethyl lactate, ethanol, acetaldehyde, 1-propanol, isopentyl, and isobutanol.

Most of the esters in the process of fermentation are produced by non-*Saccharomyces*, especially *Pichia Saccharomyces* [4]. For instance, *Pichia anomala* is the prevalent strain which can exhibit biocatalytic effect under various extreme environments. These extreme conditions include low pH, low water activity, high osmotic pressure, and anaerobic conditions [5]. Various non-*Saccharomyces* exhibit their ability to adapt to environments differently and the stages of metabolism do not mesh. Meanwhile, heat and oxygen transfer are difficult in solid state fermentation and are obviously different among different layers [6–8]. Main flavor components in earlier stage are seriously affected by oxygen. So research on the effect of different oxygen conditions on non-*Saccharomyces* has an important guiding sense to the actual production.

Three non-*Saccharomyces* strains, *Pichia kudriavzevii*, *P. anomala* and *Wickerhamomyces anomalus*, were isolated from fermenting grains in the previous study. Because it is difficult to control oxygen concentration in solid state fermentation, the amount changes of fluid in containers were utilized to control oxygen [9]. So the research on the effect on non-*Saccharomyces* fermentation characteristics in different blocks under different oxygen conditions will be an important guiding sense to the actual production.

40.1 Materials and Methods

40.1.1 Materials

Pichia kudriavzevii (Y3), *P. anomala* (Y4), and *Wickerhamomyces anomalus* (Y6) were stored in Hebei Hengshui Laobaigan liquor Co., Ltd.

40.1.2 Methods

The fermentation medium was prepared from sorghum. Shattered sorghum was proportionately added to water and boiled; starch was hydrolyzed by heat-resistant α-amylase and glucoamylase, in 1 h at 100 °C and 3 h at 65 °C, respectively. All matter was filtered and the filtrate was adjusted to 13 Brix by water. The fermentation medium was the adjusted filtrate and was separately took 50, 100, 150, 200, and 250–250 mL Erlenmeyer flasks at 121 °C for sterilization.

Three *non-Saccharomyces* strains, *P. kudriavzevii*, *P. anomala,* and *W. anomalus,* were separately incubated for 3 % yeast inoculation quantity and culture in different amount of sterilized medium. Erlenmeyer flasks were sealed by fermentation bung and stored static cultivation at 28 °C. Oxygen concentrations and yeast counts were monitored in the process of fermentation. The sample of Erlenmeyer flask was never reused. Reducing sugar, alcohol, ethyl acetate, 1-propanol, isopentyl, and isobutanol were determined on the sixth day. Reducing sugar of the fermenting liquor was determined and the other distillates were determined by means of gas–liquid chromatography.

Dissolved oxygen analyzer (SG9) is produced by Shanghai Mettler-Toledo Co., Ltd and have a probe which can drive 1 cm under the surface of medium. In this paper, Erlenmeyer flasks were sealed by a rubber stopper with two holes, one for the probe and other for the fermentation bung. All units were hermetically sealed. CO_2 produced during fermentation escaped through the fermentation bung.

Titrimetry was used to determine the reducing sugar and hydrometer method was to mensurate alcohol. In this paper, the initial reducing sugar level of the medium was 13.88 g/100 mL.

Gas chromatography (GC 2010) unit was purchased from Shimadzu Corporation, Japan and has an SPB-1701 capillary column. Column temperature: initial temperature 45 °C for 2 min, 4 °C/min risen to 65 °C, 10 °C/min risen to 220 °C; injector temperature: 200 °C; detector temperature: 240 °C; carrier gas (N_2): 0.085 Mpa (1.08 mL/min); make-up gas: 50.0 mL/min; H_2 gas: 30 mL/min; atmosphere: 300 mL/min.

10.00 mL distillates were added to 0.10 mL 3 g/100 mL internal standard and blended injection. Yeast count was measured by hemocytometer [10]. Statistical analysis of data was performed using SPSS 19.0 software and was significant at 0.05 level.

40.2 Results and Discussion

40.2.1 Changes of Oxygen Concentration in Static Fermentation

In this paper, all samples were cultured by liquid static fermentation, so oxygen of medium was obtained from the atmosphere by simple diffusion in Erlenmeyer flasks. While more liquid was in the flask, the less atmosphere was in it. A lot of flavor components, such as alcohol, CO_2, ethyl acetate, 1-propanol, isopentyl and isobutanol, were biosynthesized in the fermentation process. And more and more CO_2 from various fermentation stages escaped through the fermentation bung. As a result, fewer and fewer oxygen was kept in flask (Fig. 40.1).

Let us take *P. anomala* (Y4), for example. At the initial fermented stage (0 h), the volumes of liquid 50, 100, 150, 200, and 250 mL were corresponding to the oxygen concentrations 6.90, 6.71, 6.25, 4.32, and 4.50 mg/L, respectively. The fastest sample of oxygen decline rate was 50 mL liquid and had been reduced to 1.22 mg/L at 3 h, while the oxygen concentration of 100 mL liquid volume was reduced fewer. Oxygen of 200 and 250 mL decreased from 4.32 and 4.50 mg/L to 0.24 and 0.26 mg/L in 5.5 h, respectively; meanwhile, 150 mL had the lowest declined rate.

After 36 h at the oxygen concentration of zero, the tendency of all samples is consistent. But different liquid volume of every strain was markedly different starting point and trend of fermentation. This demonstrates that the oxygen concentration of medium controlled by liquid volume was correct.

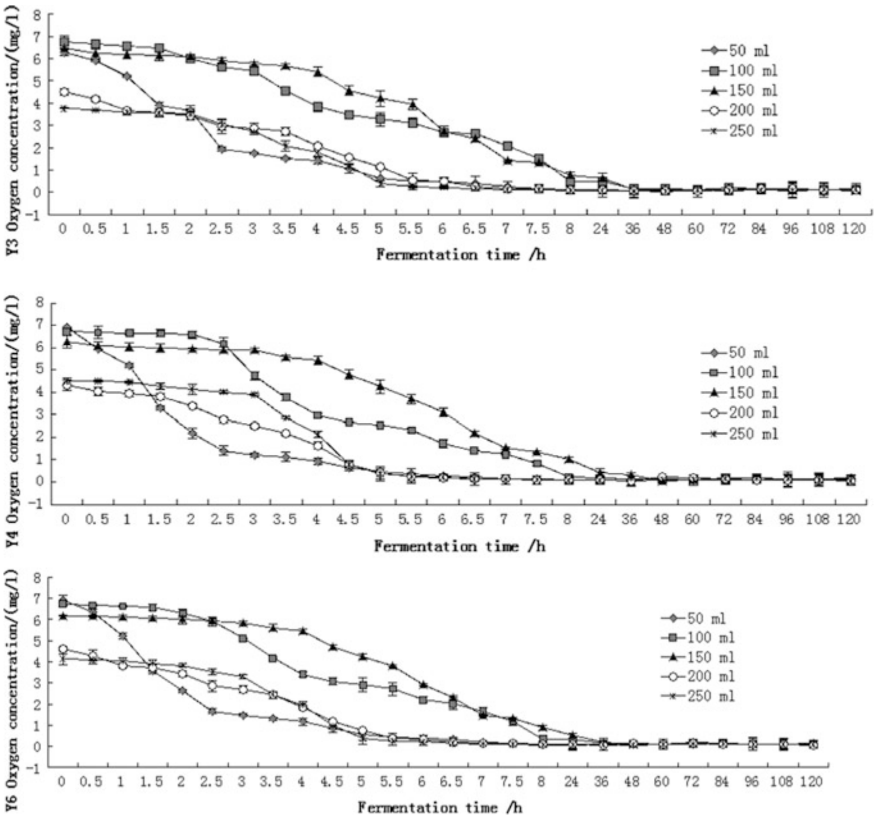

Fig. 40.1 Effects of liquid volume on dissolved oxygen

40.2.2 Effect of Oxygen on Yeast Counts of Three Strains

Effects on yeast counts of the three strains by different liquid volumes were clearly different (Fig. 40.2). Yeast counts of Y3 and Y6 in the early fermented part were closely related with liquid volumes of flask. The fastest growing period of yeast counts in the early stages was 0–24 h and was matched the fastest reducing period of oxygen concentration in Fig. 40.1. The data shows that oxygen had been largely consumed in the stage of yeast rapid reproduction. The maximum yeast counts of

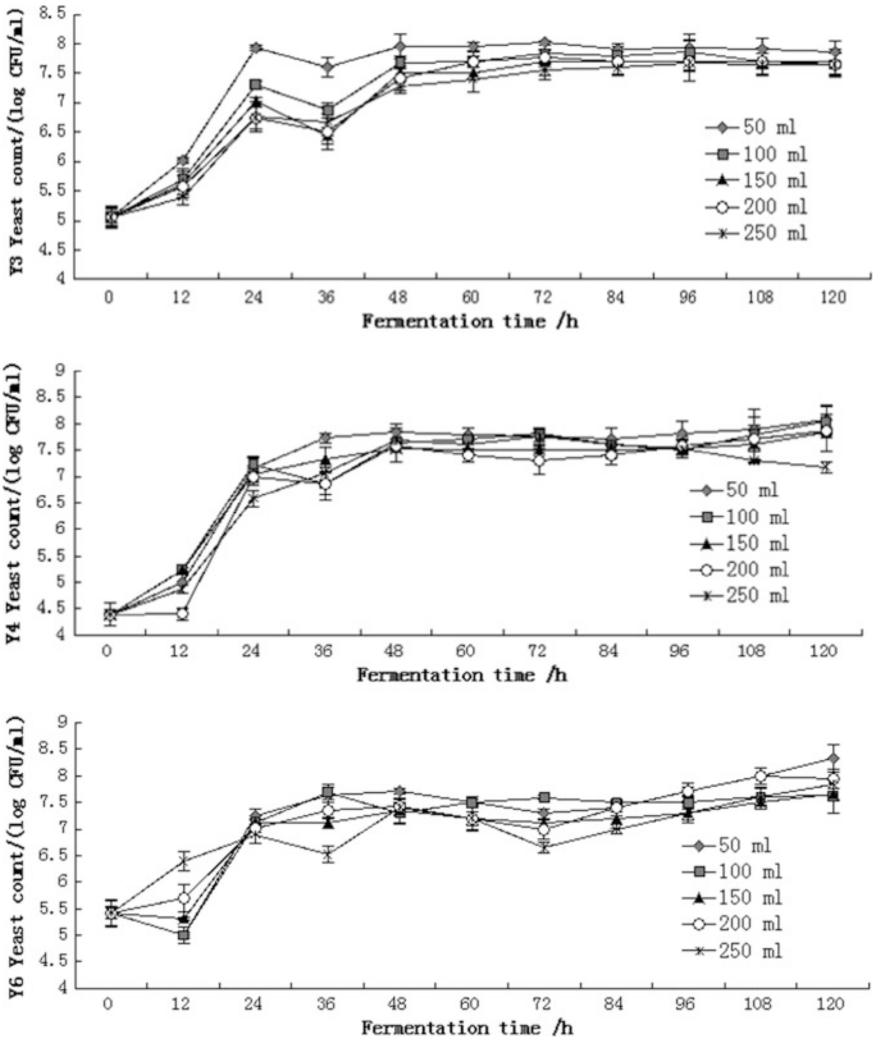

Fig. 40.2 Effects of liquid volume on yeast counts

three strains were the samples with 50 mL liquid medium and it was also proved this rule.

Y4 yeast counts were not significantly affected by liquid volumes (Fig. 40.2) in 0–96 h. While the count of 50 mL was up to 1.16×10^8 cfu/mL and 250 mL was 1.50×10^7 cfu/mL in final period.

It concluded that different oxygen concentrations have significant effects on the metabolic modulation mechanisms. This problem will need to be further gone into.

40.2.3 Effect of Oxygen on Reducing Sugar of Three Strains

After a 6 day static cultivation, the reducing sugar of Y3 every liquid volume was reduced to 2.50 g/100 mL and the utilization rate was high (Fig. 40.3). Y3 strain reducing sugar increased with liquid volume. The sugar of 50 and 250 mL was 7.21 and 12.10 g/100 mL while the utilization rates were 48.05 and 12.82 %, respectively. Trends of Y6 reducing sugar were significantly parallel with Y4, but the utilization rates were higher than the latter. In sum, reducing sugar was increased generally with increasing liquid volume.

40.2.4 Effect of Oxygen on Alcohol of Three Strains

Alcohol yield of Y3 increased generally with increasing liquid volume and Y4 was descended; Y6 alcohol had been declining in waves (Fig. 40.4).

From the results analysis, the less oxygen concentration was in the medium, the more alcohol yield of Y3; Y4 was just the opposite. The maximum alcohol yield of

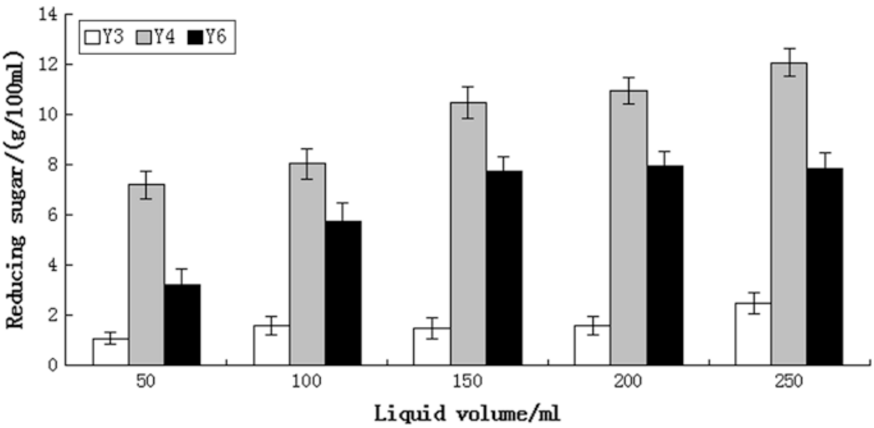

Fig. 40.3 Effects of liquid volume on reducing sugar

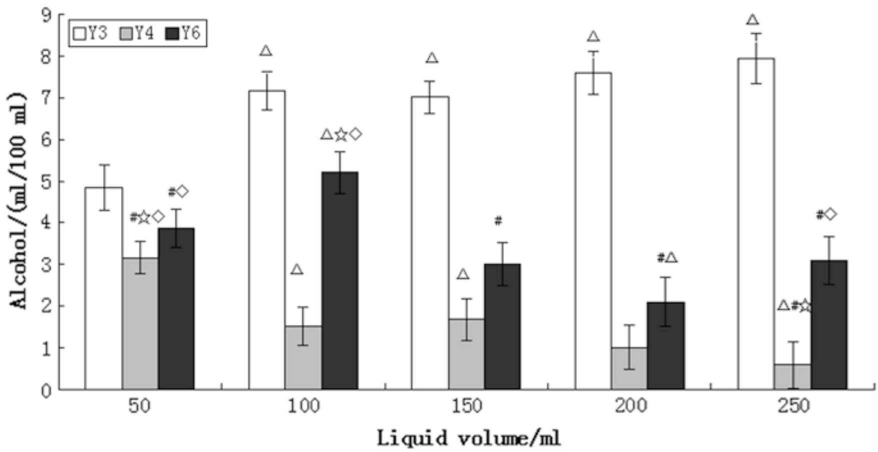

Fig. 40.4 Effects of liquid volume on alcohol. "△" Significant differences with 50 mL; "#" Significant differences with 100 mL; "☆" Significant differences with 150 mL; "◇" Significant differences with 200 mL ($P < 0.05$)

Y3 was for 100 mL liquid while the minimum was for 200 mL. Significant test of alcohol yield registered that Y3 had no significant difference by liquid volume except for 50 mL, but Y4 and Y6 had remarkable differences in every liquid volume.

40.2.5 Effect of Oxygen on Ethyl Acetate of Three Strains

Ethyl acetate yields of 3 strains were depressed generally with increasing liquid volume (Fig. 40.5). Ethyl acetate yield of Y4 was highest to 385.74 mg/100 mL for 50 mL liquid volume, which was 3.27 times than Y3, 5.80 times than Y6 in the same condition. Significance test of ethyl acetate showed that Y3 had significant difference between 50 and 100 mL liquid volume and others, while Y4 and Y6 had remarkable differences in every liquid volume. It concluded that different oxygen concentrations have significant effects on ethyl acetate.

40.2.6 Effect of Oxygen on 1-Propanol, Isobutanol, and Isopentanol of Three Strains

1-Propanol yields of Y3 were depressed generally with increasing liquid volume (Fig. 40.6). 1-propanol of Y4 and Y6 altered little when the concentration of oxygen increased. Significance test of 1-propanol was not being performed because 1-propanol was unaffected by the liquid volume.

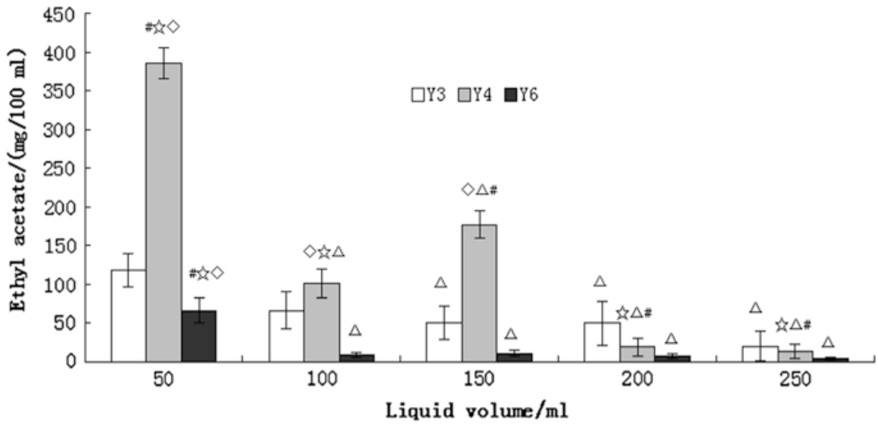

Fig. 40.5 Effects of liquid volume on ethyl acetate. "△" Significant differences with 50 mL; "#" Significant differences with 100 mL; "☆" Significant differences with 150 mL; "◇" Significant differences with 200 mL ($P < 0.05$)

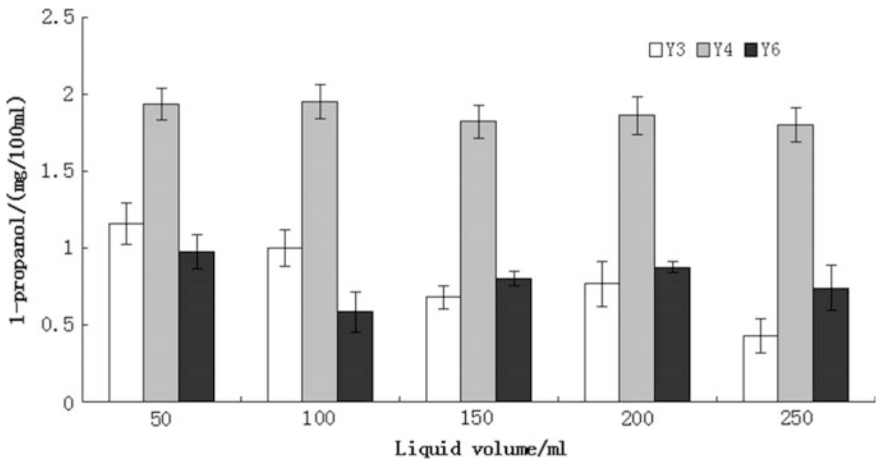

Fig. 40.6 Effects of liquid volume on 1-propanol

Isobutanol yields of Y3 and Y4 were also reduced with increasing liquid volume (Fig. 40.7). For every volume, Y6 isobutanol changed less than Y3 and Y4. Three strains had remarkable differences in every liquid volume and it concluded that different oxygen concentrations have significant effects on isobutanol.

Isopentanol yields of Y6 increased generally with increasing liquid volume (Fig. 40.8), but the Y3 and Y4 were just the opposite. In the same way, three strains had remarkable differences in every liquid volume and it concluded that different oxygen concentrations have significant effect on isopentanol.

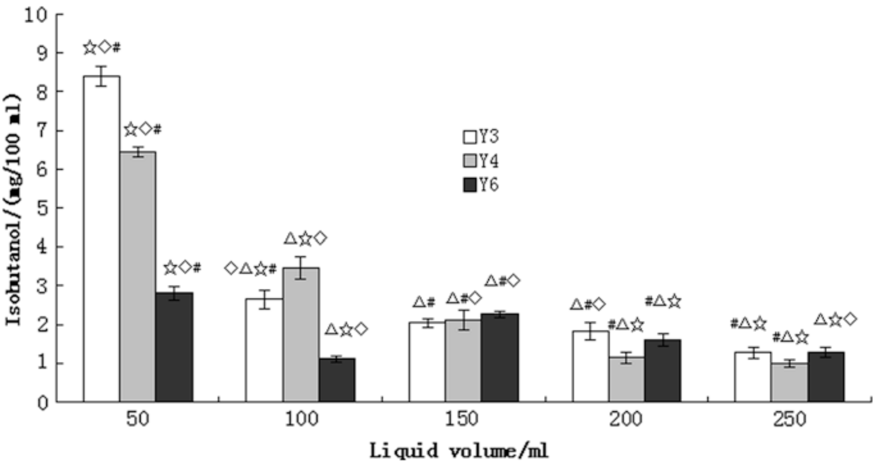

Fig. 40.7 Effects of liquid volume on isobutanol. "△" Significant differences with 50 mL; "#" Significant differences with 100 mL; "☆" Significant differences with 150 mL; "◇" Significant differences with 200 mL ($P < 0.05$)

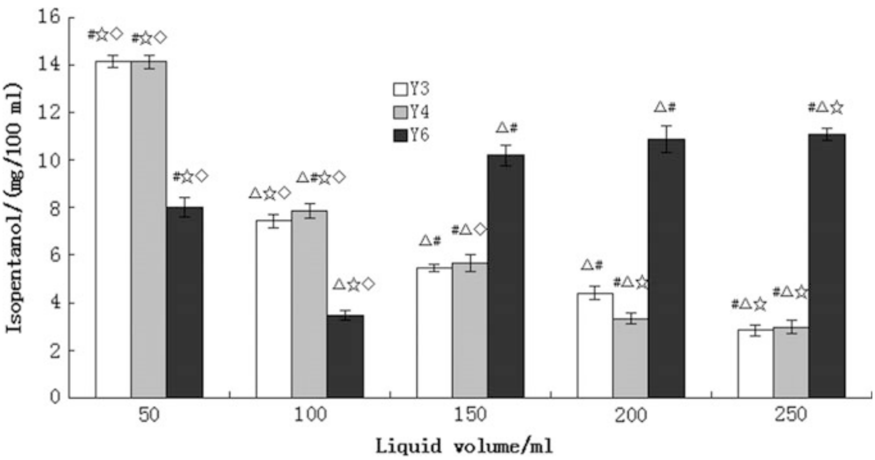

Fig. 40.8 Effects of liquid volume on isopentanol. "△" Significant differences with 50 mL; "#" Significant differences with 100 mL; "☆" Significant differences with 150 mL; "◇" Significant differences with 200 mL ($P < 0.05$)

40.3 Conclusion

At the initial fermented stage (0 h), the volumes of liquid 50, 100, 150, 200, and 250 mL were corresponding to the oxygen concentrations of 6.90, 6.71, 6.25, 4.32, and 4.50 mg/L, respectively. Three strains were separately incubated for 3 % yeast inoculation quantity and cultured in different amounts of sterilized medium for

6 days. The data shows that oxygen had been largely consumed during the stage of rapid yeast reproduction. Significance test concluded that different oxygen concentrations have significant effect on ethyl acetate. Reducing sugar was increased generally with increasing liquid volume; while alcohol yield of Y3 had no significant difference except for 50 mL, but Y4 and Y6 had remarkable differences in every liquid volume. 1-propanol was unaffected by liquid volume while different oxygen concentrations have significant effect on isobutanol.

Acknowledgments This work was supported by Hebei Postdoctoral Selected Sustentation Scientific Project (B2014002023) and Hengshui Science and Technology Fund (13067).

References

1. Zhou RP, You L, Chen YZ et al (2012) Dynamic changes of the multi-grain and flavor liquor cavities fermentation. Sci Technol Food Ind 33(18):214–216
2. Gobbi M, Comitini F, Domizio P et al (2010) Non-Saccharomyces yeasts in controlled mixed culture fermentation in winemaking: the role of metabolic interactions. J Biotechnol 50:299–300
3. Ciani M, Comitini F (2011) Non-Saccharomyces wine yeasts have a promising role in biotechnological approaches to winemaking. Ann Microbiol 61:25–32
4. Sáez JS, Lopes CA, Kirs VC et al (2010) Enhanced volatile phenols in wine fermented with Saccharomyces cerevisiae and spoiled with Pichia guilliermondii and Dekkera bruxellensis. Lett Appl Microbiol 51:170–176
5. Passoth V, Fredlund E, Druvefors UÄ et al (2006) Biotechnology, physiology and genetics of the yeast Pichia anomala. FEMS Yeast Res 6:3–13
6. Zhang WX, Yue YY, Wen-liang Xiang et al (2005) Changes and rules of chemical composition in the fermented grains of chinese strong aromatic spirits. J Sichuan Univ (Eng Sci Ed) 37:44–48
7. Zhang ZM, Wu WS, Li KF (2012) Study on the change rules of chemical composition of site-flavor fermented grains in fermentation process. Sci Technol Food Ind 33:108–113
8. Zhang MY (2007) The production mechanism of the fragrance in the Chinese spirit and the operation of the spirit brewing. Liquor Making 34:109–113
9. Aline A, Cintia MB, Henrique J et al (2014) Dissolved oxygen content in apple must: technological implications in cider processing. J Inst Brew 120:65–70
10. Walker GM (2011) Pichia anomala: cell physiology and biotechnology relative to other yeasts. Antonie Van Leeuwenhoek Int J Gen Mol Microbiol 99:25–34

Chapter 41
Microbial Transformation of Antitumor Isatin Derivatives by Fungi

Xiaolin Peng, Kailin Han, Yan Wang, Peng Yu and Hua Sun

Abstract The biotransformation of HKL-2c (**1**) and HKL-2h (**2**), the antitumor lead compounds found by our lab, were investigated. Compounds **1** and **2** were individually submitted to incubations with selected fungi *Trichoderma koningii* AS 3.4290, *Trichoderma viride* AS 2.2942, *Aspergillus flavus* AS 3.3950, *Aspergillus sydowii* AS 3.4258, *Aspergillus* AS 3.3885, and *Aspergillus niger* AS 3.3928. The products of hydrolysis from **1** and **2** by *Aspergillus* AS 3.3885 were identified based on spectroscopic methods. Those fungi, therefore, are useful for mild, selective hydrolysis of an ester of isatin substrates.

Keywords Isatin · Microbial transformation · Antitumor

41.1 Introduction

Isatin, an indole derivative, was found in many plants, such as *Isatis tinctoria*, *Calanthe discolor,* and *Couroupita guianensis* [1]. In recent years, many isatins have marked anticancer effects toward various types of cancer cell lines in vitro and in vivo. Some of them had been successfully developed to treat human cancer diseases in some therapeutic areas, including vinblastine [2], vincristine [3], and sunitinib [4]. Sunitinib (sunitinib, SU11248) is a novel multitargeted oral anticancer

X. Peng · K. Han · Y. Wang · P. Yu · H. Sun (✉)
Key Lab of Industrial Fermentation Microbiology (Tianjin University of Science and Technology), Ministry of Education, Tianjin 300457, People's Republic of China
e-mail: sunhua@tust.edu.cn

X. Peng · K. Han · Y. Wang · P. Yu · H. Sun
Tianjin Key Lab of Industrial Microbiology, Tianjin University of Science and Technology, Tianjin 300457, People's Republic of China

X. Peng · K. Han · Y. Wang · P. Yu · H. Sun
Sino-French Joint Lab of Food Nutrition/Safety and Medicinal Chemistry, Tianjin University of Science and Technology, Tianjin 300457, People's Republic of China

T.-C. Zhang and M. Nakajima (eds.), *Advances in Applied Biotechnology*,
Lecture Notes in Electrical Engineering 333, DOI 10.1007/978-3-662-46318-5_41

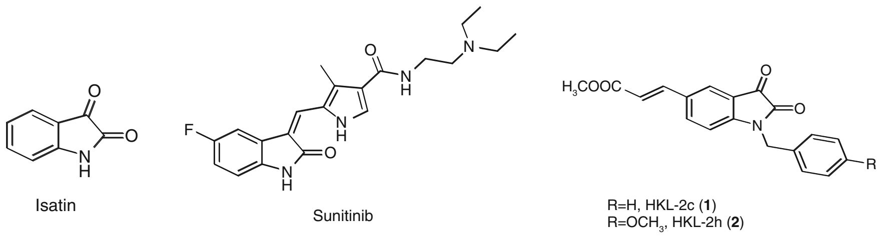

Fig. 41.1 The structures of isatin, sunitinib, HKL-2c, and HKL-2h

drug, approved by the United States FDA in 2006. It was the first cancer drug simultaneously approved for two different indications, renal cell carcinoma (RCC) and imatinib-resistant gastrointestinal stromal tumor (GIST) [5].

Our previous study successfully identified the novel isatin derivatives **1** and **2** (Fig. 41.1) as the anticancer agents with inhibitory concentrations (IC_{50}) at nanomolar level [6]. The molecular mechanism analysis showed that compound **2** treatment downregulated the expression of CDK1 and cyclin B but upregulated the level of phosphorylated CDK1. Besides, compound **2** treatment caused the dissipation of mitochondrial membrane potential, activated caspase-3, and lowered the Bcl-2/Bax ratio in K562 cells [7].

To further expand the structural diversity of isatin and investigate the potential application, compounds **1** and **2** were subjected to biotransformation by the fungi *Trichoderma koningii* AS 3.4290, *Trichoderma viride* AS 2.2942, *Aspergillus flavus* AS 3.3950, *Aspergillus sydowii* AS 3.4258, *Aspergillus* AS 3.3885, and *Aspergillus niger* AS 3.3928. This paper describes the isolation, structural elucidation, and characterization of the transformed products, as well as a discussion of their antitumor activity.

41.2 Materials and Methods

41.2.1 Reagents and Strains

All reagents and solvents were purchased from commercial suppliers and used without further purification. D(+)-sucrose, D(+)-glucose, $NaNO_3$, $MgSO_4$, KCl, $FeSO_4{\cdot}7H_2O$, K_2HPO_4, Na_2SO_4 anhydrous, and agar powder were purchased from Sinopharm Chemical Reagent Co., Ltd (China). The strains used in biotransformation were purchased from the China General Microbiological Culture Collection Center (CGMCC, Beijing, China), and stored and maintained on 20 % (v/v) glycerol stock solutions at −20 °C. It inoculated on a slant medium 28 °C cultured for 3–4 days and maintained at 4 °C.

NMR spectra were obtained at 400 MHz for ^1H and 100 MHz for ^{13}C on a Bruker Avance 400 spectrometer, in DMSO-d_6, with solvent peaks used as references. ESI–MS data were measured on an Agilent Technologies 6210 LC/TOF instrument. Column chromatography was performed with silica gel 200–300 mesh (Qingdao Marine Chemical Inc. Qingdao, China). TLC was performed on pre-coated silica gel GF_{254} plates.

41.2.2 Biotransformation

Each bacterial strain was taken from the agar slant to shaking seed bottle culture (250 mL containing 100 mL of medium) by a platinum ring and was cultivated at 30 °C on rotary shakers (120 rpm) for 48 h.

The above seedlings were transferred to fresh medium in an amount of 1 %, and incubated at 30 °C for 24 h. Each flask was fed with 10 mg of compounds **1** and **2** (dissolved in DMSO, 100 g L^{-1}) and incubated for another 7 days. Thus, the total culture volume was 10 L, and the total of 400 mg of compounds **1** and **2** were fed as substrates.

41.2.3 Extraction and Isolation of Transformed Products

At the end of the biotransformation, the cultures were filtered through cheesecloth and centrifuged to separate the mycelium. The supernatant was condensed at 40 °C to approximately 3 L and extracted with same volume of EtOAc [8]. The mycelium was immersed and extracted with EtOAc (50 mL × 3). The combined organic phases were dried over Na_2SO_4 anhydrous, and concentrated in vacuo as well as tested using TLC monitoring at 254 nm and visible light. The crude transformation products were purified by chromatography (petroleum ether/EtOAc = 100:0, 20:1, 10:1, 5:1, 3:1, 2:1, 1:1, v/v). The products were recrystallized with $CHCl_3$ and hexane to give the yellow crystals. All products (**3**–**4**) were identified on the basis of spectroscopic data. The ^{1}H, ^{13}C NMR and ESI–MS data are presented in Table 41.2.

41.2.4 Cytotoxic Assay

Cells (100 μL) were cultured in 96-well plates at a density of 5×10^4 cells/mL for 2 h (K562) or overnight (HepG2 and HT-29). Compounds (DMSO solution of 0.5 μL) were added to each well to culture for another 48 h. MTT assay was performed using thermo microplate reader. The DMSO-treated controls were calculated as a cell viability value of 100 %. The IC_{50} values were obtained by nonlinear regression using GraphPad Prism 4.0. IC_{50} measurements for each compound were done three times.

41.3 Results and Discussion

Six fungi were screened for their ability to transform compounds **1** and **2** in liquid potato-dextrose medium (*T. koningii* AS 3.4290 and *T. viride* AS 3.2942), and liquid Czapek-Dox medium (*A. flavus* AS 3.3950, *A. sydowii* AS 3.4258, *Aspergillus* AS 3.3885, and *A. niger* AS 3.3928). The secondary screening results are shown in Table 41.1. The compounds **1** and **2** could be converted into at least one product by *Aspergillus* AS 3.3885. Especially, an obvious product could be observed from the cultures of compound **1** with *Aspergillus* AS 3.3885. In addition, *T. koningii* AS 3.4290 and *A. niger* AS 3.3928 exhibited biotransform ability to compound **1**. Therefore, the fungus *Aspergillus* AS 3.3885 cultivated in the liquid Czapek-Dox medium was found to be the most effective and was selected for the preparative-scale biotransformation of both compounds **1** and **2**.

The obtained products were purified and identified by the nuclear magnetic resonance hydrogen spectrum (^{1}H-NMR), carbon spectrum (^{13}C-NMR), and Mass spectrometry (LC–MS). The spectroscopic data are shown in Table 41.2. Product **3** was obtained as a yellow crystal. The molecular weight was determined by ESI–MS from the $[M+H]^+$ peak at *m/z* 308.4. The MS spectrum indicated the absence of methyl group (CH_2) comparing with compound **1** (molecular weight 321.3). The methyl peaks of acrylic acid methyl ester disappeared in both ^{1}H-NMR and ^{13}C-NMR. Therefore, the structure of product **3** was speculated into (*E*)-3-(1-benzyl-2,3-dioxoindolin-5-yl) acrylic acid. The product **4** was a yellow crystal and $[M+H]^+$ peak at *m/z* 338.2. Comparing with compound **2** (molecular weight 351.4), the structure of product **4** could be (*E*)-3-(1-(4-methoxybenzyl)-2,3-dioxoindolin-5-yl) acrylic acid. The ^{1}H-NMR and ^{13}C-NMR analysis verified the correctness of the structure of compound **4**. The biotransforming scheme is shown in Fig. 41.2.

The anticancer activity of one of the representative products **4,** against three human tumor cell lines (K562, HepG2, and HT-29), was evaluated by MTT assay in vitro. Comparing with starting material **2**, the cytotoxicity of hydrolysis compound **4** was decreased (>10 μM) (Table 41.3). This observation suggested that the methyl ester is a necessary structure unit for the activity of **2**. However, the hydrolysis products provide the free carboxyl group, which can be modificated into other ester, amide, aldehyde, hydroxyl, etc. In our previous work [6], the compounds **3** and **4** could be obtained using basic hydrolysis. But the reaction

Table 41.1 The screening results of isatin derivatives biotransformed by 6 strains

Strain	HKL-2c	HKL-2h
Trichoderma koningii AS 3.4290	+	–
Trichoderma viride AS 3.2942	–	–
Aspergillus flavus AS 3.3950	–	–
Aspergillus sydowii AS 3.4258	–	–
Aspergillus AS 3.3885	++	+
Aspergillus niger AS 3.3928	+	–

Note (–) No products; (+) products; (++) obvious products

Table 41.2 The ^{1}H, ^{13}C NMR, and ESI–MS data of compounds **3** and **4**

Compounds	Spectroscopic data		
	^{1}H-NMR	^{13}C-NMR	ESI–MS
3	4.94 (s, 2H), 6.52 (d, 1H, J = 16.0 Hz), 7.00 (d, 1H, J = 8.0 Hz), 7.28–7.36 (m, 5H), 7.43 (d, 1H, J = 4.0 Hz), 7.55–7.59 (d, 1H, J = 16.0 Hz), 7.90 (d, 1H, J = 1.6 Hz), 7.93 (d, 1H, J = 4.0 Hz), 12.34 (s, 1H)	43.5, 111.8, 118.8, 119.1, 124.4, 127.9, 128.0, 129.1, 130.2, 135.9, 138.0, 143.0, 151.7, 159.0, 168.0, 183.0	308.4 $[M+H]^{+}$
4	3.72 (s, 3H), 4. 86 (s, 2H), 6.52 (d, 1H, J = 16.0 Hz), 6.89 (d, 2H, J = 8.8 Hz), 7.02 (d, 1H, J = 8.8 Hz), 7.37 (d, 2H, J = 8.8 Hz), 7.57 (d, 1H, J = 16.0 Hz), 7.90–7.92 (m, 2H), 12.34 (s, 1H)	42.9, 55.5, 111.9, 114.51, 114.51, 118.7, 119.1, 124.3, 127.6, 129.3, 129.3, 130.1, 137.9, 143.0, 151.6, 158.9, 159.2, 168.0, 183.1	338.2 $[M+H]^{+}$

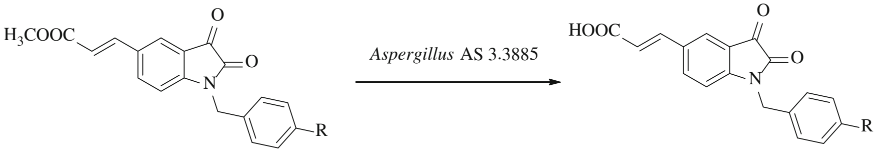

1 R_1=H
2 R_2=OCH_3

3 R_1=H
4 R_2=OCH_3

Fig. 41.2 The scheme of compounds **1** and **2** were transformed by *Aspergillus* AS 3.3885

Table 41.3 In vitro antitumor activities of compounds **2** and **4**

Compounds	IC_{50} (μM)		
	K562	HepG2	HT-29
2	0.0030 ± 0.001	0.030 ± 0.02	0.030 ± 0.01
4	>10	>10	>10
Camptothecin[a]	0.040 ± 0.02	0.050 ± 0.02	0.060 ± 0.01

Note [a] Positive control

conditions were vigorous and polluting. By contrast, the condition of microbial transformation was mild and green.

Therefore, *Aspergillus* AS 3.3885 could be useful for mild, selective hydrolysis of an ester of isatin substrates. The further microbial transformation study of antitumor isatin derivatives is ongoing in our laboratory.

Acknowledgments The authors sincerely thank the financial support from the International Science & Technology Cooperation Program of China (2013DFA31160).

References

1. Da-Silva JFM, Garden SJ, Pinto AC (2001) The chemistry of isatins: a review from 1975 to 1999. J Braz Chem Soc 12:273–324
2. Pandya P, Agarwal LK, Gupta N, Pal S (2014) Molecular recognition pattern of cytotoxic alkaloid vinblastine with multiple targets. J Mol Graph Model 54C:1–9
3. Kawasaki H, Taira N, Ichi T et al (2014) Weekly chemotherapy with cisplatin, vincristine, doxorubicin and etoposide followed by surgery for thymic carcinoma. Eur J Surg Oncol 44:1151–1155
4. Hartmann JT, Kanz L (2008) Sunitinib and periodic hair depigmentation due to temporary c-KIT inhibition. Arch Dermatol 144:1525–1526
5. US Food and Drug Administration (2006) FDA approves new treatment for gastrointestinal and kidney cancer
6. Han K, Zhou Y, Liu F et al (2014) Design, synthesis and in vitro cytotoxicity evaluation of 5-(2-carboxyethenyl) isatin derivatives as anticancer agents. Bioorg Med Chem Lett 24:591–594
7. Zhou Y, Zhao HY, Han KL et al (2014) 5-(2-Carboxyethenyl) isatin derivative induces G2/M cell cycle arrest and apoptosis in human leukemia K562 cells. Biochem Biophys Res Commun 450:1650–1655
8. Lu J, Deng S, Chen H et al (2013) Microbial transformation of cinobufotalin by *Alternaria alternate* AS 3.4578 and *Aspergillus niger* AS 3.739. J Mol Catal B Enzym 89:102–107

Chapter 42
Effect of Ultrasound on Lysine Muriate Crystallization

Aijun Hu, Zili Chen, Shuting Jiao, Huanqin Peng, Yanshu Fan, Lin Chen, Meiling Liu and Jie Zheng

Abstract Ultrasound was applied to the crystallization process of lysine muriate solution. The effects on crystal yield of lysine muriate were investigated, including ultrasonic time, ultrasonic power, and crystallization time. The experimental results showed that the crystal yield reached 84.08 % with the adequate conditions of ultrasonic power 112 W, ultrasonic time 50 min, and crystallization time 5 h. And the effects of ultrasonic power on the nucleation induction period and crystal appearance of lysine muriate were also researched, the results indicated that with ultrasound, induction period was shortened significantly compared to that without it at the same supersaturation ratio. The higher the ultrasonic power, the shorter the induction period, and the smaller the crystals. With the increase of ultrasonic power, the crystals became smaller and more uniform. It can be concluded that using ultrasound-assisted crystallization cannot only improve the crystallization rate and crystal yield, but also obtain crystalline product with the characteristics of small particles and uniform distribution by controlling ultrasonic power.

Keywords Lysine muriate · Ultrasound · Crystallization

42.1 Introduction

Lysine is not only one of the most important amino acids, but also one of the essential amino acids for people's health [1]. Except for glutamic acid, the yield of lysine is the highest. Lots of foodstuffs and feedstuffs have few of lysine, so that lysine is needed to add to both human food and animal feed in order to improve their nutritional value [2]. In recent years, the market demand for lysine has become

A. Hu (✉) · Z. Chen · S. Jiao · H. Peng · Y. Fan · L. Chen · M. Liu · J. Zheng
Key Laboratory of Food Nutrition and Safety (Tianjin University of Science & Technology), Ministry of Education, College of Food Engineering and Biotechnology, Tianjin University of Science & Technology, Tianjin 300457, People's Republic of China
e-mail: huaijun@tust.edu.cn

T.-C. Zhang and M. Nakajima (eds.), *Advances in Applied Biotechnology*,
Lecture Notes in Electrical Engineering 333, DOI 10.1007/978-3-662-46318-5_42

more great because of the rapid development of feed and food industries, as well as its applications in medical area [1].

Generally, lysine exists in the form of muriate (i.e., lysine muriate) in both production and application, and lysine muriate is transferred to lysine after it is being taken by people. The higher its purity is, the more expensive it is. Among all methods to improve its purity, crystallization is an extremely important process for obtaining highly pure lysine muriate.

Conventional crystallization methods include cooling crystallization, vacuum cooling crystallization, evaporative crystallization, and reaction crystallization [3]. Ultrasonic crystallization as a novel method is received much attention in recent years. It has been studied with various crystallization systems and its advantages in several crystallization applications [4, 5] are disputed. As a size reduction method, ultrasonic crystallization can be considered as a more attractive size reduction method compared to grinding since under ultrasound conditions the crystallinity of the crystals does not decrease in most cases. Ultrasound narrows the metastable zone which can be also concluded from shortened induction period when the nucleation rate is determined empirically under isothermal conditions, i.e., ultrasound promotes nucleation dominated by a heterogeneous primary nucleation mechanism [6]. Li et al. [7] employed ultrasound in salting out crystallization and analyzed its influence on the crystal size distribution and shape. Chow et al. [8] applied ultrasound to a melt crystallization system for ice crystallization from sugar solutions. They also studied the influence of ultrasound on the nucleation rates and cavitation effects on ice fragmentation. According to Devarakonda et al. [9], ultrasound impacts crucially on the seed size, breakage of the solute lumps, and crystallization kinetics. Amara et al. [10] found out that ultrasound increased the crystal growth rate of potash alum, while crystals grown under ultrasound were smaller than those produced in stirred crystallizer without ultrasound. Marjatta et al. [11] examined crystallization of glycine with ultrasound. Martini et al. [12] investigated the effect of high intensity ultrasound (HIU) on crystallization behavior of anhydrous milk fat, the results showed that HIU application not only decreased the induction time of crystallization (faster crystallization) at a constant crystallization temperature, but also generated smaller crystals. Patel et al. [13] studied the recovery of lactose from reconstituted lactose solutions with the aid of ultrasound.

Ultrasound is a kind of mechanical wave in elastic medium. Acoustically induced cavitation is one of the primary effects of power ultrasound in a continuum fluid. Ultrasound can impose an oscillatory pressure on the fluid. At low intensity, this pressure wave induces motion and mixing within the fluid, a process known as acoustic streaming. Mixing can be increased by above process. At higher intensity, in addition to acoustic streaming and mixing effects, the local pressure in the expansion phase of the cycle may fall below the vapor pressure of the fluid, which causes any minute bubbles or cavities to grow. If the ultrasonic intensity is increased further, negative transient pressures can be produced in the fluid medium. This pressure not only enhances the bubble growth process, but also produces new cavities by the tensioning effect on the fluid [14]. Ultrasound also has mechanical effects on crystallization systems. The shock wave which is produced by the implosion of cavitation bubbles is responsible for the effects of ultrasound on particles in suspension. At vicinity of the implosion, the pressure can reach as high as 300 MPa. According to Doktycz and Suslick [15], the shock wave can promote the mixing process as well. If the implosion of a cavitation bubble is near an interface, besides the shock wave, it can generate a liquid jet [16]. Andrew Van Hook stated further that sound wave irradiation is helpful to supplement and strengthen the wave action needed in forming critical crystal nucleus, thus, it is able to accelerate crystallization [17]. In addition, in our previous research [18], it was found that ultrasound has important effect on enhancing crystal velocity, shortening crystal time, controlling the distribution of crystalline grain diameter, improving product quality, and so on. So the application of ultrasonic crystallization of lysine muriate would have bright prospects.

The aim of this study was to extract lysine muriate crystallization with ultrasound and evaluate the influence of some critical factors on the process. The employed crystallization method was cooling crystallization enhanced with ultrasound.

42.2 Experiment

42.2.1 Materials and Instruments

Lysine muriate was crystallized from aqueous solutions. For cooling crystallization experiments, the solutions were prepared by weighing certain amounts of solid lysine muriate (purity >99.5 %), bought from Sugar Hill East King Co. Ltd. in deionized water. Ultrasonic processor (Model KQ5200DB NC) from Kunshan Ultrasonic Instrument Co. Ltd.; Electric constant temperature water bath pot from Beijing Guangming Medical Instrument Factory Wing; Electric Blast Oven from Experiment Instrument Co. Ltd. Tianjin Tianyu; Electronic Balance from Dragon Electronics Co. Ltd. Shenyang; Microscope from Shanghai Boaimei Light Instruments Manufacturing Co. Ltd.; Digital camera from Powershot 480, Nikon Instruments Sales Co. Ltd (China).

42.2.2 Ultrasonic Processor

Ultrasonic processor, Model KQ5200DB NC with a frequency of 40 kHz, was used as a ultrasonic power generator. The ultrasonic processor was equipped with a wattmeter. The ultrasonic power was changed by varying the amplitude of the ultrasound.

42.2.3 Determination and Calculation of Crystal Yield

$$\text{Crystal yield} = N \times 100\,\%/M \tag{42.1}$$

where N is the mass of lysine muriate crystals obtained by ultrasound, g; M is the mass of lysine muriate powder used to make the solutions of certain concentrations, g.

42.2.4 The Effect of Ultrasonic Time on Crystal Yield of Lysine Muriate

25 g lysine muriate powder was dissolved with 40 mL deionized water to prepare a solution with the concentration of 38.46 %, which was used for ultrasonic treatment and crystallization. The ultrasonic conditions were: ultrasonic power 160 W, temperature 35 °C, ultrasonic time was 0, 10, 30, 50, 70 and 90 min, respectively. After being treated by ultrasound each time, the solutions were kept for 3 h at 25 °C for crystallization. Crystals were filtered by using a Büchner funnel under vacuum and the crystals were collected, then dried for 3 h at 100 °C. The crystal yields were determined and calculated according to the method described in Sect. 42.2.3.

42.2.5 The Effect of Ultrasonic Power on Crystal Yield of Lysine Muriate

Ultrasonic time was 50 min, ultrasonic power was 64, 96, 112, 128 and 160 W, separately. The other ultrasonic conditions and operations were the same as those mentioned in Sect. 42.2.4.

42.2.6 The Effect of Crystal Time on Crystals Yield of Lysine Muriate

Ultrasonic time was 50 min, ultrasonic power was 112 W, and crystallization time was 3, 4, 5, 6 and 7 h, respectively. The other ultrasonic conditions and operations were the same as those mentioned in Sect. 42.2.4.

42.2.7 The Preparation of Supersaturation Solution

Rapid cooling method is used for the preparation of supersaturated solution. This method [19] shows that the supersaturated solution is obtained through rapid cooling of a certain concentration of saturated solution. For instance, when the solution is confected, which saturation solubility and supersaturation ratio S is, respectively, 85 g/100 mL and 1.4 at 35 °C, according to the definition of supersaturation ratio [20]: $S = C/C_0$ (where S is supersaturation ratio; C is solubility of supersaturation solution; C_0 is solubility of saturated solution), the solubility of supersaturation solution C = 85 g × 1.4/100 mL = 119 g/100 mL. So, firstly, the solution with the saturation solubility of 119 g/100 mL is needed to be confected, then rapidly cool to 35 °C and obtain the supersaturation solution needed.

According to the method mentioned above, the supersaturation ratios of the solutions used in our study, which were 1.45, 1.50, 1.55, 1.60, 1.65, 1.70, 1.75, 1.80, 1.85, 1.90, 1.95, and 2.0, can be confected, respectively.

42.2.8 The Measurement of Induction Period of Traditional Crystallization

Supersaturation solution of lysine muriate obtained by the above method (Sect. 42.2.7) was placed into 35 °C ultrasonic processor, however, without ultrasound. Then, the time was recorded and the record was kept until the crystals can be observed.

42.2.9 The Measurement of Induction Period of Ultrasonic Crystallization

Supersaturation solutions of lysine muriate obtained by the above method (Sect. 42.2.7) were placed into 35 °C ultrasonic processor. Then, we introduced ultrasound and started to record ultrasonic time until the crystals can be observed.

42.2.10 The Effect of Ultrasonic Power on Induction Period of Lysine Marinate Crystallization

A series of supersaturated solutions with supersaturation ratio of 1.45, 1.50, 1.55, 1.60, 1.65, 1.70, 1.75, 1.80, 1.85, 1.90, 1.95, and 2.0 were prepared, respectively, according to above method (Sect. 42.2.7). They were placed, respectively, into 35 °C ultrasonic cleaning tank, the introduced ultrasonic power was 0, 96, 112, and 128 W, respectively. Each induction period corresponding to supersaturation ratio was measured, respectively.

42.2.11 The Effect of Ultrasonic Power on Crystal Appearance of Lysine Muriate

25 g lysine muriate powder was dissolved with 40 mL deionized water to prepare a solution with the concentration of 38.46 %, which was used for ultrasonic crystallization. Ultrasonic power was 64, 96, 112, 128 and 160 W, separately, temperature 35 °C, ultrasonic time was 50 min. After being treated by ultrasound each time, the solutions were kept for 5 h at 25 °C for crystallization. Crystals were filtered by using a Büchner funnel under vacuum and the crystals were collected, then dried for 3 h at 100 °C. The crystal yields were determined and calculated according to the method described in Sect. 42.2.3.

42.3 Results and Discussion

42.3.1 Effect of Ultrasonic Time on Crystal Yield

It can be seen from Fig. 42.1 that without ultrasound, namely, ultrasonic time was 0 min, crystal yield was less than that with ultrasound. Between 0 and 50 min, crystal yield increased rapidly with the extension of ultrasonic time. Between 50 and 95 min, crystal yield kept almost the same. So, the reasonable ultrasonic time of the experimental process was 50 min.

There are several possible reasons for the above phenomenon. Cavitation bubbles may be formed because of introducing ultrasound in the crystallization of lysine muriate. The burst of cavitation bubbles will produce high temperature, pressure, and a certain degree of microjet which can shatter crystal particles and generate a large number of crystals which secondary nucleations grow into. Furthermore, the high temperature generated in the process of cavitation bubbles burst, which can accelerate the diffusion of solutes and break crystal particles, is increasing with the increase of ultrasonic power. However, the stabilization of bubbles is needed for a certain time, when ultrasonic time is shorter, ultrasound fails

Fig. 42.1 Effect of ultrasonic time on crystal yield

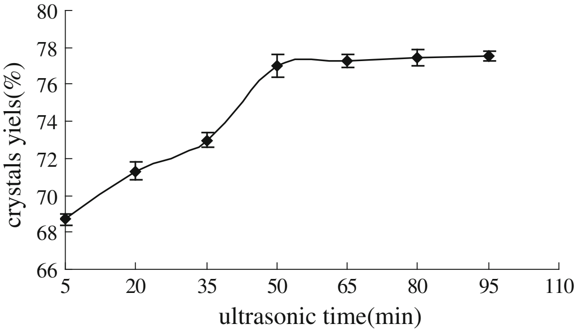

to promote nucleation, so that crystal yield will be lower; when ultrasonic time is longer, ultrasound can promote nucleation and the second nucleation will appear rapidly after the ultrasonic induction, so that more crystal nucleus will be formed. In addition, ultrasonic crushing effect will also produce more crystal nucleus and increase the crystal yield. On the other hand, for a certain volume and supersaturation ratio of lysine muriate solution, the maximal crystal yield is certain since it depends on them. As a result, the increase of crystal yield becomes slow with the extension of ultrasonic time.

42.3.2 Effect of Ultrasonic Power on Crystal Yield

As clearly shown in Fig. 42.2 that the crystal yield was increasing with the raising of ultrasonic power, but the increasing became not obvious when ultrasonic power was over 112 W. This may be because ultrasonic cavitation leads lots of bubbles to produce. And those bubbles will crack suddenly when they grow to certain extent, which will supply especial space and energy for the form of crystal nucleus, then the crystal yield is enhanced. However, whether and how much ultrasonic cavitation takes place depends on ultrasonic power, in a certain system, ultrasonic cavitation will be restrained when ultrasonic power is increased to a certain extent and then affect crystal yield. Taking all factors into consideration, ultrasonic power 112 W was relatively reasonable in the experiment.

42.3.3 The Effect of Crystallization Time on Crystal Yield

As shown in Fig. 42.3 that the crystal yield was increasing with the raising of crystallization time, but the increasing became not obvious when crystallization time was over 5 h. This phenomenon can be demonstrated as follows: solution is divided into solid–liquid two-phase once crystal nucleus is formed, crystal nucleus is enfolded with a layer of liquid film and solution in the film converts saturation from supersaturation because some of its solutes have been absorbed to the surface of crystal nucleus. However, solution out of the film is still supersaturated and its solutes

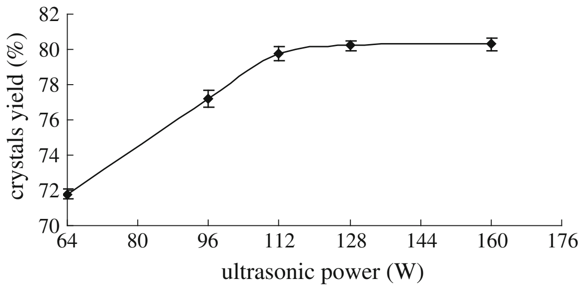

Fig. 42.2 Effect of ultrasonic power of crystal yield

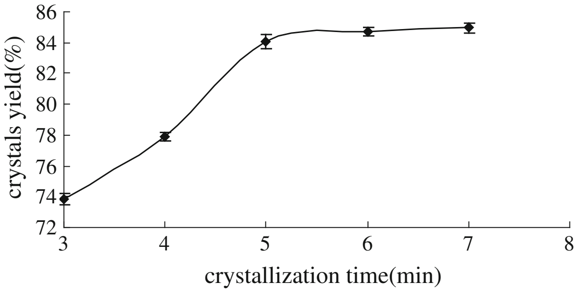

Fig. 42.3 Effect of crystallization time on crystal yield

will continually diffuse into the liquid film and also be absorbed to the surface of crystal nucleus because of the impetus of concentration difference. The solutes are arrayed layer by layer on the surface of crystal nucleus, which prompt continually the crystal growth until the concentration of solution falls to saturation [20]. So, the quality of crystal is increasing with the extension of time, as a result, crystal yield is enhanced continually until the concentration of solution falls to that solutes can no longer precipitate from the solution. Thus, in the period of 3–5 h, crystal yield increased rapidly, after 5 h it had only little increase. In the experiment, crystallization time 5 h was relatively reasonable and the crystal's yield reached 84.08 %.

42.3.4 *Effect of Ultrasonic Power on Induction Period of Lysine Muriate Crystal Nucleation*

It can be seen from Fig. 42.4 that under the circumstance of the same supersaturation ratio, the crystal induction period of lysine muriate with ultrasound was shorter than that without ultrasound. And the higher the ultrasonic power, the shorter the induction period. The shortening amplitude decreased with the increase of supersaturation ratio, and it can be concluded that the effect of ultrasound on crystal nucleation of lysine muriate in the lower supersaturation ratio solution was more significant than that in the higher.

42.3.5 *Effect of Ultrasound on Crystal Appearance of Lysine Muriate*

In the crystal growth process, the growth rates of different crystal surfaces were different. Crystal surfaces with faster growing rates eventually disappear, the final exposed surface decided the crystal shape. Introducing ultrasound can accelerate the transfer of material and heat, then strengthen crystallization [21]. The effect of ultrasonic power on crystal appearance was investigated by analyzing the pictures of lysine muriate crystals.

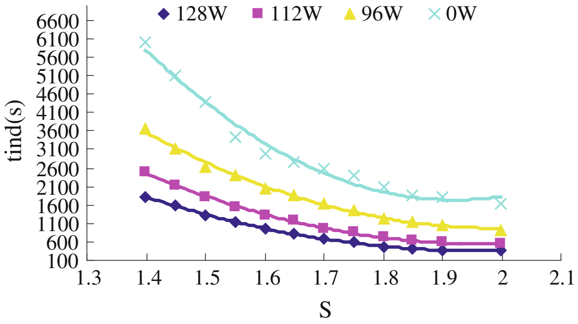

Fig. 42.4 Effect of ultrasonic power on induction period

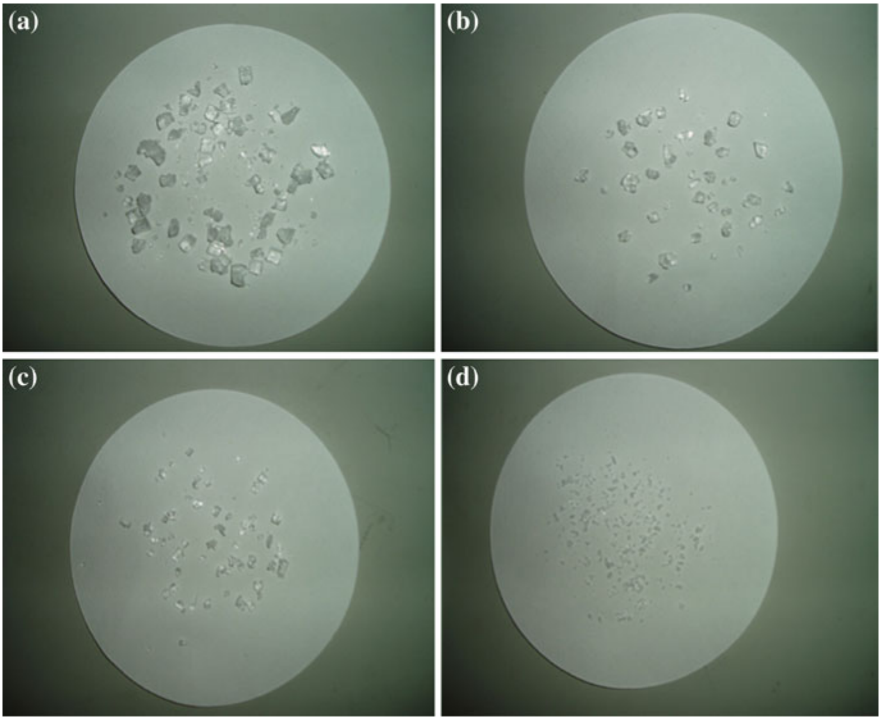

Fig. 42.5 **a** Ultrasonic power 0 W. **b** Ultrasonic power 64 W. **c** Ultrasonic power 96 W. **d** Ultrasonic power 160 W

From Fig. 42.5, the results were observed as follows: Without ultrasound, the crystals were irregular, larger, and the size distribution was broader, however, with adequate ultrasound, they were regular, smaller, and uniform, the particle size decreased with the increase of ultrasonic power from 64 to 160 W. When crystal particles were larger, the coalescence phenomenon was obvious, the dispersion of crystals was getting better and particles became more uniform.

42.4 Conclusions

In the study, the process of ultrasound-assisted crystallization and the effect of some factors including ultrasonic time, ultrasonic power, and crystallization time on crystals yield were investigated. The results showed that the crystal yield can reach 84.08 % with the adequate conditions of ultrasonic power 112 W, ultrasonic time 50 min, and crystallization time 5 h. Under the same supersaturation ratio, when ultrasound was introduced, the induction period was significantly shortened, the higher the ultrasonic power, the shorter the induction period. The crystals obtained by ultrasound were small and uniform, and become smaller with the increase of ultrasonic power. It can be concluded that using ultrasound-assisted crystallization cannot only improve the crystallization rate and crystal yield, but also obtain crystalline product with the characteristics of small particles and uniform distribution by controlling ultrasonic power.

Acknowledgments We are grateful for the financial support from the Advanced Program of Tianjin Municipal Enterprise Post-doctor Innovation Project, the China Postdoctoral Science Foundation funded project (Grant No.: 2013M540211), and the National Natural Science Foundation of China (Project No.: 31071608).

References

1. Li X (2001) Technology and market analysis of L-lysine. Shanghai Chem Ind 3(14):33
2. Zhao Z (1995) Purification and research of L-lysine muriate. Amino Acids Biotic Resour 17(2):36
3. Feng R (2002) Amino acid crystallization process. Ferment Technol Commun 31(4):11–12
4. McCausland L, Cains P, Martin PD (2001) Use the power of sonocrystallization for improved properties. Chem Eng Prog 97:56–61
5. McCausland L, Cains P (2003) Ultrasound to make crystals. Chem Ind 5:15–16
6. Lyczko N, Espitalier F, Louisnard O, Schwartzentruber J (2002) Effect of ultrasound on the induction time and the metastable zone widths of potassium sulphate. Chem Eng J 86:233–241
7. Li H, Wang J, Bao Y, Guo Z, Zhang M (2003) Rapid sonocrystallization in the salting-out process. J Cryst Growth 247:192–198
8. Chow R, Blindt R, Kamp A, Grocutt P, Chivers R (2004) The microscopic visualisation of the sonocrystallisation of ice using a novel ultrasonic cold stage. Ultrason Sonochem 11:245–250
9. Devarakonda S, Evans JMB, Myerson AS (2004) Impact of ultrasonic energy on the flow crystallization of dextrose monohydrate. Cryst Growth Des 4:687–690
10. Amara N, Ratsimba B, Wilhelm A, Delmas H (2004) Growth rate of potash alum crystals: comparison of silent and ultrasonic conditions. Ultrason Sonochem 11:17–21

11. Marjatta L-K, Milja K, Jukka R, Mikko H, Juha K (2006) Crystallization of glycine with ultrasound. Int J Pharm 320:23–29
12. Martini S, Suzuki AH, Hartel RW (2008) Effect of high intensity ultrasound (HIU) on crystallization behavior of anhydrous milk fat. J Am Oil Chem Soc 85:621–628
13. Patel SR, Murthy ZVP (2009) Ultrasound assisted crystallization for the recovery of lactose in an anti-solvent acetone. Cryst Res Technol 44:889–896
14. Cains PW, Martin PD, Price CJ (1998) The use of ultrasound in industrial chemical synthesis and crystallization. 1. Application to synthetic chemistry. Org Process Res Dev 2(1):34–48
15. Doktycz SJ, Suslick KS (1990) Interparticle collisions driven by ultrasound. Science 247:1067–1069
16. Guo Z, Jones AG, Li N, Germana S (2007) High-speed observation of the effects of ultrasound on liquid mixing and agglomerated crystal breakage processes. Powder Technol 171(3):146–153
17. Zhu T (2007) Ultrasonic crystallization and its application. Mod Phys 19(5):28–29
18. Hu A, Qiu T, Yan J et al (2002) Advances in the study of enhancement of solution crystallization by ultrasonic field. Appl Acoust 21(4):44–48
19. Zhang W (1994) Study of theory and applications of glutamate crystallization. South China University of Technology, Guangdong
20. Deng M (2007) Fermentation production technology of amino acid. China Light Industry Press, Beijing, pp 216–224
21. Meng L (2007) The effect of ultrasound on crystallization process of copper sulfate. Yangzhou University, Jiangsu

Chapter 43
Isolation and Identification of a *Bacillus amyloliquefaciens* Strain Against Grape Downy Mildew and Optimization for Its Liquid Fermentation Medium

Jiping Guo, Guang Ma, Huixia Zhu and Junfan Fu

Abstract An antagonistic bacterial strain named J12 against the grape downy mildew was isolated from 92 bacteria on grape leaves. Antagonistic strains were isolated by exploiting streak plate method. J12 was identified based on morphology observation, physiological and antibacterial characterizations, 16S rDNA sequence analysis, and the phylogenetic tree. The controlling effect of J12 on grape downy mildew was 78.6 %. The liquid fermentation medium of J12 was optimized with the response surface methodology to improve the number of live bacteria. The results showed that the strain J12 was classified as *Bacillus amyloliquefaciens*. For its liquid fermentation medium, the optimum carbon source was sucrose, the best nitrogen source was soybean meal, and the best C/N ratio was 3:1. By Plackett–Burman design and response surface methodology, the best culture medium formula is 31.18 g/L sucrose, 10.57 g/L soybean meal, 2.206 g/L K_2HPO_4, 2.5 g/L yeast, 0.5 g/L $MgSO_4 \cdot 7H_2O$. Theoretic optimum cell number was 90.87×10^8 cfu/mL. The number of bacteria in three parallel experiments was 92.54×10^8 cfu/mL, indicating that the equation fits well to the actual production.

Keywords *Bacillus amyloliquefaciens* · 16S rDNA · Phylogenetic tree · Response surface methodology

J. Guo (✉) · G. Ma · H. Zhu
Department of Life Sciences, Hengshui University, Hengshui 053000 Hebei, People's Republic of China
e-mail: guojiping888@163.com

J. Guo · J. Fu (✉)
College of Plant Protection, Shenyang Agricultural University, Shenyang 110161, Liaoning, People's Republic of China
e-mail: fujunfan@163.com

T.-C. Zhang and M. Nakajima (eds.), *Advances in Applied Biotechnology*, Lecture Notes in Electrical Engineering 333, DOI 10.1007/978-3-662-46318-5_43

43.1 Introduction

Bacillus amyloliquefaciens belongs to the aerobic or facultative anaerobic bacteria, which can produce endospores with resistance under certain conditions. It can be used as biological antagonistic bacteria [1, 2]. According to the statistics by the United Nations Food and Agriculture Organization, because the world suffered from plant diseases, 10 % of total production was lost every year [3]. 4 % of the above plant diseases are caused by fungi. At present, the main means to control fungi is chemical pesticide [4]. But environmental pollutants caused by the chemical pesticides have been threatening the health of humans. With the development of green agriculture, the use of biological means to control plant diseases are more and more concerned [5]. For example, *Bacillus subtilis* B-FS01 was used to control grape downy mildew, which effect was 88.25 %. However, the agent has not been used in factory production.

The new type of microecological preparation of *B. amyloliquefaciens* was used in agricultural production in our country from 1990s. Grape downy mildew is one of the most damaging fungal diseases of grapevine (*Vitis* spp.) worldwide [6–8]. It is caused by the heterothallic diploid *Plasmopara viticola*, a biotrophic Oomycetes native of North America. In this study, a strain named J12 was separated from the grape leaves, which has a good control effect on downy mildew of grape. After identification, the bacteria were classified as *B. amyloliquefaciens.* The nutrient requirements of this strain are relatively simple, which has a strong adaptive capacity to environment. It also has a good future as biological pesticides.

43.2 Materials and Methods

43.2.1 Separation of Bacteria on Grape Leaves

Under sterile conditions, grape leaves were cut into Erlenmeyer flask containing 50 mL of sterile water and 3 drops of Tween 80. After oscillating at 150 r/min for 30 min, the water containing bacteria was diluted to 10^{-3} and 10^{-4} with sterile water. 0.1 mL dilution was put into petri dish, and then the NA medium with 45 °C was mixed. Then the bacteria in NA medium was cultured at 28 °C for 3 days. A single colony with different forms was selected for slant culture for preservation.

43.2.2 Screening of Antagonistic Bacteria

Grape leaves infected by grape downy mildew fungus and the new shoots 4–6 wheel without downy mildew fungus were collected from the Hengshui grape garden. The grape downy mildew fungus on infected leaves was brushed away. After cultured at 22 °C for 24 h, the new grape downy mildew fungus was brushed into sterile water. The leaves without fungus were used to make leaf discs of diameter 1 cm. Leaf discs were placed in different antagonistic bacteria liquid (cell concentration = 1×10^7/mL) for 1 min. After drying, the leaf discs were placed on wet absorbent paper with back upward. The spore suspensions containing grape downy mildew fungus were sprayed on the leaf discs evenly. In each treatment, 15 leaf discs were put in a culture dish. Each treatment was replicated three times. The disease index was calculated after the leaf discs were cultured at 22 °C for 7 days.

43.2.3 Identification of Antagonistic Bacteria

Using genomic DNA as a template, the 16S rDNA was amplified. The upstream primer was 27F and the downstream primer was 1492R. The sequence of 27F is 5′-AGAGTTTGATCCTGGCTCAG-3′. And the sequence of 1492R is 5′-GGTTA CCTTGTTACGACTT-3′. PCR reaction conditions are as follows: predegeneration at 94 °C for 5 min, degeneration at 94 °C for 1 min, annealing at 55 °C for 1 min, extension at 72 °C for 1.5 min, and after 36 cycles, extension at 72 °C for 10 min, then preservation at 4 °C. The sequenced 16S rDNA gene of strain J12 was compared and analyzed by blastn software of NCBI to find the homologous sequences and determine the level of region of homology. A phylogenetic tree was constructed by the software of ClustalW and MEGA 5.05.

43.2.4 Determination of the Optimal Carbon Source, Nitrogen Source, and C/N

To determinate the optimal carbon source, the glucose, sucrose, maltose, and soluble starch were added as the only carbon sources, respectively. Then fermentation medium was cultured for 72 h with the concentration of 20 g/L. After determining the carbon source, nitrogen source was prepared with soybean meal, corn flour, peptone, fish meal, and urea (20 g/L), respectively. The determined best carbon source and nitrogen source were mixed with different C/N ratio of by 1:3, 1:2, 1:1, 2:1, 3:1, 4:1, 5:1, and 6:1, respectively. The above mediums were used to culture the J12 strain for 72 h to determine the number of live bacteria in fermentation liquid.

43.2.5 Screening the Critical Factor by Plackett–Burman Design Method

Using nine factors and three levels of Plackett–Burman (PB) design, X1, X4, X7, and X9 were void items to estimate experimental error. X2, X3, X5, X6, and X8 were sugar, soybean meal, yeast paste, $K_2HPO_4 \cdot MgSO_4 \cdot 7H_2O$, respectively. Each factor has two different level of (−1, 1), which was 30.000 and 37.500 g/L, 10.000 and 12.500 g/L, 2.500 and 3.125 g/L, 2.000 and 2.500 g/L, and 0.500 and 0.625 g/L, respectively.

43.2.6 Using the Steepest Ascent Search Experiment to Define the Optimal Concentration Range of Important Factor

In steepest ascent search experiment, the concentrations of sucrose, soybean meal, and K_2HPO_4 were changed by certain gradient and the other two factors was initial concentration. By detection of number of live bacteria in each fermentation liquid, the optimal concentration range of important factor can be determined.

43.2.7 Determine the Optimal Formula of Fermentation Culture Medium by Response Surface Method

In response surface experiments, the Box–Behnken central composite design method was selected. Three important factors were tested by three concentration levels of −1, 0, and 1, respectively. Then the data were processed by quadratic regression fitting, which can get 1° polynomial equation. In a certain range of concentration, the best culture medium formula was obtained. The equation was solved within a certain range of concentrations to get the best medium formula.

43.3 Results and Analysis

43.3.1 Separation of Bacteria on Grape Leaves

Using dilution plate method, according to colony morphology, size, color, and growth characteristics, 92 strains of bacteria were isolated from the grape leaves.

43.3.2 Screening Result of Antagonistic Bacteria

Using the leaf disc method, the 92 strains of bacteria were tested for their control effect of grape downy mildew. The results showed that there are 12 strains had the control effect of >20 %. The strain that had the best control effect is J12, which reached 78.6 %. And other strains had the control effect between 21.2–65.8 % (Table 43.1). The J12 strain was cultured 5 times for passage and its antibacterial effect was found to be stable.

Table 43.1 Control effects of different strains on grape downy mildew

Strains	J1	J2	J3	J4	J5	J6	J7	J8	J9	J10	J11	J12
Disease index	90.12	52.63	30.82	57.23	59.21	71.01	39.56	46.59	65.25	59.93	37.22	19.29
Control effect (%)		41.6	65.8	36.5	34.3	21.2	56.1	48.3	27.6	33.5	58.7	78.6

43.3.3 Sequencing and Phylogenetic Tree Analysis of 16S rDNA

The total DNA of strain J12 was amplified with universal primers of 27F and 1492R. The PCR product length is about 1.6 KB (Fig. 43.1). After sequencing, 16S rDNA length of J12 strain was 1512 bp.

By blastn software of NCBI, the 16S rDNA sequence of strain J12 and its related species were compared. Nine strains were selected to construct the phylogenetic tree with J12. It can be seen from Fig. 43.2, strain J12 and *B. amyloliquefaciens* were clustered into one branch. They have the closest genetic relationship. The morphology, growth characteristics, physiological, and biochemical characteristics of J12 strain are also similar to *B. amyloliquefaciens*. So J12 strain was finally identified as *B. amyloliquefaciens*

43.3.4 Determination of the Optimal Carbon Source, Nitrogen Source, and C/N

To get the best carbon source, 20 g/L of glucose, sucrose, maltose, and soluble starch were used as carbon source, respectively. The result showed that when sucrose was a sole carbon source, the number of live bacteria of 50.95×10^8 cfu/mL

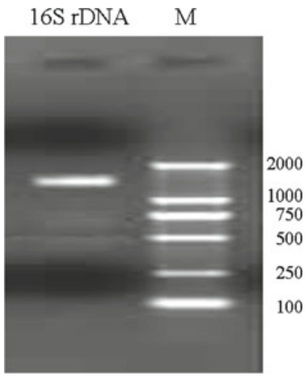

Fig. 43.1 The PCR amplification results of strain J12 16S rDNA. *M* DL2000 (DNA Maker), 16S rDNA: PCR product

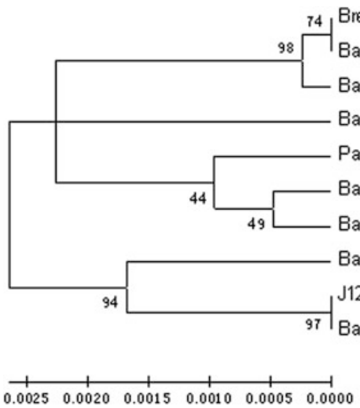

Fig. 43.2 The 16S rDNA phylogenetic tree of J12 and related strains

was highest. So the best carbon source is sucrose. 20 g/L of soybean meal, corn flour, peptone, fish meal, and urea were used to screen the best nitrogen source. The best nitrogen source is soybean meal, which number of live bacteria was 76.01×10^8 cfu/mL. Sucrose and soybean meal were mixed by different ratios of 1:3, 1:2, 1:1, 2:1, 3:1, 4:1, 5:1, 6:1, respectively to prepare different fermentation medium. The number of live bacteria was detected after fermentation for 72 h. When the C/N ratio is 3:1, the number of live bacteria was higher than other groups during which the number of live bacteria reached 77.81×10^8 cfu/mL.

43.3.5 Results of Plackett–Burman Design

Plackett–Burman design process and results were shown in Table 43.2. X2, X3, X5, X6, and X8 were sucrose, soybean meal, yeast extract, K_2HPO_4, and $MgSO_4$, respectively. X1, X4, X7, and X9 were four void items to estimate the test error.

By analysis of the obtained results (Table 43.3), it can be concluded that sugar, soybean meal, and K_2HPO_4 were the three most important influence factors. Effects of sucrose and K_2HPO_4 reached significant levels. Soybean meal reached extremely significant level.

43.3.6 The Results of Steepest Ascent Experiment

The steepest ascent experiment was designed with factors of sucrose, soybean meal, and K_2HPO_4, with initial level of yeast extract and $MgSO_4$. The ratio of sucrose and soybean meal was 3:1. The results were shown in Table 43.4. The number of live

Table 43.2 Design and results of Plackett–Burman design

No.	Factors									Number of live bacteria (10^8 cfu/mL)
	X1	X2	X3	X4	X5	X6	X7	X8	X9	
1	1	−1	−1	−1	1	−1	−1	1	1	22.70
2	1	1	−1	−1	−1	1	−1	−1	1	32.56
3	1	1	1	−1	−1	−1	1	−1	−1	24.46
4	1	1	1	1	−1	−1	−1	1	−1	22.44
5	−1	1	1	1	1	−1	−1	−1	1	62.04
6	1	−1	1	1	1	1	−1	−1	−1	26.84
7	−1	1	−1	1	1	1	1	−1	−1	32.56
8	1	−1	1	−1	1	1	1	1	−1	50.42
9	1	1	−1	1	−1	1	1	1	1	26.05
10	−1	1	1	−1	1	−1	1	1	1	63.80
11	−1	−1	1	1	−1	1	−1	1	1	92.14
12	1	−1	−1	1	1	−1	1	−1	1	34.76
13	−1	1	−1	−1	1	1	−1	1	−1	35.64
14	−1	−1	1	−1	−1	1	1	−1	1	88.56
15	−1	−1	−1	1	−1	−1	1	1	−1	40.92
16	−1	−1	−1	−1	−1	−1	−1	−1	−1	34.32

Table 43.3 Experimental factors, level and analysis of results

Factors	Levels		t	Pr > $\|t\|$	Order of importance
	1	−1			
X2	37.500	30.000	−2.63	0.031	2
X3	12.500	10.000	3.59	0.008	1
X5	3.125	2.500	−1.45	0.17	4
X6	2.500	2.000	2.52	0.042	3
X8	0.625	0.500	0.91	0.525	5

Table 43.4 Design and results of steepest ascent experiment

No.	Sucrose	Soybean meal	K_2HPO_4	Number of live bacteria (10^8 cfu/mL)
1	27.00	8.50	1.25	81.17
2	28.00	9.00	1.50	75.21
3	29.00	9.50	1.75	83.13
4	30.00	10.00	2.00	89.45
5	31.00	10.50	2.25	90.51
6	32.00	11.00	2.50	57.14
7	33.00	11.50	2.75	72.54

bacteria in No. 5 was highest, which was 90.51 × 10^8 cfu/mL. So, sucrose, soybean meal, and K_2HPO_4 content were set at 31, 10.50, and 2.25 g/L as central points of response surface experiment.

43.3.7 *Optimization Results by Response Surface Methodology*

Using Box–Behnken central composite experimental design, the amount of steepest ascent experiment result was optimized further (Table 43.5). Independent variables were sucrose = (D1 − 31)/3, soybean meal = (D2 − 10.5)/1, and K_2HPO_4 = (D3 − 2.25)/0.25. And response value was number of live bacteria. The actual value of each independent variable was shown in Table 43.5, and the experimental design and results were shown in Table 43.6.

Table 43.5 The factors and levels of response surface design

Factors	Levels		
	−1	0	1
Sucrose	28.00	31.00	34.00
Soybean meal	9.50	10.50	11.50
K_2HPO_4	2.00	2.25	2.50

Table 43.6 Design and the results of response surface

No.	Factors			Number of live bacteria (10^8 cfu/mL)
	Sucrose (g/L)	Soybean meal (g/L)	K_2HPO_4 (g/L)	
1	28.0	9.5	2.25	78.44
2	28.0	11.5	2.25	77.53
3	34.0	9.5	2.25	76.44
4	34.0	11.5	2.25	82.99
5	31.0	9.5	2.0	85.45
6	31.0	9.5	2.5	85.36
7	31.0	11.5	2.0	83.08
8	31.0	11.5	2.5	82.08
9	28.0	10.5	2.0	77.53
10	34.0	10.5	2.0	79.81
11	28.0	10.5	2.5	75.08
12	34.0	10.5	2.5	75.71
13	31.0	10.5	2.25	88.09
14	31.0	10.5	2.25	88.54
15	31.0	10.5	2.25	90.82

By response surface experiment carried out as given in Table 43.6, the experience model was obtained as Y1 = 89.15 + 0.79625X2 − 0.00125X3 − 0.955X6 − 8.63X2X2 + 1.865X2X3 − 0.4125X2X6 − 1.67X3X3 − 0.2275X3X6 − 3.4875X6X6. Correlation coefficient of the regression model is R. For R = 93.30 %, fitting degree of regression equation is good. By SAS analysis, the maximum response (Y) can be obtained when the coded value of sucrose = 0.06296, soybean meal = 0.07477, and K_2HPO_4 = −0.17448. The corresponding best culture medium formula was sucrose 31.18 g/L, soybean meal 10.57 g/L, K_2HPO_4 2.206 g/L, yeast extract 2.5 g/L, and $MgSO_4.7H_2O$ 0.5 g/L. And the best theoretical cell number is 90.87×10^8 cfu/mL. In order to test the feasibility of the used response surface, three parallel experiments were carried out. The number of live bacteria was 92.54×10^8 cfu/mL in the three experiments, which suggested that the fitting degree of the equation and the actual situation is very good. The model was correct.

43.4 Discussion and Conclusion

In the early classification systems, *B. amyloliquefaciens* was classified as a subspecies of *B. subtilis*. They were divided in the later classification systems. A lot of phenotypic characteristics of *B. amyloliquefaciens* and *B. subtilis* are very similar. It is difficult to distinguish them only by morphology, culture, biochemical characteristics, and physiological characteristics. So, further gene sequence comparison such as 16S rDNA is necessary. Physiological and biochemical characteristics are one of the important bases of microbial classification. Theoretically, 16S rDNA sequence analysis results can be verified by physiological and biochemical experiments. However, identification of microorganisms by physiological and biochemical characteristics is difficult, because of small differences in physiological and biochemical characteristics between the species, and some changes in the physiological and biochemical characteristics by the growth environment. So, the physiological and biochemical characteristics of identification are not suitable as verification by 16S rDNA sequence analysis results.

B. amyloliquefaciens had been researched and explored more and more widely with the ability to inhibit fungi and bacteria. It becomes a potential microbial biopesticide in recent years. Now, many papers on the *B. amyloliquefaciens* have been published about new discovery and applications, gene function, and molecular research methods of exploration, fermentation conditions, and medium formulation.

In this study, a strain against grape downy mildew was isolated. The strain belongs to *B. amyloliquefaciens*. The important factors for its liquid fermentation medium were screened by Plackett–Burman design and optimal fermentation medium formula was obtained by response surface methodology. The optimal liquid fermentation medium formula is 31.18 g/L sucrose, 10.57 g/L soybean meal, 2.206 g/L K_2HPO_4, 2.5 g/L yeast extract, and 0.5 g/L $MgSO_4 \cdot 7H_2O$.

Acknowledgments This work was supported by the Hengshui University Subject for Servicing Local Economic (No. 2013041) and National Nonprofit Sector (Agriculture) Scientific Research (201203035). We also thank for the support of postdoctoral research station in Shenyang Agricultural University.

References

1. Dihazi Abdelhi, Jaiti Fatima, WafaTaktak et al (2012) Use of two bacteria for biological control of bayoud disease caused by Fusarium oxysporum in date palm (*Phoenix dactylifera* L) seedlings. Plant Physiol Biochem 55:7–15
2. Bhagwat PR, Sasmita D, Pradeep KD et al (2014) Optimization of extracellular chromate reductase production by *Bacillus amyloliquefaciens* (CSB 9) isolated from chromite mine environment. Biocatalysis and Agricultural Biotechnology 3(3):1878–8181
3. Devendra KC, Bhavdish NJ (2008) Interactions of *Bacillus spp.* and plants-With special reference to induced systemic resistance (ISR). Microbiol Res 164(5):493–513
4. Dhanya G, Swetha S, Madhavan Nampoothiri K et al (2008) Response surface methodology for the optimization of alpha amylase production by *Bacillus amyloliquefaciens*. Bioresour Technol 99(11):4597–4602
5. Gobbin D, Jermini M, Loskill B et al (2005) Importance of secondary inoculum of Plasmopara viticola to epidemics of grapevine downy mildew. Plant Pathol 54:522–534
6. Lin L, Wang XP, Wang YJ (2006) cDNA clone, fusion expression and purification of the novel gene related to ascorbate peroxidase from Chinese wild Vitis pseudoreticulata in *E. coli*. Mol Biol Rep 33:197–206
7. Tari C, Genckal H, Tokatli F (2006) Optimization of a growth medium using a statistical approach for the production of an alkaline protease from a newly isolated *Bacillus sp*.L21. Process Biochem 41:659–665
8. Hq Wu, Tian L, Zhang JM et al (2005) Culture medium optimization for pigment production with RSM method. Acta Oceanologica Sinica 5:149–153

Chapter 44
The Adsorption Properties of Macroporous Resin for Fusel Oil of Luzhou—Flavor Liquor

Jinxu Sun

Abstract The D3520 resin was suited for adsorption and desorption of fusel oil by the comparison study of different types of resin. The study confirmed that macroporous resin D3520 had favorable adsorption and desorption capability by comparing different resins based on adsorption quantity, adsorption rate, and desorption rate. Temperature affected the fusel oil adsorption rate of D3520 and with more impact the temperature was high. There was little difference in the adsorption rate at 25 and 30 °C and the rate was up to 58.85 %. Among all strippant, the effect of acetone was higher than all concentration ethyl alcohol, up to 65.80 %. After treatment by D3520, there was little difference in physical, chemical, and sensory indexes of Luzhou flavor liquor and was not a bad influence on Luzhou flavor liquor. The Luzhou flavor liquor was soft and well balanced, with more rich ester aroma, and the wine quality was better by the D3520 resin treatment.

Keywords Macroporous resin · Fusel oil · D3520

44.1 Introduction

The monohydric alcohol of above of three carbons atom calls fusel oil and is brown or yellowish oily liquid in liquor of low alcohol content [1]. It is one of the main aroma substances in Chinese liquor, but more fusel oil will lead the drinker to headache and dizziness, then to be poisoned. High levels of fusel oil could damage the good qualities of Chinese liquor, like white precipitate and foreign flavor. So the level of fusel oil is one of the decisive factors in Chinese liquor quality control.

Macroporous resin is a kind of organic polymer adsorbent and has several advantages such as fast switching speed, fine heat stabilization, little pollute to extract, high mechanical strength, and convenient regeneration [2, 3]. Meanwhile,

J. Sun (✉)
Department of Life Sciences, Hengshui University, Hengshui 053000 Hebei, China
e-mail: bdsunjinxu@163.com

T.-C. Zhang and M. Nakajima (eds.), *Advances in Applied Biotechnology*,
Lecture Notes in Electrical Engineering 333, DOI 10.1007/978-3-662-46318-5_44

macroporous resin is the optimum adsorbing material which can be selective adsorption and easy desorption [4, 5]. In this paper, the different types of resin were suited for adsorption and desorption of fusel oil and the research viewed to control fusel oil content in Luzhou flavor liquor.

44.2 Materials and Methods

44.2.1 Materials

The different types (S-8, D3520, D4006, D101, NKA-9, HPD600, AB-8) of resin were purchased from Nanda synthetic resin co. (Tianjin). Butanol, *n*-propanol, isobutanol, *sec*-Butanol, *tert*-Butanol, and isopentanol were obtained from National standard network. Gas chromatograph is from Aglient HP 6890N (Aglient, USA) with FFAP column.

44.2.2 Determination of Fusel Oil [6]

44.2.2.1 Qualitative Analysis

Every alcohol of chromatographic grade standard and internal standard (*tert*-amyl alcohol) were weighed a certain amount and mixed, then dissolved in 60 % ethanol. Solution (as fusel oil in this paper) was filtered through microporous filter. Every alcohol and internal standard was determined by gas chromatograph.

44.2.2.2 Quantitative Analysis

Chromatographic grade standard and internal standard of every alcohol (*tert*-amyl alcohol) were weighed a certain amount and mixed in 100 mL volumetric flask as constant volume in 60 % ethanol. Mixed solution of 1, 2, 4, 8 and 10 mL were placed in 10 mL volumetric flask, respectively, and constant volume in 60 % ethanol. All samples of constant volume were mixed alcohol standard.

44.2.2.3 Determination of Gas Chromatography

The samples were filtered and analyzed without derivatization. FID detector; Capillary column: HP-FFAP (30.0 m × 1.00 μm × 530.00 μm); Column temperature: initial temperature 35 °C for 9 min, 4 °C/min risen to 45 °C, 10 °C/min risen to 100 °C, retain 4 min, 22 °C/min risen to 210 °C, retain 4 min; injector temperature: 200 °C; detector temperature: 240 °C; carrier gas (N_2): 0.085 MPa (1.08 mL/min); make-up gas: 35.0 mL/min; H_2 gas: 30 mL/min; atmosphere: 350 mL/min.

44.2.3 Treatment of Macroporous Resin

44.2.3.1 Pretreatment of Resin

Every resin (S-8, D3520, D4006, D101, NKA-9, HPD600 and AB-8) was soaked for 24 h in 95 % ethyl alcohol and washed by 95 % ethyl alcohol until distilled water added no muddy in washing liquor. Then the resin was washed by distilled water until no ethyl alcohol was added and dipped in HCl (5 % v/v) for a night. Distilled water was added to bring it to neutral pH value and was dipped in NaOH (5 % v/v) for a night. The resin was cleaned by distilled water to neutral pH value and dried at 60 °C.

44.2.3.2 Selection of Resin and Calculation of Adsorption Quantity and Adsorption Rate

For 1 g of every resin, 50 mL of 0.20 mg/mL fusel oil (mixed alcohol solution) was added and then vibrated for 24 h at 30 °C. Fusel oil was determined by gas chromatography and adsorption quantity and adsorption rate were calculated.

44.2.3.3 Desorption

All kinds of resin adsorbed fusel oil were stripped by 70 % ethyl alcohol and vibrated for 12 h at 30 °C. Fusel oil was determined by gas chromatography and desorption rate was calculated.

44.2.3.4 Temperature Effect of Adsorption Quantity

All kinds of resin were shocked and adsorbed fusel oil at 25, 30, 35, 40, 45, 50, and 55 °C, respectively. After adsorption, fusel oil solution was diluted, concentration was determined, and adsorption quantity was also calculated.

44.2.3.5 Comparison of Every Strippant Efficiency

The resin with adsorbed fusel oil was vibrated for 24 h at 30 °C and desorbed by absolute ethyl alcohol, 95 % ethyl alcohol, 75 % ethyl alcohol, 55 % ethyl alcohol, and acetone, respectively. Fusel oil was determined by gas chromatography and desorption rate was also calculated.

$$X = \frac{C_0 - C_1}{C_0} \times 100 \tag{44.1}$$

$$L = \frac{(C_0 - C_1) \times V}{W} \tag{44.2}$$

$$J = \frac{C_2}{C_0 - C_1} \times 100 \tag{44.3}$$

C_0 was the fusel oil concentration of initial solution (mg/mL); C_1 was the fusel oil concentration of after adsorbed solution (mg/mL); C_2 was fusel oil concentration of desorbed solution (mg/mL); V was solution volume, mL; W was the weight of resin, g; J was the desorption rate (%); L was the adsorption quantity (mg/g); and X was the adsorption rate (%).

44.3 Results and Discussion

44.3.1 Comparative Study of Different Resins on Adsorption Quantity, Adsorption Rate, Desorption Rate

Fusel oil had different adsorption quantity, adsorption rate, and the desorption rate in different resins (Figs. 44.1 and 44.2). The highest adsorption quantity was obtained in D3520 among all resins and up to 0.1662 mg/g, followed by HPD600 and D4006. Other resins had less adsorption quantity of fusel oil. Adsorption rate in different resins had the same trend with the adsorption quantity. D3520 had the

Fig. 44.1 The absorption of different resin to fusel oil

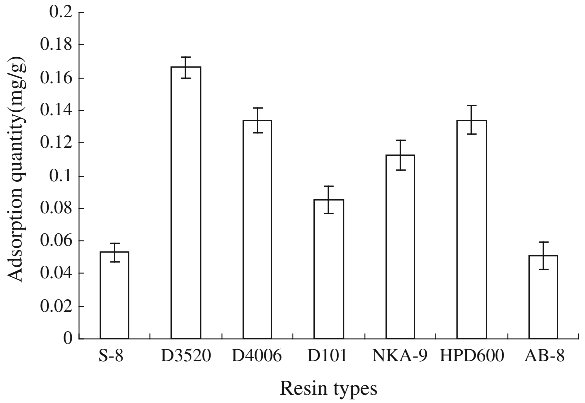

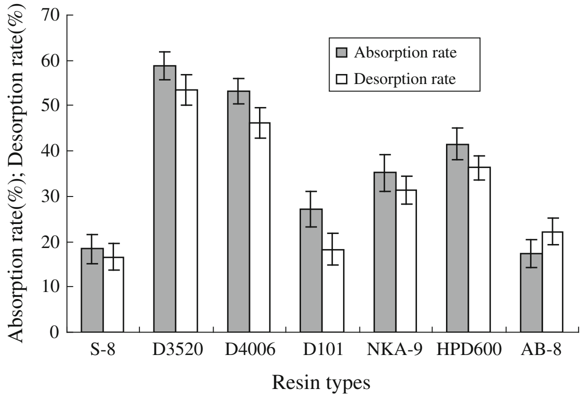

Fig. 44.2 The desorption rate and desorption rate comparison of different types of resin

highest desorption rate up to 53.56 % than others resin. By contrast, adsorption and desorption capability of D3520 was better than others. So D3520 was selected for adsorption and desorption of fusel oil.

44.3.2 Temperature Effect of Adsorption and Desorption Capability of D3520

Temperature affected the fusel oil adsorption rate of D3520 and with more impact when the temperature was high (Fig. 44.3). There was little difference in the adsorption rate between 25 and 30 °C and the rate reduced gradually as the temperature increased. All of these had the same trend with others researches. The reason for this trend was that a volatile liquid such as fusel oil was volatile at high temperature; the higher the temperature is, the more volatilization quantity it has. So temperature affected the fusel oil adsorption rate of D3520 (Fig. 44.4).

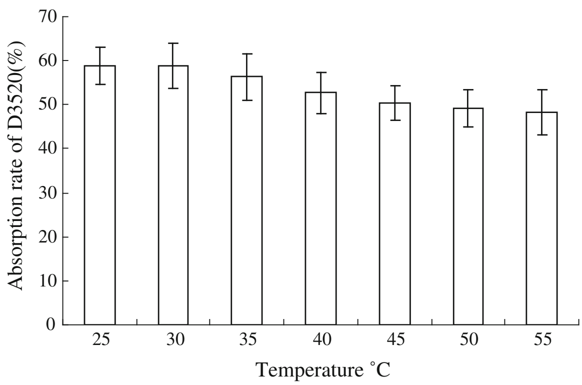

Fig. 44.3 The temperature effect to desorption rate of fusel oil in D3520

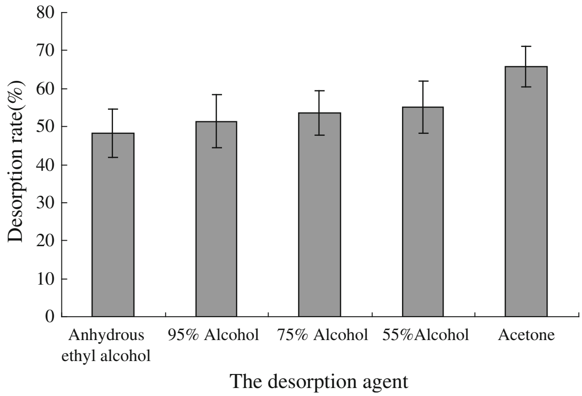

Fig. 44.4 The desorption agent effect to desorption rate of fusel oil in D3520

44.3.3 *Desorption Efficiency of Different Strippant*

Among all strippants, the effect of acetone was higher than all concentration of ethyl alcohol, up to 65.80 %. The result had the same trend with others researches. If ethyl alcohol was selected as a strippant, more desorption efficiency was obtained with less concentration of alcohol.

44.3.4 *Fusel Oil Adsorption Quantity Study of D3520 for Lu Zhou Flavor Liquor*

Fusel oil quantity of Luzhou flavor liquor was reduced by 45.81 % after treated by D3520 (Table 44.1). The data showed that D3520 resin could effectively reduce fusel oil quantity in Luzhou flavor liquor. In all ingredient of fusel oil, butanol, 1-propanol, isobutanol, and isopentanol were depressed generally when treated by D3520 while 2-butanol had no variation.

44.3.5 *Physical, Chemical, and Sensory Index Effects of D3520 for Luzhou Flavor Liquor*

There was little difference in the physical, chemical and sensory indexes of Luzhou flavor liquor before and after the treatment by D3520 (Table 44.2) and was not a bad influence on Luzhou flavor liquor. Even fusel oil quantity of Luzhou flavor liquor decreased dramatically, the total acid and ethyl alcohol decreased slightly and total ester was increased slightly. The probability of collisions between

Table 44.1 The content changes comparison of fusel oil for Luzhou flavor liquor

	Butanol	1-Propanol	Isobutanol	2-Butanol	Isopentanol	Total amount of fusel oil
Before treatment (g/L)	0.005	0.136	0.225	0.002	0.265	0.633
After treatment (g/L)	0.003	0.105	0.111	0.002	0.122	0.343

Table 44.2 The mainly liquor sensory index changes for Luzhou flavor liquor before and after treatment

	Physical and chemical indexes				Sensory index
	Total acid (g/100 mL)	Total ester (g/100 mL)	Fusel oil (g/100 mL)	Ethyl alcohol (v/v)	
Before treatment	0.0289	0.168	0.0633	42	Liquor body clear and transparent; pure and aromatic; stronger pit-flavor; penetrating odor; lingering bitterness; not clear ending wine
After treatment	0.0252	0.179	0.0343	41.8	Liquor body clear and transparent; pure and aromatic; stronger pit—flavor; mealiness; dry and refreshing aftertaste; no lingering bitterness

molecules for wine was increased with the wine through D3520 resin and the esterification reaction was accelerated and the penetrating odor was reduced, this actuated wine softer and improved wine quality.

44.4 Conclusion

The study confirmed that macroporous resin D3520 had favorable adsorption and desorption capability by comparing with other resin. Temperature affected the fusel oil adsorption rate of D3520 and with more impact the temperature was high. There was little difference in the adsorption rate 25 and 30 °C and the rate was up to 58.85 %. The effect of acetone was higher than ethyl alcohol, and the desorption rate arrived up to 65.80 %. There was little difference before and after treatment for physical, chemical, and sensory indexes of Luzhou flavor liquor and was not a bad influence on Luzhou flavor liquor. The Luzhou flavor liquor was soft and well balanced, and had more rich ester aroma. The quality of the wine was better after the treatment of D3520 resin.

Acknowledgments This work was supported by the Hengshui University students innovation key project (No. 2014025), the Hengshui University subject for servicing local economic (No. 2013039 2013004), and Hengshui city science and technology guide project research (No. 13065-1).

References

1. Jia GT, Lu XY (2008) Enrichment and purification of madecassoside and asiaticoside from Centella asiatica extracts with macroporous resins. J Chromatogr A 1193:136–141
2. Cullere L, Escudero A, Cacho J et al (2004) Gas chromatography-olfactometry and chemical quantitative study of the aroma of six premium quality Spanish aged red wines. J Agric Food Chem 6:1653–1660
3. Sáez JS, Lopes CA, Kirs VC et al (2010) Enhanced volatile phenols in wine fermented with Saccharomyces cerevisiae and spoiled with Pichia guilliermondii and Dekkera bruxellensis. Lett Appl Microbiol 51:170–176
4. Yang XL, Luo ZM, Hu SP et al (2011) Reducing total higher alcohol content in high gravity fermentation of beer. Food Sci 32:23–28
5. Zhang Y, Li SF, Wu XW et al (2010) Macroporous resin adsorption for purification of flavonoids in houttuynia cordat thunb. Chin J Chem Eng 6:872–876
6. Zhang ZM, Wu WS, Li KF (2012) Study on the change rules of chemical composition of site-flavor fermented grains in fermentation process. Sci Technol Food Ind 33:108–113

Chapter 45
Low Labeling ^{13}C Metabolic Flux Analysis of *Saccharomyces cerevisiae* Using Gas Chromatography–Combustion–Isotope Ratio Mass Spectrometry

Qi-ding Zhong, Guo-hui Li, Dong-dong Zhao, Dao-bing Wang, Shi-gang Shen and Zheng-he Xiong

Abstract The applicability of gas chromatography–combustion–isotope ratio mass spectrometry (GC–C–IRMS) for the quantification of ^{13}C enrichment of proteinogenic amino acids in metabolic tracer experiments was evaluated in this paper. We measured the ^{13}C enrichment of proteinogenic amino acids in hydrolyzates using GC–C–IRMS from a series of parallel batch cultivations of *Saccharomyces cerevisiae*, which was cultured by mixtures of natural glucose and [$1-^{13}$C] glucose, containing 0, 0.5, 1, and 2 % [$1-^{13}$C] glucose, respectively. By decreasing the [$1-^{13}$C] glucose content, kinetic isotope effects played an increasing role but could be corrected. The ^{13}C metabolic algorithm and matrix algorithms were optimized in this study. The central metabolism of vivo fluxes were determined by the calculation method optimization. The obtained flux distribution was similar to published results, which obtained from GC–MS method using conventional high labeling (99 %). The GC–C–IRMS-based method involves low labeling (0.5 %) degree of expensive tracer substrate, and suits well for larger laboratory and industrial pilot-scale fermentations.

Keywords *Saccharomyces cerevisiae* · Metabolic flux analysis · ^{13}C-labeling · GC–C–IRMS · Proteinogenic amino acid

G. Li and Q. Zhong are joint first authors.

Q. Zhong (✉) · G. Li · D. Zhao · D. Wang · Z. Xiong
China National Institute of Food and Fermentation Industries, Buliding 6, no. 24 of Middle Jiuxianqiao Road, Chaoyang District, Beijing 100015, China
e-mail: zhongqiding@163.com

G. Li · S. Shen
Key Laboratory of Analytical Science of Hebei Province, Key Laboratory of Medical Chemistry and Molecular Diagnosis, Ministry of Education, College of Chemistry and Environmental Science, Hebei University, Baoding 071002, China

T.-C. Zhang and M. Nakajima (eds.), *Advances in Applied Biotechnology*,
Lecture Notes in Electrical Engineering 333, DOI 10.1007/978-3-662-46318-5_45

45.1 Introduction

The quantitative analysis of in vivo carbon fluxes in a metabolic network is regarded a powerful tool for the optimization of industrial organisms [2, 19]. Developed from the previous methods using only metabolite balancing, flux estimation has been far advanced by supplementing the previous stoichiometry-based approach with isotopomer balances to overcome shortcomings of the previous method in many real-case situations and the ambiguity of black box model [1, 11, 17, 18, 21, 26]. Theoretically, the most complete information would be obtained by the analysis of all extracellular and intracellular metabolite isotopomers. Unfortunately, it is highly challenging to analyze all positional isotopomers in practice, e.g., using nuclear magnetic resonance spectroscopy (NMR) techniques, and also the information content finally depends on measurement sensitivity. For ^{13}C-based metabolic flux analysis (^{13}CMFA), the mass isotopomers of intracellular and extracellular metabolites and biomass constituents can be used. The analysis of intracellular metabolites is often challenging, e.g., due to low concentrations close to or below detection limits as well as often limited stability, and short time constants of certain compounds such as glycolytic metabolites. Amino acids contained in cellular proteins reflect the labeling patterns of various central key metabolites at steady state. They can be easily analyzed by NMR [13, 14, 19], gas chromatography–mass spectrometry (GC–MS) [3, 4, 6, 7, 9, 22], or matrix-assisted laser desorption time-of-flight mass spectrometry (MALDI-TOFMS) [25]. Methods have been developed to take into account natural isotope abundances of the analytes [24, 27]. In recent years, the combination of GC–MS and parameter estimation methods using network simulation techniques has been well developed and most frequently applied in metabolic flux analysis [1, 7, 16, 18, 22, 28, 29].

Another challenge in ^{13}C-based metabolic flux analysis is that experiments are limited to small scales. So far labeling experiments have been restricted to laboratory-scale fermentation, shake flasks, and microtiter plates [20, 23] due to the requirement for high degree of ^{13}C-labeled substrate (generally 100 % tracer substrate) and the resulting high cost. Experiments on a laboratory scale, however, cannot usually represent conditions on much larger scales that are industrially much more relevant. In this regard, a method of ^{13}C MFA applicable to large-scale biotechnological processes is highly desired. Here to applying a small amount of isotopic tracer substrates for labeling experiments is a possible solution, yet it leads to extremely low ^{13}C enrichments of labeling in proteinogenic amino acids and, consequently, a poor flux resolution. Since ^{13}C isotopic enrichments in amino acids present in proteins is usually low (0.001–0.05, APE) as determined in protein turnover experiments [8], the labeling patterns of metabolites cannot reliably be measured by GC–MS, which has a measurable range only higher than 0.5 APE [15]. In contrast, GC–C–IRMS is capable of measuring isotopic composition at low enrichment and even natural abundance level with high precession (0.0002 APE) and accuracy. Thus, GC–C–IRMS has a great potential for the application to cases with extremely low ^{13}C enrichments in metabolites. In 2008 and 2010, Elmar

Heinzle et al. [10, 30] had established a method to analyze microbial metabolic network using GC–C–IRMS.

In this paper, we implemented ^{13}C labeling experiments using different contents of ^{13}C glucose mixed with naturally labeled glucose. Cultivations were carried out using *Saccharomyces cerevisia* which is the most important microorganism in industry. The measured values of GC–C–IRMS in low labeling ^{13}C glucose were dealt with Matlab and quantum-behaved particle swarm optimization (QPSO). Based on the protocol, the ^{13}C fractional enrichment data were corrected from GC–C–IRMS measurements, and applied to ^{13}CMFA to verify the potential of GC–C–IRMS for an industrial scale ^{13}CMFA. Results were compared with those from conventional ^{13}CMFA using 99 % [$1-{}^{13}$C] glucose and GC–MS as well as with the literature data.

45.2 Materials and Methods

45.2.1 Chemicals, Microorganism, and Medium

Analytical amino acid and organic acid standards were obtained from Sigma–Aldrich. [$1-{}^{13}$C] glucose (99 % atom ^{13}C) was purchased from Omicion Biochemicals. *N*,*N*-Dimethylformamide (DMF, chromatographically pure), *N*-(butyldimethylsilane)-*N*-methyl fluoroacetamide (MTBSTFA, ≥95 %, Sigma–Aldrich), GC–C–IRMS (Thermo Fisher Scientific), ultraviolet spectrophotometer (UV-1240), biochemical incubator (SPX-250B-Z), refrigerated centrifuge (Sigma), constant temperature shaker, and pressure blowing concentrator (MTN-2800D).

The *S. cerevisiae* (SCFF-Y-002) was obtained from our lab and the cells were stored at −80 °C with 25 % (v/v) glycerin.

Preculture was grown in complex medium containing 20 g peptone, 10 g yeast extract, and 20 g glucose per liter. The fermentation medium contained 20 g glucose, 0.5 g $(NH_4)_2HPO_4$, 1.0 g $(NH_4)_2SO_4$, 0.05 g $MgSO_4 \cdot 7H_2O$, 0.5 g KCl, 0.03 g $CaCl_2 \cdot 2H_2O$, 3 mg $FeCl_3 \cdot 6H_2O$, 2.1 mg $MnSO_4 \cdot H_2O$, 1.8 mg $ZnSO_4 \cdot 7H_2O$, 0.5 mg $CuSO_4 \cdot 5H_2O$, 60.3 mg myoinositol, 30 mg Ca-panthotenate, 6 mg thiamin·HCl, 1.5 mg pyridoxine·HCl, 0.03 mg biotin, and 50 mmol phosphate buffer per liter.

45.2.2 Cultivation Conditions

At first, a single colony of the yeast was inoculated into 50 mL of precultivation medium in a 250 mL baffled shake flask, and incubated on a rotary shaker at 200 rpm and 30 °C for 20 h. Second, cells were transferred into fermentation medium with a starting cell concentration (OD_{660}) of 0.05 and culture for 20 h. Subsequently, cells were washed twice with fermentation medium by centrifugation at 8,500 rpm for 10 min. Then the cells were used as strain. Tracer experiments were carried out in 50 mL fermentation medium of 250 mL baffled shake flasks. The fermentation medium contained natural glucose and 0, 0.5, 1, and 2 % [1−^{13}C] glucose, respectively.

45.2.3 Determination of Physiological Parameters

Cell growth was monitored at OD_{660} during cultivation. Glucose and organic acids were analyzed by HPLC while ethanol and glycerol were determined by GC with a wax column.

45.2.4 Analysis of the ^{13}C-Labeling Patterns of Amino Acids

The isotopic labeling patterns of proteinogenic amino acids were measured by GC–C–IRMS instrument comprising an gas chromatograph, a standard GC/C III interface with a Ni/CuO/Pt combustion reactor set at 940 °C, and a MAT 253 gas isotope mass spectrometer. Biomass (100 mg) was harvested at mid-exponential period (20 h). The cells were washed twice with deionized water, mixed with 4 mL of 6 M HCl, and incubated for 24 h at 110 °C for hydrolysis. The hydrolysis was filtered through a 0.22 μm membrane and then dried with a steady stream of nitrogen at the temperature of 45 °C. Those proteinogenic amino acids were derived by the addition of 100 μL of MTBSTFA and 100 μL of DMF and then directly used for analysis.

The GC was equipped with a split/splitless injector and a HP-5 column, helium was used as a carrier gas with a constant flow of 1.0 mL/min. The injector was set to 250 °C. For analysis, 1 μL of sample was injected in split mode (split 1:10). The GC temperature parameters were set as follows: The initial temperature of 120 °C was kept for 2 min. Subsequently, the temperature was increased by 3 °C/min to 250 °C and then by 10 °C/min to 270 °C and kept for 10 min. The GC–C–IRMS was equipped with a combustion reactor set at 1,000 °C and three Faraday cup collectors for m/z 44, 45, and 46 were used for detection of CO_2. Isotope ratios were calibrated against reference CO_2 of known isotopic composition introduced directly into the ion source three times at the beginning and at the end of every run. Each measurement was performed at least in triplicate.

45.2.5 Metabolic Flux Estimation

Different from GC–MS method, during GC–C–IRMS measurement all derivatized amino acids were combusted into CO_2 which had only one carbon atom. For this case, the problem became simply the first level of the elementary metabolite units, which also corresponded to the atomic level problem. Therefore, atom mapping matrices (AMM) were used for the analysis of modeling isotope distributions.

Metabolic network simulations of yeast were performed using the MATLAB. An improved QPSO was used for the network parametrization and numerical flux estimation in this article. In short, fluxes were estimated by minimizing the variance weighted sum of squared residuals between the simulated and the experimental results of each proteinogenic amino acids.

45.3 Results and Discussion

45.3.1 ^{13}C Labeling Analysis of Amino Acids by GC–C–IRMS

GC–C–IRMS chromatograms of all proteinogenic amino acids were shown in Fig. 45.1. The ^{13}C fraction of 15 proteinogenic amino acids could be determined, the order of the peaks were alanine (Ala), glycine (Gly), valine (Val), leucine (Leu), isoleucine (Ile), proline (Pro), serine (Ser), threonine (Thr), phenylalanine (Phe), aspartic acid (Asp), glutamic acid (Glu), lysine (Lys), arginine (Arg), histidine (His), and tyrosine (Tyr). All proteinogenic amino acids present in chromatogram were found satisfactorily separated without any overlapping peaks. The δ^{13}C value for each proteinogenic amino acids were shown in Table 45.1.

45.3.2 Linearity of ^{13}C Fractional Labeling

According to the theory, the fraction of carbon atom should always be proportional to the input labeling. A series of experiments were designed to prove this theory

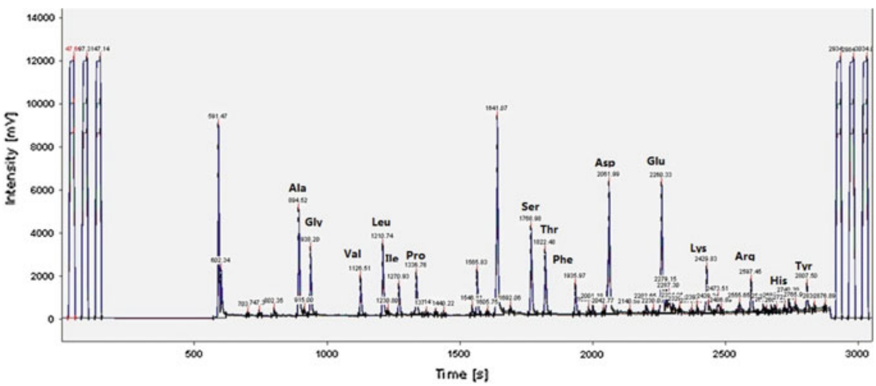

Fig. 45.1 GC–C–IRMS chromatograms of all proteinogenic amino acids for yeast

Table 45.1 $\delta^{13}C$ value for each proteinogenic amino acids

Amino acids	$\delta^{13}C$ (‰)
Ala	−0.584
Gly	−10.057
Val	22.102
Leu	27.271
Ile	30.014
Pro	25.447
Ser	−6.239
Thr	2.309
Phe	6.679
Asp	0.659
Glu	11.955
Arg	20.704
Lys	−6.266
His	−8.709
Tyr	−2.089

employing a wide range of substrate labeling. The lower fraction of ^{13}C-substrates containing 0, 0.5, 1, and 2 % [1−^{13}C] glucose, samples from the lower fraction group were measured by GC–C–IRMS due to their low ^{13}C enrichment in amino acids (<0.5 APE in derivatized analytes). The obtained δ values of individual amino acids were then converted to ^{13}C enrichment and corrected for the kinetic isotope effect as described previously. And then obtained mass isotopomer distributions of individual amino acids were converted into the fractional ^{13}C enrichment or fractional labeling (FL) using the following equation:

$$\mathrm{FL} = \frac{\sum_{i=0}^{x} i \; |y_{m+i}}{X} \tag{45.1}$$

Here, y is the carbon mass isotopomer fraction of an amino acid, i is the mass shift by ^{13}C incorporation, and x is the number of carbon atoms of the amino acid. All experimental results were listed in Table 45.2. Except glycine, the squared correlation coefficients (R^2) from the listed amino acids were close to 1 (>0.9999) at the range from 0 to 2 % of [1−^{13}C] glucose fraction obtained from GC–C–IRMS data. For the whole range from 0 to 2 %, R^2 resulting from the amino acids, again except glycine, were also quite close to 1 (>0.9999). The high linear correlation over the whole range testing allows us to predict ^{13}C enrichment of unknown labeling (e.g., 100 % [1−^{13}C] glucose fraction) using extrapolation.

Table 45.2 ^{13}C fractional labeling of proteinogenic amino acids from 0 to 2 % input [1−^{13}C] labeled glucose

Designation	$\delta^{13}C$ (‰)				R^2
	0 %	0.50 %	1 %	2 %	
Ala	−27.338	−13.143	−0.584	26.163	0.9997
Gly	−29.773	−19.981	−10.057	11.872	0.9991
Val	−25.503	−4.805	22.102	59.418	0.9948
Leu	−25.482	1.417	27.271	84.472	0.9995
Ile	−25.049	2.832	30.014	93.591	0.9984
Pro	−25.705	0.549	25.447	84.632	0.9984
Ser	−28.889	−17.298	−6.239	14.661	0.9994
Thr	−28.922	−13.007	2.309	36.4025	0.9994
Phe	−25.890	−9.156	6.679	39.848	0.9990
Asp	−28.696	−13.437	0.659	32.2035	0.9995
Glu	−27.218	−7.359	11.955	46.7465	0.9988
Arg	−25.785	−1.205	20.704	70.2065	0.9531
Lys	−28.657	−14.928	−6.266	5.075	0.9995
His	−25.909	−18.185	−8.709	12.901	0.9949
Tyr	−26.526	−13.846	−2.089	22.285	0.9999

45.3.3 Biomass Yield and Extracellular Metabolites

The yield coefficients for the formation of biomass and extracellular products on glucose during the exponential phase are listed in Table 45.3 and the precursor demands used for biomass formation in yeast are listed in Table 45.4.

Table 45.3 Anabolic demand of yeast during aerobic glucose-limited culture[a]

Compound	Demand μmol/(g dry cell mass)
Glucose 6-phosphate	2,089
Erythrose 4-phosphate	243
Ribose 5-phosphate	115
Glyceraldehyde 3-phosphate	77
Phosphoglycerate	623
Oxaloacetate	683
Phosphoenolpyruvate	457
Pyruvate	1,285
Acetyl-CoA	2,324

[a] The values were obtained from the literature [28]

Table 45.4 Biomass and metabolites yield coefficients of yeast

Biomass and metabolites	Yield (g/mmol (GLC), mmol/mmol (GLC))
Biomass	0.115
Ethanol	0.499
Acetic acid	0.0047
Lactate	0.0029
Glycerin	0.086

Biomass and metabolites yields of *Saccharomyces cerevisiae* SCFF-Y-002 cultured on glucose. All yields are given in (C-mol product)/(C-mol glucose), except the yield for biomass that is given in (g dry cellmass)/(mmol glucose)

45.3.4 Central Metabolic Network

The central metabolic network, like glycolysis, tricarboxylic acid cycle (TCA), and pentose phosphate pathway (PPP) of yeast are analyzed. The main reactions in the central metabolic network are shown as follows:

V1: G6P = F6P	V2: F6P + ATP = GA3P + DAHP + ADP
V3: DAHP = GA3P	V4: GA3P + NAD + ADP = 3-PG + NADPH + ATP
V5: 3-PG + ADP = PYR + ATP	V6: PYR + H-COA + NAD = AC-COA + NADH + CO_2
V7: G6P + NADP = RIB-5P + CO_2 + NADPH	V8: 2RIB-5P = S7P + GA3P
V9: S7P + GA3P = E-4P + F6P	V10: RIB-5P + E-4P = F6P + GA3P
V11: AC-CoA + OAA = ICI + H-CoA	V12: ICI + NADP = 2-OXO + CO_2 + NADPH
V14: SUCC + FAD + NAD = OAA + FADH + NADH	V15: PYR + ATP + PEP + 2CO_2 = 2OAA + ADP
V13: 2-OXO + NAD + H-COA + ADP = SUCC + NADH + CO_2 + ATP	

Back reactions are represented as Vir.

The atom transitions and transitions of reactants and products are shown in Tables 45.5 and 45.6, respectively.

45.3.5 Flux Estimation in Central Metabolic Pathways of Yeast

The central metabolic fluxes of *S. cerevisiae* are estimated with the measurement information, and the results are shown in Table 45.7.

The aim of this study was to develop a new straight forward and cost-efficient approach for the quantification of the in vivo flux distribution in the central

Table 45.5 Atom transitions between reactants and products

Reactants	Products	Carbon atom transitions
G6P	F6P	abcdef
F6P	G6P	abcdef
F6P	GAP	def
F6P	DHP	abc
DHP	GAP	cba
GAP	3PG	abc
3PG	PYR	abc
PYR	ACA	bc
G6P	P5P	bcdef
P5P	GAP	cde
P5P	S7P	00abcde
P5P	S7P	ab00000
S7P	P5P	cdefg
GAP	P5P	00abc
S7P	P5P	ab000
GAP	F6P	000abc
S7P	F6P	abc000
S7P	E4P	defg
F6P	S7P	abc0000
E4P	S7P	000abcd
P5P	F6P	ab0000
E4P	F6P	00abcd
P5P	GAP	cde
F6P	P5P	ab0000
GAP	P5P	00abc
F6P	E4P	cdef
OAA	ICT	dcb00a
ACA	ICT	000ba0
ICT	aKG	abcde
aKG	SUC	bcde
SUC	OAA	abcd
SUC	OAA	dcba
PYR	OAA	abc0
CO_2	OAA	000a
OAA	PYR	abc
GLC	G6P	abcdef
DHP	GLR	abc
3PG	GLY	ab
PYR	LAC	abc
F6P	GAP	def

Table 45.6 Atom transitions between intermediate metabolites and amino acids

Reactants	Products	Carbon atom transitions
PYR	ALA	abc
PYR	VAL	ab00c
PYR	VAL	00bc0
3PG	SER	abc
OAA	THR	abcd
3PG	GLY	ab
OAA	ASP	abcd
OAA	ILE	b0cd0
PYR	ILE	0b00c
PYR	aKI	00bc0
PYR	aKI	ab00c
aKI	LEU	0bcde
aKG	GLU	abcde
ACA	LEU	b0000
PYR	S5P	b0000ca
E4P	S5P	0abcd00
PYR	PHE	000000cba
S5P	PHE	abcdef000
PYR	TYR	000000cba
S5P	TYR	abcdef000
LYS	LYS	abcdef
aKG	ARG	abcde0
CO_2	ARG	00000a
P5P	HIS	0bacde
CO_2	HIS	a00000

Table 45.7 Metabolic fluxes of *Saccharomyces cerevisiae*

Reactions	Fluxs (%)
V1	80.5
V2	85.5
V3	78
V4	159.5
V5	151.5
V6	73.3
V7	17.5
V8	4.9
V9	3
V10	2
V11	18.6
V12	18.6
V13	7.4
V14	7.5
V15	25.5

metabolism of microorganisms. Based on the model-based experimental design [12], [1−^{13}C] glucose was selected as the tracer substrate because of its commercial availability and low cost. Due to the ability for the detection of extremely low isotopic enrichment and high precision, GC–C–IRMS measurement of isotope enrichment was chosen for this study. To our knowledge, GC–C–IRMS had not been applied on isotope-based in vivo flux analysis yet. Our study opens up the door for the application of GC–C–IRMS to in vivo ^{13}CMFA even at industrially relevant fermentation scales in situ. This research increased in importance with increasing competition, e.g., in the production of biopharmaceuticals [5].

The theoretically expected linear relationship between input ^{13}C labeling content and the ^{13}C enrichment of metabolic products were also observed experimentally, which suggested the GC–C–IRMS applicability for ^{13}CMFA. As verified, for the proteinogenic amino acids investigated here in, other metabolic products could also be applied to ^{13}CMFA using this novel approach, e.g., some intracellular metabolites. With this method, it is possible to calculate ^{13}C enrichment at any input ^{13}C substrate content by extrapolation with at least two or more different amounts of ^{13}C substrate in mixtures with unlabeled ones.

Typically, commercially available 99 % [1−^{13}C] glucose applied in ^{13}C labeling experiment contained 1 % ^{12}C in the first carbon, and natural abundance of isotopes of carbon and other elements at other positions. Additionally, elements with natural abundance of isotopes were introduced during derivatization, for example, silicon and nitrogen. In the case of GC–MS-based estimation, the effect of all these naturally labeled atoms could be eliminated by matrix correction [27]. The so-called correction matrix represents the abundance of naturally occurring isotopes other than the carbon atoms in the skeleton of a metabolite. Therefore, liability of carbon mass isotopomer distributions computed from measurements could be subject to the reliability of the data given for the natural abundance of isotopes.

In contrast to, all the separated derivatized analytes were combusted to CO_2 in GC–C–IRMS measurement and only CO_2 was analyzed afterwards. Therefore, only carbon and oxygen need to be considered for the correction. In this regard, the corrected GC–C–IRMS data should have a higher accuracy than the corrected GC–MS data. The new approach with the use of low degree ^{13}C substrate and GC–C–IRMS measurement allows in vivo flux estimation in central metabolism, and the final estimated fluxes showed a slightly lower precision only at very low labeling input of 0.5 % [1−^{13}C] glucose compared with those from high degree labeling and GC–MS measurement of literature date [31, 32]. The obtained flux distribution was very similar (Fig. 45.2). Contrary to the GC–MS method, many reactions in the central metabolism which were regarded as reversible, the transaldolase and transketolase reactions in the PPP; phosphoenolpyruvate carboxylase (oxaloacetate to phosphoenolpyruvate), malic enzyme (malate to phosphoenolpyruvate), and oxaloacetate decarboxylase (oxaloacetate to pyruvate) could not be determined by the new approach with [1−^{13}C] glucose as only tracer substrate. However, the net fluxes were determined with high precision and accuracy using GC–C–IRMS data in this study. The above limitation could be overcome. In terms of information content, GC–MS measurement was superior to GC–C–IRMS, since it allows the determination of mass

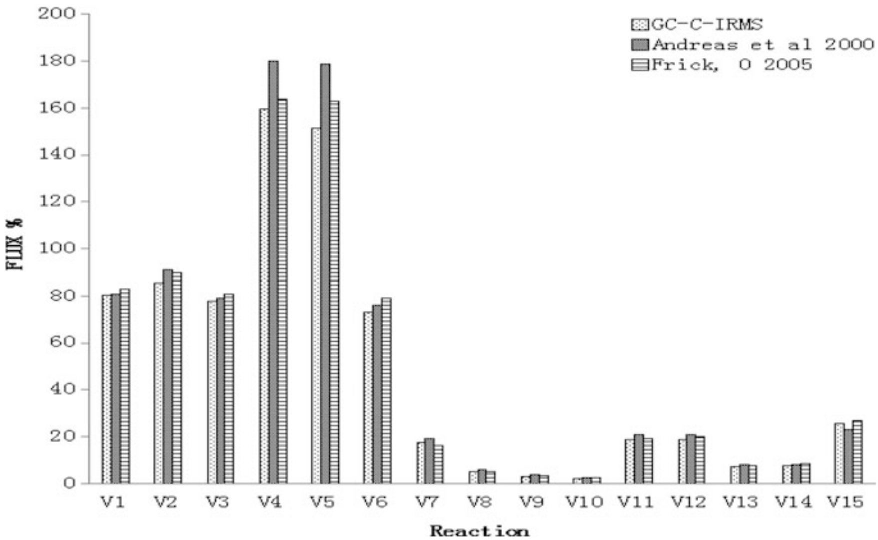

Fig. 45.2 Comparison of estimated fluxes. GC/MS-flux analysis using 99 % [1−^{13}C] glucose; literature data [31, 32]; GC–C–IRMS from single labeling experiment using 0.5 % [1−^{13}C] glucose corrected for natural isotope abundance in culture with naturally labeled glucose

isotopomer distribution for each analyte, whereas GC–C–IRMS determined only average carbon labeling. The present approach had a great potential for ^{13}CMFA at low labeling degree of substrates and, especially, was the most promising one for investigating in vivo fluxes in a large-scale bioprocess in situ.

45.4 Conclusion

Currently, ^{13}C metabolic flux analysis is the most reliable technique for measuring in vivo metabolic fluxes. The high cost of labeling is the main bottleneck of isotope tracer. This research introduced a simple and economical method to estimate metabolic fluxes of yeast using GC–C–IRMS with low labeling degree of 0.5 % (w/w) [1−^{13}C] glucose mixed with 99.5 % (w/w) natural glucose. The central metabolism flux of *S. cerevisiae* was determined by the calculation method optimization. The obtained flux distribution was similar to published results, which obtained from GC–MS method using conventional high labeling (99 %). The GC–C–IRMS-based method reduces the experiment cost greatly, and well suits for larger laboratory and industrial pilot-scale fermentations.

Acknowledgments Our research was supported by Ministry of Science and Technology Support Project (12th five year plan, Project Number: 2012BAK17B11) and Natural Science Foundation of China (Project Number: 311101333), express cordial acknowledgment here.

References

1. Antoniewicz MR, Kelleher JK, Stephanopoulos G (2007) Elementary metabolite units (EMU): a novel framework for modeling isotopic distributions. Metab Eng 9(1):68–86
2. Bailey JE (1991) Toward a science of metabolic engineering. Science 252(5013):1668–1675
3. Becker J, Klopprogge C, Herold A, Zelder O, Bolten CJ, Wittmann C (2007) Metabolic flux engineering of l-lysine production in Corynebacterium glutamicum over expression and modification of G6P dehydrogenase. J Biotechnol 132(2):99–109
4. Becker J, Klopprogge C, Wittmann C (2008) Metabolic responses to pyruvate kinase deletion in lysine producing Corynebacterium glutamicum. Microb Cell Fact 7(1):8
5. Boghigian BA, Seth G, Kiss R, Pfeifer BA (2010) Metabolic flux analysis and pharmaceutical production. Metab Eng 12(2):81–95
6. Christensen B, Nielsen J (1999) Isotopomer analysis using GC-MS. Metab Eng 1(4):282–290
7. Dauner M, Sauer U (2000) GC/MS analysis of amino acids rapidly provides rich information for isotopomer balancing. Biotechnol Prog 16(4):642–649
8. Godin J, Faure M, Breuille D, Hopfgartner GR, Fay L (2007) Determination of ^{13}C isotopic enrichment of valine and threonine by GC-C-IRMS after formation of the N (O,S)-ethoxycarbonyl ethyl ester derivatives of the amino acids. Anal Bioanal Chem 388(4):909–918
9. Hans M, Heinzle E, Wittmann C (2001) Quantification of intracellular amino acids in batch cultures of Saccharomyces cerevisiae. Appl Microbiol Biotechnol 56(5–6):776–779
10. Heinzle E, Yuan Y, Kumar S, Wittmann C, Gehre M, Richnow H et al (2008) Analysis of ^{13}C labeling enrichment in microbial culture applying metabolic tracer experiments using gas chromatography combustion isotope ratio mass spectrometry. Anal Biochem 380(2):202–210
11. Iwatani S, Yamada Y, Usuda Y (2008) Metabolic flux analysis in biotechnology processes. Biotechnol Lett 30(5):791–799
12. llney M, Wiechert W, Kownatzki D, de Graaf AA (1999) Bidirectional reaction steps in metabolic networks: IV. Optimal design of isotopomer labeling experiments. Biotechnol Bioeng 66(2):86–103
13. Maaheimo H, Fiaux J, Cakar ZP et al (2001) Central carbon metabolism of *Saccharomyces cerevisiae* explored by biosynthetic fractional ^{13}C labeling of common amino acids. Eur J Biochem 268(8):2464–2479
14. Marx A, de Graaf AA, Wiechert W et al (1996) Determination of the fluxes in the central metabolism of Corynebacterium glutamicum by nuclear magnetic resonance spectroscopy combined with metabolite balancing. Biotechnol Bioeng 49(2):111–129
15. Meier-Augenstein W (1999) Use of gas chromatography-combustion-isotope ratio mass spectrometry in nutrition and metabolic research. Curr Opin Clin Nutr Metab Care 2(6):465–470
16. Nanchen A, Fuhrer T, Sauer U (2007) Determination of metabolic flux ratios from ^{13}C-experiments and gas chromatography-mass spectrometry data. In: Weckwerth W (ed) Metabolomics. Springer, Berlin, pp 177–197
17. Schmidt K, Carlsen M, Nielsen J, Villadsen J (1997) Modeling isotopomer distributions in biochemical networks using isotopomer mapping matrices. Biotechnol Bioeng 55(6):831–840
18. Schmidt K, Marx A, de Graaf AA et al (1998) 13C tracer experiments and metabolite balancing for metabolic flux analysis: comparing two approaches. Biotechnol Bioeng 58(2/3):254–257
19. van der Werf MTJ, Takors R et al (2007) Standard reporting requirements for biological samples in metabolomics experiments: microbial and in vitro biology experiments. Metabolomics 3(3):189–194

20. Velagapudi VR, Wittmann C, Schneider K et al (2007) Metabolic flux screening of *Saccharomyces cerevisiae* single knockout strains on glucose and galactose supports elucidation of gene function. J Biotechnol 132(4):395–404
21. Wiechert W, de Graaf AA (1996) In vivo stationary flux analysis by ^{13}C labeling experiments. In: Scheper T (ed) Metabolic engineering. Springer, Berlin, pp 109–154
22. Wittmann C (2007) Fluxome analysis using GC-MS. Microb Cell Fact 6(1):6
23. Wittmann C, Kim HM, Heinzle E (2004) Metabolic network analysis of lysine producing Corynebacterium glutamicum at a miniaturized scale. Biotechnol Bioeng 87(1):1–6
24. Wittmann C, Heinzle E (1999) Mass spectrometry for metabolic flux analysis. Biotechnol Bioeng 62(6):739–750
25. Wittmann C, Heinzle E (2001) Application of MALDI-TOF MS to lysine-producing Corynebacterium glutamicum. Eur J Biochem 268(8):2441–2455
26. Wittmann C, Heinzle E (2008) Metabolic network analysis and design in Corynebacterium glutamicum. In: Burkovski A (ed) Corynebacteria-genomics and molecular biology. Caister Academic Press, Norfolk, pp 79–112
27. Yang TH, Bolten CJ, Coppi MV et al (2009) Numerical bias estimation for mass spectrometric mass isotopomer analysis. Anal Biochem 388(2):192–203
28. Yang TH, Frick O, Heinzle E (2008) Hybrid optimization for ^{13}C metabolic flux analysis using systems parametrized by compactification. BMC Syst Biol 2(1):29
29. Yang TH, Wittmann C, Heinzle E (2004) Metabolic network simulation using logical loop algorithm and Jacobian matrix. Metab Eng 6(4):256–267
30. Yuan Y, Yang TH, Heinzle E (2010) ^{13}C metabolic flux analysis for larger scale cultivation using gas chromatography-combustion-isotope ratio mass spectrometry. Metab Eng 12(4):392–400
31. Frick O, Wittmann C (2005) Characterization of the metabolic shift between oxidative and fermentative growth in *Saccharomyces cerevisiae* by comparative 13 C flux analysis. Microbial Cell Factories 4(1):1–16
32. Andreas KG, Margarida MDS, Bjarke C et al (2000) Network identification and flux quantification in the central metabolism of *Saccharomyces cerevisiae* under different conditions of glucose repression. J Bacteriol 183(4):1441–1451

Chapter 46
A Comparative Study on the Antioxidant Activity of Two Polysaccharides from *Ganoderma lucidum*

Ruyu Tao, Limin Hao, Shiru Jia, Xin Zheng, Jianyong Yu and Qingwu Jiang

Abstract Two polysaccharides from *Ganoderma lucidum* (GLP1 from fermentation broth and GLP2 from fruiting body) were obtained and investigated for their in vitro antioxidant properties. The two polysaccharides showed strong antioxidant activities in a dose-dependent manner. At 5.0 mg/mL, the reducing power and the scavenging rate on DPPH radical and hydroxyl radical of GLP1 were 1.25, 50 and 80 %, while that of GLP2 were 1.46, 85, and 78 %, respectively. GLP1 and GLP2 also showed strong protective effects on yeast cells from UV and H_2O_2 damage. At 20 mg/mL, the protective effects on yeast cells from UV and H_2O_2 of GLP1 were 57 and 49 %, and that of GLP2 were 84 and 79 %, respectively. Thus, both GLP1 and GLP2 could be considered as antioxidants for food and pharmaceutical industries.

Keywords *Ganoderma lucidum* · Polysaccharides · Antioxidant activity · Protective effect

R. Tao · L. Hao · S. Jia (✉) · X. Zheng
Key Lab of Industrial Fermentation Microbiology of the Ministry of Education,
College of Biotechnology, Tianjin University of Science and Technology,
Tianjin 300457, People's Republic of China
e-mail: jiashiru@tust.edu.cn

L. Hao (✉) · J. Yu
The Quartermaster Equipment Institute of General Logistics Department of People's Liberation Army, Beijing 100000, People's Republic of China
e-mail: hlm2005@163.com

Q. Jiang
Anhui Jinzhai Qiao Kang Pharmaceutical Co., LTD, Jinzhai 237300,
People's Republic of China

T.-C. Zhang and M. Nakajima (eds.), *Advances in Applied Biotechnology*,
Lecture Notes in Electrical Engineering 333, DOI 10.1007/978-3-662-46318-5_46

46.1 Introduction

Oxidation, which provides energy to biological process, is an essential biological process to many organisms [1]. However, overproduced oxygen free radicals under pathological conditions could generate damage to cells, such as interference and manipulation of protein, tissue loosening, genetic damage, promotion of disease, and aging [2–5]. However, recent researches suggested that using antioxidants is an effective method to reduce oxidation damage. Thus, it is essential to develop and utilize more natural antioxidants to protect human body from free radicals damage [6–8].

Ganoderma lucidum is a mushroom being widely used in China and other Asian countries [9]. It is regarded as a tonic for promoting longevity and health, which has been used to treat a variety of diseases, such as atherosis, hepatopathy, chronic hepatitis, neurasthenia, insomnia, bronchitis, nephritis, hypertension, asthma, and gastric ulcers [10–12]. Modern medical studies have shown that these functions are associated with polysaccharides, which are mainly active components of *G. lucidum*. These polysaccharides are capable of antioxidation, immunity improvement, and antitumor, etc. [13].

Ganoderma lucidum polysaccharides (GLP) are mainly extracted from fruit bodies and spores of *G. lucidum*. However, the incubation time is more than 60 days, and the yield of polysaccharides is below 100 mg/g [14]. The submerged fermentation of *G. lucidum* is another way to gain a large amount of extracellular polysaccharides [15, 16]. Compared with the artificial cultivation of *G. lucidum*, the submerged fermentation of mycelium has a short cycle, high yield, and stable product quality. Therefore, more attention has been paid to the submerged fermentation of *G. lucidum* in recent years. Although the nutritional value and pharmacologic action of the products from the fermentation broth are not lower than that of fruiting body, the contrasts of GLP from fermentation broth and fruiting body have been little studied and need further research.

In this paper, one fermentation broth polysaccharide (GLP1) and one fruiting body polysaccharide (GLP2) were extracted from *G. Lucidum*. Their antioxidant activities (DPPH, hydroxyl radical scavenging assay and reducing power) and protective effects on yeast cells with physical and chemical oxidative damage were investigated.

46.2 Materials and Methods

46.2.1 Materials

Both the strain and fruiting body of *G. lucidum* were provided by the Quartermaster Equipment Institute of General Logistics Department of People's Liberation Army. Trifluoroacetic acid solution (TFA), hydrogen peroxide (H_2O_2), ascorbic acid, ferrous sulfate, trichloroacetic acid, salicylic acid, ferric chloride, and potassium ferricyanide were purchased from Tianjin chemical factory (Tianjin, China) and of analytical grade. 1-Diphenyl-2-picrylhydrazyl (DPPH) was purchased from Sigma-Aldrich (St. Louis, MO, USA). All other chemicals used were of analytical grade.

46.2.2 Preparation of Crude Polysaccharides

The strain of *G. lucidum* was grown in a 500 mL flask containing 150 mL medium at 28 °C for 5 days with shaking at 180 rpm. After cultivation, the cultured media were filtered to remove the mycelia and the aqueous fraction obtained from filtration was concentrated with a rotary evaporator (RE3000) under reduced pressure at 50 °C and precipitation at 4 °C for 12 h with fourfold volumes of ethanol. The crude polysaccharide GLP1 was collected by centrifugation and then freeze-dried.

The fruiting body of *G. lucidum* was dried in a drying oven (DGG) at 60 °C and ground to powder. The impurities in crushed powder were removed with 80 % ethanol for 24 h at room temperature. The crude polysaccharide GLP2 was extracted from the crushed powder by hot water at 90 °C in a 1:25 (w/v) ratio for 4 h. Then, the extract was filtered and centrifuged at 10,000 rpm for 20 min at room temperature. The supernatant was concentrated, precipitated, and freeze-dried according to the method described above. So the crude polysaccharide GLP2 was obtained. The total sugar content of GLP1 and GLP2 was determined by the phenol–sulfuric acid method [17]. And the polysaccharide yield of GLP1 and GLP2 were 95.6 and 94.5 %, respectively.

46.2.3 In Vitro Antioxidant Activity of GLP1 and GLP2

46.2.3.1 DPPH Radical Scavenging Activity

The DPPH radical scavenging activities of GLP1 and GLP2 were tested according to the method of Shimada et al. [15] with some modifications. Briefly, 3 mL DPPH solution (0.4 mmol/L DPPH in ethanol) was mixed with 1 mL polysaccharide solution or ascorbic acid solution (1.0, 2.0, 3.0, 4.0, and 5.0 mg/mL) and reacted at room temperature for 30 min in dark. Then, the absorbance was measured at 517 nm and ascorbic acid was included as the positive control. The percent DPPH radical scavenging activity was calculated using the following equation:

$$\text{DPPH radical scavenging activity } (\%) = \left[\frac{A_0 - (A_1 - A_2)}{A_0}\right] \times 100$$

where A_0 was the absorbance of the control (without sample) and A_1 was the absorbance of the sample, A_2 was the absorbance without DPPH.

46.2.3.2 Hydroxyl Radical Scavenging Activity

Hydroxyl radical scavenging activity was carried out according to a literature method [16] with some modifications. Hydroxyl radical was generated from $FeSO_4$ and H_2O_2 and detected by their ability to hydroxylate salicylate. The polysaccharides solution at the concentrations of 1.0, 2.0, 3.0, 4.0, and 5.0 mg/mL (1 mL) was mixed with 5 mmol/L $FeSO_4$ (1 mL), 5 mmol/L salicylic acid–ethanol solution (1 mL), 5 mmol/L H_2O_2 (1 mL), and incubated in water bath at 37 °C for 30 min. The absorbance was measured at 510 nm and ascorbic acid was used as the positive control. The hydroxyl radical scavenging effect was calculated as:

$$\text{hydroxyl radical scavenging activity (\%)} = \left[\frac{A_0 - (A_1 - A_2)}{A_0}\right] \times 100$$

where A_1 was the absorbance of the sample or ascorbic acid, and A_0 was the absorbance of the solvent control (without sample or ascorbic acid), A_2 was the absorbance of the reagent blank without salicylic acid.

46.2.3.3 Reducing Power

The reducing power was measured according to the method of Oyaizu [18] with a minor modification. Briefly, 2.5 mL various concentrations of polysaccharide samples (GLP1 and GLP2, 1.0, 2.0, 3.0, 4.0, and 5.0 mg/mL) were mixed with 2.5 mL potassium ferricyanide (1.0 %, w/v) and were incubated at 50 °C for 20 min. Following, 2.5 mL trichloroacetic acid (10 %, w/v) was added, and the mixture was centrifuged at 5,000 rpm for 10 min. The supernatant (5 mL) was mixed with ferric chloride (0.50 mL, 0.1 %, w/v) and measured at 700 nm and ascorbic acid was used as the positive control. The reducing power was calculated as:

$$\text{Reducing Power} = A_1 - A_2$$

where A_1 was the absorbance of the sample or ascorbic acid, and A_2 was the absorbance of the reagent blank without ferric chloride.

46.2.3.4 Protective Effect on Yeast Cells from UV

Firstly, the yeast cells were cultivated to the early stage of the logarithmic phase in yeast extract peptone dextrose medium, and then 20 mL fermentation broth was centrifuged at 4,000 rpm for 5 min. Following, the precipitation was washed with phosphate buffer solution (pH 6.9) twice and then mixed with 20 mL phosphate buffer solution. A total of 1 mL yeast suspension was mixed with 4 mL various concentrations of GLP1 or GLP2 sample (4, 8, 12, 16, 20 mg/mL) and disposed with UV radiation for lethal time (1 min), respectively. The control group was added with phosphate buffer solution. Finally, the mixture was diluted to a suitable concentration and spread on a plate medium, cultured at 28 °C for 48 h. Ascorbic acid was used as the positive control. The survival rate was calculated as follows:

$$\text{The survival rate } (\%) = \left[\frac{A_1 - A_2}{A_0 - A_2}\right] \times 100$$

where A_0 was the amount of cells which had not been disposed by UV radiation, A_1 was the amount of polysaccharide sample, and A_2 was the amount of the blank control group.

46.2.3.5 Protective Effect on Yeast Cells from H_2O_2

Similar to the oxidative injury of UV irradiation above, the yeast suspension was prepared according to the method described in Sect. 46.2.3.4. A total of 1 mL yeast suspension was mixed with 4 mL polysaccharide samples (GLP1 or GLP2 of 4, 8, 12, 16, 20 mg/mL), and then disposed by 1 mL H_2O_2 solution (lethal concentration 2 %) for 30 min, respectively. The control group was mixed with 1 mL phosphate buffer solution (instead of the polysaccharide samples). The survival rate was calculated using the following equation:

$$\text{The survival rate } (\%) = \left[\frac{A_1 - A_2}{A_0 - A_2}\right] \times 100$$

where A_0 was the amount of cells which had not been disposed by H_2O_2 solution, A_1 was the amount of polysaccharide sample, and A_2 was the amount of the blank control group.

46.3 Results and Discussions

46.3.1 Scavenging Ability on DPPH Radicals

The method of scavenging the stable DPPH radicals is a widely used assay to evaluate the antioxidant activities of different compounds. The effects of scavenging DPPH radicals of GLP1 and GLP2 were measured and shown in Fig. 46.1. The results indicated that both GLP1 and GLP2 showed obvious scavenging activity on DPPH radicals in a concentration-dependent fashion. Compared with GLP2, GLP1 showed a weaker scavenging activity on DPPH radicals. The scavenging abilities at high concentration of GLP1, GLP2, and ascorbic acid were 50, 85, and 95 %, respectively. It has been reported that *G. lucidum* fruit body polysaccharides showed 46–65 % (4.0 mg/mL) of DPPH radical scavenging activities [19], similar

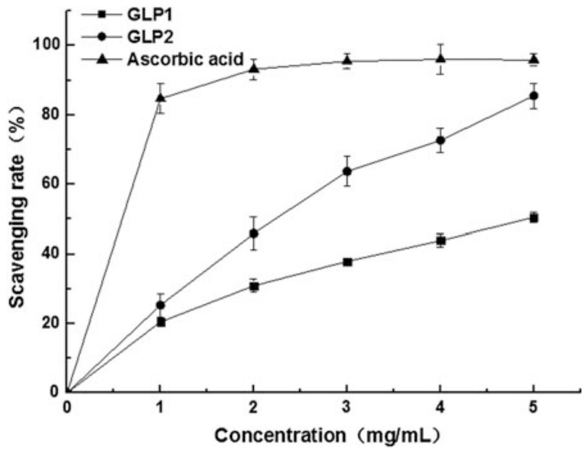

Fig. 46.1 Scavenging effects of GLP1 and GLP2 on DPPH free radicals

to the polysaccharides in this study. The difference between GLP1 and GLP2 may be related to monosaccharide component and molecular size.

46.3.2 Scavenging Ability on Hydroxyl Radicals

Hydroxyl radical reacts with most biomolecules including carbohydrates, proteins, lipids and DNA in cells, causing damage to the heterocyclic DNA bases or cell death by a variety of mechanisms [20]. Thus, scavenging hydroxyl radicals are important for the protection of living systems. The antioxidant mechanism may be related to hydrogen supplied by polysaccharides, which combines with radicals and forms a stable radical to terminate the radical chain reaction [14]. Figure 46.2

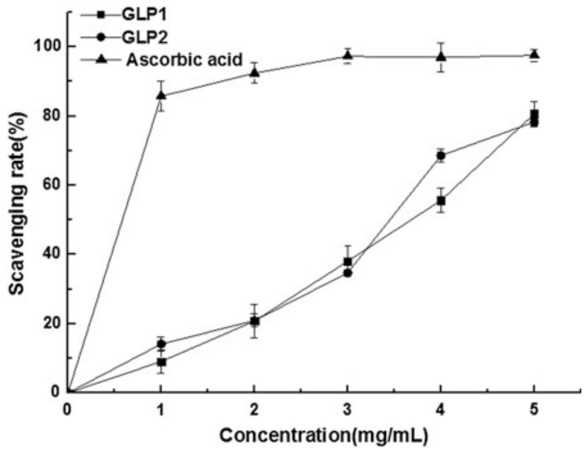

Fig. 46.2 Scavenging effects of GLP1 and GLP2 on hydroxyl free radicals

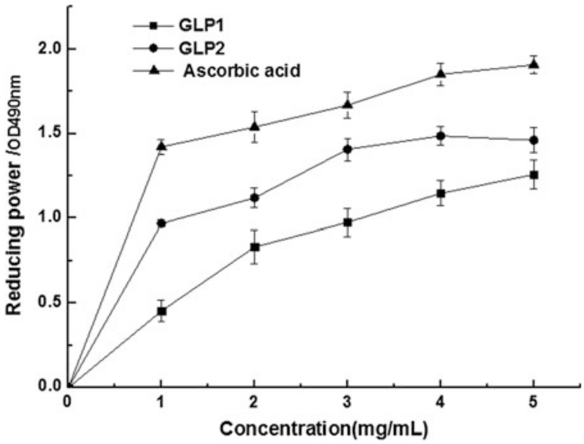

Fig. 46.3 Reducing power of GLP1 and GLP2

showed the results of the scavenging effects on hydroxyl radicals of GLP1, GLP2, and ascorbic acid. At the test concentrations, the scavenging activities of various samples increased with the increase of sample concentration ranging from 1.0 to 5.0 mg/mL. At 5.0 mg/mL, the scavenging activities of GLP1 and GLP2 were 80 and 78 %, respectively. The results were agreed with the previous report by Fan et al. [21]. They found that the scavenging ability on hydroxyl radicals of *G. lucidum* polysaccharides were 33.6–63.6 % at 2.5 mg/mL. Our data on the activities of scavenging hydroxyl radical of two polysaccharides suggested that they were potential antioxidants.

46.3.3 Reducing Power

In the reducing power assay, the antioxidants in the samples would result in the reduction of Fe^{3+} to Fe^{2+} by donating an electron. The antioxidant activity was concomitant with the reducing power. The reducing capacity of GLP1, GLP2, and ascorbic acid was tested and the results were shown in Fig. 46.3. The results showed that the reductive potential of GLP1 and GLP2 increased to 1.25 and 1.46 as the concentrations increased to 5 mg/mL, respectively. While ascorbic acid showed a stronger reducing power (1.91 at 5 mg/mL) than the polysaccharides samples. The results were much higher than the previous report [14], in which the reducing power of *G. lucidum* fruit body polysaccharides were 0.68–1.48 at 10.0 mg/mL. The reducing capacity of a compound may be considered as a significant marker of its potential antioxidant activity.

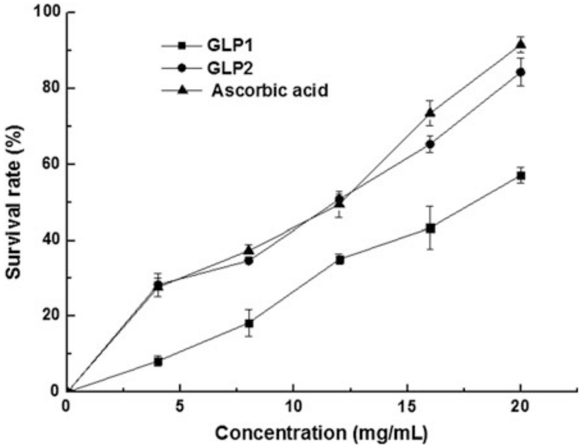

Fig. 46.4 Protective effects of GLP1 and on yeast cells from UV oxidative damage

46.3.4 Protective Effect on Yeast Cells from UV

Studies have proved that UV radiation may cause oxidative-induced DNA damage or cell death, which is induced by the generation of oxygen-derived species including free radicals, such as $O_2\cdot^-$, O_2, H_2O_2, ·OH, ROO· [19]. The presence of antioxidants could effectively reduce the DNA damage caused by UV radiation. The yeast cells were used in the assay to measure the protective effects of polysaccharides samples (at the dose of 4, 8, 12, 16, 20 mg/mL) on yeast cells from UV. The antioxidant activity was related to the survival rate of the yeast cells. As shown in Fig. 46.4, GLP1 and GLP2 demonstrated protective effects on yeast cells in a dose-dependent tendency at the concentrations examined. At 20 mg/mL, the protective effects on yeast cells of GLP1 and GLP2 were 57 and 84 %, respectively. However, the protective effect of ascorbic acid was a little stronger (91 % at 20 mg/mL) than GLP1 and GLP2. The protective effect on yeast cells of two polysaccharides were closely correlated with their antioxidant activities.

46.3.5 Protective Effect on Yeast Cells from H_2O_2

H_2O_2 is an interesting class of cytotoxic agents that tends to arise naturally from a wide variety of chemical and biochemical oxidations. Hydrogen peroxide is an essential component for toxicity and it can interact with macromolecules (e.g., DNA), cells and tissues to produce damage [22]. Thus, in this assay, the protective effect on yeast cells from H_2O_2 was used to determine the antioxidant activities of GLP1 and GLP2, and the survival rate of yeast cells is shown in Fig. 46.5. At the test concentrations, GLP1 and GLP2 exhibited protective effects on yeast cells from H_2O_2 in a dose-dependent manner. At 20 mg/mL, the protective effects on yeast

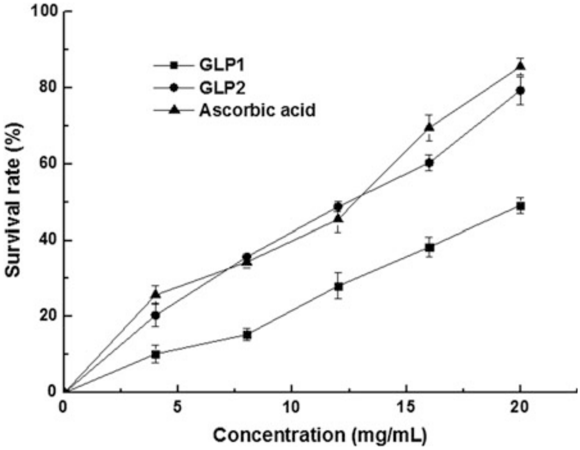

Fig. 46.5 Protective effects of GLP1 and GLP2 on yeast cells from H_2O_2 oxidative damage

cells of GLP1 and GLP2 were 49 and 79 %, respectively. However, the results were a little less than that of ascorbic acid (85 % at 20 mg/mL).

From the above results, both GLP1 and GLP2 exhibited potential antioxidant capacities and could be explored as a source of bioactive compounds.

46.4 Conclusion

In this study, two polysaccharides from the fermentation broth and fruiting body of *G. lucidum* were isolated. Moreover, the antioxidant activities of GLP1 and GLP2 indicated that they had significant scavenging effects on free radicals (DPPH, hydroxyl radicals), reducing power and protective effect on yeast cells from UV and H_2O_2. The results showed that both the two polysaccharides exhibited antioxidant activities in a concentration-dependent manner and the antioxidant activities of GLP2 were superior to GLP1. Above all, the polysaccharides of *G. lucidum* could be utilized as antioxidant for food and pharmaceutical industries. Further research is needed to elucidate the mechanism of their antioxidant activities.

Acknowledgments This research is supported by the army scientific research program AX110C002.

References

1. Yuan JF, Zhang ZQ, Fan ZC, Yang JX (2008) Antioxidant effects and cytotoxicity of three purified polysaccharides from *Ligusticum chuanxiong Hort*. Carbohydr Polym 74:822–827
2. Guo S, Mao W, Han Y, Zhang X et al (2010) Structural characteristics and antioxidant activities of the extracellular polysaccharides produced by marine bacterium *Edwardsiella tarda*. Bioresour Technol 101:4729–4732

3. Wang CC, Chang SC, Inbaraj BS, Chen BH (2010) Isolation of carotenoids, flavonoids and polysaccharides from *Lycium barbarum L.* and evaluation of antioxidant activity. Food Chem 120:184–192
4. Hu T, Liu D, Chen Y, Wu J, Wang S (2010) Antioxidant activity of sulfated polysaccharide fractions extracted from *Undaria pinnitafida* in vitro. Int J Biol Macromol 46:193–198
5. Luo AX, He XJ, Zhou SD, Fan YJ, Luo AS (2010) Purification, composition analysis and antioxidant activity of the polysaccharides from *Dendrobium nobile Lindl*. Carbohydr Polym 79:1014–1019
6. Sun Y, Li T, Liu J (2010) Structural characterization and hydroxyl radicals scavenging capacity of a polysaccharide from the fruiting bodies of *Auricularia polytricha*. Carbohydr Polym 80:377–380
7. Xie JH, Xie MY, Nie SP, Shen MY, Wang YX, Li C (2010) Isolation, chemical composition and antioxidant activities of a water-soluble polysaccharide from *Cyclocarya paliurus* (Batal.) lljinskaja. Food Chem 119:1626–1632
8. Singh N, Rajini PS (2004) Free radical scavenging activity of an aqueous extract of potato peel. Food Chem 85:611–616
9. Paterson RRM (2006) *Ganoderma*-A therapeutic fungal biofactory. Phytochemistry 67: 1985–2001
10. Liu GQ, Zhang KC (2005) Mechanisms of the anticancer action of *Ganoderma lucidum* (Leyss. ex. Fr.) Karst.: a new understanding. J Integr Plant Biol 4:129–135
11. Tang YJ, Zhong JJ (2004) Modeling the kinetics of cell growth and ganoderic acid production in liquid static cultures of the medicinal mushroom *Ganoderma lucidum*. Biochem Eng J 21:259–264
12. Xie JT, Wang CZ, Wicks S, Yin JJ, Kong J, Li J, Li YC (2006) *Ganoderma lucidum* extract inhibits proliferation of SW 480 human colorectal cancer cells. Exp Oncol 28:25–29
13. Zhang J, Liu Y, Park H, Xia Y, Kim G (2012) Antitumor activity of sulfated extracellular polysaccharides of *G. lucidum* from the submerged fermentation broth. Carbohydr Polym 87:1539–1544
14. Shi M, Zhang Z, Yang Y (2013) Antioxidant and immunoregulatory activity of *Ganoderma lucidum* polysaccharide (GLP). Carbohydr Polym 95:200–206
15. Shimada K, Fujikawa K, Yahara K, Nakamura T (1992) Antioxidative properties of xanthan on the autoxidation of soybean oil in cyclodextrin emulsion. J Agric Food Chem 40:945–948
16. Zhong XK, Jin X, Lai FY, Lin QS, Jiang JG (2010) Chemical analysis and antioxidant activities in vitro of polysaccharide extracted from *Opuntia ficus indica Mill*. cultivated in China. Carbohydr Polym 82:722–727
17. Davies OL, George EP, Lewis RC (1978) The design and analysis of industrial experiments. Longman Group Limited, London, pp 45–48
18. Oyaizu M (1986) Studies on products of browning reaction: antioxidative activities of products of browning reaction prepared from glucose amine. Jpn J Nutr 44:307–315
19. Wang JG, Wang YT, Liu XB, Yuan YH, Yue TL (2013) Free radical scavenging and immunomodulatory activities of *Ganoderma lucidum* polysaccharides derivatives. Carbohydr Polym 91:33–38
20. Dizdaroglu M (2012) Oxidatively induced DNA damage: mechanisms, repair and disease. Cancer Lett 327:26–47
21. Fan LP, Li JW, Deng KQ, Ai LZ (2012) Effects of drying methods on the antioxidant activities of polysaccharides extracted from *Ganoderma lucidum*. Carbohydr Polym 87:1849–1854
22. Giandomenico AR, Cerniglia GE, Biaglow JE (1997) The importance of sodium pyruvate in assessing damage produced by hydrogen peroxide. Free Radic Biol Med 23:426–434

Chapter 47
Biofortification Using Bacteria Containing an Atrazine-Degrading Gene and Its Effects on Reactor Operating Efficiency

Yue Wang and Jinxu Sun

Abstract To investigate the effects of biofortification of activated sludge reactors using genetically engineered microbes containing a plasmid encoding atrazine chlorohydrolase, we compared biodegradation efficiency and sludge properties during three operating stages in a conventional activated sludge (CAS) reactor and a MBR. Our results show that with the addition of genetically engineered bacteria and the selection for indigenous biodegrading microbes, membrane fouling was reduced. Atrazine has a certain level of biotoxicity toward activated sludge and shows an inhibitory effect toward pollutant removal. After biofortification, atrazine degradation was superior in MBR than that in CAS reactors. The atrazine removal rate was 92.6 % in the MBR, while it was 82.6 % in the CAS reactor. Following biofortification, the sludge concentration in the MBR was maintained at 7.3 g/L, while the sludge concentration in the CAS reactor was 2.3 g/L.

Keywords Biofortification · Genetically engineered bacteria atrazine degradation · Conventional activated sludge reactor · Membrane bioreactor

47.1 Introduction

Biodegradation-resistant organic pollutants, particularly synthetic compounds, can only be broken down through the actions of complex series of cooperative metabolic mechanisms found in different species of biodegradative bacteria [1]. Superbiodegrading bacteria overcome this need for interspecies collaboration, as they are genetically engineered to contain recombinant genes coding for degradative enzymes originating from different bacterial species. This type of genetic

Y. Wang (✉) · J. Sun
Department of Life Sciences, Hengshui University, Hengshui 053000, Hebei, China
e-mail: jyailn@163.com

T.-C. Zhang and M. Nakajima (eds.), *Advances in Applied Biotechnology*,
Lecture Notes in Electrical Engineering 333, DOI 10.1007/978-3-662-46318-5_47

engineering can effectively improve the biodegradative activity of the superbiodegrading bacteria and increase pollutant removal.

Biofortification is a process that can help improve the removal efficiency of biodegradation-resistant organic pollutants. Beginning in the late 1980s, researchers studied the use of genetically engineered bacteria for the biofortification of wastewater treatment reactors [2]. Since then, there has been a growing interest in using genetically engineered bacteria to assist in the removal of organic pollutants through biofortification. Experimental evidence shows that the use of genetically engineered bacteria can effectively improve the removal efficiency of biodegradation-resistant pollutants, greatly improving both the rate of degradation of pollutants and the ability of the reactors to handle a greater pollutant load [3–8].

47.2 Materials and Methods

47.2.1 Reactor Parameters

Our experimental setup consisted of a CAS reactor and an MBR system. The main portion of the reactor was made of plexiglass.

The CAS reactor is shown in Fig. 47.1 and was constructed using aeration and sedimentation tanks. Artificially prepared wastewater used in this study was fed into the reactor via a peristaltic pump. The reactor was made of plexiglass and its dimensions are 150 mm × 300 mm × 350 mm, with an effective volume of 9 L.

The MBR system is shown in Fig. 47.2. Artificially prepared wastewater was fed into the reactor via the intake pump. The dimensions of the reactor are 140 mm × 250 mm × 660 mm, with an effective volume of 15 L. The membrane was a hollow fiber PVDF ultrafiltration membrane.

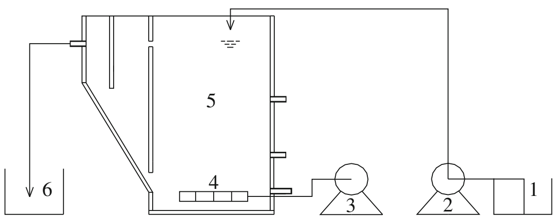

Fig. 47.1 Conventional activated sludge system schematic diagram. *1* Water supply tank. *2* Peristaltic pump. *3* Air pump. *4* Revealed the trachea. *5* The reactor. *6* Out of the water tank

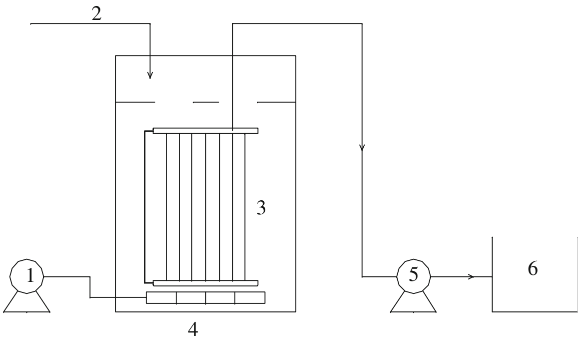

Fig. 47.2 The MBR system schematic diagram. *1* Air pump. *2* The water. *3* Membrane module. *4* Reactor. *5* Out of the water pump. *6* Out of the water tank

47.2.2 Source of Sludge and Artificially Prepared Wastewater

In this study, secondary settling tank sludge reflux was collected from the sewage treatment plant at Shijiazhuang Bridge West. The sludge concentration was 4 g/L, with high floc density and good settling characteristics.

The experimental wastewater was artificially prepared [9]. After initiating the reactor with the appropriate startup operations, atrazine was added to the influent water at a concentration maintained between 10 and 20 mg/L. The reactor's operating temperature was maintained at approximately 25 °C.

Using the same hydraulic retention time (HRT), the reactor operation was divided into two major stages:

(1) Sludge culture stage (Run-0);
(2) Sludge operation stage, which was further divided into three shorter stages, as shown in Table 47.1.

47.2.3 Preparation of Bacterial Strains and Suspensions

The genetically engineered bacteria used in this study were Escherichia coli DH5α cells containing the pACYC184 plasmid encoding atrazine chlorohydrolase and the

Table 47.1 Table experiment contents and operating conditions

Table experiment contents	Operating conditions
Blank operation phase (Run-1)	COD concentration in the influent water was 300–500 mg/L; ammonia was 40–50 mg/L; HRT was 24 h; no atrazine
Abiotic strengthen the operating period (Run-2)	Atrazine concentration was 25–30 mg/L; other conditions the same as Run-1
Biological strengthen the operating period (Run-3)	Genetic engineering bacteria in the influent water was 2.16 × 107 CFU/mL; other conditions the same as Run-2

pUC18-gfp plasmid encoding green fluorescent protein [10]. As a result, the cells are resistant to ampicillin and chloramphenicol.

A single colony was picked and grown overnight in the LB medium (containing 25 μg/mL of chloramphenicol) at 37 °C with shaking at 120–140 rpm. The culture was centrifuged and washed with phosphate buffer (pH 7.0). Cells were harvested to prepare bacterial suspensions for subsequent experiments.

47.2.4 Detection of Pollutants

COD and ammonia were measured using national standardized methods.

Atrazine concentrations were measured by high-performance liquid chromatography (Shimadzu) analysis of water samples filtered through a 0.45 μm membrane. A C18 reverse phase column and UV detector were used and the methanol:water ratio was 70:30. The detection wavelength was 223 nm.

47.2.5 Sludge Performance Testing

Measurements were performed in accordance with national standards.

Sludge floc particle sizes were measured using a laser particle size distribution analyzer (BT-9300H).

Sludge activity was measured using the total oxygen uptake rate (OUR).

47.3 Results and Analyses

47.3.1 Membrane Pressure Changes in the MBR

Changes in membrane pressure during the three stages of reactor operation are shown in Fig. 47.3.

The membrane must be cleaned when the pressure reaches 180 kPa. The regular rapid decreases in pressure shown in Fig. 47.3 reflect the times when the membrane was cleaned during reactor operation. During the different stages, membrane fouling took place quickly during Run-1, resulting in membrane cleaning every 2 months. During Run-2, the addition of atrazine disrupted the activity of the microbes in the system, resulting in rapid increases of membrane pressure due to increased membrane fouling. The frequency of membrane cleaning during this stage was once a month. During Run-3, when the genetically engineered bacteria were added, atrazine was degraded, and it took longer for the membrane pressure to increase to the maximum tolerable value of 180 kPa than during Run-2. On average, the membrane was cleaned once in every 2 months.

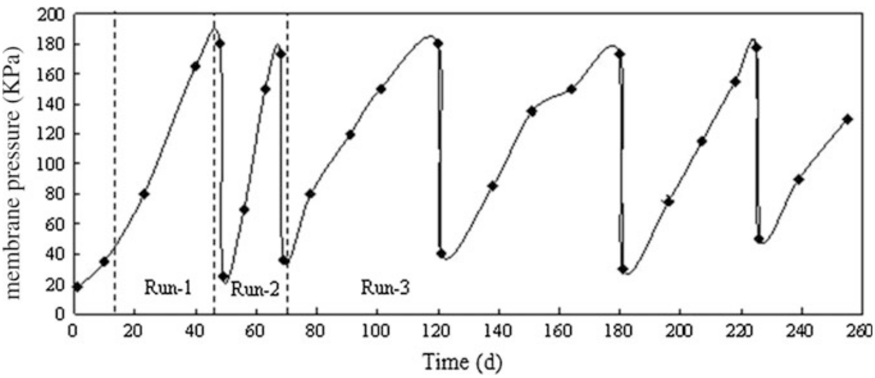

Fig. 47.3 Membrane pressure difference along with the change of running time

Bacterial growth, metabolites, organic molecules from wastewater, dissolved substances, and solid particles all contribute to the film formation on the surface of the membrane or to membrane obstruction. We show that atrazine toxicity toward sludge microbes results in accelerated membrane fouling, likely due to increased secretion of extracellular polymers and the accumulation of the secretions. However, the addition of genetically engineered bacteria improved the sludge properties, resulting in decreased membrane fouling.

47.3.2 Analysis of Pollutant Removal

47.3.2.1 Conventional Pollutants

The COD removal efficiency of the MBR and CAS reactors during all four operating stages is shown in Fig. 47.4.

As shown in Fig. 47.4, at each of the four operating stages, the MBR showed an average COD removal efficiency of 80.6, 95.6, 75.6, and 97.3 %. The average COD removal efficiency of the CAS reactor was 73.8, 83.8, 77.9, and 88.4 % during the same four stages of operation.

Clearly, the MBR has significantly higher COD removal efficiency than the CAS reactor, due to more efficient sludge and microbe retention by its membrane. Sludge is easily lost in the CAS reactor, and the effluent water contains suspended solids, indicating lower effluent water quality.

Meanwhile, in the two reactors, the trends of the rate of COD removal were roughly the same. The addition of atrazine during Run-2 led to a significant decrease in the rate of COD removal, which is reflective of the negative effect of atrazine on the biological activity of the activated sludge. During Run-3, the efficiency of COD removal returned to the levels similar to Run-1, indicating that

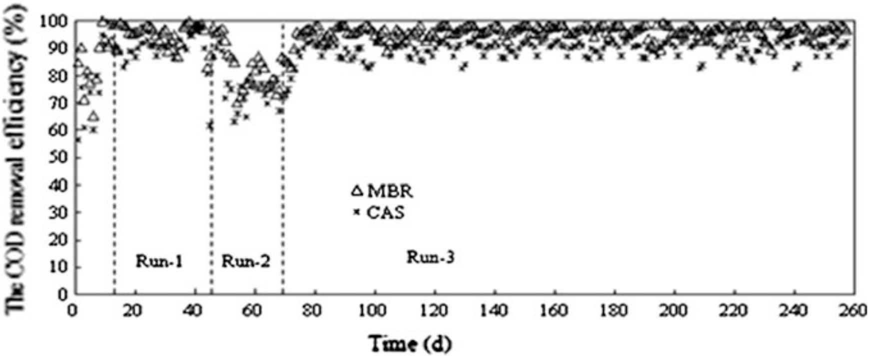

Fig. 47.4 The COD removal efficiency of the MBR and CAS reactors

biofortification using our genetically engineered bacteria helped remove atrazine in the system and reduced the adverse effects of atrazine on sludge bioactivity.

The ammonia removal efficiency of the MBR and CAS reactors during the four operating stages is shown in Fig. 47.5.

Figure 47.5 shows that the average concentration of ammonia in the influent water in both the reactors was 52.3 mg/L. The average rates of ammonia removal by the MBR during the four stages of operation were 65.4, 83.4, 71.9, and 87 %. The rates were 52.0, 78.3, 63.4, and 80 % in the CAS reactor.

These results show that the MBR is significantly better than the CAS reactor at removing ammonia. As the membrane in the MBR traps a large quantity of nitrifying bacteria, ammonia removal efficiency was improved.

Meanwhile, the ammonia removal efficiency shows the same trend in both the reactors. Addition of atrazine during the Run-2 stage significantly decreases the ammonia removal efficiency in the MBR, from 83.4 to 71.9 %. This suggests that

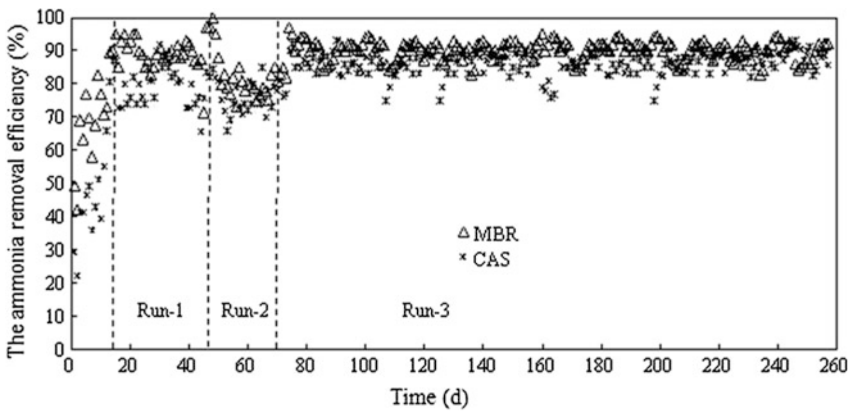

Fig. 47.5 The ammonia removal efficiency of the MBR and CAS reactors

atrazine has an inhibitory effect on nitrifying bacteria and their ability to remove ammonia. However, the addition of genetically engineered bacteria during Run-3 led to the increase of ammonia removal efficiency to 87 %, indicating that biofortification using genetically engineered bacteria reduced the quantity of atrazine in the system and further reduced the adverse effects of toxic compounds on the bioactivity of nitrifying bacteria.

Our genetically engineered bacteria showed high biodegradation activity toward atrazine. Their effect on reactor efficiency following biofortification is well demonstrated through the efficiency of atrazine removal.

The efficiency of atrazine removal by both the MBR and CAS reactors during the Run-2 and Run-3 operation stages is shown in Fig. 47.6.

During the Run-2 stage, reactors with no biofortification were not able to biodegrade atrazine.

During the Run-3 stage, the average rate of atrazine removal was 92.6 and 82.6 %, respectively. Initially after biofortification, the atrazine removal rate of the MBR increased rapidly to over 85 %. Soon after, the efficiency of atrazine biodegradation decreased due to indigenous bacteria preying on and competing with the genetically engineered bacteria, but atrazine removal remained at a steady rate during the later stage of operation. Atrazine removal by the CAS reactor gradually increased from 30 % to approximately 50 % during the early stage. However, due to the loss of genetically engineered bacteria from lack of retention or predation and competition by indigenous microbes, there was a slight decrease in atrazine removal during the subsequent stage of operation. When the efficiency of atrazine removal was compared between both the reactors, the MBR showed superior removal efficiency under the same operating conditions, likely due to microbial retention by the membrane in the MBR. This phenomenon may also be explained by the selection for indigenous atrazine biodegrading microbes.

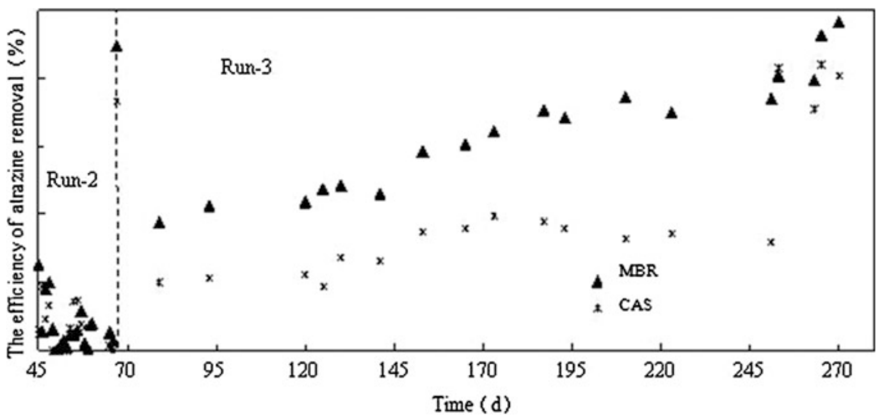

Fig. 47.6 The efficiency of atrazine removal by both the MBR and CAS reactors

47.3.3 Sludge Characteristics

We analyzed the sludge particle size distribution, which indirectly reflects the operating conditions of the reactor. The distribution of sludge particle sizes is shown in Fig. 47.7.

As shown in the figure, during the early stages of Run-1, when the sludge was first added, the particles had rather large diameters in both the MBR and the CAS reactors. After a certain time of operation, the sludge particle diameters decreased and finally stabilized at approximately 50 μ. During Run-2, the sludge particle diameters gradually decreased in both the MBR and the CAS reactors, indicating deterioration in sludge settling and reactor performance. In Run-3, sludge particle sizes grew larger in both the reactors. Overall, sludge particles in the MBR were larger than those in the CAS reactor, and showed good settling properties.

The activity of the sludge on organic matter degradation and nitrification are reflected by the reactor's treatment of COD and ammonia. We measured the rate of oxygen consumption during all three operational stages: Run-1, Run-2, and Run-3 to calculate the sludge activity in both the reactors. The results are shown in Figs. 47.8, 47.9 and 47.10.

Based on our results, the activity of the MBR was higher than that of the CAS reactor in Run-1, Run-2, and Run-3. We believe that this is due to microbial retention by the membrane in the MBR, leading to higher quantities of retained microorganisms and higher sludge activity. For this reason, the MBR showed superior COD and ammonia removal efficiencies to the CAS reactor. Meanwhile, both the MBR and the CAS reactors showed decreased activity in Run-2, which we believe to be due to the biotoxicity of the added atrazine toward the reactor microorganisms, which consequently negatively affected sludge activity, ultimately resulting in a decrease in the removal efficiency of COD and ammonia. Both the reactors recovered their initial sludge activity in Run-3.

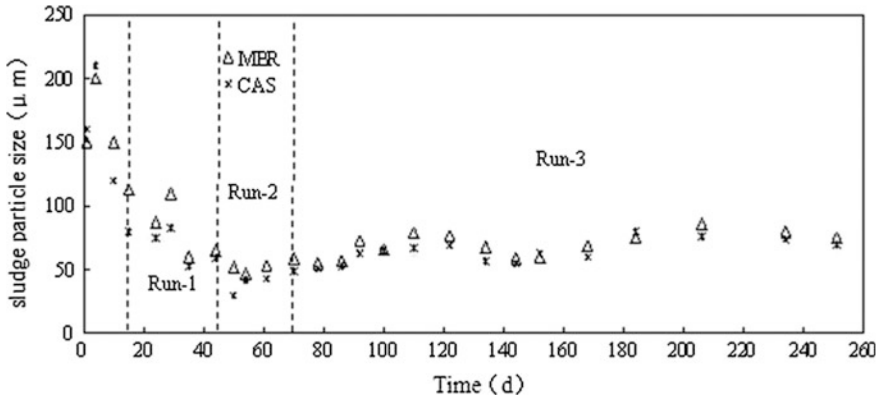

Fig. 47.7 The distribution of sludge particle sizes

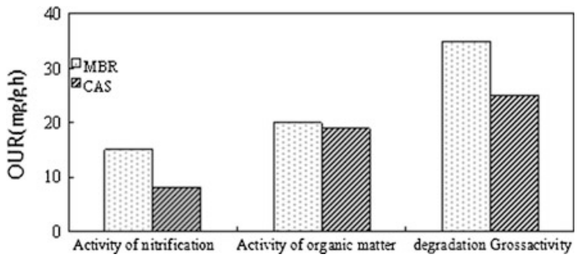

Fig. 47.8 The sludge activity of Run-1 operational stage

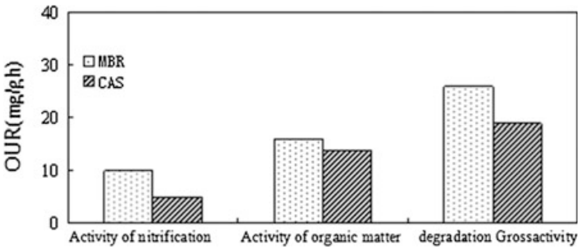

Fig. 47.9 The sludge activity of Run-2 operational stage

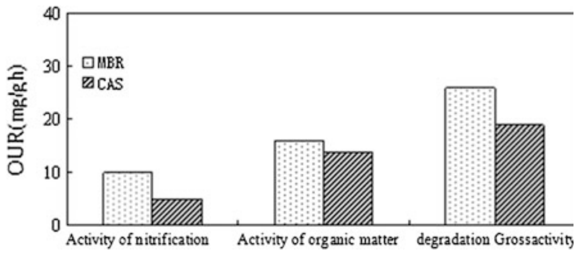

Fig. 47.10 The sludge activity of Run-3 operational stage

47.4 Conclusion

Atrazine is biotoxic and can negatively affect sludge settling, cause sludge floc dispersion, and increase extracellular secretions, thereby leading to accelerated membrane fouling in the MBR. With the use of genetically engineered bacteria and the colonization of indigenous biodegrading bacteria, membrane fouling was alleviated.

After biofortification, the MBR showed higher atrazine removal efficiency than the CAS reactor. Physical adsorption of atrazine by the activated sludge leads to lower effluent atrazine concentrations immediately after its addition to the influent water. After adsorption saturation, the effluent atrazine concentration increases. Loss of genetically engineered bacteria due to predation by the indigenous microbes in the activated sludge, as well as the loss of sludge, can lead to a decrease in the density of genetically engineered bacteria in the sludge. With bacterial growth and selection for indigenous atrazine-degrading microbial species, atrazine removal efficiency grows progressively higher. Ultimately, the efficiency of atrazine removal by the MBR was 92.6 %, while the efficiency of the CAS reactor was 82.6 %.

Under the same conditions of HRT, influent water load, and addition of the same concentration of genetically engineered bacteria, both the reactors showed similar changes in the removal of conventional pollutants. During the Run-2 stage, the addition of atrazine to the influent water decreased the removal efficiency of conventional pollutants, indicating that atrazine has some biotoxicities toward activated sludge as well as inhibitory activity toward pollutant removal. During the Run-3 stage, the efficiency of pollutant removal was restored to pre-atrazine levels, indicating that biofortification using genetically engineered bacteria reduces the adverse biological effects of atrazine on sludge activity, which is reflected by the restoration of removal efficiency of conventional pollutants by biofortified activated sludge.

References

1. Meclure NC, Weightman AJ et al (1989) Survival of pseudomonas putida UWC1 containing cloned catabolic genes in a model activated sludge unit. Appl Environ Microbiol 55:2627–2634
2. Fujita M, Ike M et al (1991) Feasibility of wastewater treatment using genetically engineered microorganisms. Water Res 25(8):979–984
3. Fujita M, Ike M et al (1993) Accelerated phenol removal by amplifying the gene expression with a recombinant plasmid encoding catechol-2, 3-oxygenase. Water Res 27(1):9–13
4. James DB, Robert RS (1997) Retention and expression of recombinant plasmids in suspended and biofilm bound bacteria degrading trichloroethene (TCE). Water Sci Technol 36(10):1–8
5. Erb RW, Wagner I et al (1997) Bioprotection of microbial communities from toxic phenol mixtures by a genetically designed pseudomonas. Nat Biotechnol 15(4):378–382
6. Soda S (1998) Effects of inoculation of a genetically engineered bacterium on performance and indigenous bacteria of a sequencing batch activated sludge process treating phenol. Ferment Bioeng 86(1):90–96
7. Eichner C (1999) A thermal gradient gel electrophoresis analysis of bioprotection from pollutant shocks in the activated sludge microbial community. Appl Environ Microbiol 65 (1):102–109
8. Nico B (2003) Bioaugmentation as a tool to protect the structure and function of an activated sludge microbial community against a 3-chloroaniline shock load. Appl Environ Microbiol 69 (3):1511–1520
9. Huang X, Liu R, Qian Y (2011) Behavior of soluble microbial products in a membrane bioreactor. Process Biochem 36:401–406
10. Lisa SC, Hugh MT, Michael SJ et al (2010) Field-scale remediation of atrazine-contaminated soil using recombinant Escherichia coli expressing atrazine chlorohydrolase. Environ Microbiol 2(1):91–98

Chapter 48
A Novel One-Pot Five-Component Synthesis of Tetrahydro-pyrrolo[3,4-*b*] pyridine-5-one via Ugi/Aza-Diels–Alder Tandem Reaction

Yan Liu, Tianyi Shang, Chuanming Xu, Hui Yang, Peng Yu and Kui Lu

Abstract A novel five-component domino processes to tetrahydro-pyrrolo[3,4-b] pyridine-5-one (**8**) were developed. Reaction of 5-phenyloxazole-2-carbaldehyde (**1**), *p*-toluidine (**2**), (Z)-4-methoxy-4-oxobut-2-enoic acid (**3**), and *t*-butyl isocyanide (**4**) in methanol at 60 °C provides an efficient access to the drug-like bicycle compound (**8**) in a good yield. In this one-pot process, a traditional oxo-bridged tricycle intermediate was formed via Ugi/ara-Diels–Alder tandem reaction and then the solvent, methanol, sequentially attacks and cuts off the oxo bridge under mild conditions via SN2 reaction. Formation of one C–N, two C–O, and three C–C bond with the triple domino sequence (Ugi/IMDA/SN2) is involved in this new scaffold generating reaction. The operational simplicity and maximizing the buildup of structural complexity makes this novel multicomponent reaction valuable in diversity-oriented synthesis of tetrahydro-pyrrolo[3,4-b]pyridine-5-one.

Keywords MCR · Ugi/aza-Diels–Alder tandem reaction · SN2 reaction · Domino process · Diversity-oriented synthesis

Y. Liu · T. Shang
Department of Biotechnology, Xinyang College of Agriculture & Forestry, Xinyang 464000, China

C. Xu · H. Yang · P. Yu · K. Lu (✉)
Key Laboratory of Industrial Fermentation Microbiology, Ministry of Education,
Tianjin Key Laboratory of Industry Microbiology, College of Biotechnology, Sino-French Joint Lab of Food Nutrition/Safety and Medicinal Chemistry, Tianjin University of Science & Technology, 13th Avenue, Tianjin Economic and Technological Development Area, Tianjin 300457, China
e-mail: lukui@tust.edu.cn

T.-C. Zhang and M. Nakajima (eds.), *Advances in Applied Biotechnology*,
Lecture Notes in Electrical Engineering 333, DOI 10.1007/978-3-662-46318-5_48

48.1 Introduction

Multicomponent reaction (MCR) is being recognized as one of the most promising approaches in diversity-oriented synthesis and is undoubtedly well suited for the drug discovery program [1]. Among named MCRs, the Ugi four-component reaction (Ugi-4CR) is without doubt one of the most powerful transformations [2]. By saving synthetic operations while maximizing the buildup of structural and functional complexity, this highly step economic reaction is particularly appealing in application of diversity-oriented synthesis [3]. Clearly, a proper union of Ugi with other reactions in a sequential or a domino process will further expand its potential [4, 5].

Indeed, pyrrolopyridine has attracted increased attention as biologically active compounds such as central nervous system agents [6], as herbicides [7] and as antidiabetic agents [8]. This skeleton has also been found in medically important natural product such as camptothecine [9] and meppicine ketone [10] (Fig. 48.1). As part of our research program directed at synthesizing drug-like heterocycles, we were interested in the development of a novel multicomponent synthesis to generate new scaffolds such as polysubstituted pyrrolo[3,4-b]pyridine-5-one.

One possible new scaffold generating reaction was illustrated by Ugi/aza-Diels–Alder tandem reaction with Lewis acid to afford the pyrrolopyridine (Scheme 48.1) [11].

Janvier et al. [12] have already shown that MCR/IMDA reaction cascades of 5-amideoxazole with a dienophile was possible leading to [4+2] cycloaddition product (Scheme 48.2).

To further apply this strategy to diversity-oriented synthesis, we set out to examine the previously unexplored Ugi reaction subsequentially combined with intramolecular Diels–Alder cycloaddition reaction of 5-phenyloxazole. According to the references, the reaction sequence we envisaged is highlighted in Scheme 48.3.

A reaction of 5-phenyloxazole-2-carbaldehyde (**1**), *p*-toluidine (**2**), (Z)-4-methoxy-4-oxobut-2-enoic acid (**3**), and *t*-butyl isocyanide (**4**) in methanol with Lewis acid in one pot was designed to provide a key pyrrolo[3,4-b]pyridine-5-one (**9**), which could then be used as a point to produce diverse bioactive libraries.

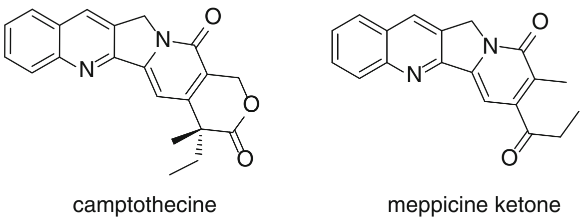

Fig. 48.1 Pharmaceutically important natural products camptothecine and meppicine ketone

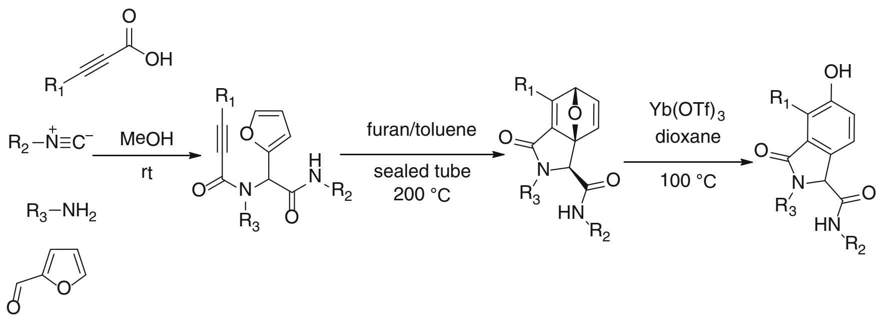

Scheme 48.1 Construction of heterocycle via sequential Ugi reaction/Diels–Alder cycloaddition reaction

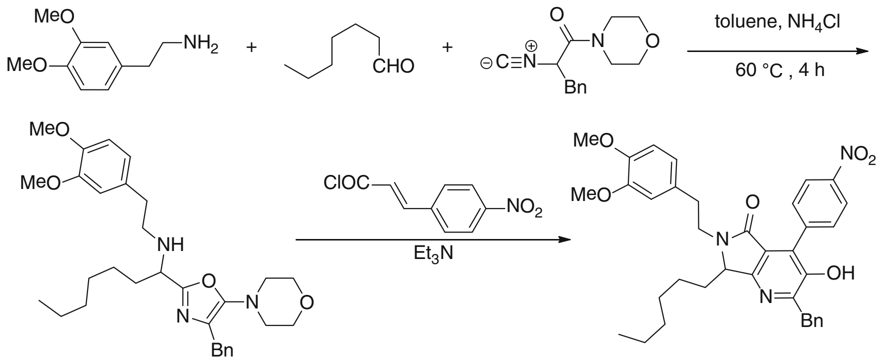

Scheme 48.2 Construction of pyrrolo[3,4-b]pyridine-5-one via MCR/IMDA reaction cascades of 5-amideoxazole

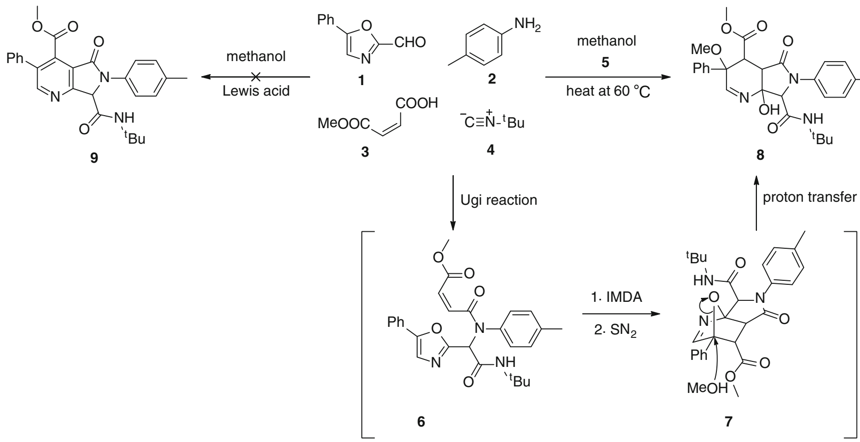

Scheme 48.3 Synthesis of tetrahydro-pyrrolo[3,4-b]pyridine-5-one

However, to our surprise, there is no **9** producing in the reaction instead of **8**. From the results of the experiment, a sequence of reaction involving intramolecular Diels–Alder cycloaddition and SN2 reaction was proposed to explain the formation of adduct **8**. In this one-pot process, a traditional oxo-bridged tricycle intermediate **7** was formed via Ugi/Aza-Diels–Alder tandem reaction.

48.2 Results and Discussions

Using 5-phenyloxazole-2-carbaldehyde (**1**), *p*-toluidine (**2**), (Z)-4-methoxy-4-oxobut-2-enoic acid (**3**), and *t*-butyl isocyanide (**4**) as substrates, we got the adduct **8** in 62 % yield. In this one-pot process, a traditional oxo-bridged tricycle intermediate **6** was formed via Ugi/aza-Diels–Alder tandem reaction, and then the solvent, methanol, sequentially attacks α-atom of –C=N and cuts off the oxo bridge in mild conditions via SN2 reaction. In order to get the tetracyclic intermediate **7**, we performed a survey of reaction conditions varying the solvents (MeOH, THF, H_2O, DCM, toluene, MeCN). The experimental results are summarized in Table 48.1. It is proved that the presence of MeOH was of utmost importance for the success of this reaction. Indeed, in its absence, there is no product **8** was obtained in other solvents. So MeOH may act as solvent as well as an activator for the domino sequence of Ugi reaction, intramolecular Diels–Alder reaction, and subsequent SN2 reaction.

In summery, we have developed an efficient five-component synthesis of tetrahydro-pyrrolo[3,4-b]pyridine-5-one. The optimized conditions we found for this five-component reaction consisted of heating a MeOH solution of **1**, **2**, **3**, and **4** at 60 °C for 10–12 h. Taking advantage of the chemical reactivity of 5-phenyloxazole and by fine-tuning the structure into the starting materials, we are expecting that this new five-component reactions can be devised for the synthesis of a number of tetrahydro-pyrrolo[3,4-b]pyridine-5-one. It is worth noting that one C–N, two C–O, and three C–C bonds were formed with the triple domino sequence (Ugi/IMDA/SN2) in this one-pot process. The efficiency of this reaction was thus truly remarkable if one looks at the yield per bond formation. At the same time, the

Table 48.1 Reaction conditions varying the solvents[a]

Entry	Sovelution	[**1**] (M)	Temp (°C)	Time (h)	Yield (%)[b]
1	MeOH	1.0	60	12	62
2	THF	1.0	60	12	n.r.
3	H_2O	1.0	60	12	n.r.
4	DCM	1.0	60	12	n.r.
5	Toluene	1.0	60	12	n.r.
6	MeCN	1.0	60	12	n.r.

[a] Reaction conditions: **1** (1.0 mmol), **2** (1.0 mmol), **3** (1.0 mmol), **4** (1.0 mmol) in 2 mL MeOH

[b] Isolated yield

significant feature of this procedure is the exploitation of methanol to cut off oxo bridge under mild conditions. It was the first time to report herein full details in development of this five-component reaction via the triple domino sequence (Ugi/IMDA/SN2) to successfully synthesize tetrahydro-pyrrolo[3,4-b]pyridine-5-one.

48.3 Experimental

48.3.1 General Procedure for the Three-Component Synthesis of Methyl 7-(tert-butylcarbamoyl)-7a-hydroxy-3-methoxy-5-oxo-3-phenyl-6-(p-tolyl)-4,4a,5,6,7,7a-hexahydro-3H-pyrrolo[3,4-b]pyridine-4-carboxylate (8)

In a 10 mL vial equipped with a magnetic stir bar, 5-phenyloxazole-2-carbaldehyde (**1**) (173 mg, 1.0 mmol), *p*-toluidine (**2**) (107 mg, 1.0 mmol), (Z)-4-methoxy-4-oxobut-2-enoic acid (**3**) (130 mg, 1.0 mmol) in MeOH (2.0 mL) was added *t*-butyl isocyanide (**4**) (83 mg, 1.0 mmol). The mixture was stirred at 60 °C for 10–12 h. Once the product formation deemed completed by TLC analysis, stopped the reaction. The mixture was cooled to room temperature and concentrated under reduced pressure to give a residue which was purified by silica gel column chromatography with hexane/ethyl acetate/CH_2Cl_2.

48.3.2 Characterization of Compound 8

Compound 8 (314 mg, 62 %) was obtained as white solid. ^1H NMR (400 MHz, d_6-DMSO): δ 7.68 (s, 1H), 7.61 (d, J = 3.2 Hz), 7.48–7.44 (m, 4H), 7.25–7.22 (m, 3H), 7.07 (d, J = 8.4 Hz, 2H), 5.27 (s, 1H), 5.16 (s, 1H), 4.47 (d, J = 2.8 Hz, 1H), 3.55 (s, 1H), 3.53 (s, 3H), 3.30 (s, 3H), 2.23 (s, 3H), 1.15 (s, 9H). 13C NMR (100 MHz, d_6-DMSO): δ 20.8, 28.4, 45.7, 51.3, 52.1, 55.4, 56.7, 62.9, 73.6, 88.7, 98.7, 117.8, 125.9, 127.7, 128.1, 129.4, 131.1, 137.7, 144.1, 153.7, 164.3, 169.9, 171.1. LRMS (ESI) m/z 508.4 $[M+H]^+$.

References

1. Zhu J, Bienaymé H (2006) Multicomponent reactions. Wiley, Weinheim
2. Dömling A (2002) Recent advances in isocyanide-based multicomponent chemistry. Curr Opin Chem Biol 6(3):306–313

3. Zhu J (2003) Recent developments in the isonitrile-based multicomponent synthesis of heterocycles. Eur J Org Chem 2003(7):1133–1144
4. Lee D, Sello JK, Schreiber SL (2000) Pairwise use of complexity-generating reactions in diversity-oriented organic synthesis. Org Lett 2(5):709–712
5. Sello JK, Andreana PR, Lee D et al (2003) Stereochemical control of skeletal diversity. Org Lett 5(22):4125–4127
6. Anzini M, Cappelli A, Vomero S et al (1996) Molecular basis of peripheral vs central benzodiazepine receptor selectivity in a new class of peripheral benzodiazepine receptor ligands related to alpidem. J Med Chem 39(21):4275–4284
7. Duerr D, Brunner HG, Szczepanski H (1988) US Patent US4721522. Chem Abstr 109:170430b
8. Hitzel V, Geisen K, Werner R et al (1981) Patent US2948522. Chem Abstr 95:150632h
9. Potmesil M, Pinedo HM (1994) Camptothecins new anticancer agents. CRC Press, Boca Raton
10. Pendrak I, Barney S, Wittrock R et al (1994) Synthesis and anti-HSV activity of A-ring-deleted mappicine ketone analog. J Org Chem 59(9):2623–2625
11. Wright DL, Robotham CV, Aboud K (2002) Studies on the sequential multi-component coupling/Diels-Alder cycloaddition reaction. Tetrahedron Lett 43(6):943–946
12. Janvier P, Sun X, Bienaymé H et al (2002) Ammonium chloride-promoted four-component synthesis of pyrrolo[3, 4-b]pyridin-5-one. J Am Chem Soc 124(11):2560–2567

Chapter 49
Study on Preparation and Application of High Esterification Green-Liquor Daqu

Xiao-Dan Wang, Bei Xiao, Shi-Dong Ban, Si-Xia Xu, Xi-Cui Shen and Shu-Yi Qiu

Abstract The optimal conditions of esterification Daqu production requires medium temperature to be used in the Daqu making process. The ratio of raw materials is 6:3:1 (wheat: barley: pea), the inoculation of *Monascus* (*Monascus purpureus*) FBKL3.0018 is 10 g/kg, and the water of Daqu is controlled at 40 %. The highest temperature is more suitable, which is controlled at 55 °C, and the culture time is 25–28 days. The best storage period of Daqu esterification is 2–3 months. This study could improve the quality of Daqu, the development, and research of fortified Daqu, which will become a hot point in increasing the quality rate of Luzhou-flavor liquor.

Keywords Esterification · Vinosity · Daqu

The yield, quality, and style of Luzhou-flavor liquor are directly affected by the quality of Luzhou-flavor Daqu. The bacteria, enzyme, and composite carrier of Daqu are made by environmental microorganisms. Fortified Daqu is used by the isolation technique of microorganisms, screening of beneficial bacteria, which could fully improve the biochemical properties, Then adding the beneficial bacteria into the Daqu improves the fortified Daqu [1, 2]. The combination of traditional brewing technology and modern biological engineering technology is used for screening and breeding of beneficial bacteria. The development and research of

X.-D. Wang · B. Xiao · S.-D. Ban · S.-Y. Qiu
Gui Zhou Provincial Key Laboratory of Fermentation Engineering and Biological Pharmacy, Guiyang 550025, Guizhou, China

S.-X. Xu · X.-C. Shen
Guizhou Green Liquor Co., Ltd, Zhenyuan 557702, Guizhou, China

X.-D. Wang · S.-D. Ban
College of Life Sciences, Guizhou University, Guiyang 550025, Guizhou, China

X.-D. Wang · B. Xiao · S.-Y. Qiu (✉)
School of Liquor-Making and Food Engineering, Guizhou University, Guiyang 550025, Guizhou, China
e-mail: syqiu@gzu.edu.cn

T.-C. Zhang and M. Nakajima (eds.), *Advances in Applied Biotechnology*,
Lecture Notes in Electrical Engineering 333, DOI 10.1007/978-3-662-46318-5_49

fortified Daqu became a hot point to increase the quality rate of Luzhou-flavor liquor [3–7].

This study used the strong esterifying power of *Monascus purpureus* (FBKL3.0018) to make Daqu. In order to improve the quality of Daqu and yeast wine, the conditions and parameters of starter-making technology should be explored.

49.1 Materials and Methods

49.1.1 Raw Materials

Monascus purpureus (FBKL3.0018), wheat, barley, and pea.

49.1.2 Equipment

Agilent GC 6890 FID (NYSE:A); U-3010 ultraviolet-visible light detector (Hitachi).

49.1.3 Medium

Rose Bengal agar, malt agar medium, NA.

49.1.4 Adding the Proportion of Monascus purpureus

Starter-making technology:

Raw materials (wheat, barley, pea) → Crushing → Water mixing → Strain breeding → Strain culturing → Then inoculate → Bacterium suspension → Artificial on Daqu → Entry → Arrangement → Mildew-growing → Tide phase → Fire stage → Insulating → Out of the house → Storage → Product Daqu.

Before the production of esterification Daqu, the room must be cleaned up. The ground is covered with a layer of fresh rice husk of about 5 cm.

The medium temperature is used in the Daqu making process. The ratio of raw materials is 6:3:1 (wheat: barley: pea), 1 kg material with *Monascus* and respective quantities of 2, 5, 8, 10 and 15 g. Through the evaluation of physical and chemical indexes and aesthetic quality, the proportion of *Monascus* is determined.

Table 49.1 Different ratio of raw material

Test number	Wheat (mass fraction %)	Barley (mass fraction %)	Pea (mass fraction %)
1	100	0	0
2	80	10	10
3	70	20	10
4	60	30	10
5	50	40	10

49.1.5 The Different Ratios of Raw Materials

The medium temperature is used in the Daqu making process. Daqu are made by the different ratios of raw materials through the evaluation of physical and chemical indexes and aesthetic quality to determine the proportion of raw materials (Table 49.1).

49.1.6 Effect of Water Addition on the Quality of Daqu

Water addition is key during the experiments; excess water can lead to difficulty in molding of grains, and it is also not conducive to make beneficial bacteria grow in Qu Xin. Excess heat causes rancidity; however, if the water is too little, the grains do not bond easily and this would also prevent the microbial from growing. The mass fraction of water, respectively, is controlled at 37, 40, 43 % of the raw materials through the evaluation of physical and chemical indexes and aesthetic quality to determine the best temperature.

49.1.7 Effect of Cultivation Time on Daqu Quality

During the cultivation process of Daqu, take samples which have been cultivated at 15, 20, 25, 30 days, respectively, for analysis. Through the evaluation of physical and chemical indexes and aesthetic quality the best time of starter-making is determined.

49.1.8 Determination of Moisture Content [8]

49.1.9 Determination of Acidity [8]

49.1.10 The Determination of Fermenting Power [8]

49.1.11 Determination of Starch Content [8]

49.1.12 The Determination of Enzyme Activity

49.1.12.1 Determination of the Liquefying Power: Iodine Color-Fading-Photometric Method at 30 °C [9]

49.1.12.2 Determination of the Proteolytic Power: Precipitation [10]

49.1.12.3 Determination of the Saccharifying Power: Lam Method [10]

49.1.12.4 Determination of the Esterifying Power [9]

49.1.13 Determination of Microorganisms

Colony counting method.

49.2 Results and Analysis

49.2.1 Addition of Monascus

Before starter-making, the bacteria suspension is made by the *Monascus* and water (1:20), then 2, 5, 8, 10, 15 g in 1 kg raw materials, respectively, is added while mixing in water to make the Daqu.

We can see from Table 49.2 that there is a big difference between esterification and medium temperature Daqu in acidity, which indicates that the acidity of the medium temperature Daqu changes to bigger than esterification Daqu.

We can see the following from Table 49.3:

(1) Compared with ordinary Daqu, the esterifying power of the esterification Daqu is much higher.
(2) With the increasing addition of *Monascus*, the esterifying power, diastatic power, fermenting power, and liquefaction power of the esterification Daqu are all improved and the esterifying power is most appreciated. The highest increase can be by 84.15 %, while the minimum increase can be by 50 %.

Table 49.2 The physiochemical indexes comparison of esterification Daqu and ordinary Daqu

Different Daqu	Number	Moisture (mass fraction %)		Acidity		Addition of *Monascus* (g/kg)
		Into the room	Out of the room	Into the room	Out of the room	
Esterification Daqu	1	37.0	15.5	0.20	1.04	2
	2	37.1	15.9	0.20	1.07	5
	3	37.4	16.0	0.21	1.05	8
	4	37.1	16.4	0.23	1.08	10
	5	37.0	15.5	0.21	1.09	15
Ordinary Daqu	1	37.0	15.5	0.19	1.35	0

The above data are means of three samples

Table 49.3 The diastatic power, fermenting power, liquefaction power and esterifying power comparison of esterification Daqu and ordinary Daqu

Different Daqu	Number	Diastatic power (mg/g h)	Fermenting power (g/kg)	Liquefaction power (g/g h)	Esterifying power (mg/g 100 h)	Esterifying growth (%)
Esterification Daqu	1	320	30.7	6.35	110.8	50.14
	2	300	32.8	6.35	114.5	55.15
	3	345	33.1	6.36	129.8	75.88
	4	360	32.4	6.33	133.1	80.35
	5	330	33.4	6.45	135.9	84.15
Ordinary Daqu		720	31.2	6.35	73.8	0.00

The above data are means of three samples

(3) There is a slight difference in esterifying power between tests 4 and 5. In order to reduce the costs of production, it is more suitable that the inoculum concentration be 10 g/kg.

49.2.2 Different Ratios of Raw Materials

From Table 49.4 we can see that when the esterification Daqu is produced with pure wheat, the esterifying power is lower, which may be due to the strength adhesion of wheat. When the Daqu is stepped too tight, due to poor permeability in Qu Xin, the growth of *Monascus* is restrained. With the decreasing of wheat and adding other materials, the esterifying power of Daqu increases gradually. Through the comprehensive analysis of the above data, test no. 4 is chosen (wheat: barley: pea = 6:3:1) to make the esterification Daqu.

Table 49.4 The test results of different ratio of raw materials

Item	Test no. 1	Test no. 2	Test no. 3	Test no. 4	Test no. 5
Moisture (%)	16	15.3	16.5	16.4	15.8
Diastatic power (mg glucose/g h)	387	314	380	385	337
Fermenting power (g/kg)	31.5	32.1	34.5	32.4	32.1
Esterifying power (mg/g 100 h)	94.5	109.8	123.6	130.2	115.5
Liquefaction power (g/g h)	6.32	6.50	6.41	6.42	6.57
Acidity	1.35	1.28	1.30	1.34	1.36

The test no. 1 is making by pure wheat, the barley and peas are being added respectively

49.2.3 Effect of Water Addition on the Quality of Daqu

We can see the following from Table 49.5:

(1) The more water is added into the room, the more it is when it is taken out of the room. At the same time the acidity also improves, thus we can see that when the Daqu has taken in too much water, it will improve the acidity.
(2) More or less water can have a measure of influence on the diastatic, fermenting, and esterifying powers, indicating that water can prevent the growth of microorganisms. So we choose the water of Daqu to be controlled at 40 %.

49.2.4 Effect of Temperature on the Quality of Daqu

We can see from Table 49.6 that esterification Daqu is made at medium temperature. The highest temperature is more suitable which is controlled at 55 °C.

49.2.5 Effect of Cultivation Time on Daqu Quality

We can see from Table 49.7 that with extension of time, the physical and chemical indexes are increased. Considering the concrete operation, the best storage period of esterification Daqu is 2–3 months.

Table 49.5 The Daqu physiochemical indexes comparison of different water

Added water (%)	Moisture (%)	Acidity	Diastatic power (mg glucose/g h)	Fermenting power (g/kg)	Esterifying power (mg/g 100 h)	Liquefaction power (g/g h)
37	16.0	1.04	341	31.4	100.3	6.41
40	16.5	1.07	359	32.5	124.5	6.46
43	17.5	1.09	336	30.1	98.8	6.16

Table 49.6 The quality comparison of different culture temperature

Temperature (°C)	Moisture (%)	Acidity	Diastatic power (mg glucose/g h)	Fermenting power (g/kg)	Esterifying power (mg/g 100 h)	Liquefaction power (g/g h)
60	15.5	1.32	335	32.5	114.5	6.42
55	15.4	1.29	356	32.1	124.8	6.56
50	15.4	1.24	308	31.8	120.9	6.50

Table 49.7 The comparison of cultivation time on Daqu quality

Time (day)	Moisture (%)	Acidity	Diastatic power (mg glucose/g h)	Fermenting power (g/kg)	Esterifying power (mg/g 100 h)	Liquefaction power (g/g h)
15	25.0	1.75	105	21.0	46.5	4.54
20	21.5	1.58	268	25.2	84.5	4.83
25	17.4	1.45	325	30.1	105.8	5.76
30	15.4	1.29	343	32.0	117.3	6.41

Through the production conditions of high esterification Daqu, the suitable parameters of production are selected and management operation is also developed:

1. The Daqu should be taken into the room quickly when the starter-making is completed because the Daqu heats up quickly and the heat dissipating capacity is big. In order to control temperature and prevent the moisture to evaporate from the surface, the length is increased by 2 cm and the total Daqu is decreased by 20 % than ordinary Daqu. When being taken into the room, the Daqu are arranged in two layers. The four sides of Daqu are enclosed well with straw and covered with a layer of thin straw on top, at the same time, choosing a room of ordinary Daqu for reference.
2. After 24 h, the temperature can be up to 40 °C, 12–15 h faster than ordinary Daqu. So after about 33 h the Daqu must be turned, and the layer increased by one. The surface of Daqu is covered with white or milky white fungus colony. The room temperature and humidity are strictly controlled to prevent moisture evaporating from the surface. When the temperature of the room is raised, it is cooled down. The other management methods are the same as with ordinary Daqu, where the layers are increased from three to four, the starter-making time is 28 days, 2 days shorter than ordinary Daqu, with the highest temperature controlled at 55 °C.

49.2.6 Physicochemical Indexes Compared with Esterification and Ordinary Daqu

We can see from Table 49.8 that compared with ordinary Daqu, the fermenting and esterifying powers are improved, and esterifying power is increased more than

Table 49.8 The physiochemical indexes comparison of esterification Daqu and ordinary Daqu

Physicochemical indexes	Esterification of Daqu	Ordinary Daqu
Moisture (%)	16.0	15.8
Acidity	1.29	1.35
Diastatic power (mg glucose/g h)	349	720
Fermenting power (g/kg)	39.0	35.0
Esterifying power (mg/g 100 h)	118.3	67.5
Liquefaction power (g/g h)	6.47	6.35

once. The esterification Daqu is covered with a milk-white covering significantly, the mycelium is more thickset and consistent, the cross-section is thin and yellow, the Daqu gives out a sweet aroma, and no spoilage or other flavors. The ordinary Daqu has little surface colony and clothing is not obvious, the section is slightly thick, the mycelium is white and red with yellow spots, and the Daqu has strong atmosphere with no spoilage or other taste.

49.2.7 Effect of Cultivation Time on Daqu Quality

We can see the following from Table 49.9:

(1) The water is dropped quickly after the Daqu out of the room, but a few months later the water is increased again.

Table 49.9 The physiochemical indexes comparison of cultivation time

Index	Daqu	January	February	March	April	May	June	July
Moisture (%)	16.0	13.2	12.4	12.2	13.0	14.5	14.0	14.7
Acidity	1.29	1.30	1.42	1.32	1.38	1.40	1.40	1.28
Diastatic power (mg glucose/g h)	349	398	402	385	365	342	336	339
Fermenting power (g/kg)	39.0	40.0	39.0	38.0	35.0	35.0	33.0	31.0
Liquefaction power (g/g h)	6.47	6.67	6.52	6.47	6.42	6.40	6.00	5.32
Esterifying power (mg/g 100 h)	118.3	125.5	134.4	142.3	135.7	130.2	121.5	115.7
Total plate count (104/g)	897.5	944.9	1165	1055	984	871	800	610
Total number of yeast (104/g)	45.3	47.2	45.5	42.1	40.5	39.7	36.2	30.6
Total counts of molds (104/g)	146.7	192.1	201.8	208.1	155.2	125.7	118.4	131.5

(2) After being stored for 2 months, the acidity reaches a maximum, then it is reduced gradually. When stored for 7 months, the acidity is equal to the Daqu out of room.
(3) After being stored for 2 months, the liquefaction, fermenting, and diastatic powers reaches a maximum. Compared with the Daqu stored for 2 months, the liquefaction, fermenting, and diastatic powers all decrease by the Daqu stored for 7 months. That is to say, when Daqu is stored for 7 months, the index of saccharification and fermentation decreases.
(4) In the first 3 months, the esterification power of Daqu rises from month to month, but from the fourth month, the esterification decreases every month; when the Daqu is stored at 7 months, esterification is decreased by 2.2 %.
(5) From the results of microbial test, yeast, bacteria, molds increase month by month, then reduce gradually. That is, the microorganisms do not stop their growth, so management at this time is particularly important for all. When stored at 7 months, the total bacterial decreases by 32.03 %, yeast decreases by 32.45 %, and molds decrease by 10.36 %.

According to the results, the best storage period of esterification Daqu is 2–3 months.

49.3 Conclusions

The optimal conditions of esterification Daqu production is the ratio of raw materials at 6:3:1 (wheat: barley: pea), the inoculation of *Monascus* (*M. purpureus*) FBKL3.0018 is 10 g/kg, and the water of Daqu is controlled at 40 %. The highest temperature is more suitable which controlled at 55 °C, and the time of cultivation is always between 25 and 28 days. Fermenting, liquefaction, and esterifying powers are higher than the ordinary Daqu, and esterifying power increases more than once. The sensory quality of esterification Daqu is better than ordinary Daqu. During storage, the esterification power of Daqu rises from month to month, but from the fourth month, the esterification power decreases every month. Based on the analysis of other factors, the best storage period of esterification Daqu is 2–3 months.

References

1. Luo CQ, Yao JC, Zeng Da B et al (2004) Application of esterified red rice starter in the production of fortified Daqu. Liquor-Making 6:23–24
2. Su FG (1995) Cultication and application of strengthen Luzhou-flavour liquor daqu. Science 4:17–19
3. Chen WD, Ding Chao-cheng C, Guan QC et al (1993) The development and application of strengthen Daqu. Liquor-Making 1:25–30

4. Hu F (2008) Application in microorganisms technologies of Luzhou-flavour liquor production. Liquor-Making 12:56–59
5. Liu XV, Miao ZJ, Wang XC (2012) Application research of Monascus in the production of Luzhou-flavor Daqu. Liquor-Making 5:33–35
6. Fu WX, Feng XS, Meng QY et al (2010) Application of monascus starter in the production of xifeng-wheat-daqu. Liquor-Making Sci 1:46–48
7. Chen X, Gan GD, Jiang L et al (2013) The research and application of beneficial microorganisms in the production of liquor. Liquor-Making 5:33–40
8. Xiong ZG, Zhao JH, Chen L et al (2011) General methods of analysis for Daqu (QB/T 4257-2011), Beijing
9. Fan Y, Jiang YM (1995) Protease to the effects of Bacillus amyloliquefaciens a-amylase activity. Microbiology 22(1):22–24
10. Wang FR (2005) Wine analysis and detection, Beijing

Chapter 50
Metabolomics Analysis Between Wild-Type and Industrial Strains of *Streptomyces avermitilis* Based on Gas Chromatography–Mass Spectrometry Strategy

Gang Guo, Ping-ping Tian, Dan Tang, Xiaoxia Wang, Hong-jin Yang, Peng Cao and Qiang Gao

Abstract *Objective* To conduct a metabolic analysis of the intracellular metabolites in *Streptomyces avermitilis,* so as to search for possible biomarkers and to discover the mechanism of higher avermectin production. *Methods* GC–MS analysis was used to obtain the fingerprint of wild-type and industrial *S. avermitilis* 9-39 strains. *Results and conclusion* multivariate statistical analysis demonstrated that D-cellobiose, D-galactose, D-glucopyranose, D-mannose, D-turanose, glutamine, L-serine, and maltose were mainly responsible for distinguishing the wild-type *S. avermitilis* and industrial strain 9-39, and most of them belong to glycometabolism. Thus, strengthened glycometabolism is the reason for high yield of avermectin in *S. avermitilis*.

Keywords *Streptomyces avermitilis* · Metabolomics · Gas chromatography–mass spectrometry · Multivariate

50.1 Introduction

Streptomyces avermitilis is a Gram-positive bacterium in the genus *Streptomyces* (family Streptomycetaceae, class Actinobacteria) [1, 2]. The major interest in this genus *Streptomyces* is the diversity of its production of secondary metabolites as an industrial microorganism. *Streptomyces avermitilis* carries out not only a complex morphological differentiation but also production of various secondary metabolites

G. Guo · P. Tian · D. Tang · X. Wang · H. Yang · P. Cao · Q. Gao (✉)
Key Laboratory of Industrial Microbiology, Ministry of Education,
College of Biotechnology, Tianjin University of Science and Technology,
Tianjin 300457, People's Republic of China
e-mail: gaoqiang@tust.edu.cn

T.-C. Zhang and M. Nakajima (eds.), *Advances in Applied Biotechnology*,
Lecture Notes in Electrical Engineering 333, DOI 10.1007/978-3-662-46318-5_50

[3, 4], one of which, avermectin, is used as a major commercial antiparasitic agent in the fields of animal health, agriculture, and human infections. Although much progress has been made, the detailed avermectin production mechanism by *S. avermitilis* is unclear up to now [4, 5].

Metabolomics aims to systematically analyze the entire small molecule metabolite composition and dynamic response in microorganisms [6–8]. Metabolomics analysis also assesses the last step in the series of changes under an external stress or a pathological insult [9, 10], and the changes of composition of metabolites directly reveals the phenotypic changes in a living system [11, 12]. By this way, we can have further insight into the difference of *S. avermitilis* industrial mutant 9-39 and its wild-type on microbial metabolism via the study of variation of intracellular metabolites, which is important for further understanding of higher production mechanism of avermectin.

In the present study, we applied a GC–MS-based metabolomics approach [13–15] and employed a multivariate analysis to explore the global metabolite profiles of industrial strain 9-39 and wild-type *S. avermitilis* at different fermentation time point. The aim is to reveal their difference in metabolomics, and the intermediate metabolites related with higher production, and find out the correlated pathway of avermectin in *S. avermitilis*.

50.2 Materials and Methods

50.2.1 Strains, Media, and Culture Conditions

A wild-type (WT) strain of *S. avermitilis* and one of its industrial mutants, strain 9-39, were offered by Microbiology Institute of CAS, China used for the metabolosome comparison in this study. All strains were maintained as spore stocks on agar slant at 4 °C. About 1 cm^2 of frozen spore culture was scalped from the agar surface and transferred into 250-mL flasks containing 40-mL seed medium [16] and incubated at 28 °C on a rotary shaker at 220 r/min for 40 h. Fermentation medium [16] were then inoculated with 5 % seed cultures and incubated on a rotary shaker at 220 r/min at 28 °C for 10 days.

50.2.2 Preparation of Metabolome Samples

Cell samples were, respectively, collected on the 6th, 8th, and the 10th day's cultivation for both 9-39 and WT. Metabolome samples were quenched and extracted in 4 replicates for each sample as described below. Cell suspensions were immediately quenched at −40 °C for 5 min with 40 % (v/v) methanol in water. The quenching solution was prechilled at −80 °C and used at a ratio of 4:1 (v/v) of quenching solution to cell suspension. Then cells were harvested by centrifugation at 8,000×*g* for 5 min with 4 °C and washed twice with 0.6 % NaCl to remove the residual culture medium [17]. Then the cells (100 mg) were disrupted with bead mill by 3 cycles for 48 s each time which contain 1 mL of extraction buffer (chloroform: ethanol: water = 2:2:1, v/v/v). The mixture was frozen in liquid nitrogen for 2 min and then was thawed, this freeze-thaw process was repeated five times. After centrifugation at 1,000×*g* for 5 min, 200 μL supernatant was mixed with 10 μL of internal standard solution and dried in a vacuum centrifuge dryer.

50.2.3 Sample Derivatization

Before GC–MS analysis, a two-stage chemical derivatization was carried out. First, methoximation was performed by dissolving the dried metabolite samples in 50 μL methoxamine hydrochloride (20 mg/mL in pyridine, Sigma), and the solution was incubated at 40 °C for 80 min. Then, 80 μL *N*-methyl-*N*-(trimethylsilyl)trifluoro-acetamide (MSTFA, Sigma) were added to the samples, which were subsequently incubated at 40 °C for 80 min for trimethylsilylation.

50.2.4 GC–MS Analysis

Gas chromatography analysis was performed on a GC–MS system (Agilent Technologies, Palo Alto, CA, USA) equipped with an HP-5 capillary column (60 m × 320 μm i.d., 0.25 μm film thickness; Agilent J&W Scientific, Folsom, CA, USA). Samples (1 μL each) were injected into HP-5 capillary column by split injection mode with a split ratio of 8:1 using an autoinjector. Helium was used as the carrier gas at a constant flow of 1 mL/min. The injection, ion source, and ion source surface temperatures were set to 280, 250 and 280 °C, respectively. The GC oven temperature was set to 70 °C for 2 min, then raised to 290 °C at a rate of 5 °C/min, and maintained at 290 °C for 3 min. The electron impact ionization (70 eV) was set at a full scan mode (*m*/*z* 50–800). MSD Productivity ChemStation software (version E.02 01.1177, Agilent Technologies) was used to acquire mass spectrometric data. Compound identification was performed by comparing the mass spectra with a commercially available standard library, the National Institute of Standards and Technology mass spectral library 2008. The compounds were also identified by comparing their mass spectra and retention times with those of commercially available reference compounds.

50.2.5 Data Analysis

The relative intensity of each metabolite peak was expressed as the ratio of its peak area to that of the internal standard on the same chromatograph. The generated normalized peak areas (variables) were imported into SIMCA package (ver. 11.5) (Umetrics, Umea, Sweden) for the multivariate statistical analysis. Principal component analysis (PCA) and partial least-squares-discriminant analysis (PLS-DA) were applied to analysis the data after mean-centering and UV-scaling.

50.3 Results and Discussion

50.3.1 Typical GC–MS TIC Chromatograms of 9-39 and WT

The wild-type and industrial strains of *S. avermitilis* were cultured in 250-mL flasks with 5 replicates. After extraction and derivatization, the typical GC–MS TIC chromatograms obtained by GC–MS analysis system were shown in Fig. 50.1.

50.3.2 Metabolites Analyzed by PCA and PLS-DA

The generated normalized peak areas were imported into SIMCA for the multivariate statistical analysis. Firstly, PCA was used to investigate the metabolic differences between 9-39 and WT at different sampling time point, and the PC1/PC2 scores plots ($R^2X_{\mathrm{cum}} = 0.977$, $Q^2_{\mathrm{cum}} = 0.918$) were performed to represent the sample distribution in the new multivariate space (Fig. 50.2a). Distinct clustering was observed among WT at each time point and 9-39 on the 6th day. There was no clear difference between 9-39 on the 8th day and on the 10th day. To confirm the

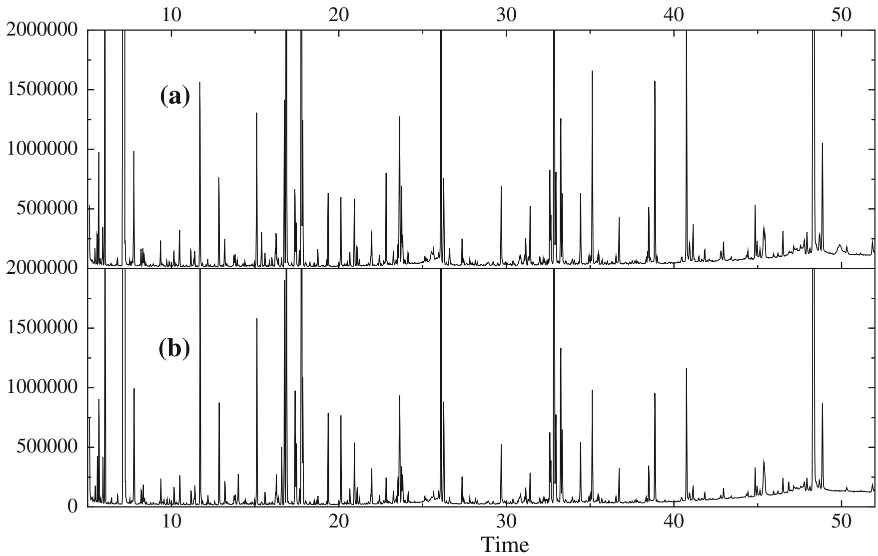

Fig. 50.1 Typical GC–MS TIC chromatograms of 9-39 (**a**) and WT (**b**)

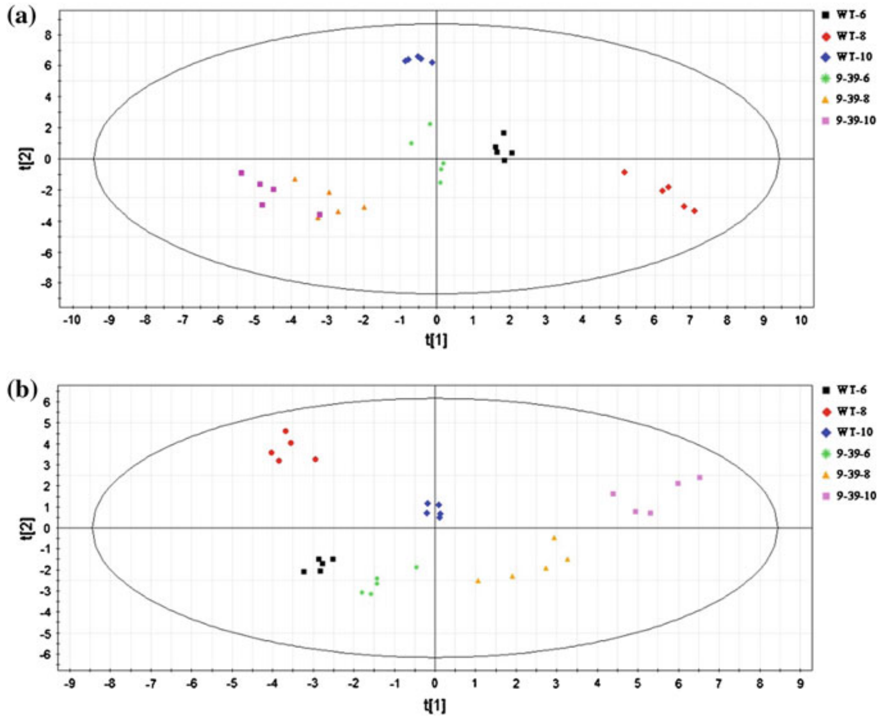

Fig. 50.2 Scores plot for 9-39 and WT. **a** PCA-derived metabolites profiles and **b** PLS-DA-derived metabolite profiles. In the scores plot, the confidence interval is defined by the Hotellin's T2 ellipse (95 % confidence interval), and observations outside the confidence ellipse are considered outliers

difference of every sampling points in metabolite variations, the class separation was further optimized using the PLS-DA model ($R^2X_{\mathrm{cum}} = 0.965$, $Q^2_{\mathrm{cum}} = 0.946$), and good discrepancy was observed (Fig. 50.2b).

To further verify the differences, multivariate data analysis was also performed by HCA. The HCA plot of the 52 differential metabolites reflected a clustering pattern that was similar to the result of the PLS-DA middle, and good discriminability was observed (Fig. 50.3).

50.3.3 Changes in Intracellular Metabolites Between 9-39 and WT at Different Time Points

The intracellular metabolites of 9-39 and data were analyzed with PLS model at different culture time. As shown in scores plots (Fig. 50.4a, c, e), good discrepancy was observed. It indicated that 9-39 were metabolically distinct from WT in all

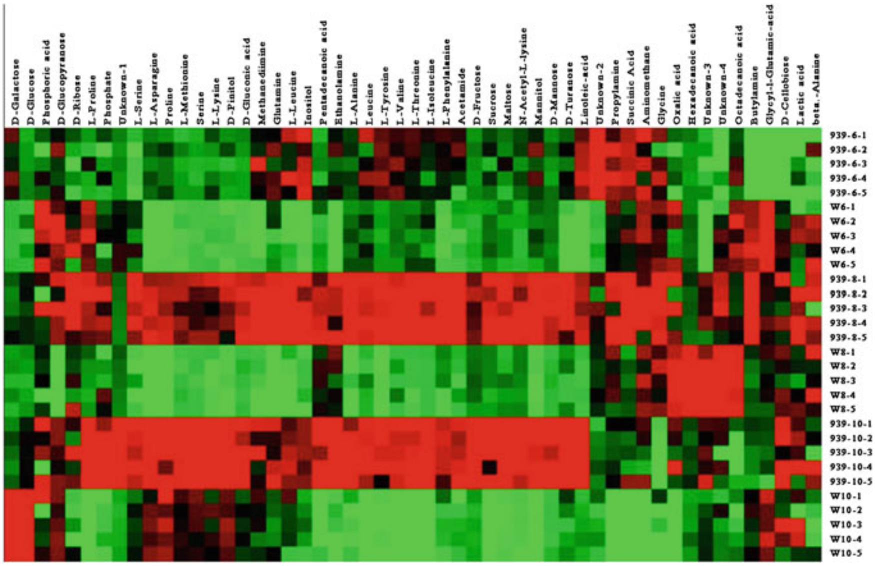

Fig. 50.3 Hierarchical cluster analysis of the 52 identified differential metabolites

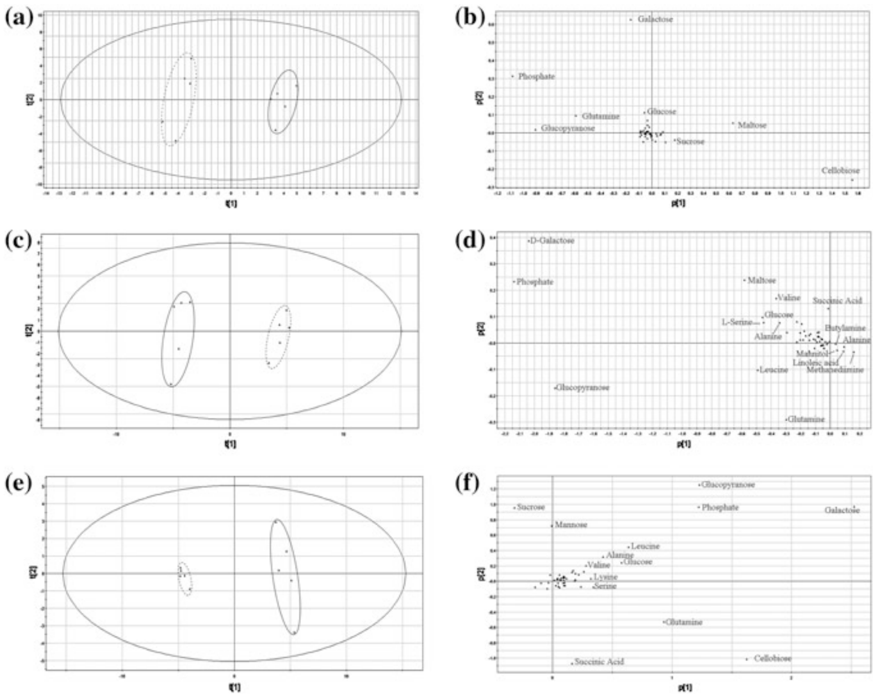

Fig. 50.4 Scores plot and loading plot generated by PLS: **a**, **b** sampling time on the 6th day ($R^2X_{\mathrm{cum}} = 0.980$, $Q^2_{\mathrm{cum}} = 0.949$); **c**, **d** sampling time at 8th day ($R^2X_{\mathrm{cum}} = 0.984$, $Q^2_{\mathrm{cum}} = 0.957$); **e**, **f** sampling time on the 10th day ($R^2X_{\mathrm{cum}} = 0.986$, $Q^2_{\mathrm{cum}} = 0.981$)

those days. The major metabolic perturbations that caused these discriminations were identified from the PLS loading plot (Fig. 50.4b, d, f). In the loading plots, points far away from the cross central means these metabolites have a larger contribution. Also, the points in loading plots have positive effect on the same quadrant in scores plots.

In the PLS models, the VIP coefficient reflects the contribution of each metabolite, the higher VIP value means the metabolite has a larger contribution. A metabolite with a VIP value greater than 1 demonstrates a significant contribution to the separation of groups within PLS model. When *S. avermitilis* fermentation was conducted for 6 days, D-cellobiose, phosphate, D-glucopyranose, maltose, glutamine, succinic acid, D-turanose, and D-galactose were responsible for the differentiation between 9-39 and WT (Fig. 50.5a). On the 8th day, the difference of intracellular metabolites between WT and 9-39 were from phosphate, D-galactose, D-glucopyranose, D-turanose, maltose, and L-serine (Fig. 50.5b). On the 10th day, the difference came from D-turanose, D-galactose, D-glucopyranose, D-mannose, and phosphate (Fig. 50.5c).

On the whole, phosphate, D-galactose, D-glucopyranose, and D-mannose were involved in variable importance of the projection plots of three sampling time

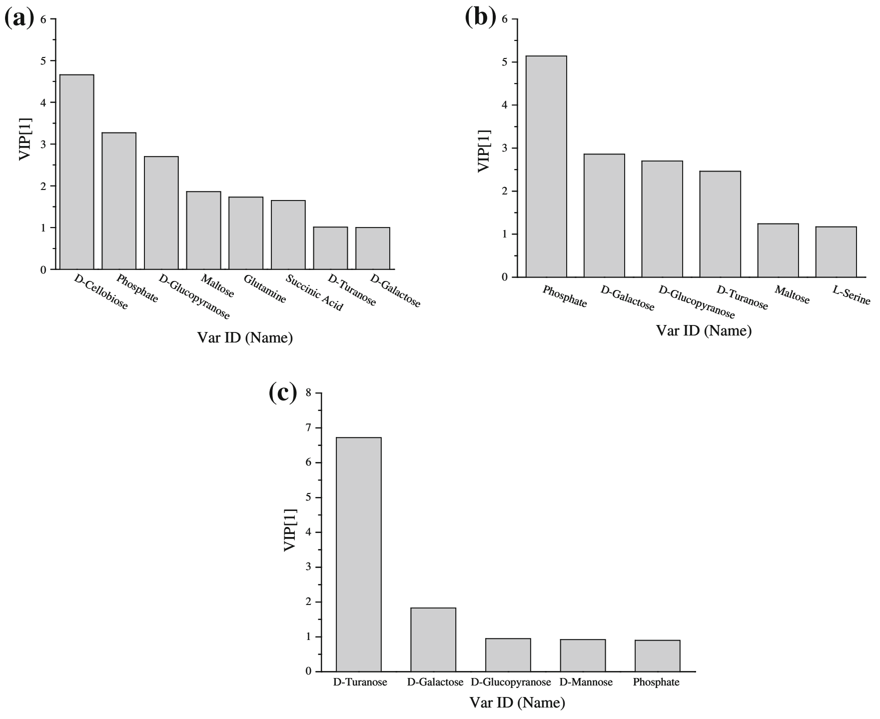

Fig. 50.5 Variable importance of the projection plots for the intracellular metabolites along component 1. **a** WT versus 9-39 on the 6th day using PLS-DA model, **b** WT versus 9-39 on the 6th day using PLS-DA model, and **c** WT versus 9-39 on the 6th day using PLS-DA model

points. By comparison of PLS-DA scores plots and loading plots, phosphate expresses higher level in WT than 9-39 on the 6th day. While on the 8th day and the 10th day, 9-39 got higher phosphate level than WT. High levels of phosphate represent vigorous intracellular energy metabolism. Avermectin synthesis process requires a lot of energy and reducing power. In other words, the intracellular energy metabolism was enhanced in high-yielding strain, while the avermectin production reached the highest. The result coincides with the fact, so metabolomics strategy can be used to research into the mechanism of high avermectin yield in *S. avermitilis*. Compared VIP of three sampling time points, these marker substances (VIP > 1) mainly focused on the glycometabolism, and 9-39 got higher level than WT. As macrolide antibiotics, avermectins production requires a large amount of carbon source. Research has shown that all carbon skeleton synthesis of avermectin from sugar [18].

50.4 Conclusion

In this study, the variation of metabolites in wild-type and industrial strains of *S. avermitilis* were investigated. Over 200 intracellular metabolites were detected and a total of 52 among them were identified by GC–MS at different culture time points. The difference between 9-39 and WT were clearly separated by PCA or PLS methods in the scores plot. Furthermore, it was found that D-cellobiose, D-galactose, D-glucopyranose, D-mannose, D-turanose, glutamine, L-serine and maltose were mainly responsible for distinguishing 9-39 and WT, and most of which belong to glycometabolism. It could be inferred the enhancement of glycometabolism is the reason of high yield of avermectin in *S. avermitilis*. Overall, this work is conducive to shed light on the avermectin high-yielding mechanism, and provides a rational strategy of metabolic engineering and synthetic biotechnology for improving avermectin production.

Acknowledgments This work was financially supported by National 973 Program of China (2013CB734004), National 863 Program of China (2012AA021302), and Natural Scientific Foundation of China (31370075 & 31471725).

References

1. Burg RW, Miller BM, Baker EE et al (1979) Avermectins, new family of potent anthelmintic agents: producing organism and fermentation. Antimicrob Agents Chemother 15(3):361–367
2. Kim SB, Goodfellow M (2002) Streptomyces avermitilis sp nov., nom. rev., a taxonomic home for the avermectin-producing streptomycetes. Int J Syst Evol Microbiol 52:2011–2014
3. Xu ZN, Cen PL (1999) Stimulation of avermectin B1a biosynthesis in Streptomyces avermilitis by feeding glucose and propionate. Biotechnol Lett 21(1):91–95

4. Yoon YJ, Kim ES, Hwang YS et al (2004) Avermectin: biochemical and molecular basis of its biosynthesis and regulation. Appl Microbiol Biotechnol 63(6):626–634
5. Ikeda H, Nonomiya T, Ōmura S (2001) Organization of biosynthetic gene cluster for avermectin in *Streptomyces avermitilis*: analysis of enzymatic domains in four polyketide synthases. J Ind Microbiol Biotechnol 27(3):170–176
6. Kell DB, Brown M, Davey HM et al (2005) Metabolic footprinting and systems biology: the medium is the message. Nat Rev Microbiol 3(7):557–565
7. Somerville GA, Proctor RA (2009) At the crossroads of bacterial metabolism and virulence factor synthesis in Staphylococci. Microbiol Mol Biol Rev 73(2):233–248
8. Han PP, Yuan YJ (2009) Metabolic profiling as a tool for understanding defense response of *Taxus cuspidata* cells to shear stress. Biotechnol Prog 25(5):1244–1253
9. Aliferis KA, Cubeta MA, Jabaji S (2013) Chemotaxonomy of fungi in the Rhizoctonia solani species complex performing GC/MS metabolite profiling. Metabolomics 9(1):S159–S169
10. Jozefczuk S, Klie S, Catchpole G et al (2010) Metabolomic and transcriptomic stress response of *Escherichia coli*. Mol Syst Biol 6:364
11. Bolten CJ, Kiefer P, Letisse F et al (2007) Sampling for metabolome analysis of microorganisms. Anal Chem 79(10):3843–3849
12. Fiehn O (2002) Metabolomics—the link between genotypes and phenotypes. Plant Mol Biol 48(1–2):155–171
13. Koek MM, Muilwijk B, van der Werf MJ et al (2006) Microbial metabolomics with gas chromatography/mass spectrometry. Anal Chem 78(4):1272–1281
14. Taymaz-Nikerel H, de Mey M, Ras C et al (2009) Development and application of a differential method for reliable metabolome analysis in *Escherichia coli*. Anal Biochem 386 (1):9–19
15. Meyer H, Liebeke M, Lalk M (2010) A protocol for the investigation of the intracellular *Staphylococcus aureus* metabolome. Anal Biochem 401(2):250–259
16. Gao H, Liu M, Liu JT et al (2009) Medium optimization for the production of avermectin B1a by *Streptomyces avermitilis* 14-12A using response surface methodology. Bioresour Technol 100(17):4012–4016
17. Bolten CJ, Wittmann C (2008) Appropriate sampling for intracellular amino acid analysis in five phylogenetically different yeasts. Biotechnol Lett 30(11):1993–2000
18. Ikeda H, Omura S (1997) Avermectin biosynthesis. Chem Rev 97(7):2591–2610

Chapter 51
Application of Orthogonal Design to Optimize Fermentation Conditions of *Bacillus amyloliquefaciens* BI_2

Yajun Wang, Zhanglei Cao, Miao Yu and Depei Wang

Abstract *Bacillus amyloliquefaciens* BI_2, isolated from corn straw silage, exhibits to be antagonistic against many kinds of molds, especially *Aspergillus flavus*. In this work, optimization of the medium and culture conditions was studied by adopting the combining single-factor tests and an orthogonal experiment. On the study of the medium optimization, yeast powder, monosodium glutamate, sodium nitrate, and the proportion of starch and maltose were selected as four factors at three levels each. On the study of the optimizing culture conditions, medium volume, culture temperature, fermentation time, and inoculums size were used as four factors at three levels each. The results demonstrated that yeast powder and monosodium glutamate have significant effects on medium optimization; medium volume, culture temperature, and fermentation time give crucial influences on culture conditions, and the influences of the other factors are not remarkable. The optimized medium results shown by the interaction tests were as following: yeast powder 1.5 %, monosodium glutamate 2 %, sodium nitrate 0.8 %, starch 0.17 %, and maltose 0.33 %; the optimal culture conditions were displayed as following: medium volume 60 mL, culture temperature 30 °C, inoculums size 2 %, and fermentation time 36 h.

Keywords *Bacillus amyloliquefaciens* BI_2 · Orthogonal experiment · Optimal medium · Optimal culture conditions

51.1 Introduction

Widely distributed in nature, *Aspergillus flavus* is one of the common food spoilage organisms and often appears in the moldy grains such as corn, peanuts, seeds, and nuts. Aflatoxins, the metabolite of *A. flavus*, can induce gene mutation, suppress the

Y. Wang · Z. Cao · M. Yu · D. Wang (✉)
Key Laboratory of Industrial Fermentation Microbiology, Ministry of Education,
College of Biotechnology, Tianjin University of Science & Technology,
Tianjin 300457, People's Republic of China
e-mail: wangdp@tust.edu.cn

T.-C. Zhang and M. Nakajima (eds.), *Advances in Applied Biotechnology*,
Lecture Notes in Electrical Engineering 333, DOI 10.1007/978-3-662-46318-5_51

immune system, and are highly toxic and carcinogenic to human beings and animals [1, 2]. Therefore, there are long-term economic benefits in developing biological control methods which can decrease the toxicity and inhibit the growth of pathogen. Recent research has shown that certain *Bacillus* sp. can inhibit *A. flavus* and its toxin [3].

The antifungal mechanism includes several aspects and the substances mainly inhibit the growth of the pathogenic fungus. *Bacillus* sp., which can produce a variety of metabolites with antifungal activity, including amino acids, peptides, grease peptide, phospholipids, polyene, nucleic acid, have a good inhibitory effect for many plant and animal pathogens [4]. Thus, they are commonly used for biological controlling of crop diseases and expected to be applied in the field of food antiseptics.

Bacillus amyloliquefaciens BI_2 is a beneficial bacterium with strong environmental adaptability and resistance because of its tolerance spores. Its secondary metabolites can also antagonize a variety of pathogens, especially aflatoxin-producing *A. flavus* [5]. In this research, we investigated the optimal medium and culture conditions by adopting the method of combining the single-factor experiment and the orthogonal design for improving its antifungal effect.

51.2 Materials and Methods

51.2.1 Microorganisms

Bacillus amyloliquefaciens BI_2 was isolated from silage feed by our previous work, and preserved by China General Microbiological Culture Collection Center, preservation number CGMCC No. 3413. *Aspergillus flavus* was preserved in the Laboratory of Industrial Fermentation Microbiology in College of Biotechnology, Tianjin University of Science & Technology.

51.2.2 Media and Culture Conditions

Strain BI_2 was cultured in nutrient broth (pH 7.2) containing 0.5 % beef extract, 1 % peptone, 0.5 % NaCl, and in addition 2 % agar for solid medium, sterilized at 1.0×10^5 Pa for 20 min. The components of the initial fermentation medium were 0.5 % beef extract, 0.5 % soluble starch, 0.5 % NaCl, 1.2 % $NaNO_3$, 1.2 % corn pulp, 0.06 % Tween 80, and 2 % sodium glutamate (pH 7.5), sterilized at 1.0×10^5 Pa for 20 min. Potato Dextrose Agar: weigh 200 g potato, dice them, add 1 L distilled water and boil for 30 min, six layers of cotton gauze filter, add the filtrate water to 1,000 mL, add 20 g glucose, pH natural, 1.0×10^5 Pa sterilized for 20 min.

51.2.3 Single-Factor Experiments for Medium Optimization

To determine the optimal factors for the following orthogonal experiment, a series of single experiments were designed. The optional carbon sources were glucose (1 %), sucrose (0.5 %), maltose (0.5 %), starch (0.5 %), and dextrin (0.5 %) to replace starch in the initial fermentation medium. The optional nitrogen sources were ammonium sulfate, ammonium nitrate, sodium nitrate, peptone, corn steep liquor, yeast extract, and beef extract. 1.5 % of sodium nitrate and corn steep liquor were added in the initial fermentation medium to replace beef extract respectively (Sect. 51.2.4).

The method of comparing the inhibition rates of *A. flavus* spore germination was used. First, the concentration of *A. flavus* spore suspension was made to be 5×10^4 cfu/mL. The centrifuged fermentation broth and the unset PDA medium were well mixed in 1:6 proportion, and poured onto the plate, coat 100 μL of the spore suspension on the medium in plate after solidification, with the blank PDA medium as the control. The colonies of *A. flavus* were reckoned after being cultured at 30 °C for 36 h, and the inhibition rates were calculated. Each group has three parallels.

51.2.4 Method of Calculating Antifungal Rate [6]

$$\alpha(\%) = \frac{N_C - N_E}{N_C} \times 100$$

where α represents antifungal rate, N_C represents the colony number of control group, and N_E represents the colony number of experimental group.

51.2.5 Orthogonal Design of Medium Optimization

For the interaction tests, a group of orthogonal tests on yeast extract (0.5, 1, 1.5 %), sodium glutamate (1, 1.5, 2), $NaNO_3$ (0.4, 0.8, 1.2 %), and the ratio of starch and maltose (1:2, 1:1, 2:1) were designed according to the results of single-factor experiments (Table 51.1). In addition, the orthogonal experiment needs to consider three nitrogen sources and the interaction between any two factors. So, 27 experiments were designed according to the orthogonal array (Table 51.2). All the experiments were carried out in triplicate.

Table 51.1 Orthogonal array of medium optimization

Factor	Level		
	1	2	3
A	0.5	1	1.5
B	1	1.5	2
C	0.4	0.8	1.2
D	1:2	1:1	2:1

Note A, B, and C represent yeast extract, sodium glutamate, and $NaNO_3$, respectively. The data of A, B, and C represents the percentage of the volume of medium, the data of D represents the ratio of starch and maltose content

Table 51.2 The $L_9(3^4)$ orthogonal test was used for culture condition

Factor	Level		
	1	2	3
A′	50	60	70
B′	30	33	37
C′	1	2	3
D′	32	36	40

Note A′ medium volume; B′ culture temperature; C′ inoculums size; D′ fermentation time. Each factor has three levels

51.2.6 Orthogonal Experiments of Culture Conditions

For the combinational effect trial, an $L_9(3^4)$ orthogonal test [7, 8] on medium volume (50, 60, and 70 mL), culture temperature (30, 33, 37 °C), inoculums size (1, 2, 3 %), and fermentation time (32, 36, 40 h) was designed according to the results of the single-factor experiments (Table 51.2). All the experiments were carried out in triplicate.

51.3 Results and Discussion

51.3.1 The Results of Single-Factor Experiments for Medium Optimization

From the results of the single-factor experiments for carbon sources in Fig. 51.1, maltose and starch among the tested factors were selected as the optimal carbon sources for fermentation. The results of adding sodium nitrate, yeast extract, and beef extract showed high inhibition rates and there is no significant difference between any two factors. But the ingredient beef exact is instable; accordingly, sodium nitrate and yeast extract are selected to optimize the combination of them in the orthogonal tests (Fig. 51.2).

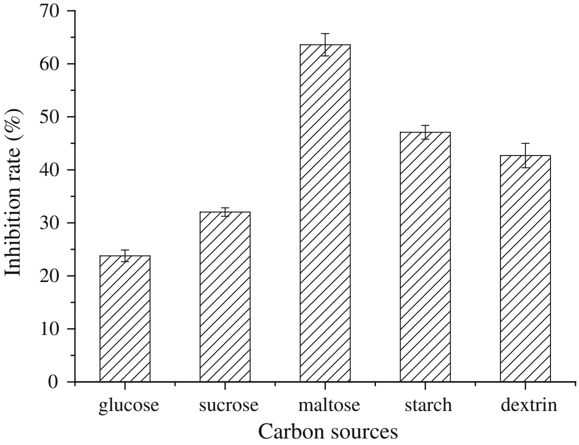

Fig. 51.1 The single-factor experiments of carbon sources for medium optimization

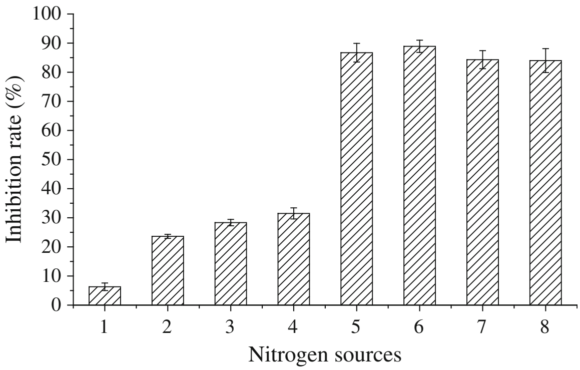

Fig. 51.2 The single-factor experiments of nitrogen sources for medium optimization. No. *1*, *2*, *3*, *4*, *5*, *6*, *7*, and *8* represent ammonium sulfate, ammonium nitrate, corn steep liquor, peptone, sodium nitrate, yeast extract, beef extract, the initial nitrogen sources, respectively

51.3.2 The Experimental Data of Orthogonal Array for Medium Optimization

According to the components of the medium, the orthogonal array was designed in Table 51.3. Six columns were picked to show the interactions of the three nitrogen sources: yeast extract, sodium glutamate, and sodium nitrate. Three blank columns were added to reduce the error of orthogonal test. Thus, specific operation in experiments did not involve the interaction columns and blank columns.

By the analysis of SPSS software [9–11], the optimized medium was obtained. As indicated in Table 51.4, A, B and the interaction between A and B had

Table 51.3 The results of medium optimization by orthogonal experiment including interaction

No.	Factor													Inhibition rate (%)
	A	B	A × B	A × B	C	A × C	A × C	B × C	D		B × C			
1	1	1	1	1	1	1	1	1	1	1	1	1	1	75.67
2	1	1	1	1	2	2	2	2	2	2	2	2	2	77.94
3	1	1	1	1	3	3	3	3	3	3	3	3	3	76.91
4	1	2	2	2	1	1	1	2	2	2	3	3	3	81.65
5	1	2	2	2	2	2	2	3	3	3	1	1	1	75.67
6	1	2	2	2	3	3	3	1	1	1	2	2	2	74.64
7	1	3	3	3	1	1	1	3	3	3	2	2	2	76.70
8	1	3	3	3	2	2	2	1	1	1	3	3	3	70.10
9	1	3	3	3	3	3	3	2	2	2	1	1	1	71.75
10	2	1	2	3	1	2	3	1	2	3	1	2	3	73.81
11	2	1	2	3	2	3	1	2	3	1	2	3	1	73.40
12	2	1	2	3	3	1	2	3	1	2	3	1	2	66.39
13	2	2	3	1	1	2	3	2	3	1	3	1	2	73.81
14	2	2	3	1	2	3	1	3	1	2	1	2	3	76.29
15	2	2	3	1	3	1	2	1	2	3	2	3	1	81.65
16	2	3	1	2	1	2	3	3	1	2	2	3	1	85.77
17	2	3	1	2	2	3	1	1	2	3	3	1	2	84.54
18	2	3	1	2	3	1	2	2	3	1	1	2	3	86.39
19	3	1	3	2	1	3	2	1	3	2	1	3	2	78.97
20	3	1	3	2	2	1	3	2	1	3	2	1	3	79.79

(continued)

Table 51.3 (continued)

No.	Factor													Inhibition rate (%)
	A	B	A × B	A × B	C	A × C	A × C	B × C	D		B × C			
21	3	1	3	2	3	2	1	3	2	1	3	2	1	80.82
22	3	2	1	3	1	3	2	2	1	3	3	2	1	88.45
23	3	2	1	3	2	1	3	3	2	1	1	3	2	85.36
24	3	2	1	3	3	2	1	1	3	2	2	1	3	88.66
25	3	3	2	1	1	3	2	3	2	1	2	1	3	92.16
26	3	3	2	1	2	1	3	1	3	2	3	2	1	87.22
27	3	3	2	1	3	2	1	2	1	3	1	3	2	89.28

Table 51.4 The results of the orthogonal experiment analyzed by SPSS

Source	Type III sum of squares	df	Mean square	F	Sig.
Calibration model	1090.211 a	20	54.511	6.852	0.012
Intercept	171807.828	1	171807.828	21597.374	0.000
A	488.835	2	244.417	244.417	0.001
B	212.746	2	106.373	13.372	0.006
C	15.802	2	7.901	0.993	0.424
D	30.167	2	15.084	1.896	0.230
A × B	291.991	4	72.998	9.176	0.010
A × C	19.386	4	4.847	0.609	0.671
B × C	31.283	4	7.821	0.983	0.482
Error	47.730	6	7.955		
Total	172945.769	27			
Total correction	1137.941	26			

significant effects on the inhibition rates, that is to say, yeast powder, monosodium glutamate, and the interaction between them had significant influences on the experiment ($P < 0.05$). Meanwhile, the results of Level 3 of yeast exact had more significant difference comparing with the results of Level 1 and Level 2. Therefore, 1.5 % yeast powder was selected to add into the medium. In a similar way, Level 3 of sodium glutamate and Level 2 of sodium nitrate were chosen to be the optimal levels. Considering the interaction of A and B, the combination A_3B_3 test had the highest inhibition rates. The results of factors C and D did not show significant differences. The level 2 of them was chosen to be the optimal one by comparing the inhibition rates. The final medium formula was $A_3B_3C_2D_1$ combination: yeast powder 1.5 %, monosodium glutamate 2 %, sodium nitrate 0.8 %, the ratio of starch to maltose 1/2, i.e., starch 0.17 %, maltose 0.33 %, and the remaining was Tween-80 0.06 % and NaCl 0.5 %.

51.3.3 The Experimental Data of Orthogonal Array for Culture Conditions Optimization

According to Table 51.5 for optimizing experiment of culture conditions, the analysis was using SPSS in Table 51.6.

From Table 51.6, medium volume, temperature, and fermentation time had remarkable influences on the results of culture conditions, but inoculums size had no significant impact on it. The optimal culture conditions were obtained as $A_2B_1C_2D_2$ combination: medium volume 60 mL, culture temperature 30 °C, inoculums size 2 %, and fermentation time 36 h.

Table 51.5 The result of the $L_9(3^4)$ orthogonal test for the culture conditions optimization

No.	A′	B′	C′	D′	Inhibition rate (%)
1	1	1	1	1	88.39
2	1	2	2	2	89.06
3	1	3	3	3	84.15
4	2	1	2	3	90.18
5	2	2	3	1	89.73
6	2	3	1	2	89.51
7	3	1	3	2	91.07
8	3	2	1	3	87.50
9	3	3	2	1	86.16

Table 51.6 The analysis of the culture conditions optimization by SPSS

Source	Type III sum of squares	df	Mean square	*F*	Sig.
Calibration model	116.534 a	8	14.567	53.707	0.000
Intercept	211589.357	1	211589.357	780122.165	0.000
A′	33.770	2	16.885	62.254	0.000
B′	46.726	2	23.363	86.138	0.000
C′	0.911	2	0.456	1.680	0.214
D′	35.127	2	17.563	64.756	0.000
Error	4.882	18	0.271		
Total	211710.772	27			
Total correction	121.416	26			

51.4 Conclusions

From the tests and analyses above, the optimal medium formula is determined as: yeast powder 1.5 %, monosodium glutamate 2 %, sodium nitrate 0.8 %, starch 0.17 %, maltose 0.33 %; medium volume 60 mL, and culture temperature 30 °C. Also, inoculums size 2 % and fermentation time 36 h are the optimal culture conditions. According to the optimal medium and culture conditions for the experiments, the inhibition rate of strain BI_2 reaches 92 % in line with the experimental predicted results.

Acknowledgments This work was supported by Key Projects in the Tianjin Science & Technology Pillar Program (No. 12ZCZDNC016000).

References

1. Gourama H, Bullerman LB (1995) Antimycotic and antiaflatoxigenic effect of lactic acid bacteria. A review. J Food Protect 57(11):1275–1280
2. Romero D, Perez-Garcia A, Rivera ME et al (2004) Isolation and evaluation of antagonistic bacteria towards the cucurbit powdery mildew fungus *Podosphaera fusca*. Appl Microbiol Biotechnol 64(2):263–269
3. Bluma RV, Etcheverry MG (2006) Influence of *Bacillus* spp. isolated from maize agroecosystem on growth and aflatoxin B1 production by *Aspergillus* section *Flavi*. Pest Manag Sci 62:242–251
4. Moyne AL, Shelby R, Cleveland T et al (2001) Bacillomycin D: aniturin with activity against *Aspergillus flavus*. J Appl Microbiol 90(4):622–629
5. Zhang T, Shi ZQ, Hu LB et al (2008) Compounds from *Bacillus subtilis* B-FS06 inhibit the growth of *Aspergillus flavus*. World J Microbiol Biotechnol 24(6):783–788
6. Benitez LB, Velho RV, Lisboa MP et al (2001) Isolation and characterization of peptides produced by *Bacillus amyloliquefaciens* LBM5006. J Microbiol 48(6):791–797
7. Chary GH, Dastidar MG (2012) Investigation of optimum conditions in coal-oil agglomeration using Taguchi experimental design. Fuel 98:259–264
8. Brasil JL, Ev RR, Milcharek CD, Martins LC et al (2006) Statistical design of experiments as a tool for optimizing the batch conditions to Cr (VI) biosorption on *Araucaria angustifoliawastes*. J Hazard Mater B 133:143–153
9. Huynh H, Feldt LS (1976) Estimates of the correction for degrees of freedom for sample data in randomised block and split-plot designs. J Educ Stat 1:69–82
10. Everitt BS, Pickles A (2000) Statistical aspects of the design and analysis of clinical trials. ICP, London
11. Davidson ML (1972) Univariate versus multivariate tests in repeated measures experiments. Psychol Bull 77:446–452

Chapter 52
Optimization of Fermentation Medium for Citric Acid Production by *Aspergillus niger*

Jianhua Zhang, Kun Li, Juan Huang and Depei Wang

Abstract A statistically based method was used to optimize the fermentation medium for enhancing citric acid production by *Aspergillus niger* TCCC 41661. The optimization of single-factor experiments (soy peptone, $(NH_4)_2SO_4$, dextrin) and an orthogonal experiment were applied to determine the optimal concentration of each significant variable. The optimum values for the critical components were obtained as follows: 0.25 g/L soy peptone, 12.0 g/L dextrin, 2.0 g/L KH_2PO_4, 2.0 g/L $(NH_4)SO_4$, 0.1 % Tween 80. Under this condition, the citric acid production of 16.11 g/L was obtained.

Keywords *Aspergillus niger* · Citric acid · Morphology · Medium optimization · Orthogonal experiment

52.1 Introduction

Citric acid is widely used as pharmaceutical additive, cosmetic and detergent additive [1]. Citric acid is an important commercial product of fermentation industry, its annual production is over 700,000 tons [2]. The study found that there was too much protein in coarse corn flour [3], filamentous fungi will overgrow if it takes coarse corn flour as raw material. There are unique advantages in using the corn liquefied clarifying solution as raw material for its low content of fat and protein, it helps to improve oxygen level and the conversion rate, shorten the

J. Zhang · K. Li · J. Huang · D. Wang
Tianjin Key Laboratory of Industrial Microbiology, Ministry of Education,
College of Biotechnology, Tianjin University of Science and Technology,
Tianjin 300457, China

D. Wang (✉)
Key Laboratory of Industrial Fermentation Microbiology, Ministry of Education,
College of Biotechnology, Tianjin University of Science and Technology,
Tianjin 300457, China
e-mail: wangdp@tust.edu.cn

T.-C. Zhang and M. Nakajima (eds.), *Advances in Applied Biotechnology*,
Lecture Notes in Electrical Engineering 333, DOI 10.1007/978-3-662-46318-5_52

fermentation period [4]. In this paper, factors affecting the production of citric acid and mycelium pellet shape of *Aspergillus niger* prefermentation were studied using the corn liquefied clarifying solution as raw material and *A. niger* TCCC 41661 as a research strain [5]. It laid a foundation for further optimization of citric acid production process.

52.2 Materials and Methods

52.2.1 Material and Equipment

A high-yield strain (*A. niger* TCCC 41661) is kept at the Microorganism Preservation Center in Tianjin University of Science and Technology. The experimental equipment consists of professional digital microscope OLYMPUS DP7 (Olympus (China) Co., Ltd.), table model high-speed centrifuge (Hunan Xiang Yi Laboratory Instrument Development Co., Ltd), the citric acid test kit was purchased from Boehringer Mannheim Company, FRG.

The initial liquid seed medium: 10 % corn liquefied serum, 0.1 % soy peptone, 0.15 % $(NH_4)_2SO_4$, 0.5 % dextrin, 0.270 g/L KH_2PO_4, 0.065 g/L $MgSO_4 \cdot 7H_2O$, 0.0792 g/L $MnCl_2 \cdot 4H_2O$, 0.016 g/L $CoCl \cdot 6H_2O$, 0.0647 g/L $ZnSO_4 \cdot 7H_2O$.

Culture conditions: the optimal fermentation conditions were: 36.5 °C, 30 mL/250 mL medium volume, 330 rpm for 24 h.

52.2.2 Analytical Methods

Determination of citric acid: approximately 20 mL fermentation broth at different time points was taken in a 50 mL Eppendorf tube and centrifuged at 10,000×g and 4 °C for 5 min. The supernatant was removed in a 10-mL Eppendorf tube was placed in a water bath at 80 °C for 10 min to stop the possible enzymatic reactions. Then the supernatant was centrifuged again for the assay. Citric acid was measured enzymatically according to the manufacturer's instruction (test kit Cat. No. 10139076035). All the assays in this study were performed in triplicate.

52.2.3 The Effect of Nitrogen on Citric Acid Fermentation

Nitrogen plays an important role in cellular material synthesis and metabolism regulation. To determine the optimal nitrogen content, a series of experiments were performed using a range of values. The effect of the nitrogen was determined by varying the amounts of soy peptone.

52.2.4 The Effect of Carbon on Citric Acid Fermentation

The carbon source for the citric acid fermentation has been the focus of much study. To determine the effect of carbon, different amounts of dextrin were added to the fermentation medium. Single-factor experiments were carried out to determine the optimal carbon content.

52.2.5 Orthogonal Experiment

The best ratio of dextrin, KH_2PO_4, soy peptone, $(NH_4)_2SO_4$ was elected in L_9. (3^4) Orthogonal experiment.

52.2.6 The Effect of Tween 80 on Citric Acid Fermentation

Tween 80, an important surfactant has a crucial impact on the spread of mycelium pellets. There are conflicting reports about the importance and influence of morphology. For example, it has been reported that citric acid titer was higher when the morphology was filamentous and dispersed [6, 7]. To determine the optimum value, a series of experiments were performed using a range of values.

52.2.7 The Effect of Inoculum Size on Citric Acid Fermentation

The effect of inoculum size on citrate production was determined by varying the number of spores added as inoculum to fermentation broth [8].

52.3 Results and Discussion

52.3.1 Effect of Nitrogen on Citric Acid Fermentation

The roles of nitrogen are synthesis of cellular material and regulate metabolism [9]. From the perspective of growth, *A. niger* can take advantage of inorganic nitrogen and organic nitrogen [10]. Soy peptone is easy absorbed and used by microorganism; the results (Fig. 52.1) showed an increase in citrate production with the increase of soy peptone concentration. The optimized soy peptone was 0.05 %, when the citric acid production was maximum and mycelium pellet shape was

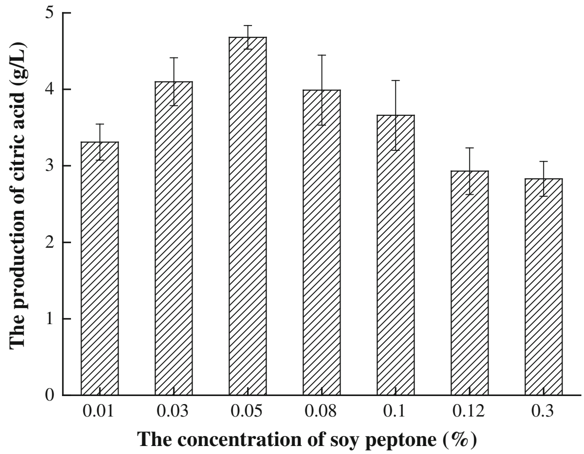

Fig. 52.1 The influence of soy peptone on citric acid fermentation

relatively homogeneous. The citric acid production decreased with the continuous increase of soy peptone concentration. Mycelium pellets (Fig. 52.2) were larger and more irregular at the soy peptone concentration of 0.01–0.03 % and 0.08–0.30 % compared to that at 0.05 %. At the soy peptone concentration of 0.01–0.03 %, the citric acid production decreased continually, because the nitrogen content was too low for bacterial growth and development. At the soy peptone concentration of 0.08–0.30 %, the rich nitrogen content accelerated the growth of filamentous fungi, which was not conducive to the accumulation of citric acid, although it was advantageous for shortening the fermentation period.

$(NH_4)_2SO_4$ as inorganic nitrogen directly affects citric acid fermentation. As showed in Fig. 52.3, with the increase of $(NH_4)_2SO_4$, citric acid yields gradually increased and citric acid yield was maximum at 0.24 % $(NH_4)_2SO_4$. Figure 52.4 showed mycelium pellet was large and irregular at the $(NH_4)_2SO_4$ concentrations of 0.16 and 0.18 % compared to that at 0.24 %. At the $(NH_4)_2SO_4$ concentration of 0.24 %, bacteria pellet were uniform and round which was conducive to the citric acid fermentation.

52.3.2 Effect of Dextrin on Citric Acid Fermentation

Carbon nitrogen ratio is a key factor in the citric acid fermentation and directly affects the fermentation period, the rate of acid production. If carbon nitrogen ratio is high, it will cause poor cell growth and slow cell metabolism, if carbon nitrogen ratio is too low, also leads to a large and loose state of mycelium pellet, and low yield of citric acid. Carbon nitrogen ratio can be adjusted, though adding different amounts of dextrin. The carbon source for the citric acid fermentation has been the

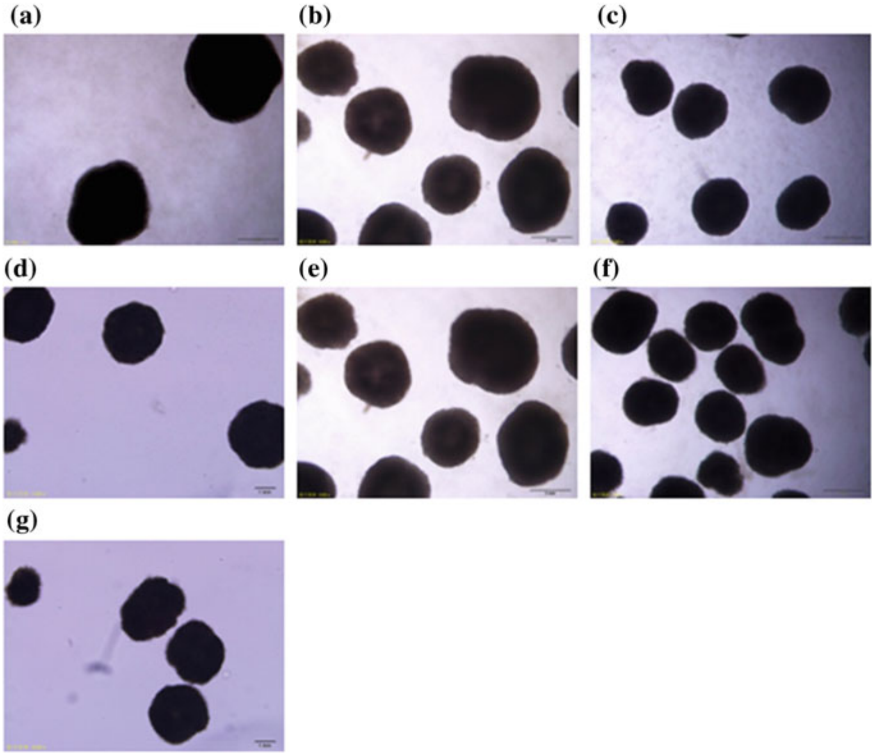

Fig. 52.2 The mycelium pellet morphology of *Aspergillus niger* in fermentation 24 h. **a** 0.01 % soy peptone, **b** 0.03 % soy peptone, **c** 0.05 % soy peptone, **d** 0.08 % soy peptone, **e** 0.10 % soy peptone, **f** 0.12 % soy peptone, **g** 0.30 % soy peptone. Magnification ×10, with the edges of the images being 1.0 mm

Fig. 52.3 The influence of different concentration of $(NH_4)_2SO_4$ on citric acid fermentation

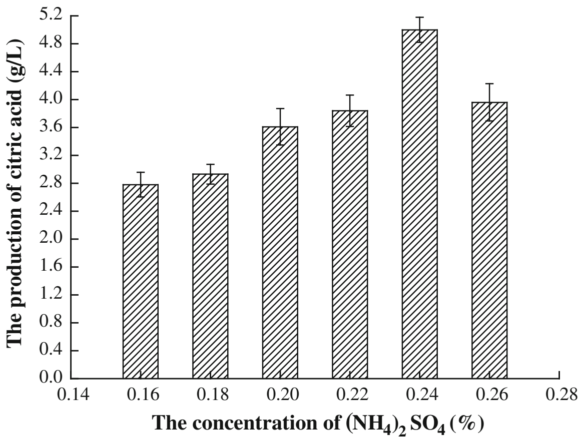

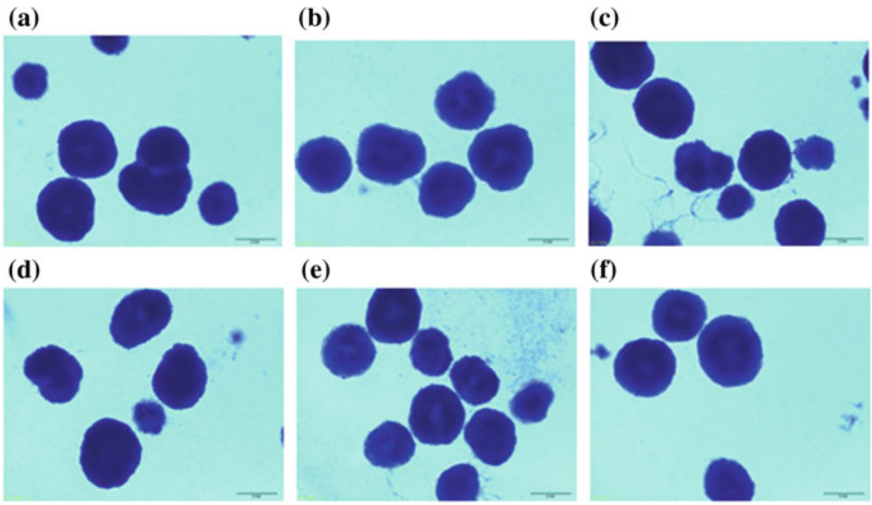

Fig. 52.4 The mycelium pellet morphology of *A. niger* infermentation 24 h. **a** 0.16 % $(NH_4)_2SO_4$, **b** 0.18 % $(NH_4)_2SO_4$, **c** 0.20 % $(NH_4)_2SO_4$, **d** 0.22 % $(NH_4)_2SO_4$, **e** 0.24 % $(NH_4)_2SO_4$, **f** 0.26 % $(NH_4)_2SO_4$. Magnification ×10, with the edges of the images being 2.0 mm

Fig. 52.5 The influence of dextrin on citric acid fermentation

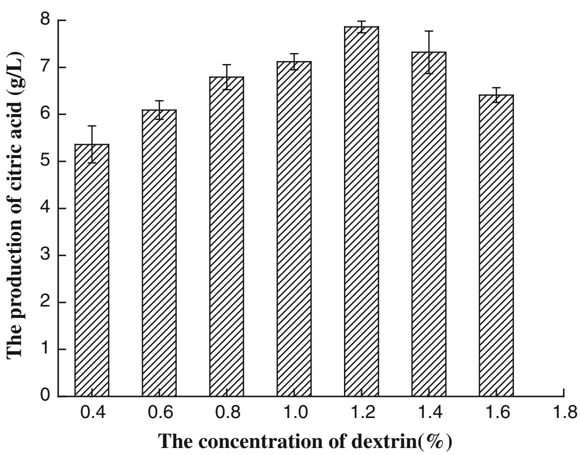

focus of much study [11]. In general, dextrin is rapidly taken up by *A. niger* [12]. Figure 52.5 shows that with the increase of dextrin concentration citric acid production gradually increased, acid production was maximum at 1.2 %. As showed in Fig. 52.6, mycelium pellets were uniform, dense, and had less broken mycelium. As dextrin increased continually, citric acid production declined.

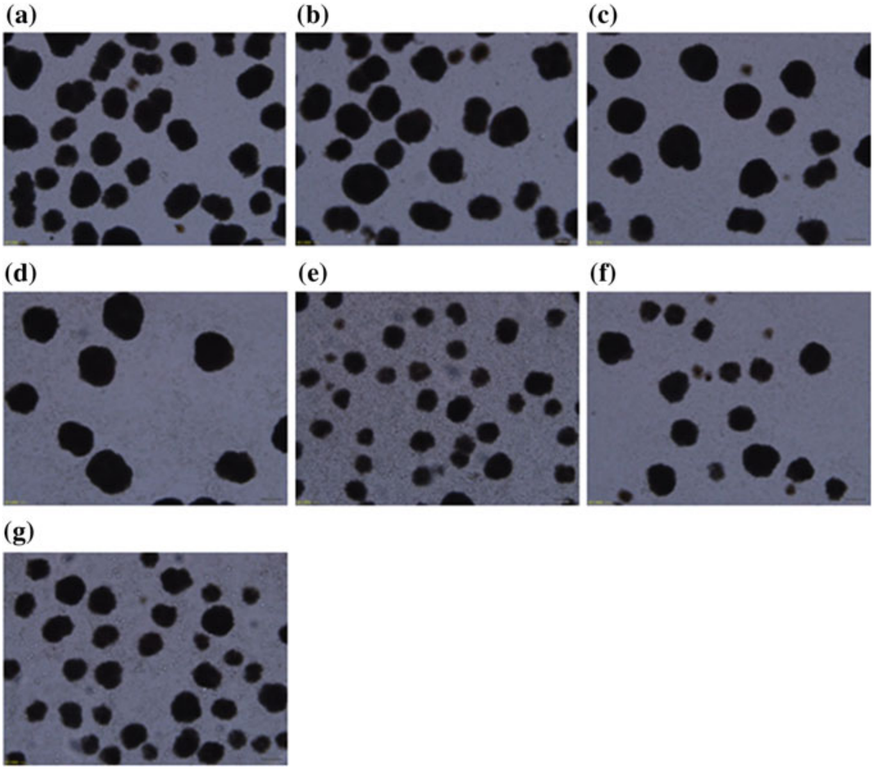

Fig. 52.6 The mycelium pellet morphology of *A. niger* infermentation 24 h. **a** 0.40 % dextrin, **b** 0.60 % dextrin, **c** 0.80 % dextrin, **d** 1.0 % dextrin, **e** 1.2 % dextrin, **f** 1.4 % dextrin, **g** 1.6 % dextrin. Magnification ×10, with the edges of the images being 100 μm

52.3.3 Orthogonal Experiment

L_9 (3^4) orthogonal experiment was used to screen the best ratio of dextrin, KH_2PO_4, soy peptone, $(NH_4)_2SO_4$. The results were shown in Table 52.1.

As showed in Table 52.1, in different proportions of four media components, the combination with the maximum production of citric acid was: dextrin 12 g/L, KH_2PO_4 2.0 g/L, soy peptone 0.25 g/L, $(NH_4)_2SO_4$ 2.0 g/L. The degrees of influence of four factors were showed though range analysis: $(NH_4)_2SO_4$ > KH_2PO_4 > Soy peptone > Dextrin.

The theoretically optimized medium was coincident with medium of the ninth group in orthogonal table. According to verification experiment, production of citric acid was 10.59 g/L.

Table 52.1 Results and variance analysis of orthogonal experiment of medium components

Experiment no.	Dextrin (g/L)	KH_2PO_4 (g/L)	Soy peptone (g/L)	$(NH_4)_2SO_4$ (g/L)	Citric acid (g/L)
1	5.0	1.0	0.10	2.0	6.50
2	5.0	1.5	0.25	2.5	5.77
3	5.0	2.0	0.50	3.0	4.84
4	8.0	1.0	0.25	3.0	4.69
5	8.0	1.5	0.50	2.0	6.85
6	8.0	2.0	0.10	2.5	5.82
7	12.0	1.0	0.50	2.5	4.95
8	12.0	1.5	0.10	3.0	4.80
9	12.0	2.0	0.25	2.0	8.61
K_1	0.5703	0.5380	0.5707	0.7320	
K_2	0.5787	0.5807	0.6357	0.5513	
K_3	0.6120	0.6423	0.5547	0.4777	
R	0.0417	0.01043	0.0810	0.2543	

52.3.4 Effect of Tween 80 on Citric Acid Fermentation

As shown in Fig. 52.7, the optimized concentration of Tween 80 was 0.10 %. With the continual increase of Tween 80, citric acid production gradually decreased. Tween 80 had damaging effects on the cell membrane. Too much Tween 80 will inhibit the growth of filamentous fungi, which leads to low citric acid production. From Fig. 52.8, the Tween 80 concentration of 0.10 %, the mycelium pellets were relatively homogeneous and dense, the hyphae was stubby, which was consistent with normal morphology of *A. niger* strains [13]. With the increase of Tween 80 concentration, the large and irregular mycelium pellets were disadvantageous to the production of acid.

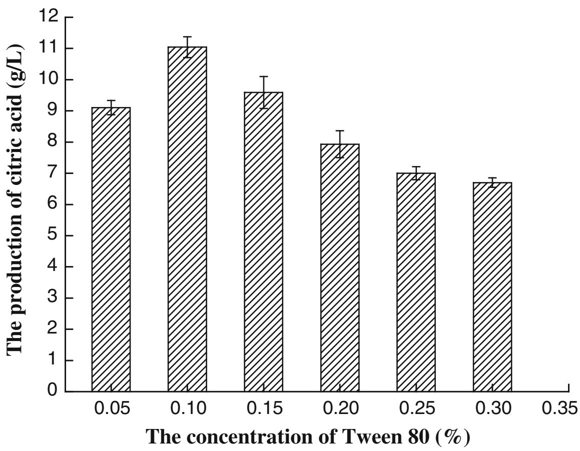

Fig. 52.7 The influence of Tween 80 on citric acid fermentation

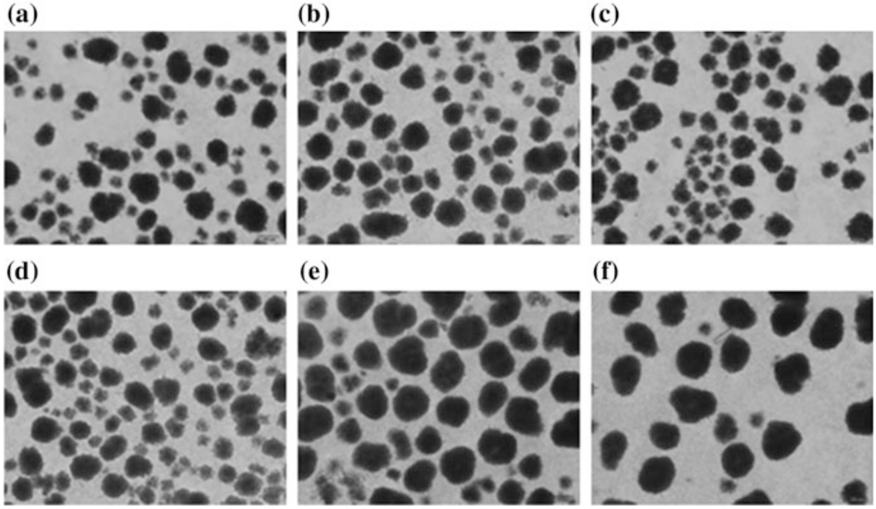

Fig. 52.8 The mycelium pellet morphology of *A. niger* infermentation 24 h. **a** 0.050 % Tween 80, **b** 0.10 % Tween 80, **c** 0.15 % Tween 80, **d** 0.20 % Tween 80, **e** 0.25 % Tween 80, **f** 0.30 % Tween 80. Magnification ×10, with the edges of the images being 100 μm

52.3.5 Effect of Inoculum Size on Citric Acid Fermentation

Generally speaking, the adequate dissolved oxygen level under small inoculum size brought excess nutrients [14] and led to large mycelium pellets and low acid production rate. In contrast, the excessive inoculum size will lead to the lack of dissolved oxygen and active anaerobic metabolism. As shown in Fig. 52.9, with the increase of inoculum size the citric acid production gradually increased. When the inoculum size was 5×10^5 spores/mL, the citric acid production was the maximum.

Fig. 52.9 The influence of inoculum size on citric acid fermentation

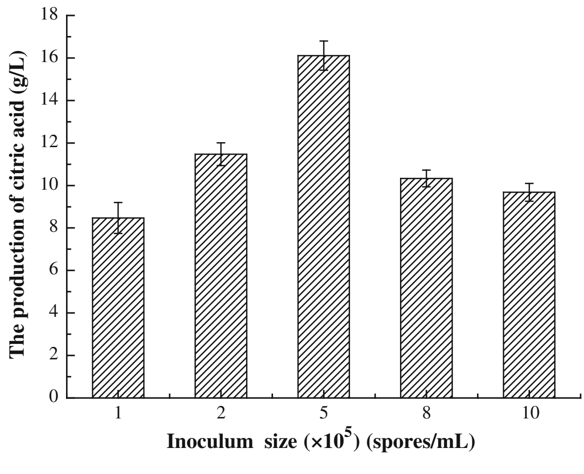

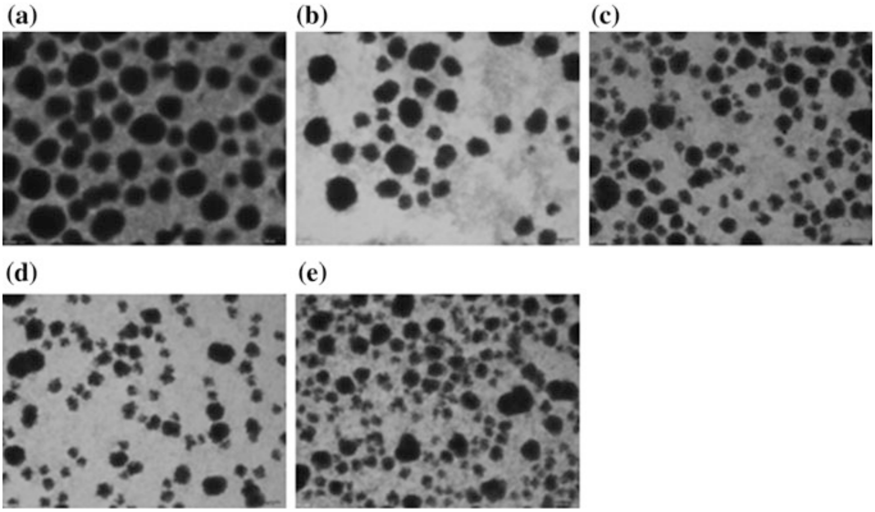

Fig. 52.10 The mycelium pellet morphology of *A. niger* in fermentation 24 h. **a** 10^5 spores/mL, **b** 2×10^5 spores/mL, **c** 5×10^5 spores/mL, **d** 8×10^5 spores/mL, **e** 10^6 spores/mL. Magnification ×10, with the edges of the images being 100 μm

From Fig. 52.10, mycelium pellets were too large under the inoculum size of 10^5 spores/mL. The optimum inoculum size was 5×10^5 spores/mL when mycelium pellets were relatively homogeneous and dense. If the inoculum size was increased continually, mycelium pellets were loose relatively, which was unsuitable for citric acid production.

52.4 Discussion

According to the results, the optimized fermentation medium consists of 10 % corn liquefied serum, 0.25 g/L soy peptone, 2.0 g/L $(NH_4)_2SO_4$, 12.0 g/L dextrin, 2.0 g/L KH_2PO_4, 0.10 % Tween 80. The fermentation conditions were 36.5 °C, 330 rpm for 24 h. The inoculation size and medium volume were 5×10^5 spores/mL and 30 mL/250 mL, respectively. Under the optimized conditions above, a maximized citric acid yield of 16.11 g/L was obtained.

Acknowledgments The author appreciated Lin Huang for equipment support, Lu Wang for technical assistance Pingping Tian and Yibing Cheng for continuous encouragement. This work was supported by The National High-tech R&D Program of China (2012AA021302), The National Basic Research Program of China (2013CB734004) and National Natural Science Foundation of China (31471725 and 31370075).

References

1. Jiang C, Xu L (2001) Development and utilization of microbial resources [M]. China Light Industry Press, Beijing
2. Lu MY, Maddox IS, Brooks JD (1998) Application of a multilayer packed-bed reactor to citric acid production in solid-state fermentation using *A. niger*. Process Biochem 33(2):117–123
3. Ma T (2008) Corn processing [M]. Chemical Industry Press, Beijing
4. Pallares J, Rodríguez S, Sanromán A (1996) Citric acid production in submerged and solid state culture of *Aspergillus niger* [J]. Bioprocess Eng 15:31–33
5. Papagianni M, Mattey M, Kristiansen B (1998) Citric acid production and morphology of *Aspergillus niger* function of the mixing intensity In a stirred tank and tubular loop bioreactor. Biochem Eng J 2:197–205
6. Ujcová E, Fencl Z, Musílková M, Seichert L (1980) Dependence of release of nucleotides from fungi on fermenter turbine speed. Biotechnol Bioeng 22:237–241
7. Seichert L, Ujcová E, Musílková M, Fencl Z (1982) Effect of aeration and agitation on the biosynthetic activity of diffusely growing *A. niger*. Folia Microbiol 27:333–334
8. Lu MY, Maddox IS, Brooks JD (1995) Citric acid production by *A. niger* in solid-substrate fermentation. Bioresour Technol 54(3):235-239
9. Zhou J, Wu D, Yao M et al (2006) Medium optimization of production of citric acid ofaging indica valley solid state fermentation [J]. Food Sci 27(12):283–286
10. Sun J, Zang W, Jiang S, Li J, Wu G (2008) Effect on citric acid production by *A. niger* utilizing corn meal as raw material in different fermentation conditions [J]. China Condiment 6:84–86
11. Papagianni M (2007) Advances in citric acid fermentation by *A. niger*. Biochemical aspects membrane transport and modeling. Biotechnol Adv 25(3):244–263
12. Mattey M (1992) The production of organic acids. Crit Rev Biotechnol 12:87–132
13. Pan S (2010) Process research on fermentation of citric acid by using corn clarifying solution. J Anhui Agric Sci 29:16700–16701
14. Chen J, Du G, Yin L et al (2003) Fermentation engineering experimental techniques [M]. The Chemical Industry Publisher, Revere, pp 70–71

Chapter 53
Study on the Soxhlet's Extraction of Star Anise Oil and Preliminary Investigation of Its Antibacterial Activity

Lin Tian and Ping Li

Abstract In this study, Soxhlet extraction method using ethyl acetate as a solvent was used to extract the volatile oil from star anise fruits. The best technological extraction conditions were obtained by a series of single-factor experiments. The antibacterial activity of star anise oil obtained by Soxhlet extraction method was preliminary determined. The result showed that the most important factor affecting the extraction rate of oil from star anise fruits was extraction temperature, followed by powder granularity, solid–liquid ratio, and extraction time. The best extraction conditions were as follows: 1:22 (w/v), 40 min, 120 °C, and 60–80 mesh, respectively. Under these conditions, the yield of star anise oil reached 25.9827 %. It was proved that star anise oil extracted by Soxhlet extraction method could reduce the cost of investment equipments, improve production significantly, and keep the high-quality and natural flavor of the essential oil. Antibacterial experiment demonstrates that star anise oil method has a strong inhibitory effect against *Escherichia coli* and *Bacillus subtilis*, so that it could be applied as a natural and environment-friendly antibacterial agent in many areas, such as food products and pharmaceutical sectors.

Keywords Star anise oil · Soxhlet extraction method · Inhibitory effect

53.1 Introduction

Star anise is an important "Medicinal and Edible" species, mainly in Guangxi, Guangdong, Yunnan, and other provinces. Star anise oil, which is extracted from fresh leaves or ripe fruits, is colorless to light yellow, odor fragrance, and tastes sweet. Anise fruit contains volatile oil, organic acids, flavonoids, anisole, and some

L. Tian (✉) · P. Li
College of Basic Sciences, Tianjin Agricultural University, Tianjin 300384, People's Republic of China
e-mail: 13752368407@126.com

T.-C. Zhang and M. Nakajima (eds.), *Advances in Applied Biotechnology*,
Lecture Notes in Electrical Engineering 333, DOI 10.1007/978-3-662-46318-5_53

active ingredients such as anise aldehyde which is reported to have certain antibacterial effect [1–3].

In the traditional food industry, the utilization of star anise oil is relatively low compared to star anise fruit. With the development of the food industry, the use of star anise oil is far more than the fruit, because of its small size, health, easy to use, and other advantages [4, 5].

Star anise oil has a good bactericidal ability to *Mycobacterium tuberculosis*, *Bacillus subtilis*, *Staphylococcus aureus*, *Streptococcus pneumoniae*, *Aspergillus flavus*, and *Aspergillus niger*. Star anise extract, extracted with ethanol, has certain inhibition against *S. aureus*, *S. pneumoniae*, *Paratyphoid bacillus*, and some common pathogenic Candida [6, 7].

In this paper, we extracted star anise oil from star anise dried fruit with Soxhlet method. Meanwhile, several major factors that affect the oil yield were investigated, such as extraction time, the degree of material crushing, extraction temperature, solid–liquid ratio, etc. Conditions of star anise oil extracted by Soxhlet method were optimized by orthogonal test on the basis of single-factor experiment. Finally, the inhibitory effect of star anise oil against *Escherichia coli* and *B. subtilis* was preliminary studied to provide some references for anise oil on drugs for antibacterial agents.

53.2 Materials and Methods

53.2.1 Drugs and Instruments

53.2.1.1 Materials

Ingredients: Dried star anise

Reagents: ethyl acetate (AR), cyclohexane, petroleum ether, 95 % ethanol, and acetone

Drugs: anhydrous sodium sulfate (AR)

Experimental apparatus: thermostatic bath with magnetic stirring mill, flat-bottomed flask (150 mL), silica gel plate, and a fat extractor

53.2.1.2 Antimicrobial Experimental Material

strains: *E. coli*, *B. subtilis*
medium: agar gel medium

53.2.2 Methods

53.2.2.1 Plant Material

The star anise was dried at 60 °C for 48 h in a electric air blowing drying oven and then were ground in different periods in order to obtain different powder granularity.

53.2.2.2 Microbial Strains and Bacteria Suspension Preparation

Escherichia coli (gram negative) and *B. subtilis* (gram positive) were selected as representative bacteria to determine antibacterial activity of star anise oil. After activated, the bacteria were inoculated into liquid standard nutrient broth medium, and cultured at 37 °C with regularity shaking at 180 rpm for 18 h. The number of bacteria was counted using plate dilution method. The final concentration of colonies was 106 CFU/mL. Solid nutrient broth medium was supplemented with 2 % agar into liquid medium.

53.2.2.3 Preparation of Essential Oil

The extraction process was performed by a Soxhlet extraction method. Star anise powder was put into a fat extractor, extraction solvent was added, and then the experiment was conducted under set conditions. After extraction, the solution was filtered and dried under anhydrous sodium sulfate. After drying, the extract was again filtered and the filtrate was concentrated by vacuum rotary evaporator to recover solvent. Anise oil was calculated using the following (53.1):

$$X(\%) = \frac{Q_1}{Q_2} \times 100\ \% \qquad (53.1)$$

where Q_1 is the quality of extracted star anise oil; Q_2 is the quality of star anise powder in test.

53.3 Results and Discussion

In the study, extraction conditions of star anise oil by Soxhlet method were optimized by a series of single-factor tests and orthogonal test.

53.3.1 *Single-Factor Tests for the Extraction of Star Anise Oil*

53.3.1.1 Extraction Solvent Selection

In the extraction process, ethyl acetate, cyclohexane, petroleum ether (30–60 °C), petroleum ether (60–90 °C), 95 % ethanol, and acetone were applied as extraction solvents to examine their effects on the oily yield. Results were shown in Fig. 53.1.

As can be seen from Fig. 53.1, ethyl acetate was the best extraction solvent with the highest extraction yield; hence, ethyl acetate was selected as the solvent to extract star anise oil in the following tests.

53.3.1.2 Effect of Powder Granularity on the Extraction Yield of Star Anise Oil

In this study, star anise was crushed into powder with the mill and was sieved into five different sizes, i.e., using 10–20, 20–40, 40–60, 60–80 and 80–100 meshes, was extracted at 100 °C, the solid–liquid ratio was 1:20, and the extraction time was 40 min. The result was shown in Fig. 53.2.

As shown in Fig. 53.2, the extraction rate of star anise oil was increased because of improved powder granularity, and reached maximum when the star anise powder was 60–80 mesh. After 60–80 mesh, the rate decreased. The possible reason is that crushing anise into powder could increase the specific surface area and promote the leaching of anise oil. However, excessive grinding could lead to large specific surface area which could cause enhanced adsorption and gradually reduced yield.

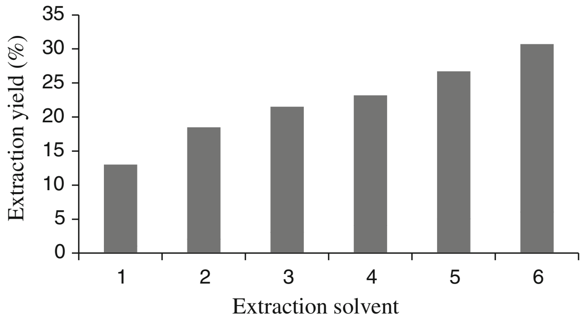

Fig. 53.1 Effect of different solvents on the extraction yield of star anise oil. *1* Ethanol (95 %); *2* petroleum ether (b.p. 30–60 °C); *3* petroleum ether (b.p. 60–90 °C); *4* cyclohexane; *5* acetone; *6* ethyl acetate

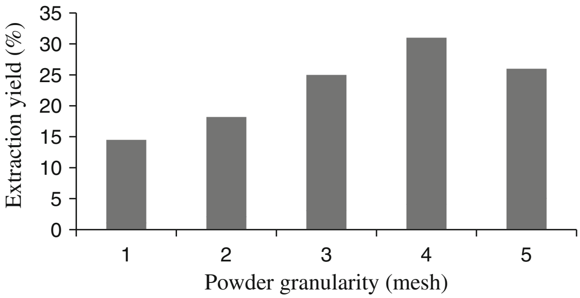

Fig. 53.2 Effect of powder granularity on the extraction yield of star anise oil. *1* 10–20 mesh; *2* 20–40 mesh; *3* 40–60 mesh; *4* 60–80 mesh; *5* 80–100 mesh

53.3.1.3 Effect of Solid–Liquid Ratio on the Yield of Star Anise Oil

Some experiments were carried out to determine the effect of solid–liquid ratio on the yield of star anise oil (Fig. 53.3). The results showed that with increased amount of ethyl acetate, the yield was relatively gentle rise. When the solid–liquid ratio was 1:22 (w/v), the yield reached 21.97 %. And after that, the yield was little changed with the increase of ethyl acetate.

53.3.1.4 Effect of Extraction Time on the Yield of Star Anise Oil

Seven experiments were conducted to study the impact of different extraction time on the yield of star anise oil. As illustrated in Fig. 53.4, with the increase of extraction time, star anise oil yield also improved. The highest rate was achieved at 60 min. After that, there was no significant increase in yield. This showed that the star anise oil had been completely extracted for 60 min.

Fig. 53.3 Effect of solid–liquid ratio on the extraction yield of star anise oil

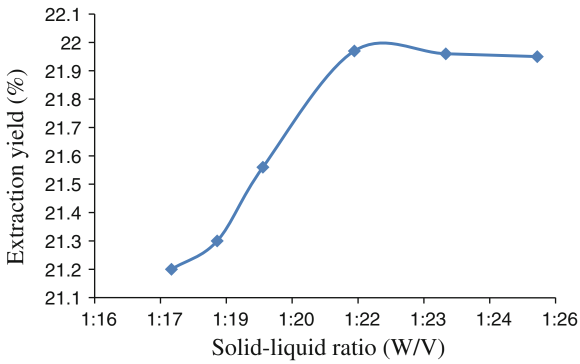

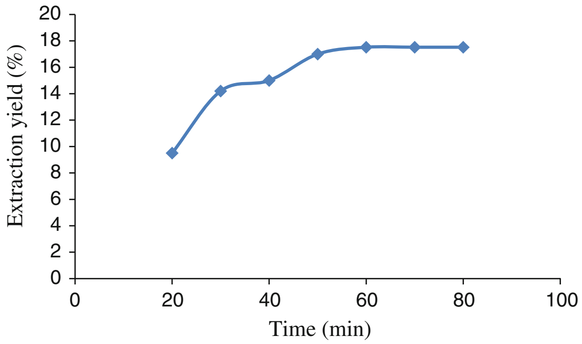

Fig. 53.4 Effect of extraction time on the extraction yield of star anise oil

53.3.1.5 Effect of Extraction Temperature on the Yield of Star Anise Oil

It can be seen from Fig. 53.5, with the rising of temperature, the rate of extraction of star anise oil raised, but gradually reduced after 110 °C. It is because the extraction temperature was too high which led to some low-boiling-point components (such as terpenoids) volatilizing.

53.3.2 *Orthogonal Test for the Extraction of Star Anise Oil*

53.3.2.1 Design and Result of the Orthogonal Test

An orthogonal experiment on four factors and four levels was designed and conducted, in order to optimize the extraction conditions of Soxhlet extraction of star anise oil, based on the previous single-factor experiments (listed in Tables 53.1 and 53.2).

As shown in Tables 53.1 and 53.2, extraction temperature had the most significant influence on the yield. But the over-high temperature could result in the

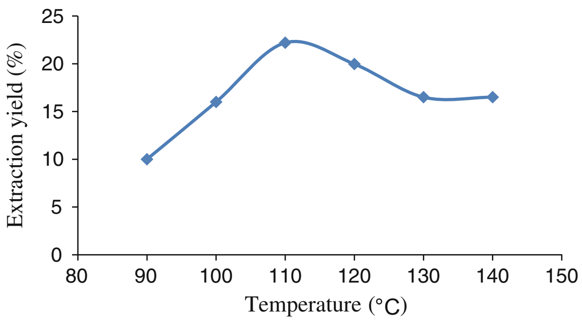

Fig. 53.5 Effect of extraction temperature on the extraction yield of star anise oil

Table 53.1 The design of experiment factors and levels

Levels/factors	A solid–liquid ratio (w/v)	B time (min)	C temperature (°C)	D powder granularity (mesh)
1	1:18	40	100	20–40
2	1:20	50	110	40–60
3	1:22	60	120	60–80
4	1:24	70	130	80–100

Table 53.2 Four-level orthogonal test and experimental results

Number	A solid–liquid ratio (w/v)	B time (min)	C temperature (°C)	D powder granularity (mesh)	Yield (%)
1	1	1	1	1	13.9754
2	1	2	2	2	19.9848
3	1	3	3	3	25.9621
4	1	4	4	4	21.9829
5	2	1	2	3	21.9811
6	2	2	1	4	15.9728
7	2	3	4	1	15.9831
8	2	4	3	2	19.9760
9	3	1	3	4	23.9741
10	3	2	4	3	25.9631
11	3	3	1	2	17.9860
12	3	4	2	1	19.9812
13	4	1	4	2	23.9842
14	4	2	3	1	19.9732
15	4	3	2	4	17.9870
16	4	4	1	3	13.9835
K_1	81.9052	83.9148	61.9187	69.9129	
K_2	73.9140	81.8949	79.9341	81.9310	
K_3	87.9044	77.9182	89.8854	87.8898	
K_4	75.9279	75.9236	87.9133	79.9178	
k_1	20.4763	20.9787	15.4797	17.4782	
k_2	18.4785	20.4737	19.9835	20.4828	
k_3	21.9761	19.4796	22.4714	21.9725	
k_4	18.9820	18.9809	21.9783	19.9795	
R	3.4976	1.9978	6.9917	4.4943	

reduction of the yield. The possible reason is that the enhancement of the temperature led to some losses of volatile components of essential oil and the decline of the yield. In addition, the powder granularity also had a great effect on the yield, which illustrated smaller powders caused more dissolution of the oil.

Besides, long extraction time was not conducive to the extraction rate. And the optimum conditions by Soxhlet extraction of star anise oil: 1:22 (w/v), 40 min, 120 °C, 60–80 mesh.

53.3.2.2 Verification Test

Three tests were carried out to verify the repeatability of optimum extraction conditions above, and the results were listed in Table 53.3. The result of verification test demonstrated that the optimum extraction technology had good stability, and under this condition, the oily yield could reach 25.9827 % in average.

53.3.3 Purification of Star Anise Oil

Since the color of the star anise oil extracted through Soxhlet extraction method was very deep (dark green), silica gel column chromatography separation and purification method was used to separate pigments or other impurity out, in order to obtain higher purity of the star anise oil. Before the separation experiments, thin layer chromatography tests were conducted to determine the best ratio of eluent (petroleum ether:ethyl acetate). Finally, the ratio of 1:10 eluent was used for column chromatography separation experiment, so that the high purity of star anise oil was obtained.

53.3.4 Antibacterial Activity of Star Anise Oil Against Escherichia coli and Bacillus subtilis

Disc-diffusion method was conducted in the study of antibacterial activity of star anise oil against *E. coli* and *B. subtilis*. The diameters of inhibition zone and the percentage of growth inhibition were listed in Tables 53.4, 53.5, 53.6, and 53.7.

It can be seen from the results, that star anise oil has a strong antibacterial activity against *E. coli* and *B. subtilis*. This might be due to the presence of its main constituent in star anise oil, such as anisic aldehyde, limonene, and transanethole which were reported to have strong antibacterial activity. However, with the decreased concentration, the inhibitory effect of star anise oil also weakened, and

Table 53.3 Verification test and results

Number	1	2	3
Yield (%)	25.8653	25.9051	26.0112
Average (%)		25.9827	
Relative standard deviation (%)		0.0080	

Table 53.4 Antibacterial activity of star anise oil (without purification) against *Bacillus subtilis*

Concentration (mg/mL)	Diameter of the inhibition zone (mm)	Inhibition percentage (%)
1.00	25.3	76.3
0.50	12.7	52.8
0.25	9.0	33.3
0.17	8.0	25.0
Control	6.0	0

Table 53.5 Antibacterial activity of star anise oil (after purification) against *B. subtilis*

Concentration (mg/mL)	Diameter of the inhibition zone (mm)	Inhibition percentage (%)
1.00	28.3	78.8
0.50	15.2	60.5
0.25	12	50.0
0.17	10	40.0
Control	6.0	0

Table 53.6 Antibacterial activity of star anise oil (without purification) against *Escherichia coli*

Concentration (mg/mL)	Diameter of the inhibition zone (mm)	Inhibition percentage (%)
1	17.7	67.1
0.50	11.7	40
0.25	8.0	25.0
0.17	7.0	14.3
Control	6.0	0

Table 53.7 Antibacterial activity of star anise oil (without purification) against *E. coli*

Concentration (mg/mL)	Diameter of the inhibition zone (mm)	Inhibition percentage (%)
1	18.3	66.1
0.50	13.0	53.8
0.25	9.0	33.3
0.17	8.0	25.0
Control	6.0	0

this was probably due to the dilution effect of essential oil, which resulted in the content of antibacterial active ingredients declining. Second, inhibitory effect of star anise oil on *B. subtilis* was better than that on *E. coli*. Finally, the oil treated by separation and purification methods displayed stronger inhibitory effect on the two strains than that without purification. This is because the wax, pigment, and other impurities could be removed through the purification experiments which improved the purity of star anise oil.

53.4 Conclusion

In conclusion, our research showed that the most important factor affecting the extraction rate of oil from star anise fruits was extraction temperature, followed by powder granularity, solid–liquid ratio, and time. The best extraction conditions were as follows: 1:22 (w/v), 40 min, 120 °C, and 60–80 mesh, respectively. Under this condition, the yield of star anise oil extracted from star anise fruits was 25.9827 %. It was proved that star anise oil extracted by Soxhlet method could reduce the cost of investment equipments and improve production significantly, and keep the high-quality and natural flavor of the essential oil. In addition, antibacterial experiment demonstrated that star anise oil obtained by Soxhlet extraction method had a strong inhibitory effect against *E. coli* and *B. subtilis*, so that it could be applied as a natural and environment-friendly antibacterial agent in many areas, such as food products, healthcare products, and pharmaceutical sectors.

References

1. Zhao JL (2004) Study on the in vitro anti candida activity of the essential oil of Illicium verum. J Dept Dermatol 475–477 (in chinese)
2. Xiong YZ (2008) Research progress of star anise. J Chin Condiment 28–30 (in chinese)
3. Zhang ZP (2006) Study of star anise, production and market situation of the shikimic acid. J Chin Mod Tradit Chin Med 41–42 (in chinese)
4. Wang GY (2006) Research progress of application of plant essential oil. J Food Sci Technol 11–14 (in chinese)
5. Liu HX (2007) Extraction and chemical composition analysis of volatile oil of anise seeds by Soxhlet method. J Food Res Dev 145–147 (in chinese)
6. Ling JN (2009) Optimization of ultrasonic extraction of star anise oil by response surface method. J Zhejiang Univ Sci Technol 111–114
7. Nikoletta G, Federico F, Ioannis G et al (2010) Phytochemistry and nematicidal activity of the essential oils from 8 Greek Lamiaceae aromatic plants and 13 terpene components. J Agric Food Chem 58:7856–7863

Part III
Biological Separation and Biological Purification

Chapter 54
Production of Diosgenin from *Dioscorea zingiberensis* by Mixed Culture of Three Filamentous Fungi

Hua Xiao, Linlin Huang, Jinxia Xie, Songtao Bie and Yu Li

Abstract The mixed culture of *Aspergillus oryzae*, *Phanerochaete chrysosporium,* and *Aspergillus niger* was explored for the production of diosgenin from *Dioscorea zingiberensis*. Conditions for biotransformation of saponin using mixed culture of three fungi were optimized. The maximum production of diosgenin (40.06 ± 0.53 mg/g) was obtained with *D. zingiberensis* concentration (50.00 g/L), inoculation size (2.0 mL of spore suspension, 1:2:3 ratio of *A. oryzae, P. chrysosporium*, and *A. niger*, v/v/v), initial pH (5.0), and cultivation time (6 days). In the optimization conditions, mono and mixed cultures were tested, with mixed culture of three fungi giving better yields of diosgenin and β-glucosidase. The diosgenin yield of optimization biotransformation increased by 50.54 % compared to the traditional acid hydrolysis method (26.61 ± 0.78 mg/g). The use of mixed culture of these fungi proposes an approach for more efficient and clean diosgenin production by *D. zingiberensis*.

Keywords Diosgenin · *Aspergillus oryzae* · *Phanerochaete chrysosporium* · *Aspergillus niger* · *Dioscorea zingiberensis*

54.1 Introduction

Diosgenin (25R-Spriost-5-en-3β-ol) is an important precursor for the synthesis of adrenal cortex hormone, sex hormone, progestational hormone, and anabolic steroid [1, 2]. *Dioscorea zingiberensis* (DZW) tuber is one of the most important resources for diosgenin production, as it has high content of steroidal saponins. DZW tubers contain 1–2 % diosgenin, 30–40 % starch, 10–15 % lignin, and 40–50 % cellulose

H. Xiao · L. Huang · J. Xie · S. Bie · Y. Li (✉)
Key Laboratory of Industrial Fermentation Microbiology, Ministry of Education,
National Engineering Laboratory for Industrial Enzymes, The College of Biotechnology,
Tianjin University of Science & Technology, Tianjin 300457, China
e-mail: liyu@tust.edu.cn

T.-C. Zhang and M. Nakajima (eds.), *Advances in Applied Biotechnology*,
Lecture Notes in Electrical Engineering 333, DOI 10.1007/978-3-662-46318-5_54

[3, 4]. Diosgenin occurs in plants in the form of saponins attaching glucose or rhamnose to aglycone by glycosidic bonds at C-3 and C-26 [5]. Production of diosgenin from plant tubers depends not only on decomposition starch, lignin, and cellulose which prevent the saponins from releasing, but also on the hydrolysis of these chemical bonds of saponins. It is reported that the glucosyl residue at C-3 sugar chain of steroidal saponins hardly could be hydrolyzed by currently available glycosidases such as β-glucosidase, amylase, and cellulase [6, 7]. The glucose unit at C-26 on furostanol saponins is easily hydrolyzed to form the corresponding spirostanol saponins [8, 9]. The structure of the saponins and diosgenin are shown in Fig. 54.1.

In the traditional method, acids are used to hydrolyze DZW to produce diosgenin. However, the acid hydrolysis causes the structure of diosgenin damaged and generates numerous byproducts, which results in higher chemical oxygen demand (COD, 80,000 mg/L in the waste water) [10] and serious environmental pollution.

Attempts to reduce oxygen consumption during diosgenin production from DZW were reported. For instance, fiber and starch were recovered by physical methods and used to produce ethanol, and then diosgenin was generated by acid hydrolysis. In this way, COD in wastewater could be decreased by at least 50 %, but resulted in the loss of 20 % diosgenin [11] and the process of recovering fiber and starch is complex. Previous studies showed that multiple enzymes (cellulase, β-glucosidase and pectinase) could transform saponins in DZW to diosgenin [11].

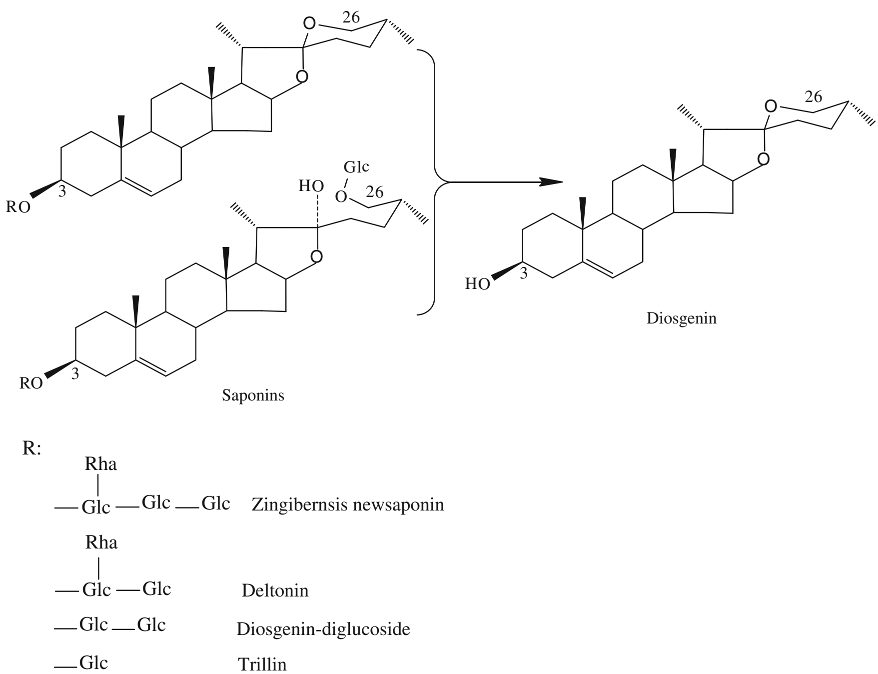

Fig. 54.1 The structure of saponins and diosgenin

However, the high costs of enzymes are the major drawback for their application and very few reports are available in the literature regarding using enzymes alone to generate diosgenin from saponin.

Diosgenin production through microbial transformation is another potential technique [12]. For example, biotransformation of DZW by *Aspergillus oryzae* [13], *Trichoderma reesei* [4], and *Trichoderma harzianum* [14] have been applied to improve tradition process efficiency. However, the yield of diosgenin is not high. Because of high contents of lignin and cellulose in DZW, the releasing of saponins and the hydrolysis of glycosidic bonds of saponins require the cooperation of many microbial enzymes to accomplish. Mixed culture of fungi thus may produce the optimal combination of enzymes for the most efficient biodegradation process in increasing diosgenin yield. So far, there are few references regarding the use by mixed microbial culture for diosgenin production. With countless possible microbe combinations, the potential for mixed fermentation in natural product drug discovery is huge [15]. Complex mixed cultures have been widely used in biotechnology for many processes, e.g., for the production of antibiotics, enzymes, fermented food, composting, dairy fermentation, bioconversion of apple distillery, and domestic wastewater sludge [12].

The aim of this work was to increase diosgenin yield from DZW and reduce environmental pollution by the mixed culture of three fungi: *A. oryzae*, *Phanerochaete chrysosporium*, and *Aspergillus niger*. The biotransformation consists of two stages: hydrolysis of lignin and cellulose of DZW to release saponins and hydrolysis of the saponins to diosgenin.

54.2 Materials and Methods

54.2.1 Materials

The dried DZW tubers were supplied by Kangsheng Company, Qingyang, Gansu, China. The materials were ground by a pulverator (DJ-048 Pulverator, Beijing Huanya Tianyuan Co. Ltd., Beijing, China) and the powder was screened through a 40-mesh stainless steel sieve (0.2 cm). Chemical reagents used were of analytical grade commercial products. HPLC-grade acetonitrile was purchased from TEDIA (USA). Diosgenin standard and *p*-Nitrophenyl β-D-glucopyranoside (pNPG) were obtained from Sigma-Aldrich Co. (USA).

54.2.2 Microorganisms and Microbial Transformation

Phanerochaete chrysosporium was preserved in Tianjin University of Science and Technology Microbiological Culture Collection Center. *A. niger* and *A. oryzae* were purchased from China Center of Industrial Culture Collection (Beijing, China). These strains were stored at 4 °C on potato dextrose agar slant temporarily. All culture and biotransformation experiments were performed in 250 mL Erlenmeyer flasks. To prepare the inocula, spores in a 7-day-old agar slant were suspended in 0.01 % Tween 80 solution (10^7 spores/mL). The optimal inoculation ratio (1:2:3 ratio of *A. oryzae*, *P. chrysosporium,* and *A. niger*) for each fungus was determined in a preliminary experiment (unpublished data). Fermentation media incubated at 30 °C on a rotary shaker at 180 r/min for diosgenin production. All experiments were done in triplicate and data expressed as average values.

54.2.3 Extraction and Analysis Diosgenin

At the end of cultivation, the steroidal saponins extraction was performed according to Zhu et al. [4]. The fermentation culture was centrifuged, precipitated, and dried at 80 °C, extracted with chloroform, and ultrasonicated for 30 min (KQ 3200B ultrasonicator). The samples were centrifuged and analyzed on Agilent 1,100 Multisolvent Delivery System equipped with a Diamonsil C18 column, 250 mm × 4.6 mm (5 μm), and detector at 203 nm, the eluent was A (CH_3CN) and B (HCOOH: H_2O = 0.01:300, v/v) with a gradient time program: 0–24 min, 55 % A → 60 % A; 24–30 min, 60 % A → 80 % A; 30–64 min, 80 % A. The flow rate of the mobile phase was 1.0 mL/min and the temperature of column was 25 °C.

$$\text{Yield of Diosgenin}\,(\text{mg/g}) = \text{diosgenin content}\,(\text{mg})/\text{DZW content}\,(\text{g})$$

54.2.4 Acid Hydrolysis Conditions

The traditional method uses acids to hydrolyze DZW to produce diosgenin. As a comparison experiment of microbial transformation, the acid hydrolysis conditions: 5.0 g DZW was mixed with 100 mL 1 mol/L H_2SO_4 and heated with a reflux condenser at 100 °C for 4 h, then centrifuged and pH was adjusted until it became neutral. The centrifuged residue was dried at 80 °C and diosgenin extraction was the same as mentioned above.

54.2.5 Analysis β-Glucosidase, Glucoamylase, Carboxymethyl Cellulase, and Lignin Peroxidase Activity

A culture in each flask was centrifuged at 4 °C with 8,000 r/min for 10 min, the supernatants were crude enzyme diluted for enzymes activity analysis.

β-Glucosidase activity was determined at 400 nm by using 1 mol/L pNPG as the substrate as described previously [16]. The reaction mixture containing 0.5 mL pNPG and 0.5 mL enzyme solution was incubated at 50 °C for 10 min. The reaction was terminated by adding 2 mL 1 mol/mL Na_2CO_3. One unit (U) of β-glucosidase activity was defined as the amount of enzyme catalyzing the formation of 1 μmol p-nitrophenyl per minute.

Carboxymethyl cellulase was determined at 540 nm by measuring the increase in reducing sugar formed by enzymatic hydrolysis of sodium carboxymethyl cellulose [17]. One unit (U) of enzyme activity was expressed as the amount releasing 1 mg of glucose per mL of enzyme in 1 h.

Glucoamylase activity was determined at 540 nm by measuring the increase in reducing sugar formed by enzymatic hydrolysis of starch described previously [6]. One unit of enzyme activity was expressed as the amount releasing 1 μmol of glucose per milliliter of enzyme per minute.

Lignin peroxidase activity was measured using veratryl alcohol oxidation [18]. The standard reaction mixture (2 mL) contained 0.2 mmol veratryl alcohol, 0.15 mmol H_2O_2, and 11.4 nmol LiP in 100 mmol/L sodium tartrate buffer pH 3.0. The reaction was assayed at 310 nm. One unit (U) of enzyme activity was expressed as the amount of generating 1 μmol of oxidation of veratryl alcohol per minute.

54.3 Results and Discussion

54.3.1 The Optimization of Culture Conditions for DZW

In order to determine the optimum concentrations of DZW, inoculation size, initial pH, and cultivation time for diosgenin yield, mixed spore suspension was inoculated into fermentation medium that consisted of only DZW in tap water at different concentrations (16.67, 33.33, 41.67, 50.00, 58.33, and 66.67 g/L). The results show that diosgenin yield increased with increasing DZW concentrations up to 50.00 g/L and decreased with further increasing DZW concentrations (Fig. 54.2).

The inoculum size is also an important factor for diosgenin production. Inoculation size for DZW fermentation was optimized by inoculating the mixed spore suspension with 1.0, 1.5, 2.0, 2.0, 2.5, 3.0, and 3.5 mL. The results obtained are shown in Fig. 54.3. The highest yield of diosgenin was obtained with 2 mL spore suspension. Using spores for inoculation offered several benefits compared with vegetative cells. For instance, they can serve as a biocatalyst in bioconversion reactions because of their ability to carry out the same reactions as the corresponding mycelia [19, 20].

pH is important for fermentation process as it may affect various metabolic activities through its effect on several components transferred across the cell membrane [21]. The effect of initial pH on diosgenin yield by mixture fermentation was carried out at pH 3.5, 4.0, 4.5, 5.5, and 6.0. The results obtained are shown in

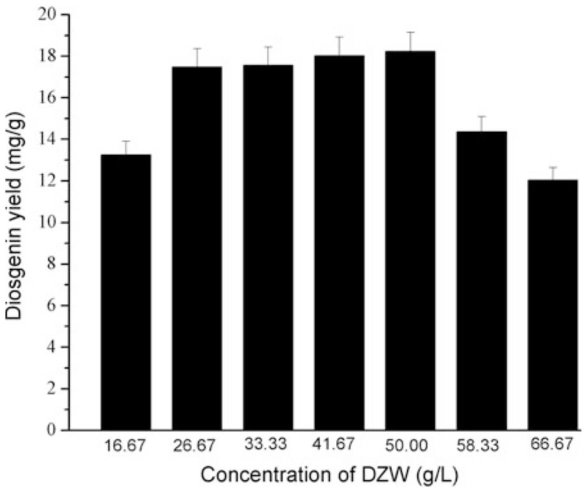

Fig. 54.2 The effect of DZW concentration on diosgenin yield by mixed culture (*A. oryzae*:*P. chrysosporium*: *A. niger* = 1:2:3); inoculum size: 2 mL; culture time: 4 days; unadjusted pH

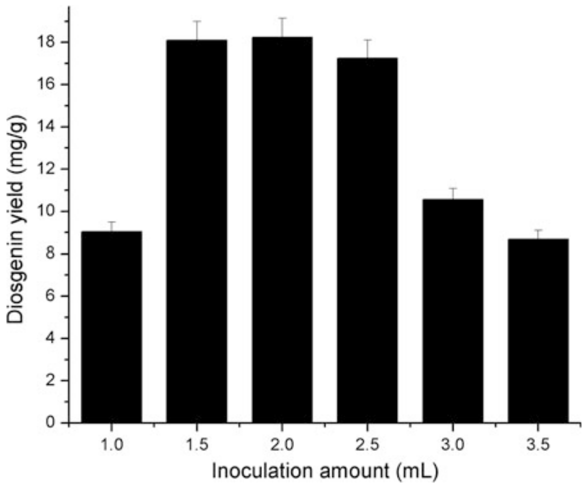

Fig. 54.3 The effect of inoculum size on diosgenin yield by mixed culture (*A. oryzae*:*P. chrysosporium*: *A. niger* = 1:2:3); DZW concentration: 50.00 g/L; culture time: 4 days; unadjusted pH

Fig. 54.4. Diosgenin yield gradually increased with increasing pH from 3.5 to 5.0 and reached the optimum level at 5.0.

The effects of culture time on diosgenin yield for mixture culture were carried out at different growth stages. The highest yield of diosgenin was obtained at 6 days, not changed in further increasing culture time (Fig. 54.5). The results of optimization showed that a combination of concentration of DZW 50.00 g/L, inoculation size 2.0 mL, initial pH 5.0, and cultivation time 6 days, the diosgenin yield was 40.06 ± 0.53 mg/g. The final diosgenin yield of optimization process increased by 50.54 % compared to the traditional acid hydrolysis method for DZW production (26.61 ± 0.78 mg/g). The use of mixed culture of these fungi proposes an approach for more efficient and clean diosgenin production from *D. zingiberensis*.

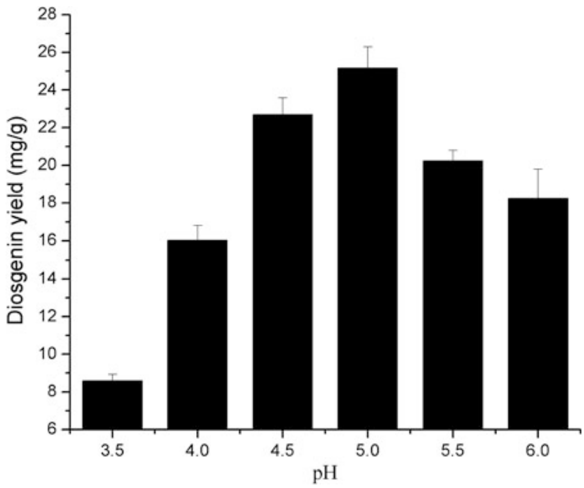

Fig. 54.4 The effect of initial pH on diosgenin yield by mixed culture (*A. oryzae*: *P. chrysosporium*:*A. niger* = 1:2:3); DZW concentration: 50.00 g/L; inoculum size: 2 mL; culture time: 4 days

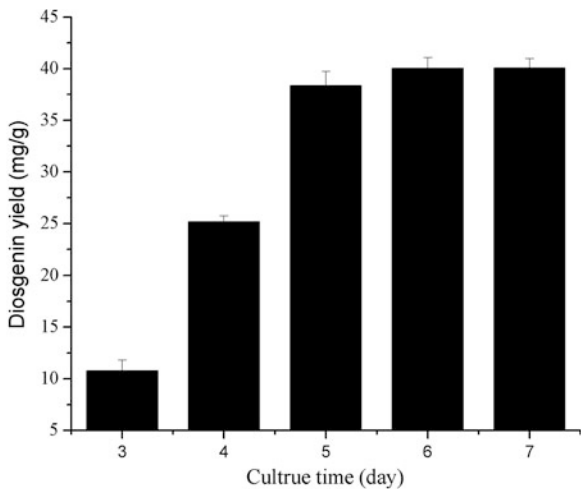

Fig. 54.5 The effect of culture time on diosgenin yield by mixed culture (*A. oryzae*:*P. chrysosporium*: *A. niger* = 1:2:3); DZW concentration: 50.00 g/L; inoculum size: 2 mL; initial pH: 5.0

54.3.2 Biotransformation of Monoculture and Mixed Culture

In the optimized conditions, as shown in Fig. 54.6, the diosgenin yield using monoculture of *A. oryzae*, *P. chrysosporium*, and *A. niger* and the mixed culture were 28.44 ± 0.89, 12.59 ± 0.67, 30.67 ± 0.23 and 40.06 ± 0.53 mg/g, respectively, after 6 days of fermentation. The final diosgenin yield of optimization process increased by 28.58, 68.57, and 23.44 % compared to that using monoculture of *A. oryzae*, *P. chrysosporium*, and *A. niger*. The results showed that the mixed culture system gave better results than monocultures for diosgenin production. The mixed culture obviously depends more on a multiple enzymatic hydrolysis strategy

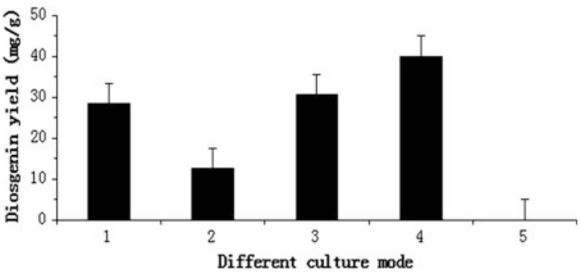

Fig. 54.6 The results of hydrolyzed product by monoculture (*1 A. oryzae*, *2 P. chrysosporium*, *3 A. niger*), mixed culture (*4 A. oryzae*:*P. chrysosporium*:*A. niger* = 1:2:3), and control (*5* not inoculation fungus). DZW concentration: 50.00 g/L; Inoculum size: 2 mL; initial pH: 5.0 the diosgenin was extracted with chloroform after culturing for 6 days

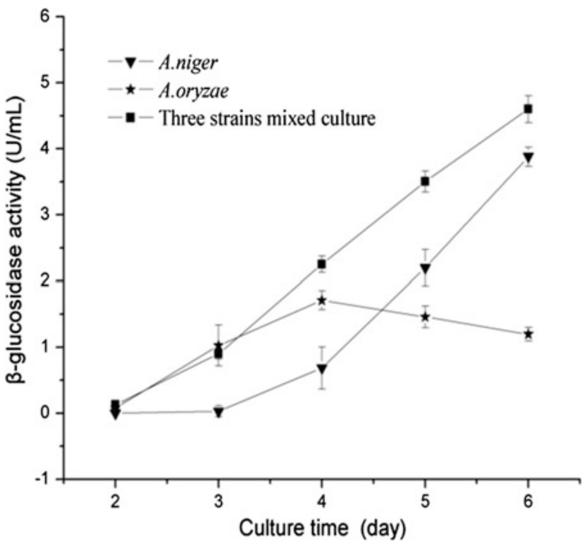

Fig. 54.7 The β-glucosidase activity of by *A. oryzae* or *A. niger* monoculture and by mixed culture (*A. oryzae*: *P. chrysosporium*:*A. niger* = 1:2:3). DZW concentration: 50.00 g/L; inoculum size: 2 mL; initial pH: 5.0 the β-glucosidase activity of *P. chrysosporium* was undetectable

for decomposition of DZW cellulose, lignin, and for transformation of saponins. The multiple enzyme system contains β-glucosidase, cellulase, glucoamylase, and lignin peroxidase which has a direct or indirect effect on production of diosgenin.

The β-glucosidase activity by mixed culture was higher than by *A. niger* or *A. oryzae* monoculture (Fig. 54.7). This result was in agreement with that of Raza et al. who reported that mixed cultures of *A. oryzae* and *A. niger* gave better production yield of β-glucosidase than single culture [22]. β-Glucosidase is one of the key glycosidases for conversion of saponin to diosgenin. Lei et al. reported

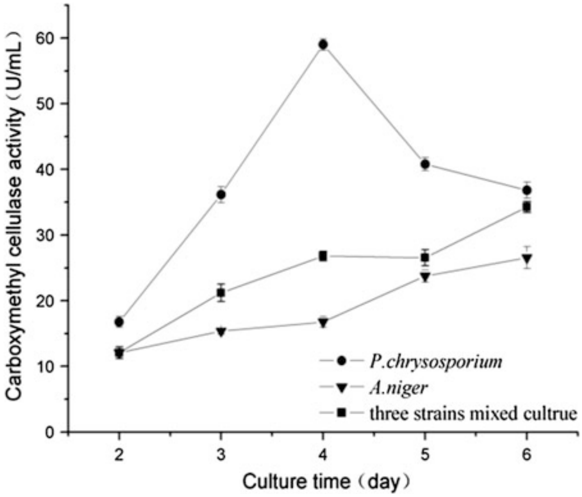

Fig. 54.8 The carboxymethyl cellulase activity of by *A. niger* or *P. chrysosporium* monoculture and by mixed culture (*A. oryzae*:*P. chrysosporium*:*A. niger* = 1:2:3). DZW concentration: 50.00 g/L; inoculum size: 2 mL; initial pH: 5.0. the carboxymethyl cellulase activity of *A. oryza* was undetectable

that β-glucosidase from *Aspergillus fumigates* could hydrolyze terminal a-1,2-linked glucopyranosyl of saponins [16]. In addition, Su et al. reported a novel β-glucosidase from *Fusarium proliferatum* ECU 2042 exhibiting almost no activity toward cellobiose, but showing relatively high activity on ginsenoside Rg3 [23].

Filamentous fungi possess powerful abilities to decompose the extensive plant material lignocellulose, and are unique organisms specified to degradation of the xylem cell wall components (cellulose, hemicelluloses, lignins and extractives) [24]. *P. chrysosporium*, the most widely researched white-rot fungus, produces two families of lignin-degrading peroxidases designated lignin peroxidase and manganese peroxidase [25, 26]. *P. chrysosporium* not only produced carboxymethyl cellulase production (Fig. 54.8), but also secreted lignin peroxidase (188.03 ± 18.95 U/L) for degrading the lignin of the DZW, thus playing an important role in generating saponins.

Furthermore, as shown in Fig. 54.9, *A. oryzae* secreted both β-glucosidase and glucoamylase. Glucoamylase from *Curvularia lunata* and *A. niger* were shown to be capable of hydrolyzing the terminal 1,2-linked rhamnosyl residues of sugar chains at C-3 position of steroidal saponins [6, 27]. Thus glucoamylase could be used to increase diosgenin yield.

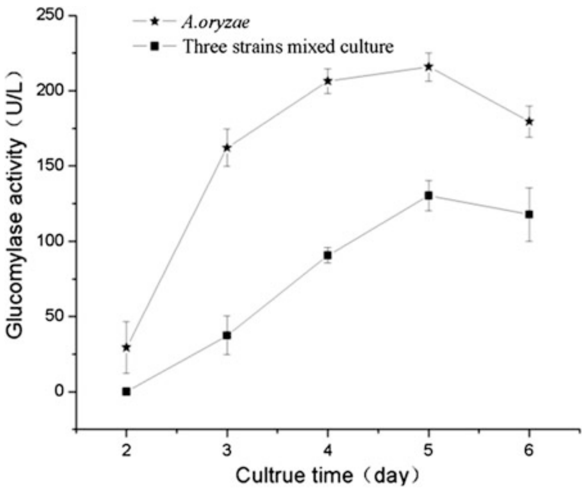

Fig. 54.9 The glucoamylase activity of by *A. oryzae* monoculture and by mixed culture (*A. oryzae*: *P. chrysosporium*:*A. niger* = 1:2:3). DZW concentration: 50.00 g/L; inoculum size: 2 mL; initial pH: 5.0 the glucoamylase activity of *P. chrysosporium* and *A. niger* was undetectable

54.4 Conclusion

The potential of mixed culture with *A. oryzae*, *P. chrysosporium,* and *A. niger* for optimal diosgenin production was demonstrated. In the optimized conditions, the maximum production of diosgenin was 40.06 ± 0.53 mg/g, an increase of 50.54 % compared to the acid hydrolysis method for DZW production (26.61 ± 0.78 mg/g). The mixed culture system gave better results than monocultures regarding diosgenin production.

Acknowledgments This work was financially supported by The Tianjin Science and Technology Support Plan Project (10ZCKFSH0060) and the Natural Science Foundation of China (No. 20906071).

References

1. Alam MZ, Fakhru'l-Razi A, Abd-Aziz S, Iris A (2001) Bioconversion of wastewater sludge by immobilized microbial treatment. In: Proceedings of international water association (IWA) conference on water and waste water management for developing countries, Kuala Lumpur, Malaysia, pp 344–353
2. Fernandes P, Cruz A, Angelova B, Pinheiro HM, Cabral JMS (2003) Microbial conversion of steroids compounds: recent developments. Enzyme Microb Technol 32:688–705
3. Li M, Hu S, Wang Y et al (2010) Optimizated conditions of acid-microorganism-enzyme co-degradation to process residue of Dioscorea zingiberensis saponin production. Acta Agric Boreali-Occidentalis Sin 19:196–201
4. Zhu Y, Ni J, Huang W (2010) Process optimization for the production of diosgenin with *Trichoderma reesei*. Bioproc Biosyst Eng 33:647–655
5. Qian SH, Yuan LH, Yang NY, Ouyang PK (2006) Study on steroidal compounds from Dioscorea zingiberensis. Zhong Yao Cai 29:1174–1176

6. Feng B, Hu W, Ma BP et al (2007) Purification, characterization, and substrate specificity of a glucoamylase with steroidal saponin-rhamnosidase activity from *Curvularia lunata*. Appl Microbiol Biotechnol 76:1329–1338
7. Feng B, Huang HZ, Zhou WB et al (2010) Substrate specificity, purification and identification of a novel pectinase with the specificity of hydrolyzing the α-1,4-glycosyl residue in steroidal saponin. Process Biochem 45:1383–1392
8. Inoue K, Ebizuka Y (1996) Purification and characterization of furostanol glycoside 26-O-beta-glucosidase from Costus speciosus rhizomes. FEBS Lett 378:157–160
9. Liu W, Huang W, Sun W et al (2010) Production of diosgenin from yellow ginger (*Dioscorea zingiberensis* C.H. Wright) saponins by commercial cellulase. World J Microbiol Biotechnol 26:1171–1180
10. Zhao HZ, Cheng P, Zhao B et al (2008) Yellow ginger processing wastewater treatment by a hybrid biological process. Process Biochem 43:1427–1431
11. Wen H, Zhao HZ, Ni JR et al (2008) The best utilization of *D. zingiberensis* C.H. Wright by an eco-friendly process. Bioresour Technol 99:7407–7411
12. Alvarez G, Pabon A, Carmona J et al (2004) Evaluation of clastogenic potential of the antimalarial plant Solanum nudum. Phytother Res 18:845–848
13. Dong YS, Teng H, Qi SS et al (2010) Pathways and kinetics analysis of biotransformation of Dioscorea zingiberensis by *Aspergillus oryzae*. Biochem Eng J 52:123–130
14. Liu L, Dong YS, Qi SS et al (2010) Biotransformation of steroidal saponins in *Dioscorea zingiberensis* C.H. Wright to diosgenin by *Trichoderma harzianum*. Appl Microbiol Biotechnol 85:933–940
15. Pettit RK (2009) Mixed fermentation for natural product drug discovery. Appl Microbiol Biotechnol 83:19–25
16. Lei J, Niu H, Li T et al (2012) A novel β-glucosidase from *Aspergillus fumigates* releases diosgenin from spirostanosides of *Dioscorea zingiberensis* C.H. Wright (DZW). World J Microbiol Biotechnol 28:1309–1314
17. Ghose TK (1987) Measurement of cellulase activities. Pure Appl Chem 59:257–268
18. del Pilar CM, Ander P, Stenström J (1997) Lignin and manganese peroxidase activity in extracts from straw solid substrate fermentations. Biotechnol Tech 11:701–706
19. Krishna C (2005) Solid-state fermentation systems—an overview. Crit Rev Biotechnol 25:1–30
20. Lazim H, Mankai H, Slama N et al (2009) Production and optimization of thermophilic alkaline protease in solid-state fermentation by *Streptomyces* sp. CN902. J Ind Microbiol Biotechnol 36:531–537
21. Moon SH, Parulekar SJ (1991) A parametric study of protease production in batch and fed-batch cultures of *Bacillus firmus*. Biotechnol Bioeng 37:467–483
22. Raza F, Raza NA, Hameed U (2011) Solid state fermentation for the production of β-glucosidase by co-culture of *Aspergillus niger* and *A. oryzae*. Pak J Bot 43:75–83
23. Su JH, Xu JH, Yu HL et al (2009) Properties of a novel β-glucosidase from *Fusarium proliferatum* ECU2042 that converts ginsenoside Rg_3 into Rh_2. J Mol Catal B Enzym 57:278–283
24. Lundell TK, Mäkelä MR, Hildén K (2010) Lignin-modifying enzymes in filamentous basidiomycetes-ecological, functional and phylogenetic review. J Basic Microbiol 50:5–20
25. Gold MH, Kuwahara M, Chiu AA et al (1984) Purification and characterization of an extracellular H_2O_2-requiring diarylpropane oxygenase from the white rot basidiomycete, *Phanerochaete chrysosporium*. Arch Biochem Biophys 234:353–362
26. Heinzkill M, Bech L, Halkier T et al (1998) Characterization of laccases and peroxidases from wood-rotting fungi. Appl Environ Microbiol 64:1601–1606
27. Feng B, Kang L, Ma B et al (2007) The substrate specificity of a glucoamylase with steroidal saponin-rhamnosidase activity from *Curvularia lunata*. Tetrahedron 63:6796–6812

Chapter 55
Characterization of Volatile Constituents of Chinese Hawthorn (*Crataegus* spp.) Fruit Juices

Yuping Zhao, Yangyang Wang, Jiwu Wang, Zhilian Wu, Zuli Sun, Tiantian Tian, Hao Niu, Lili Jing, Zhengyu Fang and Jianrong Yang

Abstract All hawthorn fruits used in this study were collected from four provinces of the China namely Shandong, Shanxi, Hebei, and Liaoning. Hawthorn fruits were prepared for hawthorn fruit juices. Volatile compounds in the juices of 12 cultivars of hawthorn were determined by gas chromatography and mass spectrometry (GC–MS) coupled with headspace solid-phase micro-extraction (HS–SPME) method. Semi-quantitative analysis was employed for the analysis of volatile constituents in hawthorn juice. Among 61 volatile compounds detected in the 12 samples, 21 volatiles were found in all samples. Esters and alcohols were the main volatiles present in the hawthorn fruit. Aldehydes, aromatic compounds, furans, terpenes, acids, and sulfurs also made great contributions to the total volatiles of the hawthorn fruits. Ethyl acetate, 3-methylbutanol, 3-octanone, acetic acid, furfural, dimethyl sulfide, and *p*-menth-1-en-8-ol were suggested to the major volatile compounds in all samples. For most volatile compounds identified in the current research, their content in sample 7 was highest than the others and the sample with lowest contents was sample 6.

Keywords Hawthorn fruit · Volatile constituents · Gas chromatography-mass spectrometry · Headspace solid-phase micro-extraction

55.1 Introduction

Hawthorn fruits, which are well known for their health benefits, are used as raw materials in the field of food and medicine [3, 13]. Hawthorn is considered as a "cardiotonic" herb and has been used in traditional medicine to reduce the risk of

Y. Zhao (✉) · Y. Wang · Z. Sun · T. Tian · H. Niu · L. Jing · Z. Fang · J. Yang
Institute of Life Science, Yantai University, Yantai 264005, Shandong, People's Republic of China
e-mail: water15689@163.com

J. Wang · Z. Wu
LvJie Company Limited, Longkou 265718, People's Republic of China

T.-C. Zhang and M. Nakajima (eds.), *Advances in Applied Biotechnology*,
Lecture Notes in Electrical Engineering 333, DOI 10.1007/978-3-662-46318-5_55

cardiovascular diseases such as chest pain, irregular heartbeat, and congestive heart failure [1, 14]. The hypolipidemic, free radical scavenging effects and anti-inflammatory potentials of hawthorn have also been reported, together with their vasorelaxing and antioxidative activities [21]. Such wide beneficial effects have been mainly attributed to the presence of phenolic compounds. As one of the commonly cultivated varieties, hawthorn fruits have long been consumed by Chinese and the long history of application supports their health and safety benefits [8].

In China, hawthorn is widely distributed, such as Shandong, Liaoning, Henan, Hunan, and Shanxi provinces. Hawthorn, belonging to the Rosaceae family, involves 18 species in China, of which *Crataegus pinnatifida* Bge. and its variety Shanlihong (*C. pinnatifida*. Bge. var. major N.E.Br.) are the most important [9]. Chinese hawthorn fruit presents intense and unique aroma which influences the acceptability and flavor of formulation of various food products including jam, confect, juice, and canned food [19].

Previous studies have determined the antioxidant activity, phenolic compounds, acids, and sugars of the hawthorn [1–13]. However, to the best of our knowledge, there is to date little research determining the flavor of hawthorn fruits [6, 15]. Hence, our research is focused on the qualitative and quantitative analysis of volatile components in 12 cultivars hawthorn fruits. The analytical technique used to determine aromatic compounds of hawthorn fruits is headspace solid phase microextraction combined with gas chromatography-mass spectrometry (HSSPME–GC–MS). From a practical standpoint, the research was performed to provide sufficient information for further study of volatile components in hawthorn fruits and the development of hawthorn fruit products.

55.2 Materials and Methods

55.2.1 Plant Materials

All hawthorn fruits used in this research were collected in China and picked at commercial maturity during the harvest season. Samples 1–2 were collected in Yantai city and Weifang city of Shandong province. Samples 3–5 were collected in Jincheng city, Yuncheng city and Linfen city of Shanxi province. Samples 6–9 were collected in Chengde city, Baoding city, Zhangjiakou city, and Cangzhou city of Heibei province. Samples 10–12 were collected in Anshan city, Dalian city, and Shenyang city of Liaoning province.

55.2.2 Chemicals

The pectic enzyme preparation was purchased from Novozymes Co. LTD in China (Beijing, China). Sodium chloride was obtained from China National

Pharmaceutical Ground Corporation (Shanghai, China). The internal standard (IS) solution of 3-octanol used in the GC–MS analysis was purchased from Aldrich (Milwaukee, Wis., USA). All other chemicals used were of analytical grade.

55.2.3 Preparation of Hawthorn Juice

The hawthorn juice was prepared according to the method proposed by Zhao et al. [21].

55.2.4 HS–SPME Analysis

A portion of 5 mL hawthorn juice, saturated with 2.0 g of sodium chloride was added into a 20 mL headspace vial spiked with 5 μL of 3-octanol (101 mg/L standard solution in ethanol), and a 10 mm stirring bar. The vial capped a Teflon-faced silicone septum and was placed in a thermostat bath adjusted to 50 °C with constant agitation in a magnetic stirrer for 10 min.

The fiber of 50/30 μm DVB/CAR/PDMS employed in the analyses was obtained from Supelco (Aldrich, Bellefonte, PA, U.S.A.). Before extraction, the fiber was conditioned by being inserted into the GC injector at the 250 °C for 2 h to prevent contamination. After that, the fiber was exposed to the headspace of the prepared glass vial for 15 min. Finally, the fiber was immediately inserted into the injection port of GC at 250 °C for thermal desorption over 5 min.

55.2.5 GC–MS Analysis

GC–MS analyses were carried out using an Agilent 6890 N gas chromatograph fitted with an Agilent 5975 mass selective detector. The above extraction was analyzed on a DB-Wax column (30 m × 0.25 mm i.d., 0.25 μm film thickness, J&W Scientific, Folsom, CA) and the injection technique was splitless. The carrier gas was helium with a constant flow of 2 mL/min. The injector and detector temperature were both 250 °C. The analysis conditions were programmed with an initial temperature of 40 °C for a 2 min hold, then to 230 °C at 4 °C/min with a 5 min hold. Electron ionization mass spectrometric data from *m/z* 34 to 348 were recorded with an ionization voltage of 70 eV and the temperature of ion source was 230 °C.

55.2.6 Compound Identification

A majority of compounds were identified by comparison of their mass spectra and retention times with those of standard compounds or by comparison of the mass spectrum with those in the National Institute of Standards and Technology (NIST) 05 MS database or a custom database [20].

55.2.7 Quantitative Analysis

Semi-quantitative analysis was employed for the determination of volatile component in hawthorn juice. The IS solution (3-octanol) was individually prepared in ethanol and stored at 4 °C prior to analysis in GC–MS. All analyses were carried out in triplicate, so the average was taken as the final peak area. The integral for all chromatogram peaks used selective ion method (SIM) [2, 12].

$$\text{Semi-quantitative concentrations} = (\text{peak area}/\text{IS peak area}) \times \text{IS concentration} \tag{55.1}$$

55.2.8 Statistical Analysis

The results were reported as means of three parallel measurements. Statistical analysis was conducted using the SPSS version 19.0 statistical package for windows (SPSS Inc., Chicago, Illinois).

55.3 Results and Discussion

For a better characterization of the volatile components of the hawthorn juice, a detailed research by GC–MS was conducted. Table 55.1 presents the corresponding volatile composition identified in the hawthorn juice, along with the relative concentrations in the extract. A total of 61 primary volatile compounds were identified and quantified, including 11 esters, 16 alcohols, 12 aromatic compounds, 8 terpenes, 5 furans, and 4 carboxylic acids, 4 ketones, 1 sulfur. According to semi-quantitative concentrations, esters and alcohols had higher concentrations among the volatiles in 12 hawthorn juices, followed by the sulfurs, terpenes, and aromatic compounds.

Table 55.1 Volatile compounds identified in 20 Chinese hawthorn juices by GC–MS analysis

Compounds	Concentration (mg/L)					
	1	2	3	4	5	6
Alcohols						
Methyl alcohol	1.259	0.754	0.887	1.044	1.065	0.777
2-Methyl-3-buten-2-ol	0.224	0.356	0.154	0.093	0.213	0.329
2-Methyl-1-propanol	0.022	0.049	0.020	0.065	0.052	0.008
1-Butanol	0.018	n.i.	n.i.	0.015	0.073	n.i.
3-Methyl-1-butanol	1.056	1.381	0.890	3.285	1.765	0.288
1-Pentanol	0.223	0.484	0.195	0.078	0.190	0.192
1-Hexanol	0.163	0.229	0.096	0.335	0.291	0.163
3-Hexen-1-ol	0.128	0.153	0.061	0.084	0.119	0.084
1-Heptanol	n.i.	n.i.	0.093	0.528	0.119	n.i.
2-Ethyl-1-hexanol	0.159	0.078	0.040	0.454	0.125	0.071
(*E*)-2-Hepten-1-ol	0.009	0.015	0.017	n.i.	n.i.	0.016
1-Octanol	0.061	0.114	0.121	0.085	0.167	0.102
(*Z*)-5-Octen-1-ol	n.i.	n.i.	0.012	0.260	0.006	n.i.
1-Nonanol	0.063	0.026	0.013	0.221	0.047	0.016
(*E*,*Z*)-3,6-Nonadien-1-ol	0.019	n.i.	n.i.	0.086	n.i.	n.i.
3-Methyl-2-buten-1-ol	0.217	0.382	0.103	0.216	0.106	0.192
Totals	3.612	4.021	2.702	6.849	4.338	2.238
Esters						
Methyl acetate	1.247	n.i.	2.752	1.290	n.i.	0.813
Ethyl acetate	9.027	3.888	3.641	6.995	6.833	3.070
2-Methylpropyl acetate	n.i.	0.105	0.038	0.520	0.072	n.i.
Butyl acetate	0.022	0.108	0.006	0.017	0.050	0.061
2-Methyl-1-butanyl acetate	0.098	0.881	0.811	0.232	0.172	0.266
3-Methyl-1-butanyl acetate	0.021	n.i.	n.i.	0.010	0.274	0.542
Ethyl hexanoate	0.077	0.093	0.006	0.063	n.i.	0.049
(*Z*)-3-Hexenyl acetate	n.i.	n.i.	n.i.	0.024	n.i.	n.i.
2-Furanmethanyl acetate	0.066	0.020	0.056	n.i.	n.i.	0.037
Methyl benzoate	0.135	0.056	0.015	0.051	0.061	0.027
1.2-Ethyl-3-hydroxyhexyl 2-methylpropanoate	0.073	0.037	0.079	0.054	0.017	0.014
Totals	10.766	5.188	7.404	9.256	7.479	4.879
Aldehydes and ketones						
3-Octanone	0.013	0.415	0.055	0.017	0.066	0.192
3-Hydroxy-2-butanone	0.016	0.040	n.i.	0.063	0.036	0.003
6-Ethyl-7-hydroxy-4-octen-3-one	0.100	0.061	0.103	0.028	0.039	n.i.

(continued)

Table 55.1 (continued)

Compounds	Concentration (mg/L)					
	1	2	3	4	5	6
6-Methyl-5-hepten-2-one	0.020	0.083	0.039	0.014	0.075	0.042
Totals	0.149	0.599	0.197	0.122	0.216	0.237
Compounds	Concentration (mg/L)					
	7	8	9	10	11	12
Alcohols						
Methyl alcohol	1.076	0.625	0.832	3.281	0.840	0.683
2-Methyl-3-buten-2-ol	0.114	0.118	0.470	0.151	0.088	0.215
2-Methyl-1-propanol	0.043	0.062	n.i.	0.209	0.008	0.024
1-Butanol	n.i.	0.047	n.i.	0.033	0.067	0.006
3-Methyl-1-butanol	0.517	0.270	0.294	6.040	0.213	0.457
1-Pentanol	0.657	0.606	0.102	0.317	0.223	0.331
1-Hexanol	0.182	0.145	0.127	0.207	0.104	0.289
3-Hexen-1-ol	0.077	0.048	0.110	0.136	0.056	0.237
1-Heptanol	0.157	n.i.	n.i.	0.427	n.i.	n.i.
2-Ethyl-1-hexanol	0.412	0.021	0.030	0.282	0.061	0.135
(*E*)-2-Hepten-1-ol	0.010	0.039	n.i.	0.033	0.005	0.018
1-Octanol	0.093	0.074	0.072	0.307	0.058	0.102
(*Z*)-5-Octen-1-ol	n.i.	0.025	n.i.	0.015	n.i.	n.i.
1-Nonanol	n.i.	n.i.	0.005	0.078	n.i.	0.046
(*E*,*Z*)-3,6-Nonadien-1-ol	n.i.	n.i.	n.i.	n.i.	n.i.	n.i.
3-Methyl-2-buten-1-ol	0.075	0.270	0.006	0.073	0.163	0.735
Totals	3.413	2.35	2.048	11.589	1.886	3.278
Esters						
Methyl acetate	1.531	n.i.	0.543	2.732	0.569	0.767
Ethyl acetate	9.001	4.728	4.106	7.897	4.504	2.329
2-Methylpropyl acetate	n.i.	n.i.	n.i.	n.i.	n.i.	n.i.
Butyl acetate	0.662	0.563	0.011	0.038	0.081	0.043
2-Methyl-1-butanyl acetate	3.278	0.820	n.i.	0.435	0.231	0.939
3-Methyl-1-butanyl acetate	3.486	0.078	1.234	0.417	0.961	1.588
Ethyl hexanoate	n.i.	0.098	n.i.	0.105	0.048	0.695
(*Z*)-3-Hexenyl acetate	n.i.	n.i.	n.i.	n.i.	n.i.	n.i.
2-Furanmethanyl acetate	0.009	0.058	0.033	0.063	0.038	0.104
Methyl benzoate	0.019	0.038	0.026	0.046	0.010	0.112
1.2-Ethyl-3-hydroxyhexyl 2-methylpropanoate	0.274	0.011	0.022	0.128	0.019	0.057
Totals	18.26	6.394	5.975	11.861	6.461	6.634

(continued)

Table 55.1 (continued)

Compounds	Concentration (mg/L)					
	7	8	9	10	11	12
Aldehydes and ketones						
3-Octanone	0.814	0.066	0.119	0.049	0.223	0.063
3-Hydroxy-2-butanone	0.021	0.023	0.052	0.075	n.i.	n.i.
6-Ethyl-7-hydroxy-4-octen-3-one	n.i.	n.i.	n.i.	n.i.	n.i.	n.i.
6-Methyl-5-hepten-2-one	0.009	0.098	0.082	0.059	0.088	0.142
Totals	0.844	0.187	0.253	0.183	0.311	0.205
Compounds	Concentration (mg/L)					
	1	2	3	4	5	6
Aromatic compounds						
1-Methyl-3-(1-methylethyl)benzene	0.009	0.075	0.062	0.031	n.i.	0.062
Acetic acid phenyl methyl ester	0.010	0.009	0.026	0.032	n.i.	n.i.
Methoxy-phenyl-oxime	0.037	0.008	n.i.	0.017	0.025	0.013
2-Methyl-3-phenylpropanal	0.146	0.072	0.034	0.330	n.i.	0.008
Acetic acid 2-phenylethyl ester	0.089	0.009	0.053	0.021	n.i.	0.044
α,α,4-Trimethyl-benzene methanol	0.118	0.104	0.088	0.111	0.072	0.078
Benzyal alcohol	n.i.	n.i.	n.i.	0.026	n.i.	n.i.
Phenyl ethyl alcohol	0.009	0.007	0.012	0.036	0.015	n.i.
Benzothiazole	0.009	0.004	0.010	0.028	n.i.	n.i.
Phenol	0.059	0.006	0.011	0.391	0.007	n.i.
2-Ethyl phenol	0.025	0.029	0.004	0.034	0.017	n.i.
Phenol, 2-methoxy-3-(2-propenyl)	0.024	0.005	0.008	0.077	0.012	0.007
Totals	0.535	0.328	0.308	1.134	0.148	0.212
Terpenes						
Eucalyptol	0.012	0.030	0.007	0.013	0.005	n.i.
3,7-Dimethyl-1,6-Octadien-3-ol	0.108	0.279	0.290	0.466	0.175	0.247
1-Methyl-4-(1-methylethyl)-3-Cyclohexen-1-ol	0.061	0.042	0.019	n.i.	0.027	0.030
4-Methyl-1-(1-methylethyl)- 3-cyclohexen-1-ol	0.253	0.622	0.145	0.308	0.161	0.174
1-Methyl-4-(1-methylethenyl)-cyclohexanol	0.080	0.034	0.019	0.101	0.039	0.025
p-Mentha-1,8-dien-6-ol	0.082	0.131	0.117	0.149	0.104	0.091
(*Z*)-3,7-Dimethyl-2,6-Octadien-1-ol	n.i.	0.014	0.016	0.018	n.i.	n.i.
p-Menth-1-en-8-ol	0.841	0.928	0.694	0.308	0.467	0.880
Totals	0.596	1.152	0.613	1.055	0.511	0.567
Furans						
5-Methyl-2(3H)-furanone	0.012	n.i.	0.003	0.011	0.016	0.004
Furfural	0.627	0.170	n.i.	n.i.	0.076	0.128
5-Methyl-2-furancarboxaldehyde	0.138	0.009	0.004	0.632	n.i.	n.i.
2-Furanmethanol	0.061	n.i.	n.i.	0.155	n.i.	n.i.

(continued)

Table 55.1 (continued)

Compounds	Concentration (mg/L)					
	1	2	3	4	5	6
5-Hydroxymethyl-2-furancarboxaldehyde	0.043	0.009	0.012	0.028	n.i.	n.i.
Totals	0.881	0.188	0.019	0.826	0.092	0.132
Acids						
Acetic acid	0.361	0.151	0.103	1.739	0.107	0.129
Propanoic acid	0.045	0.078	0.005	0.059	n.i.	n.i.
2-Methyl-butanoic acid	0.072	0.035	0.014	0.756	0.040	0.019
Octanoic acid	0.006	n.i.	0.003	0.059	n.i.	n.i.
Totals	0.484	0.264	0.125	2.613	0.147	0.148
Sulfurs						
Dimethyl sulfide	0.814	0.855	0.610	0.686	1.571	0.784
Totals	0.814	0.855	0.610	0.686	1.571	0.784
Compounds	Concentration (mg/L)					
	7	8	9	10	11	12
Aromatic compounds						
1-Methyl-3-(1-methylethyl)benzene	0.038	0.055	n.i.	0.147	0.067	0.090
Acetic acid phenyl methyl ester	0.041	n.i.	n.i.	0.016	n.i.	0.021
Methoxy-phenyl-oxime	0.026	0.015	n.i.	0.072	0.008	0.024
2-Methyl-3-phenylpropanal	0.140	0.013	0.017	0.044	0.004	0.024
Acetic acid 2-phenylethyl ester	0.108	0.003	0.019	0.051	0.012	0.020
α,α,4-Trimethyl-benzene methanol	0.027	0.079	0.106	0.058	0.066	0.068
Benzyal alcohol	n.i.	n.i.	n.i.	n.i.	n.i.	n.i.
Phenyl ethyl alcohol	0.030	n.i.	n.i.	0.158	0.007	0.013
Benzothiazole	0.060	0.004	n.i.	0.005	n.i.	0.020
Phenol	0.037	0.007	0.006	0.027	n.i.	0.018
2-Ethyl phenol	n.i.	n.i.	n.i.	0.016	n.i.	n.i.
Phenol, 2-methoxy-3-(2-propenyl)	0.042	0.007	n.i.	0.011	0.005	0.008
Totals	0.549	0.183	0.148	0.605	0.169	0.306
Terpenes						
Eucalyptol	0.127	0.015	n.i.	0.543	0.003	0.018
3,7-Dimethyl-1,6-Octadien-3-ol	0.239	0.195	0.220	0.241	0.232	0.287
1-Methyl-4-(1-methylethyl)-3-Cyclohexen-1-ol	0.018	0.030	0.027	0.034	0.013	0.022
4-Methyl-1-(1-methylethyl)- 3-cyclohexen-1-ol	0.109	0.162	0.187	0.148	0.122	0.141
1-Methyl-4-(1-methylethenyl)-cyclohexanol	0.027	0.023	0.021	0.033	0.015	0.020
p-Mentha-1,8-dien-6-ol	0.057	0.091	0.116	0.125	0.077	0.059
(*Z*)-3,7-Dimethyl-2,6-Octadien-1-ol	n.i.	n.i.	n.i.	0.022	n.i.	0.024
p-Menth-1-en-8-ol	0.336	0.581	0.854	0.345	0.617	0.577
Totals	0.577	0.516	0.571	1.146	0.462	0.571

(continued)

Table 55.1 (continued)

Compounds	Concentration (mg/L)					
	7	8	9	10	11	12
Furans						
5-Methyl-2(3H)-furanone	0.021	n.i.	0.012	0.033	0.004	n.i.
Furfural	0.057	0.134	0.126	n.i.	0.086	0.352
5-Methyl-2-furancarboxaldehyde	0.077	0.020	n.i.	n.i.	n.i.	0.048
2-Furanmethanol	n.i.	n.i.	n.i.	n.i.	n.i.	n.i.
5-Hydroxymethyl-2-furancarboxaldehyde	0.038	n.i.	n.i.	n.i.	n.i.	0.010
Totals	0.193	0.154	0.138	0.033	0.09	0.41
Acids						
Acetic acid	0.022	0.221	n.i.	0.211	0.066	0.215
Propanoic acid	0.025	n.i.	0.036	0.035	n.i.	n.i.
2-Methyl-butanoic acid	n.i.	0.003	0.029	0.018	0.008	0.021
Octanoic acid	0.024	n.i.	n.i.	0.009	n.i.	0.008
Totals	0.071	0.224	0.065	0.273	0.074	0.244
Sulfurs						
Dimethyl sulfide	2.125	0.051	0.501	0.195	0.838	0.475
Totals	2.125	0.051	0.501	0.195	0.838	0.475

n.i. Not identified

55.3.1 Esters

Esters contribute to the "fruity" and "floral" sensory properties, along with sweet, pineapple, apple, and rose odors [4, 7]. The total concentration of the esters in all samples (100.6 mg/L) was greater than the other volatile compounds accounting for 55 % of the total volatile compounds, so esters were the most important volatile compounds in the hawthorn juices. According to the results reported by Gao [5], esters were also the most abundant volatiles in the hawthorn fruits accounting for 78.41 % of the total volatile compounds. As seen in Table 55.1, a total of 16 esters were detected in the hawthorn juices and ethyl acetate, butyl acetate, methyl benzoate, and 1,2-ethyl-3-hydroxyhexyl 2-methylpropanoate were the most common compounds.

The total ester content of the juice ranged from 4.879 to 18.26 mg/L. The highest ester contents were found in sample 7 (18.26 mg/L) and the sample with lowest ester contents was sample 6 (4.879 mg/L). In the current study, ethyl acetate was present at levels of 2.329–9.027 mg/L, the most abundant volatile ester in practically all samples. Methyl acetate was second most abundant ester in the samples accounting for 12.2 % of the total volatile esters; its largest concentration was found in sample 3, while the lowest was with sample 9. The other important esters detected in most samples included 2-methyl-1-butanyl acetate (0.098–3.278 mg/L) and 3-methyl-1-butanyl acetate (0.01–3.486 mg/L).

55.3.2 Alcohols

Alcohols were the second most abundant volatile group in the tested samples. A total of 16 alcohols were identified in the 12 hawthorn juices. Among these compounds, methyl alcohol, 2-methyl-3-buten-2-ol, 3-methyl-1-butanol, 1-pentanol, 1-hexanol, 3-hexen-1-ol, 2-ethyl-1-hexanol, 1-octanol, and 3-methyl-2-buten-1-ol were found in all samples. The total alcohol content of the hawthorn juices ranged widely from 1.886 to 11.589 mg/L. Sample 10 had the highest alcohol content, while, the lowest was detected in Sample 11. Two alcohols, i.e., 3-methyl-1-butanol, methyl alcohol were considered as predominant alcohol compounds (concentration ≥10 mg/L) in all hawthorn juices. Of these, 3-methylbutanol, imparting a fusel-like odor [11], was the most important volatile alcohol due to its highest concentration. Its largest amount (6.04 mg/L) was detected in sample 10.

55.3.3 Sulfurs

Dimethyl sulfide was the only sulfur detected in all tested samples which imparted juices unpleasant flavors, such as cooked onion, rubber, garlic, and asparagus. Although the low contents, sulfur plays an important role in the flavor profile of juices because of the low sensory threshold values [10]. The content of dimethyl sulfide varied from 0.051 to 2.125 mg/L. High sulfur contents were found in sample 7, while the sample with low sulfur contents was sample 8.

55.3.4 Terpenes

Terpenes own a very pleasant aroma and low olfactory threshold, so they are easy to perceive, even at low concentrations [16]. A total of eight terpenes were identified in all tested samples including eucalyptol, 3,7-dimethyl-1,6-Octadien-3-ol, *p*-menth-1-en-8-ol, 1-methyl-4-(1-methylethyl)-3-Cyclohexen-1-ol, 4-methyl-1-(1-methylethyl)-3-Cyclohexen-1-ol, 1-methyl-4-(1-methylethenyl)-cyclohexanol, *p*-mentha-1,8-dien-6-ol and (*Z*)-3,7-dimethyl-2,6-octadien-1-ol. Total values of this group showed higher levels in sample 2 (2.08 mg/L) and the lowest level in sample 7 (0.913 mg/L).

3,7-Dimethyl-1,6-octadien-3-ol, 4-methyl-1-(1-methylethyl)-3-cyclohexen-1-ol, *p*-mentha-1, 8-dien-6-ol, 1-methyl-4-(1-methylethenyl)-cyclohexanol and *p*-menth-1-en-8-ol were found in all tested samples, which accounted for 92.4 % of the total terpenes. *p*-Menth-1-en-8-ol was the key terpenes and detected in sample 2 with highest concentrations (0.928 mg/L) in this study.

55.3.5 Aromatic Compounds

A total of 12 aromatic compounds were found in all samples. The total aromatic compounds content of the samples ranged from 0.148 to 1.134 mg/L. Its largest concentration was found in sample 4, whereas, its lowest level was with sample 5. Aromatic compounds contribute to the honey aroma in juice [17]. Although accounting for 2.4 % of the total volatile compounds, aromatic compounds were very important to the sensory characteristics of juice because of their high perception thresholds. Among this group, α,α,4-trimethyl-benzene methanol and 2-methyl-3-phenylpropanal were the predominate representatives according to their higher contents. Only one aromatic compound, i.e., α,α,4-trimethyl-benzene methanol was detected in all samples.

55.3.6 Acids

The volatile acids which usually contribute to rancid and sweaty odors did not damage the flavor of beverages [18]. The total acid content varied between 0.065 and 2.613 mg/L. Sample 5 had the highest acid among all sample, whereas sample 15 had the lowest. In all 20 samples, only 4 carboxylic acids (acetic acid, propanoic acid, 2-methyl-butanoic acid and octanoic acid) were detected using SPME because of their poor affinity with the SPME fiber [11]. Acetic acid, which had the largest content in sample 5 (1.739 mg/L) was the major acids in tested samples. 2-Methyl-butanoic acid was detected in all tested samples except sample 13.

55.3.7 Furans

Fives furans were found by HS–SPME in the hawthorn juices, including 5-methyl-2(3H)-furanone, furfural, 5-methyl-2-furancarboxaldehyde, 2-furanmethanol, 5-hydroxymethyl-2-furancarboxaldehyde. The total content of these compounds in sample 3 and sample 10 were far less than the other samples. 2-Furanmethanol was only found in sample 1 and 4 by our research. Furfural, responsible for sweet and almond-like aroma [18], could be the major furan compounds in all samples due to its largest content. The largest concentration of furfural was found with sample 1 (0.627 mg/L) and the lowest was in sample 7 (0.057 mg/L).

55.3.8 Ketones

The total ketone content of the samples ranged from 0.122 to 0.844 mg/L. Its largest concentration was found in sample 7, whereas, its lowest level was with sample 4.

A total of four ketones were identified in the 12 hawthorn juices, including 3-octanone, 3-hydroxy-2-butanone, 6-ethyl-7-hydroxy-4-octen-3-one, and 6-methyl-5-hepten-2-one. 3-Octanone and 6-methyl-5-hepten-2-one were common in all samples. The most abundant ketone was 3-octanone which had a concentration of 0.013–0.814 mg/L in these samples. The highest concentration was detected in sample 7 and the lowest was in sample 1.

55.4 Conclusions

This research provides much information about the volatile compositions of 12 hawthorn juices. A total of 61 volatile compounds were identified by GC–MS in all tested samples, including 16 alcohols, 12 aromatic compounds, 11 esters, 8 terpenes, 5 furans, 4 carboxylic acids, 4 ketones, and 1 sulfur. 21 volatiles were detected in all samples.

Esters and alcohols made great contributions to the total volatiles comparing with ketones, acids, furans, sulfurs, terpenes, and aromatic compounds. Ethyl acetate, 3-methylbutanol, 3-octanone, acetic acid, furfural, dimethyl sulfide, and *p*-menth-1-en-8-ol were suggested to the predominant volatile compounds in all samples according to their higher concentrations. For most volatile compounds detected in the current study, their content in sample 7 was higher than other samples.

Generally, the volatile compositions of the 12 hawthorn juices tested in this work were rather different and the major reasons for the differences among these hawthorn juices were due to the hawthorn species. The hawthorn fruits of different species can be distinguished according to the valuable information provided by the study.

References

1. Sokol-Letowska A et al (2007) Antioxidant activity of the phenolic compounds of hawthorn, pine and skullcap. Food Chem 103:853–859
2. Caven Q et al (2006) Comparison of micro-scale simultaneous distillation–extraction and stir bar sorptive extraction for the determination of volatile organic constituents of grape juice. J Chromatogr A 1117:121–131
3. Chang Q et al (2002) Hawthorn. J Clin Pharmacol 42:605–612
4. Fang Y et al (2005) Aroma compounds in Oregon Pinot Noir wine determined by aroma extract dilution analysis (AEDA). Flavour Frag J 20:22–29
5. Gao TT et al (2013) Analysis of volatile components in fresh hawthorn by solid-phase micro-extraction combined with gas chromatography-mass spectrometry. Food Sci 34(20):144–147
6. Gao Z et al (2013) GC/MS analysis of flavoring components of hawthorn wine. Liquor-Making Sci Technol 8:95–97

7. Gurbuz O et al (2006) Comparison of aroma volatiles in commercial Merlot and Cabernet Sauvignon wines using gas chromatography–olfactometry and gas chromatography–mass spectrometry. J Agric Food Chem 54:3990–3996
8. Liu PZ et al (2010) Acids, sugars, and sugar alcohols in Chinese hawthorn (*Crataegus* spp.) fruits. Agric Food Chem 58:1012–1019
9. Liu PZ et al (2011) Quantitative analysis of phenolic compounds in Chinese hawthorn (*Crataegus* spp.) fruits by high performance liquid chromatography–electrospray ionisation mass spectrometry. Food Chem 127:1370–1377
10. Mestres M et al (2000) Analysis of organic sulfur compounds in wine aroma. J Chromatogr A 881:569–581
11. Molina AM et al (2009) Differential synthesis of fermentative aroma compounds of two related commercial wine yeast strains. Food Chem 117:189–195
12. Mo XL et al (2009) Changes in volatile compounds of Chinese rice wine wheat qu during fermentation and storage. J Inst Brew 115:300–307
13. Qu FX et al (2012) Study on the adsorption kinetics of organic acids and total flavonoids in hawthorn fruit juice. Sci Technol Food Ind 33(22):109–112
14. Song JP et al (2012) Degrading organic acids in hawthorn fruit juice by D301G resin. Acad Periodical Farm Prod Process 5:43–45
15. Xie BJ et al (1997) Studies on volatile compounds of hawthorn. Food Ferment Ind 23 (2):42–46
16. Zhao YP et al (2009) Profile of volatile compounds in 11 brandies by headspace solid-phase micro-extraction followed by gas chromatography-mass spectrometry. J Food Sci 74:90–99
17. Zhao YP et al (2011) Comparison of volatile compounds in two brandies using HS–SPME coupled with GC–O, GC–MS and sensory evaluation. S Afr J Enol Vitic 32:9–20
18. Zhao YP et al (2012) A comparison of the influence of eight commercial yeast strains on the chemical and sensory profiles of freshly distilled Chinese brandy. J Inst Brew 118:315–324
19. Zhao YP et al (2012) Enrichment of flavonoids and removal of organic acid by treatment of weak-base anion resins. Proc Int Conf Appl Biotechnol 176:1645–1655
20. Zhao YP et al (2013) Characterization of volatiles in the six most well-known distilled spirits. Am Soc Brew Chem 71(3):161–169
21. Zhao YP et al (2013) The screening of resins reducing organic acids in hawthorn fruit juice. Food Res Dev 34(4):57–60

Chapter 56
Optimization of Extraction Conditions for Crude Antibacterial Proteins/Peptides from *Clarias gariepinus* By-products

Yan Wang, Yunxia Xu, Junyan Mei, Chengxun Chen and Xiaomei Wang

Abstract In this paper, acetic acid was used for extracting crude antimicrobial proteins/peptides from by-products of healthy *Clarias gariepinus* reared at high stocking density. For the extraction process, three variables, namely the concentration of acetic acid, extraction time, and the ratio of liquid to solid were optimized by using orthogonal design $L_9(3^3)$ with the yield and antibacterial activity of the crude proteins/peptides extracts as test indices. The yields of extracted crude proteins were analyzed by range analysis. The results showed that the yield of crude proteins/peptides was different among nine groups, the highest was group 7, producing 1.5842 g (dialyzed in 1,000 MWCO and lyophilized) per 100 g raw material. All the nine extracted samples had similar inhibitory activity against *Aeromonas hydrophila, Escherichia coli*, *Staphylococcus aureus, Citrobacter* sp., and *Microbacterium* sp. except that groups 7 and 9 exhibited higher inhibitory activity against *A. hydrophila* and *E. coli*; moreover, the inhibitory activity of group 7 was higher than group 9 against the two bacteria strains. Nine groups did not display obvious different patterns on the SDS-PAGE gel. Based on these results above, the final conclusion was that group 7, namely 10 % acetic acid, 12 h extraction, and 5:1 liquid to solid ratio was the best combination for isolating the crude antimicrobial proteins/peptides from by-products of *C. gariepinus*.

Keyword *C. gariepinus* · By-product · Antimicrobial proteins/peptides · Yield · Acetic acid · Bacteriostatic test · Electrophoresis

---

Y. Wang · J. Mei · C. Chen · X. Wang (✉)
College of Fisheries, Tianjin Agricultural University, Tianjin Key Laboratory of Aqua-Ecology & Aquaculture, No. 22, Jinjing Street, Xiqing District, 300384 Tianjin, China
e-mail: xiaomeiw@tjau.edu.cn

Y. Xu
Tianjin Aquatic Animal Infectious Disease Control and Prevention Center, 300221 Tianjin, China

T.-C. Zhang and M. Nakajima (eds.), *Advances in Applied Biotechnology*, Lecture Notes in Electrical Engineering 333, DOI 10.1007/978-3-662-46318-5_56

56.1 Introduction

The first antibacterial protein is reported and named cecropin by Steiner [1]. It is becoming clear that antimicrobial proteins or peptides are an abundant and diverse group of molecules produced by many tissues and cell types in various organisms and are an important component of the innate immune system of all species of life [2, 3]. Such proteins or peptides display stable physical and chemical properties, broad-spectrum antimicrobial activity, and do not induce bacterial resistance.

Fish are aquatic creatures, which are constantly exposed to relatively high concentrations of bacteria, virus, and fungi, many of them that may be harmful to the fish. Under normal conditions fish maintain a healthy state by especially heavily relying on innate defenses for initial protection against pathogen invasion [4]. Antimicrobial proteins or peptides are among the earliest developed molecular effectors of innate immunity and are significant in the first line of host defense response of diverse invaders [5]. It is generally acknowledged that raising fish at relatively high stocking densities means maximizing the usage of fish production infrastructure and is an effective measure for improving farm profitability [6]. However, this results in disease outbreaks in farmed fish and causes significant losses in aquaculture. To avoid economic loss caused by disease, chemicals and antibiotics are being used as prophylactic and therapeutic agents. The inevitable residues of the agent in the end product, in addition to being harmful to consumer's health, the use of antibiotics can also result in the development of resistant strains of bacterial pathogens [7]. The evolution of resistance of pathogenic bacteria to currently available antibiotics has stimulated enormous efforts to develop alternative antimicrobial agents from alternative natural sources to prevent and control disease [8]. Because antimicrobial proteins or peptides have some properties, especially, they kill bacteria very rapidly and their mode of action is considered unlikely to lead to development of resistance, they may be possibly exploited as promising candidates for new antibiotics [9]. However, because of extraction of natural antibacterial proteins or peptides from tissue with lower yield and higher processing cost, researchers need to make heroic efforts at better yields and cost reduction for the wide application of natural antibacterial proteins or peptides.

African catfish, *Clarias gariepinus* is native to the River Nile of Africa and was introduced to China in 1981. It has become an economically important aquaculture species in China owing to its fast growth and high disease resistance. The latter property of this fish might be attributed to its innate immunity system. In previous work published from our laboratory, it was mentioned that many bioactive antibacterial compounds, obtained with gradient ammonium sulfate fractionation, presented in skin mucus, skin, gill, suprabranchial organ, and intestine of *C. gariepinus* [10]. In contrast to other cultured fish, *C. gariepinus* has little intermuscular bones, processing products of muscles of the fish have good color and elasticity, so a certain proportion of commercial size individuals have been circulated to aquatic products processing factories and there are a large number of by-products during the process. The purpose of this study was, by applying acetic acid as extract solvent, to gain a better protocol for isolating crude antibacterial proteins/peptides from by-products of *C. gariepinus*.

56.2 Materials and Methods

56.2.1 Fish and Sample Collection

Healthy *C. gariepinus* obtained from Deren aquaculture center, Tianjin, China, was maintained in static aerated tanks at a stocking density of 180 kg/m^3 at temperature of 25 ± 1 °C. Fish weight were 359.7–588.9 g at the time of sampling.

By-products including gill, suprabranchial organ, and viscera, such as hepatopancreas, spleen, kidney, digestive tract, and head kidney were collected and pooled for proteins/peptides isolation. Before sampling, experimental fish were anesthetized with a sub-lethal dose of tricaine methanesulphonate (MS222, sigma). The organs obtained above were flushed gently with cold sterilized physiological saline and intestinal contents were flushed out gently. The collected samples were stored at −20 °C for the subsequent protein extraction.

56.2.2 Extraction of Crude Antibacterial Proteins/Peptides

Acetic acid was used for extracting crude antibacterial proteins/peptides from *C. gariepinus* by-products. In this study, the concentration of acetic acid, extraction time, and ratio of liquid to solid levels were chosen for independent variables. Orthogonal design L9 (3^4) [11] was used to optimize the extraction variables and the actual values of coded levels of each variable are shown in Table 56.1. Crude proteins/peptides were isolated from *C. gariepinus* by-products according to the procedure reported by Ji et al. [12] with some modifications. 100 g of *C. gariepinus* by-products were homogenized in a certain volume and concentration of acetic acid, the homogenates were placed at 4 °C for a few hours and stirred frequently at the same time. After that the homogenates were centrifuged at 8,000 rpm for 30 min at 4 °C. The pellets were weighed and treated with acetic acid using the same protocol mentioned above. The supernatants obtained twice were mixed, incubated

Table 56.1 Three independent variables and their coded and actual values in the orthogonal design

Independent variables	Symbol	Coded levels		
		1	2	3
Concentration of acetic acid (%)	A	1	5	10
Extraction time (h)	B	12	24	36
The ratio of liquid to solid (mL/g)	C	1	2	5

in a water bath at 80 °C for 20 min and centrifuged at 8,000 rpm for 30 min at 4 °C for removing high molecular weight proteins. The supernatants were adjusted pH with 1 % NaOH to 7 and then lyophilized at 5 mbar and −60 °C (Alpha 2-4, Marin Christ Company, Germany). The lyophilized crude protein/peptide extracts were redissolved in sterile deionized water and dialyzed in 1,000 MWCO (molecular weight cut-off) dialysis bag against sterile deionized water for at least 24 h at 4 °C with tenfold changes of dialysis water. Crude protein/peptide extracts obtained were lyophilized again, then weighed and kept at −20 °C. The data of the yields of the crude proteins/peptides were analyzed using range analysis method [11].

56.2.3 Antibacterial Activity Testing

Aeromonas hydrophila and *Escherichia coli* stored in Tianjin Aquatic Animal Infectious Disease Control and Prevention Center (Tianjin, China), *Staphylococcus aureus* purchased from Guangdong Microorganism Germplasm Resource Bank (Guangzhou, China), *Citrobacter* sp. and *Microbacterium* sp. provided by Prof. Liying Sui of Tianjin University of Science and Technology (Tianjin, China) were used as the main test bacteria. All strains were maintained in LB media with 30 % glycerol at −80 °C. Before the experiments, strains were sub-cultured in LB media at optimal temperature to logarithmic phase, harvested by centrifugation at 5,000 rpm for 15 min at 4 °C, washed twice with sterilized physiological saline and resuspended, and finally counted using a Neubauer hemocytometer.

The lyophilized crude proteins/peptides extracts were resuspended in sterilized physiological saline, respectively, to give a concentration of 200 mg/mL. The bacteriostasis tests were conducted according to the procedure described previously [10]. Briefly, 20 mL of 1.5 % (w/v) agar in LB medium were poured into sterile petri dishes and a layer was formed. The bacterial suspension was added aseptically to 5 mL agar medium at 45 °C to a final concentration of approximately 10^6 cfu/mL, then mixed well and poured immediately to form the second layer. After hardening, sterile Oxford cups (7.8 mm outer diameter and 6 mm inner diameter) were placed on this bilayer medium. 200 μL of resuspended samples were separately pipetted into Oxford cups and allowed to diffuse for 12 h at 4 °C. After incubation for 24 h at appropriate temperatures for bacteria growth, such as *E. coli* and *S. aureus* at 37 °C, others at 30 °C, the activity was evaluated based on the diameter of the inhibition zone. 200 μL of sterile water and 200 μL of 25 μg/mL oxytetracycline hydrochloride were used as negative and positive controls, respectively, for all assays. All inhibition assays and controls were carried out in triplicate.

56.2.4 Electrophoresis

SDS-polyacrylamide gel electrophoresis of Laemmli system was performed according to the method of Xia et al. [13] with some modifications. Acrylamide-bisacrylamide (30 % T, 2.67 % C) stock solution was used for making 15 % separating gel and 4 % stacking gel. 20 μg/μL crude proteins/peptides was mixed in equal volumes with protein loading buffer (4 % SDS, 8 % mercaptoethanol, 20 % glycerol, 0.05 % bromophenol blue, 100 mM Tris-HCl, pH 6.8), boiled for 10 min, and then loaded 10 μL supernatant to each well of the gel. Electrophoresis started with an initial current of 11 mA until the dye formed a line and maintained at this current for 20 min, and then ran at current of 24 mA until the dye front migrated to 1 cm from the bottom of the gel. After that, the gel was stained with 0.05 % Coomassie brilliant blue R-250 in 10 % acetic acid for 2 h and destained in 10 % acetic acid until clear bands were observed. The gel was transferred to deionized water for removing the acetic acid. The gel image was photographed with GeneSnap Version 6.0 software in the gel image system (GENEGENUS™, Syngene Company, UK).

56.3 Results

Nine samples of crude proteins/peptides extracted from by-products of *C. gariepinus* with acetic acid were obtained, and termed as group 1 to group 9 in order. The yields of the 9 groups and the range analysis results on yields are shown in Table 56.2.

In this paper, all of nine samples at concentration of 200 mg/mL exhibited antibacterial activity against all of the five tested bacterial strains (*A. hydrophila*, *E. coli*, *S. aureus*, *Citrobacter* sp. and *Microbacterium* sp.) by producing clear zones of inhibition, but all of the diameters of inhibition zone were the same as outer diameter of Oxford cup (results not shown) except that groups 7 and 9 exhibited bigger zones of inhibition against *A. hydrophila* and *E. coli* as shown in Fig. 56.1. The diameters of zone inhibition against *A. hydrophila* and *E. coli* produced by group 7 were 12.11 ± 0.27 and 10.10 ± 0.59 mm, respectively, while those produced by group 9 were separately 9.40 ± 0.43 and 9.35 ± 0.29 mm.

The SDS-PAGE profiles of *C. gariepinus* by-products extracts showed a broad range of proteins/peptides, including those of small proteins with molecular weights from 4.1 to 6.5 kDa that were abundant in each sample (Fig. 56.2).

56.4 Discussion

The ability of fish to avoid infection depends on their mechanisms of innate immunity. Antibacterial proteins or peptides are one of the key innate immune factors. *Clarias gariepinu* possess high disease resistance and fast growth rate at high stocking density, and bioactive antibacterial proteins or peptides exist in

Table 56.2 The yields of crude proteins/peptides and range analysis results on yields

Group no.	Coded levels				Yield (dialyzed lyophilized weight, g)
	A	B	C	Blank	
1	1	1	1	1	0.5028
2	1	2	2	2	0.626
3	1	3	3	3	0.4931
4	2	1	2	3	0.7002
5	2	2	3	1	1.3543
6	2	3	1	2	0.6564
7	3	1	3	2	1.5842
8	3	2	1	3	0.7692
9	3	3	2	1	0.7970
K_1	1.6219	2.7872	1.9284	2.6541	
K_2	2.7109	2.7495	2.1232	2.8666	
K_3	3.1504	1.9465	3.4316	1.9625	
$\overline{K}_1$	0.5406	0.9291	0.6428	0.8847	
$\overline{K}_2$	0.9036	0.9165	0.7077	0.9555	
$\overline{K}_3$	1.0501	0.6488	1.1439	0.6542	
R	0.5095	0.2802	0.5011	0.3014	
Best levels	A3	B1	C3		

K_1, K_2 and K_3 mean the sum of yields at the same level of each variable. $\overline{K}_1$, $\overline{K}_2$ and $\overline{K}_3$ = K_1, K_2 and K_s is divided respectively by n, here $n = 3$. R means range each variable, $R = \overline{K}_{max} - \overline{K}_{min}$

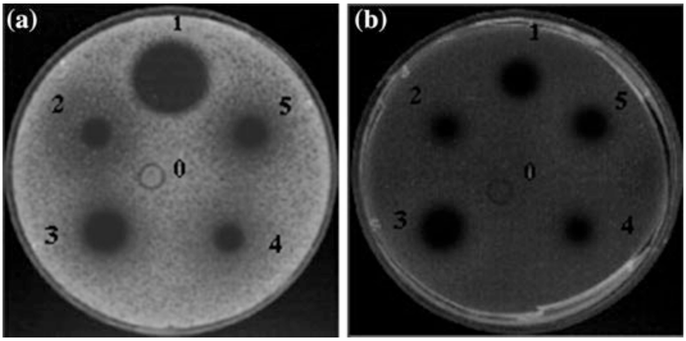

Fig. 56.1 Antimicrobial activity of crude proteins/peptides isolated from *Clarias gariepinus* by-products against *Aeromonas hydrophila* (**a**) and *Escherichia coli* (**b**). *Number 0 and 1* negative (*0*) and positive control (*1*), *Number 2–5* crude proteins/peptides samples, group 6–9

various tissues of the healthy bodies [10, 14]. Such fish are very good sources of antimicrobial proteins or peptides.

It is clearly noted that acid soluble proteins/peptides of *C. gariepinu* by-products showed different yields among 9 groups. The highest yield of the crude proteins/

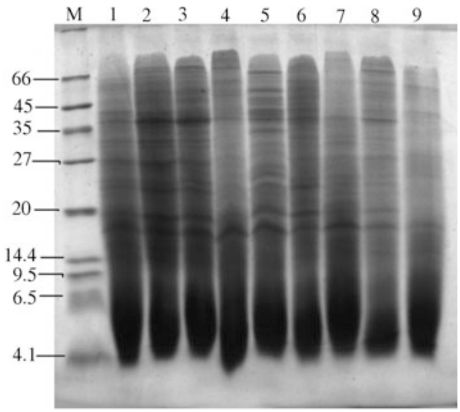

Fig. 56.2 Coomassie brilliant blue R-250 stained SDS-PAGE of soluble proteins extracted with acetic acid from *C. gariepinus* by-products. *Lane M* broad range protein markers. *Lane 1–9* crude proteins/peptides samples, group 1–9 extracted under the conditions shown in Table 56.2. Numbers on the *left side* of the gel correspond to the molecular weight of the markers in kDa

peptides extracted with group 7 condition (10 % acetic acid and 5:1 liquid to solid ratio for 12 h), was 1.5842 g (dialyzed in 1,000 MWCO and lyophilized) per 100 g raw material. According to the range analysis (Table 56.2), the values of R_A were greater than R_C and both were greater than R_D. This indicates that the concentration of acetic acid was the most influential factor, and the ratio of liquid to solid was the second one for yields of crude extracts. While the value of R_B was less than R_D, it means that the influence of extraction time on yields could not be proven in this study.

In this paper, groups 7 and 9 exhibited higher inhibitory activity against *A. hydrophila* and *E. coli*; moreover, the inhibitory activity of group 7 was higher than group 9 against the two bacterial strains. The observed variation in antimicrobial activity among 9 samples extracted under different conditions from same raw material in this paper was also observed in other organisms in previous research findings. For example, Jin et al. [15] reported that for *Rana chensinensis*, the highest antibacterial activity was from the sample extracted with pH 3.0 acetic acid at 0 °C and 22.5 of liquid to solid ratio for 24 h. Antibacterial peptides could be obtained from blue mussels (*Mytilus edulis*) by using 0.5 % acetic acid at 4 °C and 1 of liquid to solid ratio for 12 h [16]. These results indicate that different extraction protocols are suited for different organisms for extracting active antibacterial proteins or peptides.

From the image of the SDS-PAGE, it is obvious that there were a number of bands in each line, which were due to the extract samples not being subjected to any purification process. The homogeneous protein or peptide is obtained and the inhibitory activity against bacteria is improved through purification of the crude antibacterial proteins/peptides extracts [17, 18]. Further work is under progress in this laboratory for purification of active proteins or peptides and analysis of physical and chemical stability and antimicrobial activity of the purified samples, and the results will be reported in the near future.

According to the results of the yield of crude extracted proteins/peptides, antibacterial activity testing as well as SDS-PAGE in the present study, group 7 (10 % acetic acid, 12 h extraction and 5:1 liquid to solid ratio) had the best combinations for isolating the crude antimicrobial proteins/peptides from the by-products of *C. gariepinus*.

To our knowledge, this study is the first report on optimization of extraction conditions and bacteriostatic analysis of crude antimicrobial protein/peptide from by-products of healthy *C. gariepinus* in China. This study provides a scientific evidence, in other words, *C. gariepinus* can serve as a valuable source of antimicrobial proteins or peptides.

Acknowledgments This work was supported by a Science and Technology Planning Project of Tianjin (Extraction and identification of antibacterial peptides from African catfish, molecular characterization of some nonspecific immune factors of the fish). This work was supported by the Large-scale Instrument Foundation of Tianjin Agricultural University. We thank the personnel of Integrative Laboratory of College of Agronomy and Resource Environment for lyophilizing the extracted proteins/peptides samples.

References

1. Steiner H, Hultmark D, Engström Å et al (1981) Sequence and specificity of two antibacterial proteins involved in insect immunity. Nature 292(5820):246–248
2. Hancock REW, Scott MG (2000) The role of antimicrobial peptides in animal defenses. Proc Natl Acad Sci 97(16):8856–8861
3. Brogden KA (2005) Antimicrobial peptides: pore formers or metabolic inhibitors in bacteria? Nat Rev Microbiol 3(3):238–250
4. Ellis AE (2001) Innate host defense mechanisms of fish against viruses and bacteria. Dev Comp Immunol 25:827–839
5. Cole AM, Weis P, Diamond G (1997) Isolation and characterization of pleurocidin, an antimicrobial peptide in the skin secretions of winter flounder. J Biol Chem 272(18):12008–12013
6. Blancheton JP (2000) Developments in recirculation systems for Mediterranean fish species. Aquacult Eng 22(1–2):17–31
7. Grave K, Hansen MK, Kruse H et al (2008) Prescription of antimicrobial drugs in norwegian aquaculture with an emphasis on "new" fish species. Prev Vet Med 83(2):156–169
8. Beaulieu L, Thibodeau J, Desbiens M et al (2010) Evidence of antibacterial activities in peptide fractions originating from snow crab (*Chionoecetes opilio*) by-products. Probiotics Antimicro Prot 2:197–209
9. Haug T, Kjuul AK, Styrvold OB (2002) Antibacterial activity in *Strongylocentrotus droebachiensis* (Echinoidea), *Cucumaria frondosa* (Holothuroidea), and *Asterias rubens* (Asteroidea). J Invertebr Pathol 81:94–102
10. Wang X, Dai W, Xing K et al (2012) Antibacterial activities of antibacterial proteins/peptides isolated from organs and mucus of *Clarias gariepinus* reared at high stocking density. Adv Mater Res 455–456:455–460
11. Wang J (2006) Experimental design and SPSS application (in Chinese). Chemical Industrial Press, Beijing

12. Ji Y, Wang X, SU Y et al (2011) Isolation and characterization of a novel antimicrobial peptide from the gastrointestinal tract of large yellow croaker *Pseudosciaena crocea* (in Chinese). Oceanologia et Limnologia Sinica 42(3):448–454
13. Xia Q, Zeng R (2004) Protein chemistry and proteomics (in Chinese). Science Press, Beijing
14. Wang X, Dai W, Chen CH et al (2012) Antibacterial activities of antibacterial proteins/peptides isolated from organs and mucus of *Clarias gariepinus* reared at high stocking density. LNEE 137:303–309
15. Jin L, Ding ZH, Wang Q (2008) Optimization of extraction conditions for antimicrobial peptides from skin of *Rana chensinensis* (in Chinese). Food Sci 29(10):223–227
16. Li ZH, Zhang B, Gu M et al (2012) Isolation and purification of antibacterial peptides from mussel (in Chinese). J Anhui Agric Sci 40(10):5768–5770
17. Ernoult E, Bourreau A, Gamelin E et al (2010) A proteomic approach for plasma biomarker discovery with iTRAQ labelling and OFFGEL fractionation. J Biomed Biotechnol. doi:10.1155/2010/927917
18. Yuan D, Wang L, Hu Y (2001) Extraction and determination of antibiotic peptide from skin of forest frog (in Chinese). J Jilin Agric Univ 23(2):113–116

Chapter 57
Screening, Isolation, and Identification of *Bacillus coagulans* C2 in Pu'er Tea

Cuixia Feng, Zhongyuan Li, Kun Li, Minghui Zhang, Cuiqiong Wang, Xuegang Luo and Tongcun Zhang

Abstract Pu'er Tea is a popular post-fermented tea and has a variety of health benefits. Many microorganisms, especially lactobacillus, exist and play an important role in the fermentation process of Pu'er tea. In this study, we try to screen some lactobacillus by plate method from the Pu'er tea, and strain C2 with significant cycle isolated from Pu'er tea. 16S rRNA gene sequencing results showed that strain C2 had 99 % sequence similarity to that of the type strain of three *Bacillus coagulans* (NR 102791.1, CP002472.1, NR 115727.1), and the results show that methyl red test and V&P test were positive. Sugar fermentation test suggested that strain C2 produced acid but not gas, which is identical to *B. coagulans*. This study confirmed that lactic acid bacteria play a role in Pu'er tea fermentation.

Keywords Pu'er tea · *Bacillus coagulans* · 16S rRNA · Lactic acid bacteria

57.1 Introduction

Pu'er tea is a distinctive post-fermented tea produced mainly in Yunnan province, China. Modern clinical medicine has shown that Pu'er tea has a variety of healthcare functions in the human body, like lowering blood pressure, [1] reducing weight, [2] moderating the risk of cancer, [3], and preventing cardiovascular disease [4]. The large leaves of *Camellia sinensis* (*C. sinensis assamica*) were used as raw material, and it was further processed by a manufacturing technology called 'pile fermentation'. Complex biological transformations were implemented in this important fermentation process, Pu'er tea is characterized by its unique color, savory flavors, and aroma.

C. Feng · Z. Li · K. Li · M. Zhang · C. Wang · X. Luo · T. Zhang (✉)
Key Laboratory of Industrial Fermentation Microbiology, Ministry of Education and Tianjin City, College of Biotechnology, Tianjin University of Science and Technology, Tianjin, China
e-mail: tony@tust.edu.en

T.-C. Zhang and M. Nakajima (eds.), *Advances in Applied Biotechnology*,
Lecture Notes in Electrical Engineering 333, DOI 10.1007/978-3-662-46318-5_57

Previous studies have shown that many microorganisms play an important role in the fermentation process of Pu'er tea. Bacterial and fungal communities involved in Pu'er tea pile fermentation have also been reported, but the results obtained are different [5, 6]. A large number of studies show that fungi including yeast, *Aspergillus* sp., and *Penicillium* sp. were the dominant fungi in Pu'er tea samples. [7, 8]. Jeng [9] identified numerous *Actinomyces* such as *Actinoplanes* sp. and *Streptomyces* sp. in Pu'er tea. *Candida* sp. and *Aspergillus* sp. [10, 11] were also separately found to be dominant microbes in Pu'er tea. However, a metagenomic study [12] of Pu'er tea shows that the dominant microbes of Pu'er tea fermentation were bacteria and yeasts rather than molds accounting for the overwhelming majority of Eukaryota. These differences in microorganism communities are due to the different Pu'er tea samples [13]. In the previous study, several lactobacillus were isolated in the Pu'er tea which indicated that it played a role in the pile fermentation process. Lactobacillus is a major part of the lactic acid bacteria groups, which could convert lactose and other sugars into lactic acid. The production of lactic acid makes its environment acidic, which inhibits the growth of some harmful bacteria. In the human gastrointestinal tract, they could make up a small portion of the gut flora to regulate intestinal health [14]. In this study, we explored the useful lactic acid bacteria in Pu'er tea, *Bacillus coagulans* C2 was isolated, and the physiological and biochemical characters were identified.

57.2 Materials and Methods

57.2.1 Pu'er Tea Sample Collection

Pu'er tea samples of days 0, 15, 30, and 45 during pile fermentation were obtained from the courageous tea reprocessing factory in Yunnan, China. Each tea samples of different fermentation time were first soaked with sterile water for 30 min, and then centrifuged at 5,000 rpm for 10 min to remove the leaf residue. After filtration using six layers of gauze filter, the liquor samples containing the microbe, were used to isolate the probiotics.

57.2.2 Separation Probiotics

MRS medium, used to isolate the probiotics in the Pu'er tea, was purchased from Shanghai source Biotechnology Co. Ltd., which contains 2 % calcium carbonate and the final concentration of 10 ng/mL cycloheximide. Each tea liquor sample of 200 μL was coated on the solid MRS culture medium, and cultivated under 30 °C in an anaerobic incubator (Yiwu Refrigeration Factory, Zhejiang, China). After 48 h, the isolated clones with dissolved calcium which might produce acid was selected, and was cultured in MRS medium at 30 °C in an anaerobic incubator for further screening and identification. The isolated microorganisms were maintained in agar slants consisting of MRS medium supplemented with 2 % (w/v) agar.

The strain was by Gram staining test [15] and bacteria morphology was observed using a microscope.

57.2.3 DNA Extraction

Each isolated microbe with 5 mL medium was centrifuged at 12,000 rpm for 1 min to collect microbial cell. The cell residues were suspended by 750 μL CTAB-SDS lysis buffer at 55 °C for 1 h. The cell residues were suspended by 500 μL TE buffer (10 M Tris-HCl, 1 M ethylence diamine tetraacetic acid disodium salt), the cell lysis by 6 μL RNase enzymes (10 μg/μL), 30 μL lysozyme at 37 °C for 1 h, 30 μL 10 % SDS, 10 μL proteinase K (20 μg/μL) at 55 °C for 15 min, 100 μL 5 M NaCl, 80 μL CTAB/NaCl (10 % CTAB, 0.7 M NaCl) at 65 °C for 10 min. The DNA of the microbial cell was extracted by 750 μL phenol/chloroform/isoamyl alcohol (25:24:1), the supernatant of 300 μL was added to precooling of isopropyl alcohol and stored at −20 °C for 1 h. and centrifuged 12,000 rpm for 10 min. The residues was washed with 200 μL of 70 % ethanol twice, and then dissolved with 40 μL sterile water and stored at −20 °C. The extracted DNA was loaded on agarose and electrophoresed at 100 V for 30 min.

57.2.4 16S rRNA Sequencing of the Strain C2

Identification of the isolates was confirmed by 16S rRNA sequencing. DNA of the strain C2 was used as DNA template, the universal primer 27F (AGAGTTTGA TCCTGGCTCAG) and 1492R (TACGGCTACCTTGTTACGACTT) was used for amplification of 16S rRNA of these isolated microbes, and the product was approximately 1,600 bp. The PCR conditions were as follows: pre-heating at 94 °C for 5 min, 30 cycles of denaturation at 94 °C for 30 s, annealing at 55 °C for 30 s and extension at 72 °C for 2 min, and a final extension for 10 min at 72 °C. The PCR fragments were purified by agarose gel electrophoresis and PCR purification kit (TaKaRa Biotechnology Co. Ltd., China), and were ligated to the linearized vector pMD18-T (TaKaRa Biotechnology Co. Ltd., China). The ligated products were transformed into competent Escherichia coli DH5α cells and coated on the LB medime plate, which contained 100 μg/μL ampicillin. After culture at 37 °C overnight, the positive clone with correctly inserted PCR fragment was selected by PCR and was sequenced by Shanghai Invitrogen Technology Co. Ltd., China. The DNA sequences were analyzed using the BLAST program (http://blast.ncbi.nlm.nih.gov/Blast.cgi).

57.2.5 Physiological and Biochemical Identification

The strain C2 was cultured for 12 h. Sugar fermentation test, [14] methyl red reaction test, [15] V&P test [16] detected the physiological and biochemical characters of the strain C2.

57.3 Result

57.3.1 Isolation of LAB in Pu'er Tea

After being cultured at 37 °C for 48 h, about 25 clones showed a significant dissolved calcium cycle. Clone C2 shows the largest dissolved calcium cycle at the first and second screenings as shown in Fig. 57.1a. Gram staining test shows that C2 is Gram-positive bacteria (Fig. 57.1b).

57.3.2 DNA Extraction and 16S rRNA Identification

The DNA of strain C2 was successfully extracted and the correct size is shown in Fig. 57.2a. With strain C2 genome DNA as template, 16s rRNA sequence was successfully amplificated, and the PCR products verified by electrophoresis detection with nonspecific amplification (Fig. 57.2b). The PCR products were purified and ligated into PMD18-T vector, the positive clone was selected by PCR method, and the rRNA sequence of strain C2 was approximately 1,600 bp. Based on BLAST analysis, strain C2 shared 99 % identity with 16s rRNA sequence of

(a) (b)

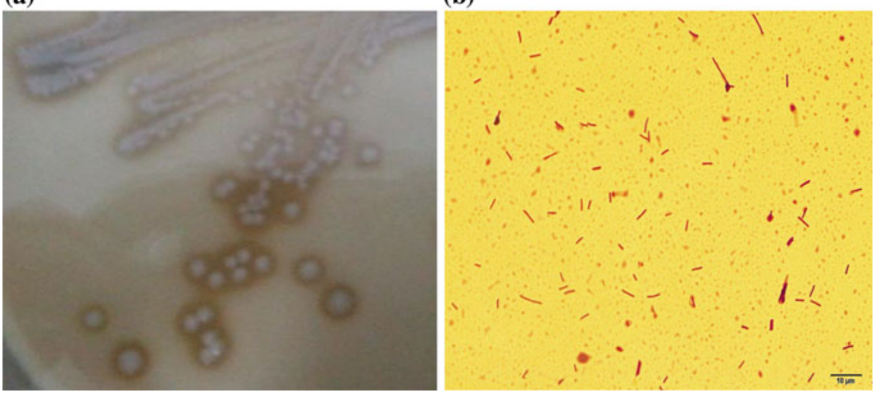

Fig. 57.1 Observed the morphology of strain C2. **a** Dissolved calcium *circle* of the culture medium. **b** The strain morphology was observed under a microscope

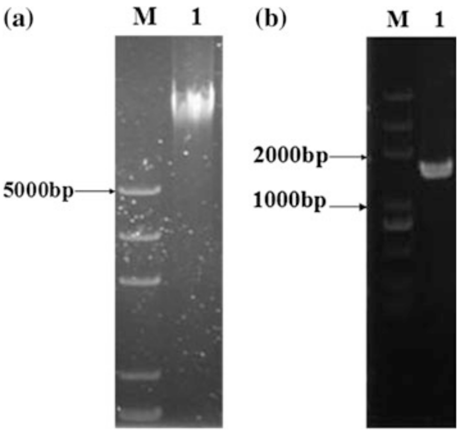

Fig. 57.2 DNA extraction and 16s rRNA identification. **a** DNA extracted from strain C2. **b** PCR product of 16s rRNA gene sequence of strain C2

B. Coagulans, (NR 102791.1, CP002472.1, NR 115727.1), which suggests strain C2 belongs to the *B. coagulans*. It was named *B. coagulan* C2 (KM980629).

57.3.3 Physiological and Biochemical Identification

Physiological and biochemical identification of strain C2 included sugar fermentation test, methyl red reaction test, V&P test, etc. The result shows methyl red test and V&P test was positive, sugar fermentation test suggested that the strain C2 produced acid but not gas. The experimental data are given in Fig. 57.3.

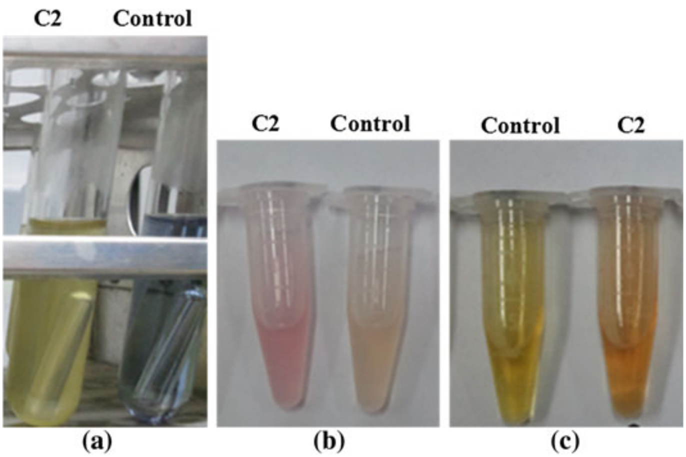

Fig. 57.3 The physiological and biochemical characteristics of strain C2. **a** Sugar fermentation test of strain C2. **b** Methyl red test of strain C2. **c** V&P test of strain C2

57.4 Conclusion

A large number of microorganisms in Yunnan's Pu'er tea has a very important effect on the human body. Probiotics in Pu'er tea plays a very important role. In our previous work, we were separated from probiotics in Pu'er Tea. We successfully isolated a strain C2. Strain C2 16s rRNA sequence by comparing gene bank, the strain C2 was identified as *B. coagulans*. The similarity is 99 %.

References

1. Anderson RA, Polansky MM (2002) Tea enchances insulin activity. J Agric Food Chem 50:7182–7186
2. Chiang CT, Weng MS, Lin-Shiau SY, Kuo KL, Tsai YJ, Lin JK (2005) Puerh tea supplementation suppresses fatty acid synthase expression in the rat liver through downregulating Akt and JNK signalings as demonstrated in human HepG2 cells. Oncol Res 16:119–128
3. Hayakawa S, Kimura T, Saeki K, Koyama Y, Aoyagi Y, Noro T et al (2002) Apoptosis-inducing activity of high molecular weight fractions of tea extracts. Biosci Biotechnol Biochem 65:459–462
4. Yang DJ, Hwang LS (2006) Study on the conversion of three natural statins from lactone forms to their corresponding hydroxy acid forms and their determination in Pu-erh tea. J Chromatogr A 1119:277–284
5. Pasha C, Reddy G (2006) Nutritional and medicinal improvement of black tea by yeast fermentation. Food Chem 89(3):449–453
6. Wen Q, Liu S (1991) Variation of the microorganism groups during the pile-fermentation of dark green tea. J Tea Sci 11:10–16
7. Abe M, Takaoka N, Idemoto Y, Takagi C, Imai T, Nakasaki K (2008) Characteristic fungi observed in the fermentation process for Puer tea. Int J Food Microbiol 124:199–203
8. Chen C, Ye Y, Kong X, Han B, Xiong X, Ge F et al (2011) A primary study on the thermophilic fungi from pile-fermentation of Pu-er tea. In: Proceedings of international symposium on medical informatics and education, pp 696–699
9. Jeng KC, Chen CS, Fang YP, Hou RC, Chen YS (2007) Effect of microbial fermentation on content of statin, GABA, and polyphenols in Pu-Erh tea. J Agric Food Chem 55:8787–8792
10. Zhou H, Li J, Zhao L, Han J, Yang X, Yang W et al (2004) Study on main microbes on quality formation of Yunnan puer tea during pile-fermentation process. J Tea Sci 24:212–218
11. Xu X, Yan M, Zhu Y (2005) Influence of fungal fermentation on the development of volatile compounds in the puer tea manufacturing process. Eng Life Sci 5:382–386
12. Lyu C, Chen C, Ge F, Liu D et al (2013) A preliminary metagenomic study of puer tea during pile fermentation. J Sci Food Agric 93(13):3165–3174
13. Zhao J, Chen Q, Huang X, Fang CH (2006) Qualitative identification of tea categories by near infrared spectroscopy and support vector machine. J Pharm Biomed Anal 41:1198–1204
14. Chen C, Zhang W, Lv C, Han B, Xiong X, Ge F et al (2011) Primary study on thermophilic during pile-fermentation of Pu-er tea. In: Proceedings of international symposium on medical informatics and education, pp. 691–695
15. Gram C (1884) Fortsch Der Medicine 2:185
16. Murray PR (2007) Manual O/F clincial microbilogy, 9th edn. ASM Press, Washington

Chapter 58
Production and Identification of Antifungal Compounds Produced by *Bacillus subtilis* B579

Fang Chen, Yu Zheng, Jianmei Luo, Deduo Han and Min Wang

Abstract Biological control has become an important approach to suppress many pathogens. *Bacillus subtilis* is considered to be an excellent biocontrol agent not only due to its ability on inducing plant systematic resistance, but also on producing various hydrolytic enzymes and antibiotics. In this study, polymerase chain reaction (PCR) was used to detect the 12 genes related to the antifungal compounds biosynthesis. Six genes were detected that exist in the genome DNA of B579 by the sequence homology analysis. Five genes were related to biosynthesis of lipopeptide antifungal compounds, and one gene was related to biosynthesis of protein antifungal compounds. Lipopeptide antifungal compounds were obtained from the supernatant of B579 using the method of acid deposition and methanol extraction. Two homologies with the molecular weight of *m/z* 1043.59 and *m/z* 1057.35 were detected in the lipopeptide antifungal compounds, which had the similar molecular weight with iturin A. Three homologies with the molecular weight of *m/z* 1008.32, *m/z* 1022.06, and *m/z* 1036.13 were detected in the lipopeptide antifungal compounds, which had the similar molecular weight with surfactin. The antifungal compounds produced by B579 could be of a good prospect for being used as a new tool for biological control.

Keywords *Bacillus subtilis* · Production · Identification · Antifungal compounds

---

F. Chen · D. Han
School of Pharmaceutical, Liaocheng University, Shandong 252059, China

Y. Zheng · J. Luo · M. Wang (✉)
Key Laboratory of Industrial Fermentation Microbiology, Ministry of Education, College of Bioengineering, Tianjin University of Science and Technology, Tianjin 300457, China
e-mail: minw@tust.edu.cn

T.-C. Zhang and M. Nakajima (eds.), *Advances in Applied Biotechnology*,
Lecture Notes in Electrical Engineering 333, DOI 10.1007/978-3-662-46318-5_58

58.1 Introduction

Soilborne disease was considered to be the major cause of yield loss on vegetable crops all over the world [1]. Pathogenic fungi, such as *Fusarium oxysporum* and *Rhizoctonia solani*, are soilborne and worldly distributed in many soil types [2]. They could infect plants through the roots, and eventually resulted in the wilt of entire plants. They could grow and survive in soil for long periods about 10–15 years as pathogenic saprophytes to many plant species, including cucumber, pepper, tomato and potato, throughout vegetable growing regions [3–6].

Synthetic chemical fungicides have long been used as active agents in reducing the incidence of soilborne diseases. However, they are costly, can cause environmental pollution, and may also induce pathogen resistance to chemical fungicides. Considering the limitations of chemical fungicides, it seems appropriate to search for a supplemental control strategy which was environmental friendly and safe to human being [7]. Biological control, the use of microorganisms or their secretions to prevent soilborne diseases, offers an attractive alternative or supplement to chemical fungicides for the management of soilborne plant diseases without the negative impact of chemical fungicides. It could also avoid the genetic resistance of pathogens to chemical fungicides. Therefore, biological control tactics have become an important approach to facilitating sustainable agriculture.

As *Bacillus subtilis* has the characteristics of omnipresence in soils, thermal tolerance, rapid growth, and ready formation of resistant spores, it is considered to be a good biological control agent. *B. subtilis* has a direct antagonistic activity not only by inducing plant systematic resistance [8], but also by producing various hydrolytic enzymes (for example, chitinase, β-1,3-glucanase) and antibiotics [9]. From the large amount of antimicrobials produced, lipopeptides stand among the most representative. *Bacillus* lipopeptides may be divided into three families—iturin, fengycin, and surfactin. These antifungal lipopeptides are either linear or cyclic. They frequently contain amino acid residues, which are unique and not commonly found in proteins, with high stability to pH, heat, and protease [10]. The specific hydrophobous section of the antifungal peptides could insert to the cell wall of hyphae, and resulted in the leakage of cytoplasm. Antifungal peptide TasA produced by *B. subtilis* is a translocation-dependent antimicrobial spore component. It could inhibit the growth of some relative bacteria [11]. These antifungal peptides have been proved safe to people and no pollution to environment [12, 13]. So, they have high potential for being used in biological control, food antisepsis, medicine, and so on.

Bacillus subtilis B579 (deposition number CGMCC No. 2270) was isolated from rhizosphere of cucumber in Tianjin, China. It could effectively inhibit the growth of 13 species plant pathogenic fungi, and exhibited a broad spectrum antifungal ability [14]. The primary objective of this study was to identify the antifungal compounds produced by B579. Genes involved in the biosynthesis of four families of antibiotics, surfactin, iturin, fengycin and TasA, were amplificated by polymerase chain reaction (PCR) with the genomic DNA of B579 as template. Lipopeptide antifungal compounds were obtained from the fermentation supernatant of B579, and were identified through HPLC and molecular weight.

58.2 Materials and Methods

58.2.1 Microorganisms and Growth Conditions

Bacillus subtilis B579 was grown in LB broth at 37 °C in a rotary shaker with 180 r/min for 24 h. They were maintained on LB agar plate at 4 °C. For antibiotic preparation, the synthetic medium was used with (g L^{-1}): dextrose, 10; DL-glutamic acid, 10; $MgSO_4 \cdot 7H_2O$, 1.02; K_2HPO_4, 1.0; KCl, 1.0; and 1 mL trace elements ($MnSO_4 \cdot H_2O$, 0.25; $CuSO_4 \cdot 5H_2O$, 8; and $FeSO_4 \cdot 7H_2O$, 0.0075 in 50 mL medium). The pH was adjusted to 7.5 prior to autoclaving. *B. subtilis* B579 was grown at 37 °C for 48 h with continuous shaking with 180 r/min.

58.2.2 PCR Conditions for Detection Antibiotic Biosynthesis-Related Genes

Genomic DNA of *B. subtilis* B579 and *B. subtilis* 168 were extracted by standard protocols [14]. The primers used in PCR were either previously described or designed with sequences obtained from GenBank using Primer Premier 5.0 (Table 58.1). PCR amplifications were carried out in 50 μL reaction mixtures containing 1 × PCR buffer (TaKaRa Inc. China), 2.5 mM $MgCl_2$, 1.5 U rTaq DNA polymerase (TaKaRa Inc. China), 400 nM of each forward and reverse primers, 200 μM dNTP (dATP, dGTP, dCTP, and dTTP), and 3 μL of template DNA (~100 ng of bacterial genomic DNA). The PCR were performed in a thermocycler (Bio-Rad 2001) with an initial denaturation at 94 °C for 5 min, followed by 30 cycles of denaturation at 94 °C for 1 min, annealing at 55 °C for 1 min, and extension at 72 °C for 1.5 min. There was a final extension at 72 °C for 10 min. Each amplification reaction was analyzed by electrophoresis using a 1.2 % agarose gel. Expected PCR products were eluted using the DNA purification kit (DingGuo Inc. China). The amplicons were sequenced by Invitrogen Co. Ltd. (Shanghai, China). The sequences were compared using the BLAST (http://www.ncbi.nlm.nih.gov/BLAST/) for identification of the homology.

58.2.3 Purification and Identification of Lipopeptide Antifungal Compounds

Antifungal compounds were extracted using the method of acid deposition and methanol extraction basically according to Bie et al. [15]. The antifungal activity

Table 58.1 PCR detection of antibiotic biosynthesis genes

Antibiotic	Gene	Sequences	Expected size of PCR product/ detected in B579	References accession number
Fengycin	*fenA*	F1:AAGGACTCGGCAGAAATGAA	900 bp/no	CP000560, AJ576102
		R1:TGAATGTGAAGCGCAGGTAG		
Iturin	*ituB*	F1:ATCCAGAATATCCGCAAGAC	1479 bp/yes	AB050629, EU263005
		R1:GCTCGATATGCGGACTCAAT		
Surfactin	*srfA*	F1:GGAGCAAAGGTGCTTCTCAC	1200 bp/yes	Z99105, BSU03480
		R1:GAAACGTTGGCATCAGGAAT		
TasA	*tasA*	F1: CACCATGGGTATGAAAAAGAAATT	790 bp/yes	Z99116, BSU03480
		R1: TTAATTTTTATCCTCGCTATGCGCTT		
Bacillomy-cin D	*bamC*	F1: AGTAAATGAACGCGCCAATC	957 bp/no	AY137375
		R1: CCCTCTCCTGCCACATAGAG		
Bacilysin	*bacD*	F1: AAAAACAGTATTGGTTATCGCTGA	749 bp/yes	AF396779
		R1: CCATGATGCCTTCGATACTGAT		
Ericin	*eriB*	F1: GCACAGATGGAAAATCTGAAG	688 bp/no	AF233755, BSU09819
		R1: GAAAATTGCTCCCCAAATGA		
Mersacidi-n	*mrsA*	F1: GGGTATATGCGGTATAAACTTATG	579 bp/no	AJ250862
		R1: GTTTCCCCAATGATTTACCCTC		
Mycosubti-lin	*mycC*	F1: AATCAATTGGCACGAACCTT	1026 bp/no	AF184956
		R1: ATCGCCCGTTTTGTACATTC		
Sublancin	*sunT*	F1: GCTTTGTTAGAAGGGGAGGAAT	974 bp/yes	AF014938
		R1: CTTGTCCCAACCCATAGGATAA		
Subtilin	*spaB*	F1: GCACAGATGGAAAATCTGAAG	688 bp/no	AF233755
		R1: GAAAATTGCTCCCCAAATGA		
Subtilosin	*albF*	F1: TCAACAGCTGGATGAACGAAC	888 bp/yes	AJ430547
		R1: AGGCGGTATGTTTGCTGTATCT		

Note “yes” representation the genes were detected; “no” representation the genes was not detected in *B. subtilis* B579

was determined according to the bioassay method described earlier [16]. The crude antifungal compounds were further purified using reverse phase high-pressure liquid chromatography (HPLC) with a C_{18} column (Agilent 1100 C_{18} semi-preparative column, 21.4 mm × 250 mm) at 30 °C. The aqueous methanol solution of the active fraction was injected into the column, and eluted with a linear gradient at 1 mL/min. Elution was monitored at 215–280 nm with a diode array UV monitor. Liquid chromatography–mass spectrometry (LC–MS) analysis were conducted for each active peak, using reverse phase HPLC with a C_{18} column (Agilent 1100 C_{18} semi-preparative column, 4.6 mm × 250 mm), and electrospray ionization mass spectrometry (ESI–MS) with quadrupole mass analyzer at 30 °C.

58.3 Results

58.3.1 PCR Detection of Antibiotic Biosynthesis-Related Genes

Specific primers were designed according to sequences related to biosynthesis of antagonistic compounds published on GenBank. Twelve genes related to the antifungal compounds biosynthesis were detected (Table 58.1). Six genes were detected that exist in the genome DNA of B579 by the sequence homology analysis [14]. Five genes were related to biosynthesis of lipopeptide antifungal compounds, and one gene was related to biosynthesis of protein antifungal compounds.

The DNA sequences obtained from these amplicons showed high homology to genes accessed in NCBI. Analysis of the 1022 bp PCR product with the ituB-F1/R1 primer pair showed 99 % identity with a region of the iturin biosynthesis operon. PCR products of sunT and albF (934 and 845 bp, respectively) also showed 99 % identity with the genes involved in the biosynthesis of sublancin and subtilosin. Bacilysin biosynthesis-related gene bacD showed 98 % identity. Analysis of the 1153 bp PCR product using the srfA-F1/R1 primer pair showed 98 % identity with a region of srfAA, a gene involved in the biosynthesis of surfactin. Finally, analysis of the 766 bp PCR product with the tasA-F1/R1 primer pair showed 99 % identity to gene involved in the biosynthesis of tasA.

58.3.2 HPLC Analysis of Antifungal Compounds

Lipopeptide antifungal compounds were obtained from the fermentation supernatant of B579 using the method of acid deposition and methanol extraction. Four major active peaks (named 24.05, 29.00, 67.54, and 69.75) were selected for further study (Fig. 58.1).

58.3.3 LC–MS Analysis of Antifungal Compounds

The active peaks of 24.05 and 29.00 were further analyzed, respectively, using LC–MS. Two homologies with the molecular weight of *m/z* 1043.59 (Fig. 58.2a) and *m/z* 1057.35 (Fig. 58.2b) were detected in the lipopeptide antifungal compounds, which

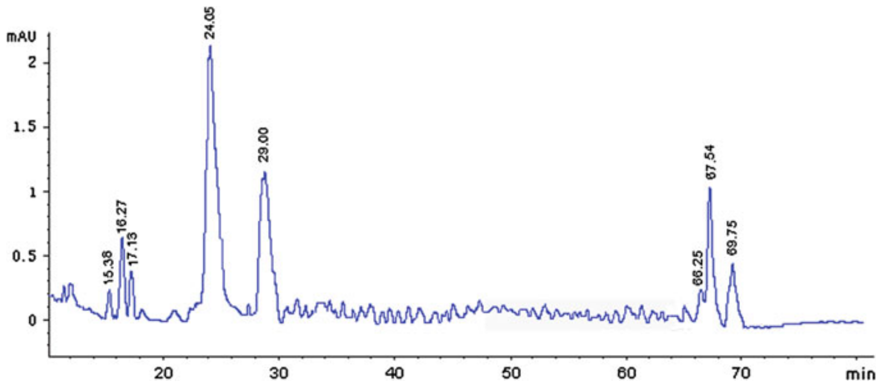

Fig. 58.1 HPLC analysis of lipopeptide antifungal compounds produced by *Bacillus subtilis* B579

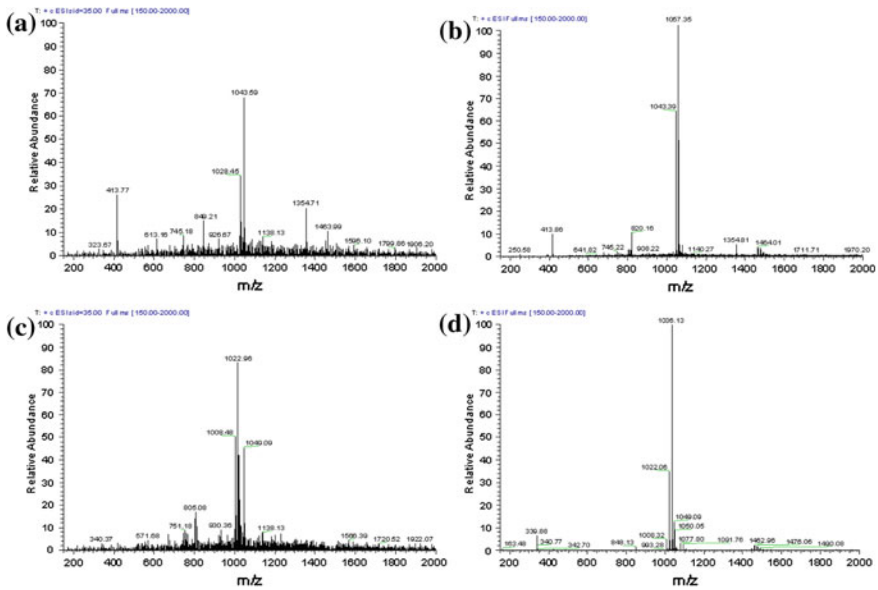

Fig. 58.2 Analysis of lipopeptide antifungal compounds produced by *B. subtilis* B579 using ESI-MS

had the similar molecular weight with the two homologies of iturin A. Two homologies with the molecular weight of *m/z* 1008.48 and *m/z* 1022.96 (Fig. 58.2c) were detected by analyzing the active peak 67.54, and the active peak 69.75 showed the molecular weight of *m/z* 1036.13 and *m/z* 1022.06 (Fig. 58.2d). The molecular weight of *m/z* 1008.48, *m/z* 1022.96, and *m/z* 1036.13 with one $–CH_2$ molecular weight difference in turn, which had the similar molecular weight with three homologies of C_{13}–C_{15} surfactin.

58.4 Discussions

So far, numerous microorganisms with antagonistic ability have been identified, and many have been confirmed effective in field experiments [1–3]. The gram-positive bacteria, like *B. subtilis*, have been studied intensively in recent years, because many *B. subtilis* strains are considered to be safe biocontrol agents [17]. So, *B. subtilis* is not only an organism known for protease production [18], but also a good bacteria used for fungicide production. Previous reports by other researchers have shown that antagonistic *B. subtilis* could produce β-1,3-glucanase, chitinase, and antibiotics such as iturin A and surfactin [19]. Iturin is a cyclolipopeptide containing seven residues of α-amino acids and one reside of a β-amino acid. It is a small molecule yet displays strong antifungal activity. The other lipopeptide, surfactin, in contrast has weak antibiotic activity. However, it exhibits a stronger antifungal ability when is synergism with iturin [10].

In the present study, genes involved in the biosynthesis of six antifungal compounds were detected in genomic DNA of B579. Two kinds of lipopeptide antifungal compounds were identified by HPLC and LC–MS. The separation of antifungal compounds and the effect of these antifungal compounds on the morphology of the pathogens are under extensive investigation in our laboratory. The related genes for biosynthesis of bacilysin, sublancin, subtilosin were detected by PCR, but they were not been detected by HPLC and LC–MS which need us for further study. They probably were produced too little to separation and identification, or need to find better conditions for their production and separation.

In our previous studies, *B. subtilis* B579 not only exhibited effective biological control ability against Fusarium wilt of cucumber under greenhouse conditions, but also could induce plant systematic resistance and promote plant growth in biological control of Fusarium wilt [16]. Formulation of powder preparation of B579 endospores had been developed (Chinese patent registration number: 200810153180.1). Some isolates of Bacillus have been successfully commercialized and marketed, such as the Gustafson product Kodiak is widely used for suppression of cotton disease in the US [20]. As the interest in biological control of soilborne plant pathogens has increased considerably in the last few decades, we believe that *B. subtilis* will be used more in production agriculture and horticulture based on the recent progress shown in implementing microbial inoculants.

Acknowledgments This work was supported by the Natural Science Foundation of Shandong, China (Project No. ZR2013CQ019), and Scientific Research foundation for Doctor, Liaocheng University, China (Project No. 3010).

References

1. Cook RJ (2000) Advances in plant health management in the twentieth century. Annu Rev Phytopathol 38:95–116
2. Fravel D, Olivain C, Alabouvette C (2003) *Fusarium oxysporum* and its biocontrol. New Phytol 157:493–502
3. Chung S, Kong H, Buyer JS et al (2008) Isolation and partial characterization of *Bacillus subtilis* ME488 for suppression of soilborne pathogens of cucumber and pepper. Appl Microbiol Biotechnol 80:115–123
4. Uppal AK, Hadrami AE, Adam LR et al (2008) Biological control of potato Verticillium wilt under controlled and field conditions using selected bacterial antagonists and plant extracts. Biol Control 44:90–100
5. Siddiqui IA, Shaukat SS (2004) Systemic resistance in tomato induced by biocontrol bacteria against the root-knot nematode, *Meloidogyne javanica* is independent of salicylic acid production. J Phytopathol 152:48–54
6. Ahn IP, Chung HS, Lee YH (1998) Vegetative compatibility groups and pathogenicity among isolates of *Fusarium oxysporum* f. sp. cucumerinum. Plant Dis 82:244–246
7. Wang SL, Shih IL, Wang CH et al (2002) Production of antifungal compounds from chitin by *Bacillus subtilis*. Enzym Microb Technol 31:321–328
8. Thilagavathi R, Saravanakumar D, Ragupathi N et al (2007) A combination of biocontrol agents improves the management of dry root rot (*Macrophomina phaseolina*) in greengram. Phytopathol Mediterr 46:157–167
9. Lee HJ, Park KH, Shim JH et al (2005) Quantitative changes of plant defense enzymes in biocontrol of pepper (*Capsicium annuum* L.) late blight by antagonistic *Bacillus subtilis* HJ927. J Microbiol Biotechnol 15:1073–1079
10. Kavitha S, Senthilkumar S, Gnanamanickam S et al (2005) Isolation and partial characterization of antifungal protein from *Bacillus polymyxa* strain VLB16. Process Biochem 40:3236–3243
11. Stover AG, Driks A (1999) Secretion, localization, and antibacterial activity of TasA, a *Bacillus subtilis* spore-associated protein. J Bacteriol 181:1664–1672
12. Chen H, Yuan CL, Cai KZ et al (2008) Purification and identification of iturin A from *Bacillus subtilis* JA by electrospray ionization mass spectrometry. Acta Microbiol Sin 48:116–120
13. Tsuge K, Inoue S, Ano T et al (2005) Horizontal transfer of iturin A Operon, *itu*, to *Bacillus subtilis* 168 and conversion into an iturin A producer. Antimicrob Agents Chemother 49:4641–4648
14. Chen F (2010) Biocontrol effect and action mechanism of *Bacillus subtilis* B579. Tianjin University of Science and Technology, Tianjin, pp 55–66
15. Bie XM, Lv FX, Lu ZX et al (2006) Isolation and identification of lipopeptides produced by *Bacillus subtilis* fmbJ. Chin J Biotechnol 22:644–649
16. Chen F, Wang M, Zheng Y et al (2010) Quantitative changes of plant defense enzymes and phytohormone in biocontrol of cucumber Fusarium wilt by *Bacillus subtilis* B579. World J Microbiol Biotechnol 26:675–684
17. Chu IM, Lee C, Li TS (1992) Production and degradation of alkaline protease in batch cultures of *Bacillus subtilis* ATCC 14416. Enzym Microb Technol 14:755–761
18. Romero D, de Vicente A, Olmos JL et al (2007) Effect of lipopeptides of antagonistic strains of *Bacillus subtilis* on the morphology and ultrastructure of the cucurbit fungal pathogen *Podosphaera fusca*. J Appl Microbiol 103:969–976
19. Leelasuphakul W, Sivanunsakul P, Phongpaichit S (2006) Purification, characterization and synergistic activity of β-1, 3-glucanase and antibiotic extract from an antagonistic *Bacillus subtilis* NSRS 89-24 against rice blast and sheath blight. Enzym Microb Technol 38:990–997
20. Choudhary DK, Johri BN (2009) Interactions of *Bacillus* spp. and plants—with special reference to induced systemic resistance (ISR). Microbiol Res 164:493–513

Chapter 59
Application of Molecularly Imprinted Polymers in Purification and Separation for Epothilones

Ruicheng Sun, Lin Zhao, Jikun Yang, Naiqiang Wang and Xinli Liu

Abstract A highly effective purification process combined with molecularly imprinted polymers (MIPs) was developed to selectively isolate Epothilones (Epos) from a complex milieu. The MIPs of Epos were successfully synthesized by precipitation polymerization, and the optimal ratio of the template molecule to functional monomer and cross-linker was 1:4:20 (with the molar ratio). Under the optimized condition, the resulted products were characterized by scanning electron microscope (SEM). The binding properties of the MIPs were evaluated by the adsorption kinetics and static adsorption. From the correlation coefficients (R^2) of the fitting models, the equilibrium data fitted well to Freundlich model ($R^2 = 0.9987$), indicating multilayer adsorption. Finally, we successfully applied the MIPs in the solid-phase extraction (SPE) process of Epos, and its purity was improved more than 40 % than the origin. It achieved an effectively selective Epos cleanup procedure, sequentially established a favorable foundation for later research on Epos.

Keywords Molecularly imprinted polymers · Epothilones · Static adsorption · Adsorption kinetics · Solid-phase extraction

R. Sun and L. Zhao have contributed equally to this work.

R. Sun · L. Zhao · J. Yang · X. Liu (✉)
Shandong Provincial Key Laboratory of Microbial Engineering, Qi Lu University of Technology, Jinan 250353, People's Republic of China
e-mail: vip.lxl@163.com

N. Wang
Baolingbao Biology Co. Ltd., Yucheng 251200, People's Republic of China

T.-C. Zhang and M. Nakajima (eds.), *Advances in Applied Biotechnology*,
Lecture Notes in Electrical Engineering 333, DOI 10.1007/978-3-662-46318-5_59

59.1 Introduction

Epothilones (Epos, Fig. 59.1) belong to the macrocyclic lactone class of antibiotics, which consist of several structurally related groups: Epothilone A, B, C, D, E, F, and K. They were first described by G. Höfle et al. in 1993, as secondary metabolites synthesized by *Sorangium cellulosum* strain SMP44, which was collected at the banks of the Zambezi river in the Republic of South Africa [1–4]. Epothilones were confirmed to be able to kill dividing cells by stabilizing microtubules at nanomolar and subnanomolar concentrations, and considered as potential advantageous successors to cancer treatment, which can be effective against taxol-resistant cells [5, 6]. Unfortunately, the inefficiency in purification seriously restricted the industrialization of Epos. For the isolation of epothilones, macroporous adsorption resins were added into the medium during fermentation, but some impurities with similar polarities or structures just as antifoaming agents and other hydrophobic component were coinstantaneous adsorbed and hard to be eliminated by later traditional column chromatography. Therefore, developing a fast, convenient, and stable method for the isolation and purification of Epos is expected.

In recent years, molecular imprinting technology (MIT) has attracted considerable attentions and molecularly imprinted polymers (MIPs) have been widely applied in many fields, such as capillary electrochromatography, solid-phase extraction (SPE), artificial enzymes, and chemical sensors. That is because of their outstanding advantages, involving mechanical and chemical stabilities, desired selectivity, as well as relative ease and low cost of preparation [7–13].

In this study, we synthesized the MIPs of Epos by precipitation polymerization, and evaluated them on the morphological characterization and binding ability. Finally, we applied the MIPs in the SPE, achieving an effectively selective Epos cleanup procedure, which remarkably simplified the purification process.

59.2 Experimental

59.2.1 Reagents

Epothilones was obtained from Shandong Provincial Key Laboratory of Microbial Engineering, Qilu University of technology (Jinan, China). Methanol and

Fig. 59.1 Chemical structures of epothilones

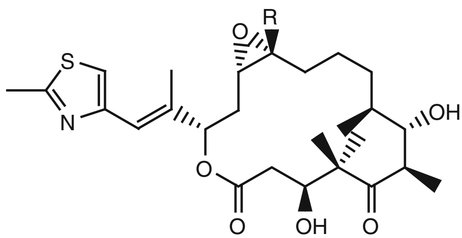

chloroform were purchased from Tianjin Chemical Reagent Company (Tianjin, China). Methacrylic acid (MAA) and Ethylene glycol dimethacrylate (EGDMA) were purchased from Aladdin Industrial Corporation (Shanghai, China). 2,2-azoisobutyronitrile (AIBN) was supplied by Tianjin Damao Chemical Reagent Factory (Tianjin, China).

59.2.2 Preparation of the MIPs for Epos

The MIPs of Epos were synthesized by precipitation polymerization method. The general synthesis route was shown in Fig. 59.2. Using MAA as functional monomer, chloroform as porogen, EGDMA as cross-linker and AIBN as initiator, a traditional preparation procedure was carried out as follows: A certain amount of Epos and MAA were dissolved in 40 mL chloroform. After being placed for 3 h, EGDMA and AIBN were added. Then the solution was purged with nitrogen for 10 min, sealed, and polymerization took place at 60 °C for 24 h in a thermostat water bath. The obtained polymers were extracted in a Soxhlet apparatus with methanol/acetic acid (4:1, v/v) for 48 h, until no Epos could be detected. Then the polymers were washed with methanol for 24 h to remove the remained acetic acid and dried at 60 °C to reach a constant weight. The NIPs were prepared and treated under identical conditions without template present during polymerization.

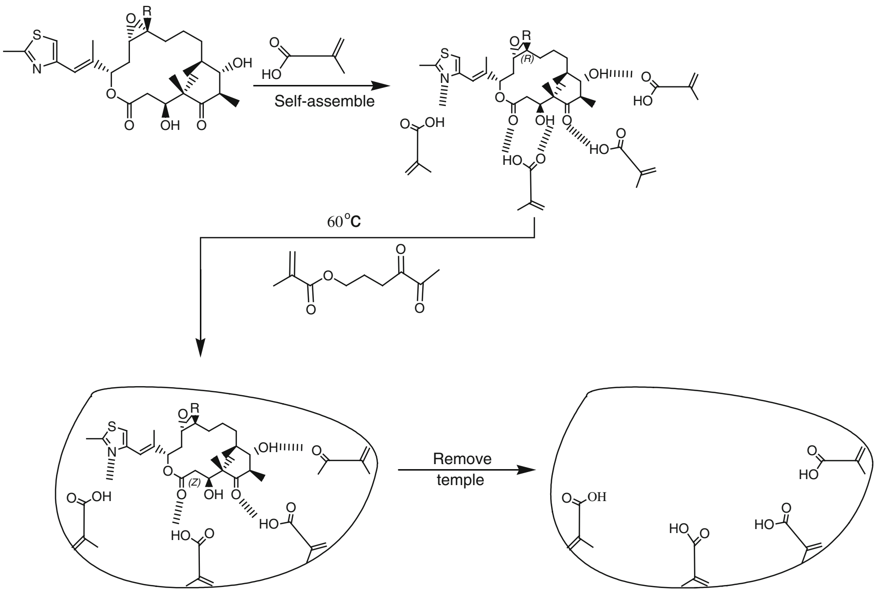

Fig. 59.2 Scheme of the synthesis route of MIPs using epothilones as template molecule

59.2.3 Morphological Characterization

The morphology of the polymers was observed by a scanning electron microscope (SEM) at 15.0 kV.

59.2.4 Binding Analysis

To evaluate the binding property of the MIPs and NIPs, 15 mg MIPs and NIPs were each added into a 20 mL vial and mixed with 10 mL Epos solution in chloroform. After being vertical shaken at room temperature for 3 h, the supernatant was centrifuged at 10,000 rpm for 10 min, then the concentration of Epos was measured. The amount of Epos which bound to the polymers was counted by subtracting the amount of Epos in the final solution from the initial amount. The adsorption property value Q could be evaluated by the following equation:

$$Q = (C_0 - C) \times V/W \tag{59.1}$$

C_0 and C were the initial and final concentrations of Epos, V was the solution volume, and W was the mass of polymer.

59.2.5 SPE Experiments

Polypropylene 1 mL SPE cartridge secured by glass-fiber frits was packed with 25 mg of the MIPs or NIPs. The cartridge was conditioned consecutively with 1 mL methanol and 1 mL water. Then, 2 mL Epos dissolved in chloroform were passed through the cartridge at a rate of 0.1 mL min^{-1}, and rinsed with 1 mL methanol/water (4:1, v/v) to wash off the interferences. Finally, for the elution step, the cartridge was eluted with mixture containing methanol and acetic acid (4:1, v/v) to release the bound analytes. All the fractions were collected; quantification of Epos was carried out by HPLC analysis.

59.3 Results and Discussions

59.3.1 Synthesis of the MIPs

The main factors affecting the adsorption behavior of the MIPs were estimated by the ratios of the template to functional monomer and cross-linker, as shown in Table 59.1.

Table 59.1 The MIPs and NIPs of Epos for preparation with different ratios and adsorption capacity

No.	Epos (mmol)	MAA (mmol)	EGDMA (mmol)	Q (mg g^{-1})	IF
MIP1	0.5	1.0	10.0	57	1.78
NIP1	–	1.0	10.0	32	
MIP2	0.5	2.0	10.0	128	2.25
NIP2	–	2.0	10.0	57	
MIP3	0.5	3.0	10.0	112	1.49
NIP3	–	3.0	10.0	75	
MIP4	0.5	2.0	7.5	78	1.73
NIP4	–	2.0	7.5	45	
MIP5	0.5	2.0	12.5	98	1.19
NIP5	–	2.0	12.5	82	

In this study, the imprinting factor IF (IF = $Q_{\mathrm{MIPs}}/Q_{\mathrm{NIPs}}$) was employed to confirm the optimal synthesis conditions. From the results in Table 59.1, we could see that insufficient amount of functional monomer was not be able to synthesis enough binding sites (MIP1), the overdosing functional monomer lead to association by themselves, forming little effective binding sites (MIP3). Furthermore, low cross-linker amount could not ensure the rigidity of the polymers (MIP4), and high cross-linker amount could promote the formation of nonspecific binding cavities (MIP5).

In conclusion, after survey in the main factors affecting the adsorption behavior to the MIPs, the optimal synthesis ratios were 1:4:20 (template molecule:functional monomer:cross-linker, with the molar ratio), and the imprinting factor IF reached maximum to 2.25.

59.3.2 Morphological Characterization of the MIPs

For both polymers, the particles possed a porous surface due to pores with irregular shapes and sizes, which could play an important role in the adsorption process. In the MIPs, the roughness of the particle surface itself causes the increase in the surface area than the NIPs, which possessed a uniform, compact, and smooth shape. The nonporous structure in the NIPs particles was due to the lack of specific binding sites which were created for Epos-MIPs and suggested that the MIPs had great potential applied for sorbents (SEM, as shown in Fig. 59.3).

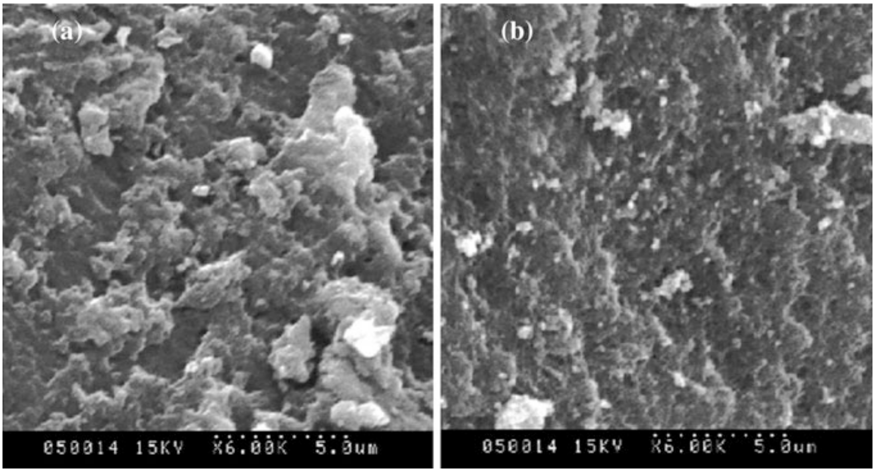

Fig. 59.3 Scanning electron micrographs of the MIPs (**a**) and NIPs (**b**)

59.3.3 Adsorption Kinetics of the MIPs

In order to explore the capacity of MIPs, the adsorption kinetics experiments for both MIPs and NIPs were carried out. 15 mg MIPs and NIPs were mixed with 10 mL Epos solution in chloroform, then incubated at room temperature with continuous vertical shaking for 5 h. The initial concentration of Epos was kept in 1.0 mg mL^{-1}, and the amount of Epos bound to the polymers was measured every 30 min. The results were shown in Fig. 59.4. It could be seen that the adsorption rate of MIPs for Epos increased rapidly in the first 30 min, which is mainly because many binding cavities existed on the MIPs surface. Furthermore, the adsorption saturation of MIPs was attained after 3 h, while NIPs was about 1 h, it showed that MIPs had many specificity binding cavities compared with NIPs.

59.3.4 Adsorption Isotherms of the MIPs

Furthermore, the static adsorption experiments of MIPs were also investigated. Compared with the adsorption kinetics experiments, the initial concentration of Epos was ranged from 0.2 to 1.0 mg mL^{-1}. The results were shown in Fig. 59.5. It could be seen that the amount of Epos bound to the polymers were raised with the initial concentration increased.

To explain how the adsorbate distributed on the adsorbent, the adsorption system were designed and established. Two classical isotherm models were used to analyze the equilibrium data: the Langmuir model (Eq. 59.2) and the Freundlich model (Eq. 59.3).

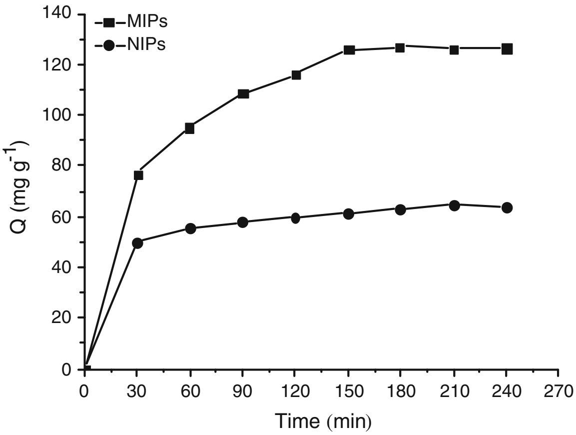

Fig. 59.4 Absorption kinetics of the MIPs and NIPs for Epos

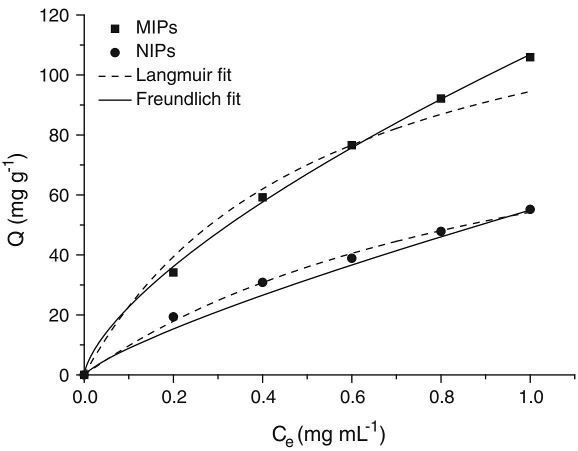

Fig. 59.5 Adsorption isothermic of the MIPs and NIPs for Epos

$$Q = K_L Q_e C_e / (1 + K_L C_e) \tag{59.2}$$

where C_e was the initial concentration, Q was the amount of Epos bound at equilibrium, Q_e was the theoretical maximum monolayer capacity, and K_L was the Langmuir constant related to the affinity of the active sites.

$$Q = K_F C_e^{1/n} \tag{59.3}$$

where C_e was the initial concentration, Q was the amount of Epos bound at equilibrium, and n and K_F are Freundlich constants, which were related to the adsorption favorability and adsorption capacity, respectively.

A comparison of the isotherm models for Epos adsorption onto the MIPs and NIPs using nonlinear regression (Eqs. 59.2 and 59.3) were also presented in Fig. 59.5,

Table 59.2 Adsorption isothermic parameters for the adsorption of Epos onto MIPs and NIPs

Polymers	Langmuir			Freundlich		
	Q_e	K_L	R^2	n	K_F	R^2
MIPs	145.15	1.86	0.9684	1.49	106.84	0.9987
NIPs	110.13	0.97	0.9965	1.26	54.95	0.9736

and the parameters obtained from the isotherm models were also listed in Table 59.2. As shown in Fig. 59.5 and Table 59.2, the correlation coefficients (R^2) of 0.9684 and 0.9987 were obtained on the MIPs for the Langmuir and Freundlich models, respectively. While on the NIPs were 0.9965 and 0.9736, respectively. From that we could see the Freundlich model was better than the Langmuir model in describing the adsorption behavior of Epos on the MIPs in terms of the higher correlation coefficients (R^2) values, it demonstrated that the MIPs belongs to multilayer adsorption, they probably exhibited a logarithmic distribution of the binding sites in multilayers [14, 15]. However, for the NIPs, the Langmuir model was better than the Freundlich model in terms of the higher correlation coefficients (R^2) values, which indicated that the NIPs belong to homogeneous adsorption [16, 17].

59.3.5 SPE Analysis for the MIPs

For the Epos extraction, the offline SPE was employed with the MIPs as sorbents, the results were shown in Fig. 59.6. A quantity of 25 mg the MIPs was packed into 1 mL SPE cartridges with two polypropylene frits between the stuffing. The initial complex milieu (the metabolites containing Epos and impurities dissolved in chloroform, the purity of Epos were 40.62 % (in peak area), chromatogram A in

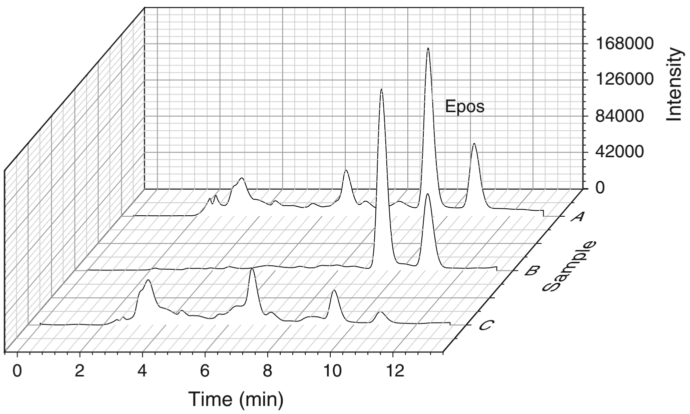

Fig. 59.6 Separation of Epos with the MIPs as a adsorbent in SPE procedure: **a** Initial complex milieu before SPE, **b** final milieu after SPE, **c** the solutions washing impurities

Fig. 59.6) were passed through at a rate of 0.1 mL min^{-1}. After all the steps were completed, collecting the elution fractions and HPLC analysis. The final milieu after SPE was eluted (chromatogram B in Fig. 59.6) successfully separating Epos from the solution. The purity of Epos in the solution was 83.83 %, improving more than 40 % compared with the initial solutions. Although most the interferences were washed off from the Epos solutions, as shown in Fig. 59.6 chromatogram C, there is still a small amount of Epos that was washed off together with impurities, and we will continue to follow up work. From the results we indicated that the MIPs of Epos could be successfully applied as an adsorbent into SPE process for separation of Epos.

59.4 Conclusions

In this paper, we successfully synthesized the MIPs of Epos by precipitation polymerization. The optimal ratio of the template to functional monomer and cross-linker is 1:4:20. Under the optimal composed conditions, a series of experimental analyses including SEM, FT-IR, adsorption kinetics, and adsorption isotherms were carried out to demonstrate the formation of the MIPs for Epos. The results showed that the equilibrium data fitted well to the Freundlich model, indicating multilayer adsorption. Moreover, the MIPs of Epos were successfully applied as sorbent into SPE process, brought about an effectively and simply Epos cleanup procedure.

Acknowledgments The work was financially supported by Research Projects of Science and Technology Division, Shandong (2012GSF12107), and Provincial Post-Doctoral Innovation Foundation (201203006).

References

1. Höfle G, Bedorf N, Steinmetz H, Schomburg D, Gerth K, Reichenbach H (1996) Epothilone A and B—Novel 16-membered macrolides with cytotoxic activity: isolation, crystal structure, and conformation in solution. Angew Chem Int Edit 35:1567–1569
2. Gerth K, Bedorf N, Höfle G, Irschik H, Reichenbach H (1996) Epothilones A and B: antifungal and cytotoxic compounds from Sorangium cellulosum (myxobacteria) production, physico-chemical and biological properties. J Antibiot 49:560–563
3. Gerth K, Steinmetz H, Höfle G, Reichenbach H (2000) Studies on the biosynthesis of epothilones: the biosynthetic origin of the carbon skeleton. J Antibiot 53:1373–1377
4. Gerth K, Steinmetz H, Höfle G, Reichenbach H (2001) Studies on the biosynthesis of epothilones: the PKS and epothilone C/D monooxygenase. J Antibiot 54:144–148
5. Domling A, Richter W (2005) Myxobacterial epothilones and tubulysins as promising anticancer agents. Mol. Divers. 9:141–147
6. Julien B, Shah S, Ziermann R, Goldman R, Katz L, Khosla C (2000) Isolation and characterization of the epothilone biosynthetic gene cluster from Sorangium cellulosum. Gene 249:153–160

7. Alexander C, Smith CR, Whitcombe MJ, Vulfson EN (1999) Imprinted polymers as protecting groups for regioselective modification of polyfunctional substrates. J Am Chem Soc 121:6640–6651
8. Haupt K, Mosbach K (2000) Molecularly imprinted polymers and their use in biomimetic sensors. Chem Rev 100:2495–2504
9. Ge Y, Turner APF (2009) Molecularly imprinted sorbent assays: recent developments and applications. J Chem Eur 15:8100–8107
10. Haginaka J (2009) Molecularly imprinted polymers as affinity-based separation media for sample preparation. J Sep Sci 32:1548–1565
11. Sumaoka J, Komiyama M (2009) Molecularly imprinted polymers for the recognition of biomolecules in water. Kobunshi Ronbunshu 66:191–201
12. Wulff G (2002) Enzyme-like catalysis by molecularly imprinted polymers. Chem Rev 102:1–27
13. Ye L, Mosbach K (2008) Molecular imprinting: synthetic materials as substitutes for biological antibodies and receptors. Chem Mater 20:859–868
14. Vieira AC, Zampieri RA, Siqueira ME, Martins I, Figueiredo EC (2012) Molecularly imprinted solid-phase extraction and high-performance liquid chromatography with ultraviolet detection for the determination of urinary trans, trans-muconic acid: a comparison with ionic exchange extraction. Analyst 137:2462–2469
15. Yang W, Zhou W, Xu W, Li H, Huang W, Jiang B, Zhou ZP, Yan YS (2012) Synthesis and characterization of a surface molecular imprinted polymer as a new adsorbent for the removal of dibenzothiophene. J Chem Eng Data 57:1713–1720
16. Dai J, Pan J, Xu L, Li X, Zhou Z, Zhang R, Yan Y (2012) Preparation of molecularly imprinted nanoparticles with superparamagnetic susceptibility through atom transfer radical emulsion polymerization for the selective recognition of tetracycline from aqueous medium. J Hazard Mater 205(206):179–188
17. Ren Y, Ma W, Ma J, Wen Q, Wang J, Zhao F (2012) Synthesis and properties of bisphenol A molecular imprinted particle for selective recognition of BPA from water. J Colloid Interface Sci 367:355–361

Chapter 60
Identification of Peanut Intersectional Hybrids with SSR Markers

Shuo Meng, Xiu Zhen Wang, Yue Yi Tang, Qi Wu, Quan Xi Sun, Chen Jiang, Chuan Tang Wang and Li Feng Liu

Abstract Wild peanut relatives constitute an invaluable gene source for broadening the narrow gene base of the cultivated peanut. However, severe pre-/post- fertilization obstacles impeded the utilization of incompatible species within the *Arachis* genus. In the present study, through SSR profiling, three true intersectional F_1 hybrids of Qunyu 101 × *Arachis pusilla* and a true intersectional F_1 hybrid of Huayu 40 × *A. pusilla* resulting from post-pollination hormone treatment of flower bases were identified, providing strong evidence for the effectiveness of the in vivo hormone treatment method in overcoming cross-incompatibility in the genus *Arachis*.

Keywords *Arachis pusilla* · Hybrid · Intersectional cross · SSR · Wild species

60.1 Introduction

The cultivated peanut, *Arachis hypogaea* L., as an important cash crop in the world, provides over 30 essential nutrients and phytochemicals including oil and protein [1]. Plumpy'Nut, a ready-to-use peanut-based paste, was invented and used to treat severe acute child malnutrition in Africa [1, 2]. However, as pointed out by Mallikarjuna et al. [1], the peanut crop, an amphidiploid member of the *Arachis* section with *A. duranensis* and *A. ipaensis* as its progenitors [3–5], is the product of evolution after a series of six bottlenecks [1]. It was estimated that the cultivated peanut contains no more than 13 % of the genetic diversity present in its closest

S. Meng · C.T. Wang · L.F. Liu (✉)
Hebei Agricultural University, Baoding 071001, China
e-mail: liulifeng@hebau.edu.cn

X.Z. Wang (✉) · Y.Y. Tang · Q. Wu · Q.X. Sun · C. Jiang · C.T. Wang (✉)
Shandong Peanut Research Institute, Qingdao 266100, China
e-mail: xzhw2000@126.com

C.T. Wang
e-mail: chinapeanut@126.com

T.-C. Zhang and M. Nakajima (eds.), *Advances in Applied Biotechnology*,
Lecture Notes in Electrical Engineering 333, DOI 10.1007/978-3-662-46318-5_60

wild relatives in the section [1, 6]. Narrow genetic base of the peanut crop accounts for its genetic vulnerability to various biotic/abiotic stresses and limited productivity potential [7].

The *Arachis* genus, now with 80 named species, is partitioned into 9 sections by Krapovickas and Gregory [8]. Reportedly, some of the genetically diversified wild *Arachis* species contained high protein/oil content [9]. It is believed that wild peanut also possesses high-yielding factors [10]. Moreover, high levels of stress resistances have been identified in wild peanut specie, some of which have never been found in the peanut cultigen [7]. Hence wild peanut relatives constitute an invaluable gene source for the genetic improvement of the cultivated peanut [7, 9]. Nevertheless, only species from section *Arachis* are cross-compatible with *A. hypogaea*. Owing to severe pre-/post- fertilization barriers, fertile hybrids between the cultivated peanut and species outside section *Arachis*, viz., incompatible species, are not readily available [7].

The aim of this study was to identify true peanut intersectional hybrids resulting from post-pollination hormone treatment of flower bases using simple sequence repeat markers.

60.2 Materials and Methods

60.2.1 Peanut Materials

Two intersectional crosses were made between peanut cultivars, Qunyu 101 and Huayu 40 (female parents) and wild peanut *Arachis pusilla* PI289628, a *Heteranthae* section species (male parent). Through post-pollination hormone treatment of flower bases, resultant seeds were harvested in fall and sown in the field under polythene film mulch in the next spring. Routine agronomic practices were followed as per the description by Wan et al. [11]. Genomic DNA was extracted from unexpanded leaves of field-grown peanut plants using EasyPure Plant Genomic DNA kit (TransGen Biotech, Beijing) according to manufacturer's instructions.

60.2.2 SSR Profiling

In primary evaluation, of the 12 SSR primer pairs evaluated, 3 primer pairs, PM201 [12], PM468 [13] and IPAHM123 [14], were found to be informative and capable of producing reproducible and distinguishable bands. Therefore, the three primer pairs were used to identify true hybrids in the study (Table 60.1). SSR analysis was conducted in three replications.

The PCR mixture (20 μL total volume) consisted of 1 μL of DNA template (30 ng), 0.5 μL of upstream and downstream SSR primers (10 μM) each, and 10 μL

Table 60.1 List of informative SSR primer pairs

Primer ID	Forward primer (5′–3′)	Reverse primer (5′–3′)
PM201	CCTTTATAGAGGACCTTCCCTCTC	GCCTATTTGGTATCGGCTCA
PM468	TCAAGCCATAATATGTTCCACA	AAAACAACCCAAGCACCTCT
IPAHM123	CGGAGACAGAACACAAACCA	TACCCTGAGCCTCTCTCTCG

of 2× *Taq* PCR Master Mix (DBI Bioscience, Catalog # DBI-2028). Thermal cycling profile was denaturing at 95 °C for 3 min, followed by 35 cycles of 95 °C for 45 s, 55 °C for 45 s, and 72 °C for 45 s, and a final extension of 72 °C for 5 min.

Bands were separated on a 6 % denaturing polyacrylamide gel. Gel was washed with distilled water twice (1 min). Fixation and silver staining were conducted in a single step. Gel was placed in solution containing 0.2 % $AgNO_3$, 1 % glacial acetic acid, and 10 % ethanol for 10 min. Then the gel was washed with distilled waterr twice (2 min). Later, gel was placed in developing solution (3 % NaOH, with 1 mL formaldehyde added in 200 mL total volume just prior to developing). Generally, 13 min was enough to develop clear bands [15].

60.3 Results and Discussion

For both crosses, no difference was detected among banding patterns of the 3 replications. Judged by ployacrylamide gel electrophoresis profile, true hybrids could be easily selected in both crosses.

60.3.1 *Qunyu 101* × *A. pusilla*

In the cross, a total of 8 single plants were tested by PCR using the 2 SSR primer pairs, PM468 and PM201. Merely three single plants (37.5 %) were identified as true F_1 hybrids (Fig. 60.1a, b). PM468 and PM201 resulted in the same results. True hybrids were characterized by the presence of a band co-immigrating with the band from *A. pusilla*, whereas the female parent Qunyu 101 and selfs did not produce such a band (Fig. 60.1a, b). The results were supported by SSR profiling with a third primer pair, IPAHM123, where totally 16 single plants were utilized. Not surprisingly, with this new primer pair, all of the three "hybrid" plants previously identified using primer pairs PM468 and PM201 produced a characteristic band co-immigrating with the band from the male parent, *A. pusilla* (Fig. 60.2a).

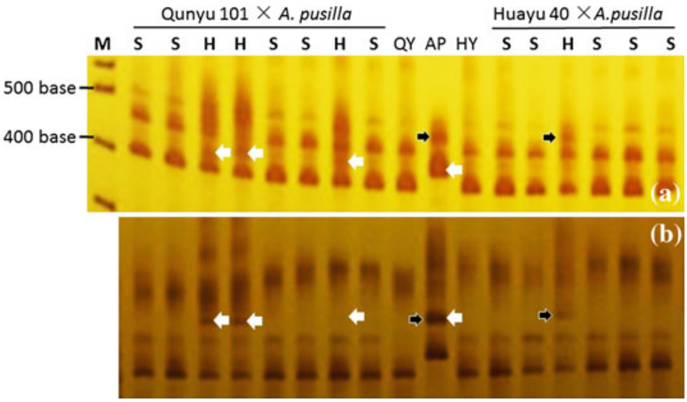

Fig. 60.1 PM468 (**a**) and PM201 (**b**) identified true F_1 hybrids (H) and selfs (S) resulting from Qunyu 101 × *A. pusilla* and Huayu 40 × *A. pusilla*, *arrow* indicating characteristic band present in *A. pusilla* (AP, male parent) but absent in female parents, Qunyu 101 (QY) and Huayu 40 (HY). *M* 50 bp DNA Ladder (Fermentas) *S* self. *H* hybrid

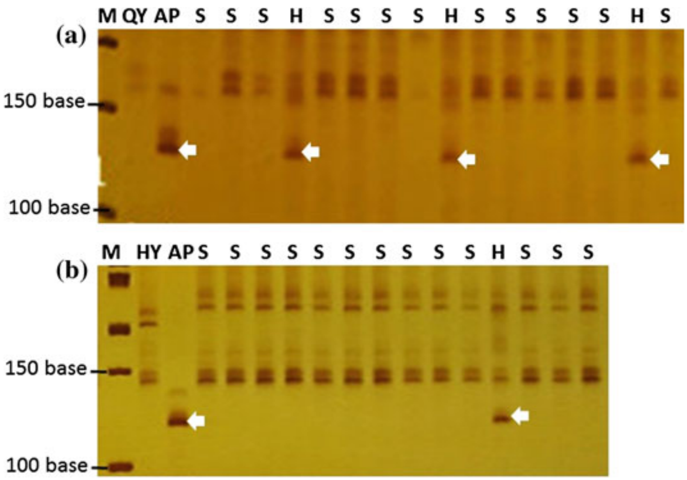

Fig. 60.2 IPAHM123 identified true F_1 hybrids (H) and selfs (S) resulting from Qunyu 101 × *A. pusilla* (**a**) and Huayu 40 × *A. pusilla* (**b**), *arrow* indicating characteristic band present in *A. pusilla* (AP, male parent) but absent in female parents, Qunyu 101 (QY) and Huayu 40 (HY). *M* 50 bp DNA Ladder (Fermentas) *S* self. *H* hybrid

60.3.2 Huayu 40 × A. pusilla

In this cross, totally six single plants were tested by PCR using primer pairs, PM468 and PM201, among which one plant (16.67 %) was identified as true F_1 hybrids only (Fig. 60.1a, b). Similar to the situation in Qunyu 101 × *A. pusilla*, both the true hybrid and the male parent *A. pusilla* produced a 100–150 nt band absent in Huayu 40. When more single plants (a total of 14 single plants) were included in SSR profiling using primer pair IPAHM123, the true hybrid identified previously produced a characteristic band co-immigrating with the band from *A. pusilla* (Fig. 60.2b).

60.4 Conclusions

In the present study, through SSR profiling, three true intersectional F_1 hybrids of Qunyu 101 × *A. pusilla* and a true intersectional F_1 hybrid of Huayu 40 × *A. pusilla* were identified, providing evidence for the effectiveness of the in vivo hormone treatment method in overcoming cross-incompatibility in the genus *Arachis*. The easy-to-use in vivo hormone treatment method may facilitate the utilization of wild incompatible peanut species in the genetic improvement of the cultivated peanut.

Acknowledgments We wish to express our sincere thanks to the financial support from China Agricultural Research System (CARS-14) and the Major Scientific and Technological Innovation Project of Shandong Academy of Agricultural Sciences (2014CGPY09) for providing financial support for this study.

References

1. Mallikarjuna N, Shilpa K, Pandey M, Janila P, Varshney R (2014) Groundnut. In: Singh M, Bisht IS, Dutta M (ed) Broadening the genetic base of grain legumes, Springer, Heidelberg, pp 161–172
2. http://en.wikipedia.org/wiki/Plumpy'nut. Accessed 1 Nov 2014
3. Kochert G, Halward T, Branch WD, Simpson CE (1991) RFLP variability in peanut (*Arachis hypogaea* L.) cultivars and wild species. Theor Appl Genet 81:565–570
4. Kochert G, Stalker HT, Gimenes M, Galgar L, Lopes CR, Moore K (1996) RFLP and cytogenetic evidence on the origin and evolution of allotetraploid domesticated peanut, *Arachis hypogaea* (Leguminosae). Am J Bot 83:1282–1291
5. Seijo JG, Lavia GI, Fernández A, Krapovickas A, Ducasse DA, Bertioli DJ, Moscone EA (2007) Genomic relationships between the cultivated peanut (*Arachis hypogaea,* Leguminosae) and its close relatives revealed by double GISH. Am J Bot 94:1963–1971
6. Varshney RK, Bertioli DJ, Moretzsohn MC, Vadez V, Krishnamurthy L, Aruna R, Nigam SN, Moss BJ, Seetha K, Ravi K, Knapp HSJ, Hoisington DA (2009) The first SSR-based genetic linkage map for cultivated groundnut (*Arachis hypogaea* L.). Theor Appl Genet 118:729–739
7. Wang CT, Tang YY, Wang XZ, Wu Q, Yang Z, Song GS, Gao HY, Yu ST, Ni WL, Yang TR, Li M, Qian L (2014) Utilizing wild incompatible *Arachis* species in the genetic improvement of the cultivated peanut (*A. hypogaea* L.). In: Kumar PA (ed) Biotechnology, vol 2, Plant biotechnology. Studium Press LLC, Houston, pp 91–114 (in press)
8. Krapovickas A, Gregory WC (1994) Taxonomy of the genus *Arachis* (Leguminosae). Bonplandia 1–4:1–186

9. Wang CT, Zhang JC, Tang YY, Guan SY, Wang XZ, Wu Q, Shan L, Zhu LG, Su JW, Yu ST (ed) (2013) Peanut Genetic Improvement. Shanghai Science and Technology Press, Shanghai, 531 pp
10. Nigam SN, Dwivedi SL, Gibbons RW (1991) Groundnut breeding: Constraints, achievements and future possibilities. Plant Breed Abstr 61:1128–1136
11. Wan SB (ed) (2003) Peanut cultivation science in China. Shanghai Science and Technology Press, Shanghai, 531 pp
12. He G, Meng R, Newman M, Gao G, Pittman RN, Prakash CS (2003) Microsatellites as DNA markers in cultivated peanut (*Arachis hypogaea* L.). BMC Plant Biol 3(1):3. doi:10.1186/1471-2229-3-3
13. He G, Meng R, Gao H, Guo B, Gao G, Newman M, Pittman RN, Prakash SC (2005) Simple sequence repeat marker for botanical varieties of cultivated peanut (*Arachis hypogaea* L.). Euphytica 142:131–136
14. Cuc LM, Mace ES, Crouch JH, Quang VD, Long TD, Varshney RK (2008) Isolation and characterization of novel microsatellite markers and their application for diversity assessment incultivated groundnut (*Arachis hypogaea*). BMC Plant Biol 15(8):55. doi:10.1186/1471-2229-8-55
15. Liang H, Wang C, Li Z, Luo X, Zou G (2008) Improvement of the silver-stained technique of polyacrylamide gel electrophoresis. Hereditas (Beijing) 30(10):1379–1382

Chapter 61
Partial Purification and Chemical Characterization of a Bioemulsifier and Its Application in MEOR

Dayuan Dong, Xingbiao Wang, Mingyu Cai, Jingjing Wang, Yifan Han, Xiaoxia Zhang and Zhiyong Huang

Abstract The bioemulsifier secreted by strain XS2, which was isolated from oil-contaminated soil samples in Yumen oil field, China, was partially purified and analyzed. Protease hydrolysis and heat treatment results showed that the protein composition of the bioemulsifier played a significant role in emulsification activity. High-performance liquid chromatography (HPLC) study suggested that the protein composition may exist as glycoprotein. Monosaccharide analysis by gas chromatograph–mass spectrometer (GC–MS) showed that galactose, glucose, xylose, and mannose presented in the bioemulsifier. The emulsification activity of this bioemulsifier was relatively high due to different carbohydrates (*n*-hexadecane 61 %, liquid paraffin 60 %, Toluene 77 %). Furthermore, single well stimulation trial in Changqing oil field, was done to explore the potential application in Microbial-enhanced oil recovery (MEOR). Up to September 2014, the cumulative increased crude oil production was about 88 T in total 240 days, and the water content of the well-produced liquid decreased from 85 to 25 %. These data illustrated that the bioemulsifier performed a high potential in applications and had important economic values.

Keyword Bioemulsifier · XS2 · Chemical characterization · MEOR · Single well stimulation

---

D. Dong and X. Wang are contributed equally to this work.

D. Dong · X. Wang · M. Cai · J. Wang · Y. Han · X. Zhang · Z. Huang (✉)
Tianjin Key Laboratory for Industrial Biological Systems and Bioprocessing Engineering,
Tianjin Institute of Industrial Biotechnology, Chinese Academy of Sciences,
Tianjin 300308, People's Republic of China
e-mail: huang_zy@tib.cas.cn

T.-C. Zhang and M. Nakajima (eds.), *Advances in Applied Biotechnology*,
Lecture Notes in Electrical Engineering 333, DOI 10.1007/978-3-662-46318-5_61

61.1 Introduction

Bioemulsifiers were compounds with surface emulsifying activity, which were usually amphipathic polysaccharides, proteins, lipopolysaccharides, lipoproteins, or complex mixtures of these biopolymers [1]. The ability to form stabilized o/w or w/o emulsion and keep the condition was the typical feature of these substances, which ensured its potential application in microbial-enhanced oil recovery (MEOR) [2, 3]. Plentiful studies about bioemulsifiers nowadays were done which mainly focused on isolation, screening of active strains, and the characteristics of their products [4–8]. De Sousa and Bhosle [5] studied the isolation and character of a lipopeptide bioemulsifier, which the emulsification activity (E24) was varied from 40 to 60 % for various tested hydrocarbons [5], while it was a pity that no further application test was carried. The study of Colin [7] was more comprehensive with an applied research for bioremediation besides the basic character of the bioemulsifier, nevertheless a more wonderful work will be presented if added the exploration of the bioemulsifier field application [9]. Although extensive researches have been conducted on variety of aspects of different bioemulsifiers including production, emulsification activity and cell surface hydrophobic activities, however, few analysis of the field application of bioemulsifiers based on the emulsification activity and production were carried out further. The most likely application of bioemulsifier was in MEOR [2, 3], which of low requirements toward the emulsifier concentration and purity. Bioemulsifiers played a significant role in extracting the remaining oil from oil reservoirs, which was cost-effective, environmental-friendly, and efficient particularly in the exploitation of oil remained trapped in capillary pores of the formation rock or in areas not swept by the classical or modern-enhanced oil recovery (EOR) methods [3]. Here, the partial purification and chemical characterization of the bioemulsifier produced by XS2 was reported and its application potential was explored in Changqing oil field by single well stimulation trial.

61.2 Materials and Methods

61.2.1 Microorganism and Media

Strain

The strain XS2, identified as *Geobacillus pallidus*, was isolated from oil contaminated soil samples in Yumen oil field, China. It could produce bioemulsifier at 60 °C with water-soluble carbon source glucose and the E24 of the fermentation liquid was about 60 %. Former chemical composition studies exhibited that the bioemulsifier consisted of carbohydrates (68.6 %), lipids (22.7 %), and proteins (8.7 %) [10].

Media

Luria-Bertani liquid medium (LB) (g/L), NaCl 10, tryptone 10, yeast extraction 5, pH 7.2, sterilized at 121 °C for 20 min.

Glucose–inorganic salt medium (GS) (g/L), glucose 20, $NaNO_3$ 3, KH_2PO_4 0.42, K_2HPO_4 1.2, $FeSO_4$ 0.05, $MgSO_4$ 0.5, $CaCl_2$ 0.05, pH 7.2, sterilized at 121 °C for 20 min [11].

The strain was cultured at 60 °C, 200 rpm with a 10 % inoculum size in 250 mL flasks. The XS2 cells as seed was incubated in LB medium for 10 h and then harvested and transferred into GS medium and cultured at 60 °C, 200 rpm for 24 h.

61.2.2 Purification of the Bioemulsifier

After culturing, the fermentation broth was centrifuged at 10,000 rpm for 20 min at 4 °C to remove the cells, and then the supernatant was obtained and precipitated with three volumes cold methanol for crude bioemulsifier isolation. The precipitate was redissolved in distilled water, dialyzed against distilled water for 48 h by dialysis bag (8,000–14,000 Da) to remove the excess inorganic salts and small molecular saccharides [10]. Then the free proteins were removed used sewage methods for three times until there was no protein layer existing. And the proteins were further dialyzed against with distilled water again for 24 h, and lyophilized.

61.2.3 Proteins Activity Identification of the Bioemulsifier

Two different treatments were carried to explore the protein role in the whole bioemulsifier. (1) Dealt with 20 mg/mL final concentration protease K at 37 °C for 30 min, (2) Set the bioemulsifier solution (5 mg/mL) at 100 °C in a water bath for 2 h, and tested the emulsification activity after treatment.

61.2.4 Gel Filtration Chromatography for the Protein Component in the Bioemulsifier

20 mg purified bioemulsifier was dissolved in 1 mL Tris-NaCl buffer (20 mmol/L Tris, 150 mmol/L NaCl) to separate the different protein components. The column used was Hiload 16/60 Superdex 200 with 0.15 Mpa column pressure and a 0.5 mL/min flow rate. The sample volume was 1.0 mL [12].

61.2.5 HPLC Analysis for the Glycosyl of the Bioemulsifier

High-performance liquid chromatography (HPLC) was used to study the glycosyl of the bioemulsifier. The chromatography column was used Agilent PL aquagel-OH MIXED-H (300 × 7.5 mm, 8 μm), and the column temperature was set at 35 °C. Double-distilled H_2O was used as the mobile phase with 0.8 mL/min flow velocity. And the injection volume was 10 μL. The Refractive index detector (RID) was set to detect the carbohydrates, at the same time an ultraviolet detector was set at 280 nm to detect proteins.

61.2.6 GC–MS Analysis for the Monosaccharide Components of the Bioemulsifier

For GC–MS analysis, the carbohydrate was first hydrolyzed by trifluoroacetic acid (TFA) and then subjected to trimethylsilylation (TMS) according to the references [13, 14]. The specific steps were done according to the method described by Peng [14]. The carrier gas was nitrogen at a flow rate of 30 mL/min. The oven temperature was set to 70 °C for 0.5 min. The temperature gradient was 130–280 °C at a rate of 10 °C/min.

61.2.7 Microbial Community Structure Analysis of the Test Well

Total DNA was extracted from the well production water sample of the test well Liu55-4 before the field trial by Ultra Clean TM Soil DNA Isolation Kit (Mo Bio Laboratories, Inc., USA) according to the operation manual. The microbial community was tested by 16S rDNA gene clone library, DNA sequencing, alignment, and phylogenetic analysis according to the reported method [15]. Aiming to compound a nutrient liquid to stimulate the indigenous bacteria, the community consisted was studied by the above method.

61.2.8 Field Study of MEOR

A pilot test in oil field was carried out to examine the applicability of the bioemulsifier produced by the strain XS2 after laboratory studies. To get a better effect, fermentation broth of XS2 and glycolipid were mixed by different ratios. The perfect ratio that the mixed liquid could make the solution keep a relative low surface tension and a high E24 activity at the same time was set as the final used ratio. Microbial inorganic salt nutrients were determined by the microbial community structure, which was learned from the oil well production water samples. Then the compounds mixture used as the composite oil displacement agent in MEOR including bioemulsifier of XS2, glycolipid, and inorganic salt nutrients was injected into Liu55-4 well, Changqing oilfield, China. The well had been closed for three months after composite oil displacement agent injection, and then begun to exploit crude oil. Two data mainly, crude oil production and water content of the well production liquid were recorded as the parameters to evaluate the bioemulsifier efficiency in MEOR.

61.3 Results and Discussions

61.3.1 Protein Activity Identification of the Bioemulsifier

For the protein activity identification of the bioemulsifier, an interesting phenomenon suggested that the protein component in bioemulsifier acted as a vital role for its emulsification activity. After treated by protease K for 30 min at 37 °C, the emulsification ability of the bioemulsifier was disappeared, but thermal treatment at 100 °C for 2 h acted slight influence on the emulsion ability of the bioemulsifier (Fig. 61.1). From this test, two conclusions were gotten. One conclusion was that the protein component performed a significant role in emulsification ability, the

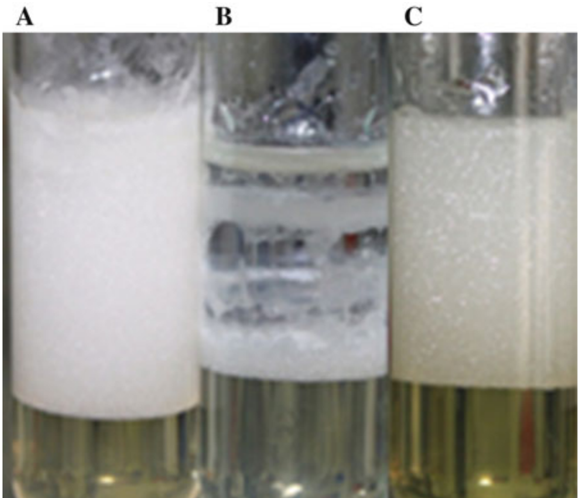

Fig. 61.1 The emulsification activity of the bioemulsifier, *A* stands for the bioemulsifier solution with no treatment, *B* stands for treated by protease K, and *C* stands for treated by high temperature

other was that the bioemulsifier performed certain thermo stability. A reasonable interpretation may be that the optimum growth temperature of this strain was 60 °C, the thermal protein was a result of evolving to adapted the environment in the heat oil reservoir. This may strengthen the theoretical support of the bioemulsifier of this strain application in MEOR.

61.3.2 Gel Filtration Chromatography for the Protein Components of the Bioemulsifier

To further purify the bioemulsifier, gel filtration chromatography of the protein components was done. Figure 61.2 showed that the protein in bioemulsifier was consisted of 3 fractions, and then the fractions were collected, respectively, and carried out the emulsification activity test for each fraction. The results showed that the second fraction performed the central emulsion activity, while the first and third fractions had no emulsification activity. SDS-PAGE was done for fraction 2, and there were totally four bands about 72, 70, 42, 24 KDa, respectively (Fig. 61.3). From the analysis of the Gel filtration chromatography, fraction 2 was consisted of totally four protein fragments and played a key role in the emulsion activity of the bioemulsifier. And further components research was carried out by HPLC.

61.3.3 HPLC Analysis for Fraction 2 of the Bioemulsifier

To explore the existing form of the protein in fraction 2, HPLC analysis was performed. The HPLC data showed that when there was a peak in the RID, there appeared a peak in ultraviolet detector almost the same time, which mean that the saccharine component and the protein component were detected almost at the same time. There comes a hypothesis that the protein component may exist as glycoprotein in the bioemulsifier (Fig. 61.4).

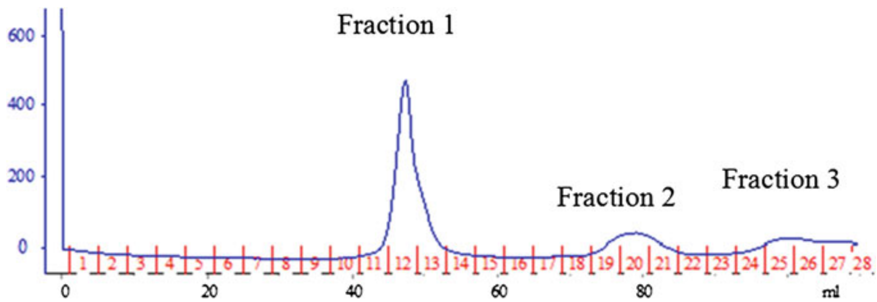

Fig. 61.2 Results of the bioemulsifier gel filtration chromatography

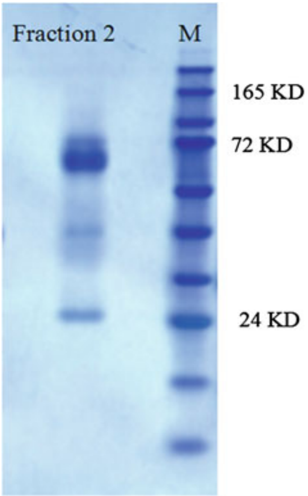

Fig. 61.3 SDS-PAGE for fraction 2

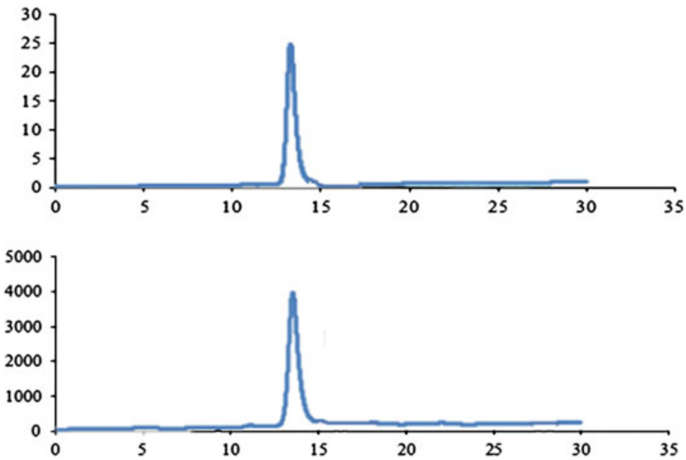

Fig. 61.4 HPLC result of fraction 2, the *above* peak was detected by RID detector, standing for the saccharide detected, and the *below* peak was detected by ultraviolet detector, standing for the protein detected

61.3.4 Monosaccharide Components Analysis of the Bioemulsifier

GC–MS analysis was done to analyze the monosaccharide composition of the bioemulsifier. Figure 61.5 showed there were four main peaks, and each peak

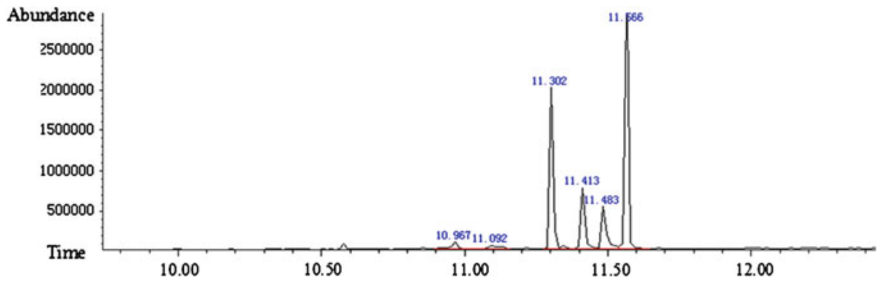

Fig. 61.5 GC–MS analysis of the monosaccharide of the bioemulsifier

stands for one silanized saccharide. Compared to the database, the monosaccharide components were likely to be galactose, glucose, xylose, and mannose (Table 61.1). A certain result will be obtained followed by further study. Research conducted by Llamas et al. [16] reported that the monosaccharide composition of the EPS was mannose, glucose, and rhamnose. Monteiro et al. [17] also mentioned the bioemulsifier produced by CLA2 had xylose, mannose, and glucose. Glucose and mannose were the shared monosaccharide in the high-molecular polymer. The unique monosaccharide of the bioemulsifier produced by XS2 was galactose compared to the other two researches. Although different products from various bacteria have diverse monosaccharide composition, there may be some usual monosaccharide. The different monosaccharides and the composition ratio of the high-molecular polymers may present on various activity and function.

61.3.5 Microbial Community Structure Analysis of the Test Well

Microbial community structure in the well Liu55-4 was analyzed, which could provide much more useful and abundant information for selecting appropriate inorganic salt as the injected nutrients for MEOR. Based on the analysis data, a total of 7 genera were discovered in Liu55-4, which were *Pelobacter*, *Petrotoga*, *Bacillus*, *Acinetobacter*, *Synergiste*, *Sedimentibacte*, and *Halabaerobiu*. The dominant species was *Palobacter*, about 38.3 % of total bacteria. *Sedimentibacte* and *Halanaerobiu* were infrequent species, about 4.26 %. Most microorganisms existed in the oil well could utilize the hydrocarbons in the oil reservoir, and according to

Table 61.1 The monosaccharide component of the bioemulsifier

Remain time	Compound	Structure formula
11.302	Galactopyranose	$C_{21}H_{52}O_6$
11.413	Glucopyranose	$C_{21}H_{52}O_6$
11.483	D-Xylose tetrakis	$C_{17}H_{42}O_5$
11.566	Mannose	$C_{21}H_{52}O_6$

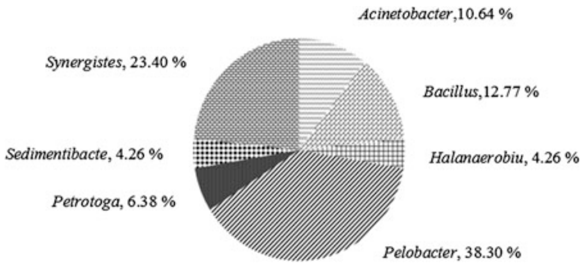

Fig. 61.6 The microbial community structure of 55-4 oil water

nutrients necessary for these bacteria and XS2, a nutrient solution including nitrates, phosphate, trace elements, and vitamins was determined for pilot research in oil field (Fig. 61.6).

61.3.6 Field Study of MEOR

XS2 fermentation by various scale fermenters (7, 30, 200, 2,000 L) was performed to obtain enough fermentation liquid, all the cell concentration maintained more than 5 × 108/mL in the fermentation broth. Aimed at getting effective oil displace agent, the fermentation broth was compound with glycolipid solution (1 g/L). Finally, an 87 % emulsion activity on paraffin and the surface tension of the oil displace agent solution kept 33.8 mN/m. At the same time, 5 % (w/v) crude oil, 75 % inorganic salt medium (v/v) were mixed and added the following three liquids, respectively: (1) 20 % fermentation broth of XS2, (2) 20 % glycolipid solution (1 g/L), (3) 20 % compound agent of XS2 fermentation broth and gly-colipid. The flasks were incubated at 60 °C and 180 rpm in shaker for 5 min, and then observed the emulsification state of crude oil (Fig. 61.7). The system added compound agent showed the crude oil dispersed as small droplets and the emulsification state could keep more than 15 days. While the other two systems added fermentation broth and glycolipid solution separately, both presented a weaker effect. This oil displacement agent compound consisted of fermentation broth and glycolipid gathered both the advantages of bioemulsifier and glycolipid which could decrease the surface/interfacial tension, meanwhile maintain a high emulsification state more than 15 days.

Liu55-4 well, Changqing oilfield, China, was chosen as the experimental well. Since November 2011, the water content of the well-produced liquid increased from 20 to 85.7 % and the yield of crude oil fall down to 0.23 m^3/d (0.03 T). The oil displacement agent was injected into the Liu55-4 well in December, 2013, and then closed the well for three months before exploitation. Crude oil production and water content of the produced liquid were recorded as the main parameters. The oil yield and water content gradually tended to stable after 20 days extraction. The oil

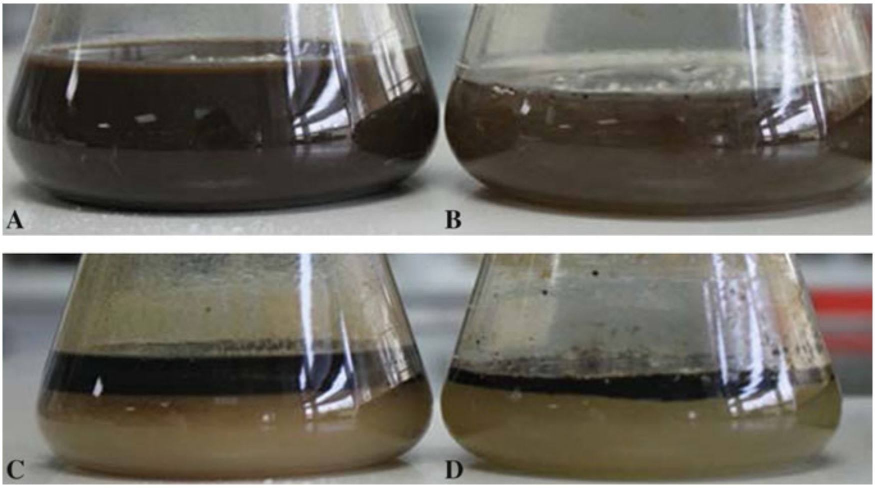

Fig. 61.7 The comparison of single liquid and compound liquid acting on crude oil, *A* and *C* were compound liquid of XS2 fermentation broth and glycolipid, *B* and *D* stands for the result added glycolipid only. *A* and *B* were uniformed by shaking, and *C* and *D* were the static condition

production was 0.65 m^3 (0.36 T), with 25 % water content. To date, the well had produced crude oil for more than 8 months, and the average daily output was 0.45 T. Partial data after trial was displayed in Table 61.2 and Fig. 61.6, which showed the comparison of oil production and water content before and after the oil displacement agent injection. The data showed crude oil production was increased more than 12 times and the water content was decreased more than 70 %. Totally, 100 T crude oil was extracted after this trial, and compared to the data before, the increased production of the crude oil was 88 T. Oil displacement agent performed a sound effect for oil extraction, and the bioemulsifier played a significant role in the process, which give a robust proof that the strain XS2 has a huge application potential in MEOR (Fig. 61.8).

Table 61.2 The results of oil recovery

Time (d)	Liquid (m^3)	Water content (%)	Oil production (T)
1	6.72	100	0
4	3.41	95	0.13
6	2.19	23.4	1.43
12	2.19	25.6	1.38
17	0.63	26.6	0.39
24	0.6	26.6	0.36
40	0.6	26.6	0.36
55	0.6	26.6	0.36

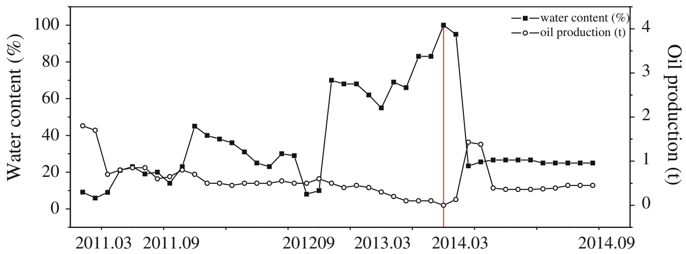

Fig. 61.8 Oil production and water content curve of the Liu55-4 well in Changqing oil field. The *red vertical line* was a mark. On the *left* and *right of the red line* were the oil production data before and after oil displacement agent injection, respectively

Acknowledgments This work was supported by cooperation projects of China Academy of Sciences (Xinjiang), Major projects of beautiful Tianjin (Tianjin Municipal Science and Technology Commission), The Youth Foundation of National Natural Science Fund (31300098), Top Priority Open Fund Projects in Zhejiang Province (xkzsc10) and The National High Technology Research and Development Program (2012AA092001).

References

1. Rosenberg E, Ron EZ (1999) High- and low-molecular-mass microbial surfactants. Appl Microbiol Biotechnol 52(2):154–162
2. Camacho-Chab JC, Guezennec J, Chan-Bacab MJ, Rios-Leal E, Sinquin C, Muniz-Salazar R et al (2013) Emulsifying activity and stability of a non-toxic bioemulsifier synthesized by microbacterium sp MC3B-10. Int J Mol Sci 14(9):18959–18972
3. Campos JM, Stamford TLM, Sarubbo LA (2014) Production of a bioemulsifier with potential application in the food industry. Appl Biochem Biotechnol 172(6):3234–3252
4. Colin VL, Pereira CE, Villegas LB, Amoroso MJ, Abate CM (2013) Production and partial characterization of bioemulsifier from a chromium-resistant actinobacteria. Chemosphere 90 (4):1372–1378
5. de Sousa T, Bhosle S (2012) Isolation and characterization of a lipopeptide bioemulsifier produced by Pseudomonas nitroreducens TSB.MJ10 isolated from a mangrove ecosystem. Bioresour Technol 123:256–262
6. Pereira JFB, Gudina EJ, Costa R, Vitorino R, Teixeira JA, Coutinho JAP et al (2013) Optimization and characterization of biosurfactant production by Bacillus subtilis isolates towards microbial enhanced oil recovery applications. Fuel 111:259–268
7. Leticia Colin V, Fernanda Castro M, Julia Amoroso M, Beatriz Villegas L (2013) Production of bioemulsifiers by Amycolatopsis tucumanensis DSM 45259 and their potential application in remediation technologies for soils contaminated with hexavalent chromium. J Hazard Mater 15(261):577–583
8. Lazar I, Petrisor I, Yen T (2007) Microbial enhanced oil recovery (MEOR). Pet Sic Technol 25(11):1353–1366
9. Brown LR (2010) Microbial enhanced oil recovery (MEOR). Curr Opin Microbiol 13(3): 316–320
10. Zheng C, He J, Wang Y, Wang M, Huang Z (2011) Hydrocarbon degradation and bioemulsifier production by thermophilic Geobacillus pallidus strains. Bioresour Technol 102 (19):9155–9161

11. Wang M, Wang X, Zheng C, Chang Y, Wang Y, Huang Z (2014) Study on process optimization for bioemulsifier production. In: Proceedings of the 2012 international conference on applied biotechnology (ICAB 2012), vol 249, pp 367–379
12. Moon SM, Kim JS, Kim HJ, Choi MS, Park BR, Kim SG et al (2014) Purification and characterization of a novel fibrinolytic alpha chymotrypsin like serine metalloprotease from the edible mushroom, Lyophyllum shimeji. J Biosci Bioeng 117(5):544–550
13. Wang XB, Nie Y, Tang YQ, Wu G, Wu XL (2013) *n*-Alkane Chain Length Alters Dietzia sp Strain DQ12-45-1b Biosurfactant Production and Cell Surface Activity. Appl Environ Microbiol 79(1):400–402
14. Peng F, Liu Z, Wang L, Shao Z (2007) An oil-degrading bacterium: rhodococcus erythropolis strain 3C-9 and its biosurfactants. J Appl Microbiol 102(6):1603–1611
15. Filteau M, Lagace L, LaPointe G, Roy D (2010) Seasonal and regional diversity of maple sap microbiota revealed using community PCR fingerprinting and 16S rRNA gene clone libraries. Syst Appl Microbiol 33(3):165–173
16. Llamas I, Amjres H, Mata JA, Quesada E, Bejar V (2012) The potential biotechnological applications of the exopolysaccharide produced by the halophilic bacterium halomonas almeriensis. Molecules 17(6):7103–7120
17. de Souza Monteiro A, Domingues VS, Souza MVD, Lula I, Gonçalves DB, de Siqueira EP et al (2012) Bioconversion of biodiesel refinery waste in the bioemulsifier by *Trichosporon mycooxinivorans* CLA2. Biotechnol Biofuels 5(29)

Chapter 62
Optimization of a Whey Containing Medium for β-Galactosidase Production by *Lactobacillus reuteri*

Mengfei Li, Huiming Zhu, Huibin Qin, Yan Zhang and Hongjiang Yang

Abstract *Lactobacillus reuteri* MF2-2 was screened out for producing a high level of β-galactosidase from chicken fecal samples and identified with 16S rRNA gene sequence analysis. To reduce production cost, a new whey containing medium was formulated on the basis of MRS medium and optimized. Nutrients including whey, yeast extract, $NH_4H_2PO_4$, and vitamin B_1 were investigated at the individual and interactive level by the Taguchi orthogonal tests. The production of β-galactosidase was improved from 490.0 U/g in lactose-based MRS (L-MRS) medium to 814.6 U/g in the optimized whey-based MRS (W-MRS) medium. W-MRS medium did not comprise of lactose, peptone, and beef extract and was expected to cut the raw material cost approximately in half compared to L-MRS medium.

Keywords *Lactobacillus reuteri* · β-Galactosidase · Whey-based MRS medium (W-MRS)

62.1 Introduction

β-Galactosidases are mainly used to hydrolyze lactose in milk for producing low-lactose dairy products [1]. β-Galactosidases are widely present in plants, bacteria, fungi, yeast, and animal cells. The industrial β-galactosidases are mainly obtained from the probiotic microorganisms, such as *Aspergillus* sp. and *Kluyveromyces* sp. [2, 3].

M. Li · H. Zhu · H. Qin · H. Yang (✉)
Key Laboratory of Industrial Microbiology, Ministry of Education, Tianjin Key Laboratory of Industrial Microbiology, College of Biotechnology, Tianjin University of Science & Technology, Tianjin 300457, China
e-mail: hongjiangyang@tust.edu.cn

Y. Zhang
Tianjin Shuang Lian Ke Xin Biotechnology Co., Ltd, Tianjin, China

T.-C. Zhang and M. Nakajima (eds.), *Advances in Applied Biotechnology*,
Lecture Notes in Electrical Engineering 333, DOI 10.1007/978-3-662-46318-5_62

Lactic acid bacteria (LAB) are a taxonomically diverse group of gram-positive bacteria and usually categorized as “generally regarded as safe” (GRAS) organisms. All LAB strains produce lactic acid as the only or main end product of carbohydrate metabolism [4, 5]. Due to their GRAS status and ability to hydrolyze lactose, a number of strains may have the potential to be starters for industrial production of β-galactosidases [6]. Among them, *Streptococcus thermophilus*, which is the most important species in the manufacture of cheese and yogurt, has been well studied for β-galactosidases production [7]. Bifidobacteria are obligate anaerobes existing in the intestinal tract of humans and animals, and β-galactosidase productions have been investigated in strains of this genus [8–10]. Moreover, a wide variety of Lactobacillus species have also been assessed as potential source of β-galactosidases, such as *L. acidophilus*, *L. bulgaricus*, *L. helviticus*, *L. kefiranofaciens*, *L. lactis*, *L. sporogenes*, *L. themophilus*, *L. delbrueckii*, and *L. fermentum* [2, 11].

In this work, lactose-based MRS (L-MRS) medium was used in isolation of lactic acid bacteria (LAB) producing β-galactosidase. The highest β-galactosidase producer was selected and the lactase was characterized. In addition, a whey-containing medium was formulated and optimized based on L-MRS medium to improve the enzyme productivity and reduce production cost in the β-galactosidase fermentation process.

62.2 Materials and Methods

62.2.1 *Media, Growth Conditions, and Isolation of β-Galactosidase Producing Lactobacilli*

MRS medium was composed of 20 g/L glucose, 10 g/L peptone, 8 g/L beef extract, 4 g/L yeast extract, 5 g/L sodium acetate, 2 g/L ammonium citrate, 0.2 g/L $MgSO_4$, 0.05 g/L $MnSO_4$, 2 g/L KH_2PO_4, and 0.1 % Tween-80 [12]. Lactose-MRS (L-MRS) agar (pH 5.0) was used in isolating β-galactosidase producing *lactobacilli* by replacing glucose in MRS with 20 g/L lactose. L-MRS broth (pH 6.4) was used for the cultivation of *lactobacilli* isolates and β-galactosidase production. Both plates and liquid cultures were statically incubated at 35 °C. Thirty fresh chicken fecal samples were collected from five henneries located in Beijing and Henan Province, respectively. To isolate β-galactosidase producing *lactobacilli*, the chicken fecal samples were suspended in 1× PBS buffer. Serial dilutions were spread on L-MRS agar containing 20 μg/mL X-gal and incubated.

62.2.2 Determination of β-Galactosidase Activity

β-Galactosidase activity was tested by a modified method [13, 14]. In brief, 3 mL Z-buffer (pH 7.0) and 80 μL chloroform were added to 1 mL culture and mix thoroughly by vortex. The crude permeabilized cell suspension was added with 0.8 mL of 4 mg/mL ONPG (o-nitrophenol-β-D-Galactopyranoside) and incubated at 37 °C. The reaction was terminated by adding 1 mL of 1 M Na_2CO_3 when the mixture turned yellow. The mixture was centrifuged at 12,000 rpm for 3 min and the supernatant was measured spectrophotometrically at 420 nm. One unit of β-galactosidase activity was defined as the enzyme quantity that liberated 1 μmol o-nitrophenol per minute. Lactase concentration (U/g) was determined as the number of the enzyme units per gram of dry cell weight.

62.2.3 Identification of the Isolated Organism

Genomic DNA of the isolated *lactobacilli* was extracted and used as template for amplification of 16S rRNA gene with primers described previously [15]. The PCR reaction system was 50 μL and the parameters include denaturation at 94 °C for 5 min, 1 cycle; denaturation at 94 °C for 45 s, annealing at 53 °C for 45 s, and extension at 72 °C for 1.5 min, 30 cycles; 72 °C for 10 min. Sequence similarity was analyzed by using the tool BLAST from the NCBI web site.

62.2.4 Time Course of β-Galactosidase Production

To study the β-galactosidase production of different periods, fermentations were performed in 250 mL shake flasks containing 100 mL L-MRS medium with 1 % inoculums of seed cultures. Samples were collected at 2 h time intervals for measuring cell density (OD_{600}) and β-galactosidase activity during fermentation process.

62.2.5 Formulation and Optimization of a Whey Containing Medium

Whey contained high content of lactose and it was often used as an alternative carbon source to lactose. On the basis of L-MRS medium, a whey medium was formulated by using dry whey (sweet type) powder as the carbon source. The effect of different nitrogen sources and vitamin B_1 on β-galactosidase production was investigated. Fermentation parameters were tested at individual and interactive level. An L_{16} (4^4) array used in the Taguchi orthogonal tests was designed to optimize the whey containing medium for improvement of β-galactosidase production. Lactose content in whey was determined by Lane-Eynon's method [16].

62.3 Results and Discussions

62.3.1 Isolation of β-Galactosidase Producing Lactobacilli

L-MRS agar containing 20 μg/mL X-gal was used to isolate β-galactosidase producing lactobacilli. From 30 chicken fecal samples, 13 strains were obtained and purified. The β-galactosidase production was measured after fermentation in L-MRS for 24 h. Strain MF2-2 produced the highest level of β-galactosidase with the activity of 517.7 U/g.

62.3.2 Identification of Strain MF2-2

16S rRNA gene of strain MF2-2 was amplified and sequenced. The obtained sequence was deposited in GenBank with the accession number KJ495694. 16S rRNA gene comparison was conducted and the result showed that strain MF2-2 exhibited a 99 % sequence homology with *L. reuteri* TD1 [17]. *L. reuteri* is the most abundant species of the heterofermentative *lactobacilli* in the gastrointestinal tract in humans and animals. The bacterium is responsible for hydrolyzing lactose inside the gastrointestinal tract with β-galactosidase. *L. reuteri* MF2-2 was deposited in China Center for Industrial Culture Collection and the number was CICC No. 10855.

62.3.3 Time Course of β-Galactosidase Production

Time course of cell growth and β-galactosidase production of *L. reuteri* MF2-2 were analyzed and shown in Fig. 62.1. As the bacterium began to grow, the bacterial cells began to produce β-galactosidase. The cultures entered stationary phase after 16 h incubation at an OD_{600} of 4.0, while β-galactosidase production reached maximum level of 509.3 U/g at 24 h. Only a limit amount of β-galactosidase was accumulated after 20 h and the result indicated the enzyme could be harvested at the window of 20–24 h.

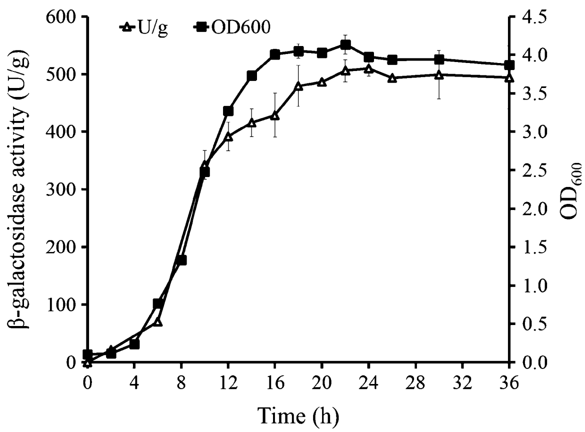

Fig. 62.1 Time course of the growth and β-galactosidase production by *Lactobacillus reuteri* MF2-2

62.3.4 Formulation of a Whey Containing Medium for β-Galactosidase Production

Several ingredients in L-MRS medium were expensive, including lactose, yeast extract, peptone, beef extract, and ammonium citrate. To reduce the high production cost, L-MRS medium was modified by testing different formulas. Sweet type whey powder was determined containing 71.1 % lactose by Lane-Eynon's method, and it was used as an alternative carbon source to lactose. In W-MRS-1 (whey-based MRS) medium with 20 g/L whey, the β-galactosidase yield was 957.5 U/g which was much higher than L-MRS (490.0 U/g) (Table 62.1). However, beef extract and peptone were present in both media which were still very expensive for β-galactosidase production.

In L-MRS-2 and L-MRS-3 media, whey was used as a nitrogen source to replace peptone or beef extract, the cultures produced higher levels of β-galactosidase, 594.0 and 622.7 U/g, respectively, compared to fermentations in L-MRS medium (Table 62.1). The result indicated that the whey could provide nitrogen sources for fermentation of the strain MF 2-2. To test this hypothesis, W-MRS-4 medium was further tested and the strain produced 517.1 U/g of β-galactosidae in the absence of both peptone and beef extract (Table 62.1). The production level was comparable to L-MRS medium (Table 62.1). Furthermore, $NH_4H_2PO_4$ was used to replace inorganic nitrogen source ammonium citrate and KH_2PO_4 in W-MRS-5 medium, and the β-galactosidase production was 520.2 U/g which was at the same level with L-MRS medium (490.0 U/g) (Table 62.1). The results demonstrated that whey and $NH_4H_2PO_4$ were able to provide enough nitrogen for the enzyme production.

Vitamin B_1, also called thiamine or thiamin, is a cofactor of a variety of enzymes which are involved in carbohydrate catabolism. The effect of vitamin B_1 on β-galactosidase production was also investigated. The result showed that vitamin

Table 62.1 Investigation of the nutrients affecting β-galactosidase production

Medium	Components (g/L)									β-Galactosidase activity (U/g)
	Whey	Lactose	Peptone	Beef extract	Yeast extract	Ammonium citrate	KH_2PO_4	$NH_4H_2PO_4$	VB_1 ($\times 10^{-3}$)	
L-MRS	0	20	10	8	4	2	2	0	0	490.0 ± 35.0
L-MRS-1	0	20	10	8	8	2	2	0	0	453.4 ± 20.0
L-MRS-2	0	20	10	8	4	2	2	0	4.5	700.6 ± 15.1
W-MRS-1	20	0	10	8	4	2	2	0	0	957.5 ± 34.7
W-MRS-2	10	20	0	8	4	2	2	0	0	594.0 ± 35.9
W-MRS-3	8	20	10	0	4	2	2	0	0	622.7 ± 52.1
W-MRS-4	20	0	0	0	4	2	2	0	0	517.1 ± 11.3
W-MRS-5	20	0	0	0	4	0	0	4	0	520.2 ± 36.7
W-MRS-6	20	0	0	0	4	0	0	4	4.5	742.0 ± 23.9
W-MRS-7	20	0	0	0	2	0	0	4	4.5	349.4 ± 4.3

In addition to the components listed in the table, all media also contain CH_3COONa 5 g/L, $MgSO_4$ 0.2 g/L, $MnSO_4$ 0.05 g/L, and Tween-80 0.1 %

B_1 could increase β-galactosidase production significantly in both L-MRS-2 and W-MRS-6 media, 700.6 and 742.0 U/g, respectively (Table 62.1).

Yeast extract content was also monitored. When its concentration was increased to 8 g/L, no increase of β-galactosidase production was obtained in L-MRS-1 compared L-MRS medium (Table 62.1). However, the decrease of yeast extract content brought a significant reduction of β-galactosidase production, only 349.4 U/g was obtained in W-MRS-7 medium (Table 62.1). Based on the obtained results, the final formula of W-MRS medium was determined and composed of whey 20 g/L, yeast extract 4 g/L, $NH_4H_2PO_4$ 4 g/L, CH_3COONa 5 g/L, $MgSO_4$ 0.2 g/L, $MnSO_4$ 0.05 g/L, 0.1 % Tween-80, and vitamin B_1 4.5 mg/L.

62.3.5 The Optimization of W-MRS Medium

To further improve β-galactosidase production, W-MRS medium was optimized by orthogonal array. The effects of whey, yeast extract, $NH_4H_2PO_4$, and vitamin B_1 in W-MRS medium on fermentation performance were investigated at the individual level first. As shown in Fig. 62.2, each factor with five concentrations was evaluated by measurement of β-galactosidase production in the cultures. The optimum

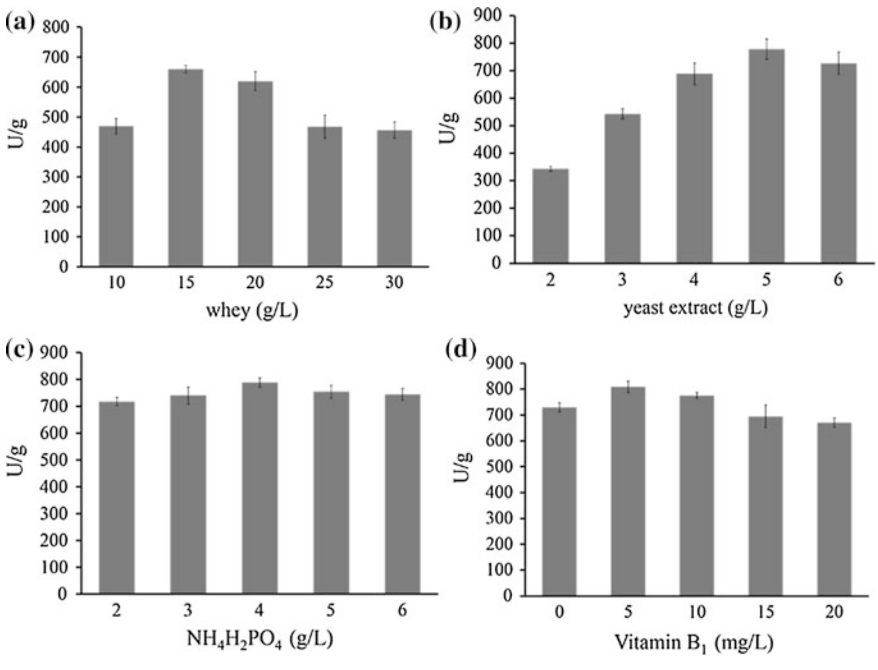

Fig. 62.2 Effect of different whey **a** yeast extract, **b** $NH_4H_2PO_4$, **c** and vitamin B_1, **d** concentrations on β-galactosidase production

Table 62.2 Selected factors and their assigned levels for the orthogonal experimental design

Factors		Levels			
No.	Descriptions	1	2	3	4
A	Whey (g/L)	12.5	15.0	17.5	20.0
B	Yeast extract (g/L)	4.5	5.0	5.5	6.0
C	$NH_4H_2PO_4$ (g/L)	3.5	4.0	4.5	5.0
D	Vitamin B_1 (mg/L)	2.5	5.0	7.5	10.0

concentration was 15 g/L whey, 5 g/L yeast extract, 4 g/L $NH_4H_2PO_4$, and 5 mg/L vitamin B_1, respectively, which was indicated by the highest corresponding β-galactosidase activity in each set of fermentations (Fig. 62.2).

According to the obtained optimum concentration for each nutrient, an L_{16} (4^4) array used in the Taguchi orthogonal tests was designed as described in Tables 62.2 and 62.3. Fermentations using 16 different media were conducted. Based on the R value obtained, factors affecting β-galactosidase activity were ranked from high to low as whey, vitamin B_1, yeast extract, and $NH_4H_2PO_4$. The optimal conditions were determined as $A_3B_4C_3D_3$, which was whey powder 17.5 g/L, vitamin B_1

Table 62.3 Orthogonal experiment design for optimization of W-MRS medium

No.	Factor levels				β-Galactosidase activity (U/g)
	A	B	C	D	
1	1	1	1	1	614.1 ± 30.3
2	1	2	2	2	610.1 ± 29.7
3	1	3	3	3	720.6 ± 92.8
4	1	4	4	4	616.5 ± 59.3
5	2	1	2	3	680.6 ± 40.6
6	2	2	1	4	652.8 ± 61.7
7	2	3	4	1	658.4 ± 32.5
8	2	4	3	2	789.8 ± 52.1
9	3	1	3	4	679.5 ± 46.7
10	3	2	4	3	721.9 ± 52.8
11	3	3	1	2	751.1 ± 13.0
12	3	4	2	1	713.6 ± 76.6
13	4	1	4	2	664.3 ± 33.8
14	4	2	3	1	616.3 ± 43.4
15	4	3	2	4	651.0 ± 56.3
16	4	4	1	3	779.6 ± 51.7
T1/4	640.3	659.6	699.4	650.6	
T2/4	695.4	650.3	663.8	703.8	
T3/4	716.5	695.3	701.5	725.7	
T4/4	677.8	724.9	665.3	649.9	
R	76.2	74.6	37.7	75.7	

7.5 mg/L, yeast extract 6 g/L, and $NH_4H_2PO_4$ 4.5 g/L. Together with other components, including CH_3COONa 5 g/L, $MgSO_4$ 0.2 g/L, $MnSO_4$ 0.05 g/L, and 0.1 % Tween-80, the optimum parameters of W-MRS medium was defined. Under the same fermentation conditions, the β-galactosidase production was 814.6 U/g in the optimized medium, much higher than L-MRS medium.

62.4 Conclusion

Whey was a by-product generated in the cheese processing industry. More than 55 % of milk nutrients were remained in the whey liquid, including lactose (4.5–6.0 % w/v), protein (0.6–1.1 % w/v), and other nutrients. After dehydration, lactose and protein constituted approximately 70 and 10 % of whey powder, respectively [18]. Whey products provided carbon and nitrogen source to the microorganisms capable of metabolizing lactose. Currently, whey has been widely applied in a variety of fermentation processes to produce a number of bioproducts, such as ethanol, lactic acid, bacteriocins, and enzymes [19–21].

In this study, W-MRS medium was formulated and optimized. The medium did not contain lactose, peptone, and beef extract and the medium cost was reduced approximately to 50 % of L-MRS medium with a relatively high β-galactosidase activity 814.6 U/g. However, there is still room for further improvement of β-galactosidase production if more nutrients were supplemented. W-MRS-1 medium gave 957.5 U/g of β-galactosidase even without optimization of the related fermentation parameters, though the enzyme production cost went up significantly. Our results suggested strain MF2-2 might be used as a starter strain for β-galactosidase production and W-MRS medium had the potential to cut down the production cost during fermentation process.

Acknowledgments This work was partly supported by the Tianjin Key Technology R&D Program (Grant No. 13ZCZDNC00600).

References

1. Oliveira C, Guimaraes PM, Domingues L (2011) Recombinant microbial systems for improved beta-galactosidase production and biotechnological applications. Biotechnol Adv 29 (6):600–609
2. Husain Q (2010) β Galactosidases and their potential applications: a review. Crit Rev Biotechnol 30(1):41–62
3. Panesar PS, Panesar R, Singh RS, Kennedy JF, Kumar H (2006) Microbial production, immobilization and applications of β-D-galactosidase. J Chem Technol Biotechnol 81 (4):530–543
4. Foligne B, Daniel C, Pot B (2013) Probiotics from research to market: the possibilities, risks and challenges. Curr Opin Microbiol 16(3):284–292

5. Konings WN, Kok J, Kuipers OP, Poolman B (2000) Lactic acid bacteria: the bugs of the new millennium. Curr Opin Microbiol 3(3):276–282
6. Husain Q (2010) β-Galactosidases and their potential applications: a review. Crit Rev Biotechnol 30(1):41–62
7. Rao MV, Dutta SM (1977) Production of beta-galactosidase from *Streptococcus thermophilus* grown in whey. Appl Environ Microbiol 34(2):185–188
8. Goulas T, Goulas A, Tzortzis G, Gibson G (2009) Comparative analysis of four β-galactosidases from *Bifidobacterium bifidum* NCIMB41171: purification and biochemical characterization. Appl Microbiol Biotechnol 82(6):1079–1088
9. Hinz SA, Broek LM, Beldman G, Vincken J-P, Voragen AJ (2004) β-Galactosidase from *Bifidobacterium adolescentis* DSM20083 prefers β-(1,4)-galactosides over lactose. Appl Microbiol Biotechnol 66(3):276–284
10. Hsu CA, Yu RC, Chou CC (2005) Production of β-galactosidase by *Bifidobacteria* as influenced by various culture conditions. Int J Food Microbiol 104(2):197–206
11. Panesar PS, Kumari S, Panesar R (2010) Potential applications of immobilized beta-galactosidase in food processing industries. Enzym Res 2010:4731–4737
12. De Man JC, Rogosa M, Sharpe ME (1960) A medium for the cultivation of lactobacilli. J Appl Bacteriol 23(1):130–135
13. Dagbagli S, Goksungur Y (2008) Optimization of β-galactosidase production using *Kluyveromyces lactis* NRRL Y-8279 by response surface methodology. Electron J Biotechnol 11(4):1–12
14. Lodi T, Donnini C (2005) Lactose-induced cell death of beta-galactosidase mutants in *Kluyveromyces lactis*. FEMS Yeast Res 5(8):727–734
15. Lane DJ (1991) 16S/23S rRNA sequencing. In: Stackebrandt E, Goodfellow M (eds) Nucleic acid techniques in bacterial systematics. Wiley, New York, pp 115–175
16. AOAC (1984) Official methods of analysis, 14th edn. Association of Official Analytical Chemists, Arlington, p 1141
17. Leonard MT, Valladares RB, Ardissone A, Gonzalez CF, Lorca GL, Triplett EW (2014) Complete genome sequences of *Lactobacillus johnsonii* strain N6. 2 and *Lactobacillus reuteri* strain TD1. Genome Announc 2(3):e00397–14
18. Prazeres AR, Carvalho F, Rivas J (2012) Cheese whey management: a review. J Environ Manage 110:48–68
19. Guimarães PMR, Teixeira JA, Domingues L (2010) Fermentation of lactose to bio-ethanol by yeasts as part of integrated solutions for the valorisation of cheese whey. Biotechnol Adv 28 (3):375–384
20. Panesar PS, Kennedy JF, Gandhi DN, Bunko K (2007) Bioutilisation of whey for lactic acid production. Food Chem 105(1):1–14
21. Siso MIG (1996) The biotechnological utilization of cheese whey: a review. Bioresour Technol 57(1):1–11

Chapter 63
Enzymatic Bioconversion for γ-Aminobutyric Acid by *Lactobacillus brevis* CGMCC No. 3414 Resting Cells

Xiu-feng Shi, Bo Zheng, Chuan-you Chang, Peng Cao, Hong-jin Yang and Qiang Gao

Abstract In this work, γ-aminobutyric acid (GABA) was prepared by the decarboxylation of L-glutamate via L-glutamate decarboxylase in the resting cells of *Lactobacillus brevis* CGMCC No. 3414. The influence of cell concentration, cell age, buffer system, reaction time, and substrate concentration were investigated. The optimal composition of bioconversion system was composed of 50 g/L resting cells, cell age at 48 h fermentation, 0.2 M disodium hydrogen phosphate–citric acid buffer, and 25 mM monosodium glutamate. When the bioconversion system was performed at pH 4.6, 30°C, and 180 r/min shaking for 4 h, GABA production in biotransformation solution was 23.29 mM and the molar yield rate of bioconversion reached 93.15 %.

Keywords γ-Aminobutyric acid (GABA) · *Lactobacillus brevis* · Resting cells · L-Glutamate decarboxylase · Bioconversion

63.1 Introduction

γ-Aminobutyric acid (GABA), an ubiquitous natural nonprotein amino acid, is widely distributed in plants and animals [1]. GABA, which acts as an important type of inhibitory neurotransmitter in mammal brain and spinal cord, could play an important role in hormone and nutritional factors in non-nerve tissues [2]; so GABA has an important regulating effect on the normal physiological functions of an organism [3]. GABA has several well-known physiological functions, such as antihypotension effects, improving cerebral function, delaying senility, tranquilizer

X. Shi · B. Zheng · C. Chang · P. Cao · H. Yang · Q. Gao (✉)
Key Laboratory of Industrial Fermentation Microbiology, Ministry of Education,
College of Biotechnology, Tianjin University of Science and Technology,
Tianjin 300457, People's Republic of China
e-mail: gaoqiang@tust.edu.cn

T.-C. Zhang and M. Nakajima (eds.), *Advances in Applied Biotechnology*,
Lecture Notes in Electrical Engineering 333, DOI 10.1007/978-3-662-46318-5_63

effects, activating renal and liver functions, and promoting the secretion of growth hormone [4–9]. GABA, therefore, has the potential as a bioactive component in foods and pharmaceuticals due to its bioactive effects. Glutamate decarboxylase (GAD, EC 4.1.1.15), which is widely distributed in prokaryotic and eukaryotic cells [10, 11], is the unique enzyme to catalyze the conversion of L-glutamate or its salts to GABA and CO_2 via the single-step α-decarboxylation [12–14].

With the increasing commercial demand for GABA, various chemical and biological synthesis methods for GABA have been studied [15–17]. Chemical synthesis of GABA has a high cost and a low production ratio. Furthermore, it cannot be used in the food industry due to dangerous or poisonous solvents used in the synthesis. Microbiological fermentation method is characterized by easy operation, moderate reaction conditions, safety, and low cost, whereas the downstream process and production cycle is long. Bioconversion method of GABA may be a much more promising method due to simple reaction procedure, high catalytic efficiency, saving production cost, shortening production cycle, less by-product, less pollution, and environmental compatibility [18]. In the current study, the process of enzymatic conversion for γ-aminobutyric acid by *Lactobacillus brevis* CGMCC No. 3414 resting cells and the influence of several factors on GABA production were investigated and the optimal composition of bioconversion system was determined in order to provide reference for using GAD of GRAS lactic acid bacterium to catalyze the conversion of L-glutamate or its salts to GABA.

63.2 Materials and Methods

63.2.1 Materials and Equipment

The *L. brevis* strain used in the present work was isolated from naturally pickled Chinese vegetables in our previous work, and it is stored at the China General Microbiological Culture Collection Center as *L. brevis* CGMCC No. 3414. The experimental equipments are high performance liquid chromatography (Agilent 1,260 infinity, Agilent Technologies, USA) with an Agilent ZORBAX StableBond C18 column (4.6 × 250 mm), Hitachi CR22GIII high-speed refrigerated centrifuge (Hitachi Koki Co., Ltd., Japan), and desk high speed centrifuge (Hunan Xiang Yi Laboratory Instrument Development Co., Ltd., China).

The glucose-yeast extract-peptone (GYP) medium for seed preparation contained (g/L): glucose, 10; yeast extract, 10; peptone, 5; sodium acetate, 2; $MgSO_4 \cdot 7H_2O$, 0.02; $MnSO_4 \cdot 4H_2O$, 0.001; $FeSO_4 \cdot 7H_2O$, 0.001; NaCl, 0.001; and pH 6.8.

The fermentation medium consisted of the following (g/L): glucose, 30; yeast extract, 30; peptone, 5; sodium acetate, 3; $FeSO_4 \cdot 7H_2O$, 0.001; $MgSO_4 \cdot 7H_2O$, 0.03; NaCl, 0.001; $MnSO_4 \cdot 4H_2O$, 0.019; L-sodium glutamate (L-MSG), 10; pH 6.8.

GABA standard was purchased from Sigma-Aldrich. L-MSG (purity ≥ 99 %) was provided by Tianjin Red Rose Food Co., Ltd, China. Chromatography reagents were obtained from Tianjin Kemiou Chemical Reagent Co., Ltd, China. Other reagents were of analytical reagent grade and biochemical reagents.

63.2.2 GABA Biotransformation by L. brevis CGMCC No. 3414 Resting Cells

One loop of slant culture of *L. brevis* CGMCC No. 3414 was inoculated into a 50-mL seed medium in a 500-mL Erlenmeyer flask and incubated without agitation at 30 °C for 24 h. The seed culture was then inoculated at 10 % (v/v) into 200 mL fermentation medium in a 500-mL Erlenmeyer flask and cultivated without agitation at 30 °C. After 16–72 h cultivation, the cells were harvested by centrifugation at 5,000×*g* for 10 min at 4 °C, washed twice with sterile water, and then resuspended in 0.2 M disodium hydrogen phosphate–citric acid buffer (containing 25 mM L-MSG, pH 4.6) containing 50 g wet cells per liter. The bioconversion was performed at 30 °C and 180 r/min shaking for 4 h, and then the bioconversion broth was detected after centrifugal filtration.

63.2.3 Analytical Methods

The volume of 1 mL bioconversion broth was centrifuged at 12,000 r/min for 2 min, then a 10-μL supernatant was pipetted into a 1.5-mL centrifuge tube, added with 100 μL derived buffer, 100 μL derivative agent (2,4-dinitro-1-fluorobenzene), and 790 μL potassium dihydrogen phosphate buffer, uniformly mixed, water bath at 60 °C for 1 h. After that, the derivation mixture was filtered by a 0.22 μm cellulose acetate membrane filter, and the filtrate was stored at 4 °C for HPLC assay. Gradient elution conditions: Agilent ZORBAX StableBond C18 column, 30 °C column temperature, 360 nm ultraviolet detection wavelength, 0.8 mL/min flow velocity, 10 μL sample amount, mobile phase A: water, mobile phase B: acetonitrile, mobile phase C: methyl alcohol, and mobile phase C: 0.05 M sodium acetate solution [19].

63.3 Results and Discussion

63.3.1 Effect of Cell Age on GABA Production by L. brevis CGMCC No. 3414 Resting Cells

The glutamate decarboxylase produced by lactic acid bacteria is an inducible enzyme [20]. The current study evaluated the resting cell of different cell age

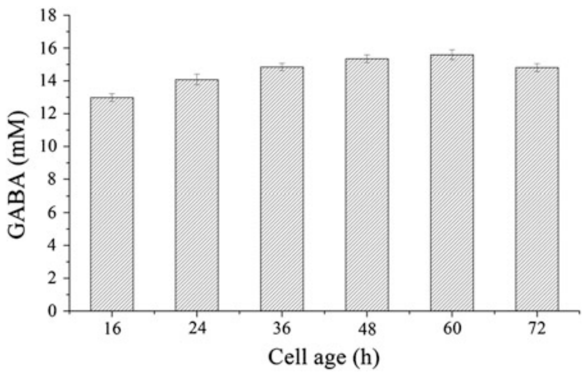

Fig. 63.1 The influence of cell age on GABA production

bioconversion of MSG to GABA. *L. brevis* CGMCC No. 3414 cells were harvested at culture time of 16, 24, 36, 48, 60, and 72 h, respectively, which is collected according to the above methods. The resting cells with the same concentration were resuspended in bioconversion system, and then the bioconversion broth was detected after a period of reaction time.

As shown in Fig. 63.1, the GABA yield was greatly improved with the increase of culture time. When the *L. brevis* CGMCC No. 3414 cells were harvested at culture time of 60 h, the cells had the strongest transformation ability, whereas at 72 h, the transformation ability of cells decreased. This is mainly because that a great amount of secondary metabolites produced by the cells began to accumulate after strains were developed to the stationary phase, especially the glutamate decarboxylase. When *L. brevis* CGMCC No. 3414 cells were harvested in this period for transformation, the yield of GABA could reach the highest. However, we conjecture that the content of GAD had little difference between the cells cultivated at 48 and 60 h. Therefore, the yield of GABA is of no significant difference between them. Considering the fermentation period and cost, culture time of 48 h was used for subsequent studies on GABA production by *L. brevis* CGMCC No. 3414 resting cells.

63.3.2 Effect of Cell Concentration on GABA Production by L. brevis CGMCC No. 3414 Resting Cells

Generally speaking, the yield of GABA will increase with the increased cell concentration. As shown in Fig. 63.2, the yield of GABA increased rapidly in the concentration range of 10–25 g/L. When the cell concentration increased further, the yield of GABA increased little. The specific conversion ratio was investigated in the current study. Figure 63.2 indicates that the specific conversion ratio decreases with the increased cell concentration, and the turning point appears at cell concentration of 50 g/L. Given the yield of GABA, training cost, and efficiency of the

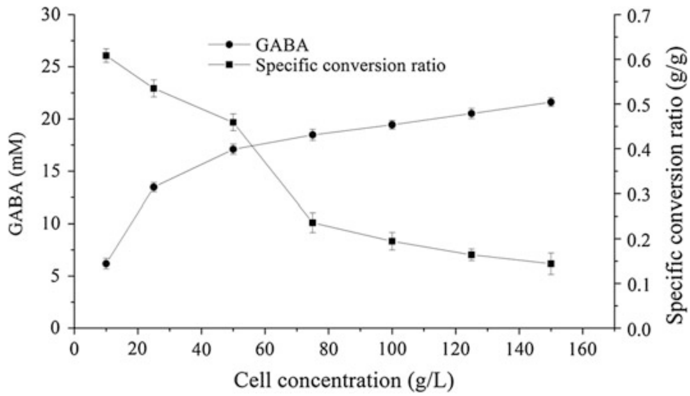

Fig. 63.2 The influence of cell concentration on GABA production

cell culture, 50 g/L cell concentration was used for subsequent studies on GABA production by *L. brevis* CGMCC No. 3414 resting cells.

63.3.3 Effect of Bioconversion Time on GABA Production by L. brevis CGMCC No. 3414 Resting Cells

When GABA is produced by bioconversion, glutamate reacts with GAD after penetrating the cell membrane and getting into the cell cytoplasm. The reaction ratios of GABA bioconversion were the highest at (0–3) h, slowed down at (4–5) h, and then became almost constant after 5 h (Fig. 63.3). This is mainly because that substrate consumption and product accumulation reach relative balance, and the

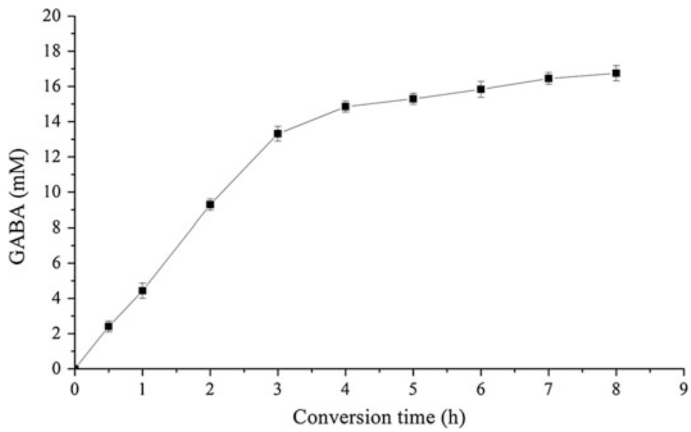

Fig. 63.3 The influence of bioconversion time on GABA production

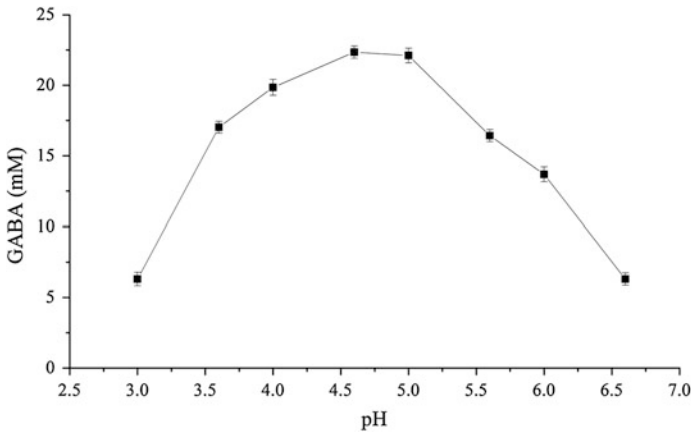

Fig. 63.4 The influence of pH on GABA production

decrease of substrate has an effect on reaction ratio. Thus, considering product accumulation and reaction ratio, a conversion time of 4 h was used for subsequent studies on GABA production by *L. brevis* CGMCC No. 3414 resting cells.

63.3.4 Effect of pH on GABA Production by L. brevis CGMCC No. 3414 Resting Cells

The reaction pH of GAD from different sources has a great difference. GADs of plant origin show the highest activity at pH 5.5–6.6 [21]. Nomura et al. [22] reported that the optimum pH of GAD produced by *Lactococcus lactis* subsp. *lactis* was 4.7. Huang and Mei [23] reported that the optimum pH of GAD produced by *L. brevis* CGMCC 1306 was 4.4. Figure 63.4 exhibits that the effect of pH has influence on bioconversion. The result showed that the suitable pH range of GAD was 4.6–5.0. The study proves that *L. brevis* GAD displays good pH stability in the pH 4.0–5.0 and the optimum pH is about 4.5. The optimum pH of bioconversion in the current study is 4.6 which is similar with the references. Thus, pH 4.6 was used for subsequent experiments.

63.3.5 Effect of MSG Substrate Concentration on GABA Production by L. brevis CGMCC No. 3414 Resting Cells

Substrate concentration has great influence on reaction ratio in enzymatic reaction. Substrate usually has double effects of accelerating the reaction speed and inhibiting

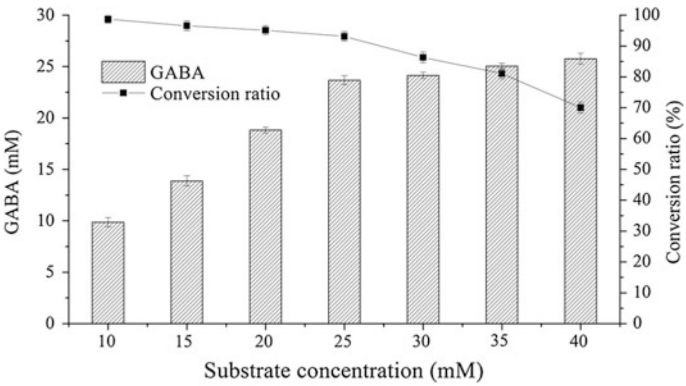

Fig. 63.5 The influence of MSG substrate concentration on GABA production

enzyme activity. The influence of initial MSG concentration on GABA production and the ratio of bioconversion by *L. brevis* CGMCC No. 3414 resting cells were studied in current research. In Fig. 63.5, the yield of GABA by resting cell transformation at lower ranges of MSG substrate concentration (10–25 mM) gradually increased with the increase of MSG concentration by 4-h biotransformation. The final GABA yield was almost constant while the substrate concentration increased to over 25 mM; however, the conversion ratio decreased significantly. This result indicates that low concentration of substrate has little effect on enzymatic reaction and the product inhibition is not found during this bioconversion. Thus, 25 mM MSG was used for GABA bioconversion by *L. brevis* CGMCC No. 3414 resting cells.

63.4 Discussion

Lactobacillus brevis, which has full GAD activity and is the preferable species to catalyze the conversion of L-glutamate or its salts to GABA, is a GRAS microorganism. Using bioconversion method for GABA production not only has advantages like high yield and short production cycle, but also obtains high purity product and overcomes the limitation of microbiological fermentation method. Since each influencing factor of GABA production by *L. brevis* CGMCC No. 3414 resting cells was analyzed and discussed, the optimal composition of bioconversion system contained 50 g/L resting cells, cell age at 48 h fermentation, 0.2 M disodium hydrogen phosphate–citric acid buffer, and 25 mM MSG. When the bioconversion system was performed at pH 4.6, 30 °C, and 180 r/min shaking for 4 h, GABA production in biotransformation mixture was 23.29 mM, and the molar yield rate of bioconversion reached 93.15 %. Overall, this study laid a foundation for catalyzing the conversion of L-glutamate or its salts to GABA by *L. brevis* resting cells.

Acknowledgments This research was supported by the National 863 Program of China (2012AA021302), the National 973 Program of China (2014CB734004), and the National Natural Science Foundation of China (31370075 & 31471725).

References

1. Kinnersley AM, Turano FJ (2000) Gamma aminobutyric acid (GABA) and plant responses to stress. Crit Rev Plant Sci 19(6):479–509
2. Manyam BV, Katz L, Hare TA et al (1981) Isoniazid-induced elevation of CSF GABA levels and effects on chorea in Huntington's disease. Ann Neurol 10(1):35–37
3. Yang S, Lu Z, Lu F et al (2005) Research progress on microbial glutamate decarboxylase. Food Sci 26(9):546–551
4. Okada T, Sugishita T, Murakami T et al (2000) Effect of the defatted rice germ enriched with GABA for sleeplessness, depression, autonomic disorder by oral administration. J Jpn Soc Food Sci 47(8):596–603
5. Omori M, Yano T, Okamoto J et al (1987) Effect of anaerobically treated tea (Gabaron tea) on blood pressure of spontaneously hypertensive rats. J Agr Chem Sci Jpn 61:1449–1451
6. Jones EA (2002) Ammonia, the GABA neurotransmitter system, and hepatic encephalopathy. Metab Brain Dis 17(4):275–281
7. Hagiwara H, Seki T, Ariga T (2004) The effect of pre-germinated brown rice intake on blood glucose and PAI-1 levels in streptozotocin-induced diabetic rats. Biosci Biotech Biochem (BBB) 68(2):444–447
8. DeFeudis FV (1983) γ-Aminobutyric acid and cardiovascular function. Experientia 39(8): 845–849
9. Cavagnini F, Invitti C, Pinto M et al (1980) Effect of acute and repeated administration of gamma aminobutyric acid (GABA) on growth hormone and prolactin secretion in man. Endocrinol Acta 93(2):149–154
10. Zhao Y, Liang XL, Zhang H (2006) The Structure and function of the glutamate decarboxylase and its genes expression regulation in *Escherichia coli*. Food Ferment Ind 32 (7):75–78
11. Peng C, Huang J, Hu S et al (2013) A two-stage pH and temperature control with substrate feeding strategy for production of gamma-aminobutyric acid by *Lactobacillus brevis* CGMCC 1306. Chinese J Chem Eng 21(10):1190–1194
12. Ueno H (2000) Enzymatic and structural aspects on glutamate decarboxylase. J Mol Catal B-Enzym 10(1):67–79
13. Battaglioli G, Liu H, Martin DL (2003) Kinetic differences between the isoforms of glutamate decarboxylase: implications for the regulation of GABA synthesis. J Neurochem 86(4):879–887
14. Gao Q, Duan Q, Wang D et al (2013) Separation and purification of γ-aminobutyric acid from fermentation broth by flocculation and chromatographic methodologies. J Agr Food Chem 61 (8):1914–1919
15. Plokhov AY, Gusyatiner MM, Yampolskaya TA et al (2000) Preparation of γ-aminobutyric acid using *E. coli* cells with high activity of glutamate decarboxylase. Appl Biochem Biotech 88:257–265
16. Komatsuzaki N, Shima J, Kawamoto S et al (2005) Production of γ-aminobutyric acid (GABA) by *Lactobacillus paracasei* isolated from traditional fermented foods. Food Microbiol 22(6):497–504
17. Choi SI, Lee JW, Park SM et al (2006) Improvement of gamma-aminobutyric acid (GABA) production using cell entrapment of *Lactobacillus brevis* GABA 057. J Microbiol Biotech 16:562–568

18. Zhang Y, Song L, Gao Q et al (2012) The two-step biotransformation of monosodium glutamate to GABA by *Lactobacillus brevis* growing and resting cells. Appl Microbiol Biotech 94(6):1619–1627
19. Chen HM, Gao Q, Su Z et al (2012) Screening, identification and flask fermentation optimization of a high-yield γ-aminobutyric acid *Enterococcus raffinosus* strain. Microbiol China 39(11):1642–1652
20. Fu YX, Zhang T, Jiang B et al (2008) Enzymatic conversion for γ-aminobutyric acid by *Lactococcus lactis*. Sci Tech Food Ind 09:166–169
21. Satyanarayan V, Nair PM (1985) Purification and characterization of glutamate decarboxylase from *Solanum tuberosum*. Eur J Biochem 150(1):53–60
22. Nomura M, Nakajima I, Fujita Y (1999) *Lactococcus lactis* contains only one glutamate decarboxylase gene. Microbiology 145(6):1375–1380
23. Huang J, Mei LH (2007) Purification and characterization of glutamate decarboxylase of *Lactobacillus brevis* CGMCC 1306 isolated from fresh milk. Chinese J Chem Eng 15(2): 157–161

Part IV
Progress of Biotechnology

Chapter 64
[FeFe]-Hydrogenase: Catalytic Center and Modification by Genetic Engineering

Jiayi He and Chunfei Wu

Abstract In this review, we highlight the [FeFe]-hydrogenase, which is capable of catalyzing the splitting of molecular hydrogen to produce electrons and protons or catalyzing the reversible reaction: $2H^+ + 2e^- = H_2\uparrow$ as a potential renewable fuel. We have focused on [FeFe]-hydrogenase because of structural studies have shed more light on the hydrogenase activity than the [NiFe]-hydrogenase. Our studies on the [FeFe]-hydrogenase from *Chlamydomonas reinhardtii* CC-503 ($HydA_1$) have also been highlighted. There are two factors influencing the multiplexed hydrogenase activity: a single hydrophobic channel of catalytic center, which is known as the H-cluster active site based on site-directed mutagenesis, moreover, some promising results have already been obtained. Modifications of [FeFe]-hydrogenase can improve its stabilization and activity in vitro, increase the efficiency of bioenergy utilization, and promote industrial amplification of biofuel production.

Keywords Renewable energy resource · Biohydrogen synthesis · [FeFe]-hydrogenase · Gene mutation

64.1 Introduction

Driven by the growing appetite for energy consumption and increasing severity of global environment issue, the requirement for replacing traditional fossil fuel with alternative energy becomes urgent. Sustainable, secure energy supply plays a crucial role in stabilizing global economic development. Thus, to seek reproducible, clean and effective new energy source has become the primary task in the field of

J. He (✉) · C. Wu
China University of Petroleum (East China), No. 66, Chang Jiang West Road, Economic & Technological Development Zone, Qingdao 266580, People's Republic of China
e-mail: hjy0085@126.com

C. Wu
e-mail: chunfeiw2006@126.com

T.-C. Zhang and M. Nakajima (eds.), *Advances in Applied Biotechnology*,
Lecture Notes in Electrical Engineering 333, DOI 10.1007/978-3-662-46318-5_64

energy research [1]. Biohydrogen synthesis technology can be one preferred solution to these conflicts in future energy supply, using water as substrate and solar energy as power supply, possessing varieties of incomparable advantages, such as high transformation efficiency, environmental amity and mild reaction conditions, for which this technology has been enrolled in strategic agenda and environment protection issue around the world.

Currently, biohydrogen synthesis technology can be performed in three ways: by photosynthetic bacteria, by fermentation and by microalgae, among which microalgae hydrogen production technology is considered to be the most promising one, for its high energy conversion efficiency, unlimited resource of solar power and relatively low pollution [2]. The major subclasses of microalgae that can be used for hydrogen synthesis are *cyanophyta* and *chorophyta*. Reversible hydrogenase is the predominant hydrogen production source for these microalgae. The activity of reversible hydrogenase in *chlorophyta* is higher than that of nitrogen-based hydrogen production enzyme in *cyanophyta*, for mechanism of hydrogen production varies with organisms. Hydrogenase can transform proton into hydrogen directly, with no consumption of ATP (adenosine triphosphate), which in turn result in spontaneous accumulation of solar energy. Research on reversible hydrogenase in *chlorophyta* has become a hot topic in the field of biohydrogen synthesis recently [3].

64.2 Mechanism for Hydrogen Production in *Chorophyta* and Key Enzymes

64.2.1 Mechanism of Biohydrogen Synthesis

It was reported by Jackson that *Cyanobacterium Anabaena* has the ability to generate hydrogen as early as 1896 [4]. Gaffron and Rubin discovered that green algae Scenedesmus *obliquus* can produce hydrogen in the condition of hypoxia [5]. Researchers also reported that *Chlamydomonas reinhardtii* and *Chlorella* could generate hydrogen persistently under certain condition. The basic advantage of hydrogen synthesis by green algae is that solar energy can be fully used—water act as a direct raw material. Solar transformation efficiency is 10 times more than the other plants which live on photosynthesis, sometimes 10 % (lower limit of transformation efficiency in the field of hydrolysis of hydrogen production with applicable economic benefit). Increasing number of microorganisms and their hydrogen synthesis mechanisms have been studied in recent years and significant progress has been made.

Based on the metal ion that hydrogenase contains, hydrogenase fall into the following major classes: [FeFe]-hydrogenase, [NiFe]-hydrogenase, and metal-free hydrogenase. However, [FeFe]-hydrogenase is considered to be the most promising hydrogen synthesis catalyzed at its unique catalytic center and with higher efficiency than the other two classes [6, 7]. In green algae, light is captured by specialized Light

Harvest Complex (LHC), which confers the energy to photosynthetic reaction centers of photosystem I (PSI) and photosystem II (PSII). Hydrogen activation is mediated by a family of enzymes, termed hydrogenases, which either provide these organisms with reducing power from hydrogen oxidation or act as electron sinks, following the reaction: $2H^+ + 2e^- = H_2\uparrow$ [8].

The electrons are passed down via chain reaction of plastoquinone (PQ), cytochrome b6f complex (Cytb6f), and plastocyanin (PC) to PSI, and then electrons are transmitted to Ferredoxin (Fd), which helps hydrogenase produce H_2 (Fig. 64.1) [9, 10]. Aerobic photosynthesis and mitochondrial respiration action can be changed in the absence of sulfur during algae culturing, because sulfur is an essential component of protein residue cysteine and methionine, and the repair cycle can be blocked without the presence of sulfur [6]. Eventually, respiration reaction can exceed photosynthesis action, as a result of the absence of sulfur, leading to the decrease of oxygen concentration, which can provide an ideal environment to maintain the activity of hydrogenase [7].

64.2.2 Key Enzyme Hydrogenase and Its Reaction Center

[FeFe]-hydrogenase is found in single cell green algae (e.g. *Chlamydomonas reinhardtii*), anaerobic fungi, and some procaryotic organisms so far. [FeFe] H_2ases house four iron–sulfur (FeS) clusters in addition to the active-site "H-cluster". Each H-cluster is coordinated by diatomic molecules CN- and CO ligand [11, 12]. In

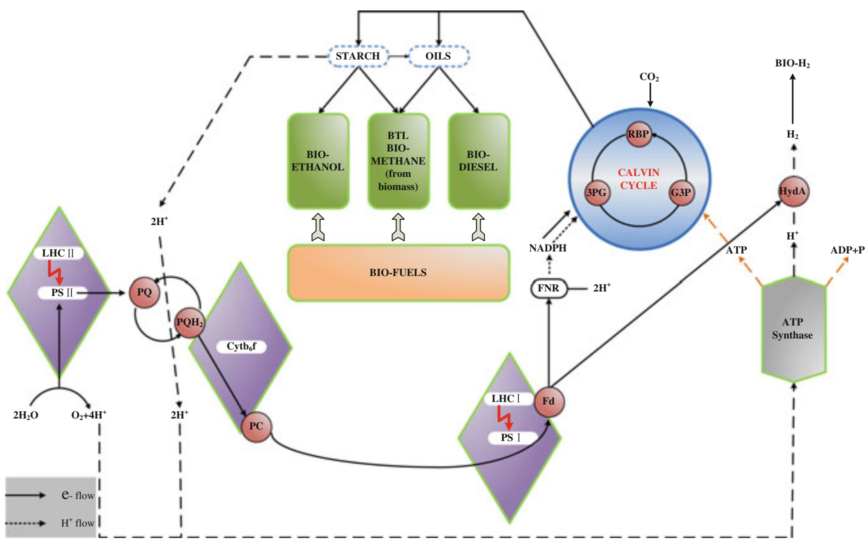

Fig. 64.1 Mechanism for biohydrogen synthesis in *green* algae

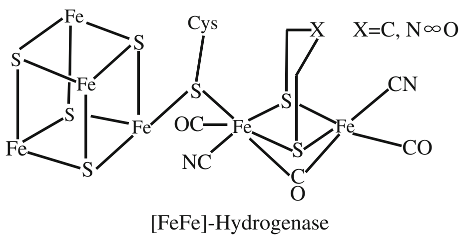

Fig. 64.2 H-cluster active site of [FeFe]-hydrogenase [15]

addition, there is also a Fe bridge ligand exiting, apart from the structure that each Fe atom is bridged to each other by two S atoms in H-cluster active site. The known [FeFe]-hydrogenase atomic structures, respectively, show a common core, which contains a moiety, deeply buried inside the protein, with an Fe–Fe dinuclear center, nonproteic bridging, terminal CO and CN^{-} ligands attached to each of the iron atoms, and a dithio moiety, which also bridges the two iron atoms and has been tentatively assigned as a di(thiomethyl)amine (Fig. 64.2) [8].

Hydrogenase has its own active channel to generate hydrogen. Current data indicate that *HydF*, *HydE*, and *HydG* would have the key role of a scaffold upon chemically modifying the [FeFe]-hydrogenase, a carrier that transfers the latter *HydA*, thus completing the maturation process, which means that if these proteins are expressed alone or two, the activity of hydrogenase will be very low with little hydrogen production ability [13, 14].

64.2.3 Tolerance to Oxygen

H-cluster active site, the activity site of hydrogenase, is highly sensitive to O_2, which is produced by PSII and can make hydrogenase lose its activity. In order to improve its tolerance to oxygen, the mechanism of oxygen sensitivity of [FeFe]-hydrogenase was studied. It is reported that this sensitivity is related to the catalytic center [2Fe–2S]. When O_2 reaches its catalytic site, an irreversible oxidation reaction will take place, in which O_2 binds to Fe_2 of [2Fe–2S], causing H^+ to lose its ability to bind to Fe_2 of the H-cluster active site [15]. One plausible way to increase oxygen endurance ability of hydrogenase is to modify its structure, preventing O_2 from reaching the catalytic site of [FeFe]-hydrogenase by shrinking the diameter of gas channel, through which only H_2 can pass other than O_2. It is proven that the oxygen sensitivity of [FeFe]-hydrogenase is related to its amino acid sequence.

64.3 Application of Biotechnology in the Study of Hydrogenase

Researchers have attempted to optimize the amino acid residue inside the hydrogen synthesis channel, in order to solve the problem that hydrogenase can be easily poisoned by O_2. Several plausible ways, including decreasing the diameter of gas channel, shrinking the cubage of catalytic site on this enzyme, was experimented to increase hydrogen production efficiency. Next, we discuss some of the genetically modified strains that led to improved hydrogen production.

64.3.1 Recombination of Gene In Vitro

DNA recombinant method is used to introduce extracellular DNA into cell, making it possible for exchanging genes between species. It includes homologous recombination, site specific recombination, transposon recombination, and abnormal recombination, which is a common way of mutation in nature.

Vanabendroth reported that the production of hydrogenase protein can doubly increase when the original gene $HydA_1$ of C. acetobutylicum was replaced by a homologous gene [16]. Many attempts have been made to generate O_2-tolerant hydrogenases through random mutagenesis in vivo and in vitro [17]; Yacoby used protein engineering method to fuse Fd to the N terminal of *HydA*, as a result, the expression levels of protein increased by about four times. The activity and purification of enzyme increased dramatically, which was proven by the following experiment [18, 19].

64.4 Gene Mutation Method

Two main types of gene mutation method systems exist: site specific mutation and random mutation. Cycle PCR and Quick-change Kit are used in the method of site-specific mutation to produce key mutated sites. Random mutation method runs in other way. The reaction condition, including concentration of Mg^{2+}, Mn^{2+}, dNTP, or low-cost polymerase was modified during amplification of DNA to optimize the frequency of mutation, in order to generate random mutation site in gene of interest.

64.5 Selection of Mutation Site

The key site of interest is the one that can affect the gas channel and can be modified by protein engineering method. It is reported that the hydrophobic amino acid residue, which is vital to the surface of protein, is essential for the diffusion of oxygen. One way to select mutation site is to choose the amino acid which is small in the channel in nature. If the small residue can be replaced by larger one, it can prevent oxygen from reaching the active site of hydrogenase. The structure of hydrogenase of *Clostridium pasteurianum* has been revealed by X-ray method. The arrangement of amino acid inside the hydrophobic environment can be acquired by computer simulation (Fig. 64.3). It was reported that the activity of hydrogenase can increase when Leu-238 was changed into trp, Val-423 was mutated into Ala-321 was replaced [20].

The other choice of mutation sites is that highly conserved amino acid residues. The H-cluster active site has its unique [Fe-s] diatomic center, in which each Fe has CN and CO ligand. The function of CN and CO is to stabilize Fe, making it easier to bond to hydrogen. The helper genes *HydE*, *HydF,* and *HydG* have its unique domain that can help synthesize these ligands, such as [Fe–S] binding site. In order to obtain high activity mutation of hydrogenase, the amino acid sequence of helper genes was chosen for mutation, The residues Cys 302, 354, 356 and residues His 304, 352 of *HydF* were mutated in new Apollo hot mantle bacteria by Berto in 2012, which has demonstrated that the three Cys residue help the binding of *HydF* with [4Fe-4S] and the activation of hydrogenase [22].

Modification of hydrogenase active site is done by genetic engineering based on the above theory in our experiments. The fact that co-expression of active [FeFe]-hydrogenase requires strictly anaerobic conditions has always been interpreted as revealing the extreme oxygen sensitivity of these enzymes. Compared with wild

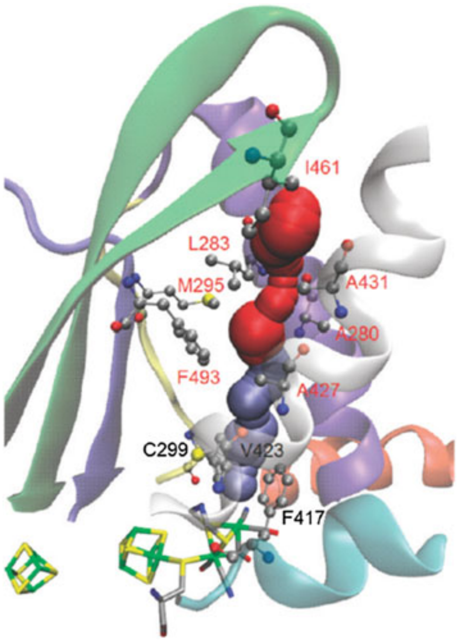

Fig. 64.3 X-ray analysis of gas channel [21]

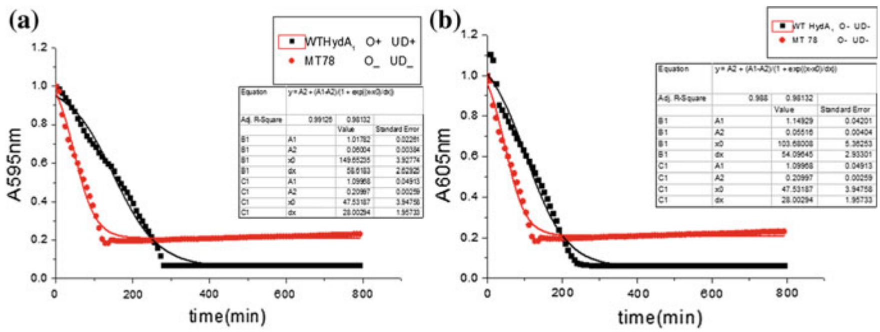

Fig. 64.4 **a**, **b** Specific activities of wile-type and mutant $HydA_1$. *Dark red*, mutant 78 (residues Ala to Leu); *black*, wild-type $HydA_1$; O^+, aerobic treatment; O^-, anaerobic treatment; UD^+, cell disruption with sonic oscillator in aerobic; UD^-, cell disruption with sonic oscillator in anaerobic. **a** Specific activities of MT 78(O^-, UD^-) and WT $HydA_1$(O^+, UD^+). **b** Specific activities of MT 78 (O^-, UD^-) and WT *HydA*1(O^-, UD^-)

type, our data and quantitative analysis show that the rate of hydrogen synthesis by mutant is increased significantly. Some promising results have been obtained already by regulatory factor experiment, and regulation experiments showed that the control system of reliable, stable operation, high universality, moreover establishment of calculation and related model is under study, all of the further researches are in progress (Fig. 64.4a, b).

64.6 Outlook

As a promising ideal energy, hydrogen has relatively high efficiency without apparent pollution to the environment. However, much more need to be done in terms of expression, tolerance to oxygen, and the activity of the hydrogenase. Genetic engineering or protein engineering methods have been used major tools in the study of hydrogen biosynthesis. Moreover, modern molecular biology methods have been discussed in this paper, such as gene modification, site specific mutation method [23], and molecular dynamics calculations [21]. In addition, it is a very urgent problem to be solved, which will require further studies on the specific activities, dynamics calculations, and mechanistic modeling of different mutant strains.

References

1. Nocera D-G (2009) Chemistry of personalized solar energy. Inorg Chem 48(21):10001–10017
2. Gaffron H, Rubin (1942) Fermentative and photochemical production of hydrogen in algae. J Gen Physiol 26:219
3. Elam C (2001) International energy agency agreement on the production and utilization of hydrogen. NREL/CP-570-30535

4. Benemann J-R (2000) Hydrogen production by microalgae. J Appl Phycol 12(3–5):291–300
5. Gaffron H (1939) Reduction of CO_2 with H_2 in green plants. J Gen Physiol 143:204–205
6. Chen J-S, Mortenson L-E (1974) Purification and properties of hydrogenase from Clostridium pasteurianum W5. Biochim Biophys Acta 371:283–298
7. Nicolet Y, Cavazza C (2002) Fe-only hydrogenases: structure, function and evolution. Inorg Chem 91:1–8
8. Michel Frey (2002) Hydrogenases: hydrogen-activating enzymes. ChemBioChem 3:153–160
9. Asada Y, Miyake J (1999) Photobiological hydrogen Production. J Biosci Bioeng 88(1):1–6
10. Das D, Veziroglu T (2001) Hydrogen production by biological processes: a survey of literature. Int Hydrogen Energy 26(1):13–28
11. Zhang L, Zhang W, Jin M et al (2005) Cloning and structure analysis of hydrogenase gene from Chlamydomonas reinhardtii SE. Process Biochem 40(9):2968–2972
12. Roseboom W, De Lacey A-L, Fernandez V-M et al (2006) The active site of the [FeFe]-hydrogenase from Desulfovibrio desulfuricans. II. Redox properties, light sensitivity and CO-ligand exchange as observed by infrared spectroscopy. J Biol Inorg Chem 11(1):102–118
13. Peters J-W, Lanailotta W-N, Lemon B-J et al (1998) X-ray crystal structure of the Fe-only hydrogenase (CpI) from Clostridium pasteurianum to 1.8 angstrom resolution. Science 282:1853–1858
14. Stripp S-T, Goldet G, Brandmayr C et al (2009) How oxygen attacks [FeFe] hydrogenases from photosynthetic organisms. Proc Natl Acad Sci 106(41):17331–17336
15. Lemon B-J, Peters JW (1999) Binding of exogenously added carbon monoxide at the active site of the iron-only hydrogenase (CpI) from Clostridium pasteurianum. Biochemistry 38 (40):12969–12973
16. Vonabendroth G, Stripp S, Silakov A et al (2008) Optimized over-expression of [FeFe] hydrogenases with high specific activity in clostridium acetobutylicum. Int J Hydrogen Energy 33(21):6076–6081
17. Dubini A, Ghirardi ML (2014) Engineering photosynthetic organisms for the production of biohydrogen. Photosynth Res. doi: 10.1007/s11120-014-9991-x
18. Happe T, Kaminski A (2002) Differential regulation of the Fe-hydrogenase during anaerobic adaptation in the green alga Chlamydomonas reinhardtii. Eur J Biochem 269(3):1022–1032
19. Roessler P-G, Lien S (1984) Purification of hydrogenase from Chlamydomonas reinhardtii. Plant Physiol 75(3):705–709
20. Ghirardi M- L, Cohen J, King P et al. (2006) [FeFe]-hydrogenases and photobiological hydrogen production. Annu Rev Plant Biol 6340–6346
21. Hong G, Pachter R (2012) Inhibition of biocatalysis in [FeFe] hydrogenase by oxygen: molecular dynamics and density functional theory calculations. ACS Chem Biol 7(7):1268–1275
22. Zhang L, Zhang W, Jin M et al (2005) Cloning and structure analysis of hydrogenase gene from Chlamydomonas reinhardtii SE. Process Biochem 40(9):2968–2972
23. Knörzer P, Silakov A, Carina E-F et al (2011) Importance of the protein framework for catalytic activity of [FeFe]-hydrogenases. J Biol Chem 287(2):1489–1499

Chapter 65
Characteristics of *Staphylococcus aureus* Isolates from Raw Milk

Xiaomei Zhang, Qian Li and Hongjiang Yang

Abstract *Staphylococcus aureus* has raised great health concerns worldwide. In this work, with the traditional culture-based methods, totally 70 bacterial isolates on Barid–Parker medium from raw milk samples are collected from 181 healthy cows in a dairy farm located in Northern China. With comparative sequence analysis of 16S rDNA genes, 18 isolates were identified as *S. aureus*. One isolate was resistant to cefoxitin and tentatively considered as a methicillin-resistant *S. aureus* (MRSA) strain. *Spa* typing was performed to discriminate the strains. Four *spa* types were determined, including t3104 in 12 strains, t267 in 3 strains, t521 in 2 strains, and t528 in strain Z1584. The type t11557 was a new *spa* type discovered in this work and its repeats succession was 07-12-21-13-34-34-33-13. Our work suggested that the prevalence of MARA strains was quite low in fresh raw milk produced in the dairy farm located in Northern China.

Keywords Microbial communities · Methicillin-resistant *Staphylococcus aureus* (MRSA)

65.1 Introduction

Currently, a few molecular techniques have been developed that can identify bovine mastitis causing agents. Numeral bacterial genes were selected as targets and detected with such methods, including conventional PCR [1], multiplex PCR [2], real-time PCR [3]. Commercial kits were already available for this kind of assay with relatively high accuracy and sensitivity [4].

X. Zhang · Q. Li · H. Yang (✉)
Key Laboratory of Industrial Fermentation Microbiology, Ministry of Education, Tianjin Key Laboratory of Industrial Microbiology, College of Biotechnology, Tianjin University of Science & Technology, Tianjin 300457, People's Republic of China
e-mail: hongjiangyang@tust.edu.cn

T.-C. Zhang and M. Nakajima (eds.), *Advances in Applied Biotechnology*,
Lecture Notes in Electrical Engineering 333, DOI 10.1007/978-3-662-46318-5_65

In this work, we collected raw milk samples from 181 healthy cows in one dairy farm located in Togtoh County, a relatively remote area in northern rural China. Bacteria were isolated from raw milk via traditional culture-based methods. By comparative analysis of bacterial 16S rDNA genes, the isolates were further determined to species level. Finally, we investigated the phenotypic and genotypic traits of the *Staphylococcus aureus* isolates with various methods.

65.2 Materials and Methods

65.2.1 Cultivation of Bacteria in Raw Milk

Raw milk samples were collected from 181 healthy dairy cows without clinical signs of mastitis in one dairy farm in Togtoh County of Inner Mongolia Autonomous Region.

Prepare tenfold serial dilutions of milk samples and spread 100 μL samples of each dilution on Baird–Parker agar plates. After incubation at 35 °C for 24–48 h, colony morphology was recorded to discriminate bacteria in all experiments.

65.2.2 Identification of the Isolates with Comparative Sequence Analysis of the 16S rDNA Genes

Genomic DNA of the isolates was extracted from cultures as described previously. Universal primers 27f (5′-AGAGTTTGATCCTGGCTCAG-3′) and 1492r (5′-GGTTACCTTGTTACGACTT-3′) were used for 16S rDNA gene amplification and sequencing of PCR products [5]. Sequence similarity was analyzed with BLAST program provided by NCBI for species identification.

65.2.3 Antibiotics Resistance Test of S. aureus Isolates

Antibiotic resistance in *S. aureus* strains was determined with disk diffusion test. Cefoxitin, oxacillin, tetracycline, ciprofloxacin, and gentamicin were tested and the results were recorded according to the CLSI documents (CLSI 2009). Gene *mecA* was detected with primers mecA1 and mecA2 [6].

65.2.4 Detection of Virulence Genes of S. aureus Isolates

Virulence genes were tested as described previously [7]. Briefly, *S. aureus* fibronectin binding protein A precursor gene *fnbA* was amplified with primers FNBA-1 and FNBA-2. *Staphylococcus aureus* fibronectin binding protein B precursor gene *fnbB* was amplified with primers FNBB-1 and FNBB-2. *Staphylococcus aureus* clumping factor A gene *clfA* was amplified with primers CLFA-1 and CLFA-2. *Staphylococcus aureus* clumping factor B gene *clfB* was amplified with primers CLFB-1 and CLFB-2.

65.2.5 Spa Typing

Staphylococcus aureus spa gene coding for protein A was amplified with primers 1113f (5′-AAAGACGATCCTTCGGTGAGC-3′) and 1514r (5′-CAGCAGTAGT-GCCGTTTGCTT-3′). The sequence data was analyzed for *spa* typing with the Bionumerics software (http://www.ridom.de) [8].

65.3 Results

65.3.1 Isolation and Identification of S. aureus Isolates

In Baird–Parker medium, 70 isolates with colonies displaying gray-black color, opaque zone surround, and an outer clear halo were selected as presumptive *Staphylococcus* strains.

To identify the isolates, sequence analysis of 16S rDNA gene was performed in 70 presumptive *Staphylococcus* strains. Totally, 18 *S. aureus* isolates were identified.

65.3.2 Antibiotic Resistance Analysis of S. aureus Isolates

Strain Z1395 was resistant to cefoxitin (zone diameter = 17.7 mm), and it is tentatively considered as methicillin resistance according to the recommendation of CLSI (CLSI 2009). Strain Z1395 was also resistant to oxacillin, ciprofloxacin, and tetracycline showing its multiple drug resistance characteristics. Strain Z16004 was intermediate to cefoxitin (zone diameter = 21.2 mm) and ciprofloxacin, and susceptible to oxacillin, gentamicin, and tetracycline (Table 65.1). However, no *mecA* gene was detected by PCR in all 18 strains, suggesting non-*mecA*-mediated methicillin resistance mechanism might exist in strain Z1395.

Table 65.1 Analysis of antimicrobial drug resistance of *S. aureus* strains

Strains	Antibiotics resistance				
	Cefoxitin	Oxacillin	Ciprofloxacin	Gentamicin	Tetracycline
Z160004	I	S	I	S	S
Z164	S	S	S	S	I
Z191	S	S	S	S	S
Z221	S	S	S	S	S
Z222	S	S	R	S	I
Z37002	S	S	S	S	I
Z1126	S	S	S	S	I
Z1127	S	S	S	S	S
Z1186	S	S	I	R	R
Z1261	S	S	R	R	R
Z1263	S	S	S	S	S
Z1394	S	S	I	R	R
Z1395	R	R	R	S	R
Z1583	S	S	S	S	R
Z1584	S	S	I	S	I
Z1585	S	S	I	S	R
Z1587	S	S	I	S	I
Z1588	S	S	S	S	S

S susceptible; *I* intermediate; *R* resistant

65.3.3 Characterization of Virulence Factors of the S. aureus Isolates

Clinical strains C123 and C126 were used as positive controls in coagulase and hemolytic activity tests. Eighteen strains were coagulase positive. Twelve strains displayed alpha hemolysis, five strains displayed beta hemolysis, and one strain displayed gamma hemolysis (Table 65.2). In virulence gene test, PCR results showed both *clfA* and *clfB* genes were positive in all 18 strains (Table 65.2). Their sequences were subjected to further analyses (accession no. KC212097–KC212118).

65.3.4 Spa Typing

Partial *spa* gene was amplified and sequenced (accession no. KC212119–KC212140). Four *spa* types were determined, including t3104 in 12 strains, t267 in 3 strains, t521 in 2 strains, and t528 in strain Z1584. These *spa* types were different from t11557 of strain C123 and t2310 of strain C126 (Table 65.2). The type t11557

Table 65.2 Characterization of virulence factors in the isolated *S. aureus* strains

Strains	Virulence genes				Coagulase	Hemolysis	Ridom type
	fnbA	*fnbB*	*clfA*	*clfB*			
Z160004	−	−	+	+	+	γ	t3104
Z164	−	−	+	+	+	β	t3104
Z191	−	−	+	+	+	α	t3104
Z221	−	+	+	+	+	α	t267
Z222	−	+	+	+	+	β	t267
Z37002	−	+	+	+	+	β	t267
Z1126	−	−	+	+	+	α	t3104
Z1127	−	−	+	+	+	α	t3104
Z1186	−	−	+	+	+	β	t3104
Z1261	−	+	+	+	+	β	t521
Z1263	+	+	+	+	+	α	t521
Z1394	+	−	+	+	+	α	t3104
Z1395	+	−	+	+	+	α	t3104
Z1583	−	−	+	+	+	α	t3104
Z1584	−	−	+	+	+	α	t528
Z1585	−	−	+	+	+	α	t3104
Z1587	−	+	+	+	+	α	t3104
Z1588	+	−	+	+	+	α	t3104
C123			+	+	+	β	t11557
C126			+	+	+	β	t2310

was a new *spa* type discovered in this work and its repeats succession was 07-12-21-13-34-34-33-13.

65.4 Discussion

In this work, culture-based method was used for the first round isolation of microorganisms in raw milk samples. Colony morphology was the primary criterion for discrimination of different isolates. Other characteristics, including growth on Baird–Parker medium, hemolysis, and coagulase activity, were also taken into considerations for isolates screening and discriminating. Genus *Staphylococcus* was the predominant group isolated from bovine milk samples, including 18 *S. aureus* isolates and 13 coagulase-negative staphylococci. It had been shown that *S. aureus* was the major pathogen causing bovine mastitis [9], and the coagulase-negative staphylococci were minor pathogens isolated from clinical or subclinical mastitis cases [10].

A variety of gram-negative bacteria were isolated and identified in our work. Some species were opportunistic pathogens normally existing in bovine milk including *Citrobacter freundii*, *Escherichia coli*, *Enterococcus cloacae*, *Enterococcus faecalis*, and *Serratia marcescens*. These coliform bacteria could possibly be responsible for the infections in some mastitis cases [11].

MRSA strains can be isolated from clinical samples, communities, and livestock-associated sources across the world. The emergence of MRSA in dairy cows has raised a great public health concern. In this work, one isolate was considered as a tentative MRSA strain without *mecA* gene detected. However, it was possible that *mecA* homologs including *mecC* gene may be responsible for its MRSA phenotype [12].

Spa typing method has been used extensively in discrimination of *S. aureus* isolates from various environments. In this study, 18 *S. aureus* isolates were determined belonging to four *spa* types. Most of them (12/18) were of t3104, which was first assigned to strains isolated from intensive care unit in Netherlands [13]. Clinical isolates C123 and C126 had different *spa* types compared with the 18 isolates from raw bovine milk, especially C123 had a new *spa* type t11557 (Repeats Succession: 07-12-21-13-34-34-33-13) assigned by the database. The results indicated that the strains might originate from different lineages [14].

Acknowledgments This work was partly supported by The National Natural Science Foundation of China (Grant No. 31370205) and The National Key Technology R&D Program of China (Grant No. 2011BAC11B05).

References

1. Riffon R, Sayasith K, Khalil H et al (2001) Development of a rapid and sensitive test for identification of major pathogens in bovine mastitis by PCR. J Clin Microbiol 39(7):2584–2589
2. Shome BR, Das Mitra S, Bhuvana M et al (2011) Multiplex PCR assay for species identification of bovine mastitis pathogens. J Appl Microbiol 111(6):1349–1356
3. Amagliani G, Petruzzelli A, Omiccioli E et al (2012) Microbiological surveillance of a bovine raw milk farm through multiplex real-time PCR. Foodborne Pathog Dis 9(5):406–411
4. Ruegg PL (2009) The quest for the perfect test: phenotypic versus genotypic identification of coagulase-negative *staphylococci* associated with bovine mastitis. Vet Microbiol 134(1–2):15–19
5. Weisburg WG, Barns SM, Pelletier DA et al (1991) 16S ribosomal DNA amplification for phylogenetic study. J Bacteriol 173(2):697–703
6. Fluit AC, Wielders CL, Verhoef J et al (2001) Epidemiology and susceptibility of 3,051 *Staphylococcus aureus* isolates from 25 university hospitals participating in the European SENTRY study. J Clin Microbiol 39(10):3727–3732
7. Tristan A, Ying L, Bes M et al (2003) Use of multiplex PCR to identify *Staphylococcus aureus* adhesins involved in human hematogenous infections. J Clin Microbiol 41(9):4465–4467
8. Harmsen D, Claus H, Witte W et al (2003) Typing of methicillin-resistant *Staphylococcus aureus* in a university hospital setting by using novel software for *spa* repeat determination and database management. J Clin Microbiol 41(12):5442–5448
9. Syring C, Boss R, Reist M et al (2012) Bovine mastitis: the diagnostic properties of a PCR-based assay to monitor the *Staphylococcus aureus* genotype B status of a herd, using bulk tank milk. J Dairy Sci 95(7):3674–3682
10. Jarp J (1991) Classification of coagulase-negative *staphylococci* isolated from bovine clinical and subclinical mastitis. Vet Microbiol 27(2):151–158

11. Boehmer JL, Ward JL, Peters RR et al (2010) Proteomic analysis of the temporal expression of bovine milk proteins during coliform mastitis and label-free relative quantification. J Dairy Sci 93(2):593–603
12. Ito T, Hiramatsu K, Tomasz A et al (2012) Guidelines for reporting novel *mecA* gene homologues. Antimicrob Agents Chemother 56(10):4997–4999
13. Rijnders MI, Deurenberg RH, Boumans ML et al (2009) Population structure of *Staphylococcus aureus* strains isolated from intensive care unit patients in The Netherlands over an 11-year period (1996 to 2006). J Clin Microbiol 47(12):4090–4095
14. Said KB, Ismail J, Campbell J et al (2010) Regional profiling for determination of genotype diversity of mastitis-specific *Staphylococcus aureus* lineage in Canada by use of clumping factor A, pulsed-field gel electrophoresis, and spa typing. J Clin Microbiol 48(2):375–386

Chapter 66
EST-SSR Marker-Based Assay for Purity Identification of Melon “Green Angle”

Ou-Jing Li, Xiao-Mu Chen, Pu-Xian Xia, Zhong-You Pei, Yong Wang, Qing-Kuo Lan and Ruo-Wei Zhang

Abstract In order to define the purity of melon (*Cucumis melo* L.) “Green Angle” variety F1 seed, PCR amplification, detection, and analysis were carried out with leaf DNA, using EST-SSR molecular marker technology. The results show that, among 57 SSR primers, PCR products with one pair of primer showed polymorphism from parents. For this marker, parents showed single allele whereas the hybrids showed both the parental alleles indicating the heterozygosity of the hybrids. 51 seeds were tested using the marker, and one seed was off-type. The same lot of seeds was also tested in the field and the purity was 98.4 %. It showed that the EST-SSR marker-based PCR assay is effective in determining the purity of F1-hybrid seeds of melon “Green Angle”.

Keywords Melon (*Cucumis melo* L.) · SSR marker · Hybrid seed purity

66.1 Introduction

Melon is one of the most important horticultural crops in the world. At present, the production has been widely used in hybrids [1]. Seeds are the most basic means of production in agricultural production, and its purity is the main indicators of seed quality.

Innovation team project of Tianjin “crop quality and genetic improvement of resistance”; Innovative talent training plan between Young and middle-aged backbone in Tianjin.

O.-J. Li · X.-M. Chen · P.-X. Xia · Z.-Y. Pei (✉)
Tianjin Agricultural University, Key Laboratory of Crop Genetic Breeding, Tianjin, China
e-mail: peizhy@126.com

O.-J. Li
e-mail: lioujing123@126.com

Y. Wang · Q.-K. Lan
Tianjin Institute of Agicultural Quality Standard and Testing Technology, Tianjin, China

R.-W. Zhang
Tianjin Academy of Agricultural Sciences, Institute of Vegetables, Tianjin, China

T.-C. Zhang and M. Nakajima (eds.), *Advances in Applied Biotechnology*,
Lecture Notes in Electrical Engineering 333, DOI 10.1007/978-3-662-46318-5_66

Reducing seed purity will decrease crop yield and product quality, so the peasants will suffer huge economic losses. Conventionally, hybrid seed purity assessment is done through grow out test (GOT) which is based on the morphological and floral characters of plants grown to maturity [2]. Being land and labor intensive, time consuming, and influenced by the environment, there is an immense need to replace GOT with a simple, rapid, unbiased, and cost-effective DNA-based assay for hybrid purity assessment.

With the continuous development of modern agriculture technology, the seed purity identification tag technology from the traditional form developed to a comprehensive appraisal technology system which set morphological marker identification, biochemical marker identification, and DNA molecular marker identification as a whole. DNA molecular marker is the direct reflection of DNA genetic variation at the molecular level [3], and they have stability genetic, large amount of information, not affected by internal and external environment, and has nothing to do with gene expression or not, rapid detection and such outstanding advantages as easy operation, therefore, DNA molecular markers become one of the ideal of rapid detection methods for the identification of seed purity, including RAPD (random amplified polymorphic DNA), RFLP (restriction fragment length polymorphism), SSR (simple sequence repeat), and ISSR (inter-simple sequence repeat) markers. Because of its codominance, the advantages of high polymorphism, and simple experimental procedure, SSR markers are one of the most commonly used tags in the study of crop variety and seed purity identifications.

The use of SSR markers for assessing seed purity has been reported in agricultural crops like rice [4–6], maize [7], sunflower [8] and horticultural crops like tomato [9], cabbage [10], and melon [11]. However, genomic SSR markers have been developed in melon only recently. The current development of SSR markers are mainly genomic SSR and EST-SSR. Relative to the SSR genome, EST-SSR makes full use of existing sequencing data, eliminates some steps in the process of development of SSR primers, such as library construction and sequencing, and reduces the cost. In recent years, with the continuous improvement of sequencing technologies and molecular biology research, a large number of melons have been EST sequenced; so far, the international cucurbitaceae genome project team recorded 7,856 ESTs markers in watermelon, 126,940 markers in melon, and 359,105 markers in cucumber [12].

Through DNA extraction, PCR amplification, and EST-SSR analysis, this report confirms the codominant complementary belt type of stable hybrids and their parents, thus identifying the melon hybrid purity.

66.2 Materials and Methods

66.2.1 Plant Material and DNA Extraction

F1 hybrid of melon "Green Angle" (LV) and their parents were analyzed in this study. These materials were provided by the Tianjin academy of agricultural sciences' institute of vegetables.

DNA was extracted from young leaves using the CTAB extraction protocol. About 100 mg of tissue was placed in a 2.0 mL microfuge tube and incubated in 800 mL of CTAB extraction buffer (2 % CTAB, 100 mM Tris-HCl, pH 8.0, 20 mM EDTA, pH 8.0, 1.4 M NaCl) at 65 °C for 1 h. Centrifuged for 10 min and the supernatant was collected. To each tube, 500 mL of chloroform was added, mixed, and centrifuged for 10 min. DNA was precipitated by mixing 300 μL of supernatant with 240 μL 95 % isopropanol. The precipitation was washed with 70 % ethanol, dried to remove alcohol, and dissolved in 100 mL TE (10 mM Tris, pH 8.0). The DNA quantity for each sample was assessed on 1 % agarose gel and the DNA concentrations were normalized at 50 ng/μL.

66.2.2 Primers

Primers used for SSR reactions were designed using CMD SSR Server online. A set of 57 SSR primer pairs were used to assess hybrid purity. The length of the primer is 18–25 bp, the content of GC is 40–60 %. The primers were synthesized by Shanghai biological engineering Co., Ltd.

66.2.3 PCR Conditions

PCRs were performed in a 20 μL reaction volume [10× Buffer (Mg^{2+}) 2.0 μL, dNTP (2.5 mM each) 1.6 μL, TagE (5 U/L) 0.1 μL, Primer (10 μmol/L) 0.5 μL, DNA(50 ng/μL) 2.0 μL] in 96-well microtiter plate using ABI veriti 96-well Thermal cycler. An initial denaturation for 2 min at 95 °C was used. This was followed by initial 35 cycles of denaturation for 45 s at 94 °C, annealing for 45 s at 55 °C, and extension for 45 s at 72 °C. Subsequently, followed by 7 min final extension at 72 °C.

The amplification products were analyzed by 8 % polyacrylamide gel and visualized by silver staining. Take photos with the "Typhoon" Multifunction scanner.

66.3 Results

66.3.1 EST-SSR Polymorphism in the Parental Lines

In a preliminary study, a set of 57 simple sequence repeat (SSR) primer pairs were used to assess hybrid purity. These 57 EST-SSR markers were used for the polymorphism survey among the parental lines of melon hybrids. Only one EST-SSR marker (Table 66.1) detected polymorphism between the parents of the hybrids.

Table 66.1 Details of the polymorphic EST-SSR markers used in the study

No.	Marker	Sequence (5′–3′)	Expected product (bp)
Pri73	M548-F	AACAGGTAGAGGAAAGCATG	145
	M548-R	TGACCCACTAGTACATCTCTC	

For the marker, parents showed single allele whereas the hybrids showed both the parental alleles indicating the heterozygosity of the hybrids (Fig. 66.1).

66.3.2 Genetic Purity Testing of Safflower Hybrids

This report chose the EST-SSR marker (M548) which shows polymorphism between LV-1 and LV-2 were used to amplify the genomic DNA of LV hybrid seedlings through PCR (Fig. 66.2). The result showed that the hybrid purity analysis of these 51 seedlings with EST-SSR marker M548 could identify the same number of off-types which are consistent with the field test results and the purity of F1 generation is 98.04 %. It indicates the reliability of genetic purity assessment of hybrid and it also indicated that a single polymorphic marker should be sufficient to ascertain the genetic purity as suggested by Yashitola et al. [4] and Nandakumar et al. [5].

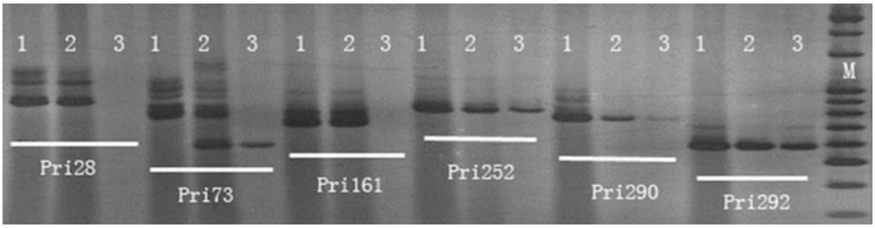

Fig. 66.1 EST-SSR markers polymorphism between parental lines of melon. *1* is female parent ‘LV-1’, *3* is male parent ‘LV-2’, *2* is ‘LV’ hybrid

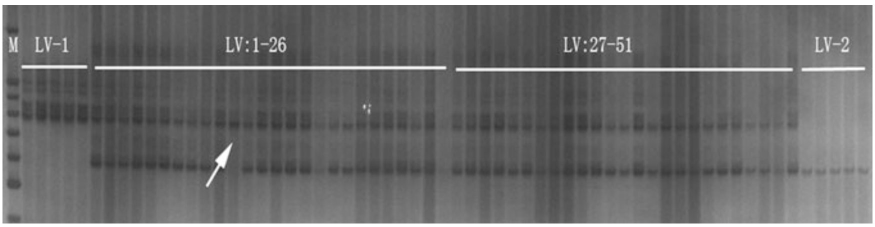

Fig. 66.2 Single seedling assay for detecting the genetic purity of the melon hybrid LV

66.4 Discussion

Though morphological and biochemical markers have been used for the characterization of genotypes, there are very few reports on the use of molecular markers for melon. In recent years, there are some reports on the use of molecular markers for cucurbitaceae [13, 14]. Though the utility of EST-SSR markers has been demonstrated in many species for applications discussed above, to the best of our knowledge, this is the first report of the EST-SSR marker-based genetic purity assessment of melon "Green Angle" hybrids.

In conclusion, molecular marker-based genetic purity assays will be highly useful in rapid and large-scale screening of hybrid seed lots. EST-SSR marker-based genetic purity testing would save the cost of hybrid seed storage for a whole season and the cost incurred on GOT. But, this pair of primer is only for melon "Green Angle" varieties; it is unknown for other varieties. The follow-up can be validated in other varieties and core primers of melon purity identification can be developed.

References

1. Chengxiang A, Lu L(2005) Application of SSR markers in melon hybrid seed purity test. Acta Hortic Sinica 32(5):902–904
2. Naresh V, Yamini KN, Rajendrakumar P, Dinesh Kumar V (2009) Euphytica 170:347–353
3. Xiaohui L, Congyan W (2008) The application of molecular marker technology in the watermelon genetic breeding. Mol Plant Breed 6(2):329–334
4. Yashitola J, Thirumurugan T, Sundaram RM, Naseerullah MK, Ramesha MS (2002) Assessment of purity of rice hybrids using microsatellite and STS markers. Crop Sci 42:1369–1373
5. Nandakumar N, Singh AK, Sharma RK, Mohapatra T, Prabhu KV, Zaman FU (2004) Molecular fingerprinting of hybrids and assessment of genetic purity of hybrid seeds in rice using microsatellite markers. Euphytica 136:257–264
6. Sundaram RM, Naveenkumar B, Biradar SK, Balachandran SM, Mishra B, IlyasAhmed M, Viraktamath BC, Ramesha MS, Sarma NP (2008) Identification of informative SSR markers capable of distinguishing hybrid rice parental lines and their utilization in seed purity assessment. Euphytica 163:215–224
7. Mingsheng W, Xihai J, Lei T, Baochun L (2006) Rapid and reliable purity identification of F1 hybrids of maize (Zea mays L.) using SSR markers. Mol Plant Breed 4:381–384
8. Antonova TS, Guchetl SZ, Tchelustnikova TA, Ramasanova SA (2006) Development of marker system for identification and certification of sunflower lines and hybrids on the basis of SSR-analysis. Helia 29:63–72
9. Smith JSC, Register JC (1998) Genetic purity and testing technologies for seed quality: a company perspective. Seed Sci Res 8:285–293
10. Liu L, Liu G, Gong Y, Dai W, Wang Y, Yu F, Ren Y (2007) Evaluation of genetic purity of F1 hybrid seeds in cabbage with RAPD, ISSR, SRAP and SSR markers. Hort Sci 42:724–727
11. Jianli L, Xiaohua S, Shouchun Z, Jianshe W (2006) Purity test of melon hybrid with SSR molecular markers. Mol Plant Breed 4:23–26

12. Shengjie. Z, Wenge. L, Zhihong. Y. Mainly melons EST—the development and application of SSR markers in cucurbitaceae crops. Biotechnol Bull 2011 10:72–75
13. Zhou S, Zhang P, Zhu P, Chen X, Chen L (2013) Application of SSR markers in ‘Zhexiu 1’ hybrid seed purity test of cucumber. Mol Plant Breed 11(5):557–561
14. Zhou Z, Wang H, Wang X, Li G (2014) Genetic purity test of melon variety ‘Red Moon’ F1 using SSR marker. Chinese Vegetables 27(1):21–24

Chapter 67
Exposure to Static Magnetic Fields Affects Insulin Secretion in INS Cells

Libin Mao, Zhixia Guo, Huiqin Wang, Qiongyao Wu, Nan Wang and Tong-Cun Zhang

Abstract The exposure to static magnetic fields (SMFs) has rapidly increased and is recently accompanied with the wide use of more and more electrical appliances. Although few researches have been reported on other types of magnetic fields that may have the effects on clinical therapy of diseases, it is rarely seen reports on the effects of moderate static magnetic fields on human health. In this study, in order to evaluate the influence of exposure to moderate static magnetic fields on biological systems, we cultured the INS-1 under exposure to moderate intensity of 400 mT and sham conditions for different times from 6 to 18 h, insulin secretion to medium and mRNA expression will be tested after exposure. Insulin secretion has significantly increased after exposed to SMFs with moderate intensity of 400 mT for 18 h compared with the sham condition. Furthermore, similar to the insulin secretion, insulin 1 and insulin 2 mRNA expression also increased after exposure. These results suggest that exposure to SMFs at 400 mT position for specific times might have positive stimulation in both insulin secretion and insulin mRNA expression, and these will be used hopefully in further investigations in vitro, even in the therapy clinically.

Keywords Static magnetic fields · INS-1 cells · Insulin secretion · Clinical therapy

67.1 Introduction

There is no doubt that with more and more electrical appliances being used in our daily life [1], man has got more exposure to static magnetic fields (SMFs) than ever before. Previously, the beneficial effects of magnetic fields on inflammation [2],

L. Mao · Z. Guo · H. Wang · Q. Wu · N. Wang · T.-C. Zhang (✉)
A Key Laboratory of Industrial Microbiology, Ministry of Education and Tianjin City, College of Biotechnology, Tianjin University of Science and Technology, Tianjin 300457, People's Republic of China
e-mail: tony@tust.edu.cn

T.-C. Zhang and M. Nakajima (eds.), *Advances in Applied Biotechnology*, Lecture Notes in Electrical Engineering 333, DOI 10.1007/978-3-662-46318-5_67

osteoporosis [3], wound healing [4], and pain reduction [5] have been demonstrated by a plenty of intriguing studies using laboratory animals in vivo. Meanwhile, the frequency of exposure to SMFs has also increased rapidly, such as magnetic resonance imaging (MRI) and nuclear magnetic resonance (NMR) [6], which have been used in hospitals as noninvasive diagnostic tools. Therefore, it has become important to systematically elucidate the influence of SMFs on biological systems.

In an attempt to explain the biological effects of SMFs, it is useful to classify them as weak (<1 mT), moderate (1 mT–1 T), strong (1–5 T), and ultrastrong (>5 T). Previous studies have shown that SMF alone does not exhibit lethal effects on cell growth, survival, and DNA damage [7, 8], but are still controversial [9, 10]. It is urgent for us to provide a clear answer regarding the impact of SMFs on cell function, which is due to the use of SMFs of certain intensities and different cell types.

Pancreatic islets play a vital role in regulating the blood glucose levels of the body through the secretion of hormones such as glucagon and insulin, and the insufficient release of insulin is the basis of various forms of diabetes. Previously, Sakurai et al. reported that the effects of magnetic fields on insulin-secreting cells. Although the effects of strong static magnetic fields whose magnetic flux density is from 3 to 10 T has already been reported [11, 12], the effects of moderate intensity of SMFs were rarely seen before. In addition, insulin-secreting cells are appropriate for evaluating the effects of SMFs on biological systems, because insulin secretion is affected by calcium and its channel [13, 14], which was considered to be a candidate for interaction with SMFs.

Accordingly, in this study, we have investigated the effects of exposure to moderate SMFs at 400 mT on insulin mRNA expression by the insulinoma cell line, INS-1, under exposure to sham and SMFs conditions.

67.2 Materials and Methods

67.2.1 SMF Exposure System and SMF Exposure

SMF exposure (purchased from Tianjin Nibboh Magnets Co., Ltd), a static magnetic field at a intensity of 400 mT, was supplied by the xxx company. Briefly, the SMF exposure system was formed by a magnet with 10 mm thickness, 20 mm inner diameter, and 35 mm outer diameter into a CO_2 incubator where the atmosphere is maintained with 5 % CO_2 and 95 % humidified air and, the direction of the field is vertical. The temperature in the incubator was monitored by thermocouple sensor probes and is maintained at 37 ± 0.2 °C. For the sham-exposure system, we utilized another magnet of the same shape, but without the magnetic field. The SMF in the sham-exposure space was less than 5 μT.

67.2.2 Cell Culture

INS-1 cells were cultured in RPMI-1640 medium supplemented with 10 % fetal bovine serum (FBS), 10 mM 2-[4-(2-hydroxyethyl)-1-piperazinyl] ethanesulfonic acid (HEPES), 2 mM L-Glutamine, 1 mM Sodium Pyruvate, 50 µM β-mercapto-ethanol, 100 U/mL of penicillin, and 100 µg/mL of streptomycin at 37 °C with 95 % humidified air and 5 % CO_2.

67.2.3 Insulin Secretion

Cells were seeded on the dishes of 35 mm with 2 mL culture medium at a density of 1.5×10^5 cells/cm^2. After cultured for 48 h, cells were washed once using the fresh medium, then the medium was changed to another 800 µL/dish fresh culture medium. After INS-1 cells were exposed to SMF in 6, 12 or 18 h at 37 °C with 95 % humidified air and 5 % CO_2, The supernatant was collected and insulin secreted into the culture medium was measured by ELISA assay kits for rat insulin (WUHAN BEINGLAY BIOTECH CO.). Total protein was used to normalize the insulin secreted into the medium.

67.2.4 RNA Extraction, cDNA Synthesis, and PCR Reaction

Cells were seeded on the dishes of 35 mm in diameter at a density of 1.5×10^5 cells/cm^2 and cultured as described in cell culture. After culture for 48 h, cells were washed once with PBS, the culture medium was then changed to another 1 mL fresh medium in each dish. After cells were exposed to SMF at 37 °C with 5 % CO_2 and 95 % humidified air for 6, 12 or 18 h, total RNA was extracted from cells with TRIzol reagent (Invitrogen). After that, the cDNA synthesis was performed using the reverse transcription with random primers. The thermal cycle profile was as follows: denaturation for 30 s at 95 °C, annealing for 30 s at 54–57 °C depending on the primers used, and extension for 30 s at 72 °C. PCR products were visualized on 2 % agarose gels stained with ethidium bromide under ultraviolet (UV) trans-illumination. The primers used in this study are summarized in Table 67.1.

Table 67.1 Primers used in the present study

Gene	Primer sequence
GAPDH	F: 5'-ATTCAACGGCACAGTCAAGG-3'
	R: 5'-GCAGAAGGGGCGGAGATGA-3'
Rat Insulin 1	F: 5'-CCGTCGTGAAGTGGAGGA-3'
	R: 5'-CAGTTGGTAGAGGGAGCAGAT-3'
Rat Insulin 2	F: 5'-TGGGGAGCGTGGATTCTTCTA-3'
	R: 5'-ACCTCCAGTGCCAAGGTCTGA-3'

[1] *F* Forward, *R* Reverse

Glyceraldehyde-3-phosphate dehydrogenase (GAPDH) was used as an internal control to show equal loading of the cDNA samples.

67.3 Results

67.3.1 Insulin Secretion

INS-1 cells were exposed to SMF at 400 mT position for 6, 12, or 18 h, respectively, and insulin secretion were measured by rat ELISA assay Kit. Compared with the sham-exposed cells, insulin secretion was significantly increased under the exposure to SMF at 400 mT position for 18 h (Fig. 67.1). A slight increase in insulin secretion was observed following exposure to SMF for 6 and 12 h. The results show that 400 mT SMF can significantly enhance intracellular insulin concentration in INS cells in a time-dependent manner.

67.3.2 Effects of SMF on the Expression of Insulin mRNA

Next, the effect of SMF on the expression of insulin1 and insulin2 mRNA was evaluated by RT-PCR. When cells were exposed to SMF at 400 mT for 6, 12, and 18 h, the insulin secretion was significantly enhanced in a time-dependent manner, compared with sham-exposure conditions (Figs. 67.2 and 67.3).

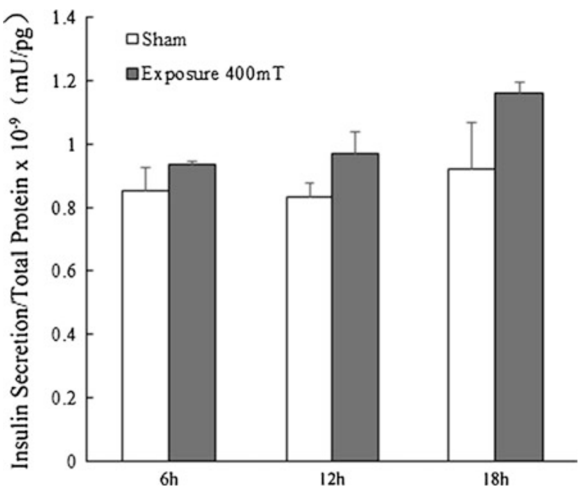

Fig. 67.1 Alternations of insulin secretion levels during exposure to static magnetic fields (SMF). INS-1 cells were exposed to SMF at 400 mT position for 6, 12 or 18 h, respectively, compared with the sham-exposure cells. Insulin secretion levels in the culture medium were normalized by total protein

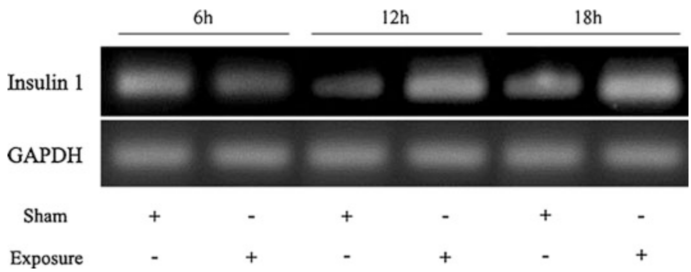

Fig. 67.2 Alternation of the expression of insulin 1 following exposure to static magnetic fields (SMF). INS-1 cells were exposed to SMF at 400 mT position for 6, 12 or 18 h, respectively, compared with the sham-exposure cells. Insulin 1 mRNA levels were normalized to GAPDH

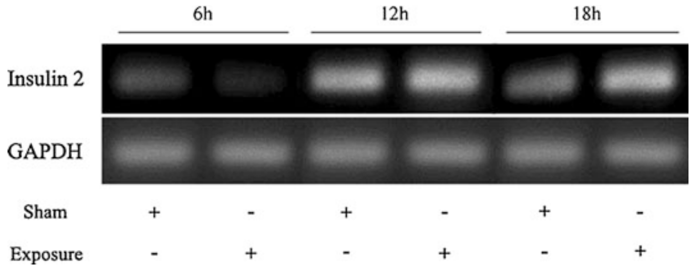

Fig. 67.3 Alternation of the expression of insulin 2 following exposure to static magnetic fields (SMF). INS-1 cells were exposed to SMF at 400 mT position for 6, 12 or 18 h, respectively, compared with the sham-exposure cells. Insulin 2 mRNA levels were normalized to GAPDH

67.4 Discussion

Diabetes mellitus has already become a deadly threat to human life. Its occurrence rate rapidly increased in recent years. The insufficient insulin secretion is recognized as one of the main causes of diabetes. There are a few studies that have already evaluated the influence of exposure to magnetic fields on pancreas islet function, including strong SMF [9] and ELFMF [15, 16], it is still difficult to compare the results which have been performed, not only because of the cells used are different from each other [13], but also the methods used were quite inconsistent in different researches. Therefore, the association between pancreas islet function and magnetic fields exposure is still controversial and uncertain [17]. In this study, we explored the effects of a medium SMF exposure on INS cells by measuring insulin secretion and the expression of mRNA. Exposure to SMF at 400 mT position for 18 h significantly increased insulin secretion. Similar to the results on insulin secretion, the expression of insulin 1 and insulin 2 mRNA were also obviously increased after exposure to SMF at 400 mT position for 18 h.

In conclusion, SMF might be used clinically as a new medical therapy in diabetes. Of course, the precise underlying mechanisms remain unclear and need further studies.

Acknowledgments Thanks to SINO-GERMAN LIDE BIOLOGICAL TECHNOLOGY CO., LTD for providing LIDE products and technical support. This work was financially supported by Program for Changjiang Scholars and Innovative Research Team in University of Ministry of Education of China (IRT1166), Science Research Foundation of Tianjin University of Science & Technology (20130109), and National Training Programs of Innovation and Entrepreneurship for Undergraduates (201310057075).

References

1. Feychting M, Ahlbom A, Kheifets L (2005) ELF and Health. Ann Rev Public Health 26: 165–189
2. Weinberger A, Nyska A, Giler S (1996) Treatment of experimental inflammatory synovitis with continuous magnetic field. Isr J Med Sci 32:1197–1201
3. Giordano N, Battisti E, Geraci S et al (2001) Effects of electromagnetic fields on bone mineral density and biochemical markers of bone turnover in osteoporosis: a single-blind, randomized pilot study. Curr Ther Res 62:187–193
4. Man D, Man B, Plosker H (1999) The influence of permanent magnetic field therapy on wound healing in suction lipectomy patients: a double-blind study. Plast Reconstr Surg 104:2261–2266
5. László J, Gyires K (2009) 3 T homogeneous static magnetic field of a clinical MR significantly inhibits pain in mice. Life Sci 84:12–17
6. World Health Organization (2006) “Static fields”, environmental health criteria, 232. Switzerland, Geneva
7. Miyakoshi J (2005) Effects of a static magnetic field at the cellular level. Prog Biophys Mol Biol 87:213–223
8. Glinka M, Gawron SA, Sieroń A et al (2013) Action of the static magnetic fields on the antioxidant activity in the fibroblasts’ culture. Prz Elektrotech 1:41–44
9. Todorovi ć D, Mirčić D, Ilijin L et al (2012) Effect of magnetic fields on antioxidative defense and fitness-related traits of Baculum extradentatum (insecta, phasmatodea). Bioelectromagn 33:265–273
10. Lee BC, Johng HM, Lim JK et al (2004) Effect of extremely low frequency magnetic field on the antioxidant defense system in mouse brain: a chemiluminescence study. J Photochem Photobiol, B 73:43–48
11. Sakurai T, Terashima S, Miyakoshi J (2009) Effects of strong static magnetic fields used in magnetic resonance imaging on insulin-secreting cells. Bioelectromagn 30:1–8
12. Sakurai T, Terashima S, Miyakoshi J (2008) Enhanced secretion of prostaglandin E2 from osteoblasts by exposure to a strong static magneticfield. Bioelectromagn 29:277–283
13. Rosen AD, Lubowsky J (1987) Magnetic field influence on central nervous system function. Exp Neurol 95:679–687
14. Coots A, Shi R, Rosen AD (2004) Effects of a 0.5 T static magnetic field on conduction in guinea pig spinal cord. J Neurol Sci 222:55–57
15. Sakurai T, Satake A, Sumi S et al (2004) An extremely low frequency magnetic field attenuates insulin secretion from the insulinoma cell line, RIN-m. Bioelectromagn 25:160–166
16. Hayek A, Guardian C, Guardian J et al (1984) Homogeneous magnetic fields influence pancreatic islet function in vitro. Biochem Biophys Res Commun 122:191–196
17. Sahebjamei H, Abdolmaleki P, Ghanati F (2007) Effect s of magnetic field on the antioxidant enzyme activities of suspension-cultured tobacco cells. Bioelectromagn 28:42–47

Chapter 68
The New Strategy of Breeding Cytidine Excessive Biosynthesis Mutants by *pyr* Operon Rearrangement of *Bacillus amyloliquefaciens*

Qing Wu, Huiyan Liu, Haitian Fang, Jianguo He, Xiaoguang He and Linan Yu

Abstract Cytidine is a good antitumor and antiviral intermediate which can also be used as a healthy food ingredients. With the market for cytidine increasing, the large-scale production of cytidine by microbial fermentation method has become a major way to solve this problem. While improving cytidine production, the regulation of pyr operon is essential to the excessive synthesis cytidine. However, its transcriptional regulation mechanism is unclear. The passage summarizes the regulation of de novo pyrimidine nucleotide biosynthesis (pyr genes) and the metabolic regulation mechanism of cytidine synthesis in *Bacillus amyloliquefaciens*. This paper makes the regulation protein pyrR as the research object, presents a series of *Bacillus amyloliquefaciens* pyrimidine operon transcriptional regulatory rearrangement strategy, effects the transcriptional regulation on cytidine biosynthesis, and aims to provide a theoretical basis for cytidine yielding strain.

Keywords *Bacillus amyloliquefaciens* · Cytidine · *pyr* operon · *pyrR*

68.1 Introduction

Cytidine was known as cytidine, and 1-β-D-furan nucleoside cytosine. As a pyrimidine nucleoside, cytidine is a structural component of DNA in organisms. It is a nucleoside molecule that is widely used as a precursor for antitumor and antiviral drugs and it is the main raw material for the manufacture of cytarabine (Ara-CR), ring cytidine (CycloC), cytidine triphosphate (CTP), citicoline

Q. Wu · H. Liu · H. Fang (✉) · J. He · X. He · L. Yu
Bioengineering Laboratory, Agricultural College of Ningxia University,
Yinchuan 750021, China
e-mail: fanght2014@163.com

T.-C. Zhang and M. Nakajima (eds.), *Advances in Applied Biotechnology*,
Lecture Notes in Electrical Engineering 333, DOI 10.1007/978-3-662-46318-5_68

(CDP-Choline), and other drugs [1]. With the deep study of antiviral and antitumor, natural pyrimidine nucleoside demand become increasingly large, the demand for natural cytidine also increased. The present production methods to generate high cytidine production involves RNA hydrolysis, the combination of fermentation and synthetic, uracil precursor for the fermentation and direct fermentation method. However, the intracellular cytidine levels are very low and tightly controlled [2]. Compared to other methods, the use of mutant strains of microorganisms in direct fermentation for mass production of the nucleoside is an outstanding achievement of modern microbiology; such methods have the simplicity, short duration, easy control, high yield and low production cost as its advantages. The fermentation obtained strains using breeding techniques have capable of producing large-scale, single-cytidine, greatly reduced the production cost, accelerate research on fermentation for the production of cytidine.

68.2 Analysis of Pyrimidine Biosynthesis Pathway in *Bacillus amyloliquefaciens*

The genes encoding the enzymes of pyrimidine nucleotide biosynthesis de novo are the same in all bacteria. The regulation of cytidine biosynthesis in *B. amyloliquefaciens* are summarized as follows (Fig. 68.1).

The first step of pyrimidine nucleotide biosynthesis de novo is to generate pyrimidine synthesis carbamoyl phosphate by carbamoyl phosphate synthetase catalyzed condensation reaction of CO_2 and glutamine. The next reaction catalyzed by aspartate transcarbamoylase (ATCase) with the condensation reaction of aspartate and carbamoylphosphate condensation to generate carbamoyl aspartate, which undergoes several reactions to produce UMP, the precursor for the synthesis of the cytidine. The de novo biosynthesis of pyrimidine nucleotides is regulated by intracellular concentrations of various nucleotides through feedback inhibition [3]. The intracellular CTP levels controls the intracellular UMP level through the control of ATCase and the feedback inhibition of CPS [4]. Further on that UDP is

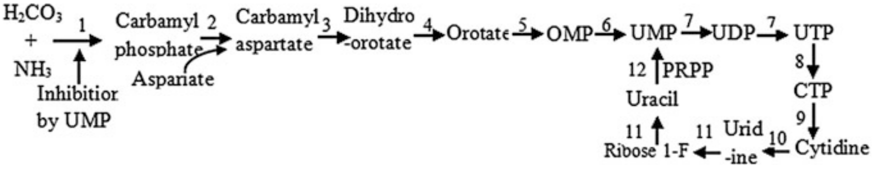

Fig. 68.1 Pyrimidine nucleotide biosynthetic pathway of *B. amyloliquefaciens*. The catalytic enzyme of each reactions are as follows: *1* Carbamylphosphate synthetase; *2* Aspartate transcarbamylase; *3* Dihydroorotase; *4* Dihydroorotate dehydrogenase; *5* Orotate phosphoribosyltransferase; *6* 5′-monophosphate decarboxylase; *7* UMP kinase; *8* CTP synthetase; *9* 5′-nucleotidase; *10* Cytidine deaminase; *11* Uridine phosphorylase; *12* Uracil phosphoribosyl transferase; *PRPP* Phosphoribosyl pyrophosphate

transformed by the UMP catalyzed by UMP kinase and CTP is transformed by the UTP catalyzed by the CTP synthase, which is regulated by CTP effectors through binding to specific allosteric sites on CTP synthase [5–7]. Moreover, the synthesis of CTP is located at a node in the cytidine biosynthesis pathway. Because of its importance, CTP synthase is also regulated by a feedback inhibition by CTP and cytidine [7]. Meanwhile, the CPS and ATCase enzyme reactions are key regulatory enzymes in the nucleotide metabolism and represent the major pathways for cytidine synthesis. It has been found that the CPS and ATCase generating UMP is a part of the overall regulation of CTP synthesis [8].

68.3 Research Progress of Pyrimidine High Yield Strains

Since 1980s to the 1990s, the Japanese scientists began to produce the pyrimidine nucleoside by fermentation [2]. High-level cytidine production depends on direct fermentation of carbohydrates by auxotrophic and regulatory mutant with *B. subtilis*, *B. pumilus*, *B. licheniformis, Escherichia coli*, and other organisms has been reported since the 1970s. Turnbough and Switzer [2, 9]. Among these species, *B. amyloliquefaciens, B. subtilis* and *E. coli* stains depending on their high growth rate and well-known physiological characteristics have been developed by mutagenesis or genetic manipulation and selected for the ability to grow on toxic cytidine analogues cytidine analogues [10–12]. The general strategy used for the development of a cytidine overproducing strain involves the alleviation of control mechanisms in key pathways [13–15]. Besides, these studies concentrated on the six operons encoding the enzymes required for the biosynthesis of UMP, the precursor of all pyrimidine nucleotides (Fig. 68.1). Nevertheless, we have never seen the report about the reconstruction of pyrimidine operon transcription regulatory system to optimize the cytidine metabolic network.

68.4 Pyrimidine Operon Regulatory Region Genes and Related to Pyrimidine Biosynthesis

Many diverse bacteria regulate the expression of genes of de novo pyrimidine nucleotide biosynthes by an transcriptional attenuation that is mediated by the PyrR, an mRNA-binding regulatory protein [2]. The genes of pyrimidine nucleotide biosynthesis in *B. amyloliquefaciens* are organized in an operon whose expression is governed by a single promoter and a regulatory protein encoded by *pyrR* [2]. The *pyr* operon of *B. amyloliquefaciens* contains 10 cistrons, which appears to be expressed as a single transcriptional unit. The first gene in the operon encodes pyrR, which has been shown to be the regulatory protein for the operon, and a uracil phosphoribosyltransferase (EC 2.4.2. 9) [2]. The second gene in the operon encodes pyrP, which is uracil permease. The remaining eight cistrons encode the six enzymes necessary for de novo biosynthesis of UMP [2]. The map of *B. amyloliquefaciens pyr* operon are summarized as follows (Fig. 68.2).

The PyrR protein binds in a uridine nucleotide-dependent manner to three attenuation sites which lie upstream of the genes, called the binding loop and that is regulated by uridine and guanosine nucleotides, allowing a terminator hairpin to form and repressing the downstream genes. These have been seen in *Bacillus* [16], *Lactobacillus* [17, 18], *Lactococcus* [19], and *Enterococcus* [20] species. These attenuation regions are located in the 5′ leader region of the operon upstream of pyrR (binding loop 1, BL1), the pyrR-pyrP intercistronic region (BL2), and the pyrR-pyrB intercistronic region (BL3) of pyr mRNA. Following transcription, the three attenuation sites within the nascent *pyr* mRNA are each predicted to fold into either an anti-antiterminator transcription terminator or a antiterminator structure. The key to regulation of the *pyr* operon lies in the ability of pyrR to favor formation of the terminator hairpins, which results in premature termination of transcription and reduces expression of the downstream genes. PyrR does this by binding to *pyr* mRNA when the protein is activated by binding of uridine nucleotides, PyrR binds to *pyr* mRNA at a site which lies upstream of the genes that it regulates. The binding of PyrR to the mRNA is dependent on the formation of a PyrR-UMP complex [2]. Previous research led to a model in which high levels of UMP stimulate PyrR to bind to a conserved sequence and secondary structure in the mRNA in each attenuation region called the anti-antiterminator or the binding loop; when UMP levels are low, the RNA-binding affinity of PyrR is reduced and the more stable antiterminator stem-loop is favored, leading to transcriptional read-through and expression of the downstream genes [2]. The pyrR protein of *B. amyloliquefaciens* also has been

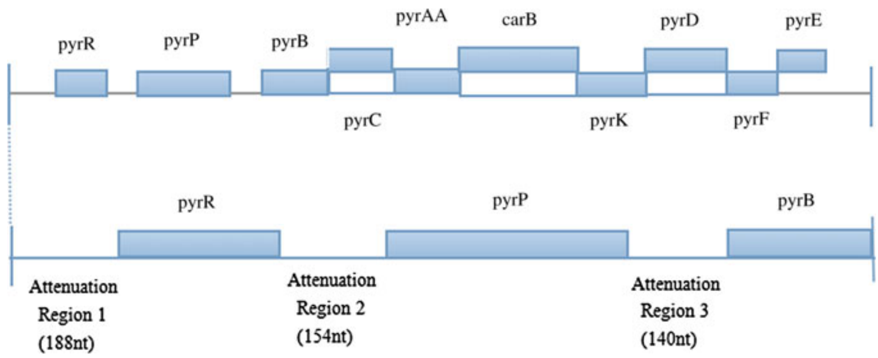

Fig. 68.2 The map of pyr operon in *B. amyloliquefaciens*. The genes shown in the figure and the encoded proteins are as follows: pyrR, pyr mRNA-binding attenuation regulatory protein; pyrP, uracil permease; pyrB, catalytic subunit of aspartate transcarbamylase; pyrC, dihydroorotase; pyrAA, glutamine-utilizing subunit of carbamylphosphate synthetase equivalent to carA; carB, catalytic subunit of carbamylphosphate synthetase; pyrK, electron-transferring accessory protein to dihdroorotate dehydrogenase; pyrD, dihydroorotate dehydrogenase; pyrF, OMP decarboxylase; pyrE, orotate phosphoribosyltransferase

shown to have the ability to catalyze the formation of UMP from uracil and PRPP, thus being a uracil phosphoribsyltransferase (UPRTase) as well as a regulatory protein [2].

68.5 Cytidine Excessive Biosynthesis Mutant Breeding Strategy-Pyrimidine Operon Regulatory Region Gene Modification

The prerequisite of cytidine fermentation is to design, build, and optimize the microbial pyrimidine nucleoside metabolic network, directional breeding high-yielding strains that have capable of production cytidine. The pyrimidine metabolism of *B. amyloliquefaciens* is flux, whole genome sequencing has been completed, clear genetic background and suitable for breeding cytidine production of bacteria strains. Pyrimidine nucleotide operon (pyr operon) plays an important role in pyrimidine nucleotide synthesis of *B. amyloliquefaciens*. At present, a lot of studies about metabolism of cytidine focus on traditional mutagenesis breeding production bacteria, the research on molecular genetic breeding, and cytidine metabolic network reconstruction optimization report a little late. While there has little report on the impact of excess synthesis of cytidine about *B. amyloliquefacien*s and has never seen about the reconstruction of pyrimidine operon transcriptional regulatory system to optimize cytidine metabolic network. Through the modification of pyrimidine operon transcriptional regulatory region in *B. amyloliquefaciens* may be relieved the negative regulation of transcription, increase expression of gene dosage in the cells, and promote the rate-limiting step in the biochemical reactions, which may lead to increased production of cytidine.

68.5.1 pyrR Gene and Effect of PyrR Regulatory Protein Inactivation on Excessive Biosynthesis of Pyrimidine

The previous reports have indirectly showed that deletion of the gene leads to very high-level constitutive expression of *pyr* genes [2], and PyrR has been previously shown to act to regulate all three attenuators [2]. Our laboratories have analyzed carbamyl phosphate synthetase gene, aspartate aminotransferase, cytidine deaminase gene and homoserine dehydrogenase gene cytidine synthesis-related genes and cytidine accumulation at the early stage. It turned out that cytidine production has accumulated after metabolic block, indicating the metabolic pathways of cytidine and metabolic pathways of aspartic acid to homoserine block to the of cytidine is very necessary for the cytidine accumulation. Fixed point mutation cytidine synthesis from the de novo pathway of two key enzymes of cytidine accumulation is very effective, But accumulation level is low, which may be influenced by many factors, series of cytidine synthesis enzyme gene transcription level lower the speed limit is the key factor. To solve this problem, we decided to try directed evolution and genetic recombination, focusing on the transformation of PyrR regulatory protein and attenuators of pyrimidine biosynthesis of *B. amyloliquefaciens*. We intend to adopt the homologous recombination to make the *pyrR* gene inactivation in *B. amyloliquefaciens.* RTFQ PCR is used to characterize the structural gene expression in transcription levels and then analyze the change in technology pyrimidine metabolism pathway protein levels by SDS-PAGE, analyzing the impact of pyrR gene inactivation pyrimidine operon transcriptional level.

68.5.2 Attenuations of pyr Operon Regulatory Region and Effects of Attenuator Gene Rearrangement on Excessive Biosynthesis of Pyrimidine

With further research that the interaction of the *B. amyloliquefaciens* regulatory protein PyrR with BL1, BL2 and BL3, which are located within the three different attenuation sites of pyr mRNA, has been analyzed in great detailing vitrousing gel mobility shift assays. Besides, It has been found that the apparent strength of the interaction between PyrR and the three different BLs was very different. PyrR bound significantly more tightly to the BLs of the second (BL2) and third (BL3) attenuation site than to the BL of the first (BL1) site. However, there has little reports about the influence of knocking out *pyrR* gene on expression of proteins in the bacterial cell about global responses of the bacterial cells affected by PyrR [21]. And still there has little reports about after knocking out pyrR gene and three attenuators like the following combinations (pyrR, pyrR, and BL in any one of pyrR and BL in any two arbitrary, pyrR and BLs), what it has impact on the level of transcription, and further effect on the cytidine synthesis. We intend to make the *pyrR* gene inactivation at first. After the *pyrR* gene inactivation and analysis of pyrimidine operon transcription level, we plan knockout attenuation in tandem to reconstruct attenuation regulatory region, even more monitor its impact on production of cytidine.

68.5.3 Blockade of Cytidine Catabolic Pathways

Aspartic acid is an important precursor in the de novo cytidine synthesis pathway of *B. amyloliquefaciens*. With carbamoyl phosphate in aspartate aminotransferase. Aspartate and carbamoyl phosphate catalyzed by aspartate aminotransferase produces carbamyl aspartic acid, and in the role of cytidine deaminase, cytidine further generate uridine. So we can delete cytidine deaminase gene to cut-off further metabolized to cytidine decomposition pathways uridine. There are studies indicating that knocking out of *cdd* gene can increase the production [12]. Therefore, we plan to use homologous recombination to make the *cdd* gene inactivation of being transformation of the deficient strain and monitor the production of cytidine by fermentation.

68.6 Summary

After a series of ways to rearrange operon expression synthetic dose at the transcriptional level by monitoring the pyrimidine creatures, in order to get an impact on the cytidine through the gene modification of measures later. Doing that what we have imagined would increase or decrease the yield of cytidine and we do not know the results. Only through the experiment to draw conclusions and the process and results that is what we should strive to get. Through the modification of pyrimidine operon transcriptional regulatory regions in *B. amyloliquefaciens*, which may be relieve the negative regulation of transcription, increasing expression of gene dosage in the cells and promoting the rate-limiting step in the biochemical reactions, which may lead to increase production of cytidine. And, analyzing the change of the pyrimidine biosynthesis transcription level and structural gene expression can provide theoretical basis to enhance the cytidine production.

Acknowledgments We thank our colleagues for critical reading of the manuscript and providing valuable suggestions. This work was supported by Chinese National Natural Science Foundation (Grant №31301542).

References

1. Bezombes C, Laurent G, Jaffrezou JP et al (2003) Implication of rafe microdomains in drug induced apoptosis. Curr Med Chem Anticancer Agents 3(4):263–270
2. Turnbough CL Jr., Switzer RL (2008) Regulation of pyrimidine biosynthetic gene expression in bacteria: repression without repressors. Microbiol Mol Biol Rev 72(2):266–300
3. Caldara M, Dupont G, Leroy F, Goldbeter A, Vuyst LD, Cunin R (2008) Arginine biosynthesis in Escherichia coli experimental perturbation and mathematical modeling. J Biol Chem 283(10):6347–6358
4. Song KH, Do YK, Sang YK, Jung KL, Hyung HH (2005) Thymidine production by Corynebacterium ammoniagenes mutants. Microbiol Biotechnol 15(3):477–483
5. Lee HC, Ahn JM, Lee SN, Kim JH (2004) Overproduction of thymidine by recombinant Brevibacterium helvolum amplified with cytidine monophosphate phosphohydrolase gene from bacteriophage PBS2. Biotechnol Lett 26:265–268
6. Palmen LG, Becker K, Bulow L, Kvassman JO (2008) A double role for a strictly conserved serine: further insights into the dUTPase catalytic mechanism. Biochemistry 47:7863–7874
7. Lee HC, Kim JH, Kim JS, Jang W, Kim SY (2009) Fermentative production of thymidine by a metabolically engineered Escherichia coli strain. Appl Environ Microbiol 75(8):2423–2432
8. Rabinowitz JD, Hsiao JJ, Gryncel KR, Kantrowitz ER, Feng XJ, Li GY, Rabitz H (2008) Dissecting enzyme regulation by multiple allosteric effectors: nucleotide regulation of aspartate transcarbamoylase. Biochemistry 47(21):5881–5888

9. Koo BS, Hyun HH, Kim SY, Kim CH, Lee HC (2011) Enhancement of thymidine production in E. coli by eliminating repressors regulating the carbamoyl phosphate synthetase operon. Biotechnol Lett 33:71–78
10. Zhang H, Switzer RL (2003) Transcriptional pausing in the Bacillus subtilis PyrR with pyr mRNA by site-directed mutagenesis of the protein. J Bacteriol 185:4764–4771
11. Switzer RL (2009) Discoveries in bacterial nucleotide metabolism. J Biol Chem 284 (11):6585–6594
12. Lee HC, Kim JS, Jang W, Kim SY (2010) High NADPH/NADP + ratio improves thymidine production by a metabolically engineered Escherichia coli strain. J Biotechnol 149:24–32
13. Fang H, Xie X, Xu Q, Zhang C, Chen N (2012) Effects of medium components and fermentation conditions on cytidine production by recombinant Escherichia coli CYT20. Lect Notes Electr Eng 249:15–22
14. Fang H, Zhang C, Xie X, Xu Q, Zhou Y, Chen N (2014) Enhanced cytidine production by a recombinant Escherichia coli strain using genetic manipulation strategies. Ann Microbiol 64(3):1203–1210
15. Fang H, Liu H, Chen N, Zhang C, Xie X, Xu Q (2013) Site-directed mutagenesis studies on the uridine monophosphate binding sites of feedback inhibition in carbamoyl phosphate synthetase and effects on cytidine production by Bacillus amyloliquefaciens. Can J Microbiol 59(6):374–379
16. Switzer RL, Turner RJ, Lu Y (1999) Regulation of the Bacillus subtilis pyrimidine biosynthetic operon by transcriptional attenuation: control of gene expression by an mRNA-binding protein. Prog Nucleic Acids Res Mol Biol 62:329–367
17. Arsene-Ploetz F, Kugler V, Martinussen J, Bringel F (2006) Expression of the pyroperon of Lactobacillus plantarumis regulated by inorganic carbon availability through a second regulator, PyrR2, homologous to the pyrimidine regulator PyrR. J Bacteriol 188:8607–8616
18. Nicoloff H, Elagoz A, Arsene-Ploetze F, Kammerer B, Martinussen J, Bringel F (2005) Repression of the pyr operon in Lactobacillus plantarum prevents its ability to grow at low carbon dioxide levels. J Bacteriol 187:2093–2104
19. Martinussen J, Schallert J, Andersen B, Hammer K (2001) The pyrimidine operon pyrRPB-carA from Lactococcus lactis. J Bacteriol 183:2785–2794
20. Ghim SY, Kim CC, Bonner ER, D'Elia JN, Grabner GK, Switzer RL (1999) The Enterococcus faecalis pyr operon is regulated by autogenous transcriptional attenuation at a single site in the 5'leader. J Bacteriol 181:1324–1329
21. Seul K-J, Cho H-S, Ghim S-Y (2011) Characterization of a PyrR-deficient mutant of Bacillus subtilis by a proteomic approach. Korean J Microbiol Biotechnol 39(1):9–19